

Copyright is owned by the Author of the thesis. Permission is given for a copy to be downloaded by an individual for the purpose of research and private study only. The thesis may not be reproduced elsewhere without the permission of the Author.



Modelling of chewing and aroma release during oral processing: model development, model validation and comprehensive examples for food design

A thesis presented in partial fulfilment of the requirements for the degree of

Doctor of Philosophy

in

Chemical and Bioprocess Engineering

Massey University,

Palmerston North, New Zealand

Muhammad Syahmeer How Mohd Firdaus How

2021

Abstract

Chewing is complex because of its sub-processes and interactions, and inter-individual differences between people. The development of mechanistic models can be a tool to explore these aspects and can lead to the development of foods with controlled digestion outcomes and improved sensory appeal.

A mechanistic chewing model was developed based on selection and breakage processes and implemented using a discretised population balance to predict the changes in bolus particle size distribution during chewing. The model was successfully implemented on peanuts, which gave confidence for its implementation to cooked white rice, which is an aromatic food system and has strong correlations with *in vitro* digestion. The relationship between panellists physiological, chewing and aroma release parameters during mastication of white rice were investigated *in vivo* to provide insights for model development. The findings showed that the dynamic behaviour of aroma release of all five subjects followed a similar trend with the breakdown pathways where subjects with smaller particles size in their bolus had higher aroma release. The study paved the first step in understanding the role of chewing on aroma release of cooked white rice and provided a range of oral processing behaviours for model validation.

A coupled chewing and aroma release model was developed and validated against experimental data. Adjusting the input parameters from the coupled model showed that the portion size, initial concentration of the studied aroma compound, initial liquid volume and the rice pasted fraction were the most sensitive product-related parameters. The oral cavity volume, pharynx volume, nasal cavity volume and the breathing frequency were the most sensitive physiological parameters. The physico-chemical parameter which had the most significant effect was the mass transfer coefficient in the saliva phase. Examples were also given to show the difference in aroma release when aroma compounds of varying partition coefficients were used.

The work from this thesis constitutes the first step in the application of mechanistic chewing models as a tool for food design. The next step will be to expand these models to a wider range of food systems and to a larger number of individuals to improve the model reliability.

Acknowledgements

This thesis becomes a reality with the constant help, support and encouragement of many individuals.

I would like to take this opportunity to extend my sincere thanks to all of them.

First and foremost, I would like to thank my primary supervisor, Professor John Bronlund for his excellent supervision throughout this PhD journey. Thank you for accepting and encouraging me to take up this project although I literally had zero knowledge about the topic when I first started. I am who I am now because of you. I would also like to thank my co-supervisors, Professor Jim Jones, Dr Eli Gray-Stuart and Mr Marco Morgenstern for constantly challenging my ideas and giving constructive feedbacks in our weekly meetings and thesis writing. Without their help, this PhD would have remained only a dream.

Special thanks also to Dr Isabelle Souchon and Professor Christian Trelea from INRAE, AgroParisTech, France, for allowing me to carry out a huge part of my PhD work in their lab. Although it was only for three months, the experience made a huge impact on my PhD experience. It was truly an honour to have learned so much from two of the best experts in the food engineering field.

I would also like to thank Associate Professor Farah Saleena Taip, Professor Siti Mazlina, Associate Professor Noriznan Mokhtar and from the Department of Process and Food Engineering, Universiti Putra Malaysia (UPM), for their support, encouragement and most importantly for their trust to take me as a future lecturer in the department. I look forward to serve UPM for many years to come.

I would also like to thank my sponsors, Riddet Centre of Research Excellence, Massey University, and UPM for their financial support throughout this PhD. I would not be able to complete this PhD, attending international conferences and making international collaboration without their support.

I would also like to thank all the technical staffs as well as interns in AgroParisTech who have helped to ensure all the experiments performed during the PhD was successful. In no particular order, Manon, Bridgitte, Anne-Claire, David. Not to forget to Lidia Motoi and Dr Esther Kim from Plant and Food Research, for all the technical support during my three weeks stay in the institute.

Thanks to my colleagues, squash partners and friends in New Zealand, France and Malaysia who have helped to make this PhD journey bearable. Special mention to Syidi, Abg Najmi, Matt Sells, Simon Tornquist, Nadeem Kako, Elena Piri Piri, Rohit Srivastava, Ana-Karen Castaneda, Cecilia Arnaud, Nick Smith, James van Kerkoff, Farzanah Desai, Aaron Warner, Emma Cormack, Sarah Blair, Joseph Williams, Kak Anis, Abg Man, Dino and Hajar. Thanks for listening to my constant complaints on my PhD struggles and giving me advice when I need them the most. I will also miss my weekly squash hit with Simon when it was the only time I could de-stress from work.

I want to acknowledge my family members who have continuously supported me behind the scene. My late father, Mohd Firdaus How bin Abdullah who was the one who strongly encouraged me to pursue this PhD. My mum, Khairun Sabibi Binti Abdul Majeed and my siblings, Achik, Aboi, Pompe and Kakak Mas, my kuku, Milo, thank you for your endless moral support especially when things were tough during this journey.

I would also like to dedicate this thesis to myself. Since I started, I have always doubted if the finishing line will become a reality especially working on such a challenging interdisciplinary topic. Four years later and almost 10 kg gained, writing this acknowledgement section still feels surreal.

Finally, I would like to thank my panellists who have participated in this work. I really appreciate their time for willing to chew hundreds of rice samples so I could submit this thesis (I mean although I eat rice every day, I don't think I can tolerate eating them without curries!)

List of publications and presentations

Journal publications

- **How, M. S.**, Jones, J. R., Morgenstern, M. P., Gray-Stuart, E., Bronlund, J. E., Saint-Eve, A., & Souchon, I. Modelling the role of oral processing on in vivo aroma release of white rice: Conceptual model and experimental validation. *LWT*, 2021.

Conference Oral Presentations

- **How, M. S.**, Gray-Stuart, E.M., Morgenstern, M., Jones, J.R. and Bronlund, J.E. Selection and breakage functions of foods during human mastication. 13th International Congress on Engineering and Food, Melbourne, 23rd - 26th September **2019**.
- **How, M. S.**, Gray-Stuart, E.M., Morgenstern, M., Jones, J.R., Bronlund, J.E., Trelea, C., and Souchon, I. Modelling the bolus formation of starch-based foods during oral processing and its impact on the dynamics of aroma release. Journee' des doctorants du GMPA, Paris, 25th June **2019**.
- **How, M. S.**, Gray-Stuart, E.M., Morgenstern, M., Jones, J.R. and Bronlund, J.E. Predicting the PSD of Starch Food Bolus During Mastication. Biomouth meeting, University of Canterbury, 29th - 30th October **2018**.
- **How, M. S.**, Gray-Stuart, E.M., Morgenstern, M. and Jones, J.R. Bronlund, J.E. A Mathematical Model of the Bolus Formation of Starch-Based Foods during Oral Processing. 5th International Conference on Food Oral Processing, University of Nottingham, 1st -4th July **2018**
- **How, M. S.**, Gray-Stuart, E.M., Morgenstern, M., Jones, J.R. and Bronlund, J.E. Modelling the bolus formation of starchy foods during oral processing. Riddet Symposium, Auckland, 5th November **2017**.
- **How, M. S.**, Gray-Stuart, E.M., Morgenstern, M., Jones, J.R. and Bronlund, J.E. Modelling of bolus formation during oral processing. Riddet Symposium, Massey University, 31st October– 2nd November **2016**. (*Awarded as runner up*)

Poster Presentations

- **How, M. S.**, Gray-Stuart, E.M., Morgenstern, M., Jones, J.R., Bronlund, J.E., and Souchon, I. Effect of Portion Size and Chewing Rate on the Retronasal Aroma release of Flavoured White Rice. Food Structures, Digestion and Health, Rotorua, 30th September-03rd October **2019**.
- **How, M. S.**, Gray-Stuart, E.M., Morgenstern, M., Jones, J.R. and Bronlund, J.E. Selection and breakage functions of foods during human mastication. 13th International Congress on Engineering and Food, Melbourne, 23rd - 26th September **2019**.

Table of Contents

Abstract	I
Acknowledgements	II
List of publications and presentations	IV
Table of Contents	V
List of Figures	VIII
List of Tables	XVI
List of Abbreviations	XVIII
List of Symbols	XIX
Chapter 1 Introduction	1
1.1 Project overview	1
1.2 Overall Goal and Research Objectives	5
Chapter 2 Literature review	8
2.1 Introduction	8
2.2 The chewing process	8
2.3 Saliva	11
2.4 Effects of mastication	17
2.5 Chewing models	19
2.6 Application of the chewing models in aroma release	35
2.7 Chapter conclusion	40
Chapter 3 Chewing model development	43
3.1 Conceptual model	43
3.2 Model formulation and implementation	48
3.3 Chapter conclusion	74
Chapter 4 Predicting the PSD of peanuts using different selection and breakage models	76
4.1 Introduction	76
4.2. The model	76
4.3 Model application	77
4.4 Model results and discussions	100
4.5 Chapter conclusion	110
Chapter 5 Chewing models as a tool for food design	111
5.1 Introduction	111
5.2 Case study one: Understanding the effect of portion size on selection	112

5.3 Case study two: Understanding the breakage function of peanuts with different initial moisture contents	123
5.4 Chapter conclusion	135
Chapter 6 Influence of mastication on aroma release of rice	137
6.1 Introduction	137
6.2 Conceptual model relating the physiology and oral processing to aroma release	139
6.3 Materials and methods	141
6.4 Results and discussions	158
6.5 Chapter conclusion	178
Chapter 7 A mathematical model for in vivo aroma release	180
7.1 Introduction	180
7.2 Conceptual model development	181
7.3 Model assumptions	186
7.4 Mathematical model formulation	187
7.5 Numerical solution	195
7.6 Coupling of the food breakdown model and the aroma release model	196
7.7 General model results	196
7.8 Chapter summary	200
Chapter 8 Validation of the aroma release model	201
8.1 Introduction	201
8.2 Objective 1: Aroma model validation using in-vivo experimental bolus properties	202
8.3 Objective 2: Validation using coupled chewing-aroma release models	229
8.4 Chapter conclusion	246
Chapter 9 Application of the aroma release model	247
9.1 Introduction	247
9.2 Using the model to provide insights for food design	247
9.3 Effect of physiological parameters on model predictions	255
9.4 Effect of physico-chemical parameters on model predictions	258
9.5 Chapter conclusion	262
Conclusions and Recommendations for Future Work	263
Conclusions	263
Recommendations for Future Work	266
References	270
Appendices	289
Appendix A: MATLAB codes used in the thesis	289

Appendix B: PSO algorithm formulation	313
Appendix C: Information sheet and consent forms	317
Appendix D: Data used in Chapter 4, 5 and 6.	322
Appendix E: Effect of chewing on in vitro digestion of brown rice	324
Appendix F: A comparison of the bolus properties of starch-based food systems	330

List of Figures

Fig. 2-1: A conceptual model of chewing described as a sequence of events. Decision boxes are shown as diamonds whereas process boxes are rectangular, from Lucas et al. (2002).	9
Fig. 2-2: The process model of feeding from Hiiemae (2004)	10
Fig. 2-3: Conceptual model of oral processing from Gray-Stuart (2016).	11
Fig. 2-4: Role of saliva in oral processing. Figure from Mosca & Chen (2017).	15
Fig. 2-5: A typical plot of number of selected particles vs number of offered particles. The data (red circle markers) was obtained from a single chew experiment performed on Subject 1 in van der glas et al. (2018) for particle size of 1.7 mm. The data is then fitted with Eq.2.3 to obtain the number of breakage sites n_b and the affinity factor, O_1	26
Fig. 2-6: Change in shape of a spherical gum bolus from Zhang et al. (2019). Left shows the shape with a natural tongue function whereas the right side is when the tongue was kept away from the bolus. ...	27
Fig. 2-7: Breakage function predictions example with varying input parameters. a. prediction with varying r values and a constant b value in Eq.2.8. b, prediction with varying b values and a constant r value in Eq.2.8. c, prediction with varying r values and a constant s value in Eq.2.9. d, prediction with varying s values and a constant r value in Eq.2.9 e, prediction with varying r values in Eq.2.10.	30
Fig. 2-8: Discretised population balance during mastication from Gray-Stuart (2016).	33
Fig. 2-9: Conceptual model showing the transfer of flavour release from a solid food from Hills and Harrison (1995). c denotes concentration, v , volume, and subscripts g,s and f refers to gas, saliva and food respectively.	35
Fig. 2-10: Two-layer stagnant film theory from Hills and Harrison (1995). Solid vertical line is the interface. In the theory it was assumed there exists the surface layer of thickness L_s adjacent to the interface (the vertical lines). The volatile concentration can then be estimated by a linear concentration gradient across the stagnant layer (dotted) line, where the volatiles diffuse into the uniform bulk saliva concentration, c_s	37
Fig. 2-11: Conceptual model of the steps involved during mastication of a solid food product from Doyennette et al (2014).	40
Fig. 3-1: Conceptual diagram describing the processes involved during mastication.	44
Fig. 3-2 Schematic model diagram showing the steps required to implement the one-way and two-way competition models.	51
Fig. 3-3 Volume fraction of particles selected at 1 chew, 15 chews and 30 chews between one-way and two-way competition models. The simulation was run three times.	54
Fig. 3-4: Examples of one-way and two-way competition model predictions using real peanut bolus PSD data. Black diamond marker represents the real PSD chewed peanuts data used as the model input for the selection models. A cumulative percentage number of particles is used here to show selected particles. For instance in a. selected particles make up around 10% of the total number of particle from the input data. Red X marker, prediction after one simulation. Black round marker, prediction after the second simulation. Blue diamond marker, prediction after the third simulation. a, One-way competition model when implemented on a 1 chew data. b, Two-way competition model when implemented on a 1 chew data. c, One-way competition model when implemented on a 15 chew data. d, Two-way competition model when implemented on a 15 chew data. e, One-way competition model when implemented on a 30 chew data. f, Two-way competition model when implemented on a 30 chew data.	55
Fig. 3-5: Scanned image of chewing with bite marks (circled in red). The projected area of the occlusal area was then measured using ImageJ.	57

Fig. 3-6: Projected occlusal area (mm^2) measured from the scanned image of the bite marks on a chewing gum for four subjects. Dashed line is the median value observed in Sumonsiri et al. (2019). 58

Fig. 3-7: Number of selected particles against the number of offered particles for Whole Orzo (Black X marker), Halved Orzo (red round marker), Whole Rice (blue triangle marker) and Halved Rice (green square marker). The error bar represents the standard deviation of a triplicate measurement..... 58

Fig. 3-8: Projected area of selected particles against the number of offered particles for Whole Orzo (Black X marker), Halved Orzo (red round marker), Whole Rice (blue triangle marker) and Halved Rice (green square marker). Dotted black line shows the projected occlusal area for the particular subject. The error bar represents the standard deviation of a triplicate measurement. 60

Fig. 3-9 Schematic diagram showing one of the two approaches used to address the conservation of occluded particles volume during breakage, which is a modelling challenge. 66

Fig. 3-10: Comparison between generating daughter particles using bins and without bins for a single particle. Black round with black face colour, breakage of a particle with bins. Black round with white face colour, breakage of a single particle without bins. Red line, breakage function, Eq. 2.10. The simulation was run once..... 69

Fig. 3-11 Schematic model diagram showing the processes required to generate daughter particles after breakage using the second numerical approach. 70

Fig. 3-12: Daughter particles distribution as a function of the number of selected particles. Black round marker, volume distribution of daughter particles. Red line, breakage function using Eq. 2.10. 71

Fig. 3-13 Schematic flow diagram showing the general process involved to apply the discretised population model 74

Fig. 4-1 Discrete Particle Size Distribution (PSD) of 4 g of peanuts generated from Flynn (2012). The dotted markers (connected with line) show the sieve data from Flynn (2012). The rest are the generated particles. The randfixedsum approach allows a population of particles to be generated from the sieve data..... 79

Fig. 4-2: The normalised mean, standard deviation and standard error at 25% of the swallow point (10th chew) using lower bound values as input parameters. 87

Fig. 4-3: The normalised mean, standard deviation and standard error at 50% of the swallow point (20th chew) using lower bound values as input parameters. 88

Fig. 4-4: The normalised mean, standard deviation and standard error at 100% of the swallow point (35th chew) using lower bound values as input parameters..... 89

Fig. 4-5: The normalised mean, standard deviation and standard error at 25% of the swallow point (10th chew) using upper bound values as input parameters. 90

Fig. 4-6: The normalised mean, standard deviation and standard error at 50% of the swallow point (20th chew) using upper bound values as input parameters. 91

Fig. 4-7: The normalised mean, standard deviation and standard error at 100% of the swallow point (35th chew) using upper bound values as input parameters..... 92

Fig. 4-8: Swarm fitted (black marker) and experimental (red marker) d_{90} , d_{50} and d_{10} values across various chew numbers using 20 swarm. 94

Fig. 4-9: Swarm fitted (black marker) and experimental (red marker) d_{90} , d_{50} and d_{10} values across various chew numbers using 40 swarm size. 94

Fig. 4-10: Swarm fitted (black marker) and experimental (red marker) d_{90} , d_{50} and d_{10} values across various chew numbers using 60 swarm size. 95

Fig. 4-11 Swarm fitted (line) and experimental (coloured dot markers) in cumulative PSD form across various chew numbers of 20, 40 and 60 swarm size..... 96

Fig. 4-12 Swarm fitted (dot markers with face colour) and experimental (dot markers with no face colour) when presented in terms of volume fraction vs sieve size classes in across various chew numbers of 20 swarm size.	97
Fig. 4-13 Swarm fitted (dot markers with face colour) and experimental (dot markers with no face colour) when presented in terms of volume fraction vs sieve size classes in across various chew numbers of 40 swarm size.	98
Fig. 4-14 Swarm fitted (dot markers with face colour) and experimental (dot markers with no face colour) when presented in terms of volume fraction vs sieve size classes in across various chew numbers of 60 swarm size.	99
Fig. 4-15: Swarm fitted (black marker) and experimental (red marker) d_{90} , d_{50} and d_{10} values at various chew numbers when different selection models and a fixed breakage function were used. a. Model fits of one-way competition and the Austin (1971) breakage model. b. Model fits of two-way competition and Austin (1971) breakage model. c. Model fits of power law model and Austin (1971) breakage model.	103
Fig. 4-16 Model predictions when the assumed initial PSD is used as the input distribution using the swarm fitted of one-way and two-way competition models in Table 4-3.	103
Fig. 4-17: Predicted (black marker) and experimental (red marker) d_{90} , d_{50} and d_{10} values at various chew numbers when the one-way competition model was used to predict the selection for chew number less than an optimum chew number, here 18 chews, and the two-way competition model for chew number greater than the optimum. The Austin (1971) breakage model was used with a fixed fragmentation index.	105
Fig. 4-18: Predicted (black marker) and experimental (red marker) d_{90} , d_{50} and d_{10} values at various chew numbers when the combined one-way and two-way competition model was used to describe particle selection process. Two breakage models in Lucas and Luke (1983b), (a) empirical breakage function (Eq. 2.8) and (b) mechanistic breakage function (Eq. 2.9) were applied and the model predictions were compared.	108
Fig. 5-1 Mean peanut bolus data of 2 g and 4 g portion sizes. Redrawn from Flynn (2012). The bolus data is a mean of 10 subjects at swallow point (17 and 26 chews for 2 g and 4 g respectively). The original figure of Flynn (2012) which consists the error bar can be referred in Appendix D.	112
Fig. 5-2: Model flow chart to generate PSD after a single chew for the 2 g portion size. PS refers to portion size and n refers to the iteration number. Miss refers to the rejected particles which will not be accounted for in the simulation.	115
Fig. 5-3: Cumulative mass fraction vs particle size (mm) for 4 g and 2 g peanuts respectively. Red marker = 2 g PSD, Black marker = 4 g PSD. The simulation was run once.	117
Fig. 5-4 A comparison of 4 g and 2 g peanuts PSD, where the 2 g peanuts PSD is plotted for the number of times the simulation was run (5, 10, 100 and 1000 simulations).	118
Fig. 5-5: The schematic diagram to take readers through the steps taken to minimise the sum of squares residuals to obtain the input parameters required to fit the particle size output for the 2 g and 4 g peanuts.	120
Fig. 5-6: A comparison between model predictions and experimental data of the PSD at swallow point for 2 g and 4 g peanuts. The one-way competition model was used to predict particles that were selected. An R^2 value of 0.99 shows the goodness of fit of the model.	122
Fig. 5-7: A comparison between model predictions and experimental data of the PSD at swallow point for 2 g and 4 g peanuts. The two-way competition model was used to predict particles that were selected. An R^2 value of 0.99 shows the goodness of fit of the model.	123
Fig. 5-8: The cumulative PSD of peanut particles in the food bolus where peanuts were served after they were removed from food matrices. Light blue marker, peanuts removed from scone (7.8 chews); Orange marker, peanuts removed from gelatine gel (7.5 chews); Grey marker; peanuts removed from	

brownie (7.5 chews), Yellow marker, peanuts removed from chocolate (7 chews); Dark blue marker, peanuts with no matrix (7.8 chews). 1 g portion of peanuts. Figure from Hutchings (2011).	125
Fig. 5-9: The new interpolated F(s) data is denoted by the blue dotted lines, and the circle marker is the original data.	127
Fig. 5-10: The probability density function, f(s).....	127
Fig. 5-11: The probability density function for the projected surface area, f(s) and the volume, f(v).	128
Fig. 5-12: The original F(s) data (blue round marker); The interpolated F(s), blue dotted line; The cumulative volume fraction F(v), red solid line.....	128
Fig. 5-13: Cumulative volume (%) for peanuts after they were removed from matrices measured at swallow point.....	129
Fig. 5-14: Cumulative mass fraction vs particle size (mm) for 4 g and 1 g peanuts respectively. Red marker = 1 g PSD, Black marker = 4 g PSD.....	131
Fig. 5-15: A schematic diagram showing the steps undertaken to solve model input parameters for peanuts with different moisture contents after being removed from matrices when chewed at swallow point. The algorithm solves for one set of selection input parameters and five sets of breakage input parameters.	132
Fig. 5-16: A comparison between model predictions and experimental data of the PSD at swallow point for the five peanuts that were removed from matrices and have different moisture contents. Dotted lines are model predictions and open circles are the data. The error bar is the standard deviation of the model predictions after 50 simulations.	135
Fig. 6-1: A diagram to demonstrate the possible factors that can influence aroma release. Physiological parameters such as oral volume, pharynx volume and nasal volume can affect aroma release. Oral processing variables include the mastication efficiency, saliva flow rate, chewing frequency (rate) and the dynamics of the particle size distribution (PSD).....	140
Fig. 6-2: Rice kept warm in 60°C water bath.	144
Fig. 6-3: Rice bolus diluted in glycerol under constant shaking at 100 rpm.....	145
Fig. 6-4 Petri dish containing particles and glycerol which are gently separated using a plastic spatula prior to image acquisition.	146
Fig. 6-5: Petri dishes containing the boluses were placed inside ScanCube 308 which conferred a standardised brightness. A camera is used to capture the image of the bolus.....	146
Fig. 6-6 The factor, f from Eq.6.2 to calculate the height of the particle at different mastication stages (3 replicates each), obtained by minimising the residual sum of squares between the total volume of particles calculated in Eq. 6.1 and the experimental recovered volume of bolus.	148
Fig. 6-7 Data showing the intensity vs number of measurement cycles (a) and area under the curve (b) of PTR-MS results of hexanal (m/z 103) in cooked rice at different equilibration time which was measured in vitro.....	151
Fig. 6-8: In vitro set up to measure aroma compounds in rice using the PTR-MS.....	152
Fig. 6-9: The 20 highest protonated molecular ion (AUC) during experimental in vivo trial of two subjects when measured in SCAN mode of the PTR-MS.....	153
Fig. 6-10: Rice samples in Schott Vials placed inside warmer that was set at 50°C.	156
Fig. 6-11: Measuring in vivo aroma release using the PTR-MS.....	157
Fig. 6-12: Aroma release curve profile. The total amount of aroma released (AUC 1 & AUC 2), the maximum intensity (I_{max1} & I_{max2}), the time at which I_{max} occurred (T_{max1} & T_{max2}) as well as the intensity and AUC during multiple stages during mastication (25%, 50%, 75% and 100% of the time when first	

swallow occurred) were determined from the aroma release curve (Image redrawn from D�el�eris et al. (2016)).	157
Fig. 6-13: Physiological volumes (Oral cavity, Pharynx and Nasal volume) of all subjects.	158
Fig. 6-14: Saliva flowrates of all subjects.	159
Fig. 6-15: Masticatory efficiency of all subjects.	159
Fig. 6-16: Number of chews and chewing time (s) required to reach swallow point for all subjects.	160
Fig. 6-17: The percentage recovery of solids and the ratio of saliva mass to solids mass (g saliva/100 g solids) at swallow point for each subject.	161
Fig. 6-18: Saliva content as a function of chew number for subjects A1-A5, showing the variation in both saliva rate and apparent initial saliva present. The initial quantity of 5 g rice was at 61.0% moisture content.	163
Fig. 6-19: Bolus particle size distribution results for all subjects. The plotted curves are to guide the eye. Subject A1 and A4 clearly have a different number of chews to completion, $N_{100\%}$, which means 25% of completion in subject A1 is about 4 chews while in subject A4 it is 6 chews.	166
Fig. 6-20: Reduction in whole particles with chew number (with (0,100) point removed).	166
Fig. 6-21: Saliva addition rate. It is assumed that if the trendline is constrained to pass through (0,0) this will draw out the salivating effects of elevating the initial saliva content	167
Fig. 6-22: Breakdown pathways of rice during oral processing from PCA analysis. (a) shows the plot when PC 1 and PC 2 of the bolus properties between subjects were compared. (b) shows the plot of the factor loadings of the bolus variables measured for all subjects and provides a guide for the breakdown pathway plot, in (a). Arrows are drawn from left to right to illustrate the breakdown pathway from the time when samples were introduced in the mouth (initial) to the swallowing point. The points between the initial and swallow point of each subject were the bolus properties at 25%, 50% and 75% of the subject's total oral processing time.	170
Fig. 6-23: The dynamics of aroma release parameters (AUC and I values) during oral processing between subjects. Subject A1 and A4 were differentiated from other subjects with higher I and AUC values while other subjects had similar I and AUC values during oral processing.	172
Fig. 6-24: Principal components of bolus properties compared with the principal components of intensity and AUC values of aroma release measured during several mastication stages. (a) shows the plot of PC 1 aroma release vs PC 1 bolus properties which explained most of the variation between subjects whereas (b) showed the impact of bolus residues on aroma release. No lines were drawn on (c) and (d) as both provided little information on the aroma release parameters.	174
Fig. 7-1: Conceptual diagram of the interconnected compartments and the mechanisms involved in flavour release during the consumption of cooked white rice.	183
Fig. 7-2: 'Cleave and paste' mechanism during mastication of cooked rice	184
Fig. 7-3 Schematic diagram showing the model flow chart to couple the particle size reduction model developed in Chapter 3 and the models describing flavour release developed in this chapter.	197
Fig. 7-4: Results of 12 model variables for the release of ethyl propanoate during the consumption of cooked white rice: (a) volume of pasted particles in the oral cavity, $V_{Opasted}$, (b) volume of saliva in the oral cavity, V_{Os} , (c) liquid bolus saturation, S , (d) Surface area of bolus, A_{Ob} , (e) Concentration of aroma in the liquid bolus of the oral cavity, C_{Os} , (f) Concentration of aroma in the mucosa layer in the oral cavity, C_{Om} , (g) Concentration of aroma in air phase in the oral cavity, C_{Oa} , (h) Concentration of aroma in the liquid bolus in the pharynx, C_{Fs} (i) Concentration of aroma in the air phase in the pharynx, C_{Fa} , (j) Concentration of aroma in the mucosa layer in the pharynx, C_{Fm} , (k) Concentration of aroma in the mucosa layer in the nasal cavity, C_{Nm} , (l) Concentration of aroma in the air phase in the nasal cavity, C_{Na} .	198

Fig. 8-1: Bolus particle size distribution results for all subjects. The line curves were plotted to guide the reader.....	204
Fig. 8-2 The mean and standard deviation of the fraction, f of diameter across all mastication stages (measured in Chapter 7) to calculate the height of the particle in Eq. 6.2 obtained by minimising the residual sum of squares between the total volume of particles calculated in Eq. 6.1 and the experimental recovered volume of bolus.....	205
Fig. 8-3: Volume of pasted particles and total surface area of particles data for subject A1. A linear model (red line) was fitted to the data. The model does not fit the data well for subject A1 as demonstrated by the low R^2 value.....	205
Fig. 8-4: Volume of pasted particles and total surface area of particles data for subject A2. A linear model (red line) was fitted to the data. The model fit the data well for subject A2 as demonstrated by the high R^2 value.....	206
Fig. 8-5: Volume of pasted particles and total surface area of particles data for subject A3. A linear model (red line) was fitted to the data. The model fit the data well for subject A3 as demonstrated by the high R^2 value.....	206
Fig. 8-6: Volume of pasted particles and total surface area of particles data for subject A4. A linear model (red line) was fitted to the data. The model fit the data well for subject A4 as demonstrated by the high R^2 value.....	207
Fig. 8-7: Volume of pasted particles and total surface area of particles data for subject A5. A linear model (red line) was fitted to the data. The model fit the data well for subject A5 as demonstrated by the high R^2 value.....	207
Fig. 8-8: An example to illustrate the dynamics of acetone signal during chewing. Data shown above is a single replicate from one of the panellists'. The arrow in the figure shows the length of time in (s) for one breathing cycle, which determines the breathing frequency. For instance, it takes about 3-4 s for the subject to finish a breathing cycle. The breathing frequency used in the model is the average of several breathing frequencies measured in all five replicates in the <i>in vivo</i> aroma release experiments.	211
Fig. 8-9: $1/A$ vs β plot of 2- nonanone. The ratio of the slope and the y-intercept is K_{ap}	215
Fig. 8-10: $1/A$ vs β plot of Ethyl propanoate. The ratio of the slope and the y-intercept is K_{ap}	215
Fig. 8-11: Typical <i>in vivo</i> experimental data results of 2-nonanone that was measured using PTR-MS (single replicate).....	218
Fig. 8-12: Subplots to demonstrate the effect of different sampling time on the experimental data. The black symbol in the subplot refers to the original model results, while the other coloured curves referred to the curves that were taken at different sampling times.....	219
Fig. 8-13: Plot to demonstrate the effect of the different starting time of the experimental data. The blue curve in the plot refers to the original model results, while the other coloured curves referred to the curves that started at different time.....	221
Fig. 8-14: Subplots to demonstrate the cumulative area the curve with different sampling time. The black dashed curve in the subplot refers to the original model results, while the other coloured curves referred to the curves that were taken at different sampling time.....	222
Fig. 8-15: Model prediction against experimental data of 2-nonanone (m/z 143) and ethyl propanoate (m/z 103) for Subject A1. Rel. AUC refers to the relative cumulative area under the curve, where the cumulative area under the curve was normalised against the total area under the curve. The model was also predicted using different pasted size threshold (0.2 mm, 0.354 mm, 0.5 mm and 1 mm) and compared against the five replicates of the experimental data.	224
Fig. 8-16: Model prediction against experimental data of 2-nonanone (m/z 143) and ethyl propanoate (m/z 103) for Subject A2. Rel. AUC refers to the relative cumulative area under the curve, where the cumulative area under the curve was normalised against the total area under the curve. The model was	

also predicted using different pasted size threshold (0.2 mm, 0.354 mm, 0.5 mm and 1 mm) and compared against the five replicates of the experimental data.	225
Fig. 8-17: Model prediction against experimental data of 2-nonanone (m/z 143) and ethyl propanoate (m/z 103) for Subject A3. Rel. AUC refers to the relative cumulative area under the curve, where the cumulative area under the curve was normalised against the total area under the curve. The model was also predicted using different pasted size threshold (0.2 mm, 0.354 mm, 0.5 mm and 1 mm) and compared against the five replicates of the experimental data.	226
Fig. 8-18: Model prediction against experimental data of 2-nonanone (m/z 143) and ethyl propanoate (m/z 103) for Subject A4. Rel. AUC refers to the relative cumulative area under the curve, where the cumulative area under the curve was normalised against the total area under the curve. The model was also predicted using different pasted size threshold (0.2 mm, 0.354 mm, 0.5 mm and 1 mm) and compared against the five replicates of the experimental data.	227
Fig. 8-19: Model prediction against experimental data of 2-nonanone (m/z 143) and ethyl propanoate (m/z 103) for Subject A5. Rel. AUC refers to the relative cumulative area under the curve, where the cumulative area under the curve was normalised against the total area under the curve. The model was also predicted using different pasted size threshold (0.2 mm, 0.354 mm, 0.5 mm and 1 mm) and compared against the five replicates of the experimental data.	228
Fig. 8-20 Initial PSD used in the model (5 g).	230
Fig. 8-21: Best-fit model against experimental data for Subject A1.....	232
Fig. 8-22: Best-fit model against experimental data for Subject A2.....	233
Fig. 8-23: Best-fit model against experimental data for Subject A3.....	234
Fig. 8-24: Best-fit model against experimental data for Subject A4.....	235
Fig. 8-25: Best-fit model against experimental data for Subject A5.....	236
Fig. 8-26 Model prediction against experimental data of 2-nonanone (m/z 143) and ethyl propanoate (m/z 103) for Subject A1. Rel. AUC refers to the relative cumulative area under the curve, where the cumulative area under the curve was normalised against the total area under the curve. The model was also predicted using different pasted size threshold (0.2 mm, 0.354 mm, 0.5 mm and 1 mm) and different selection models (one-way and two-way competition) and compared against the five replicates of the experimental data.	240
Fig. 8-27 Model prediction against experimental data of 2-nonanone (m/z 143) and ethyl propanoate (m/z 103) for Subject A2. Rel. AUC refers to the relative cumulative area under the curve, where the cumulative area under the curve was normalised against the total area under the curve. The model was also predicted using different pasted size threshold (0.2 mm, 0.354 mm, 0.5 mm and 1 mm) and different selection models (one-way and two-way competition) and compared against the five replicates of the experimental data.	241
Fig. 8-28 Model prediction against experimental data of 2-nonanone (m/z 143) and ethyl propanoate (m/z 103) for Subject A3. Rel. AUC refers to the relative cumulative area under the curve, where the cumulative area under the curve was normalised against the total area under the curve. The model was also predicted using different pasted size threshold (0.2 mm, 0.354 mm, 0.5 mm and 1 mm) and different selection models (one-way and two-way competition) and compared against the five replicates of the experimental data.	242
Fig. 8-29 Model prediction against experimental data of 2-nonanone (m/z 143) and ethyl propanoate (m/z 103) for Subject A4. Rel. AUC refers to the relative cumulative area under the curve, where the cumulative area under the curve was normalised against the total area under the curve. The model was also predicted using different pasted size threshold (0.2 mm, 0.354 mm, 0.5 mm and 1 mm) and different selection models (one-way and two-way competition) and compared against the five replicates of the experimental data.	243

Fig. 8-30 Model prediction against experimental data of 2-nonanone (m/z 143) and ethyl propanoate (m/z 103) for Subject A5. Rel. AUC refers to the relative cumulative area under the curve, where the cumulative area under the curve was normalised against the total area under the curve. The model was also predicted using different pasted size threshold (0.2 mm, 0.354 mm, 0.5 mm and 1 mm) and different selection models (one-way and two-way competition) and compared against the five replicates of the experimental data. 244

Fig. 9-1: Effect of parameters related to the product and individual which may be of interest to a food manufacturer. Using the physiological parameters of Subject A4, C_{na} of 2-nonanone was predicted. a. Aroma release (C_{na}) when portion size is varied (2.5 g, 5 g and 10 g of rice), b. Aroma release (C_{na}) when initial particle size is varied (halved, original and doubled size) for 5 g of rice c. Aroma release (C_{na}) when the initial concentration is varied for 5 g of rice, d. Aroma release (C_{na}) when the breakage function (represented by the fragmentation variable, r) is varied for 5 g of rice, e. Aroma release (C_{na}) when saliva flow rate is varied for 5 g of rice, f. Aroma release (C_{na}) when the initial liquid volume is varied for 5 g of rice, g. Aroma release (C_{na}) when the breakage function (represented by the pasted fraction, p) is varied for 5 g of rice, h. Aroma release (C_{na}) when the chewing rate (0.7 chew/s, 1.5 chew/s and 2 chew/s) is varied for 5 g of rice. 252

Fig. 9-2: Effect of physiological parameters on aroma release (C_{na}). Using the physiological parameters of Subject A4 as a reference value, C_{na} of 2-nonanone was predicted. a. Effect of breathing frequency on aroma release (C_{na}) (0.12 cycle/s, 0.25 cycle/s, 0.32 cycle/s), b. Effect of the oral cavity volume on aroma release (C_{na}) (20,000 mm³, 60,000 mm³, 100,000 mm³) c. Effect of the pharynx volume on aroma release (C_{na}) (15,000 mm³, 32,000 mm³, 60,000 mm³), d. Effect of the nasal cavity volume on aroma release (C_{na}) (12,000 mm³, 16,000 mm³, 40,000 mm³) 256

Fig. 9-3: Effect of mass transfer coefficient in saliva in oral cavity on aroma release (C_{na}) (0.00001 mm/s, 0.001 mm/s, 0.1 mm/s)..... 260

Fig. 9-4 Release of aroma compounds with different partition coefficients of air to saliva phase. 261

List of Tables

Table 2-1: Salivary flow rates in response to chewing different foods from (Watanabe & Dawes, 1988; Engelen et al., 2003; Gavião et al., 2004); *NA is defined as not applicable as the parameter was not measured in the study.....	13
Table 3-1 Summary of breakage models commonly used in milling industry	63
Table 4-1: The range of the input parameters was chosen based on the range of values found when single chew experiments were performed among five subjects in (van der Glas et al., 2018) for the selection model input parameters and in (van der Glas et al., 1987) for the breakage model input parameter, r.	84
Table 4-2: Model input parameters solved by the PSO algorithm when the swarm size (number of particles) in the PSO algorithm was varied.....	93
Table 4-3: Selection model input parameters optimised by the PSO algorithm, for a constant breakage model.	102
Table 4-4: Selection model input parameters optimised by the PSO algorithm, for a fixed fragmentation index used in the Austin (1971) breakage model.....	104
Table 4-5: Model input parameters optimised by the PSO algorithm, the global best fitness value (the sum of squared residuals minimised by the PSO algorithm) and the R-squared value when one-way and two-competition model were combined and the breakage model was varied.....	109
Table 5-1: Upper and lower bounds set in the PSO algorithm to fit the model to predict the PSD for 2 g and 4 g portion sizes.	120
Table 5-2: Best fit model input parameters solved by the PSO algorithm to predict the PSD at swallow point for the 2 g and 4 g peanuts. The input parameters of 4 g peanuts when fitted with data of various number of chews in section 4.4.1 (Table 4-3) is also added for comparison.....	121
Table 5-3: Mastication parameters for the five peanut variants from Hutchings (2011).....	124
Table 5-4: Cumulative area distribution data for the peanuts after being removed from different matrices, presented in terms of their varying moisture contents (MC) (Hutchings, 2011).	125
Table 5-5: Cumulative area distribution data (with extra points) for the peanuts after being removed from different matrices, presented in terms of their varying moisture contents (MC).	126
Table 5-6: Best fit model input parameters solved by the PSO algorithm to predict the PSD at swallow point for the five peanuts that were removed from matrices at different moisture contents. A good agreement between the model and data is found (R-squared > 0.96 for all peanuts)	134
Table 6-1 Aroma compounds of Basmati and Jasmine Rice after measurement in DHS-GC-MS.....	150
Table 6-2: Bolus properties at four stages of mastication (25%, 50%, 75% and 100%) for all five subjects (A1-A5). Each trial was performed three times, N=3. M is the mean of the bolus characteristic measured, and SE is the standard error. O/all is the overall mean and standard error for all subjects. Significance levels were encoded as follows: *: p<0.05; **: p < 0.01; ***: p < 0.001.....	161
Table 6-3: Aroma parameters extracted from subject's aroma release curve for m/z 143 (2-nonanone).	173
Table 6-4: Aroma parameters extracted from subject's aroma release curve for m/z 103 (Ethyl propanoate).	173
Table 8-1: Number of chews and time taken to swallow of all subjects determined from the PSD and <i>in vivo</i> aroma release experiments.	208
Table 8-2 Subject's physiological input values used in the model	209
Table 8-3: Model input parameters which include the mass transfer coefficient, partition coefficient and the initial concentration of the aroma compounds that were spiked in the cooked white rice.....	211

Table 8-4: Physico-chemical characteristics of the target aroma compounds	216
Table 8-5: GC peak areas and the concentration of aroma compounds in the liquid/rice/air phase when in thermodynamic equilibrium.....	217
Table 8-6: Best fit input parameters of the PSD model evaluated from the PSO algorithm.....	237
Table 9-1 PSD model input parameters which was previously fitted in Chapter 8.	248
Table 9-2 Reference physiological parameters of subject A4.	249
Table 9-3 Reference physicochemical parameters used in the simulation.....	250
Table 9-4 Product related and chewing parameters which may of interest to a food manufacturer ...	253
Table 9-5 Physiological values manipulated in the simulations.	255
Table 9-6 Physicochemical parameters manipulated in the simulations.....	258

List of Abbreviations

ODE	Ordinary Differential Equation
PSD	Particle Size Distribution
PSO	Particle Swarm Optimisation
PTR-MS	Proton Transfer Reaction- Mass Spectrometry

List of Symbols

Symbol	Description	Unit
A_{Oam}	air/lubricated mucosa contact area in the oral cavity	mm^2
A_{Ob}	air/bolus contact area in the oral cavity	mm^2
A_{Fas}	air/saliva contact area in the pharynx	mm^2
A_{Fam}	air/lubricated mucosa in the pharynx	mm^2
A_{Nam}	air/lubricated mucosa in the nasal cavity	mm^2
C_{Os}	aroma concentration in the saliva in the oral cavity	g/mm^3
C_{Oa}	aroma concentration in the air in the oral cavity	g/mm^3
C_{Om}	aroma concentration in the lubricated mucosa in the oral cavity	g/mm^3
C_{Op}	aroma concentration in the product (rice) in the oral cavity	g/mm^3
C_{Fs}	aroma concentration in the saliva in the pharynx	g/mm^3
C_{Fa}	aroma concentration in the air in the pharynx	g/mm^3
C_{Fm}	aroma concentration in the lubricated mucosa in the pharynx	g/mm^3
C_{Na}	aroma concentration in the air in the nasal cavity	g/mm^3
C_{Nm}	aroma concentration in the lubricated mucosa in the nasal cavity	g/mm^3
F_{breath}	breathing frequency	number of cycles/s
$fr_{opening}$	opening frequency of the velopharynx	occurrence number/s
fr_{chew}	chewing frequency	number of chews/s
k_{Oa}	mass transfer coefficient in the air phase in the oral cavity	mm/s
k_{Os}	mass transfer coefficient in the saliva phase in the oral cavity	mm/s
k_{Om}	mass transfer coefficient in the lubricated mucosa in the oral cavity	mm/s

k_{Fs}	mass transfer coefficient in the saliva phase in the pharynx	mm/s
k_{Fa}	mass transfer coefficient in the air phase in the pharynx	mm/s
k_{Fm}	mass transfer coefficient in the lubricated mucosa in the pharynx	mm/s
k_{Na}	mass transfer coefficient in the air phase in the nasal cavity	mm/s
k_{Nm}	mass transfer coefficient in the lubricated mucosa in the nasal cavity	mm/s
K_{Oas}	air/saliva partition coefficient in the oral cavity	[C_{Oa}/ C_{Os}] at equilibrium
K_{Oam}	air/lubricated mucosa partition coefficient in the oral cavity	[C_{Oa}/ C_{Om}] at equilibrium
K_{Osp}	saliva/product(rice) partition coefficient in the oral cavity	[C_{Os}/ C_{Op}] at equilibrium
K_{Fas}	air/saliva partition coefficient in the pharynx	[C_{Fa}/ C_{Fs}] at equilibrium
K_{Fms}	lubricated mucosa/saliva partition coefficient in the pharynx	[C_{Fm}/ C_{Fs}] at equilibrium
K_{Fam}	air/lubricated mucosa partition coefficient in the pharynx	[C_{Fa}/ C_{Fm}] at equilibrium
K_{Nam}	air/lubricated mucosa partition coefficient in the nasal cavity	[C_{Na}/ C_{Nm}] at equilibrium
V_{bolus}	volume of bolus	mm ³
V_c	current breath volume	mm ³
V_{Os}	volume of saliva in the oral cavity	mm ³
V_{Osrest}	volume of saliva at rest in the oral cavity	mm ³
$V_{Opasted}$	volume of pasted rice particles in the oral cavity	mm ³
V_{Om}	volume of mucosa in the oral cavity	mm ³
V_{Oa}	volume of air in the oral cavity	mm ³
V_{fluid}	volume of saliva surrounding a single particle	mm ³
V_{Fa}	volume of air in the pharynx	mm ³
V_{Fs}	volume of saliva in the pharynx	mm ³

V_{Fm}	volume of mucosa in the pharynx	mm^3
V_{Na}	volume of air in the nasal cavity	mm^3
V_{Nm}	volume of mucosa in the nasal cavity	mm^3
V_p	volume of a single particle	mm^3
$V_{p\ total}$	total volume of particles (non-pasted)	mm^3
V_{tot}	volume of particle and surrounding saliva	mm^3
Q_{Os}	saliva flow rate in the oral cavity	mm^3/s
Q_{Oa}	air flow rate in the oral cavity	mm^3/s
Q_{Na}	air flow rate in the nasal cavity	mm^3/s
Q_{Ta}	air flow rate in the trachea	mm^3/s
r	radius of a particle	mm
R	radius of a bolus	mm
S	saturation of the bolus	[volume of liquid bolus / volume of voids]
SA_E	surface area of expanded bolus	mm^2
SA_{sphere}	surface area of a spherical bolus	mm^2
t	time	s
ϕ	packing density of bolus	[-]
ϕ_E	packing density of expanded bolus	[-]
ε	porosity	[volume of voidage / volume of bolus]

“My father gave me the greatest gift anyone could ever give another person. He believed in me.” – Jim Valvano

In memory of my beloved father:

Almarhum Mohd Firdaus How bin Abdullah

Who passed away on the 24th May 2018 midway through my PhD journey. This is for you
Daddy.

May Allah grant you Jannah.

Chapter 1 Introduction

1.1 Project overview

With the growing health crisis with the rapid increase in people with dietary related diseases such as obesity, type 2 diabetes and cardiovascular diseases, there has been an increasing awareness amongst consumers' in food products that benefit their personal health. This interests food manufacturers to design novel foods that can manage caloric intake, increase satiety responses, provide controlled digestion, and/or delivery of bioactive molecules (Singh & Gallier, 2014). To design such foods, a detailed understanding of how food structure and matrix design interact with the physiological and behavioural processes during digestion is required. In recent years, efforts have been made to understand how different food structures are broken down in the human gastrointestinal tract. However, chewing, which is the first operation of the gastrointestinal tract, is often assumed to be less important.

Chewing, or mastication is a complex process whereby the sizes of food particles are reduced and processed with saliva to form a bolus for swallowing. Chewing is needed because it ensures food particles are fragmented small enough and are well mixed and properly lubricated with saliva to form a coherent bolus for safe swallow (Chen, 2009). In the last few decade or so, studies have explored the many benefits of chewing. It has been related to digestion by increasing the surface area of foods to allow more efficient breakdown by digestive enzymes. For instance, the glycaemic index of white rice (glycaemic response relative to their response to a standard glucose) when chewed 15 times was significantly lower (68) compared when chewed for 30 times (88) among 15 subjects (Ranawana et al., 2014). A different study from the same research group has also found that the percentage of small particles in a rice bolus (particles smaller than 500 μm) correlated significantly with *in vitro* digestion rate where the higher the proportion of small particles showed a higher percentage of digested starch at the start of gastric digestion (Ranawana et al., 2010). Saliva adds lubrication to allow safe swallowing and also adds amylase to hydrolyse starches, and bicarbonate to buffer pH in the swallowed material. It is known that once swallowed, boluses can spend significant periods of time (1-2 hours for part of a meal) in the proximal unmixed region of the stomach where amylase activity can be significant

(Bornhorst et al., 2014; Bornhorst, 2017). The design of foods that can be safely swallowed with different saliva inclusion could provide an approach to influence digestion rates.

Besides allowing a more efficient breakdown by the enzymes, the increase in the surface area through mastication also helps the release of flavour and aroma. For instance, the increase of the particle size distribution (PSD) was observed to significantly reduce the release of flavour volatile release in dark chocolate matrices (Afoakwa et al., 2009). When encapsulating oil droplets within biopolymer gelled particles of various sizes to reduce the rate of lipophilic flavour release, it was found that as the particle size increases, the maximum flavour intensity of ethyl hexanoate (one of the lipophilic flavours) was reduced (Malone & Appelqvist, 2003).

Due to the many benefits of chewing as stated above, an opportunity exists for food manufacturers to design foods to manipulate chewing behaviour and the resulting bolus for improving the sensory and nutritional benefits in manufactured foods. However, this is not a straightforward task because chewing is a complex process where individuals have their own unique chewing style in which many factors are involved. An individual's chewing behaviour is related to physiological (e.g. gender, age, dental status, saliva flow rate, muscle strength), anatomical (facial anatomy), physiological (personality type, emotion, cognitive processes) and behavioural (learned pattern) factors (Kim et al., 2020). All of these characteristics affect, for example, the duration of a mouthful, the chewing rate, the movement of the bolus within the mouth, the speed and trajectory of the jaw motion, and the forces applied to the food, which all have an impact on the bolus properties (Kim et al., 2020). The development of mechanistic models can provide tools to assess strategies to design foods that achieve different outcomes in ways that are insensitive to these variations or tailored to them. Additionally, it can also be a tool to reveal in-depth underlying relationships of any experimental observations involving chewing.

In the literature, mathematical models to predict some of the outcomes of chewing have been developed, such as the PSD. The majority of the prior research has adapted fundamental comminution theory of coal grinding (Epstein, 1947) to predict the PSD of foods during mastication (Lucas & Luke, 1983a, 1983b; van der Bilt et al., 1987, 1992; Gray-Stuart, 2016). According to the theory, mastication

can be defined as a combined process of selection and breakage. Selection can be defined as a process whereby food particles have a chance to be placed between the teeth where they are at least damaged or broken by the subsequent breakage process. The breakage process is defined by the distribution of the broken particles that originated from a selected particle.

Several attempts have been made to model the selection process during chewing. It has been shown to depend on particle size by a power function (van der Glas et al., 1987; van der Bilt et al., 1992;) or to depend on both particle size and number by two mechanistically derived competitive selection models (van der Glas et al., 2018,1992). The competitive selection models have the potential to aid in food design by providing the essential knowledge to determine the conditions for a controlled flavour release by varying particle shape, size and number ratio in mixtures and the way particles are embedded into other food matrices (van der Glas et al., 2018). Despite efforts made to develop these models, they are rarely applied to real foods due to the number of time-intensive experiments needed to generate inputs to the model. This demonstrates the need to provide simple and rapid methods to generate model input data during the model development process.

Additionally, the competitive selection models developed by van der Glas et al., (1992) have only been validated with cubic Optosil® particles, which is a silicone dental impression material, that is not affected by saliva (van der Glas et al., 2018). Optosil® is representative for natural brittle hard foods which form a loose aggregation of particles during chewing (stiffer than raw vegetables but less stiff than nuts). To date, only one study has applied the selection model to real food. This was the study by Gray-Stuart (2016), where he had successfully simulated the PSD of brown rice by applying the two-way competition model. The application of selection models is a logical starting place for more complex chewing model development that can account for some of the anatomical and behavioural differences we see between people, although these models need to be extended to a wider range of food systems.

The breakage function is determined by the internal mechanical properties of foods, which are properties that resist the formation of new surface by fracture (Agrawal et al., 2000). Previous studies which incorporate breakage in chewing simulations have used empirical and mechanistic functions to fit their experimental data. For instance, Lucas and Luke (1983b) used an empirical power function to

fit the breakage of carrot particles during chewing. Other studies have applied the mechanistic function describing the distribution of particles resulting from a single breakage event from Austin (1971) to simulate the PSD of Optosil® particles (van der Bilt et al., 1987; van der Glas et al., 1987) and brown rice (Gray-Stuart, 2016). However, because of the requirement for conservation of volume in the distribution of daughter particles during breakage, for modelling, most literature methods apportion daughters to mean bin sizes. This results in less accurate model predictions when compared against experimental data as the size of the daughter particles generated is limited to the average between two bin sizes. There is opportunity to overcome these shortcomings and to adapt breakage models to be population balances where complete distributions of particles are followed over time.

Extension to the selection and breakage models are the studies by Harrison & Cleary (2014), Harrison et al. (2014a, 2014b) who developed a coupled biomechanics-smoothed particle hydrodynamics to predict size distributions of food fragments for an agar model food. Other studies include Gray-Stuart et al. (2017), who developed a conceptual model of the decision-making criteria for bolus properties needed to ensure safe swallows, and Ng et al. (2017), who investigated slip extrusion as a function of bolus properties in a simulated swallow. Despite these extensions, the next steps to use such models for better design of foods have not been made. Comprehensive examples are needed to demonstrate the application of models to facilitate their use by industry.

In the literature, models to predict PSD of bolus during mastication have been used to predict aroma compound release. Harrison et al. (1998) simulate aroma release from foods in the mouth by incorporating the selection and breakage functions that were described by a power law relationship. The model, however, was not validated against *in vivo* experimental data. Another study that modelled flavour release of jellied sweets incorporated mastication models by empirically fitting Pearson type IV distribution to the bolus experimental data (Wright et al., 2003). However, the model was not complete as breathing was not taken into account. Additionally, the assumptions are limited to the type of food matrix explored in the study (e.g. candy) and consumption patterns (e.g. sucking) (Doyennette et al., 2014). The most comprehensive validated model of aroma release during chewing of solid foods was developed by Doyennette et al. (2014) for cheese. However, the mastication model was simplified by

assuming that the bolus surface area increases linearly with time. Clearly, there is still a gap in the literature in developing a validated and comprehensive mechanistic model which incorporates mastication models to predict flavour release.

1.2 Overall Goal and Research Objectives

Overall Goal: The purpose of this work was to develop a chewing model for solid foods during oral processing and to demonstrate model application through a series of case studies which are linked to the design of foods to influence digestion and sensorial outcomes.

1.2.1 Research Objectives

The specific objectives of this research were to:

- i. Develop conceptual and quantitative mathematical models to predict the PSD of bolus during chewing.
- ii. Validate the developed models against *in vivo* peanut chewing data to demonstrate model application in order to provide a mechanistic understanding of the chewing process and how it could lead to food design.
- iii. Develop conceptual and quantitative mathematical models which describe a combined chewing and aroma release mechanisms of a starch-rich food to expand model application for food design which influences digestion and sensorial outcomes.
- iv. Validate the coupled chewing-aroma release model using a starch-rich food by comparing model predictions to *in vivo* experimental data from human subjects.
- v. Apply the validated coupled chewing-aroma release model by demonstrating its usage on the better design of foods to influence sensorial outcomes.

1.2.2 Organisation of the thesis

The outcomes of the objectives of section 1.2.1 are documented and organised in this thesis as follows:

- Chapter 2 reviews the current literature on modelling mastication of solid foods and aroma release. From this a combined conceptual was developed.
- In Chapter 3, based on objective (i), conceptual and mathematical models to predict the bolus PSD of chewing were developed based on the adaption of existing selection and breakage processes developed in the literature. Several numerical approaches were also developed to implement the models due to several model shortcomings such as ensuring the conservation of volume when daughter particles were generated. The establishment of the mathematical model, model assumptions and the numerical approach form the basis for the model application case studies in the subsequent chapters.
- In Chapter 4, the models developed in Chapter 3 were applied to predict peanut breakdown to demonstrate model application on a real food system. The PSD predictions from the model were fitted to experimental data obtained from the literature using an optimisation tool called Particle Swarm Optimisation (PSO). A variety of mechanistic and empirical selection and breakage models in the literature were applied to determine which model provided the best fit to the experimental data. The fitted parameters were then interrogated to provide a mechanistic understanding of how peanuts were chewed.
- In Chapter 5, similar to Chapter 4, the models developed in Chapter 3 were applied to peanuts to test model application for food design. Two case studies were presented which were aimed at understanding the breakdown process when the initial portion size was varied and when the initial moisture content (and hence breakage behaviour) was different. The optimisation technique developed in Chapter 4 was applied to the case studies where the resulting input parameters solved from the algorithm were interrogated to understand the difference in chewing mechanisms from the alteration in food design. Chapter 4 and Chapter 5 fulfilled objective (ii).
- In Chapter 6, which was based on objective (iii), *in vivo* chewing and aroma release experiments were performed on five subjects using the chosen starch-rich food system. The physiological, oral processing and aroma release parameters of each subject were investigated. The results of

the study were then used to understand the relationship between physiology and chewing on aroma release as well as to generate the data for model validation.

- In Chapter 7, the results of the *in vivo* study in Chapter 6 was used as the basis for the model development of a coupled chewing and aroma release model for the chosen starch-rich food system. A conceptual model which included model assumptions were developed and used to convert into several ordinary differential equations (ODEs) to predict aroma release. The ODEs were then solved numerically using MATLAB. This chapter fulfilled objective (iii).
- Chapter 8 achieved objective (iv) by validating the combined chewing-aroma release model developed in Chapter 7 against the *in vivo* experimental data measured in Chapter 6. Two different approaches were used to validate the model; the first approach directly used the PSD outputs from experimental data to establish the coupling with the aroma release model whereas the second approach used the PSD outputs predicted from the chewing model developed in Chapter 3. The comparison made between the two different approaches provided a staged approach to validation of different parts of the combined particle breakdown-aroma release model.
- Chapter 9 completed objective (v) by showing how modelling can act as a tool to provide insights towards the betterment of food design to influence sensorial outcome. This was demonstrated by manipulating the input parameters related to the product, physiology and physicochemical properties through application of the model validated in Chapter 8 to one of the subjects characterised in Chapter 6.

In the final chapter, the work and results obtained for this research were summarised followed by recommendations for future work.

Chapter 2 Literature review

2.1 Introduction

Chewing is a complex phenomenon because various processes occur concomitantly to process the ingested food from its initial state into a safe-to-swallow bolus (Xu et al., 2007; Gray-Stuart, 2016; Almotairy et al., 2020). The objectives of this thesis revolve around extending previous work on chewing, aroma release and the existing models for these processes in the literature. Therefore, the first part of this chapter will focus on understanding the main processes involved during chewing and saliva addition, as well as their main benefits to general health, well-being and sensorial experience.

2.2 The chewing process

Chewing is needed because it ensures food particles are fragmented small enough, well mixed and properly lubricated with saliva to form a coherent bolus for safe swallowing (Chen, 2009). Mastication is influenced by factors such as the characteristics of the food (e.g. water, fat percentage and hardness), teeth (e.g. total occlusal area), bite force (which depends on muscle volume, jaw muscle activity and the coordination of chewing muscles), and neuromuscular control (i.e. the movement of the jaw and the manipulation of tongue and cheeks) (van der Bilt et al., 2006). During mastication, specific oral processing steps occur as described in a conceptual model developed (Fig. 2-1) by Lucas et al. (2002).

The conceptual model in Fig. 2-1 attempts to list the primary requirements for processing food entering the mouth. It is noted by its authors that the conceptual model does not intend to describe decisions made by the central nervous system from the sensory feedback it receives, and it is simply an analytical way of defining a general sequence of events. According to the model, any food entering the mouth must be gripped or else its movement cannot be controlled. Food can either be transported directly to the pharynx for swallowing depending on whether the food can crack or not. For example, easily swallowable food like porridge will not require a ‘crack initiation’ event, hence it will be transported straight to the pharynx. If food is perceived to be sufficiently solid such as a biscuit, the teeth will attempt to make a crack and hence the food will undergo more oral processing events such as ‘Fracture’, ‘Comminution’ and ‘Sculpture’ until it is safe to be transported to the pharynx.

Fig. 2-1: A conceptual model of chewing described as a sequence of events. Decision boxes are shown as diamonds whereas process boxes are rectangular, from Lucas et al. (2002).

Similarly, Hiiemae (2004) drew a conceptual model that describes chewing as a series of sequential stages (Fig. 2-2). The model asks three questions; the first question is whether the food is safe to be eaten. If the food is perceived to be poisonous, then it is expectorated at this stage. The second is whether the food material is suitable for swallowing. If the material is too large to be swallowed, then more chewing is needed to reduce the food particle size. At this stage, food particles are mixed with saliva to begin bolus formation. The last question is a threshold gate which asks if there is enough food to swallow. If food is not enough, it implies a lower volume limit which means food particles need to be constantly processed with saliva until the bolus volume reaches the swallowing threshold (Gray-Stuart, 2016).

Gray-Stuart (2016) combined subsets from the Hiiemae (2004) and Lucas et al. (2002) conceptual models to demonstrate how food is transformed into a bolus and how it is assessed to determine whether it is safe to swallow (Fig. 2-3). His conceptual model integrates food breakdown, mixing and testing of the food properties. The swallowing decision in his model is based on a range of

properties the food must have, which are the temperature, volume, adhesion, bolus deformation, particle deformation and particle size. The threshold properties were determined using a chemical engineering methodology called a hazard and operability study (HAZOP) which is commonly used in chemical process plant design.

Fig. 2-2: The process model of feeding from Hiimae (2004)

The conceptual models produced by Lucas et al. (2002), Hiimae (2004) and Gray-Stuart (2016) are similar in a sense that all of them are displayed as a series of ‘decision-making’ processes where a threshold gate needs to be satisfied before proceeding to later stages. All of the models describe pathways that need to be taken by food to ensure that it is safe to be swallowed. Out of the three, the model by Gray-Stuart (2016) is the most complex and provides a better explanation of what occurs in each of the stages. His conceptual model stands out from the others by not only addressing the movement of food and the action of chewing, but also includes other mechanisms occurring to food

during oral processing such as the *size reduction, work softening, dissolution, absorption, melting and mixing.*

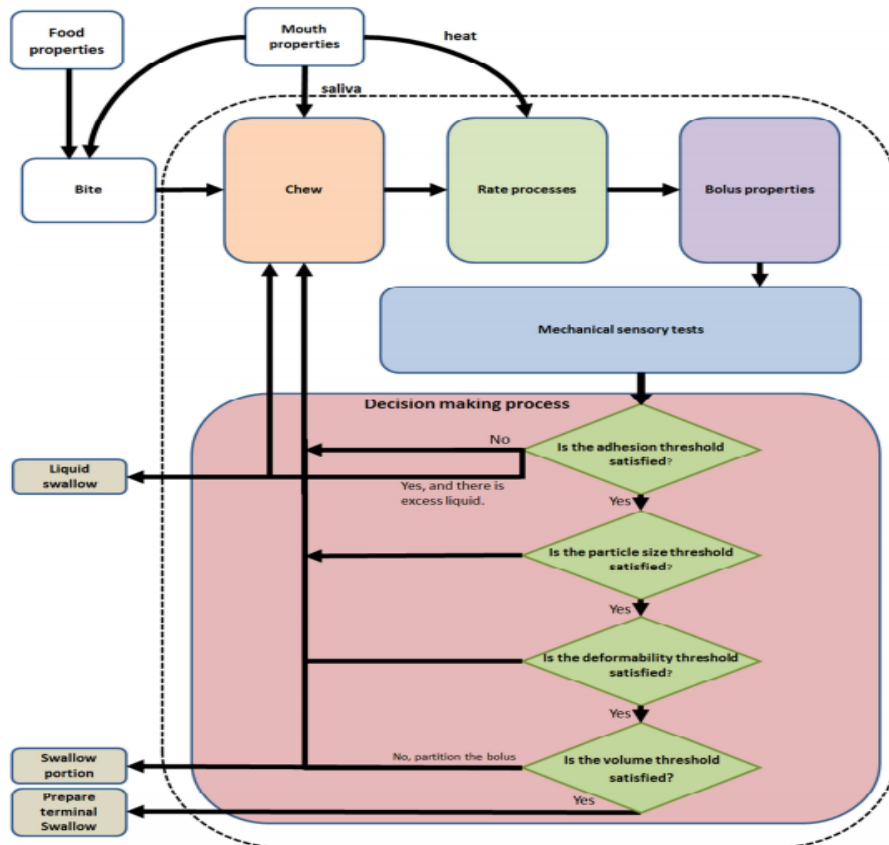


Fig. 2-3: Conceptual model of oral processing from Gray-Stuart (2016).

As mentioned above, all of the models provide a great overview of the processes involved during chewing. During chewing, saliva is produced to facilitate mastication, moisten food particles, contributes to bolus formation and assists in swallowing by providing lubrication (van der Bilt et al., 2006). In the next section, a brief background of saliva will be presented.

2.3 Saliva

During chewing, saliva is secreted due to the combination of mechanical stimulation (from chewing) and chemical stimulation from food components (i.e. tastants and aromas). Saliva plays an important role in bolus formation, as it acts as a liquid binder between food particles which are bound together to form a cohesive bolus. Other functions of saliva include destabilizing colloidal systems such as emulsions, breaking down compounds by means of salivary α -amylase and lipase, dissolution of tastants

and binding aromas, and participates in the formation of soluble and insoluble aggregates (Mosca & Chen, 2017).

2.3.1. Saliva production

Approximately 90% of saliva is produced by the three major salivary glands in the oral cavity. These are the parotid, submandibular and the sublingual glands (Bornhorst & Singh, 2012; Carpenter, 2013; Mosca & Chen, 2017). The remaining 10% of the whole saliva is contributed by the gingival crevicular sulci (area between tooth and marginal free gingiva), the minor salivary glands (situated on the tongue), the buccal mucosae, the palate and by oro-naso-pharyngeal secretions (Aps & Martens, 2005).

The flow rate of an unstimulated salivary flow is approximately 0.5 ml/min (Carpenter, 2012). Saliva flow rate and composition varies in response to gustatory stimulation (such as acid) or mechanical stimulation from chewing inert materials such as parafilm (Watanabe & Dawes, 1988). Watanabe and Dawes (1988) studied the effects of seven different foods and three concentrations of citric acid in 16 adult subjects on the saliva flow rate. The foods were steamed rice, French fries, cheeseburger, cookies, milk chocolate, apple, and rhubarb pie. The saliva flow rate was calculated by dividing the volume of saliva (calculated by subtracting the initial weight of food with the expectorated food bolus) with the chewing time. The food with the highest mean salivary flow rates was rhubarb pie (4.94 ± 1.51 ml/min) and the lowest was rice (3.15 ± 1.48 ml/min). Meanwhile, the highest concentration of citric acid (260 mmol/l) produced the highest mean salivary flow rates (7.07 ± 2.16 ml/min) which is consistent with other studies looking at measuring the saliva flow rate in response to varying citric acid concentrations (Norris et al., 1984; Froehlich et al., 1987). Table 2-1 shows salivary flow rates from three different studies, measured in response to chewing different foods.

From Table 2-1, it can be seen that saliva flow rates vary in response to chewing different type of foods. Toast and cake produce saliva flow rates significantly higher than other food types. This is because they are dry foods which require more saliva to form a bolus than the moist foods such as rice, apple and cheeseburger. Saliva flow rate can also be seen to be independent of food volume when compared within a single food type. This is shown with the saliva flow rates measured in response to

chewing different volumes of cakes. The unstimulated saliva flow rates measured in all of the studies are quite similar and lie in the range 0.38-0.72 ml/min.

Table 2-1: Salivary flow rates in response to chewing different foods from (Watanabe & Dawes, 1988; Engelen et al., 2003; Gavião et al., 2004); *NA is defined as not applicable as the parameter was not measured in the study

Stimulus	Flow rate (ml/min)		
	Watanabe and Dawes (1988)	Engelen et al. (2003)	Gavião et al. (2004)
Unstimulated	0.72 ± 0.28	0.38	0.53 ± 0.28
Parafilm	NA	1.12	1.40 ± 0.67
Rice	3.15 ± 1.48	NA	NA
French fries	3.82 ± 1.32	NA	NA
Cheeseburger	3.92 ± 1.85	NA	NA
Cookie	4.17 ± 1.32	NA	NA
Chocolate	4.18 ± 1.44	NA	NA
Apple	4.76 ± 1.53	NA	NA
Rhubarb pie	4.94 ± 1.51	NA	NA
Toast	8.84 ± 5.06	NA	NA
Toast (with margarine)	7.74 ± 4.97	NA	NA
Cake (small)	7.97 ± 5.02	NA	NA
Cake (medium)	7.32 ± 3.97	NA	NA
Cake (large)	7.42 ± 3.61	NA	NA
Odour	0.51	NA	NA
Citric acid (3 drops of 4% concentration)	1.87	NA	NA
52mmol/l citric acid	4.35 ± 1.92	NA	NA
156 mmol/l citric acid	5.94 ± 2.08	NA	NA
260 mmol/l citric acid	7.07 ± 2.16	NA	NA

It can also be seen that gustatory stimulation has more effect than mechanical stimulation, which is shown by the lower flow rates for chewing parafilm in comparison to natural foods especially if it is considered that saliva flow rate is likely to be underestimated in this measurement method as it is assumed that all the ingested food is recovered in the expectorated bolus. Dry solids recovery of ingested foods can be as low as 50% of the original mouthful for different foods (Jalabert-Malbos, 2007).

Engelen et al. (2003) also compared saliva flow rates between gender and found that saliva flow rates for females are not significantly different from their male counterparts. However, Inoue et al. (2006) claimed that the unstimulated whole saliva flow rate in females is lower than males as their gland sizes are smaller due to their smaller body sizes. Li-Hui et al. (2016) analysed the difference of saliva flow rates for 28 females and 27 males before and after citric acid stimulation and found that the saliva flow rates in females before acid stimulation was significantly lower than in males in all samples

collected. They also found that there is no difference among gender for the salivary amylase activity measured.

2.3.2 Saliva properties and components

Saliva is made of 99% water and less than 1% electrolytes or organic compounds such as proteins (Mosca & Chen, 2017). Although saliva is composed mostly of water, it is a non-Newtonian fluid as the viscosity decreases with increasing shear. The viscoelastic properties of saliva are a result of the mixture of water with mucins, glycoproteins and ionic components (Mosca & Chen, 2017). The strong viscoelastic quality of saliva is important as it allows the wetting of both hydrophobic and hydrophilic surfaces in foods (Boehm et al., 2014). Foods ingested in the mouth have different properties. They can be dry such as a biscuit or can be oily such as potato chips. To coat these foods with saliva to form a safe-to-swallow bolus, saliva needs to possess viscoelastic properties (Boehm et al., 2014).

The properties of saliva are affected by many factors such as individual characteristics (e.g. age, gender), health status, emotional stress and the use of dentures (Mosca & Chen, 2017). Extrinsic factors related to the conditions of collection, handling and preservation of saliva samples can also affect the properties of saliva (Mosca & Chen, 2017).

A component of saliva which is not well studied in the literature is the role of its most abundant protein, salivary amylase. In humans, AMY1, the salivary gene, produces the amylase enzyme present in saliva. Salivary amylase is an endoenzyme that carries out multiple attacks on linear portions of starch amylose and amylopectin with maltose and maltotriose as the principal short chain products (Butterworth et al. 2011). A purified salivary amylase has a specific activity of 1.5×10^3 U per mg (1 U is defined as milligrams of maltose produced in 3 mins at 20°C) (Butterworth et al. 2011). Using this assumption, the comparison of AMY1 gene copy number with amylase content of saliva, indicates that saliva would contain up to 2×10^4 U/ml.

2.3.3 Saliva functions

A comprehensive review of the essential functions of saliva in food oral processing has been given in Mosca & Chen, (2017). A conceptual model was drawn to summarise the roles of saliva in food oral processing (Fig. 2-4). At a food structural level, as chewing progresses and the food structure is

reduced into smaller pieces, saliva coating is essential as it helps to dissolve and release flavour compounds, prevents food particles from sticking to oral surfaces or teeth, clustering food particles and forming a safe-to-swallow bolus (Mosca & Chen, 2017).

Fig. 2-4: Role of saliva in oral processing. Figure from Mosca & Chen (2017).

At the molecular level, saliva destabilises colloidal food products such as emulsions and beverages through flocculation and coalescence. The flocculation of emulsion systems due to saliva, increases the viscosity, storage modulus and viscoelasticity of the emulsion (Mosca & Chen, 2017). Due to the action of salivary α -amylase, saliva-induced coalescence is observed in starch-stabilised emulsions. For instance, a study by Dresselhuis et al. (2008) observed that emulsions that were prepared with octenylsuccinate starch as an emulsifier had the highest scores for mouth-feel and after-feel fat-related and taste-related attributes, due to emulsion droplet coalescence induced by saliva. Saliva also forms complexes by binding basic proline-rich salivary proteins to polyphenols (tannins). This is believed to be the main reason for astringency sensations (i.e. puckering, rough, dry mouth-feel and after-feel) (Mosca & Chen, 2017).

The role of saliva on digestion is arguably one of the functions of saliva that is the most poorly understood. An enzyme in saliva, the salivary α -amylase is generally thought to be involved in the initial digestion of starch-containing foods. Hoebler et al. (1998) studied the levels of starch hydrolysis in the mouth by asking twelve volunteers to chew bread or spaghetti at their natural swallowing point. It was

found that during the short step of oral digestion (about 20-30s) about 50% of bread starch and 25% of pasta starch was hydrolysed and transformed into molecules of smaller molecular mass, however they were still mostly large molecules. Only a small fraction of the starch was broken down into oligosaccharides (mainly maltose and maltotriose). A more recent study investigating the role of salivary α -amylase in the gastric digestion of wheat bread starch found that the amylolytic activity of saliva hydrolyses up to 80% of bread starch in the first 30 min of gastric digestion (Freitas et al., 2018). This finding is significant as it shows that although the oral phase is the shortest phase of digestion and the changes to starch are relatively minor, it plays a significant role in total digestion. The action of amylase can also continue in the proximal regions of the stomach (during the gastric step), as it was found that amylase is partly protected from denaturation by acid pH in the distal region of the stomach (Rosenblum et al., 1988). In addition, salivary α -amylase has been found to influence the physical breakdown and subsequent gastric emptying by changing the texture of the bolus. Bornhorst et al. (2014) studied the effect of α -amylase on rice bolus texture after simulated mastication and found that bolus texture was significantly lower in the presence of α -amylase. Boehm et al. (2014) also conducted a similar study with potato chips and found that within the first minute of mixing with saliva, the amylase degrades only 6% of starch but leads an order of magnitude reduction in the bolus elasticity.

Lipase is another salivary enzyme that can play a role in the initiation of food digestion in the mouth. However, because of the low concentration of this enzyme in saliva, it is most likely that it does not influence fat digestion (Mosca & Chen, 2017). However, a low degree of fat hydrolysis might still have an influence on oral perception, but further investigation will be needed to confirm this hypothesis (Mosca & Chen, 2017).

Lastly, saliva at rest assists the tasting of foods. The low surface tension (a feature of resting and stimulated saliva) allows a rapid interaction of the tastant with taste receptors (Carpenter, 2012). Tastants such as salt and acids use saliva as a medium to convey the ions to the taste receptors, which enhances taste intensity. The components of saliva such as mucins can also interact with aroma compounds. When investigating the interactions between saliva components and 20 aroma compounds in water and oil model systems, mucins were showed to decrease the retention of highly volatile compounds and increase the retention of hydrophobic compounds (van Ruth et al., 2001). Salivary

enzymes in saliva can also affect aroma release and perception. A study by Buettner (2002) concluded that the persistence of odorous compounds in the mouth after food consumption is caused by the degrading action of salivary enzymes. When odor-active compounds are mixed with whole saliva, the concentrations of esters, thiols and aldehydes decrease but no change in concentration was observed when saliva was thermally treated at 100°C for 10 min.

It is clear from the literature that saliva is important in mastication. In the next section, the key importance of chewing, particularly on digestion and taste and aroma release will be reviewed.

2.4 Effects of mastication

2.4.1 Effect of mastication on digestion

In the literature, chewing has mostly been related to digestion as it increases the surface area of foods when the particle size is reduced. Studies have shown the role of chewing on the digestion of starch-based foods. For example, when investigating the effects of mastication on glycaemic response of four different carbohydrate foods (sweetcorn, white rice, diced apple and potato), it was found that swallowing the foods without chewing significantly reduced the blood glucose response compared to when they were chewed thoroughly for 15 s (Read et al., 1986). In another study, when comparing the total glycaemic response, when white rice is chewed 15 or 30 times, it was shown that the total glycaemic response was significantly lower when chewed faster (glycaemic response of 155 mmol min/l for 15 times compared to 184 mmolmin/l for 30 times) (Ranawana et al., 2014). When investigating the role of mastication on *in vitro* digestion of white rice, it was found that the percentage of particles that were reduced to smaller than 500 µm correlated significantly with *in vivo* glycaemic response at the initial digestion stage (Ranawana et al., 2010). Chewing has also been shown to influence the release of other nutrients during digestion. It has been shown to influence the amino acid assimilation of meat protein (Rémond et al., 2007), bio-accessibility (nutrient release) of lipids from almonds (Cassady et al., 2009; Grundy et al., 2014; Mandalari et al., 2018) and the release of carotenoids from fruits (Lemmens et al., 2010; Low et al., 2015).

2.4.2 Effect of mastication on taste and aroma release

The increase of surface area of foods due to the chewing process also influences the release of volatile compounds from foods, and subsequently affects the profile of volatiles in the nasal cavity. Numerous studies have shown the effects of decreasing particle size during mastication on flavour release; however they were mostly focused on *in vitro* studies due to the difficulty to characterise the bolus (e.g. the PSD) when the experiment is conducted *in vivo*. When investigating the effect of the mastication rate on temporal aroma release from ripe and unripe bananas using a model mouth system, the higher mastication rate (52 min^{-1}) had significant odour active compounds detected (18 and 7) compared to without mastication, where only 3 and 2 compounds were detected (Mayr et al., 2003). Another *in vitro* study looking at the effect of mastication of apples on volatile release using an artificial mouth device observed more volatile compounds released the longer apples were chewed (Arvisenet et al., 2008). *In vivo*, a significant correlation between chewing parameters (e.g. chewing rate and muscle activity) and aroma release was also observed during eating of a model cheese when measured *in vivo* (Pionnier et al., 2004).

Despite previous efforts to understand the role of chewing on aroma release, they were mostly focused on relating the chewing behavior (e.g. the chewing rate and muscle activity) with aroma release but very little effort was made in understanding the effects of the bolus PSD. Because of the complexity in characterizing the particle size *in vivo*, several attempts have been made to understand its role by developing mechanistic mathematical models. Although not validated with experimental data, Harrison et al. (1998) developed a model describing flavor release from solid foods during mastication based on the stagnant-layer theory of mass transfer. It showed that the fracture mechanics of food had an impact on the initial rate of flavor release. Similarly, the air-bolus contact area was shown to be one of main parameters affecting release intensity in a mechanistic model developed by Doyennette et al. (2014) to predict the flavor release of cheese.

These studies showed the importance of mastication, particularly on digestion and aroma release of foods. However, due to the complexity of chewing and the difficulty in obtaining good quality input data, there have been few efforts made to model the system. In the next sections, those attempts to model chewing will be presented.

2.5 Chewing models

Models have been developed because of the time and labour-consuming nature of chewing experiments designed to measure the change of PSD across several number of chews (Liu et al., 2020). Models to describe chewing in the literature have been based on the selection and breakdown of particles. Selection in chewing can be defined as the process in which a food particle has the probability of being arranged between the antagonistic teeth for subsequent breakage. Particles are considered selected if they are at least damaged or comminuted. The breakage process can be defined as the process in which selected particles are fractured between the teeth into smaller fragments of variable size and number. Both selection and breakage are influenced by subject-related anatomical and physiological factors and food-related factors (van der Glas et al., 2018; Zhang et al., 2019; Liu et al., 2020).

2.5.1 Selection as a function of particle size

Selection can be observed from the change in PSD (PSD) collected on a stack of sieves after consecutive a chewing cycles, N and $N+1$ (where N is a given chew number). Non-selected particles will be found on the same sieve. Selected particles will be damaged in some way. Smaller daughter fragments will be found on lower sieves, but some particles will only have been cracked or chipped, rather than broken, so may also remain on their original sieve (van der Glas et al., 1987).

Experimentally, the selection chance in cycle $N+1$ can be measured if particles are form-labelled at cycle N (e.g. cubes or cylinders) so that selected particles can be differentiated as being damaged or broken in cycle $N+1$. The selection chance can be defined as the proportion of particles of size \bar{X}_i that are damaged or broken between consecutive chew cycles. This is not easy to do experimentally as each sieve, below the largest one, has both particles arriving on and leaving the sieve after the cycle. Rather, authors observe the net change in PSD, where each sieve mean particle size, \bar{X}_i , is defined by the sieve mid-point size, (i.e., the logmean of the aperture of adjacent sieves in series), and the selection $\sqrt{\bar{X}_{i-1} \cdot \bar{X}_i}$, can be defined as the proportion of particles of size \bar{X}_i that are damaged or broken between consecutive chew cycles.

To study selection, Lucas and Luke (1983a) used carrot as a test food with ten subjects. They found that selection decreased strongly as particle size decreased but, within that, also decreased weakly

with increasing chew number. Despite this, Lucas and Luke (1983a) did not propose a relationship for the dependence of selection on particle size but did propose a relationship for the dependence of selection on chew number. For this, they assumed that the percentage of particles in a size fraction declines exponentially with the number of chews, in which case the selection function is dependent on chew number described by;

$$S(\bar{X}_l) = 1 - \left(\frac{P_{2,i}}{P_{1,i}} \right)^{\frac{1}{C_2 - C_1}} \quad (2.1)$$

where $S(\bar{X}_l)$ is the average selection function of a mid-point size of a size fraction, P_1 is the percentage of particles of average size \bar{X}_l after C_1 chew and P_2 is the percentage remaining after chew number C_2 .

Van der Glas et al. (1987) explored the size dependence of selection. From a study of four panellists during chewing of silicone rubber (Optosil®), they found that selection as a function of particle size can be described by a power function

$$S(\bar{X}_l) = v\bar{X}_l^w \quad (2.2)$$

where $S(\bar{X}_l)$ is the selection function (in the range of $0 \leq S(\bar{X}_l) \leq 1$), \bar{X}_l is the particle size, and v and w are constants. The v variable describes the mixing action of the chewing that is the ability of the teeth to lock the particles for breakage as well as the movement of the tongue to arrange particles to fit on the occlusal area of the teeth. The exponent w describes the degree of piling of the particles where damage can be applied to particles piled on top of each other on the occlusal surfaces. If $w > 2$ then piling of particles in the occlusal area of teeth might occur. They also found, like Lucas and Luke (1983a), that the selection value for the larger particles seemed to decline gradually as chewing progressed, which is captured here by the variable v increasing with chew number. So, while the power-law model for selection in Eq. (2.2) has been shown to successfully simulate the PSD during chewing in previous studies (van der Bilt et al., 1987, van der Glas et al., 1992), its weakness is that it does not mechanistically account for particle number. Nevertheless, the effect of competition is acknowledged by van der Bilt et al. (1987) where they surmise that, due to the limited occlusal area, an increase in the number of particles would saturate the available space, causing a decrease in selection chance.

2.5.2 Competitive selection as a function of particle size and number

Van der Glas et al. (1992) introduced the idea of including breakage sites, defined as the part of the occlusal area of the post-canine teeth where particles of a specific size can be broken. As the same tooth surface is utilised to break particles of various sizes, the breakage sites available for large particles to break overlaps considerably with the locations at which small particles are broken. As chewing progresses, large particles would have to compete with the increasing number of smaller particles occupying the limited occlusal surface for chewing. The selection model they developed differs from the above, where selection is expressed as the fraction of particles of a particular size selected for occlusion. Instead, here selection refers to the number of particles that occupy sites in the occlusal plane relative to the maximum number of sites available for that particle size. For single-sized particles, the number of particles selected in size class X_i , $n_s(X_i, n_{xi})$, after a single chew can be described by

$$n_s(X_i, n_{xi}) = n_b(X_i) \cdot \left[1 - (1 - O_1(X_i, 1))^{n_{xi}} \right] \quad (2.3)$$

where $n_b(X_i)$ is the number of breakage sites that are available for particles in size class X_i , and $O_1(X_i, 1)$ is an affinity factor for particles in size class X_i . If $n_b(X_i)$ is the number of breakage sites, then the term $\left[1 - (1 - O_1(X_i, 1))^{n_{xi}} \right]$ must be the fractional occupancy of these breakage sites. The term $(1 - O_1(X_i, 1))^{n_{xi}}$ therefore represents the opposing fraction, (i.e., the fraction of breakage sites free of particles). The power term indicates this fraction is affected by the number of particles within the portion of food. As the number of particles in the system grows, the fraction of breakage sites free of particles decreases, approaching zero when n_{xi} is large. Within this term, $1 - O_1(X_i, 1)$ is best considered by imagining there is only one particle, $n_{xi} = 1$. If so, it is the fraction of the breakage sites that are free of particles when one particle occupies one site. Therefore, the affinity term $O_1(X_i, 1)$ must be one divided by the number of breakage sites, $1/n_b(X_i)$. Given that this is dependent on size, $O_1(X_i, 1)$ will decrease markedly as size X_i becomes smaller, tending to zero as size becomes infinitely small. For an example, if there is one large particle in the portion that can occupy 20% of the occlusal area, the number of breakage sites is five. In this case the number selected is

$$n_s(X_i, n_{xi}) = n_b(X_i) \cdot \left[1 - (1 - O_1(X_i, 1))^{n_{xi}} \right]$$

$$n_s(X_i, n_{xi}) = 5 \times [1 - (1 - 0.2)^1] = 5 \times 0.2 = 1$$

Given that there is one particle present and one is selected, this is correct. Now imagine there are 6 particles of the same equal size in the mouth competing for 5 breakage sites. In this case the number selected is

$$n_s(X_i, n_{xi}) = n_b(X_i) \cdot [1 - (1 - O_1(X_i, 1))^{n_{xi}}]$$

$$n_s(X_i, n_{xi}) = 5 \times [1 - (1 - 0.2)^6] = 5 \times 0.748 = 3.69$$

This makes perfect sense too. So, if the above deduction is correct, the selection model for single sized particles is actually a single parameter model, requiring only $n_b(X_i)$.

The selection model for single-sized particles was extended to particles in a mixture of sizes. Two models describe how different sized particles compete for the breakage sites: the one-way and two-way competition models. The one-way competition model (Eq.2.4) assumes that the selection of smaller particles will be affected by the presence of large particles without the reverse occurring. The number of selected particles as a function of number $n_s(X_i, n_{xi})$ in the smaller size class (X_i) in the presence of p classes of larger particles of sizes ($p = 0 \dots i-1$) can be described as:

$$n_s(X_i, n_{xi}) = \left[n_b(X_i) \cdot \prod_{p=0}^{i-1} U(X_p, n_{xp}) \right] [1 - (1 - O_1(X_i, 1))^{n_{xi}}] \quad (2.4)$$

where $U(X_0, n_{x_0}) = 1$ and $U(X_p, n_{xp}) = [1 - O_1(X_p, 1)]^{n_{xp}}$. The term $n_b(X_i)$ is the number of breakage sites available for size X_i if larger sizes were not present, and $O_1(X_i, 1)$ is the affinity factor related to particle size X_i or to the other larger particle sizes X_p ($p = 0 \dots i-1$), as defined previously, which is also independent of the presence of other particle sizes.

Using the same approach as above, the one-way model competition model has the same two terms as the single size model, with the addition of the product multiplier. Each term of the product multiplier $U(X_p, n_{xp}) = [1 - O_1(X_p, 1)]^{n_{xp}}$ is the fraction of breakage sites free of particles of size X_p where the power term accounts for the number of particles of this size in the portion. This term is

calculated in the same way as for the single size selection model above. However, here there are many larger particle sizes to consider. The cumulative effect of these is obtained by multiplying their effects together. This reduces the number of available breakage sites for particles of size, $n_b(X_i)$. As an example, imagine a mixture of three particle sizes, with $n_b(X_i) = 5, 10 \text{ and } 20$. . Imagine now that the numbers of each are in the portion are 2, 4 and 8 respectively. The number selected of the smallest size are compromised by the presence of the larger particles. The terms are evaluated as follows

$$1^{\text{st}} \text{ term } n_b(X_1) = 20$$

$$2^{\text{nd}} \text{ term } [1 - O_1(X_{p2}, 1)]^{n_{xp2}} \times [1 - O_1(X_{p3}, 1)]^{n_{xp3}} = [1 - 0.1]^4 \times [1 - 0.05]^8 = 0.88$$

$$3^{\text{rd}} \text{ term } [1 - O_1(X_{p1}, 1)]^{n_{xp1}} = [1 - 0.2]^2 = 0.64$$

The number selected is $20 \times 0.87 \times 0.64 = 11.2$

This shows that without the presence of the two larger sizes, $20 \times 0.64 = 12.8$ particles would have been selected.

The two-way competition model (Eq. 2.5) accommodates the ability of the smaller particles to pile, which means piling can compensate for the height advantage of large particles and so improves the competitiveness of small particles for occupying breakage sites. Therefore, for any size class X_i , the number of selected particles as a function of particle number $n_s(X_i, n_{xi})$ in a mixture of j classes of particle sizes ($j = 1 \dots k$) can be described as:

$$n_s(X_i, n_{xi}) = n_b(X_i) \left[n_{xi} \frac{\ln(1 - O_1(X_i, 1))}{\sum_{j=1}^k [n_{X_j} \ln(1 - O_1(X_j, 1))]} \right] \left[1 - \prod_{j=1}^k (1 - O_1(X_j, 1))^{n_{xj}} \right] \quad (2.5)$$

where $n_b(X_i)$ is the number of breakage sites available for size class X_i , and $O_1(X_i, 1)$ is the affinity factor related to size class X_i or to the other available size classes, X_j ($j = 1 \dots k$). The term in the middle bracket is the fraction of breakage sites free of particles that are able to be occupied by particles of size X_i . The natural logarithm terms are the inverse of the critical particle numbers $1/n_c, X_i$ and $1/n_c, X_j$. The last term is the total fraction of breakage sites occupied by the particle mixture and will equal to 1 for a normal mouthful of food as there will be enough food particles to saturate the occlusal area. Van der

Glas et al. (1992) then went on to show the similitude between the power law model of Eq. 2.2 and the two-way competition model of Eq. 2.5. The one-way model, they concluded, is incompatible with experimental evidence. However, in a more recent work including experimental results, van der Glas et al. (2018) show that the one-way model is most appropriate for small numbers of particles at the beginning of mastication, while the two-way model is better once large numbers of smaller particles accumulate.

2.5.3 Experimental validation for the selection models

For the selection model for single-sized particles in Eq.2.3, the model validation required the data from one-chew experiments with many particles of a specific size. Subjects performed a single chewing cycle and expectorated the particles, which were then transferred to a single sieve on which undamaged and large fragments of particles were retained. The contents from the sieve was then emptied on a sheet of smooth paper where damaged and undamaged particles were separated by visual inspection and the weight of the non-damaged (un-selected) particles was determined (van der Glas et al., 1992, 2018).

The data acquisition is a time-consuming process as for each size of particles inspected, they must be repeated from six up to 50 times to obtain a reliable estimate of the number of particles selected. Due to the time-consuming nature of the single chew experiments, they were often performed in only several subjects; four subjects in van der Glas et al. (1992) and five subjects in van der Glas et al. (2018). Additionally, for small-sized particles of 1.2 mm that require a number of particles greater than 2000 to saturate the breakage sites as observed in van der Glas et al. (2018), this would take days to complete the experiment. The method was acceptable for the test food Optosil® used in their study as it avoids the risk of degradation but would not be ideal for other ‘particle-like’ real foods such as rice or peanuts due to a risk of spoilage. Moreover, despite repeating the experiments multiple times, the data obtained would still be questionable as ‘damaged particles’ may have different meanings to different individuals and could raise question such as ‘Does this damage comes from chewing or preparation defects?’

As the selection models for particles in mixtures (Eq.2.4 and Eq.2.5) contain the $n_b(X_i)$ and $O_1(X_i, 1)$ terms as model inputs, single chew experiments will still be required to determine the input

variables. For each particle size studied, a relationship between the number of selected particles versus the number of offered particles is plotted and $n_b(X_i)$ and $O_1(X_i, 1)$ are obtained by curve fitting with a selection model for single-sized particles (Fig. 2-5). If X refers to the size of any particle, the number of breakage sites as a function of size $n_b(X)$, against X relationship for each subject can be adequately described by a power-law function (Eq.2.6) after curve fitting. Hence,

$$n_b(X) = k.X^{-m} \quad (2.6)$$

where k and m are the fitted constants.

Similarly, the relationship between the affinity value and particle size can also be described by a power-law function (Gray-Stuart, 2016), hence

$$O_1(X, 1) = p.X^q \quad (2.7)$$

where the multiplication factor p and exponent q are the fitted constants.

2.5.3 Number of breakage sites and affinity factor

The number of breakage sites becomes smaller the larger the particle size, and the absolute value of the exponent g in the power function of $n_b(X)$ - X relationship found with Optosil® particles was, in general, lower than two (van der Glas et al., 2018). A value higher than two of the exponent g would indicate that the initiation of breakage would be contributed by a combination of projected area (X^2) of individual particles and a degree of piling.

Although a mixture of small and large particles was used in the study, theoretically as indicated in the assumption of the two-way competition model, small particles should pile, and this would mean in some subjects, the exponent g should be greater than 2. In contrast, the finding that the exponent g can take values lower than 2 suggests that small particles could slide along each other during further jaw-closing hence only a monolayer of particles is formed at the initiation of breakage (van der Glas et al., 2018). Additionally, a value of exponent g , smaller than 2 could also suggest that only specific tooth areas may be involved in the breakage of small particles, whereas every location on the teeth is suitable for breakage of large particles (van der Glas et al., 2018). Van der Glas et al. (2018) also indicated that the piling of small-sized particles might occur if the particle size is smaller than the buccolingual dimensions of the premolar or molar teeth. A stack of piled particles is normally composed of two to six layers of a small particle with a size of 1 to 3 mm (van der Bilt et al., 1991).

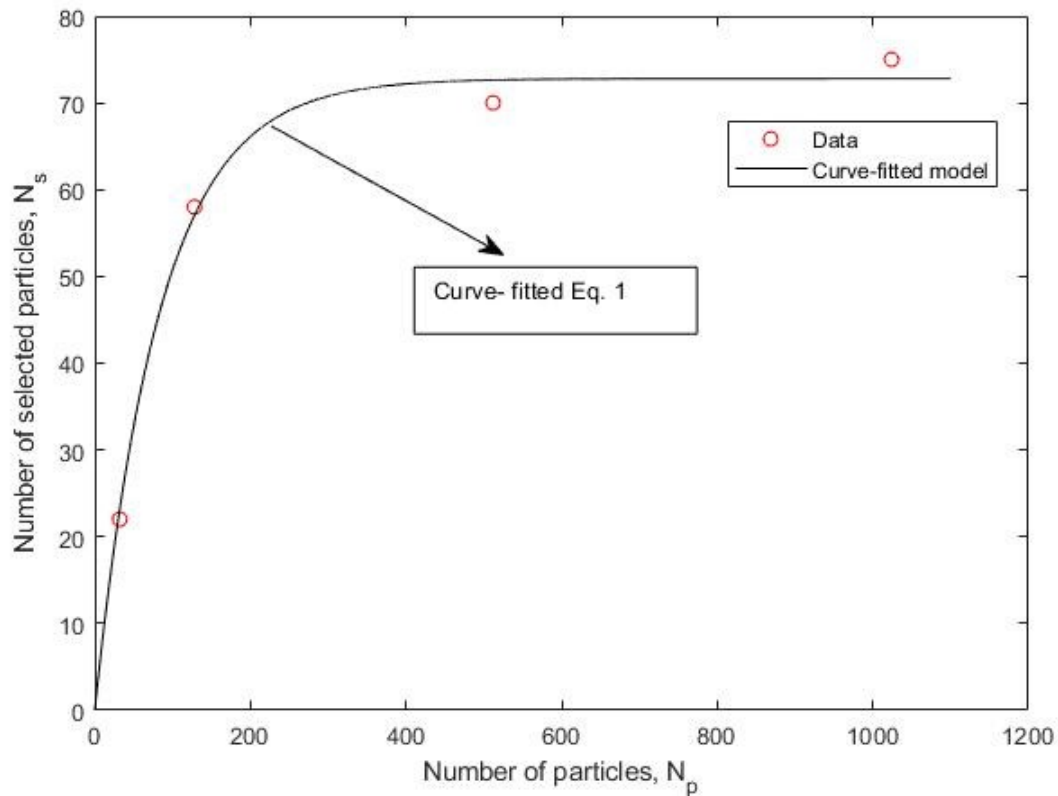


Fig. 2-5: A typical plot of number of selected particles vs number of offered particles. The data (red circle markers) was obtained from a single chew experiment performed on Subject 1 in van der glas et al. (2018) for particle size of 1.7 mm. The data is then fitted with Eq.2.3 to obtain the number of breakage sites n_b and the affinity factor, O_1 .

If the X^{-g} term in Eq. (2.6) describes the projected area of particles, the multiplication factor k of the equation would be the projected area of the occlusal teeth. Hence, the number of breakage sites is the ratio of the projected occlusal area to the projected area of a food particle. If this concept is true, the number of breakage sites can be estimated by only measuring the projected occlusal and the particle area, which is significantly faster compared to performing the traditionally single chew experiments. To date, this idea has not been explored.

2.5.4 Food locking function

During selection, the tongue collects and transports food particles towards the space between antagonistic posterior teeth. Selected particles have the tendency to escape from the space between antagonistic teeth, however it has been shown by video-fluoroscopy that a cheek and the tongue are responsible for pushing particles back between the teeth, therefore keeping the particles locked up (Zhang et al., 2019). Thus, other than the effectiveness of transporting particles to the teeth, the selection

process during mastication is also dependent on the ability to lock up particles (food locking function) between the antagonistic posterior teeth, cheek, and tongue during the closing phase of a chewing cycle.

A recent study by Zhang et al. (2019) measured the food locking function of 20 subjects by serving an artificial food that undergoes plastic deformation rather than breakage (spherical gum bolus) so that it will always be selected by the subject. The food locking function was obtained by measuring the width-length ratio of the gum bolus before and after chewing through image analysis. They found that when the tongue, cheek and teeth were involved in the food locking function, the spherical gum bolus becomes elongated following a number of chewing cycles (Fig. 2-6 left). However, when the tongue was kept away from the bolus while chewing, the shape in the plane of scanning was in general, circular (Fig. 2-6 right). The results from the study shows the importance of the tongue to ensure the locking of particles during selection.

Fig. 2-6: Change in shape of a spherical gum bolus from Zhang et al. (2019). Left shows the shape with a natural tongue function whereas the right side is when the tongue was kept away from the bolus.

Furthermore, when investigating the relationship between the food locking function and chewing efficiency, they found that subjects who had ‘good’ chewing efficiency had a significant quadratic U-shaped relationship with the food locking function. The results as suggested by the authors might be an interplay of the two functions of the tongue to manipulate particles during selection (affinity factor); first, the collection of food particles and transport towards the occlusal area, and second, the

food locking of particles in the space between antagonistic teeth and the cheek. The findings from the study by Zhang et al. (2019) signify an area where the selection model developed by van der Glas et al. (1992) can be improved.

2.5.5 Breakage functions

After selection, particles are broken between the teeth into smaller fragments of variable number and size (breakage). The breakage functions used in the literature for chewing are based on fitting a weight distribution data from a sieving analysis. The breakage function in the chewing model of Lucas & Luke (1983b) applied to carrots was estimated from the weight distribution of broken particles after a single chew. Two equations were used which produced good fit to the weight distribution data. For an initial particle size of X_o , the percentage of particles undersize by volume can be plotted for different sieve size X_i and can be given by

$$B(X_i, X_o) = b\left(\frac{X_i}{X_o}\right)^r \quad (2.8)$$

where $B(X_i, X_o)$ is the weight or volume fraction of particles of size X_o which break into particles smaller than size class X_i , and r and b are the fitted variables. A larger value of r and a smaller value of b in Eq.2.8 would show less fragmentation. For example an r value of 0.4 would have a higher proportion of smaller particles compared to $r = 0.8$ (constant b value of 1) as shown in Fig. 2-7a, but a b value of 1.0 with a constant r value of 1 had a higher proportion of smaller particles compared to a b value of 0.8 (Fig. 2-7b).

and

$$B(X_i, X_o) = 1 - s\left(1 - \frac{X_i}{X_o}\right)^r \quad (2.9)$$

where s and r are constants. Both s and r indicate the degree of fragmentation of the selected particle.

The difference between Eq.2.8 and Eq.2.9 is that Eq.2.8 has no mechanistic basis whereas Eq.2.9 was theoretically derived for a random single breakage of a solid particle from Gaudin and Meloy (1962). One of the assumptions behind the equation of Gaudin and Meloy (1962) is isotropy, therefore to use the equation; the food material should have uniform properties when force is applied in all directions. However, Lucas & Luke (1983b) indicated that it is possible that food particles are always randomly orientated on the teeth during chewing (thus, force is always applied in the same direction) hence the question if the food material is isotropic or anisotropic is not entirely critical.

Austin (1971) improved the theoretical breakage function of Gaudin and Meloy (1962) as described in Eq. 2.8. Van der Glas et al., (1987) implemented the improved equation to fit the experimental values for Optosil® after a single chew for four subjects and can be given as

$$B(X_i, X_o) = 1 - \left(1 + r \frac{X_i}{X_o}\right) \cdot \left(1 - \frac{X_i}{X_o}\right)^r \quad (2.10)$$

In contrast to Eq. 2.8, a larger r value in Eq. 2.9 and Eq. 2.10 would indicate higher degree of fragmentation, thus higher proportion of small daughter particles are produced for $r = 0.8$ compared to $r = 0.4$ as shown in Fig. 2-7c and Fig. 2-7e respectively. Fig. 2-7d shows the effect of the s value when r is constant in Eq. 2.9 where a larger s value of 1 has a smaller proportion of smaller particles compared to an s value of 0.8.

Eq. 2.10 also assumes isotropy, which was well-suited with the type of test food material, Optosil® used in the study in van der Glas et al. (1987). They found that the degree of fragmentation, r is dependent upon the initial particle size before chewing. A maximum value of r was found for particle sizes between 3.4 and 4.8 mm. Large particles which are locked between the teeth will most likely stick out, therefore a huge portion of the particles will not be subjected to breakage. Medium sized particles may possess large values of r as they will be cleaved more frequently by the teeth. Particles which are smaller with respect to the cusp size of the post-canine teeth are not likely to be cleaved and are most likely to squeeze between the antagonistic tooth surfaces without fragmentation (van der Glas et al., 1987).

When modelling the chewing process of brown rice, Gray-Stuart (2016) modified the improved Austin (1971) breakage function to include a pasted fraction term. When measuring the PSD of rice bolus for a range of chews using Mastersizer and sieve analysis, he found that the size reduction mechanism of rice follows a ‘cleave and paste mechanism’ in which selected particles are cleaved into few large particles and the remaining fraction pasted into small particles. Hence, if the pasted fraction is a constant, the breakage function can be described as

$$B(X_i, X_o) = (1 - P) * \left(1 + r \frac{X_i}{X_o}\right) * \left(1 - \frac{X_i}{X_o}\right)^r \quad (2.11)$$

where P is the pasted fraction.

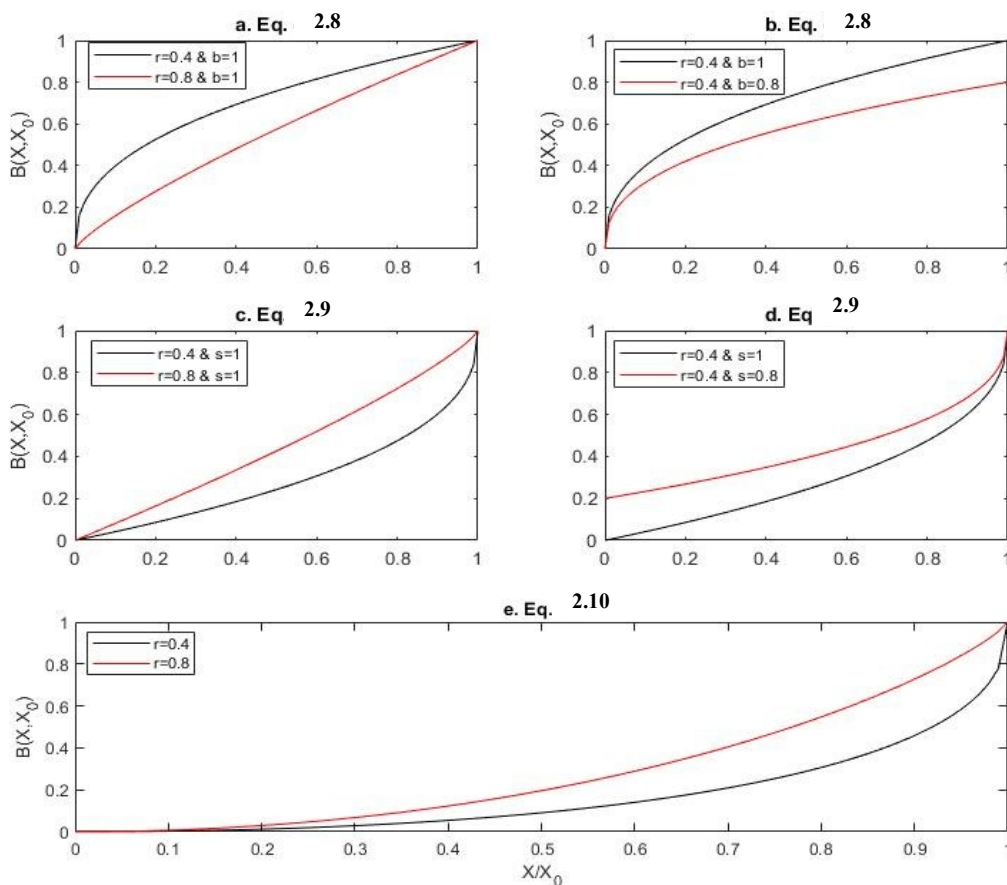


Fig. 2-7: Breakage function predictions example with varying input parameters. a. prediction with varying r values and a constant b value in Eq.2.8. b, prediction with varying b values and a constant r value in Eq.2.8. c, prediction with varying r values and a constant s value in Eq.2.9. d, prediction with varying s values and a constant r value in Eq.2.9 e, prediction with varying r values in Eq.2.10.

Peanuts are another food commonly used to fit a breakage function. For a single peanut particle, Gray-Stuart (2016) found that 17% of fragments of a single occluded particle passed a 0.355 mm sieve, which suggested that peanuts produce a bimodal distribution. The size distribution of the occluded peanut was fitted by a mixed breakage function

$$B(X_i, X_o) = Y * \left(1 - \left(1 + r_1 \frac{X_i}{X_o}\right) \cdot \left(1 - \frac{X_i}{X_o}\right)^{r_1}\right) * (1 - Y) * \left(1 - \left(1 + r_2 \frac{X_i}{X_o}\right) \cdot \left(1 - \frac{X_i}{X_o}\right)^{r_2}\right) \quad (2.12)$$

where Y is the portion of particle X_o being distributed with fragmentation variable r_1 and $1 - Y$ of X_o are distributed with r_2 .

2.5.6 Matrix models

In the literature, the selection and breakage functions were applied in matrices to predict the PSD during mastication. Van der Bilt et al. (1987) adapted the matrix methods from Broadbent & Callcott (1956) and Berenbaum (1961) which were developed for industrial comminution processes to predict the PSD during mastication. The PSD after one chewing cycle, p , can be predicted from the product of the comminution matrix, A , and the feed distribution, f . Therefore,

$$p = Af \quad (2.13)$$

The comminution matrix, A is expressed in terms of the selection, S and breakage, B matrices respectively,

$$A = [BS + (I - S)] \quad (2.14)$$

where the term $B.S$ represents the breakage of the selected particles, $I-S$ refers to the portion of non-selected particles and I is the unit matrix.

In the study, the selection process was simulated using the power law model (Eq. 2.2), where the variables v and w were not obtained experimentally but rather determined from fitting the experimentally PSD data with the comminution model using a least squares method. The selection matrix, S , was constructed as follows:

$$S = v \begin{pmatrix} x_1^w & & \\ & x_2^w & \\ & & x_3^w \end{pmatrix} \quad (2.15)$$

where in an experiment with three sieves, x_1 , x_2 and x_3 are the average sizes of particles on successive sieves.

The breakage matrix, B was constructed as follows:

$$B = \begin{pmatrix} b_{1,1} & b_{1,2} = 0 & b_{1,3} = 0 \\ b_{2,1} & b_{2,2} & b_{2,3} = 0 \\ b_{3,1} & b_{3,2} & b_{3,3} = 1 \end{pmatrix} \quad (2.16)$$

where $b_{1,1}$, $b_{2,1}$ and $b_{3,1}$ are the fractions of daughter particles originating from the particles on the top sieve, $b_{2,2}$ and $b_{3,2}$ are the fractions of fragments from the second sieve and $b_{3,3}$ is the fraction on the third sieve.

The matrix A is only related to one chewing cycle. However, p can also be calculated at any chewing number by multiplying f by the matrix A , N times:

$$p = A^N f \quad 2.17$$

The matrix model developed by van der Bilt et al. (1987) was able to predict the PSD of a bolus of Optosil® particles, where a good agreement was obtained between the experimental and model PSDs. However, the main weakness of this model is that it does not take into account the losses of particles during chewing (Gray-Stuart, 2016).

2.4.7 Population balance models

The extension to the matrix model to predict the PSD of the particles in the bolus during mastication was the study by Gray-Stuart (2016) where he developed a particle population balance model to track the particle-phase within the mouth. The population balance model was developed to define the available surface area necessary for the rate processes that occur in the mouth such as absorption, dissolution and melting. The balance also defines particle size and when particles are occluded.

The population balance is a discrete approach. Particles are labelled as ‘die’ if they are selected whereby when they give birth to new particles, they are called ‘daughter’ particles. When particles are broken below a lower limit threshold size they are not tracked, but their volumes are summed together. This is deemed as the suspended solids in the liquid phase.

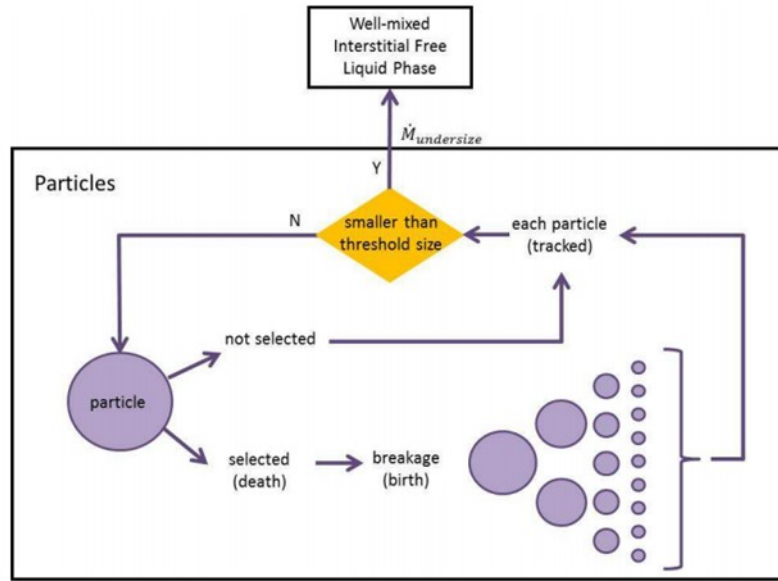


Fig. 2-8: Discretised population balance during mastication from Gray-Stuart (2016).

The population can be described mathematically by an array, V_p , where the elements are individual particles with the same volume, V_i . If particles less than the threshold size are created from breakage, their volume is summed and apportioned to the liquid-phase.

where V_p

$$= \begin{bmatrix} V_1 \\ V_2 \\ \vdots \\ V_{i-1} \\ V_i \\ V_{i+1} \\ \vdots \\ V_{max} \end{bmatrix}$$

The particles in V_p are sorted into size classes, i where i ranges from the minimum threshold size to the maximum size class used to describe the PSD. The PSD is given by the array \underline{N}_k , whose elements are the number of particles in each size class, and k , denotes the chew number.

$$\underline{N}_k = \begin{bmatrix} n_{1,k} \\ n_{2,k} \\ \vdots \\ n_{i-1,k} \\ n_{i,k} \\ n_{i+1,k} \\ \vdots \\ n_{max,k} \end{bmatrix}$$

During chewing all particles in the same size class are assumed to have the same chance of being selected. This selection chance is calculated from either the size dependent power law (Eq. 2.2) or the one-way (Eq. 2.4) and two-way competition selection model (Eq. 2.5). From the array of particles

V_p , another array is generated with the corresponding chance of selection for each particle V_i . A particle is selected when a random number (generated from a random distribution (*rand* function, Matlab)) is less than the theoretical selection chance.

These selected particles ‘die’ and undergo breakage producing daughter particles. Breakage is then approximated by a continuous breakage function $B(X, X_i)$ of ‘cumulative fraction less than’ where the particle undergoing breakage has characteristic dimension X_i and the function gives the cumulative fraction less than size X . Common breakage functions used in mastication are Eq. 2.8, 2.9 and 2.10. To discretize this, the volume fraction falling within the bin of a single size class is calculated by finding the difference of $B(X_j, X_i) - B(X_{j-1}, X_i)$ where the subscript j refers to the size classes from $j=1$ to $j=i$, after occlusion of a particle of size X_i . For a particle in size class X_i , the volume of births in size class X_j is given by

$$Volume_{births,j,i} = V_i(B(X_j, X_i) - B(X_{j-1}, X_i)) \quad 2.18$$

For each j from $j=1$ to $j=max$, the array of birth volume for all size classes for particle X_i is given by,

$$Total\ Volume_{births} = V_{births} = \begin{bmatrix} \sum_{i=1}^{i=max} B(X_1, X_i) - B(0, X_i))V_i \\ \sum_{i=1}^{i=max} B(X_2, X_i) - B(X_1, X_i))V_i \\ \vdots \\ \sum_{i=1}^{i=max} B(X_{j-1}, X_i) - B(X_{j-2}, X_i))V_i \\ \sum_{i=1}^{i=max} B(X_j, X_i) - B(X_{j-1}, X_i))V_i \\ \sum_{i=1}^{i=max} B(X_{j+1}, X_i) - B(X_j, X_i))V_i \\ \vdots \\ \sum_{i=1}^{i=max} B(X_{max}, X_i) - B(X_{max-1}, X_i))V_i \end{bmatrix} \quad 2.19$$

This matrix allows the number of birth particles in each size class to be calculated. The breakage process described by Eq. 2.19 above is applied to all the selected particles. The newly created particles are combined with the unselected particles and a new array, V_p , is obtained.

2.6 Application of the chewing models to aroma release

During mastication, solid food particles are reduced into smaller fragments which increases the surface area. The increase in surface area increases the rate of release of volatiles from foods, and subsequently affects the profile of volatiles in the nasal cavity. Although mastication plays an important role in flavor release of solid foods, very few mathematical models have been developed which couple both mastication and flavor release process in the literature. This is not surprising given the complexity of the mastication process (Hills & Harrison, 1995).

2.6.1 Two-film theory to describe flavour release

Some of the pioneering work was undertaken in the late 1990s by Hills & Harrison (1995, 1996) and Harrison et al. (1998). Hills & Harrison (1995) developed a model describing the flavor release of a perfectly spherical boiled sweet in the mouth. A conceptual model was made which describes the transportation of volatiles from the food product to the gaseous phase (Fig. 2-9).

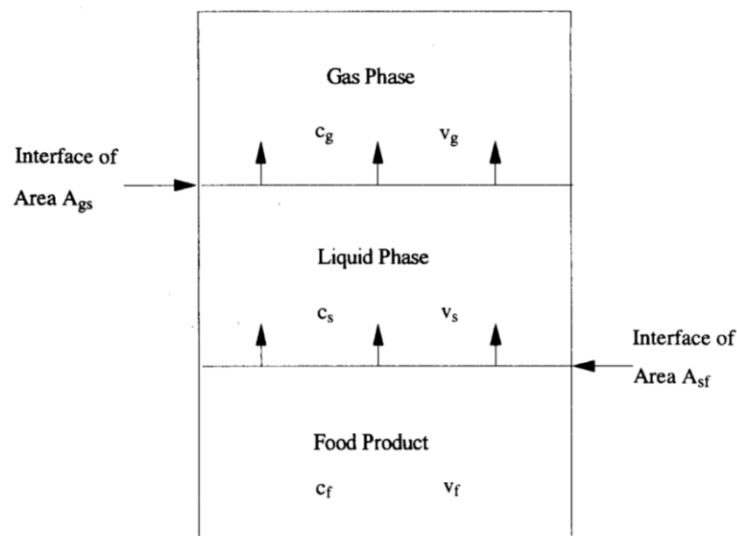


Fig. 2-9: Conceptual model showing the transfer of flavour release from a solid food from Hills and Harrison (1995). c denotes concentration, v , volume, and subscripts g , s and f refers to gas, saliva and food respectively.

In their model, the following assumptions were made:

1. Chemical equilibrium in the food matrix was assumed, as the dissociation rate constant is unlikely to be the rate-limiting step controlling flavor release.

2. The physiology of perception was ignored where the taste perception was assumed to be proportional to the concentration of flavor in saliva and aroma perception was proportional to the concentration of flavor in gas phase.
3. Interfacial mass transfer of flavor across the food/saliva and/or saliva/air interfaces is the rate limiting step controlling flavor release as mastication removes diffusion gradients and generates fresh interfaces.

A two-layer stagnant film theory was used to describe flavor release in their model (Fig. 2-10). It was assumed that all regions further from the layer are well stirred, and therefore the composition will be uniform. Across the film, transport takes place by diffusion and the concentration gradient across the laminar layer is assumed to be linear. The non-equilibrium concentration difference for volatiles between the food product and saliva or saliva and air phase in the mouth is the driving force for flavour release across the interface. Thus, the rate of mass transfer across the interface is given by

$$\frac{dM}{dt} = \frac{D}{L_s} A(t) [c_s^i(t) - c_s(t)] \quad (2.20)$$

where M is the total mass of volatile which diffuses across the interface, D is the diffusion constant, $A(t)$ is the interface surface area, L_s is the laminar thickness, and $c_s^i(t)$ and $c_s(t)$ are the concentrations of volatile at interface and the bulk region, respectively.

The predictions derived from the above theory were compared against experimental results *in vitro* and *in vivo*. *In vitro*, the predictions were compared to the change in dye concentration in water after a single coloured boiled sweet was placed inside a beaker filled with water. The change in dye concentration in the liquid phase was measured using a spectrometer, where a small sample of solution was removed from the beaker at regular time intervals. The normalized absorbance vs time curve was assumed to be equivalent to the flavour concentration vs time curve. The change in mass of the boiled sweet over time was measured *in vivo* where the results were also compared against the model predictions. The boiled sweet which was sucked in the mouth, was removed at regular time intervals and weighed. The change in the mass of sweet was assumed to be directly proportional to the flavour release. Other input parameters such as K_{sf} were determined by assuming that the solution at the

interface was saturated with sugar (dye). The initial concentration of dye in the sweet, C_f was determined by dissolving a single sweet in a fixed volume of distilled water.

The study by Hills and Harrison (1995) highlighted the importance of modelling the changes in surface area between the product of saliva by suggesting a multi-fragmentation theory to represent the chewing of the boiled sweet (assuming it was a cube). However, the theory may not be useful for real food products which do not always produce cubes where the area of fragments after each bite is essentially an increase by a factor of 2 (Doyennette et al., 2014).

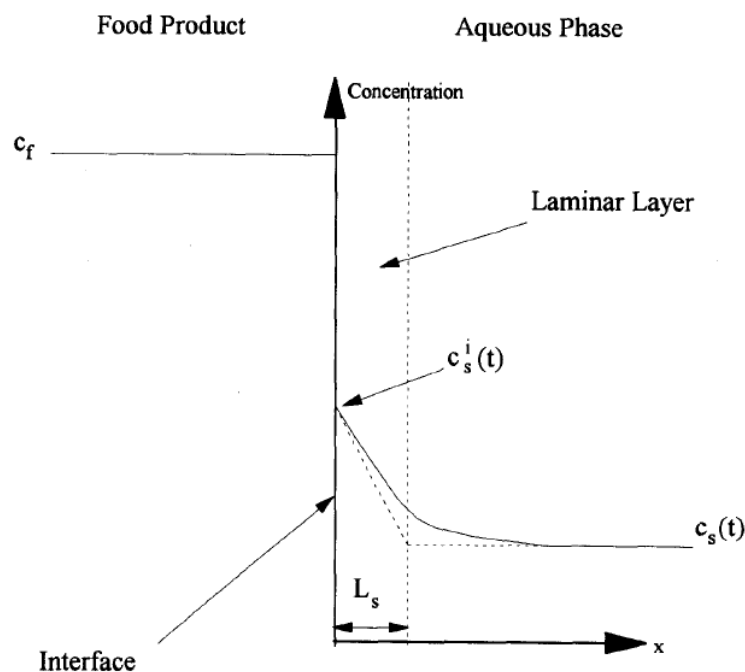


Fig. 2-10: Two-layer stagnant film theory from Hills and Harrison (1995). Solid vertical line is the interface. In the theory it was assumed there exists the surface layer of thickness L_s adjacent to the interface (the vertical lines). The volatile concentration can then be estimated by a linear concentration gradient across the stagnant layer (dotted) line, where the volatiles diffuse into the uniform bulk saliva concentration, c_s .

2.6.2 Flavour release models of solid foods

Although the model developed by Hills and Harrison (1995), as described above was incomplete as it did account for other physiological parameters (e.g. breathing) and was not validated with *in vivo* data, the model provided a framework for subsequent modelling studies related to flavour release from solid foods. Using the same theory of flavour release and combining it with heat transport, a mathematical

model was developed to describe the flavour release from gelatin-sucrose gels (Harrison & Hills, 1996). The model was found to give good agreement with *in vitro* release experiments using gelatin gels containing sucrose and dye.

The same group extended the flavour release model by incorporating a mastication model to generate PSDs after each chew (Harrison et al., 1998). The mastication model includes the selection and breakage functions which were described by a power law relationship (e.g. Eq. 2.2). If a parent particle size is y and the fragment size is x , the percentage of particles below size y after the n^{th} chew is given by

$$Q_n(y) = \int_y^\infty P_{n-1}(x)B(y,x)S(x)dx + \int_0^y P_{n-1}(x)dx \quad (2.32)$$

where $P_{n-1}(x)$ is the percentage of the total volume of size x to $x + dx$ before the n^{th} chew, and the second term on the right-hand side refers to the percentage of particles that exist below size y in the ingested feed particles before the n^{th} chew.

The percentage of particles of size x to $x + dx$ before the $(n + 1)^{\text{th}}$ chew, $P_n(x)dx$ is given by

$$P_n(x) = \frac{dQ_n(x)}{dx} \quad (2.33)$$

The integrals in Eq. 2.32 were numerically solved to generate values of $Q_n(x)$. $P_n(x)$ were then obtained by solving Eq. 2.33 using a finite difference method. The PSDs which were calculated using Eq. 2.33 were then used to calculate the surface area of the food assuming all fragments produced during mastication are spherical. The model was able to predict the concentrations of flavour in the gas phase of the mouth and sensitivity analysis of the model shows the concentration was less sensitive to the chewing frequency and salivary flow rate but was dependent on the breakage function of the food and mass transfer coefficient. Despite the extension made, the model did not include the effect of breathing and was not validated against *in vivo* experimental data.

Wright & Hills (2003) and Wright et al. (2003) took a different approach to model the mastication process during flavour release of jellied sweets in the mouth by fitting a Pearson Type IV probability distribution to the subject's electromyography (EMG) and surface area data. The model simulation produced the same trend as the sensory time-intensity (TI) data of the subjects. However,

the authors acknowledge that it needs to be compared against the actual headspace or saliva flavour concentrations to really test the model. Additionally, the model did not take the effect of breathing into account.

The most comprehensive model that describes flavour release of solid food during mastication is the one developed by Doyennette et al., (2014) for flavour release from cheese. Fig. 2-11 shows a conceptual model, which describes the mastication process of the model. The process starts with the introduction of food in the mouth, the intra-oral manipulation of the product (chewing, swallowing (e.g. contraction and relaxation)) and the release after mastication is finished (resting). Usually, the intra-oral manipulation phase only lasts until the first swallow, however, for some products (e.g. firm products), it may need more swallows. The swallowing step includes contractions of the oral cavity and pharynx which occur concomitantly, which lead to the expulsion of air and product, followed by relaxation and filling with fresh air. In each swallowing step, a small part of the liquid bolus is assumed to be deposited on the pharyngeal walls. If residual solids of the bolus are still present in the mouth, they will be chewed again and mixed with saliva to form a new bolus for swallowing.

The model was the most complex one to date as it included all physiological compartments that are involved in flavour release. Additionally, the model also included the physiological aspect of breathing and takes aroma persistence (release from lubricated mucosa) into account, which was not included in previous models describing flavour release of solid foods. Two aroma compounds were tracked; 2-nonanone and ethyl propanoate which exhibit different persistence behaviour (2-nonanone interacts with the lubricated mucosa in the nasal cavity, oral cavity and pharynx, causing a higher release post swallowing). Results from the study showed that the model predictions (relative concentration of aroma compound in the nasal cavity) were in good agreement with the *in vivo* experimental data of ten subjects, which was measured using Atmospheric-Pressure Chemical Ionisation-Mass Spectrometry (APCI-MS). A sensitivity analysis of the model showed that the product dissolution rate in the mouth, the mass transfer coefficient of aroma compound in the bolus and the air-bolus contact area had a significant positive impact on the release intensity. The respiratory frequency on the other hand had a strong negative effect on the aroma concentration by increasing the rate of removal of aroma

compounds. Additionally, it was also found that the rate of saliva addition in the bolus and the velopharynx opening had a major influence on the overall kinetics of aroma release.

Fig. 2-11: Conceptual model of the steps involved during mastication of a solid food product from Doyennette et al (2014)

The weakness of the model is the strong simplifying assumptions made to describe the mastication process. The authors acknowledge it was challenging to predict the contact area between the solid product and liquid bolus due to the type of food used in the study (cheese) which becomes pasty during mastication. Hence, it was assumed that rate of change of contact area between the solid product and liquid bolus evolves linearly over time. This highlights an area of weakness of the model which can be improved by coupling with the selection and breakage models to predict the bolus PSD. However, characterising the bolus PSD data for model validation might prove a challenge.

2.7 Chapter conclusion

The first part of this review covered the main processes involved during mastication. To help visualise the main steps involved during chewing, several researchers have developed conceptual models (Lucas et al., 2002; Hiemae, 2004; Gray-Stuart, 2016). The most comprehensive model was the one developed by Gray-Stuart, (2016) where the model integrates food breakdown, mixing and testing of the food properties, which is more closely matched to the chewing process in real life. Understanding the chewing process will not be complete without including a review on the role of saliva as it plays an important role to bind food particles for bolus formation.

Mastication has been shown to affect digestion and flavour release as the reduction of food particles increases the surface area available for enzymatic action and the release of volatiles. Current studies relating mastication and digestion were mostly focused on carbohydrate-based foods (e.g. white rice) which is not surprising given the abundance of salivary amylase in the mouth. Studies have shown that the total glycaemic response was lower when chewed faster due to the presence of more large particles in the bolus (Ranawana et al., 2010, 2014). In addition, investigation on the role of mastication on aroma release were mostly focused on performing *in vitro* studies due to the challenge of characterising the bolus PSD *in vivo* which is laborious and time consuming. Mastication has been shown to affect *in vivo* aroma release of cheese (Pionnier et al., 2004) where it was correlated with chewing behavior, but again very minimal effort was made to understand the role of the bolus PSD on flavour release.

The review also discusses previous mastication models which were developed in the literature. Selection and breakage functions which are commonly used in industrial comminution processes were adapted to chewing in previous studies (Lucas & Luke, 1983b; van der Bilt et al., 1987; Gray-Stuart, 2016). The review first discusses pioneering selection models that were used in the literature, to the most comprehensive to date, which were the competitive models developed by van der Glas et al. (1992). The weakness of the model is that it requires input parameters which had to be measured from experimental data which are labour intensive and time consuming. The experiment involves chewing a defined number of food particles until the occlusal area is saturated, where model is then fitted to obtain the input parameters. The experiments may work for artificial test food such as Optosil® as used in the study but may not work for real foods as it may be challenging to differentiate which particles that are selected or not. Therefore, to apply the competitive selection models on real foods, new methods will need to be designed to obtain the input parameters. In addition, common breakage models in the literature for different type of foods were also described and compared. Previous approaches used to predict PSDs such as the matrix and population balance models were also described.

Finally, the extension to the chewing models is its application in food design. One way is to couple with a flavour release model, as if successful, it can be used to mathematically predict the effect of varying food composition, food structure, and mastication behaviour on aroma release (Harrison et

al., 1998). Early efforts have been made to include the selection and breakage functions such as in Harrison et al., (1998) however, the model was never validated against experimental data. Similarly, Wright et al. (2003) included mastication aspects in their model based on electromyography (EMG) readings, however the model could only predict the same trend with the sensory time intensity data.

The model developed by Doyennette et al. (2014) was the most complex one to date as it includes the subject's physiological data (e.g breathing cycle, oral cavity, pharynx and nasal cavity volumes, saliva flow rate) and the model was able to be validated against *in vivo* experimental data. Despite this, a strong simplifying assumption was made where the rate of change of surface area was assumed to increase linearly with time, which is not the case in real life. This leaves a gap to incorporate a validated chewing model to improve the aroma release model developed by Doyennette et al. (2014).

Chapter 3 Chewing model development

Models have been established for the selection and breakdown of particles and changes to the PSD during the mastication process (Lucas & Luke, 1983a, 1983b; van der Glas et al., 1992; Prinz & Lucas, 1997; Gray-Stuart, 2016). In each case, they have been applied to a limited number of food types and in some cases, only to model food systems such as Optosil®.

While several selection and breakage models exist in the literature, only some have been used in previous mastication studies. Selection has been fitted by power law functions with respect to PSD during mastication of carrots, peanuts and Optosil® (Lucas & Luke, 1983; van der Bilt et al., 1987; Prinz & Lucas, 1997). It has been improved to account for both particle size and number by incorporating competition rules for occupancy of particle on the teeth before occlusion (van der Glas et al., 1992, 2018). The two models, called the one-way and two-way competition models, have been validated with Optosil®, but have not been applied to real foods experimental data. Breakage models are many and varied, but the most common one is the improved Austin, (1971) theoretical breakage function of Gaudin and Meloy (1962), which has been applied for the mastication of Optosil® (van der Bilt et al., 1987; van der Glas et al., 1987) and brown rice and peanuts (Gray-Stuart, 2016). In the literature, selection and breakage functions have been applied to matrices (van der Bilt et al. 1987) and to a discretised population balance (Gray-Stuart, 2016) to predict the bolus PSD. However, since the competitive selection models are a function of particle number, the models need to be discretised, to be able to track the number of particles in a specific size class.

This chapter aims to develop a mechanistic chewing model to predict the PSD of solid food bolus based on the selection and breakage processes.

3.1 Conceptual model

It is important to first understand the selection and breakage process involving mastication of solid foods through a conceptualised diagram. This will form the basis for the implementation of the particle size reduction model.

3.1.1 Selection and Breakage process – A conceptual model

The selection and breakage processes involved during mastication of solid food particles are illustrated in Fig. 3-1.

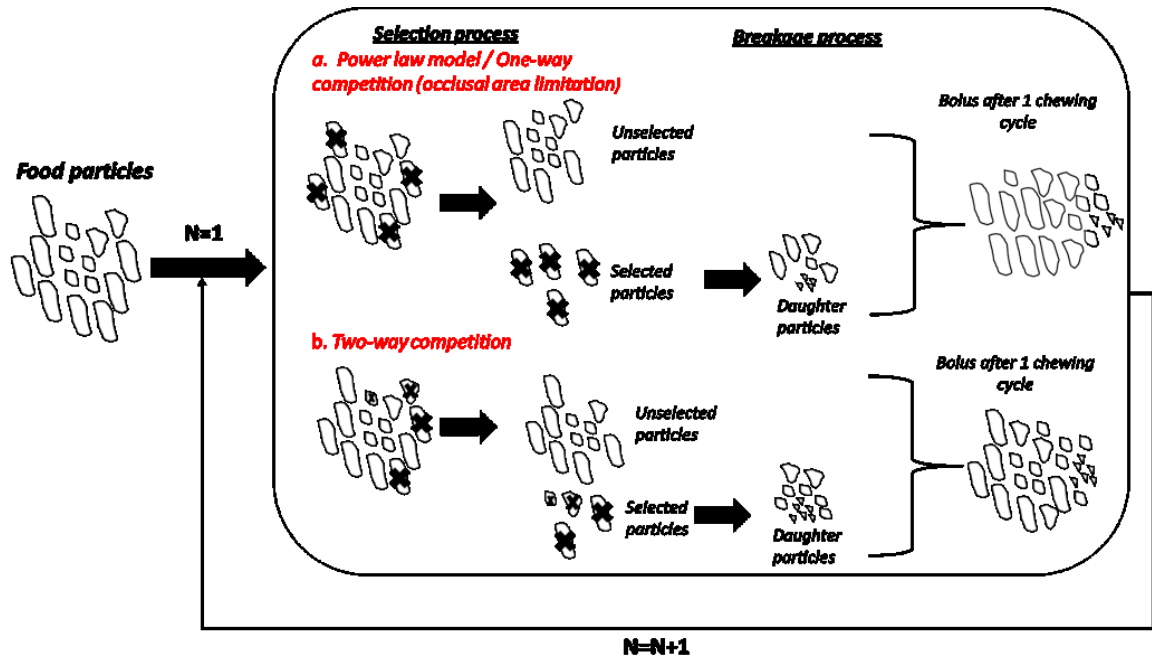


Fig. 3-1: Conceptual diagram describing the processes involved during mastication.

During mastication, food particles undergo two separate processes, selection and breakage. Selection is the consequence of the tongue and jaw movements positioning particles in the occlusal zone before occlusion and on the likelihood of a particle on the occlusal zone being subjected to compression and shear during occlusion. A selected particle is one that is subsequently damaged during jaw closure. Some particles present on the occlusal surface could escape damage by flowing away or may be positioned such that no forces can be applied for a given molar shape and jaw trajectory.

Three key selection models have been developed (van der Glas et al. 2018). The power-law model, which describes selection and particle size relationship (the larger the particle size, the higher the selection chance), has been developed based on the observations found when chewing on labelled particles (Lucas & Luke, 1983a; van der Glas et al., 1987). The power-law model has been improved to account for both particle size and number by incorporating competition rules for occupancy of particles on the teeth before occlusion (van der Glas et al., 1992, 2018). The one-way competition model is somewhat similar to the power-law model that it assumes that the large particles will hinder the

selection of smaller particles without the reverse occurring. The difference is that selection of particles based on the one-way competition model accounts for particle number, where the selection chance is also dependent to the surface area of the post-canine teeth (the number of breakage sites). In contrast, the two-way competition model assumes that both large and smaller particles can compete equally, where smaller particles can pile in the space between antagonistic teeth (forces propagate from one particle to another rather than having to be directly between the opposing molar surfaces) and so compete with larger ones for the breakage sites (van der Glas et al., 2018). Once selected, particles undergo breakage into smaller daughter particles.

After occlusion, the PSD may be significantly different. The process of size reduction is known collectively as breakage which includes a number of mechanisms. For example, the breakage of carrot produces a few small particles and two particle fragments being held together by an unbroken bridge of tissue (Lucas & Luke, 1983a). Thus, a narrow PSD is to be expected for this specific breakage mechanism after several chews. On the other hand, a wider PSD can be expected for the breakage of brown rice that follows a cleave and paste breakage mechanism. In this mechanism, several large daughter particles are produced and a fraction is pasted into many very small particles that are suspended in the liquid phase of the bolus and not further broken down (Gray-Stuart, 2016).

3.1.2 Model assumptions

The key assumptions in the model are described below; however, these assumptions will likely change as models are adapted to a wider range of foods.

- 1. There are no losses of particles.** However, the inclusion of particle loss could come later in model development. The mechanisms for losses would need to be considered in order to develop mathematical methods for how to choose which particles are lost and whether they can rejoin the bolus and undergo further breakdown. Flynn (2012) demonstrated that two ‘compartments’ of particles existed, with a growing population of residue particles as mastication continues. Some of her data suggested that larger lost particles somehow find themselves being broken down later on in the chewing process, suggesting a recirculation of particles between the active bolus and residue

compartments. The following questions/aspects should be considered in order to include the losses of particles in the model.

- a. Are losses dependent on factors such as particle size, bolus volume and food properties?
- b. Will losses reduce as saliva and hence bolus cohesion increases?
- c. Mechanisms could include sticking to teeth, solubilisation of particles, washing out, sticking to other mouth surfaces etc.

Apart from the studies by Peyron et al. (2004), Flynn (2012), and Hutchings et al. (2012), no structured experimental investigation of food losses and the mechanisms for the low recovery of ingested food in expectorated boluses has been completed. Because of this, no attempt was made to include losses in this work and therefore the application of the model will be limited to foods that incur high solids recovery.

2. Selection could change with stage of mastication.

- a. During the initial phase of chewing, the number of small particles will be small and not piled, therefore larger particles could be preferentially selected according to the one-way competition model. After a few initial cycles, the number of small particles of various sizes will start to build up and could begin to pile, which allows them to compete against the large particles for selection (two-way competition model). Therefore, the selection function could switch from one-way to two-way competitive model after a particular mastication stage. Although this mechanism has been suggested (van der Glas et al., 2018), it has not yet been applied in food breakdown modelling.
- b. The selection of smaller particles could increase due to cohesion provided by saliva which binds particles together. This cohesion effect would be negated when there is a lot of saliva or another fluid (a sip of water) where the small particle would more likely

be washed away from the occlusal surfaces during a chew. This effect could be partially accounted for in the two-way competition model where inter-particle cohesion could increase the chances of piling.

- 3. Selection is likely to vary between people because of differences in teeth shape, jaw trajectories and chewing side preference used for specific foods.** Cusps can trap food particles in lateral trajectories ensuring better selection chances than if the teeth are flat. Furthermore, it has been shown that chewing was more efficient on the side where there was a greater occlusal area (Wilding, 1993). As such it is likely that the constants for selection are likely to vary between people and potentially different selection models may be more appropriate.
- 4. Breakage could change throughout mastication due to a number of factors.** A number of factors could change the breakage behaviour of particles undergoing occlusion. Some food structures can swell with increasing moisture absorption. Others may become softer or tougher on moisture uptake. Moisture may dissolve some of the food components and if structural materials are removed, the breakdown rate can be significantly impacted. Similarly, temperature changes can occur during mastication. This could change mechanical properties or melt fat-based components which impact the breakage properties of the food. To begin with, it is assumed that the breakage properties of foods are not changing with time, limiting the model application to systems that are around physiological temperature and resist moisture uptake by being high fat or already saturated in moisture.
- 5. Breakage is likely to vary with jaw trajectory where more grinding lateral motions will apply more shear than the mainly compressive loads applied with vertical jaw trajectories.** In studying the effects of varying chewing trajectories on the breakage function of peanuts using a chewing robot, Ng (2018) found that the degree of fragmentation was larger for lateral chewing compared to vertical chewing. She postulated that the reason peanuts were broken more in the lateral trajectory is due to a higher resultant force from the lateral shear which makes contact with a larger area of particles in each chewing cycle. Furthermore, chewing trajectories can also change with stages of mastication. Little or no lateral jaw trajectories (bilateral) were observed once the

food attains the consistency, homogeneity, and cohesiveness ready to be swallowed for various type of foods (Wictoria et al., 1971; Paphangkorakit et al., 2016). Thus, differences in trajectories can change with people, meaning breakage functions may be person specific, although some changes in trajectory can occur during mastication of a food within a subject, particularly in the early phases of mastication. In this work, breakage functions are assumed to not vary with time throughout mastication but could vary between individuals who have different chewing behaviour.

3.2 Model formulation and implementation

3.2.1 Selection model equations

The selection model used in previous chewing studies was either the power-law model (Eq 2.2), the one-way competition model (Eq 2.4), or the two-way competition model (Eq 2.5). The important assumptions behind each model have been described previously in Chapter 2 (see section 2.5.1 & 2.5.2).

The selection model equations are restated here for clarity.

Power-law model:

$$S(\bar{X}_i) = v\bar{X}_i^w \quad (2.2)$$

where $S(\bar{X}_i)$ is the selection function (in the range of $0 \leq S(\bar{X}_i) \leq 1$), \bar{X}_i is the particle size, and v and w are constants.

One-way competition model:

$$n_s(X_i, n_{xi}) = \left[n_b(X_i) \cdot \prod_{p=0}^{i-1} U(X_p, n_{xp}) \right] \left[1 - (1 - O_1(X_i, 1))^{n_{xi}} \right] \quad (2.4)$$

where $n_s(X_i, n_{xi})$ in the smaller size class (X_i) is the number of selected particles as a function of number in the presence of p classes of larger particles of sizes ($p = 0 \dots i-1$). $U(X_p, n_{xp}) = [1 - O_1(X_p, 1)]^{n_{xp}}$ is the fraction of breakage sites free of particles of size X_p . The term $n_b(X_i)$ is the number of breakage sites available for size X_i if larger sizes were not present, and $O_1(X_i, 1)$ is the affinity factor related to particle size X_i or to the other larger particle sizes X_p ($p = 0 \dots i-1$).

Two-way competition model:

$$n_s(X_i, n_{xi}) = n_b(X_i) \left[n_{xi} \cdot \frac{\ln(1 - O_1(X_i, 1))}{\sum_{j=1}^k [n_{X_j} \ln(1 - O_1(X_j, 1))]} \right] \left[1 - \prod_{j=1}^k (1 - O_1(X_j, 1))^{n_{xj}} \right] \quad (2.5)$$

where $n_b(X_i)$ is the number of breakage sites available for size class X_i , and $O_1(X_i, 1)$ is the affinity factor related to size class X_i or to the other available size classes, X_j ($j = 1 \dots k$).

3.2.1.1 Selection model implementation

Two input parameters are required to implement the one-way and two-way competition equations as described above. This is described below and summarised in Fig. 3-2.

Input one: Number of particles in each size class

The first input parameter required for the models is the number of particles that has been assigned to each size classes. To obtain a finer scale of scrutiny, a greater number of size classes can be defined, sorted into a desired number of size classes, ranging from the minimum size class to the maximum size class. This is expressed by the array

$$M_P = \begin{bmatrix} M_{min} \\ \vdots \\ M_{j-1} \\ M_j \\ M_{j+1} \\ \vdots \\ M_{max} \end{bmatrix} = \begin{matrix} M_{min} \\ \vdots \\ n_{j-1} \rho_{pfood} V_{j-1} \\ n_j \rho_{pfood} V_j \\ n_{j+1} \rho_{pfood} V_{j+1} \\ \vdots \\ n_{max} \rho_{pfood} V_{max} \end{matrix}$$

where the j counter is distinct from the i counter used in the equations above.

The number of particles grouped in each size class (n_j) is numerically counted from the distribution generated above, the volumes summed, and multiplied by density to obtain the mass matrix.

Input two: Number of breakage sites and affinity factor

The number of breakage sites are required in both one-way and two-way selection models. Traditionally, this is obtained by offering a large number of particles of a particular size until the occlusal teeth area is saturated. This is the maximum number of particles that can be occluded during a chew stroke and is called the number of breakage sites. It varies with size to the power of X where

$$n_b(X) = k.X^{-m} \quad (2.6)$$

where k and m are the fitted constants.

The affinity factor, $O_1(X, 1)$, is defined as the fraction of breakage sites which is on average, occupied by the first particle that is selected by the teeth (van der Glas et al., 2018). Similarly, the relationship between the affinity value and particle size can also be described by a power-law function (Gray-Stuart, 2016), hence

$$O_1(X, 1) = p.X^q \quad (2.7)$$

where the multiplication factor p and exponent q are the fitted constants.

Selection outcome

Once all of the model inputs are obtained, it is time to calculate the selection outcome. During occlusion, all particles assigned to the same size class are assumed to have the same selection chance (Gray-Stuart, 2016). Once the theoretical number of selected particles in a size class X_j ($n_s(X, n_{xi})$) is obtained, the selection chance in a size class can be calculated as

$$S(X_j) = \frac{n_s(X_j, n_j)}{n_j} \quad (3.1)$$

where $S(X_j)$ refers to the selection chance in size class X_j .

where for a mixture of particles following the one-way competition model

and for a mixture of particles following the two-way competition model

Each of the particles within each j^{th} size class therefore has $S(X_j)$ chance of being selected. To pick the specific particles that will undergo breakage, each particle is given a random number. The particle is selected if the random number is less than $S(X_j)$. This method is stochastic, so the number of particles selected will vary between simulations.

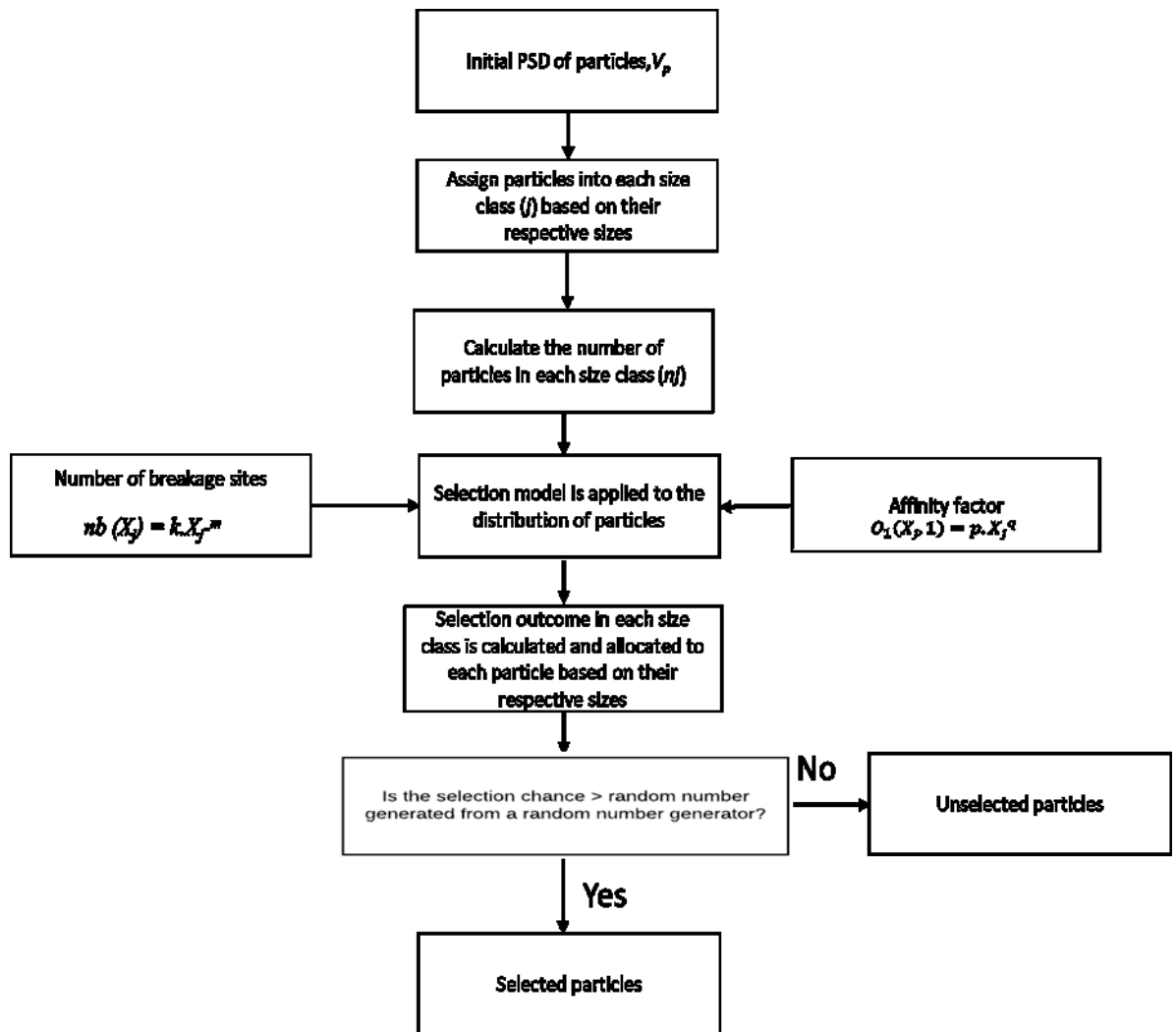


Fig. 3-2 Schematic model diagram showing the steps required to implement the one-way and two-way competition models.

3.2.1.2 One-way and two-way competition examples on peanuts data

To demonstrate the one-way and two-way competition models on real food particles, the PSD of 4 g halved peanut bolus from a single subject (Flynn, 2012) was used. The data was presented as mass fraction against a series of sieve size classes, which provided the PSD for 4 g portions of peanuts chewed for various numbers of chews (1, 2, 4, 6, 8, 10, 15, 20, 25, 30 and 35 chews). A single subject (male, age =27 years old) was used with three replicates at each stage of chewing. The raw data which included the standard error of the three replicates can be found in Appendix D. Three PSDs representing early (1 chew), middle (15 chews) and late phases of chewing (30 chews) were obtained. The mass fraction versus sieve size class data was converted to particle number versus size class, X_i and used as inputs to the one-way and two-way competition models.

Two other parameters are also required, the maximum number of breakage sites for each particle size and the affinity factor. The latter of is a size dependent term for selection of each particle size, where larger particles have higher affinity factors (van der Glas et al., 1992, 2018). Because the objective here was to demonstrate the mode and differences between the one-way and two-way competition selection models, the constants for the number of breakage sites power law model were obtained from the results for Subject no. 01 in van der Glas et al. (2018) where $k = 216.9$, $m = 1.94$, where k is the multiplication factor and m is the exponent in the power function. The affinity factor $O_1(X, 1)$ for Subject no. 01 in van der Glas et al. (2018) were converted from the critical particle number, using the equation below.

$$O_1(X, 1) = 1 - e^{\left(-\frac{1}{n_c(x)}\right)} \quad (3.2)$$

Eq.2.7 ($O_1(X, 1) = p.X^q$) was then used to fit the affinity factors vs particle size (mm) data to obtain the p and q constants (where p is the multiplication factor and q is the exponent in the power function), which were 0.0038 and 1.94 respectively.

Fig. 3-3 shows the difference in the volume fraction of selected particles (defined as the sum of the volume of particles that are selected divided by the volume of particles in the bolus) whereas Fig. 3-4 illustrates the difference in the number of selected particles when the one-way and two-way selection models were applied to the different PSD's. In every simulation, the number of particles selected is different each time. Therefore, to predict the PSD for any bolus, more than one of simulations is required to ensure the average number of particles selected reaches a convergence (e.g. 20 simulations from Gray-Stuart (2016)). In Fig. 3-3 and Fig. 3-4, the simulations were repeated 3 times and the results of each simulation were shown.

A clear difference between the one-way and two-way competition models can be observed. The results obtained from the model simulations in Fig. 3-3 and Fig. 3-4 were consistent with the assumptions of the one-way and two-way competition models developed in van der Glas et al. (1992). The number of selected particles for larger particle sizes was higher when the one-way competition model was used because it favours the selection of larger particles because they are selected first because of their height advantage. These larger particles will occupy the breakage sites which are not

available for smaller particles (van der Glas et al., 1992, 2018). Smaller particles can still be selected during jaw closing but have less area available to them. The smallest particles have the least area and therefore the least chance of selection (van der Glas et al., 1992, 2018). On the other hand, the two-way competition model recognises that the increase of the number of smaller particles, particularly later in the chew cycle, can cause piling of small particles which can compete with the larger particles (van der Glas et al., 1992, 2018).

Thus, van der Glas et al. (2018) explains that the one-way model is likely to be more applicable in the early stages of chewing but that the two-way model is more appropriate in the later stages of chewing. This is evident from the results, where the one-way model better selects more large particles at 15 and 30 chews (more particles between 2-4 mm selected) in Fig. 3-4, which was the reason why the volume fraction of selected particles was higher than when the two-way model was applied. The two-way model better selects small particles at 15 and 30 chews where it was evident from the higher number of particles less than 1 mm selected, hence the reason why the volume fractions of selected particles were much smaller than predicted using the one-way model.

It was interesting to observe the small difference in the volume fraction of selected particles between the two different models at 1 chew (Fig. 3-3). Van der Glas et al. (2018) postulated that because of a higher number of large particles in the first initial cycles, the difference between one-way and two-way model regarding selection of large particles will be small because of a small affinity for small particles. Therefore, small particles will not one-way model or hardly two-way model when they are initially present in small numbers. Thus, as the large particles were preferentially selected in both models during the initial stage of mastication, the results showing the small difference of the volume fraction of selected particles in Fig. 3-3 was expected.

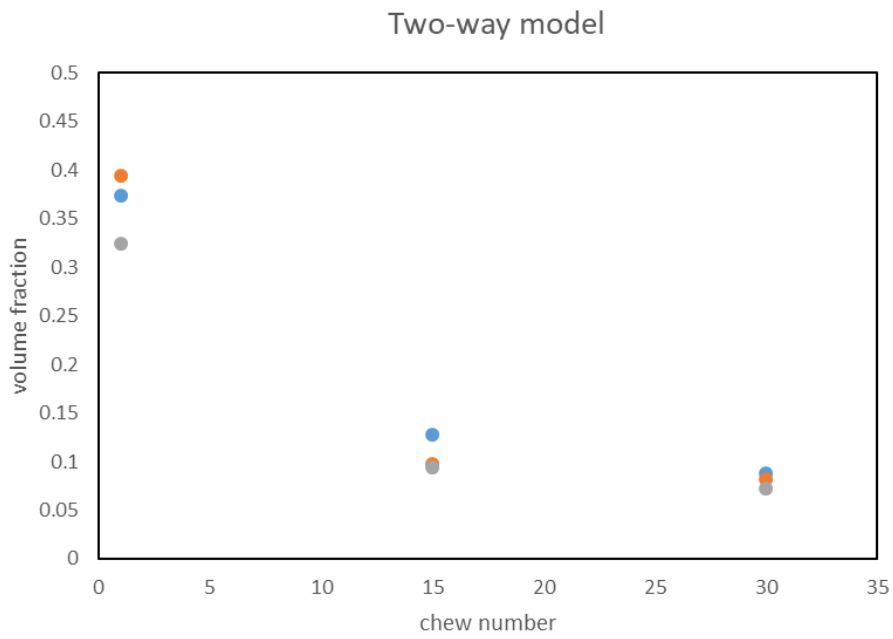
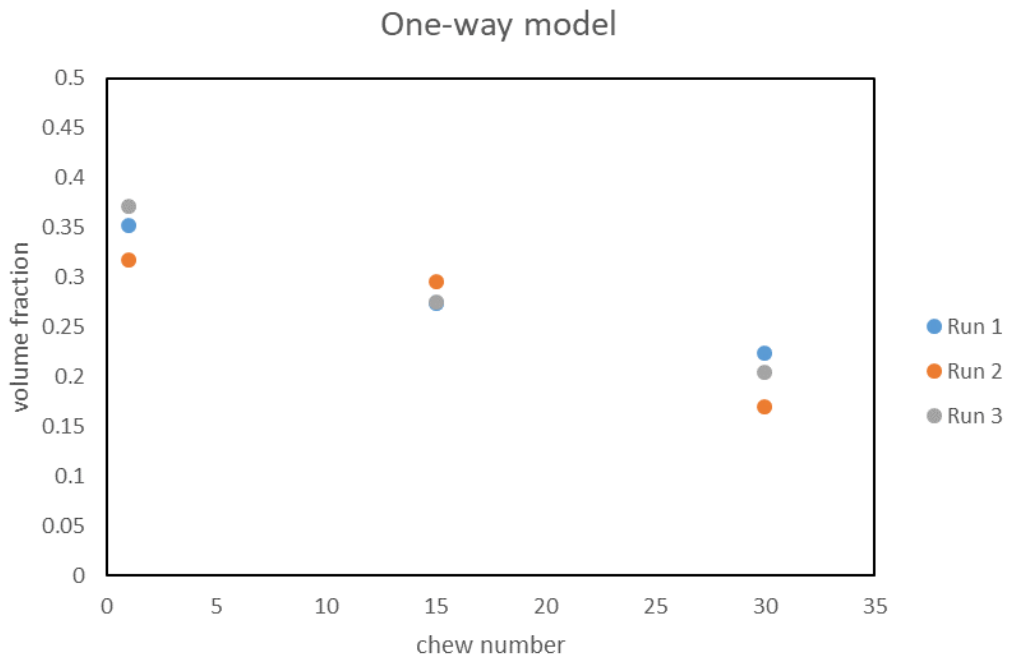


Fig. 3-3 Volume fraction of particles selected at 1 chew, 15 chews and 30 chews between one-way and two-way competition models. The simulation was run three times.

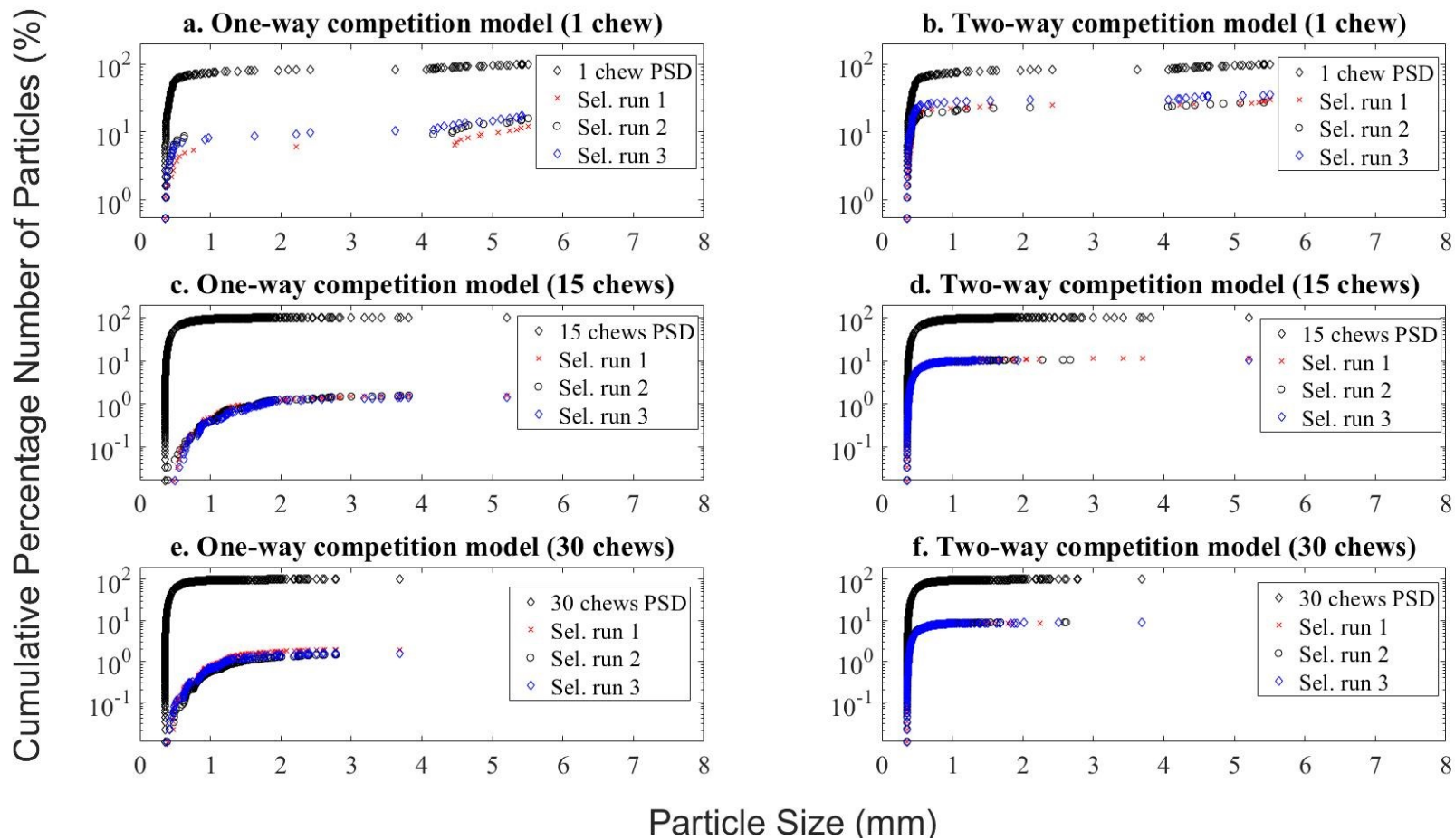


Fig. 3-4: Examples of one-way and two-way competition model predictions using real peanut bolus PSD data. Black diamond marker represents the real PSD chewed peanuts data used as the model input for the selection models. A cumulative percentage number of particles is used here to show selected particles. For instance in a. selected particles make up around 10% of the total number of particle from the input data. Red X marker, prediction after one simulation. Black round marker, prediction after the second simulation. Blue diamond marker, prediction after the third simulation. a, One-way competition model when implemented on a 1 chew data. b, Two-way competition model when implemented on a 1 chew data. c, One-way competition model when implemented on a 15 chew data. d, Two-way competition model when implemented on a 15 chew data. e, One-way competition model when implemented on a 30 chew data. f, Two-way competition model when implemented on a 30 chew data.

3.2.1.3 Occlusal area and number of breakage sites

As described above, both one-way and two-way competition models require the number of breakage sites as one of the model inputs. Usually, this is obtained by performing a number of single chew experiments. Differing numbers of the same size particle are served, subjects are asked to expectorate the bolus after a single chew. The selected particles are then differentiated from the non-selected particles by visual inspection. A detailed review of the single chew experiment has been described previously in Chapter 2 (section 2.5.3). While this method has been proven successful for an artificial test food such as Optosil®, it can be difficult to perform such experiments with real foods in a repeatable and consistent manner. Therefore, there is a need to develop a new approach to experimentally measure the number of breakage sites of a subject. Because the number of breakage sites is defined as the number of particles to saturate on the occlusal area, the number of breakage sites might be able to be determined by dividing the projected occlusal area and a projected area of a single food particle. The following section describes the procedure to obtain the number of breakage sites from the occlusal area.

3.2.1.3.1 Measurement of occlusal area using chewing gum

To test the hypothesis that the number of breakage sites can be determined from the projected occlusal and particle area, four subjects were asked to participate in a session where they were asked to chew a piece of chewing gum on the preferred side of their mouth to obtain the projected occlusal area by biting down on the gum in one action before expectorating it. The chewed gum was then placed on a petri dish (diameter: 140 mm) and the image of the chewed gum and the petri dish was scanned using a scanner (Epson Perfection, 3490) at 800 dpi. Following scanning, the portion of the chewing gum showing the bite marks was cropped (Fig. 3-5) and the projected area was measured through image analysis using ImageJ (version 1.52a, National Institutes of Health, USA) to give an approximation of the occlusal area.

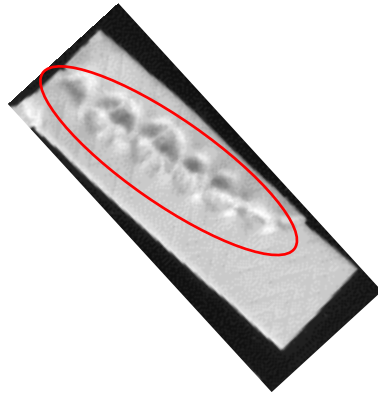


Fig. 3-5: Scanned image of chewing with bite marks (circled in red). The projected area of the occlusal area was then measured using ImageJ.

A single chew calibration experiment was also performed by a single subject to determine the suitability of the new fast method. Two different sizes of white rice ($21.4 \pm 1.2 \text{ mm}^2$ and $10.6 \pm 0.5 \text{ mm}^2$ projected area) and *Orzo* pasta ($54 \pm 4 \text{ mm}^2$ and $29 \pm 2 \text{ mm}^2$) were used. For each particle size, four different number of particles were used: 5, 20, 64, and 128. After the particles were chewed, they were transferred into a glass petri-dish where damaged and undamaged particles were separated by visual inspection. The number of selected particles vs the number of offered particles was then plotted and the number of breakage sites was assumed to be the number of selected particles when the curve started to level-off (van der Glas et al. 2018).

3.2.1.3.2 Occlusal area results

The total occlusal area (from one side of the mouth (the person's preferred side)) measured from the image analysis for all four subjects ranged from 133.71 mm^2 to 241.01 mm^2 respectively (Fig. 3-6). The results obtained were within the range reported in literature (Sumonsiri et al. 2019). The median of the occlusal area, when measured using ImageJ for 40 subjects (15 men and 25 women), was 166.3 mm^2 (Sumonsiri et al., 2019).

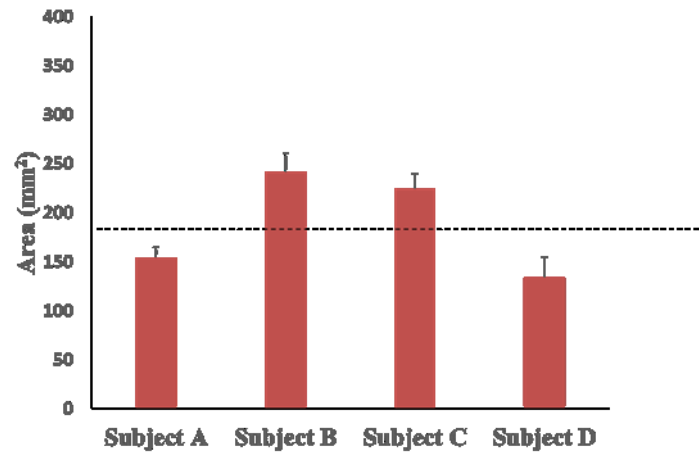


Fig. 3-6: Projected occlusal area (mm²) measured from the scanned image of the bite marks on a chewing gum for four subjects. Dashed line is the median value observed in Sumonsiri et al. (2019).

The results of the single chew calibration experiments for the single subject is shown in Fig. 3-7. Fig. 3-7 shows the plot of the number of selected particles vs number of offered particles for two types of food (rice and pasta) and sizes (whole and halves).

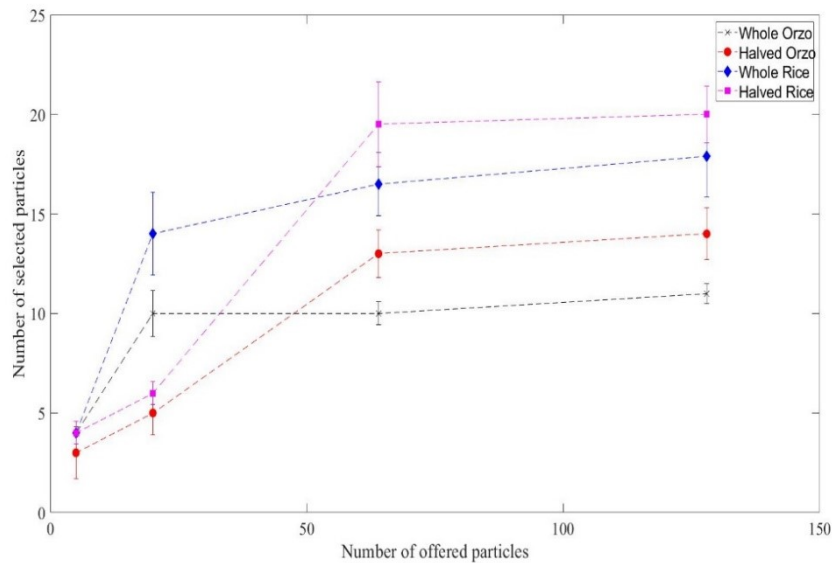


Fig. 3-7: Number of selected particles against the number of offered particles for Whole Orzo (Black X marker), Halved Orzo (red round marker), Whole Rice (blue triangle marker) and Halved Rice (green square marker). The error bar represents the standard deviation of a triplicate measurement.

For all of the food particles tested, it can be observed that the number of selected particles increases as the number of offered particles increases until a plateau is reached where the number of offered particles is sufficient to saturate the occlusal area. The number of breakage sites is the number

of selected particles when it first enters a plateau. The halved rice which was the smallest ($10.6 \pm 0.5 \text{ mm}^2$) had the most breakage sites of 20 whereas whole *Orzo* pasta which was the largest ($54 \pm 4 \text{ mm}^2$) had the smallest with 10 breakage sites. The number of breakage sites for whole rice and halved *Orzo* pasta was in between with the number of breakage sites of 14 and 13 respectively.

The results obtained here were consistent with the findings from van der Glas et al. (1992, 2018) who found that the number of breakage sites increases as the particle size decreases. Using a cubic-form of Optosil® particles, the number of breakage site obtained for an edge size of 6.8 mm was 5.3 compared to 77.6 for an edge size of 1.7 mm (data from Subject no. 01, (van der Glas et al., 2018). Particles with a larger projected area (X^2) such as for the whole *Orzo* pasta would not fit on the occlusal surface of the teeth, contributing to a smaller number of sites available for breakage. Furthermore, smaller particles also can pile at the initiation of breakage, which may explain the higher number of breakage sites (van der Glas et al., 2018).

To assess the viability of using the measured occlusal area to predict the breakage sites the number of selected particles was multiplied by the mean projected area of the particle tested and plotted against the number of offered particles (Fig. 3-8). The projected occlusal area (mm^2) determined from the image of the bite marks in the chewing gum was also indicated in the plot for comparison. Results showed that the total projected area of the selected particles when the breakage sites were exceeded was significantly higher than the measured occlusal area 225 mm for the whole and halved *Orzo* ($540 \pm 62.1 \text{ mm}^2$, $377 \pm 34.8 \text{ mm}^2$) and the whole rice ($353.1 \text{ mm}^2 \pm 34.03$) respectfully. However, the halved rice was close to the projected occlusal area of 225 mm^2 . These results indicate that the fast optical method using the chewing gum is perhaps not suited for larger particles that could not fit on the occlusal area for breakage.

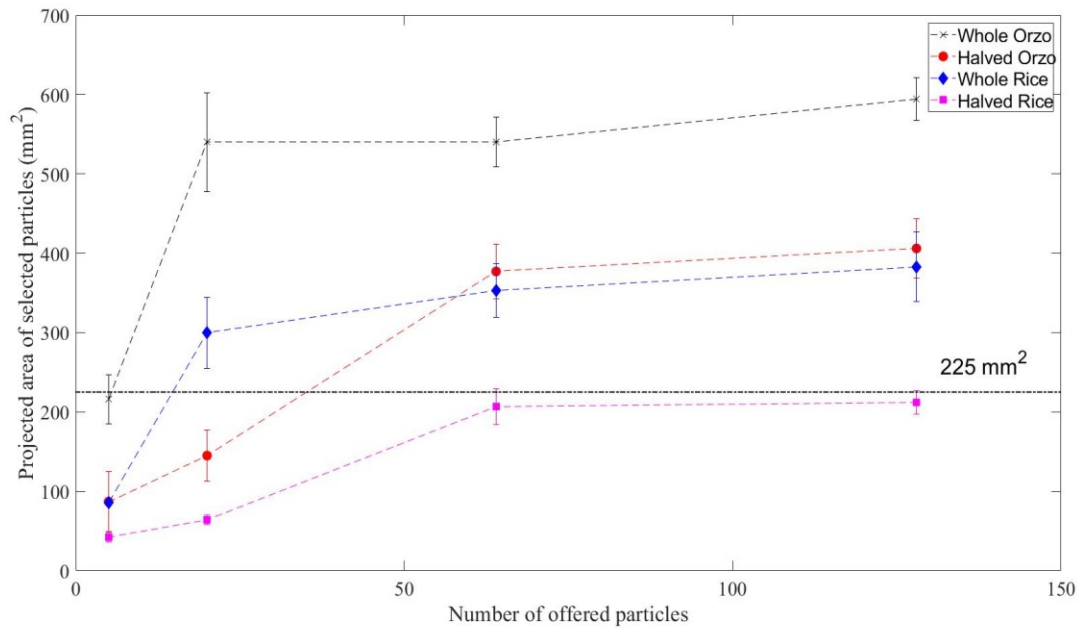


Fig. 3-8: Projected area of selected particles against the number of offered particles for Whole Orzo (Black X marker), Halved Orzo (red round marker), Whole Rice (blue triangle marker) and Halved Rice (green square marker). Dotted black line shows the projected occlusal area for the particular subject. The error bar represents the standard deviation of a triplicate measurement.

The total projected area of the whole *Orzo* pasta when it started to level off was four times greater than the total occlusal area. This is interesting and indicates that either piling or pinning is occurring, where piling is explained above and pinning is the tendency to catch part of a particle while a significant overlap remains outside the occlusal plane. Both would tend to suggest the two-way competition model is the most appropriate here. It also suggests that single chew calibration experiments may need to be performed for particles with a large projected area such as the whole pasta. Such calibration experiments on larger particles are rapid, e.g., Fig. 3-7 shows that pasta gives 10 breakage sites from 20 offered particles. The saturation number for small particles is more difficult to determine because the numbers are larger. In the limit, the maximum possible number of particles that can saturate the occlusal plane is obtained by dividing the total occlusal area by the mean projected area of the particle.

3.2.2 Breakage model equations

The breakage models used in previous mastication studies were the breakage models used by Lucas & Luke (1983b) (Eq. 2.8 and Eq. 2.9) for carrots, van der Glas et al. (1987) (Eq. 2.10) for Optosil, Gray-Stuart (2016), (Eq. 2.11) for rice and peanuts (Eq. 2.12). The breakage functions are reinstated here for clarity.

Lucas & Luke (1983b) an empirical breakage function to carrot:

For an initial particle size of X_o , the percentage of particles undersize by volume can be plotted for different sieve size X_i and can be given by a power law model

$$B(X_i, X_o) = b\left(\frac{X_i}{X_o}\right)^r \quad (2.8)$$

where $B(X_i, X_o)$ is the weight or volume fraction of particles of size X_o which break into particles smaller than size class X_i , and r and b are the fitted variables. A larger value of r and a smaller value of b in Eq.2.8 would show less fragmentation.

Lucas & Luke (1983b) a mechanistic breakage function to carrot:

$$B(X_i, X_o) = 1 - s\left(1 - \frac{X_i}{X_o}\right)^r \quad (2.9)$$

where s and r are constants. Both s and r indicate the degree of fragmentation of the selected particle where larger values indicate higher degree of fragmentation.

Van der Glas et al. (1987) applied the modified Austin (1972) breakage function to Optosil®:

$$B(X_i, X_o) = 1 - \left(1 + r\frac{X_i}{X_o}\right) \cdot \left(1 - \frac{X_i}{X_o}\right)^r \quad (2.10)$$

where r is the degree of fragmentation and a larger value indicate higher degree of fragmentation.

Gray-Stuart (2016) applied the modified Austin with pasting to brown rice:

$$B(X_i, X_o) = (1 - P) * \left(1 - \left(1 + r \frac{X_i}{X_o}\right) \cdot \left(1 - \frac{X_i}{X_o}\right)^r\right) \quad (2.11)$$

where r is the degree of fragmentation and a larger value indicate higher degree of fragmentation. P is the pasted fraction which refers to the volume fraction of daughter particles which are pasted after breakage.

Gray-Stuart (2016) applied the modified Austin to peanuts, which form a bimodal distribution after breakage:

$$B(X_i, X_o) = Y * \left(1 - \left(1 + r_1 \frac{X_i}{X_o}\right) \cdot \left(1 - \frac{X_i}{X_o}\right)^{r_1}\right) * (1 - Y) * \left(1 - \left(1 + r_2 \frac{X_i}{X_o}\right) \cdot \left(1 - \frac{X_i}{X_o}\right)^{r_2}\right) \quad (2.12)$$

where Y is the portion of particle X_o being distributed with fragmentation variable r_1 and

$1 - Y$ of X_o are distributed with r_2 . Similarly as above, r is the degree of fragmentation and a larger value indicate higher degree of fragmentation.

Other than the breakage functions described above for mastication, there is also potential to explore other breakage models particularly the ones used in the milling industry. A summary of some common breakage functions can be found in Rozenblat et al. (2012) and a modified version of the breakage functions are described in Table 3-1 below.

Table 3-1 Summary of breakage models commonly used in milling industry

Breakage model	Application	References
$B = 1 - \left[1 - \left(\frac{x}{x_0} \right)^a \right]^b$	Milling	Harris (1968)
$B = 1 - \exp \left[- \left(\frac{x}{a} \right)^b \right]$	Impact milling	Cheong et al. (2004)
$B = \left(\frac{x}{a} \right)^b$	Jaw milling	Schumann (1940)
$B = 1 - \left(1 - t_{10j} \right)^{\left(\frac{9}{D_i} \right)^{\alpha}}$	Ball milling	Tavares (2004)
$B = \phi \left(\frac{x}{y} \right)^r + (1 - \phi) \left(\frac{x}{y} \right)^{\beta}$	Ball milling	Austin (1972)
$B = \left(\frac{x}{y} \right)^q \frac{1}{2} (1 + \tanh(\frac{x-x'}{x'}))$	Impact milling	Vogel and Peukert (2002)

These breakage models however are applied to scenarios, which could be significantly different than the breakage mechanism during a chewing process. For example, in ball milling, breakage is achieved through impact and attrition of a rotated hollow cylindrical shell that is partially filled with steel balls (Kumar et al., 2018). Impact milling such as the model by Vogel and Peukert (2002) was fitted to the PSD of particles which were comminuted from a single particle impact device. In the device, single particles are first transported from a vibrational feeder into a disk-shaped rotor. Particles are then accelerated in one of four radial channels by the centrifugal force in the rotor. The particles then leave the rotor and hit the target ring at an angle of 90°. In their study, minor damages to the particles in the form of broken edges or abrasion were also found.

The breakage mechanisms such as abrasion and attrition as described above cannot be compared to chewing due to the vertical and lateral chewing trajectories, which ensures particles are either fractured or cut. The teeth used their cusps to fracture food particles if a vertical chewing motion is used and the teeth use sharp edges to function as blades to cut up food particles (Xu et al., 2008).

In addition, as these models have not been applied to mastication studies, they need to be validated against *in vivo* experimental data. To do so, subjects will be required to perform chewing experiments where they will be asked to chew a food (or several) food particles once, and the broken

particles size distribution will be measured. The single chew experiment, however, is tedious and a time-consuming process, as they have to be repeated at least 100 times to obtain a reliable fit with the breakage model as shown in the study of van der Bilt et al. (1987) for an 8 mm cube Optosil®. In addition, these breakage models often consist of more than two input parameters, which increases the degree of freedom for fitting the models to data compared to the modified Austin (1972) model that only requires one parameter (r). It is notable that overfitting may lead to irrelevant models (Frank, 2005). Thus, for the reasons stated above, this work will focus on using the breakage equations pertinent to the mastication literature.

3.2.2.1 Conservation of volume during breakage

Generating a discrete distribution of daughter particles to fit a continuous breakage function while conserving the volume of the occluded particle is a modelling challenge. Experimentally, this is obtained by a sieving procedure (Lucas & Luke, 1983a, 1983b; van der Glas et al. 1987; Peyron et al., 2004), but for modelling, most literature methods apportion daughters to mean bin sizes (Lucas & Luke 1983b, Gray-Stuart, 2016). After breakage, volume fractions of the parent particle are apportioned to a $2^{3/2}$ volume series ($\sqrt{2}$ particle diameter series) where the size and the number of particles within each size class are calculated. Conservation of volume is achieved if the size of particle is somewhere within the size class range. But, if the volume apportioned to a size class (after breakage) is less than the volume of a minimum sized particle within that size class, then modifications need to be made to ensure the distribution generated matches the distribution given by the breakage function.

Two approaches were developed to address this modelling challenge. The first approach is summarised in Fig. 3-9. To generate daughter particles, a breakage model (Eq. 2.8 – 2.12) is applied to the selected parent particle, V_i which apportions the total volume of daughter particles in each size class ($V_{births,j,i}$). If the apportioned volumes are less than the minimum sized volume a particle within the size class, then they will be added to the adjacent sieve below. This conditional statement ensures the apportion volumes are always greater than the minimum sized volume of a particle within the size class. The particles generated from the allocated volume fraction in X have sizes between two adjacent sieve aperture sizes. To generate the daughter particles, a function called *randfixedsum* in MATLAB (2019a

version, The MathWorks; www.mathworks.com) was used (the MATLAB code can be referred in Appendix A). The function can create, n particles (in random sizes) between two size limits that sum up to a fixed volume.

The following describes the procedure to use the *randfixedsum* function to generate particles of a specific size class. Firstly, the number of particles must be specified. To do so, the total volume of particles in a size class has to be divided by the minimum volume of a single particle on the size class. A size class, X_j , is the mean size of two size limits (Eq.3.3), thus, the minimum volume of a particle on a size class is assumed to be the geometric mean of the minimum volumes from the two size limits.

$$\text{Average size on sieve } \bar{X}_j = (\text{Aperture of sieve } X_j * \text{Aperture of sieve } X_{j+1})^{\frac{1}{2}} \quad (3.3)$$

The number of particles occupying the j^{th} sieve, N_j , was then calculated from the actual volume generated from the breakage function.

$$N_i = \frac{\text{Apportioned volume on sieve, } V_j}{\text{Volume of single geometric mean particle, } V_{\bar{X}_i}} \quad (3.4)$$

Each particle volume generated will always be greater than the minimum volume of its size class and less than the minimum volume of particle from size class above. The total volume of the daughter particles when summed, will always be the same to the total volume of apportioned particles within the size class ($V_{births,j,i}$), ensuring the conservation of volume.

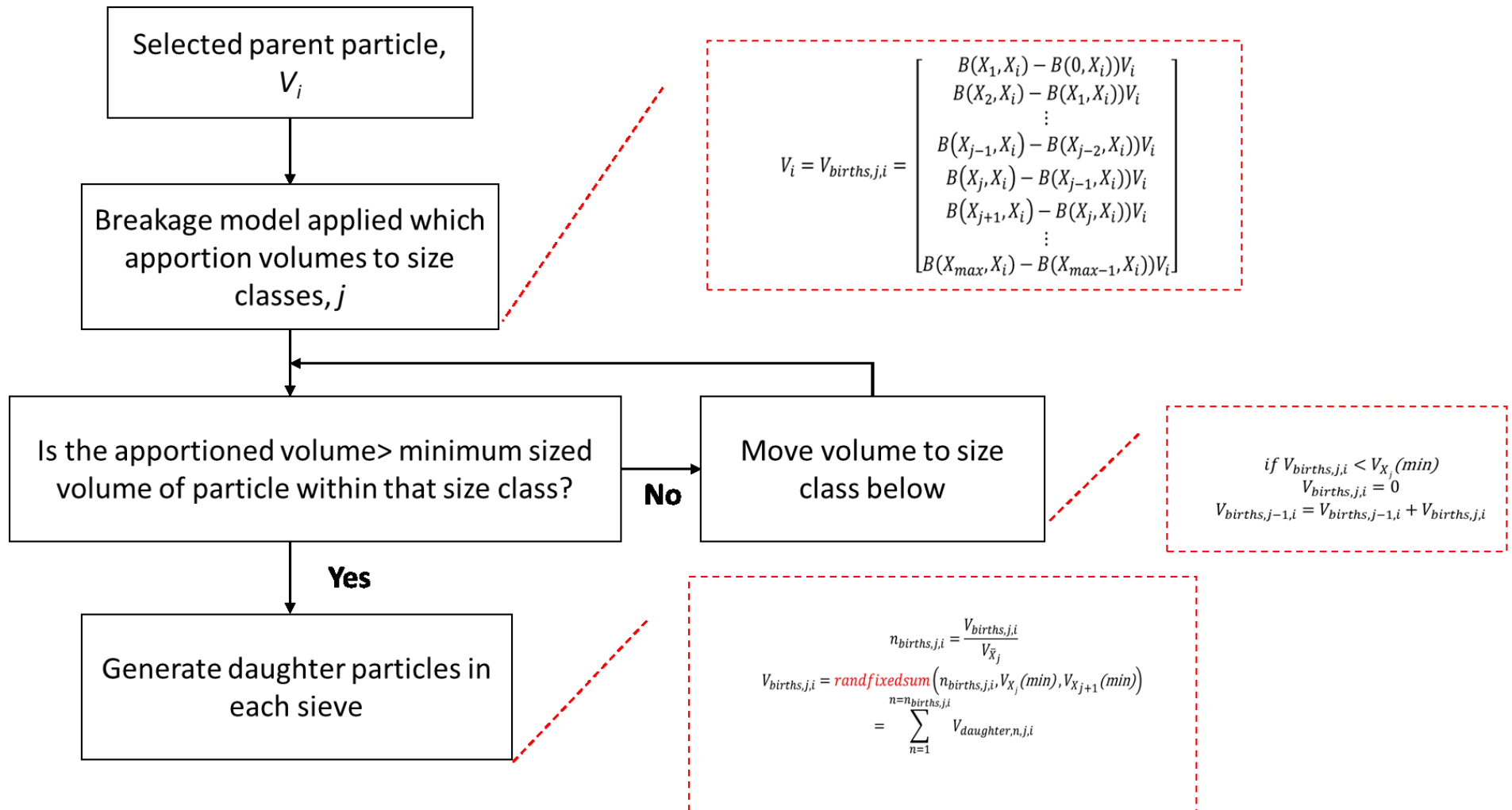


Fig. 3-9 Schematic diagram showing one of the two approaches used to address the conservation of occluded particles volume during breakage, which is a modelling challenge.

3.2.2.2 Numerical approach to generate daughter particles from breakage function

The second approach is a numerical approach to generate daughter particles without the use of bins by maintaining a fully discretised population until they reach a lower limit size where particles are assigned to the liquid suspension phase (pasted fraction) and no longer participate in selection or breakage (the MATLAB code can be referred in Appendix A). This section will describe the new numerical approach which is summarised in Fig. 3-11.

Assume a particle of size X_o follows a cleave and paste breakage mechanism according to Gray-Stuart (2016). This involves a large particle that is caught between antagonistic teeth, which, upon occlusion, is cleaved in two. Then, one part breaks free into the oral cavity and the other part is pasted, meaning it immediately reduces to a size below the small-size limit. Assuming an ellipsoid shape, the volume of the particle, V_o is calculated. Firstly, a random number of daughter particles will be generated from a large number of simulations (e.g. $n=1000$) until the sum of all the daughter particles is equivalent to V_o . In each simulation loop, if X_o is less than a pasted threshold size (e.g. 0.355 mm), the daughter particles will be part of the pasted fraction and will not undergo further breakage. To calculate the daughter particle size, X_i , a breakage function value (values from 0 to 1) is randomly generated. This random breakage function value is then interpolated linearly against the breakage function from Eq. (2.8-2.12). This gives the X/X_o value. The initial size of the particle X_o is then multiplied with this ratio to obtain the size of the potential daughter particle.

1. The potential daughter particle generated will need to pass several conditions before it is regarded as part a daughter particle for particle X_o . The conditions are described as below: **Is the size of the daughter particle less than the pasted size threshold (e.g. 0.355 mm)?**
 - a. The first condition is whether this daughter particle is less than the pasted size threshold or not. If it is less than the size threshold then this particle will be recorded as part of the pasted volume for the particle V_o . If the daughter particle size is larger than the size threshold than the particle will go through to the next condition.

2. **Is the potential daughter particle volume larger than the unallocated original particle volume?** Mathematically this is $V_p > V_o - \sum_i^n V_p - \sum_i^n V_{paste}$? where V_p is the potential daughter particle volume, V_o is the initial particle volume, V_{paste} is the pasted particle volume, i refers to the initial number of loop and n is the final number of loop.
- a. This condition is important to ensure volume is conserved. If the volume of the potential daughter particle is greater than the sum of the daughter and pasted particles from the previous loops then the particular loop will be skipped and the simulation is repeated. If the opposite occurred, the volume of the daughter particle in this loop is recorded. The simulation runs until the sum of all daughter and pasted particles are equivalent to V_o or after $n=1000$ simulations has been reached. If the maximum iterations is reached and the sum of all daughter particles is not equivalent to V_o then the remaining unallocated volume will be assigned to one additional daughter particle.

The advantage of using the new method is that it does not require bin for the apportioned particles therefore; it does not require the number of particles to be fixed to generate particles like the *randfixedsum* function as described in 3.2.2.1. A comparison of the daughter particles generated that followed the breakage function of Eq.2.10 for a single particle, X_o of 4 mm using the two different methods (bins and without bins) is displayed in Fig. 3-10. For the simulation using bins, the following sieves was used: 4.0 mm, 2.8 mm, 2.0 mm, 1.4 mm, 1.0 mm, 0.71 mm, 0.5 mm, 0.355 mm. An r value of 0.8 was used in both methods. As observed in Fig. 3-10, the daughter particles that were generated using the *randfixedsum* function have more particles on the lower size classes, whereas the new numerical approach had a single daughter particle with $X/X_o = 0.97$ and a few between 0.1 and 0.35, hence fewer particles were produced in the lower size classes. The method which implemented the breakage function using bins (*randfixedsum*) assumes that the same daughter distribution is produced in every chew, therefore is not computationally expensive. While the *randfixedsum* approach ensures conservation of volume, the downside of using this approach is that it does not match the theoretical breakage function where more small particles are generated because of shifting the volume of particles in the smaller sieve size. In contrast, the new numerical approach is stochastic, thus, a large number of

simulations is required to show that the distribution matched the breakage function. This is the trade-off of using the new numerical approach, as it is more computationally expensive therefore will result to a longer simulation time. However, the numerical approach will more closely follow the chewing process, as food particle breakdown is highly variable as shown by the data collected here and in the literature. As such, the new numerical approach will be used to apply the breakage function for the subsequent case studies explored in this thesis.

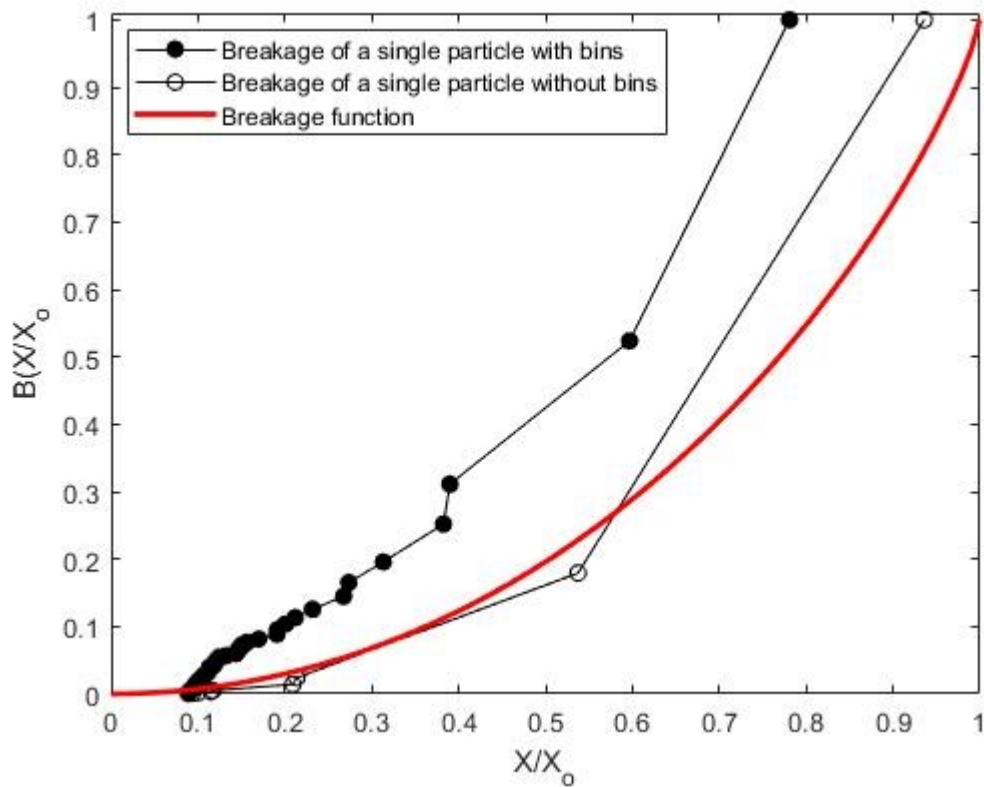


Fig. 3-10: Comparison between generating daughter particles using bins and without bins for a single particle. Black round with black face colour, breakage of a particle with bins. Black round with white face colour, breakage of a single particle without bins. Red line, breakage function, Eq. 2.10. The simulation was run once.

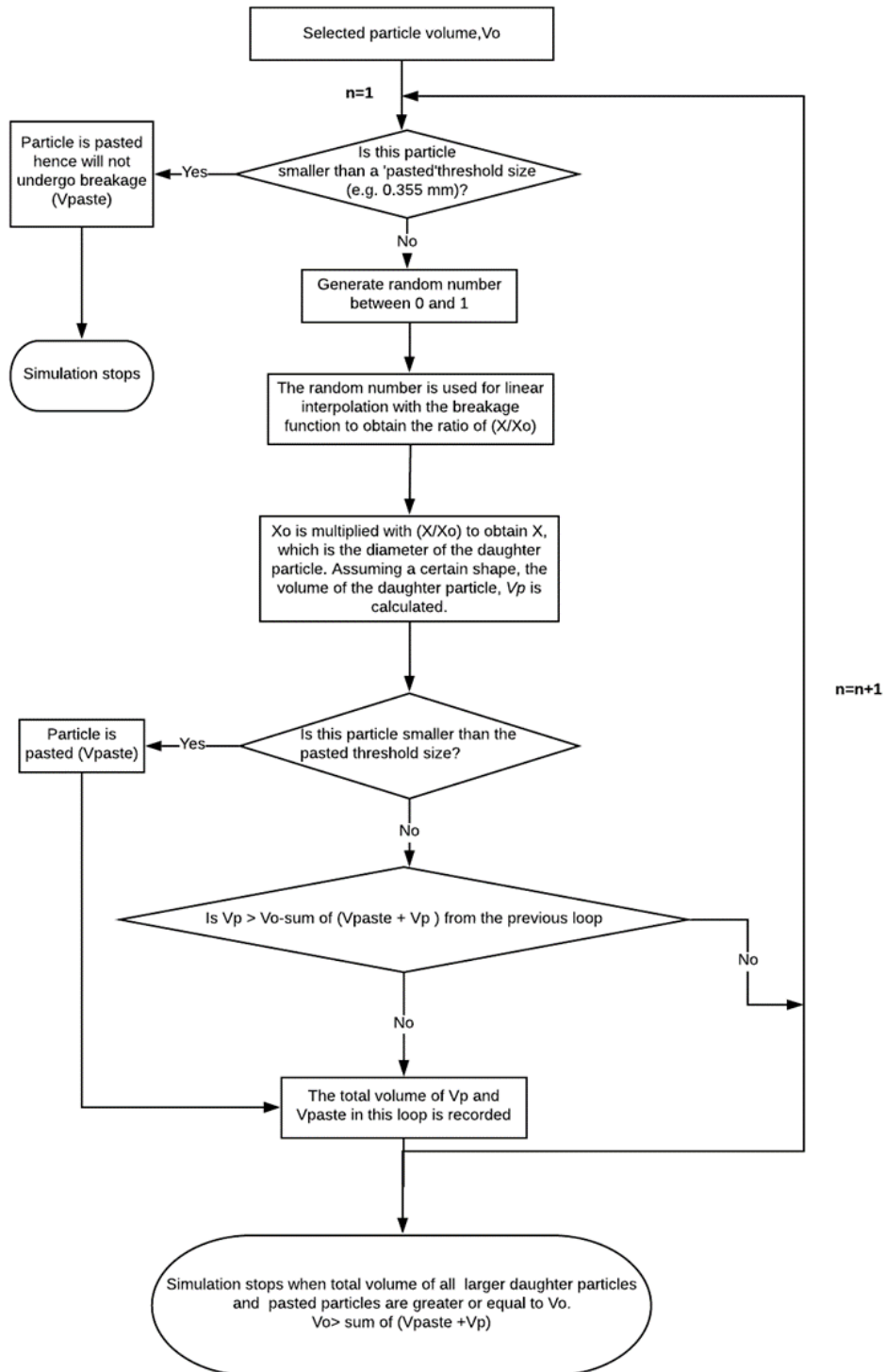


Fig. 3-11 Schematic model diagram showing the processes required to generate daughter particles after breakage using the second numerical approach.

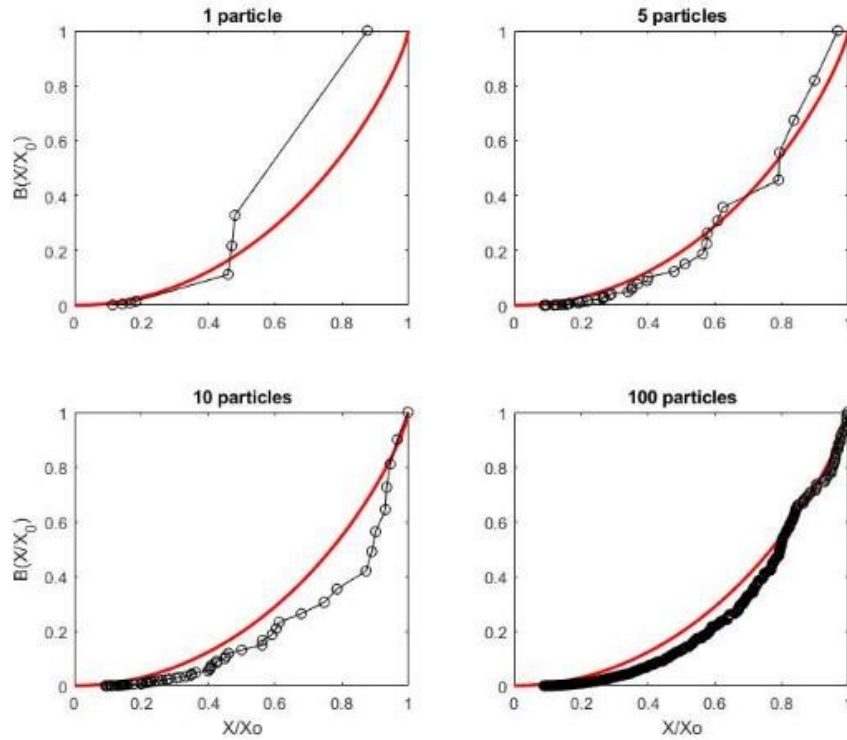


Fig. 3-12: Daughter particles distribution as a function of the number of selected particles. Black round marker, volume distribution of daughter particles. Red line, breakage function using Eq. 2.10.

3.2.3 Model implementation using the population balance model

A discretised population balance model developed by Gray-Stuart (2016) can be applied to predict the PSD of a food particle during mastication. This approach allowed individual particles to be tracked. If a parent particle was selected, that particle would ‘die’ and be reborn into a discrete number of ‘daughter’ particles. A schematic flow diagram showing the general processes involved during the comminution of a food particle based on the population balance model is shown in Fig. 3-13 (the MATLAB code can be referred in Appendix A). The population model has been described previously in section 2.4.8 but will be restated here for clarity. The implementation part of the selection model has also been described in sections 3.2.1.1 and 3.2.2.2.

Based on Fig. 3-13, a population of an initial distribution of particles can be described mathematically by an array, V_p , where the elements are individual particles with some volume, V_i

where V_p

$$= \begin{bmatrix} V_1 \\ V_2 \\ \vdots \\ V_{i-1} \\ V_i \\ V_{i+1} \\ \vdots \\ V_{max} \end{bmatrix}$$

The particles in V_p are sorted into size classes, i where i ranges from the minimum threshold size to the maximum size class used to describe the PSD. The PSD is given by the array \underline{N}_k , whose elements are the number of particles in each size class, and k , denotes the chew number.

$$\underline{N}_k = \begin{bmatrix} n_{1,k} \\ n_{2,k} \\ \vdots \\ n_{i-1,k} \\ n_{i,k} \\ n_{i+1,k} \\ \vdots \\ n_{max,k} \end{bmatrix}$$

During occlusion, all particles in the same size class are assumed to have the same chance of being selected. This selection chance is calculated from either the size dependent power law (Eq. 2.2), the one-way (Eq. 2.4) or two-way competition selection model (Eq. 2.5). From the array of particles V_p , another array is generated with the corresponding chance of selection for each particle V_i . A particle is selected when a random number (generated from a random distribution) is less than the theoretical selection chance.

These selected particles ‘die’ and undergo breakage producing daughter particles. Breakage is then approximated by a continuous breakage function $B(X, X_i)$ of ‘cumulative fraction less than’ where the particle undergoing breakage has characteristic dimension X_i and the function gives the cumulative fraction less than size X . Common breakage functions used in mastication are Eq. 2.8- Eq. 2.12. To discretize this, the volume fraction falling within the bin of a single size class is calculated by finding the difference of $B(X_j, X_i) - B(X_{j-1}, X_i)$ where the subscript j refers to the size classes from $j=1$ to $j=i$, after occlusion of a particle of size X_i . For a particle in size class X_i , the volume of births in size class X_j is given by

$$Volume_{births,j,i} = V_i(B(X_j, X_i) - B(X_{j-1}, X_i)) \quad 2.18$$

For each j from $j=1$ to $j=max$, the array of birth volume for all size classes for particle X_i is given by,

$$Total\ Volume_{births} = V_{births} = \begin{bmatrix} \sum_{i=1}^{i=max} B(X_1, X_i) - B(0, X_i))V_i \\ \sum_{i=1}^{i=max} B(X_2, X_i) - B(X_1, X_i))V_i \\ \vdots \\ \sum_{i=1}^{i=max} B(X_{j-1}, X_i) - B(X_{j-2}, X_i))V_i \\ \sum_{i=1}^{i=max} B(X_j, X_i) - B(X_{j-1}, X_i))V_i \\ \sum_{i=1}^{i=max} B(X_{j+1}, X_i) - B(X_j, X_i))V_i \\ \vdots \\ \sum_{i=1}^{i=max} B(X_{max}, X_i) - B(X_{max-1}, X_i))V_i \end{bmatrix} \quad 2.19$$

This matrix allows the number of birth particles in each size class to be calculated. The breakage process described by Eq. 2.19 above is applied to all the selected particles. To ensure the conservation of volume, the approach described in 3.2.2.1 or 3.2.2.2 is applied. If particles less than the threshold size are created from occlusion, their volume is summed and added to saliva, which becomes the liquid phase of the bolus. The newly created particles are combined with the unselected particles and a new array, V_p , is obtained.

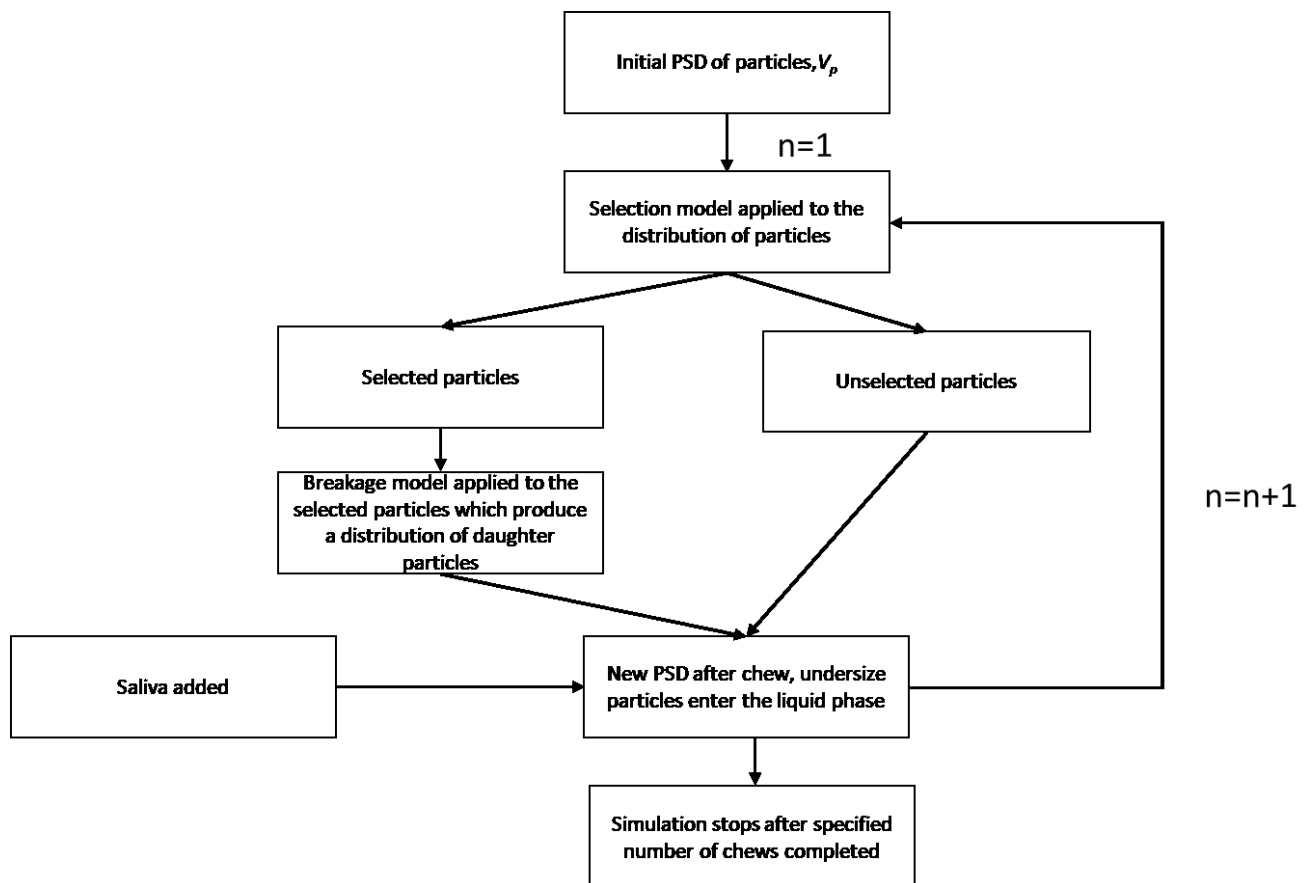


Fig. 3-13 Schematic flow diagram showing the general process involved to apply the discretised population model

3.3 Chapter conclusion

This chapter describes the development of the chewing model which forms the basis of the subsequent case studies in the remaining chapters. The first part of the chapter describes the conceptual model, followed by a discussion of model assumptions. The selection and breakage models form the basis of the chewing model. The difference in mechanism for the one-way and two-way competition models was demonstrated in real foods, using peanut bolus PSDs expected at different stages of chewing as an example. Both models have not been extensively applied in the literature, despite being the most comprehensive models developed to date. An alternative, but faster optical approach was also developed to determine selection model input parameters which is a notoriously time-consuming process. However, the method did not accurately determine the input parameters for the model, as it was shown that the occlusal area did not translate to larger size particles such as the whole *Orzo* and whole rice where portions of the particles can be caught on the edges of the teeth (and damaged), rather

than the whole area. Further experiments for a larger number of subjects will be needed in the future to support the findings.

Other breakage models also exist in the milling literature however the breakage mechanisms may not be adapted to chewing. In addition, the experimental process to fit the breakage model can be laborious and time-consuming. The breakage models from the mastication literature consists of one to two parameters which reduces the degrees of freedom required for model fitting. Because of the requirement for conservation of volume in the distribution of daughter particles during breakage, for modelling, most literature methods apportion daughters to mean bin sizes. This could result in less accurate model predictions when compared against experimental data as the size of the daughter particles generated is limited to the average between two bin sizes. A numerical approach was developed to generate daughter particles without the use of bins by maintaining a full-discretised population of particles with liquid suspension phase where particles below a threshold size are assigned and not individually tracked. The new approach also provides insights that a large number of single chew experiments are required to ensure a good fit to the breakage function.

The selection and breakage functions are then applied using a discretised population balance to predict the bolus PSD. In the next few chapters, the models developed in this chapter will be applied in a series of case studies to demonstrate the model and then integrated with models for aroma release.

Chapter 4 Predicting the PSD of peanuts using different selection and breakage models

4.1 Introduction

Chapter 3 presented the model development for chewing based on selection and breakage functions adapted from the literature. Before implementing the models to a novel food system to link mastication to digestion and flavour release, it was first important to test the models against a food system, which has been extensively applied in the mastication literature. Thus, this chapter aimed to test the models developed in Chapter 3 to predict the PSD of peanuts during chewing and compare their predictive outcomes. In addition to the power-law model which is commonly used to describe selection in previous mastication related studies (Lucas & Luke, 1983a, 1983b; van der Bilt et al., 1987; Prinz & Lucas, 1997), the one-way and two-way competition models (van der Glas et al., 1992, 2018) were investigated. The competitive selection models in particular, have not been extensively applied to real foods. Similarly, different breakage functions are explored by applying the models to published literature data in two case studies. Both case studies are applied to a data set collected by Flynn (2012) for human subjects chewing peanuts.

4.2. The model

The model consists of selection and breakage models. Each will be discussed in the sections below.

4.2.1 Selection model equations

The selection model used in this chapter was either the power-law model (Eq. 2.2), the one-way competition model (Eq. 2.4), or the two-way competition model (Eq. 2.5). The selection model equations and examples of the model implementations have been described previously in section 3.2.1.

4.2.2. Breakage model equations

For the case studies in this chapter, the breakage models of Eq. 2.8-2.10 will be used (section 3.2.2 in chapter 3).

4.2.3 Discretised population model

The PSD will be predicted using the discretised population balance model as described in section 3.2.3.

4.3 Model application

4.3.1 Food system and data source

Flynn (2012) collected PSD data for subjects chewing peanuts. The data was presented as mass fraction of expectorated bolus particles collected on a series of sieve size classes, which provided the PSD for 4 g portions of peanuts chewed for various numbers of chews (1, 2, 4, 6, 8, 10, 15, 20, 25, 30 (swallow point) and 35 chews). A single subject (male, age =27 years old) was used with three replicates for each stage of chewing. The raw data which included the standard error of the three replicates can be found in Appendix D.

This food system and data source make a good first application for the particle breakage model. Although peanuts have been widely used in mastication studies, there are few examples where particles size changes are monitored and reported at regular stages during chewing. In her study, Flynn (2012) found that the total recovered solids was between 50-90% throughout the chewing sessions. In addition, when compared with other food types investigated in the study, such as muesli bars, the amount of recovered solids for peanuts was significantly higher, particularly in the first five chews (60-90% for peanuts vs 40-50% for muesli bars). Therefore, the assumption of negligible particle losses in the model is reasonable in this case. In addition, because of the high fat content of peanuts, it is not expected that breakage behaviour will change due to moisture absorption over the period of chewing. In order to apply the model to predict particle size changes in this system, there was no need to model saliva inclusion and bolus saturation.

Because the model used a discretised population balance approach, it was necessary to convert the mass fraction data into a population of particles to allow the model to be fitted to the experimental data. The sieve sizes used in (Flynn, 2012) were 4.0 mm, 2.8 mm, 2.0 mm, 1.4 mm, 1.0 mm, 0.71 mm, 0.5 mm, 0.355 mm, 0.25 mm, 0.18 mm, 0.125 mm, and the pan. The sieves were a good starting point for discretisation; however, as some of the peanut bolus was retained on the 4.0 mm sieve, an additional size class above 4.0 mm was added (5.7 mm). In the model, particles below 0.354 mm were not tracked, and their masses were summed and regarded as suspended solids in the liquid phase (Gray-Stuart, 2016). Gray-Stuart found that particles smaller than this critical size were not broken down any further in

subsequent chewing. This assumption is also practical as it avoids the model simulation being computationally expensive with the generation of thousands of particles in the lower size range.

The particles generated from the allocated mass fraction in X have sizes between two adjacent sieve aperture sizes. These peanut particles were generated using a similar methodology used to generate particles in section 3.2.2.1. A function called *randfixedsum* in MATLAB (2019a version, The MathWorks; www.mathworks.com) was used (the MATLAB code can be referred in Appendix A). Some of the equations required to use to the function are restated here for clarity. The *randfixedsum* function requires the number of particles to be specified to generate particles of a specific size class. In order to do so, the total mass of particles in a size class (which was obtained from the mass fraction data) has to be divided by the minimum mass of a single particle on the size class. A size class, X_i , is the mean size of two size limits (Eq.3.1), thus, the minimum mass of a particle on a size class is assumed to be the geometric mean of the minimum masses from the two size limits.

$$\text{Average size on sieve } \bar{X}_i = (\text{Aperture of sieve } X_i * \text{Aperture of sieve } X_{i+1})^{\frac{1}{2}} \quad (3.1)$$

The minimum mass of a peanut particle on a size class can be calculated by multiplying the minimum volume of a peanut particle from an assumed halved ellipsoid shape (Eq. 4.1) by the density of a peanut particle of 0.00112 g/mm³ (Hutchings, 2011). The minimum volume of a halved peanut particle on X_i can be described as

$$V_{X_i} = \frac{1}{2} \left(\frac{4}{3} \cdot \pi \cdot a \cdot b \cdot c \right) \quad (4.1)$$

a is the major axis, b is the minor axis and c is the vertical axis radius. If the minor and vertical axes b and c are assumed to be related to a by a shape factor, s_f , thus

$$V_{X_i} = \frac{1}{s_f} \left(\frac{2}{3} \cdot \pi \cdot a^3 \right) \quad (4.2)$$

where a is assumed to be the mean diameter or the size class, \bar{X}_i . It was found from the experimental data that even in the 25th chew, some volume of particles was on the 4 mm sieve. This mass was between the expected mass for one and two particles. This enabled the shape factor s_f to be calculated using Eq.4.2. The s_f value was 2.03. Thus,

$$V_{\bar{x}_i} = \frac{1}{2.03} \left(\frac{2}{3} \cdot \pi \cdot \bar{x}_i^3 \right) \quad (4.3)$$

The number of particles occupying the i^{th} sieve, N_i , was then calculated from the actual mass determined from the data.

$$N_i = \frac{\text{Mass on sieve, } M_i}{\text{Mass of single geometric mean particle, } \rho_{\text{peanuts}} V_{\bar{x}_i}} \quad (4.4)$$

Fig. 4-1 shows the generated PSD for the 4 g halved peanuts using the *randfixedsum* function. The function was run once, and the generated distributions are saved to be used in subsequent simulations. Each PSD in the represents different mastication stage of a single subject.

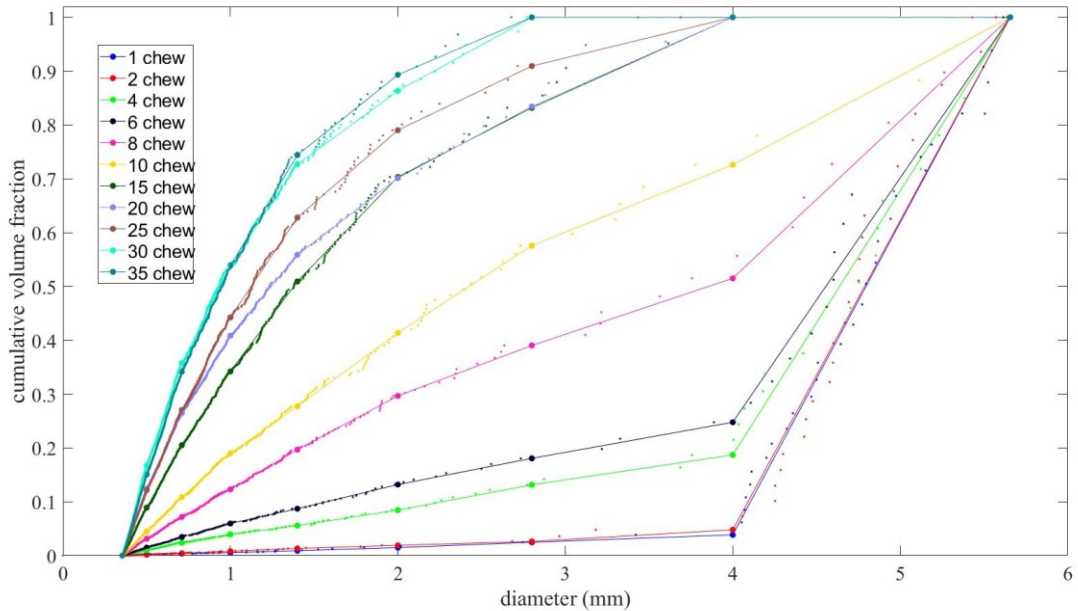


Fig. 4-1 Discrete Particle Size Distribution (PSD) of 4 g of peanuts generated from Flynn (2012). The dotted markers (connected with line) show the sieve data from Flynn (2012). The rest are the generated particles. The *randfixedsum* approach allows a population of particles to be generated from the sieve data.

4.3.2 Model inputs

To apply the model to predict the data set from Flynn (2012), several model inputs were required. Specifically, the initial mass and PSD, the selection and breakage model input parameters (depending on which model was applied).

4.3.2.1 Input 1: PSD after a single chew as model input

Because the data set from Flynn (2012) does not have the initial PSD, the PSD of the peanut bolus after a single chew from the experimental data (which is the closest to the initial) was used as the initial

distribution input to predict the PSD after 35 chewing cycles for the 4 g peanuts. However, it can be observed in Fig. 4-1 that after the 1st chew, there were few particles of sizes 5.6 mm. The mass of a single halved peanut particle of size 5.6 mm calculated using Eq. 4.3 multiplied by the density gives 0.2 g. Therefore, if these particles were assumed to be the original peanuts then this gives around 20 particles to make up the 4 g portion size. In this study, the predicted PSD using the 1st chew PSD as input will be fitted to the data set from Flynn (2012). In order to test the reliability of the fitted parameters using the 1st chew input, the fitted parameters will be used to predict the PSD using the assumed original PSD of peanuts as inputs. The model predictions using this new input will then be compared against experimental data.

4.3.2.2 Input 2: Selection and breakage model input parameters

The input parameters required for the power-law selection model were a multiplication constant and an exponential constant. The input parameters were obtained by best fitting the PSD from the model predictions to the experimental data. For the one-way and two-way competition models, the input parameters required for calculating the number of selected particles were the number of particles, the number of breakage sites and the affinity factor. Both models required particles to be apportioned into size classes. Once particles had been grouped into their respective size classes, the particles were counted. The method has been described previously in Chapter 3 (section 3.2.1.1).

The number of breakage sites and the affinity factor as a function of size class can be described in a power-law equation (see Eq 2.6 & Eq. 2.7 in Chapter 2). The multiplication factor and the exponent value were the two input parameters required in both power-law models that described the number of breakage sites and the affinity factor. As explained in Chapter 2 (Section 2.4.4), the two input parameters are obtained by fitting the theoretical model describing selection of single-sized particles as a function of their number (van der Glas et al., 1992, 2018). The fitting required offering subjects with a different number of particles and sizes (to the point until the occlusal area is saturated with particles) where the subjects are asked to chew once and the number of selected particles is determined through manual inspection. The same process applies for the breakage model where the volume distribution of the daughter particles after a single chew cycle are fitted to obtain the fragmentation variable, r .

However, because as these experiments were not performed by the subject in Flynn (2012), the model inputs were acquired by fitting the coupled selection and breakage model predictions with the experimental PSD data.

4.3.3 Model fitting

To allow the residuals to be calculated, ten percentile diameters were selected (d_{10} to d_{90} - where for d_x , d is diameter and x is the percentile) from the cumulative volume distributions after each chewing cycle prediction was obtained. The model was fitted to the experimental data by minimising a normalised sum of squares residual between the model predictions and the experimental data. By normalising against the experimental percentile diameter, the model fitting was balanced across the whole PSD. This is described as Eq 4.5 below.

$$SS_{res(norm)} = \sum_{i=1}^n \sum_{j=1}^n \left(\frac{ypred_{i,j} - ydata_{i,j}}{ydata_{i,j}} \right)^2 \quad (4.5)$$

where $ypred_{i,j}$ refers to the predicted diameter of an i th percentile intercept ($i = 1$ means 10%, $i = 2$ means 20% of the PSD) and j th chew number and $ydata_{i,j}$ refers to the experimental diameter.

To determine the goodness of the fit of the model, the R-squared value was calculated as follows.

$$R^2 = 1 - \frac{SS_{res}}{SS_{total}} \quad (4.6)$$

and

$$SS_{res} = \sum_{i=1}^n \sum_{j=1}^n (ypred_{i,j} - ydata_{i,j})^2 \quad (4.7)$$

$$SS_{total} = \sum_{i=1}^n \sum_{j=1}^n (ydata_{i,j} - y_{mean}data)^2 \quad (4.8)$$

where SS_{res} refers to the sum of squares residuals between the model and the experimental data. SS_{total} refers to the total sum of squares residuals between the data and the y_{mean} data. y_{mean} data is the mean of all experimental diameter percentiles that were used for the model fitting ($ydata$).

4.3.4 Optimisation method used to fit the experimental data

As the input parameters for the PSD model were not known, an optimisation technique was required to fit the model to the experimental data. A derivative-free optimisation method called the Particle Swarm Optimisation (PSO) was used due to the inability to choose a good starting value for the model input parameters. PSO is a stochastic search method inspired by the social behaviour of birds flocking or fish schooling (Kennedy et al., 1942). The PSO algorithm contains particles that describe possible solutions to the optimisation problem using their positions and velocities (Lim et al., 2013). Mathematically speaking, particle swarm optimisation can be used to solve optimisation problems of the form (Ebbesen et al., 2012)

$$\min_x : f(x) \quad (4.9)$$

Subject to: $A \cdot x \leq b$

$$\begin{aligned} A_{eq} \cdot x &\leq b_{eq} \\ c(x) &\leq 0 \end{aligned} \quad (4.10)$$

$$c_{eq}(x) \leq 0$$

$$lb \leq x \leq ub$$

where b , b_{eq} , lb , and ub are vectors, and A and A_{eq} are matrices. The functions $f(x)$, $c(x)$ and $c_{eq}(x)$ can be nonlinear functions. The fitness function $f(x)$ quantifies the performance of x .

The PSO algorithm used to fit the model to the experimental data was obtained from the MATLAB file-exchange server (Chen, 2009-2018). The function was called ‘Constrained Particle Swarm Optimization’. The formulation implemented in the PSO algorithm in MATLAB is shown in Appendix B-1.

4.3.4.1 Default values used in the PSO algorithm

The default values used in the PSO algorithm implemented by Chen (2009-2018) were used to solve the model (see Appendix B-1 for full details). However, an additional MATLAB code was written for

the output function called the 'OutputFcns' so the state of the swarm can be recorded after each generation. This is important to ensure the swarm can be recovered should the algorithm be terminated prematurely due to some extraordinary event. Thus, the swarm can be recovered at an intermediate state rather than restarting the optimisation. The MATLAB code can be found in Appendix B-2.

To confirm if the default swarm size (40) used in the algorithm was sufficient, the PSO algorithm was run using three different swarm sizes, and the model predictions and the global best fitness value were compared. The swarm size used were 20, 40 and 60 particles.

The PSO algorithm, was applied to determine the parameters for selection and breakage which, when used, allowed the selection and breakage function to best fit the experimental data (4 g peanuts data). To begin with, the PSD model was implemented with the one-way competition model as the selection function and Austin's (1971) breakage model as the breakage function. Clearly, selection and breakage function parameters have to be realistic. The selection function has four unknown variables (number of breakage sites = $f(k,m)$ and affinity factor = $f(p,q)$) and a breakage function with another unknown parameter (r). It was explained previously in Chapter 2 that the k variable for the number of breakage sites power-law function is related to the occlusal area. The m variable, which is the power for the function denotes the degree of particle piling at the initiation of breakage. If such piling is involved, the absolute value of the power-law relationship between the number of breakage sites and particle size would be expected to be larger than or equal to 2 (van der Glas et al., 2018). The affinity factor, which is defined as the average chance of a single particle being selected divided by the number of breakage sites is a function of p and q .

To ensure the selection function parameters solved by the PSO algorithm were realistic, the upper and lower bounds were chosen based on the range of values found in van der Glas et al. (2018). The r variable in the breakage function denotes the degree of fragmentation; larger r values mean a higher degree of fragmentation. Similarly, the upper and lower bounds for the breakage function parameter were chosen from the range of values found in previous studies (van der Glas et al., 1987; Gray-Stuart, 2016). Table 4-1 shows the range of the input parameters chosen (upper and lower bounds) to solve the selection and breakage function parameters.

Table 4-1: The range of the input parameters was chosen based on the range of values found when single chew experiments were performed among five subjects in (van der Glas et al., 2018) for the selection model input parameters and in (van der Glas et al., 1987) for the breakage model input parameter, r .

Parameter	Selection model inputs			Breakage model input	
	Number of breakage sites		Affinity factor		Fragmentation variable, r
	<i>Multiplication factor, k</i>	<i>Power, m</i>	<i>Multiplication factor, p</i>	<i>Power, q</i>	
Upper bound	90	1	0.007	1	0
Lower bound	500	3	0.004	3	3

4.3.4.2 Model convergence

Mastication involves a discrete number of particles which, in any one chew, may or may not be selected for breakage. Therefore, both selection and breakage are probabilistic and, because mastication involves only a small number of particles at the beginning of mastication, and usually fewer than forty chews, the outcome will also differ in a probabilistic way. The selection-breakage model has been constructed, as described, to match this probabilistic process. Therefore, this means that even with the same adjustable parameters for selection and breakage, many different mastication outcomes will be obtained. Therefore, optimising for the most representative set of adjustable parameters, requires a progressive optimisation method. In the particle swarm method that was adopted, the parameters are adjusted slowly by limiting the rate of their change from one iteration to another. They are also bounded to upper and lower limits as described above. Within these boundaries, it is necessary to determine the appropriate number of iterations for each set of input parameters. This is called simulation convergence. To determine the convergence point, the simulation was run for 100 times for any set of input parameters. The upper bounds and the lower bounds as described in Table 4-1 were used as the input parameters for the model to observe if a different range of parameters will reach the same convergence point. The model outputs that delivered the PSD representing early (10 chews), middle (20 chews) late (35 chews) mastication stages were recorded. Three d-values (d_{90} , d_{50} and d_{10}) were then retrieved from

the recorded PSD output. The mean of the d-values in each simulation following the first simulation was then calculated to identify the convergence point. The calculation can be described as

$$d_{x_n} = \frac{\sum_{i=1}^n d_{x_i}}{n} \quad (4.11)$$

where n refers to the current simulation number, d_x refers to the d-value (d_{90} , d_{50} or d_{10}).

The calculated mean d-value was then normalised against the mean d-value after 100 simulations. The normalised mean d-value was then plotted against the simulation number where the convergence point was identified. Fig. 4-2, Fig. 4-3 and Fig. 4-4 show the normalised mean, the normalised standard deviation and the normalised standard error of the d -values after 100 simulations for three different chewing numbers when the lower bound set of input parameters was used. A normalised mean d-value of 1 indicates that it was close to the value achieved after 100 simulations.

At the 10th chew, from Fig. 4-2, the mean of the d-value is already close to one even after only a few simulations. The same can be observed with the standard deviation for the d_{50} and d_{10} . However, the normalised standard deviation for the d_{90} value is close to one only after fifty simulations. The standard error has the same trend across all d-values, where the error is higher in the first five simulations but decreases immediately after. The standard error then becomes constant from around 30-50 simulations across all d-values. A similar trend can be observed in Fig. 4-3 at the 20th chew, where the normalised mean d-values stay constant throughout all simulations and the normalised standard deviation of the d-values stay constant after approximately 40-50 simulations. The normalised standard error also had the same trend as observed in Fig. 4-2 where it becomes constant after around 40-50 simulations. At 35 chews, which is at swallow point for the experimental subject (Fig. 4-4), the normalised mean was also constant throughout all simulations. The normalised standard deviation, however, starts to become constant from 15-20 simulations onwards. The normalised standard error also had the same trend in Fig. 4-2 and Fig. 4-3 where it becomes constant from 40-50 simulations onwards.

It was also important to check the trend in the model simulations when the upper bound values are used as the input parameters. Fig. 4-5, Fig. 4-6, and Fig. 4-7 show the normalised mean, normalised standard deviation and the normalised standard error for the first 100 simulations. In general, the trend

followed, by in large, the trend observed when the lower bound values were used as input parameters. The normalised mean was constant throughout all number of simulations and the normalised standard deviation and the normalised standard error starts to become constant from approximately 20-50 simulations. Based on these observations, it was concluded that the simulation had to be repeated for at least 50 times and the average of all the recorded d -values after 50 simulations were then used to calculate the sum of squares residuals for the optimisation.

The observation where model convergence is reached after 50 simulations can tell us that perhaps 50 chewing trials are needed to get a reliable statistics on the PSD data. Depending on the particle size parameters of interest, only a few trials or sometimes numerous trials would be needed. For example, it was observed that standard deviation and standard error of d_{10} results become constant after a few simulations but to achieve reliable d_{90} data needed at least 50 simulations. If the distribution variance is not of interest, then perhaps only a few trials are sufficient as the mean values are basically steady after a few simulations.

4.3.4.3 Comparison of model predictions and global best fitness value when different swarm sizes were used

The model predictions and the global best fitness value (the sum of squares residual value at the optimised input parameters) at a different swarm sizes were compared. Table 4-2 shows a summary of the fitted model parameters and fitting statistics. Fig. 4-8, Fig. 4-9, and Fig. 4-10 shows the d_{90} , d_{50} and d_{10} model predictions compared against the experimental data at various chew numbers for when the swarm size was 20, 40 and 60 respectively. Fig. 4-11 shows comparison between all the fitted d -values against experimental data when presented in a cumulative form. Because the original bolus peanuts PSD data used here from Flynn (2012) were based of sieve size classes (section 4.3.2), the model predictions were also compared in this form (Fig. 4-12, Fig. 4-13 and Fig. 4-14). There was no noticeable difference in the model predictions when a different swarm size was used.

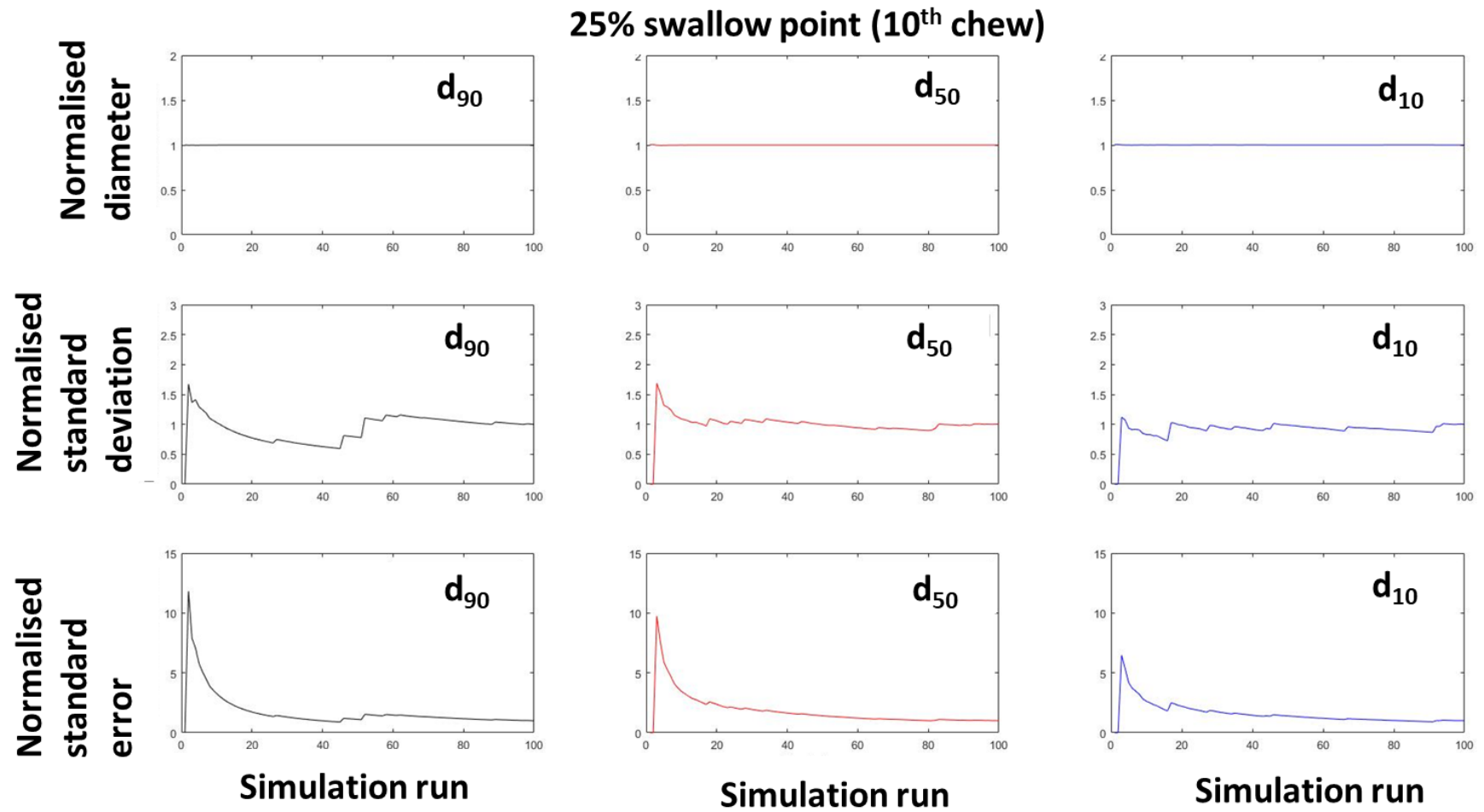


Fig. 4-2: The normalised mean, standard deviation and standard error at 25% of the swallow point (10th chew) using lower bound values as input parameters.

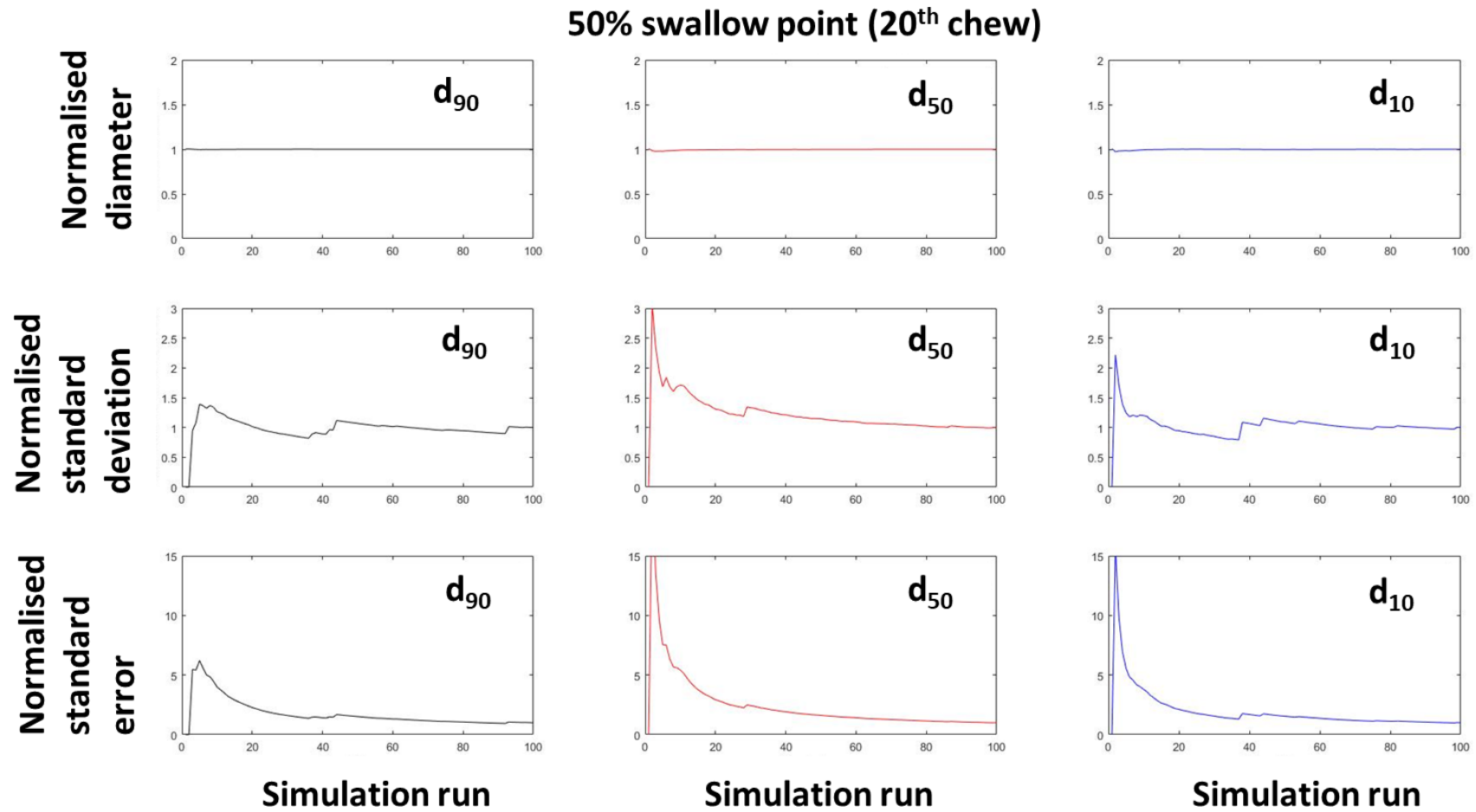


Fig. 4-3: The normalised mean, standard deviation and standard error at 50% of the swallow point (20th chew) using lower bound values as input parameters.

100% swallow point (35th chew)

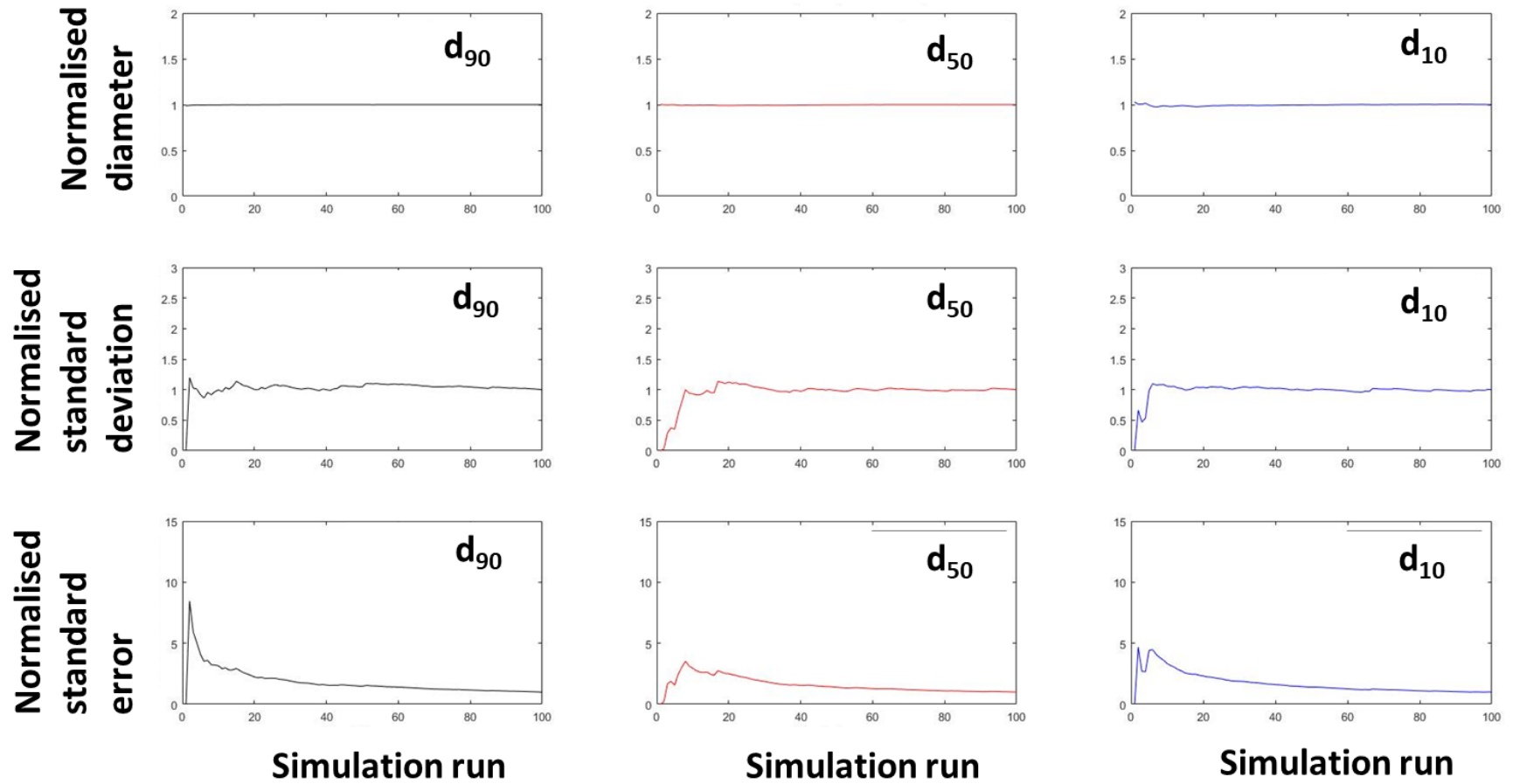


Fig. 4-4: The normalised mean, standard deviation and standard error at 100% of the swallow point (35th chew) using lower bound values as input parameters.

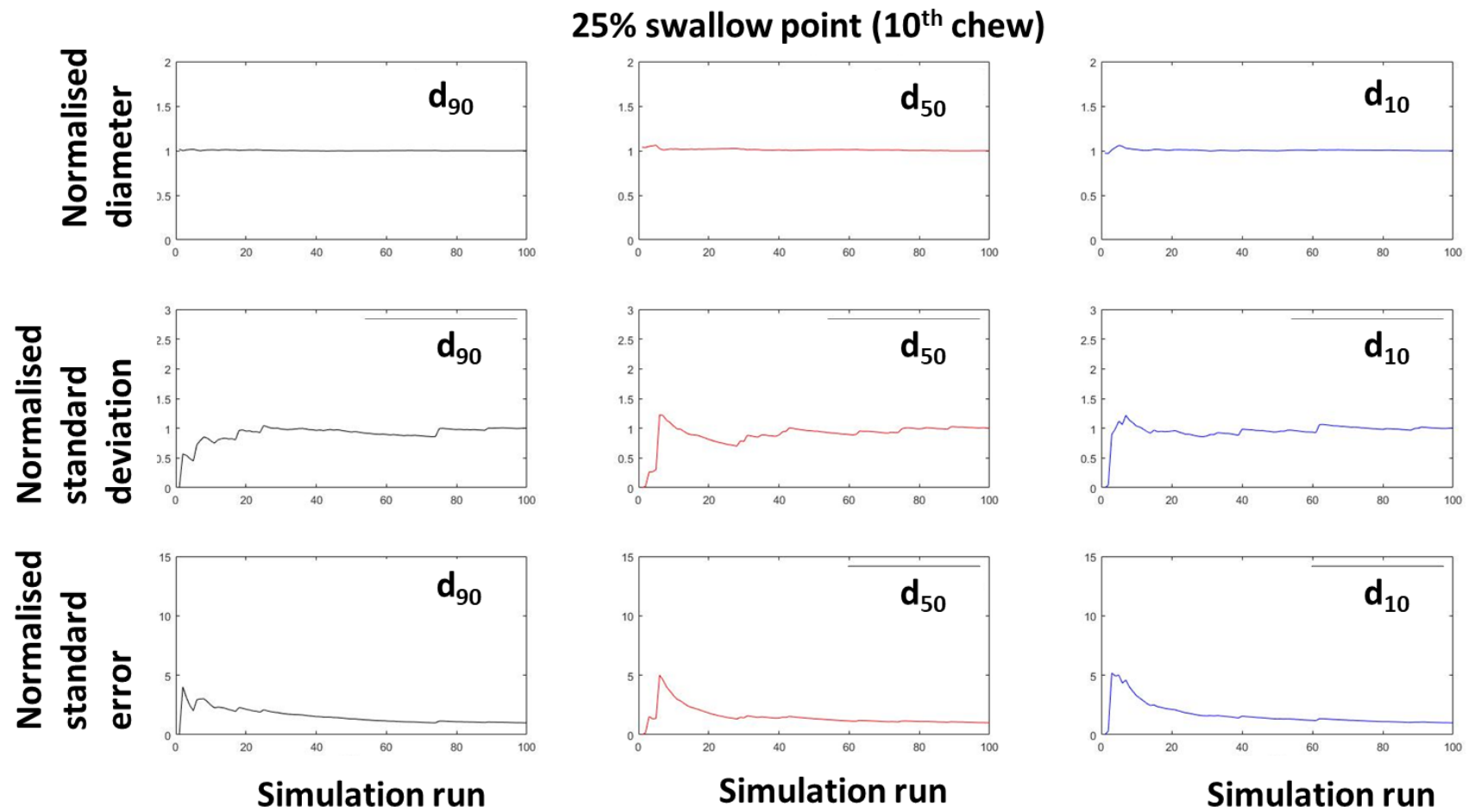


Fig. 4-5: The normalised mean, standard deviation and standard error at 25% of the swallow point (10th chew) using upper bound values as input parameters.

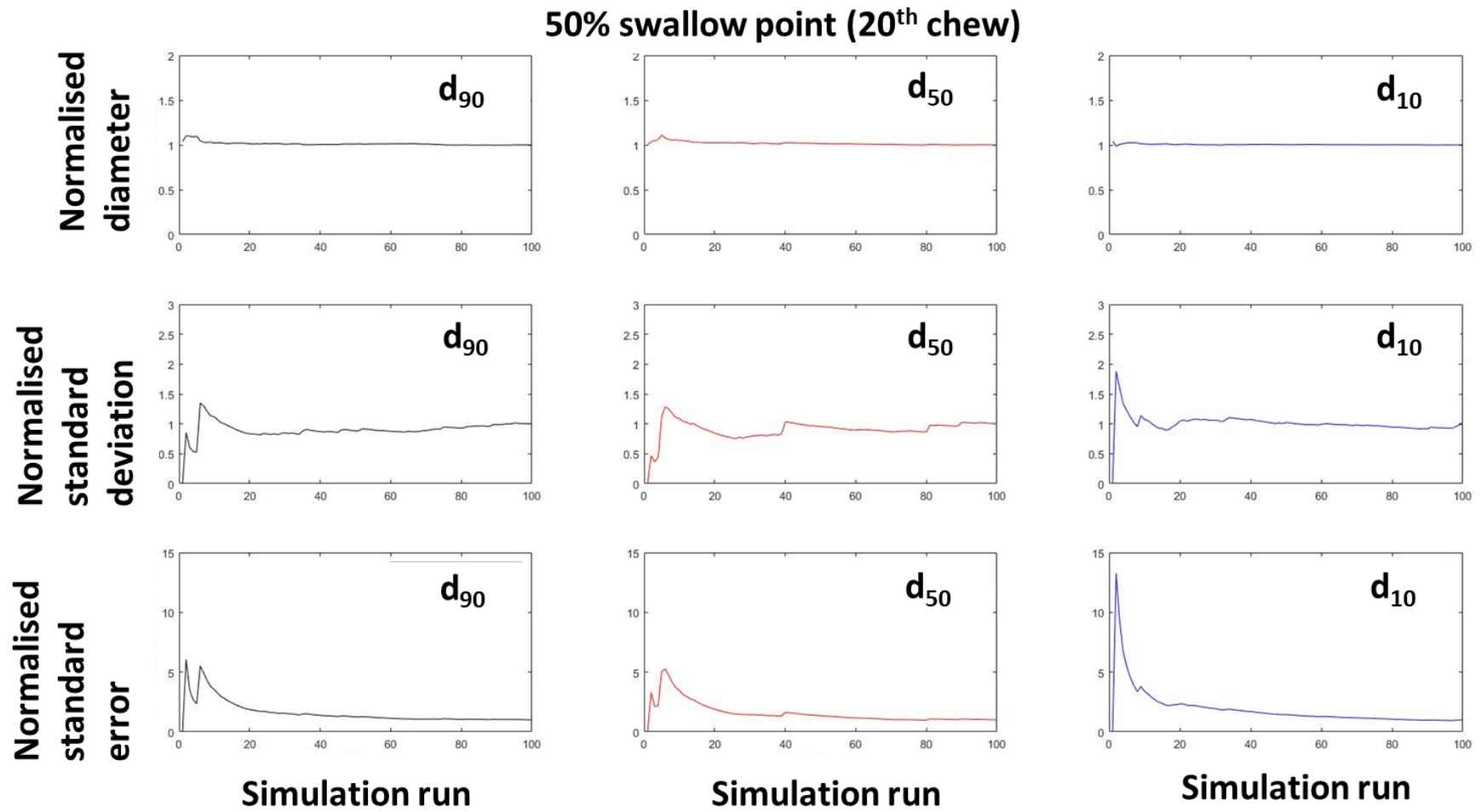


Fig. 4-6: The normalised mean, standard deviation and standard error at 50% of the swallow point (20th chew) using upper bound values as input parameters.

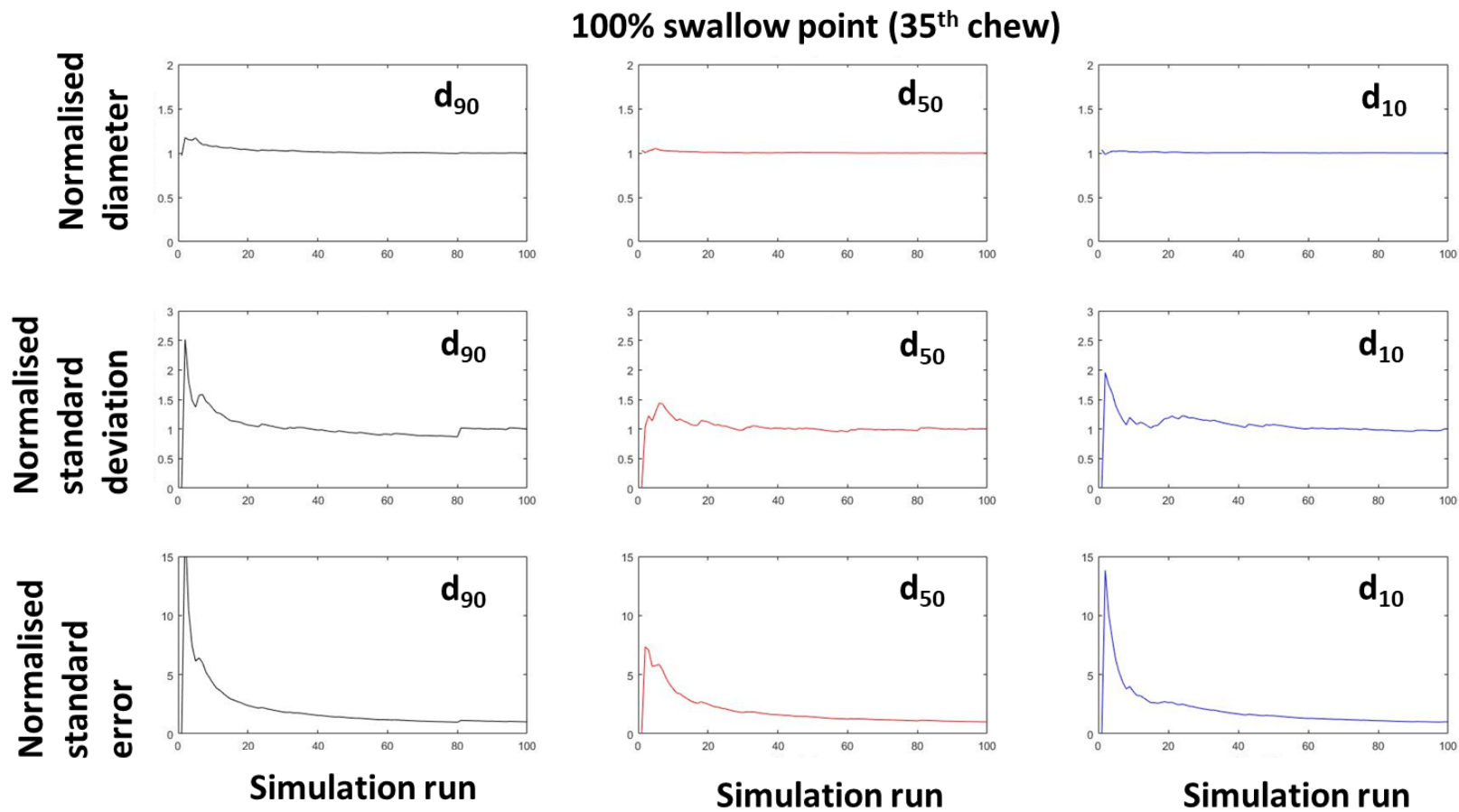


Fig. 4-7: The normalised mean, standard deviation and standard error at 100% of the swallow point (35th chew) using upper bound values as input parameters.

The model fits particularly well for the d_{90} values in the first 15 chews, and the d_{50} and d_{10} values after the first 15 chews. There is a small difference between the model fitting parameters and the global best fitness value for different swarm sizes (Table 4-2). The R-squared values for all swarm sizes were > 0.9 , which indicated that the model was a good fit. The sum of squared residuals was the lowest at 60 swarm, but it only differed by 1% with the sum of squared residuals at 20 and 40 swarms respectively. In general, because of the small difference in the sum of squared residuals and the high R-squared value, the default swarm size of 40 in the PSO algorithm was implemented. Additionally, 40 is also a standard swarm size used in the literature. For example, when comparing between 15, 30 and 60 particles per swarm used to optimise five benchmark functions, the best results were found when an average number of particles was used (Trelea, 2003). Too few particles gave a meagre success rate and required more iterations but using too many particles required too many function evaluations per iteration (Trelea, 2003). However, a noticeable difference can be seen in the simulation time where a larger swarm size took longer to solve. As the model fitting requires the simulation to be repeated 50 times where the results are averaged, it took about 41 minutes to complete one iteration when 40 swarm size was used. This means if the maximum iterations is reached (200 iterations), it can take about 136 hours (6 days) to complete the entire simulations.

Table 4-2: Model input parameters solved by the PSO algorithm when the swarm size (number of particles) in the PSO algorithm was varied.

Swarm size	Fitting	Selection model inputs				Breakage	Global best		
	simulation time per iteration (minutes)	Number of breakage sites, n_b		Affinity factor, o_1		model input	fitness value	SS	R^2
		<i>Multiplication factor, k</i>	<i>Power, m</i>	<i>Multiplication factor, p</i>	<i>Power, q</i>	<i>Fragmentation variable, r</i>	(Normalised SS residuals)		
20	28	145.62	1.83	0.0019	1.51	2.41	3.07	16.9	0.94
40	41	179.06	2.22	0.0013	2.01	2.91	3.09	16.1	0.94
60	55	185.38	1.29	0.0009	1.25	2.58	2.95	15.8	0.94

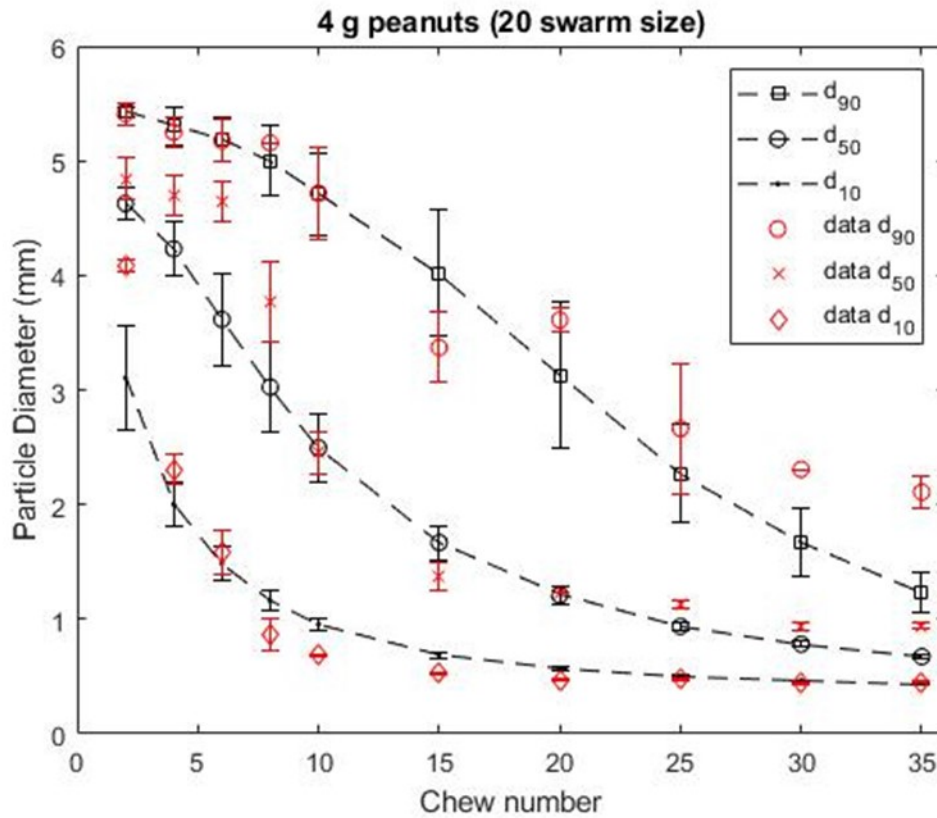


Fig. 4-8: Swarm fitted (black marker) and experimental (red marker) d_{90} , d_{50} and d_{10} values across various chew numbers using 20 swarm.

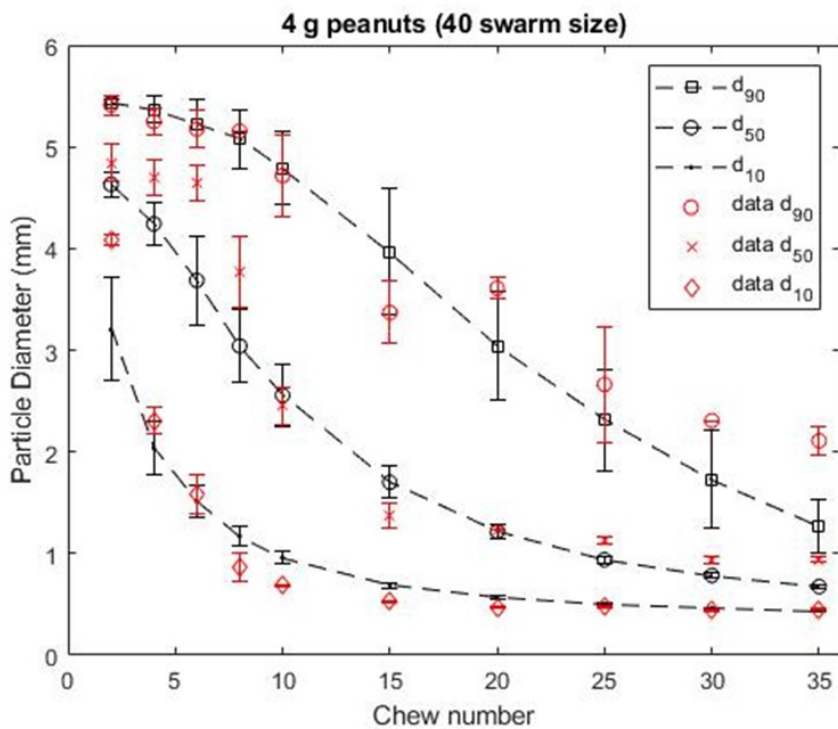


Fig. 4-9: Swarm fitted (black marker) and experimental (red marker) d_{90} , d_{50} and d_{10} values across various chew numbers using 40 swarm size.

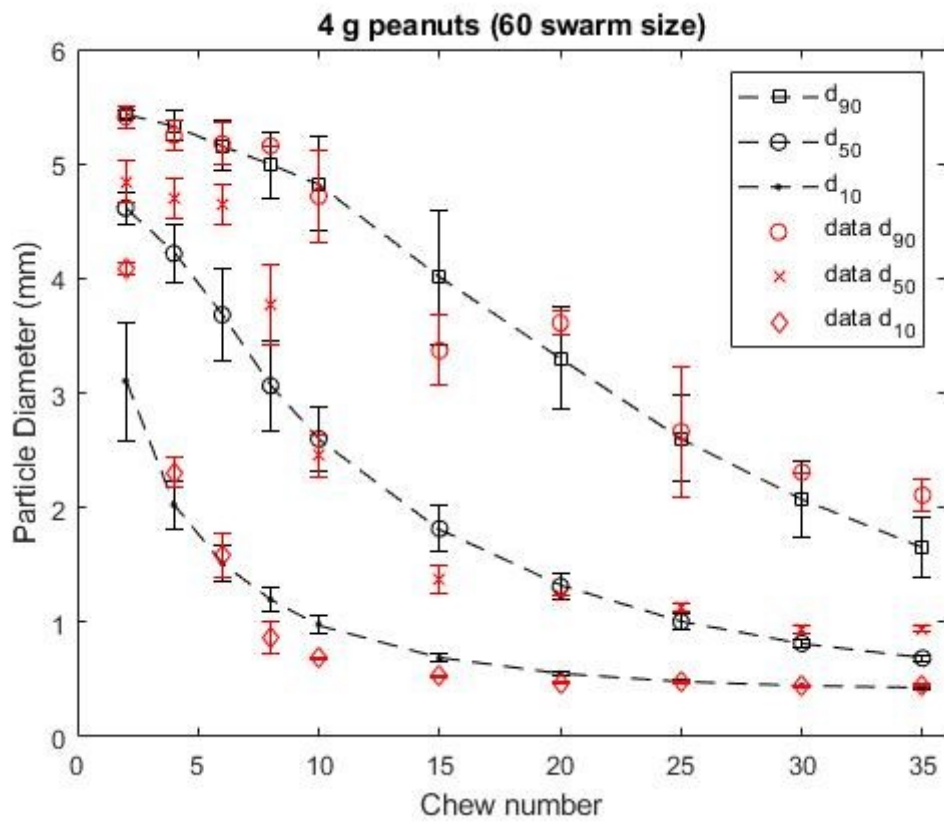
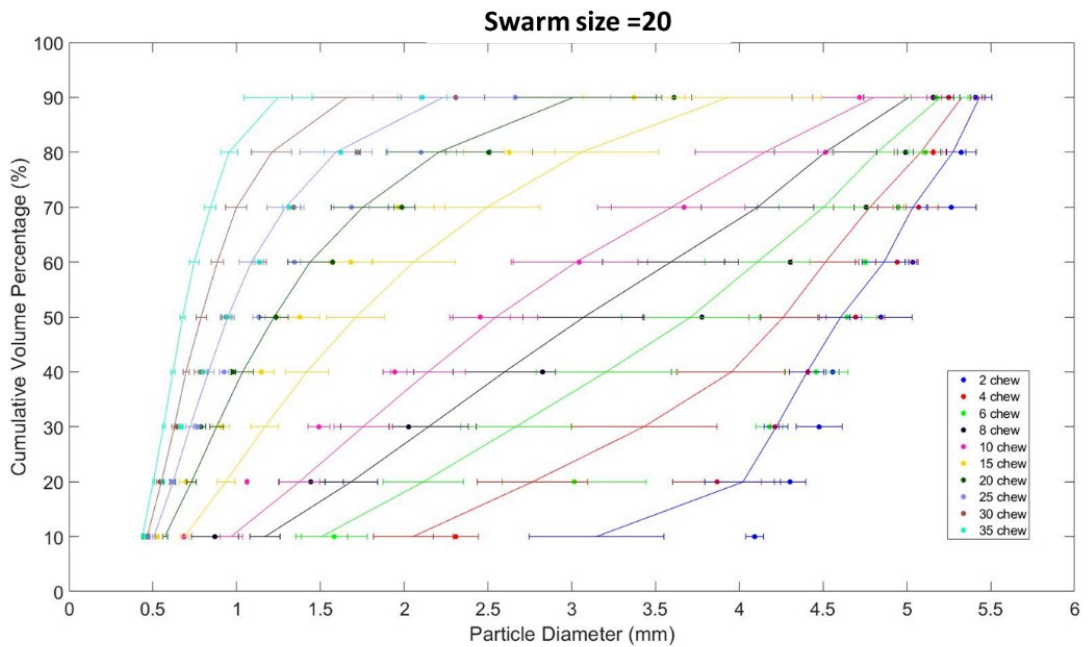


Fig. 4-10: Swarm fitted (black marker) and experimental (red marker) d_{90} , d_{50} and d_{10} values across various chew numbers using 60 swarm size.



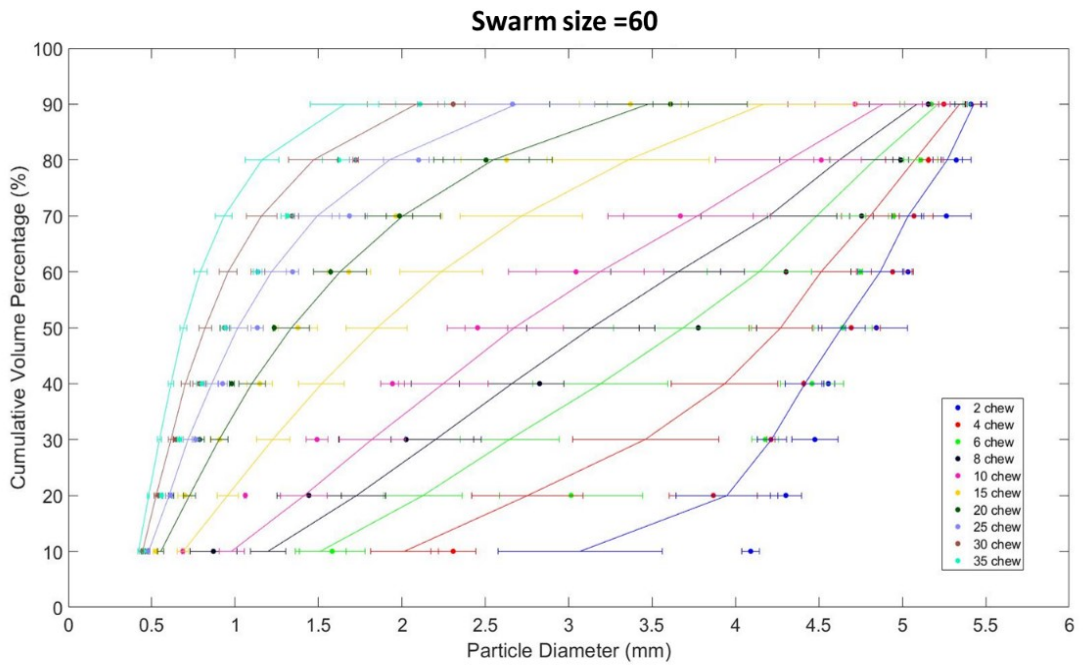
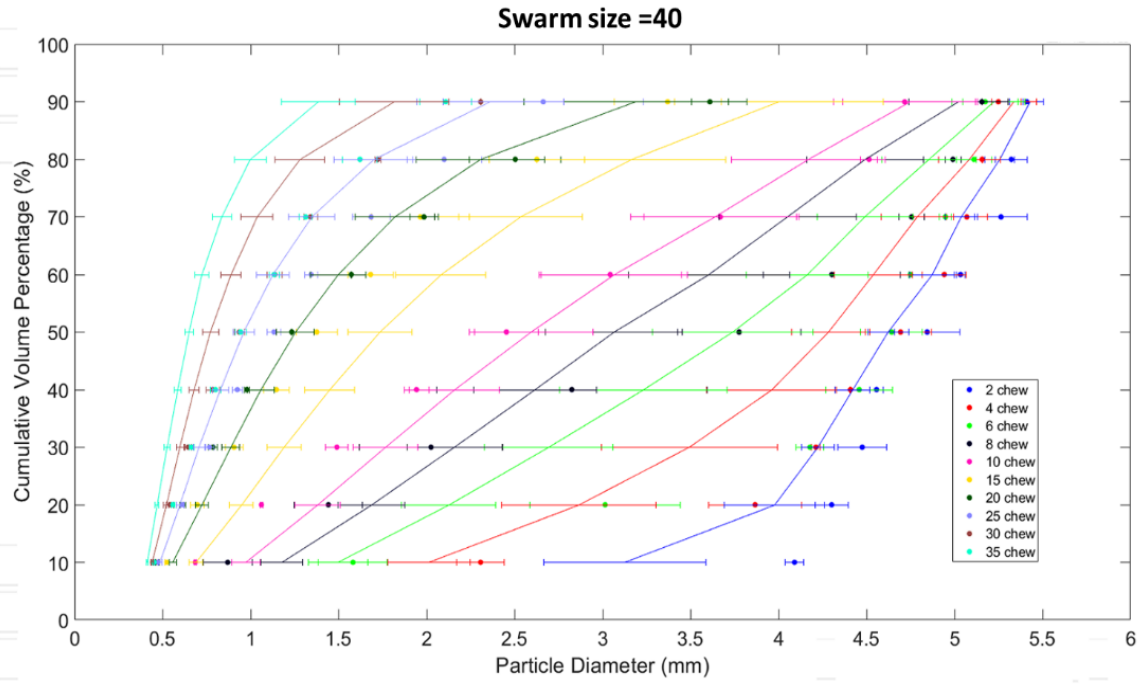


Fig. 4-11 Swarm fitted (line) and experimental (coloured dot markers) in cumulative PSD form across various chew numbers of 20, 40 and 60 swarm size.

Swarm size =20

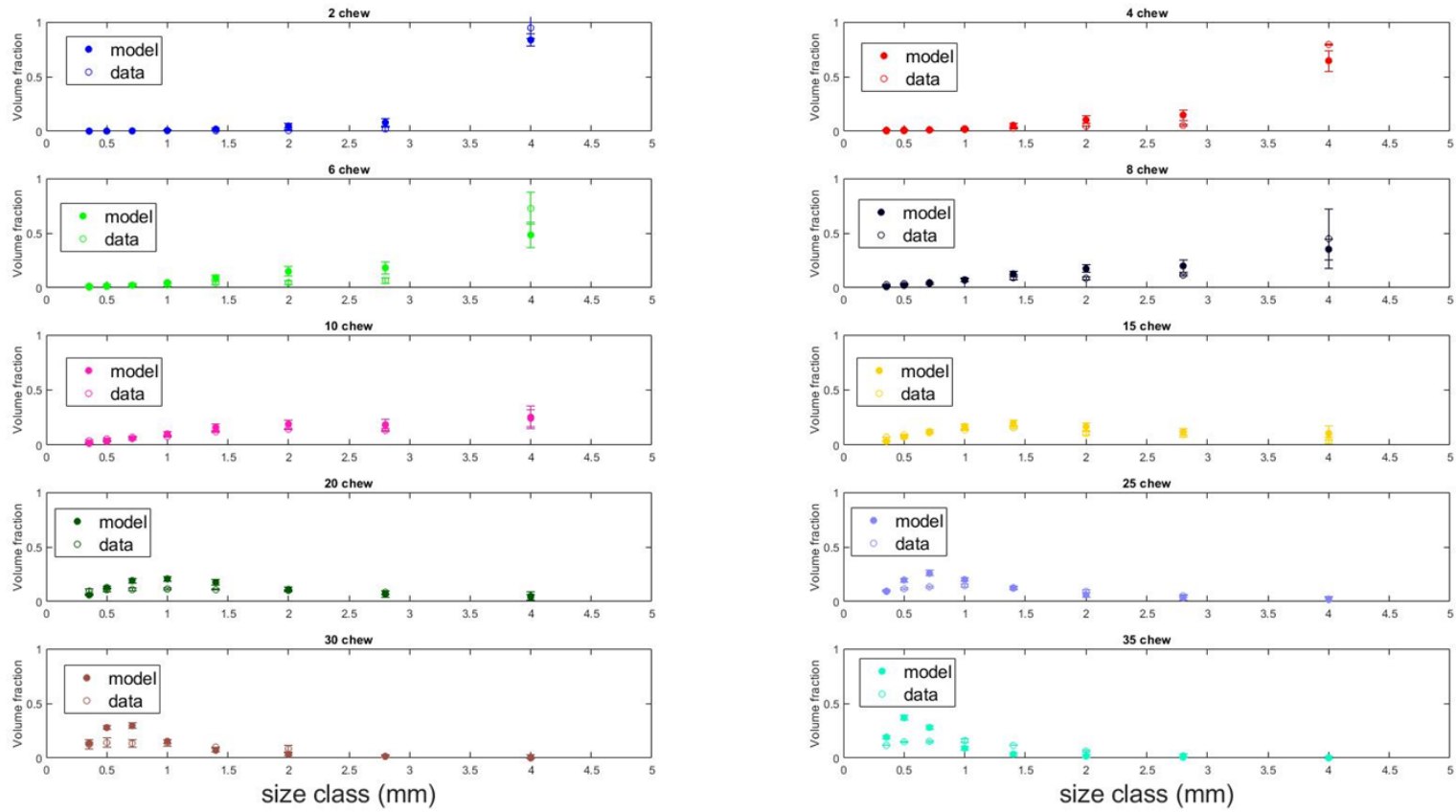


Fig. 4-12 Swarm fitted (dot markers with face colour) and experimental (dot markers with no face colour) when presented in terms of volume fraction vs sieve size classes in across various chew numbers of 20 swarm size.

Swarm size =40

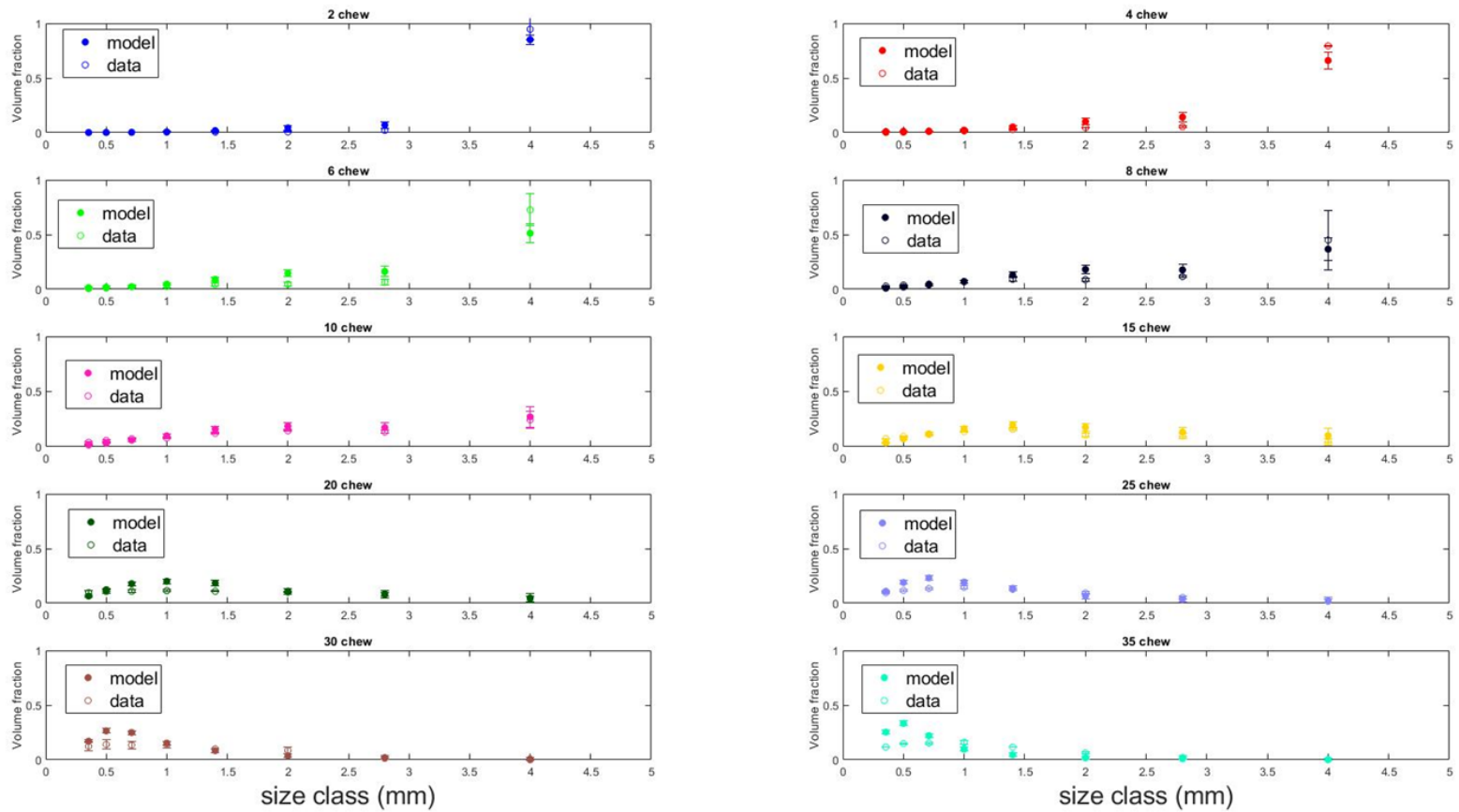


Fig. 4-13 Swarm fitted (dot markers with face colour) and experimental (dot markers with no face colour) when presented in terms of volume fraction vs sieve size classes in across various chew numbers of 40 swarm size.

Swarm size = 60

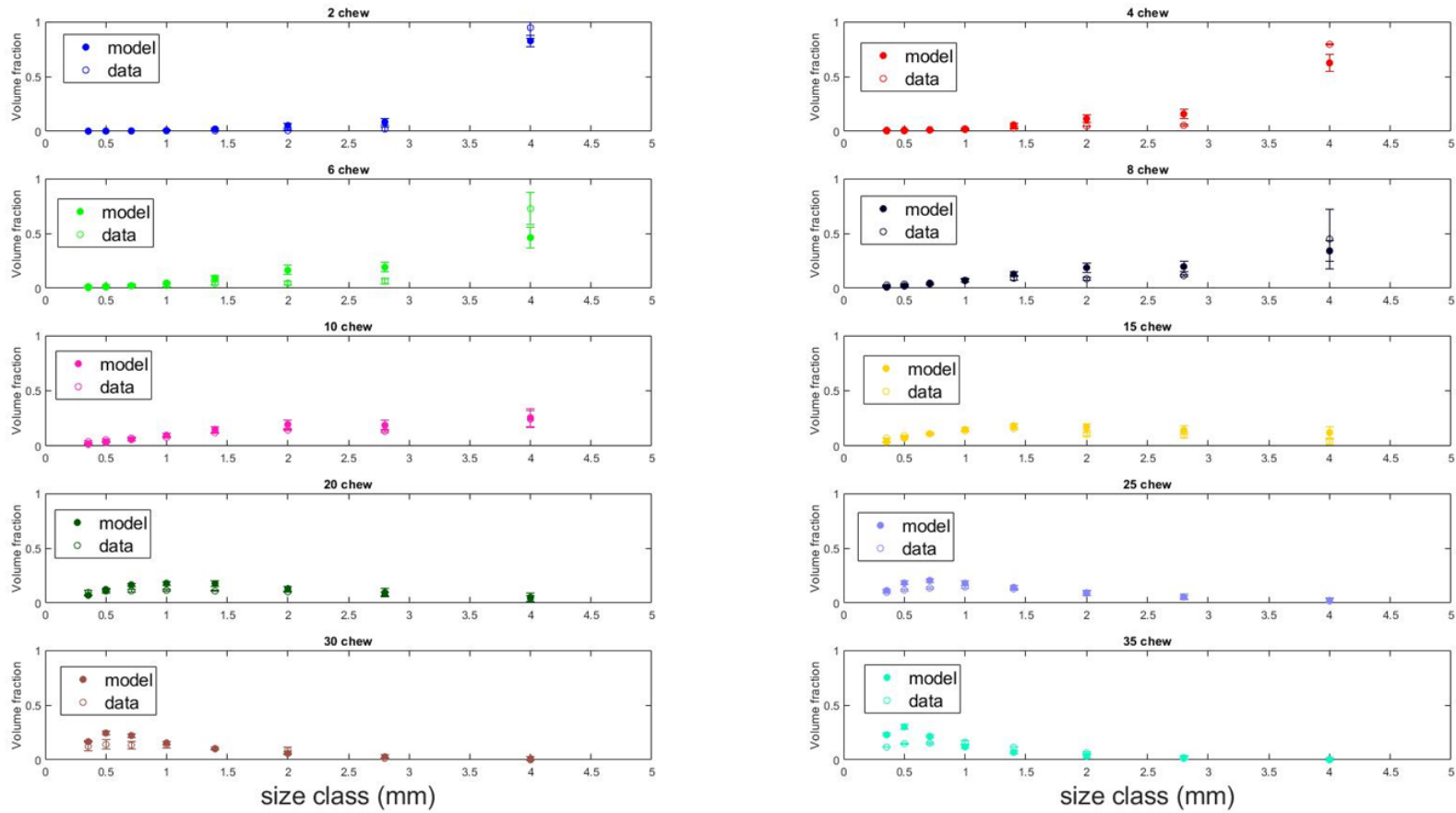


Fig. 4-14 Swarm fitted (dot markers with face colour) and experimental (dot markers with no face colour) when presented in terms of volume fraction vs sieve size classes in across various chew numbers of 60 swarm size.

4.4 Model results and discussions

The particle breakdown model was successfully applied to chewing of peanuts, showing good agreement between measured and predicted PSDs. In those predictions the one-way competition selection model (Eq. 2.4) and Austin (1971) breakage model (Eq.2.10) were used. Two case studies were carried out to explore the predictive behaviour of different selection (case study 1) and breakage (case study 2) models.

4.4.1 Case study one: Comparing model fittings when the selection model is varied, and the breakage model is fixed

This section compares the predicted PSDs to the experimental PSDs when the selection model was varied while keeping the breakage function fixed. The PSD model uses either the one-way competition, two-way competition or the power-law model as the model for selection. The breakage function of Austin (1971) was used for all simulations. The PSO algorithm was used to fit the input parameters to the model. The model was repeated for 50 times to account for the probabilistic nature of the model predictions as described in section 4.2.6.1.1 and the average of the d -values after 50 simulations were used to calculate the sum of squares residuals with the experimental data. The one-way competition model combined with Austin (1971) breakage model was fitted first, where all five (4 selection and 1 breakage model) of the fitting parameters are tabulated in Table 4-3. Following that, the k parameter which was related to the occlusal area (discussed in section 3.2 in Chapter 3) obtained from the one-way model fitting (179.06 in Table 4-3) was kept the same as the bolus data was from the same subject. The r input parameter in the breakage function was also kept the same (2.91 in Table 4-3) as the same type of food (peanuts) was tested. Therefore, for the two-way competition model, the PSO algorithm was only solved for three parameters, m , p and q .

Fig. 4-15 shows the model predictions compared to the experimental data. Overall, all selection models seem to provide a good fit to the experimental data, as shown by their high R-squared values ($R^2 > 0.9$). The one-way competition model under-predicted the d_{90} values after 15 chews, whereas the two-way competition model had a better fit. This can be explained by the fact that the one-way

competition model preferentially selects larger particles during selection whereas the two-way competition model can also select smaller particles as chewing progresses. Because the one-way competition model selects more large particles, it is expected that as chewing number increases, the number of larger particles will also decrease. This explains why it under-predicts the d_{90} value but fits d_{50} and d_{10} values quite well.

In contrast, the two-way competition model fits the d_{90} values quite well towards the latter stages of mastication but under-predicts the d_{10} values in the first few chews as smaller particles can also be selected for breakage. Comparing the fitting parameters between the one-way and two-way competition model in Table 4-3, the obvious difference can be seen in the p and q parameters that describes the affinity factor power-law model. The p and q values were higher in the two-way competition model than it is in the one-way competition model. This suggests that for any particle size, X , in the absence of any larger particles, the probability that it is selected is higher according to the two-way competition model. This makes sense because, in the two-way competition model, small particles can also compete for the breakage sites because of their ability to pile. Therefore, small particles will have a higher chance of selection than they would with the one-way competition model. In contrast, according to the one-way model, larger particles are hugely favoured to occupy breakage sites than smaller particles. This explains why, for the same particle size, the affinity value is higher in the two-way competition model than the one-way competition model.

A comparison with the power-law model was included because this is the simplest model, first proposed by researchers (Lucas and Luke, 1983b; van der Bilt et al., 1987; van der Glas et al., 1987), which does not discriminate between selection and breakage. It overestimates the breadth of the PSD, with smaller d_{50} and d_{10} values especially in the first few chewing cycles. As it does not describe a mechanism, it cannot really be compared, except to conclude that mastication is better described by assuming some competition rules for selection.

The reliability of using the one chew PSD data as the input distribution is tested when the fitted parameters in Table 4-3 for the one-way and two-way competition models were applied to an assumed original PSD of peanuts, which had a uniform particle size of 5.6 mm (section 4.3.2.1). Fig. 4-16 shows the model fits against experimental data where both had R-squared values > 0.9 . The model predictions

seem to over predict the d_{90} and under predict the d_{10} in the first few chews, but in general the predictions produced the same trend with the fits in Fig. 4-15. The result is interesting as there was evidence in a previous study where the chewing side patterns of peanuts remained unchanged when it was observed twice (Paphangkorakit et al., 2006). The authors surmise that because of the reproducibility of the chewing side patterns for brittle foods such as peanuts then the breakage can be easily reproduced. As chewing progresses and the peanuts became softer and more dissociated, they found that subjects tend to use less lateral movement. Therefore as more lateral movements are used in the first few chews and less towards the late stage, it is expected that the breakage could change in the early phase of mastication but remains constant as the food softens towards the late stage of mastication. This explains why the model predictions seem to over and under predict when the fitted values in Table 4-3 but agree well with the experimental data at the later stages of mastication. Based on these observations, it can be concluded that the fitted parameters using the 1st chew PSD as the starting distribution gave reliable predictions except over and under predicting the d_{90} and d_{10} values in the early phases of mastication.

Table 4-3: Selection model input parameters optimised by the PSO algorithm, for a constant breakage model.

Selection model	Selection model inputs				Breakage model input		Global best fitness value (Normalised SS)		R ²
	Number of breakage sites, n _b		Affinity factor, o ₁		Fragmentation variable, r	3.09	16.1		
	Multiplication factor, k	Power, m	Multiplication factor, p	Power, q					
<i>One-way competition</i>	179.06	2.22	0.0013	2.01	2.91	3.09	16.1	0.94	
<i>Two-way competition</i>	179.06	2.25	0.0019	2.62	2.91	2.72	34.4	0.87	
<i>Power law</i>	-	-	0.14	0.16	2.91	2.15	21.6	0.92	

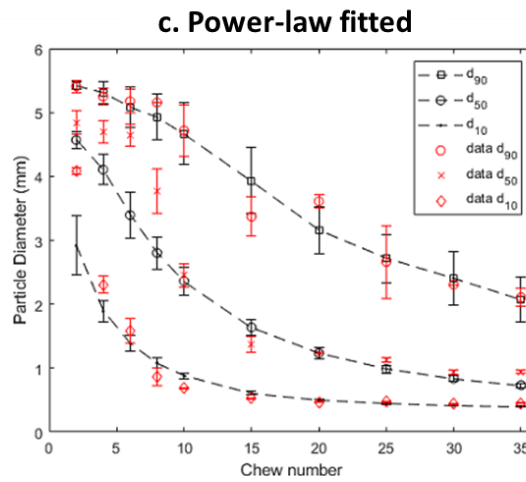
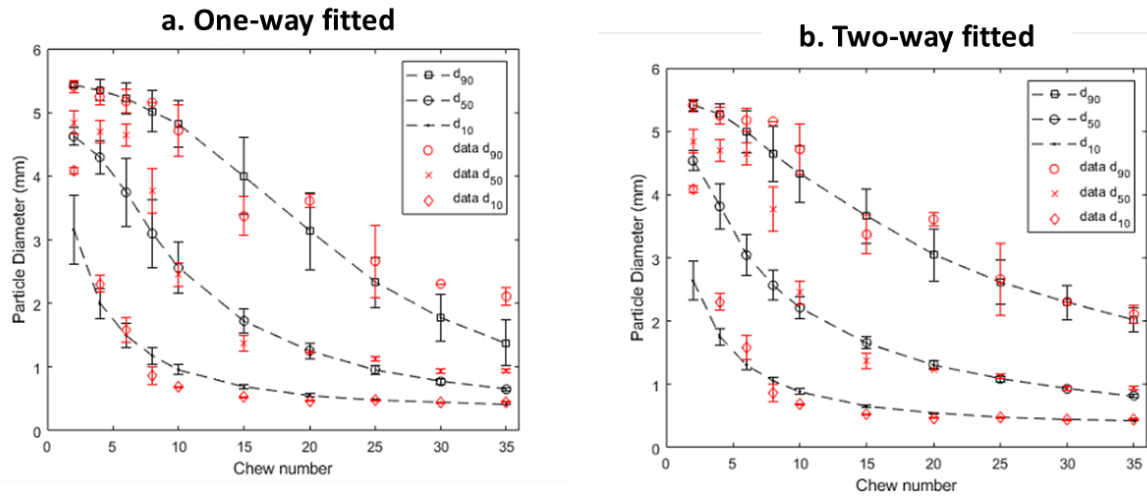


Fig. 4-15: Swarm fitted (black marker) and experimental (red marker) d_{90} , d_{50} and d_{10} values at various chew numbers when different selection models and a fixed breakage function were used. a. Model fits of one-way competition and the Austin (1971) breakage model. b. Model fits of two-way competition and Austin (1971) breakage model. c. Model fits of power law model and Austin (1971) breakage model.

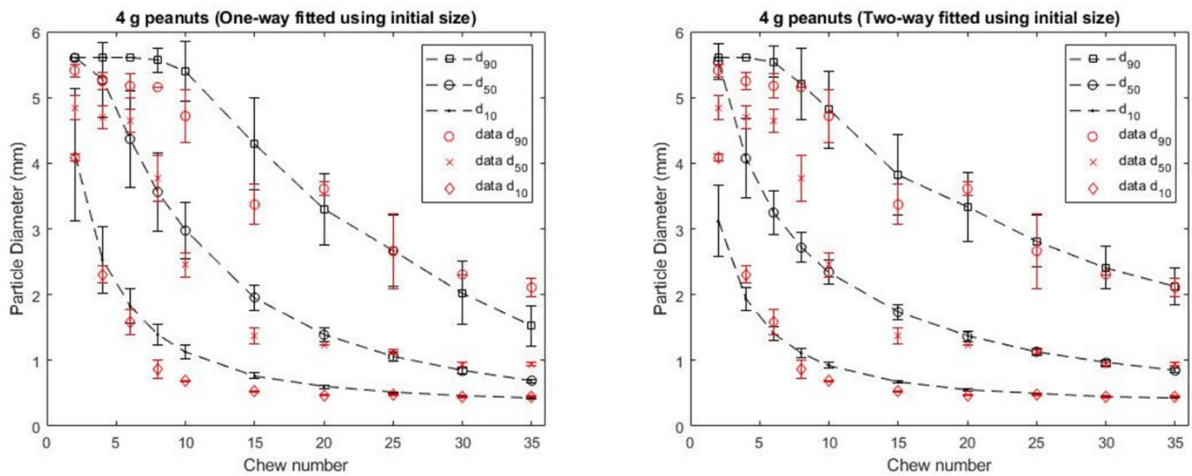


Fig. 4-16 Model predictions when the assumed initial PSD is used as the input distribution using the swarm fitted of one-way and two-way competition models in Table 4-3.

Comparison of the predictions of the one-way and two-way competition models and due to their underlying assumptions, it could be said that in the early stages of mastication, the one-way model is most appropriate, but after some time, the two-way model applies. This idea was then tested.

4.4.2 Model fitting using a combined one-way and two-way competition model

Van der Glas et al. (2018) proposed that selection will occur according to the one-way competition model in the first few cycles, after which selection then shifts into the two-way competition model. Therefore, here a combined one-way and two-way competition selection model along with the Austin (1971) breakage model was fitted to the experimental PSD data for the 4 g portion size peanut particles at various numbers of chews. The k parameter which was related to the occlusal area obtained from the one-way model fitting (179.06 in Table 4-3) was kept the same as the bolus data was from the same subject. The r input parameter in the breakage function was also kept the same (2.91 in Table 4-3) as the same type of food (peanuts) was tested. Therefore, the only additional term here (besides the selection function parameters, m , p and q) to be solved by PSO was the chew number when the selection model switches from one-way to two-way competition. Fig. 4-17 shows the model fitted against the experimental data when the combined one-way and two-way competition model was used. Table 4-4 shows the fitted parameters, the final sum of squared residuals value and the R-squared.

Table 4-4: Selection model input parameters optimised by the PSO algorithm, for a fixed fragmentation index used in the Austin (1971) breakage model.

Selection model	Selection model inputs				Breakage model input	Mechanism	Global best fitness value		
	Number of breakage sites, n_b		Affinity factor, o_1				(Normalised	SS	SS
	<i>Multiplication factor, k</i>	<i>Power, m</i>	<i>Multiplication factor, p</i>	<i>Power, q</i>	<i>Fragmentation variable, r</i>	switch chew number	residuals)		
<i>Combined one and two-way model</i>	179.06	2.08	0.002	1.67	2.91	18	1.92	22.9	0.91

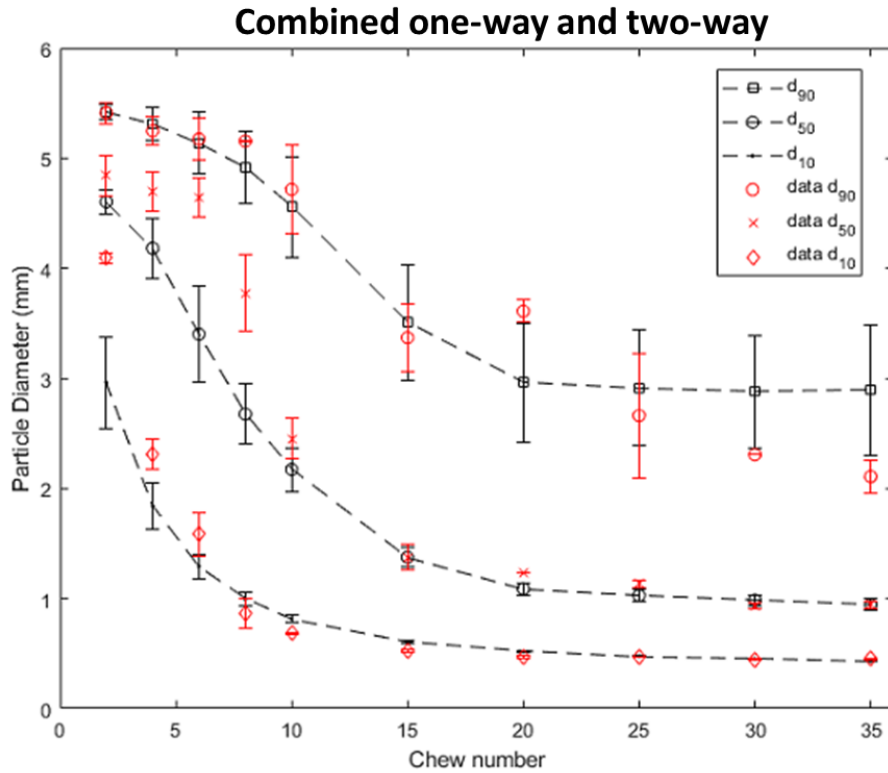


Fig. 4-17: Predicted (black marker) and experimental (red marker) d_{90} , d_{50} and d_{10} values at various chew numbers when the one-way competition model was used to predict the selection for chew number less than an optimum chew number, here 18 chews, and the two-way competition model for chew number greater than the optimum. The Austin (1971) breakage model was used with a fixed fragmentation index.

After the 18th chew number, the one-way competition model shifted to the two-way competition model to describe the particle selection process. From the 20th chew number and beyond, the predicted d_{90} remained constant. The observation makes sense as the two-way competition model assumes that the number of breakage sites available for larger particles will be reduced due to an increase in competition with small particles which could pile. Therefore, less large particles will be selected for breakage and will remain unbroken. This explains why the d_{90} values remained constant once the selection model was shifted to the two-way competition model at the 18th chew number.

Comparing the fits from the combined selection mechanisms and fits of Fig. 4-15, all models seem to under-predict the d_{50} values in the first few chewing cycles and d_{90} values at the later stages of mastication. A reason why the model was not a closer fit might be that the amount of bolus recovered in the data was quite low in the later stages of mastication. This mass balance including losses was not included in the modelling, which assumes 100% bolus recovery. In practice, the amount of food recovered reduces when subjects chew for longer (Flynn, 2012). Flynn (2012) studied this effect and

proposed a two-compartment model, where some food resides for some time within the buccal pouches and is only periodically cleared. Such a mechanism has not been included here. The selection model simply assumes all particles are always available. It also assumes the bolus recovered, although an acknowledged fraction of the ingested food is representative of the non-recovered PSD. However, this is not accurate. Flynn (2012) found that in five different food types (including peanuts), the debris from all foods contained a significantly higher proportion of particles in the 0.5 – 1.0 mm range and a lower proportion of particles > 2.8 mm compared to the bolus (Flynn, 2012). The presence of more large particles in the recovered bolus combined with the fact that the d_{50} and d_{90} of the experimental data is calculated from a reduced volume than the portion size, it could be expected that the experimental d_{50} and d_{90} values will be a lot larger than the predicted ones.

4.4.3 Case study 2: Comparing model fittings when the selection model is fixed, and the breakage model is varied

The second case study was to compare the fits when the selection model was fixed, and different breakage equations were used. The combined one-way and two-way competition model was chosen to model the selection process. The k parameter (which represents the occlusal area) for the selection model was taken from the fits obtained in section 4.3.2 (Table 4-3). Because Austin's (1971) breakage model was used in previous sections, two additional breakage functions (one mechanistic, and the other empirical) used in previous mastication studies in Lucas and Luke (1983a, 1983b) were applied (Eq. 2.8 and Eq. 2.9). Fig. 4-18 shows the model fits against the experimental PSD data. The model prediction gave good agreement with the experimental data when the empirical and mechanistic breakage functions were used ($R^2 > 0.9$).

The close fit to the experimental data when the breakage functions of Eq. 2.8 and Eq. 2.9 were interesting as they have been shown to characterise breakage well for carrots (Lucas & Luke, 1983a, 1983b). The results were interesting because the main assumption of the breakage functions was that 'all particles must break into two fragments only' but the results suggest that the same assumption can be applied to the breakage of a peanut particle. The breakage of peanuts seems to depend on the physical properties of the food where moist, soft peanuts break into larger pieces during contact with the teeth, whereas dry peanuts shatter into smaller pieces (Hutchings, 2011). Either way, a peanut particle does

not break to just two fragments during breakage. An improved version of Eq. 2.9 was the breakage function developed by Austin (1971) (Eq.2.10) which was shown to produce a good fit (R-squared >0.9) with the experimental data when implemented in section 4.3.2. This is interesting, as it seems that despite having more than one parameter in Eq. 2.8 and Eq. 2.9, they perform as well with Eq. 2.10, which only contains one parameter. Having only a single parameter in the model also prevents overfitting, which is defined as when a model includes more terms than necessary or procedures that use more complicated approaches than necessary (Hawkins, 2004). Overfitting is undesirable as it leads to wasting of resources (from measuring irrelevant parameters), makes worse predictions (as it adds random variation to other parameters) and not portable (meaning it can only be reproduced by reusing modeller's software and calibration data) (Hawkins, 2004).

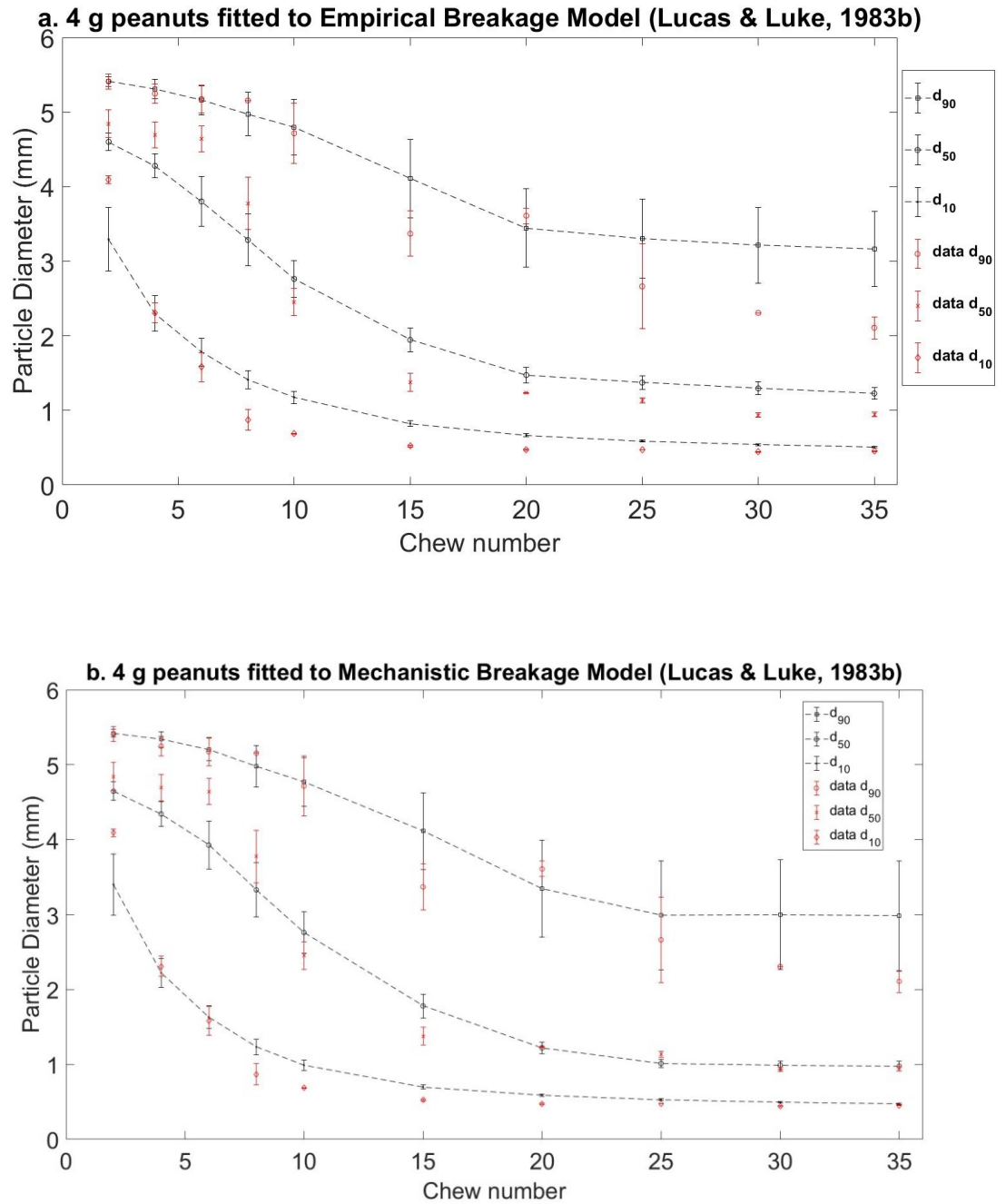


Fig. 4-18: Predicted (black marker) and experimental (red marker) d_{90} , d_{50} and d_{10} values at various chew numbers when the combined one-way and two-way competition model was used to describe particle selection process. Two breakage models in Lucas and Luke (1983b), (a) empirical breakage function (Eq. 2.8) and (b) mechanistic breakage function (Eq. 2.9) were applied and the model predictions were compared.

Table 4-5: Model input parameters optimised by the PSO algorithm, the global best fitness value (the sum of squared residuals minimised by the PSO algorithm) and the R-squared value when one-way and two-competition model were combined and the breakage model was varied.

Breakage model	Selection model inputs				Breakage model input		Mechanism	Global best		
	Number of breakage sites, n_b		Affinity factor, α_1		Fragmentation variable, r	Fragmentation variable, s	switch chew	fitness value	SS	<i>R-squared</i>
	<i>Multiplication factor, k</i>	<i>Power, m</i>	<i>Multiplication factor, p</i>	<i>Power, q</i>			number	(SS residuals)		
Empirical breakage model in Lucas & Luke (1983b) (Eq. 2.8)	179.06	1.75	0.002	1.34	1.07	1.84	18	1.95	18.7	0.93
Mechanistic breakage model in Lucas & Luke (1983b) (Eq. 2.9)	179.06	2.01	0.003	1.23	1.41	1.09	22	7.26	19.9	0.92
Austin(1971) (Eq. 2.10)	179.06	2.08	0.002	1.67	2.91	-	18	1.92	22.9	0.91

4.5 Chapter conclusion

In this chapter, the chewing models developed in Chapter 3 were applied to peanuts, to test the application of the models prior to applying them to a novel food system linking digestion and aroma release.

Different selection and breakage models were applied to predict the PSD of peanuts during mastication as reported in the literature. The competitive selection models, despite mechanistic, are difficult to implement due to the complexity in obtaining input data. As such, a powerful optimisation algorithm, called the PSO, was used to obtain the input parameters of each model. The algorithm was used as there were no obvious starting values and a large number of parameters were required.

When different selection models were compared, the combined one-way and two-way model were found to give the best fit. However, because of the difference in the rate of bolus recovery between the model and the experimental data, large discrepancies between the model and experimental data occur, particularly towards the late mastication stages. Although not a focus of this research, it is recommended in future research to include a 'bolus loss' function in the model so the predictions can be more accurately compared to real-life particle size measurements.

When different breakage models were compared, all models produced a good agreement with the experimental data, but the improved Austin (1971) breakage model, which consists of only one input parameter, may prevent overfitting, which is defined as when a model includes more terms than necessary.

The chewing models developed in Chapter 3 were successfully applied to peanuts in Chapter 4. The next step will be to test if the models can provide useful information to aid in food design. It is known that some processes such as heating, or moisture uptake can change the fracture behaviour of foods (Hutchings, 2011). Portion size is also known to impact on size reduction (Flynn 2012). The models which have been implemented here can be applied to these scenarios and will be explored in the next chapter.

Chapter 5 Chewing models as a tool for food design

5.1 Introduction

The physical properties of food are known to influence bolus PSDs before swallowing. For example, the toughness (Agrawal et al., 2000), hardness (Kohyama et al., 2004), rheological properties (Agrawal et al., 2000; Foster et al., 2006), portion size (Lucas & Luke, 1984; Flynn, 2012) and initial moisture content (Hutchings, 2011) all are known to affect food breakdown. The PSD of food boluses, which is a chewing outcome, is of growing interest to food manufacturers. This is because it has been related to digestibility (Hoebler et al., 1998; Ranawana et al., 2010; Bornhorst & Singh, 2012), texture perception (Peyron et al., 2004) and the extent of flavour and aroma release (Harrison et al., 1998; Chen, 2009; Bornhorst & Singh, 2012; Doyennette et al., 2014). Thus, understanding food structural breakdown during eating is essential not only for our basic understanding of the governing principles of eating and sensory perception but more importantly for better design and manufacturing of quality and tasty foods (Chen, 2015).

However, it can be challenging to understand these observations, because of the complexity of the number of sub-processes and their interactions occurring during chewing. Mathematical modelling can be used as a tool to propose interactions and then to compare model predictions to observed masticatory, sensory and digestion outcomes. Models are also flexible and can be used to study a range of primary food properties that affect food breakdown. Models have been established for the selection and breakdown of particles during the mastication process and the PSD after chewing in the literature (Lucas & Luke, 1983; van der Bilt et al., 1992; Prinz & Lucas, 1997; Gray-Stuart, 2016). Extension to these are the studies by Gray-Stuart et al. (2017), who developed a conceptual model of the decision-making criteria for bolus properties needed to ensure safe swallows, and Ng et al. (2017), who investigated slip extrusion as a function of bolus properties in a simulated swallow. Despite these extensions, the next steps to use such models for better design of foods has not been made.

Therefore, the main objective of Chapter 5 was to demonstrate the application of the chewing models for food design through two simple case studies. The first was to understand the breakdown process when the initial portion size of peanuts is varied. An increase in portion size is known to increase

the median particle size at swallow point (Buschang et al., 1997; Flynn et al., 2012). It will also affect the selection process during mastication. Additionally, adapting the bite-size has been shown to affect satiety by increasing the extent of retro-nasal aroma release (Ruijschop et al., 2011). A second case study was carried out to understand the breakdown of food when the initial moisture content of peanuts is varied. Moisture affects the physical properties of peanuts, which have been shown to influence the breakage function and the resulting particle size (Agrawal et al., 1997; Prinz & Lucas, 1997).

5.2 Case study one: Understanding the effect of portion size on selection

It is well-known that an increase in the initial portion size results in larger food particles being swallowed (Yurkstas, 1965). The study by Flynn (2012) showed that when two different portion peanut sizes (2 g vs 4 g) were masticated by 10 subjects, the 4 g portion size contained a significantly higher proportion of large particles (>2 mm) and a lower proportion of small particles (< 0.5 mm) as shown in Fig. 5-1 below.

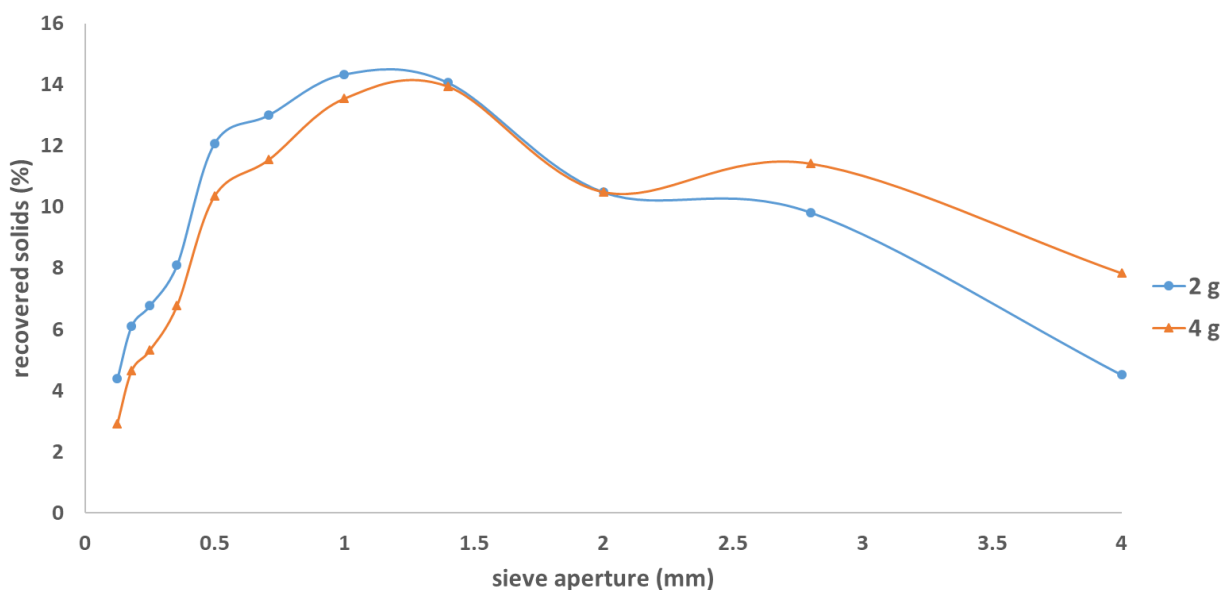


Fig. 5-1 Mean peanut bolus data of 2 g and 4 g portion sizes. Redrawn from Flynn (2012). The bolus data is a mean of 10 subjects at swallow point (17 and 26 chews for 2 g and 4 g respectively). The original figure of Flynn (2012) which consists the error bar can be referred in Appendix D.

The reason there is a higher proportion of particles at swallow point when portion size increases can be hypothesised from the mechanisms of selection. As a larger portion size indicates higher particle

numbers, the selection chance of any individual particle will be smaller, particularly as the breakage sites of the teeth become more saturated with particles. Thus, an increase in the number of non-selected particles can be expected. This could explain why more large particles are observed in the 4 g compared to the 2 g portion size.

The competitive selection models developed by van der Glas et al. (1992) may be used to explain the observation as above because the equations are mechanistic. This case study therefore aims to interrogate selection model input parameters when the model is fitted to the PSD data of two portion sizes from Flynn (2012).

5.2.1 The model

The model consists of selection and breakage sub-models. Each will be discussed.

5.2.1.1 Selection equations

The selection models used to fit the PSD of both portion sizes are the one-way (Eq.2.4) and the two-way competition (Eq. 2.5) models as both models are mechanistic models, where the equations and examples for implementation were described in section 3.2.1. Also, both seem to have parts of the mastication cycle where they are best suited. They allow investigation here of the selection process when the portion size of the food is varied.

5.2.2 Breakage model equation

In this case study, the Austin (1971) breakage model (Eq. 2.10) will be applied. The breakage model is the most widely used in previous mastication studies to predict PSD of various foods during mastication (Lucas & Luke 1983a, 1983b; van der Glas et al., 1987; Gray-Stuart, 2016). In addition, the breakage model also consists of one fitted parameter which reduces the degree of freedom of the optimisation.

5.2.3 Discretised population model

The PSD will be predicted using the discretised population balance model developed as described in section 3.2.3.

5.2.4 Model inputs

5.2.4.1 Discretised PSD of the 2 g and 4 g peanut boluses

The particle distribution of the peanut bolus data was obtained from Flynn (2012) for each reported chew number (e.g. Fig. 5-1). The data was presented as a mass fraction obtained on a series of sieve size classes, which provided the PSD for peanuts at two portion sizes, 2 g and 4 g respectively. For 4 g portions, the data was provided for the PSD at a range of chew numbers: one, two, four, six, eight, ten, fifteen, twenty, twenty-five, thirty and thirty-five chews as used before in Chapter 4 previously. However, for the 2 g portion, the data was only collected for the PSD at swallow point averaged across 10 subjects (17 chews).

Because the model (as outlined in Chapter 3) employs a discretised population balance, it was necessary to convert the data into a population of particles. The method to generate the PSD for the 4 g portion size at a various number of chews and the 2 g portion size at swallow point followed the numerical approach as described previously in Chapter 4 (see section 4.3.1), where a random and discrete number of particles were generated in each sieve size class from the experimental data. For the 2 g peanuts, the data was only provided for the PSD at swallow point. Previously in Chapter 4, the PSD after a single chew of the 4 g peanuts was used as the model input. However, as the mass is different, the single chew data could not be used as the model input for the 2 g peanuts. Thus, it was necessary to develop a numerical approach to create the PSD after a single chew for the 2 g peanuts.

The PSD after a single chew for the 2 g peanuts were created under the assumption that the volume distribution followed the distribution of the 4 g peanuts. However, to ensure mass was conserved, a numerical algorithm was written to ensure that the total mass of all particles in the distribution does not exceed 2 g. A diagram, showing the steps in the process is shown in Fig. 5-2 (the MATLAB code can be referred to in Appendix A).

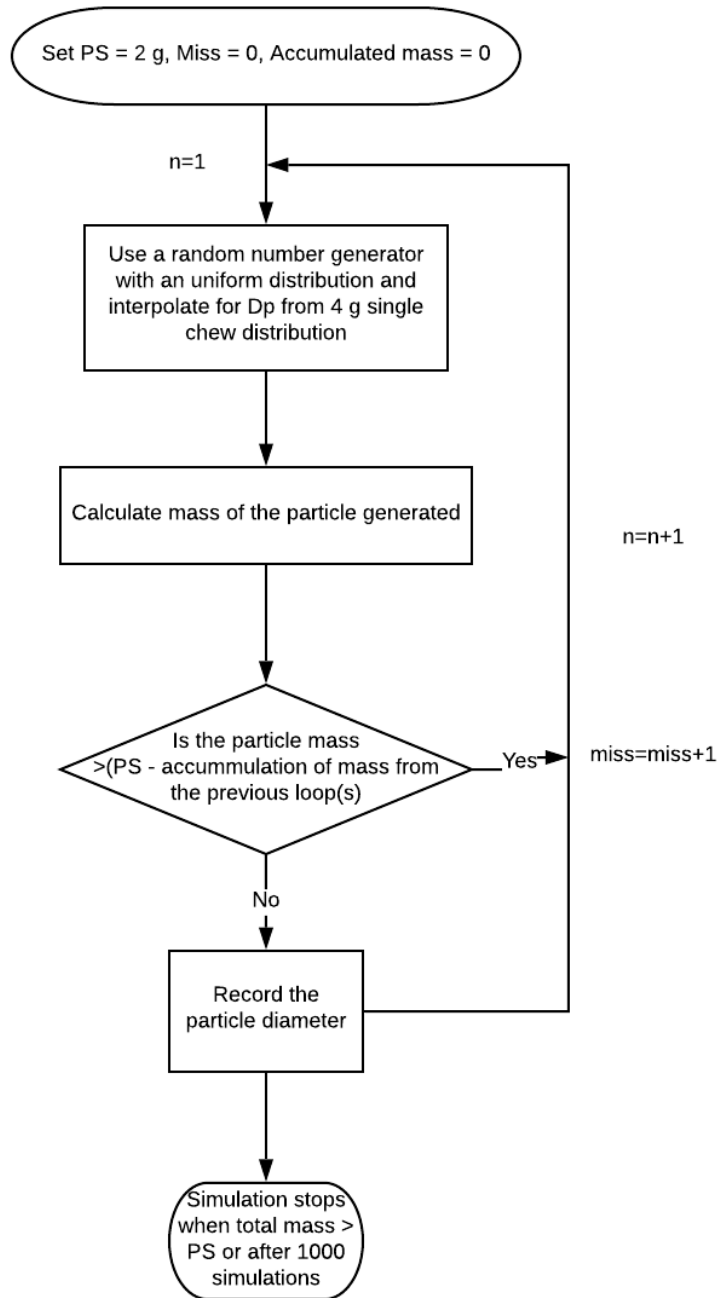


Fig. 5-2: Model flow chart to generate PSD after a single chew for the 2 g portion size. PS refers to portion size and n refers to the iteration number. Miss refers to the rejected particles which will not be accounted for in the simulation.

As can be seen from Fig. 5-2 above, from the top, the portion size (PS) was first set to a pre-defined mass, which was 2 g. An initial zero value was also set for particles that did not satisfy the conditions in the model flow chart (Miss = 0). The initial mass of particles in the distribution was first set at 0 (accumulated mass = 0). A random number generator (*rand* function, 2019b version, The MathWorks; www.mathworks.com) was used to generate a random cumulative mass fraction from 0 – 1. The random cumulative mass fraction value was then used to linearly interpolate (*interp1* function, 2019b version, The MathWorks; www.mathworks.com) the particle diameter from the single chew cumulative mass distribution of the 4 g portion size. The volume of the particle was then calculated using Eq. 4.3 assuming the peanut has a halved ellipsoid shape as described previously in Chapter 4. The mass of the particle was then determined by multiplying by the density, 0.00112 g/mm³ (Hutchings, 2011). There are certain conditions that the solution must satisfy in order to conserve mass. Firstly, with each run of the simulation, the mass of particle generated must be less than the pre-defined portion size minus the accumulated mass of particles generated thus far (i.e. the unaccounted-for mass required). Mathematically, this can be described as

$$M_p < M_o - \sum_i^n M_{p,i} \quad (5.1)$$

where M_p is the mass of the new particle generated, M_o is the pre-defined required portion size, subscript i refers to the number of the existing simulation loop, n refers to the total number of loops.

If the mass of the particle generated, M_p , was greater than the portion size minus the accumulated mass of particles, then the particle will be rejected, and it will be added as miss= miss + 1. The simulation is then repeated. If the generated particle satisfied Eq. 5.1, the diameter of that particle would be recorded, and the mass of the particles would be added as Accumulated mass = Accumulated mass + M_p . The simulation stopped when the total mass of all recorded particles was greater than 2 g. Because the numerical method was stochastic, the simulation was set to run for 1000 simulations. The number was chosen as it was found from trial and error that the simulation needed at least 1000 simulations to ensure the total mass will always be 2 g.

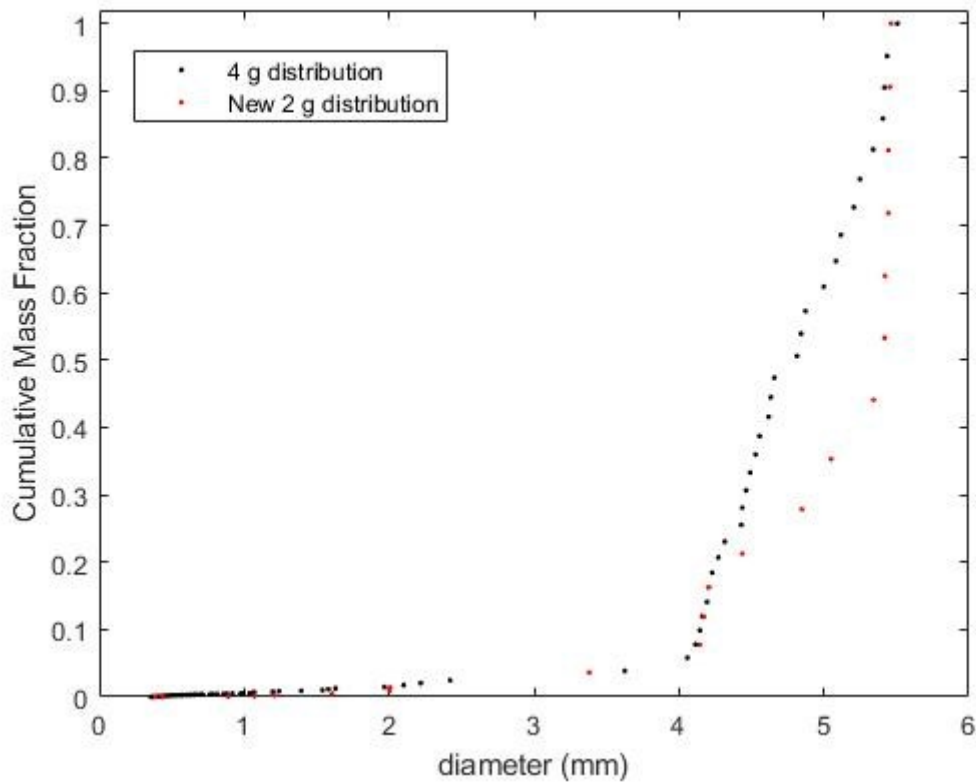


Fig. 5-3: Cumulative mass fraction vs particle size (mm) for 4 g and 2 g peanuts respectively. Red marker = 2 g PSD, Black marker = 4 g PSD. The simulation was run once.

Fig. 5-3 shows the generated PSD after a single chewing cycle for the 2 g and 4 g peanuts. Because of the randomness introduced in the simulation, this figure clearly shows the difference in PSD after a single chew for the 2 g and 4 g peanuts after 1 simulation. For example, in the 4 g peanuts, there are more particles observed in the size range between 4 to 5 mm and between 0.354 mm and 2.5 mm respectively. However, when the simulation is repeated for different number of times (5 to 1000 times) and plotted in the same graph, it can be observed that the PSD of the 2 g peanuts on average does end up the same as the 4 g peanuts (Fig. 5-4). This gives the confidence to use the numerical approach described above to generate the new PSD for the 2 g portion size.

Input 1: PSD after a single chew as a model input

Following the generation of particles as described above, the PSD of the peanut bolus after a single chew from the experimental data was used as the initial PSD input to predict the PSD at swallow point for the 2 g and the 4 g peanuts in this case study (Fig. 5-3).

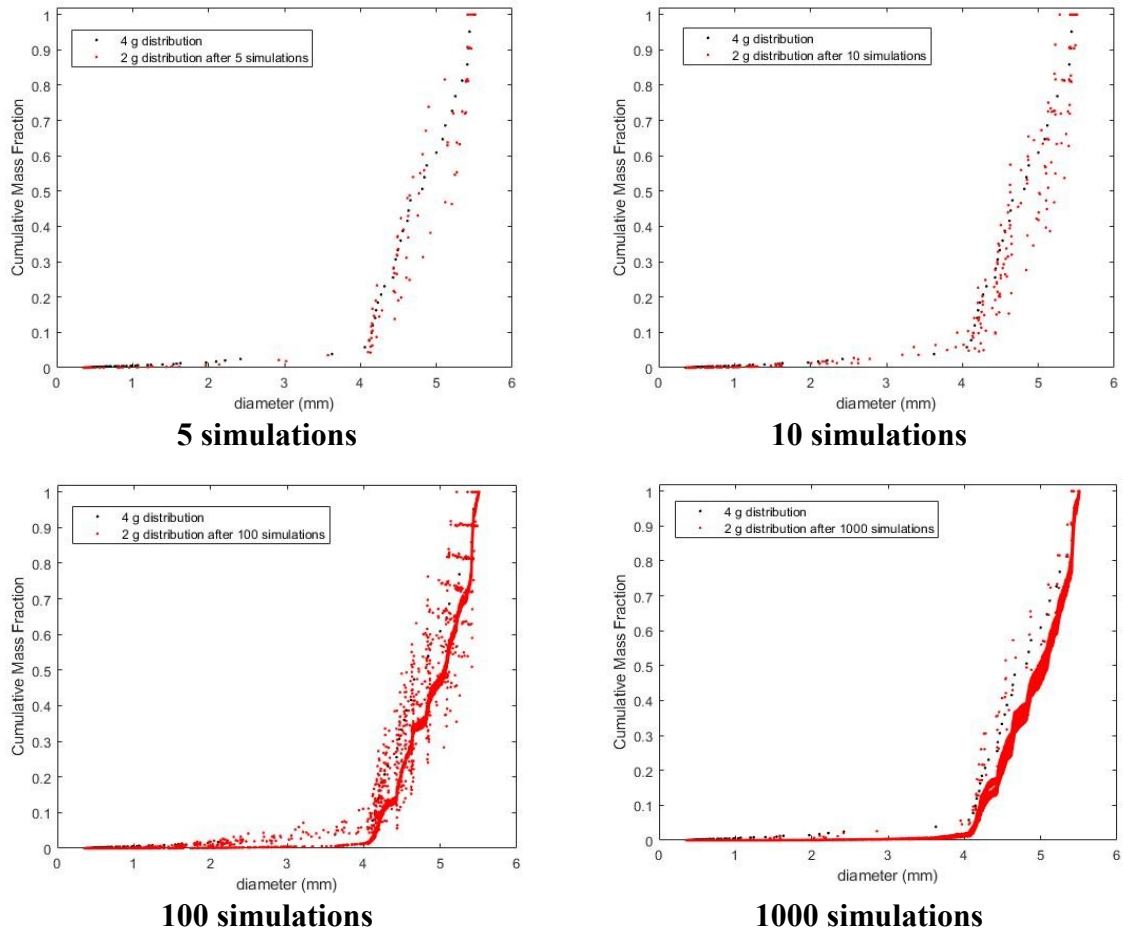


Fig. 5-4 A comparison of 4 g and 2 g peanuts PSD, where the 2 g peanuts PSD is plotted for the number of times the simulation was run (5, 10, 100 and 1000 simulations).

Input 2: Selection and breakage model input parameters

The input parameters required for the one-way and two-way selection functions are the number of particles, the number of breakage sites and the affinity factor. The degree of fragmentation variable is required for the breakage function. The full details of the input parameters required for the selection and breakage functions have been discussed previously in Chapter 3.

5.2.5 Model fitting

Similarly, to as described in Chapter 4, as one-chew experiments (as described in van der Glas et al., 1987, 1992, 2018) were not conducted to determine the selection and breakage model input parameters, the PSD outputs from the model were fitted to the experimental PSD data.

To calculate the residuals between the model outputs and the experimental data, 10 percentiles (d -values) for d_{10} - d_{90} of the cumulative volume distribution in both the model output and the experimental data were obtained.

For the 2 g peanuts, the model was set to calculate the PSD after 17 chews, which was the average natural number of chews at swallow point of the 10 subjects in Flynn (2012). To be able to understand the effect of portion size on selection, the number of chews set for the 4 g peanuts was also set at a chew number which, in the experimental data, was the closest to 17 chews (the swallow point for the 2 g peanuts). This was at 15 chews. The fitted parameters were then obtained by minimising a normalised sum of squares residuals between the model predictions and the experimental data for the 2 g (after 17 chews) and 4 g (after 15 chews) peanuts, which were run simultaneously. The PSO algorithm, as used in Chapter 4 (Section 4.3.4), was used to fit the model. The algorithm lower and upper bounds for the input parameters were also set the same as described in section 4.3.4. The fragmentation variable, r , an input parameter in the breakage function was also kept constant since the same type of peanuts were used. Thus, only the selection model input parameters were solved by the PSO algorithm, as described in Table 5-1 below. The model simulation was also repeated 50 times as the solution was shown to converge after 50 times previously in Chapter 4 (section 4.3.4.2). The R-squared coefficient was also calculated to determine the model goodness-of-fit. The full details of how the sum of squares residuals and the R-squared were calculated can be found in section 4.3.3. The model fitting provided two sets of input parameters related to each portion size studied. One set was the fitted model input parameters for the 2 g peanuts, and the other was the 4 g peanuts. A diagram, showing the steps in the process is shown in Fig. 5-5.

5.2.5 Fitted input parameters

This section outlines the results of the model input parameters to fit the PSD at swallow point at two portion sizes, 2 g and 4 g peanuts respectively. Because the focus of this section is to understand the different mechanisms of the selection process when the initial portion size is varied, the one-way or the two-way competition models were applied, and the model predictions were compared.

Table 5-1: Upper and lower bounds set in the PSO algorithm to fit the model to predict the PSD for 2 g and 4 g portion sizes.

Parameter	Selection model inputs				Breakage model
	Number of breakage sites		Affinity factor		input
	<i>Multiplication factor, k</i>	<i>Power, m</i>	<i>Multiplication factor, p</i>	<i>Power, q</i>	<i>Fragmentation variable, r (2.91)</i>
Upper bound	90	1	0.007	1	-
Lower bound	500	3	0.004	3	-

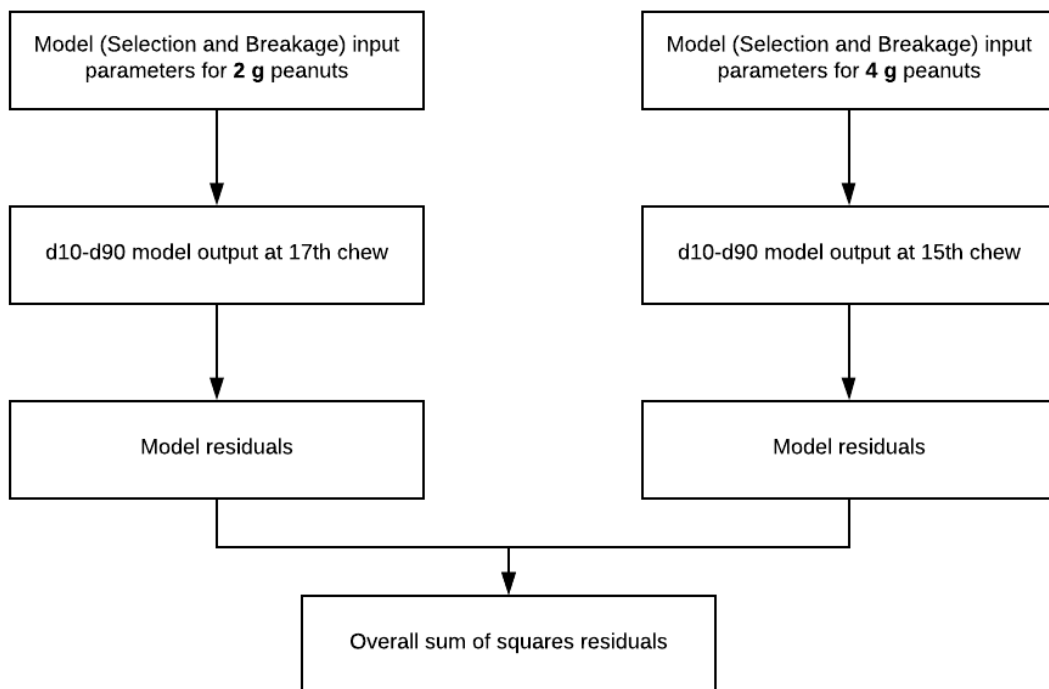


Fig. 5-5: The schematic diagram to take readers through the steps taken to minimise the sum of squares residuals to obtain the input parameters required to fit the particle size output for the 2 g and 4 g peanuts.

Table 5-2: Best fit model input parameters solved by the PSO algorithm to predict the PSD at swallow point for the 2 g and 4 g peanuts. The input parameters of 4 g peanuts when fitted with data of various number of chews in section 4.4.1 (Table 4-3) is also added for comparison.

Selection model	Selection model inputs				Breakage model input	Global best fitness		
	Portion size (g)	Number of breakage sites, n_b		Affinity factor, O_1		value (Normalised SS residuals)	R-squared	
		Multiplication	Power,	Multiplication				Power,
		factor, k	m	factor, p				q
<i>One-way competition</i>	2	242.02	2.35	0.0009	2.21	2.91	0.002	0.99
<i>One-way competition</i>	4	242.02	2.39	0.0015	2.06	2.91	0.028	0.99
<i>Two-way competition</i>	2	236.58	1.64	0.0018	1.46	2.91	0.024	0.99
<i>Two-way competition</i>	4	236.58	1.96	0.0017	2.13	2.91	0.015	0.99

The fragmentation variable, r , in the breakage model was kept the same. The best-fit parameters for the two selection models are shown in Table 5-2. A comparison between the predicted and the experimental d-values is shown in Fig. 5-6. The results illustrated in Fig. 5-6 show that the model closely predicts the experimental data, with an R^2 value of 0.99. The model predicts the PSD at the 17th chew for the 2 g peanuts and the 15th chew for the 4 g peanuts. It is observed that the largest difference between the two portion sizes are the d_{50} , d_{60} , d_{70} , d_{80} and d_{90} and these differences are larger for the 4 g peanuts. Both the one-way and two-way competition models fitted the experimental data well ($R^2 = 0.99$). When fitted using the one-way competition model, the absolute value of the power m in the power function describing the number of breakage sites and particle size relationship for both portion size of peanuts was greater than 2. A value larger than 2 would be expected if the number of breakage sites is determined by a combination of projected area (X^2) of individual particles and a degree of piling at the initiation of breakage (van der Glas et al., 2018). Therefore, the decrease in the number of breakage sites as particle size increases will be larger than $1/X^2$ (van der Glas et al., 1992).

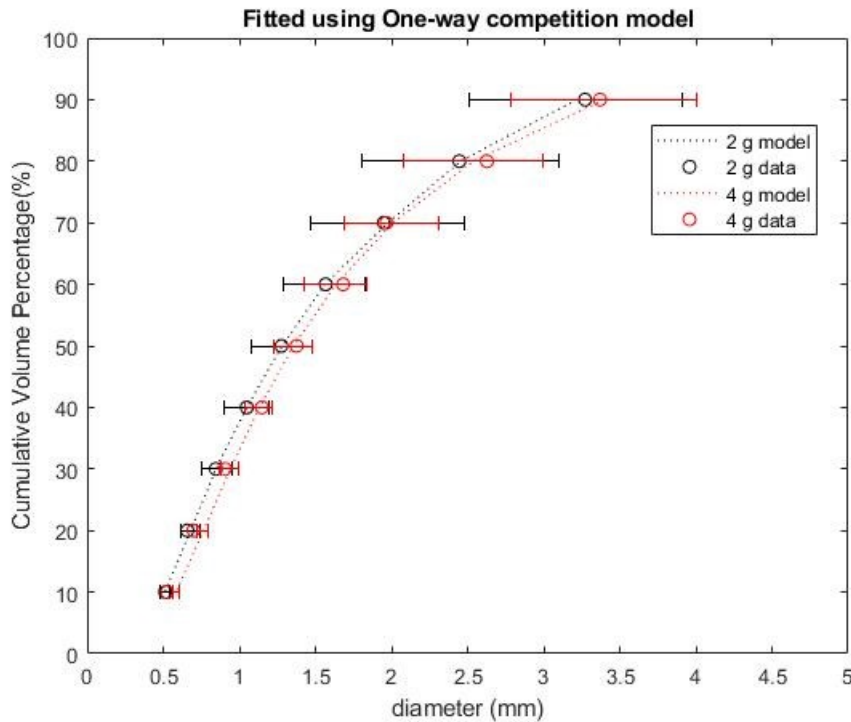


Fig. 5-6: A comparison between model predictions and experimental data of the PSD at swallow point for 2 g and 4 g peanuts. The one-way competition model was used to predict particles that were selected. An R^2 value of 0.99 shows the goodness of fit of the model.

The multiplication factor, p in the power-law model (describing the affinity factor and particle size relationship) was higher for the 4 g peanuts. The results are mainly caused by the fact that the 4 g peanuts would have contained a higher number of larger particles compared to the 2 g peanuts. The affinity factor is known to increase with particle size (van der Glas et al., 1992, 2018). It is also related to the ability of the teeth and the tongue to capture particles for breakage (van der Glas et al., 2018). The increase in the particle size, in principle, can give rise to increased effectiveness of the teeth and the tongue to select particles for breakage.

There was no notable difference between the model input parameters between the 2 g and 4 g portion sizes when the two-way model was applied. The main difference between the two portion sizes will be the most different in the volume of larger particles than for the volume of smaller particles. However, since the two-way model assumes that the small particles can be selected as well as the large particles, the small difference between the two portion size is not surprising because the larger the particle size, the higher the affinity and the smaller the particles size, the higher the number of breakage

sites. Therefore, no size of particles (large or small) will be favoured according to the two-way competition model, hence the reason for the small difference in the model input parameters.

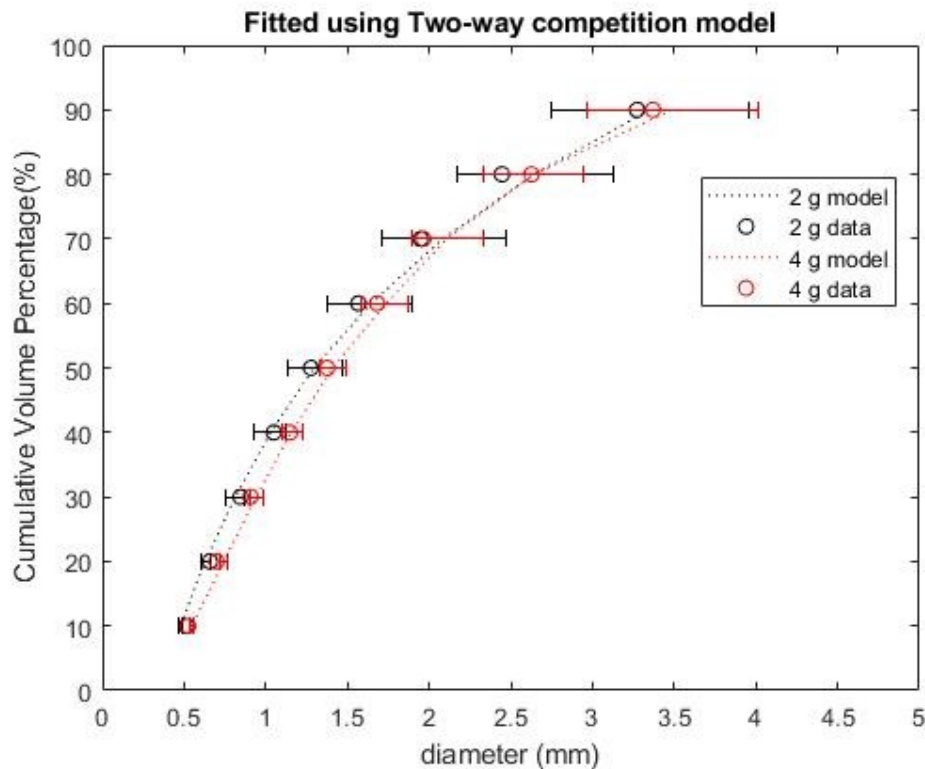


Fig. 5-7: A comparison between model predictions and experimental data of the PSD at swallow point for 2 g and 4 g peanuts. The two-way competition model was used to predict particles that were selected. An R^2 value of 0.99 shows the goodness of fit of the model.

5.3 Case study two: Understanding the breakage function of peanuts with different initial moisture contents

The second study aimed to understand if the differences in Particle Size Distribution (PSD) of peanuts of varying initial moisture content can be explained by differences in the breakage function. The study from Hutchings (2011) showed that the d_{50} of peanut bolus increases when initial moisture content increases when a 26 year old male had chewed five peanut variants of 1 g portion size. Four of the peanut variants were removed from food matrices (after moisture absorption had occurred) and one was a control (peanuts not prepared in a matrix). The aim of the study in Hutchings (2011) was to quantify the effect of preparation inside the matrices (gelatine gel, chocolate, scones and brownies) on the particle size outcome of the peanuts (because of the physical changes in the peanuts during baking or

setting inside the matrices). Nevertheless, in his preliminary experiments the peanuts also had different initial moisture contents. The parameters of mastication of the five peanut variants that were removed from matrices (prior to chewing) are shown in Table 5-3 below.

The cumulative PSD of the peanut particles in the food bolus for the five peanut variants in Hutchings (2011) is shown in Fig. 5-8. The data in Fig. 5-8 was presented on a cumulative surface projected area fraction basis by imaging of the particles on a flatbed scanner. To allow comparison with modelling, the data was subjected to additional processing to convert it into a cumulative volume fraction basis (the MATLAB code can be referred in Appendix A). In order to demonstrate this, the cumulative area distribution from the 7.2% moisture peanuts is presented.

Table 5-4 illustrates the original cumulative area distribution, $F(s)$ data for all peanuts that were removed from different matrices, presented in terms of the initial moisture content from Hutchings (2011). The data was extracted from Fig. 5-8 using WebPlotDigitizer version 4.3 (<https://automeris.io/WebPlotDigitizer>).

Table 5-3: Mastication parameters for the five peanut variants from Hutchings (2011)

Matrix (which the peanuts were removed from)	Moisture content (gH₂O/100g total mass)	Number of chews	Chewing time (s)	Mastication frequency (s⁻¹)	Volume of peanuts in bolus (mm³)
Scone	7.2 ± 0.35	7.8 ± 0.4	5.04 ± 0.18	1.58 ± 0.03	1640 ± 70
Gelatine gel	3.43 ± 0.10	7.5 ± 0.3	4.57 ± 0.10	1.64 ± 0.03	1350 ± 40
Brownie	2.69 ± 0.32	7.5 ± 0.3	4.76 ± 0.15	1.58 ± 0.04	1270 ± 20
Chocolate	1.94 ± 0.07	7.0 ± 0.4	4.57 ± 0.06	1.53 ± 0.02	1020 ± 40
Peanuts only	1.99 ± 0.10	7.8 ± 0.2	5.00 ± 0.16	1.55 ± 0.05	980 ± 20

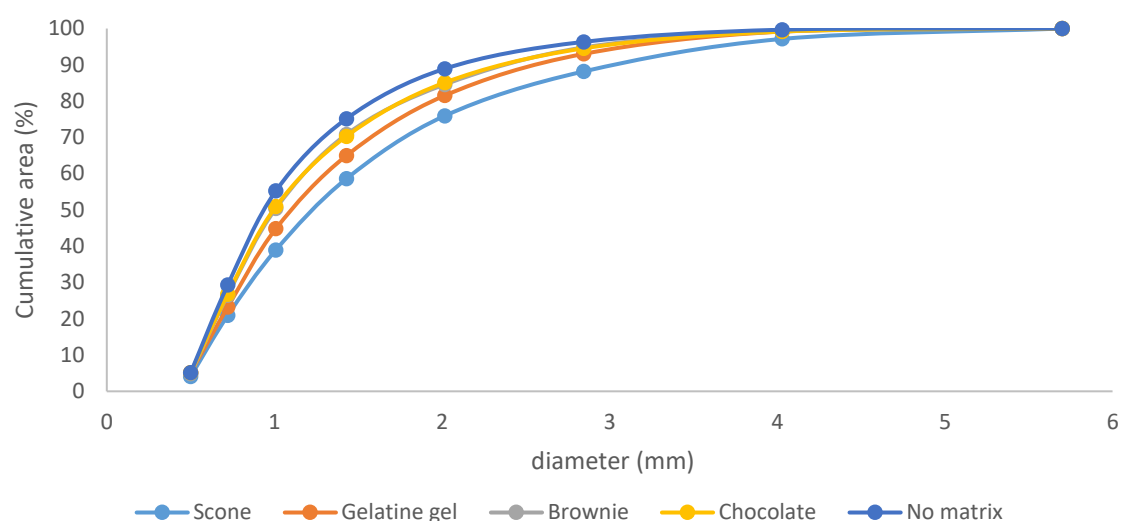


Fig. 5-8: The cumulative PSD of peanut particles in the food bolus where peanuts were served after they were removed from food matrices. Light blue marker, peanuts removed from scone (7.8 chews); Orange marker, peanuts removed from gelatine gel (7.5 chews); Grey marker; peanuts removed from brownie (7.5 chews), Yellow marker, peanuts removed from chocolate (7 chews); Dark blue marker, peanuts with no matrix (7.8 chews). 1 g portion of peanuts. Figure from Hutchings (2011).

Table 5-4: Cumulative area distribution data for the peanuts after being removed from different matrices, presented in terms of their varying moisture contents (MC) (Hutchings, 2011).

diameter (mm)	$F(s)$ (%)				
	7.2% MC (Scone)	3.4% MC (Gelatine gel)	2.7% MC (Brownie)	2.0% MC (No matrix)	1.9% MC (Chocolate)
0.50	4.10	5.11	4.86	5.11	5.11
0.72	20.90	23.19	26.49	29.29	26.75
1.01	38.98	44.83	50.43	55.27	50.94
1.43	58.59	64.95	70.81	75.13	70.29
2.02	75.93	81.52	84.58	88.91	85.09
2.85	88.18	93.01	94.79	96.32	94.54
4.03	97.14	99.18	99.18	99.68	99.18
5.70	100.00	100.00	100.00	100.00	100.00

Two extra data points were then added in Table 5-4 so that the $F(s)$ value will start at 0 %. Table 5-5 shows the $F(s)$ data with the added data points. Because the existing data is not sufficient for comparison against model predictions (all the percentiles used in fitting were not directly available), the intermediate $F(s)$ values were calculated by simple linear and curved interpolation of a diameter series. A diameter series numbered between 0 and 6 with an increment of 0.05 was created. The $F(s)$ values for the diameter between 0 and 0.47 mm were linearly interpolated, whereas the diameter between 0.47 to 6

mm was interpolated using a curve interpolation method. All interpolation was performed using the *interp1* function from MATLAB. Fig. 5-9 shows the original and the newly interpolated cumulative area data for the peanuts in the scone matrix.

Table 5-5: Cumulative area distribution data (with extra points) for the peanuts after being removed from different matrices, presented in terms of their varying moisture contents (MC).

diameter (mm)	$F(s)$ (%)				
	7.2% MC (Scone)	3.4% MC (Gelatine gel)	2.7% MC (Brownie)	2.0% MC (No matrix)	1.9% MC (Chocolate)
0	0	0	0	0	0
0.47	0	0	0	0	0
0.50	4.10	5.11	4.86	5.11	5.11
0.72	20.90	23.19	26.49	29.29	26.75
1.01	38.98	44.83	50.43	55.27	50.94
1.43	58.59	64.95	70.81	75.13	70.29
2.02	75.93	81.52	84.58	88.91	85.09
2.85	88.18	93.01	94.79	96.32	94.54
4.03	97.14	99.18	99.18	99.68	99.18
5.70	100.00	100.00	100.00	100.00	100.00

The first step to convert into a cumulative volume fraction basis was to first change the $F(s)$ data to a probability density function, $f(s)$. This is done by calculating the derivative of $F(s)$. After differentiation, the $f(s)$ value was normalised with the total $f(s)$ value to ensure the area under the curve value is equal to 1. Fig. 5-10 shows the new $f(s)$ plot. The $f(s)$ data could now be converted to a volume fraction basis, $f(v)$. This was done by multiplying the $f(s)$ data with the diameter series data. The $f(v)$ data was also normalised with the total $f(v)$ value to obtain values under 1. Fig. 5-11 shows the $f(s)$ and the newly computed $f(v)$ data plotted in the same graph. The cumulative volume distribution function, $F(v)$ can then be calculated from the probability density function by computing the cumulative sum. The computed $F(v)$ data is shown in Fig. 5-12. The above shows the steps taken to convert the cumulative projected surface area data to a cumulative volume fraction data for the 7.2% moisture peanuts (recovered from the scone matrix). The same steps were employed for the other peanut chewing data. The cumulative volume fraction results for all of the peanuts is shown in Fig. 5-13 below. Using these

data (in cumulative volume fraction form), it was then possible to compare the model predictions to the experimental data.

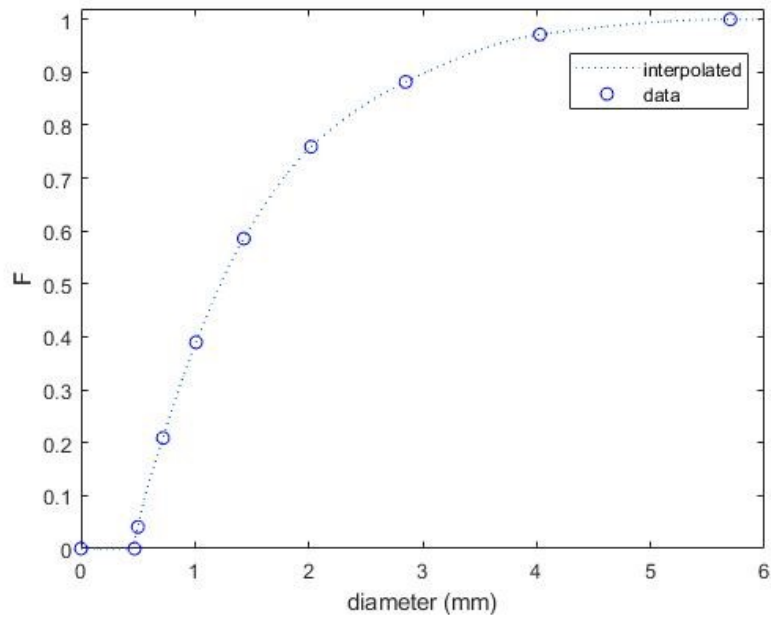


Fig. 5-9: The new interpolated $F(s)$ data is denoted by the blue dotted lines, and the circle marker is the original data.

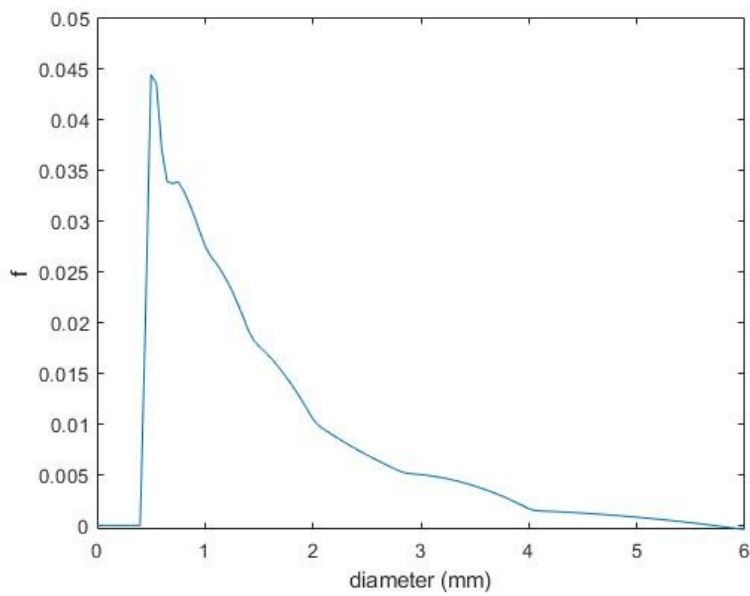


Fig. 5-10: The probability density function, $f(s)$.

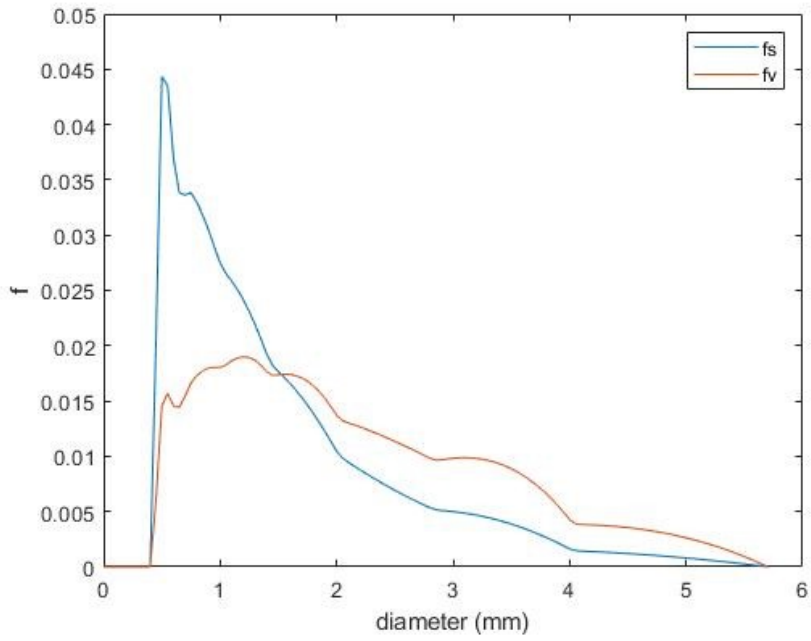


Fig. 5-11: The probability density function for the projected surface area, $f(s)$ and the volume, $f(v)$.

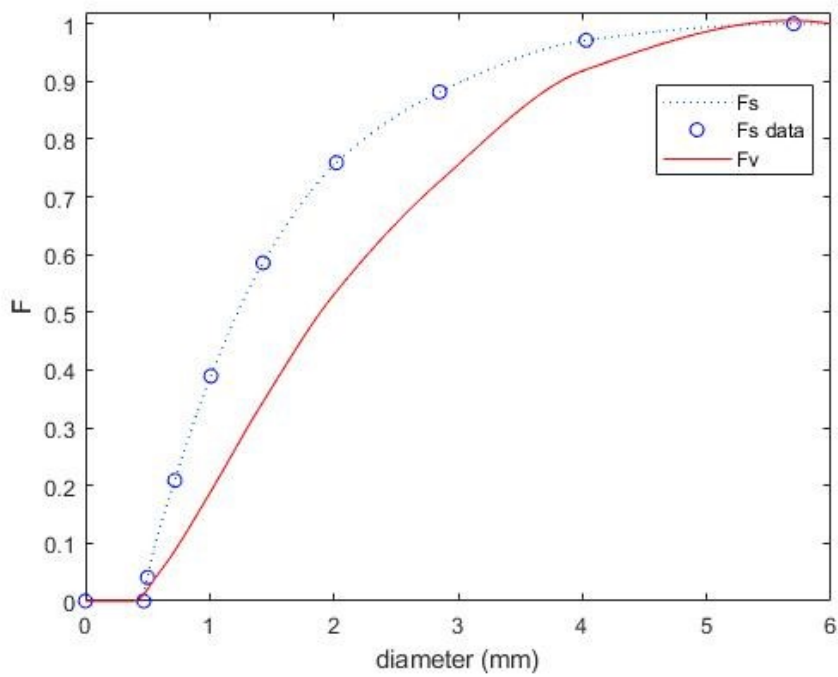


Fig. 5-12: The original $F(s)$ data (blue round marker); The interpolated $F(s)$, blue dotted line; The cumulative volume fraction $F(v)$, red solid line.

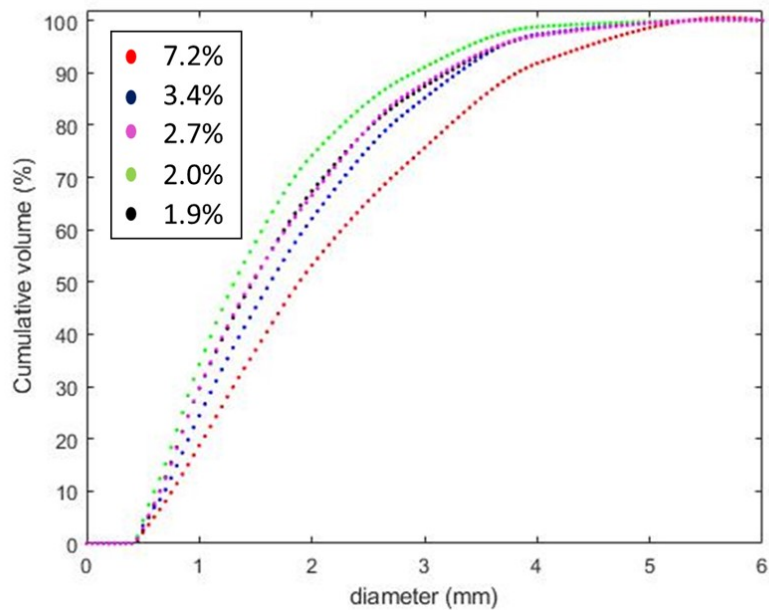


Fig. 5-13: Cumulative volume (%) for peanuts after they were removed from matrices measured at swallow point.

5.3.1 The model

Similar to case study one, the model consisted of selection and breakage sub-models. Each will be discussed.

5.3.1.1 Selection equations

The two-way competition model (Eq. 2.5) was used to describe the particle selection as it has been demonstrated to be sufficiently adequate to describe particle selection during an entire chewing sequence if chewing is started on a number of large particles (van der Glas et al., 2018). In addition, this case study aimed to understand the breakage functions of food, therefore using one selection model was sufficient as the different mechanisms of selection were not be explored. The peanuts were served in all cases with the same portion size and therefore selection should not vary.

5.3.1.2 Breakage model equation

Similar to case study one, the Austin (1971) breakage model (Eq. 2.10) was applied. Because the model is mechanistic, the fitted parameter from the model can also be used to explain the breakage properties of different food conditions during mastication (e.g. the effect of the initial moisture content on the

breakage properties of peanuts). In addition, the breakage model also consists of one fitted parameter which reduces the degree of freedom for the optimisation.

5.3.1.3 Discretised population model

The PSD was predicted using the discretised population balance model developed as described in section 3.2.3.

5.3.2 Model inputs

Input 1: PSD after a single chew as a model input

The PSD of the peanut bolus after a single chew from the experimental data was used as the initial PSD input to predict the PSD at swallow point for the 2 g and the 4 g peanuts in case study one. In case study two, which was based on Hutchings (2011), the mass of the peanuts served was 1 g. The same method employed in section 5.2.1 was used to ensure the mass of peanuts was always 1 g. Fig. 5-14 below shows the generated 1 g distribution after a single chew from Hutchings (2011) when compared against the 4 g distribution after a single chew from Flynn (2012).

Input 2: Selection and breakage model input parameters

The input parameters required for the two-way competitive model are the number of particles, the number of breakage sites and the affinity factor. The degree of fragmentation variable is required for the breakage function. The full details of the input parameters required for the selection and breakage functions have been discussed previously in Chapter 3.

5.3.2 Model fitting

The same model-fitting approach that was taken in section 5.2.4 was employed to fit the model for the peanuts of different moisture contents which were removed from matrices from Hutchings (2011). The ten cumulative volume percentile diameters (d_x -values) were extracted from the model output and the experimental data at swallow point, where the sum of squares residuals was minimised with a PSO algorithm to find the best-fit input parameters. Although a similar approach was taken in section 5.2.4, this work differs in the number of input parameters solved by the PSO algorithm. Because the subject in Hutchings (2011) is a different person to the subject in Flynn (2012), all of the selection input parameters including the multiplication constant, k , were solved by the PSO algorithm. It was thought

that the difference in breakage function of the peanuts in matrices was the reason for the difference in PSD at swallow point (Hutchings, 2011). For this reason, the PSO algorithm was set up in such a way to solve one set of selection model input parameters and five sets of input parameters relating to the breakage function. Fig. 5-15 presents a diagram to understand this process, where the algorithm is solved for one set of selection model input parameters (as it is based from the same person) and one fragmentation variable, r , for each peanut system.

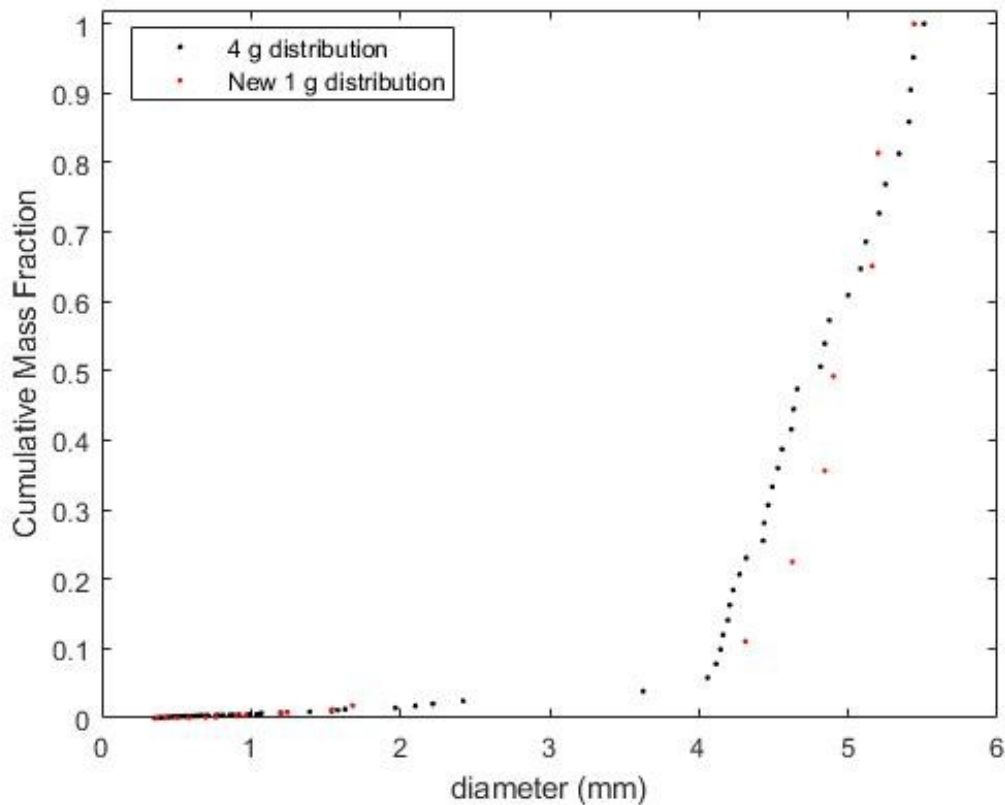


Fig. 5-14: Cumulative mass fraction vs particle size (mm) for 4 g and 1 g peanuts respectively. Red marker = 1 g PSD, Black marker = 4 g PSD.

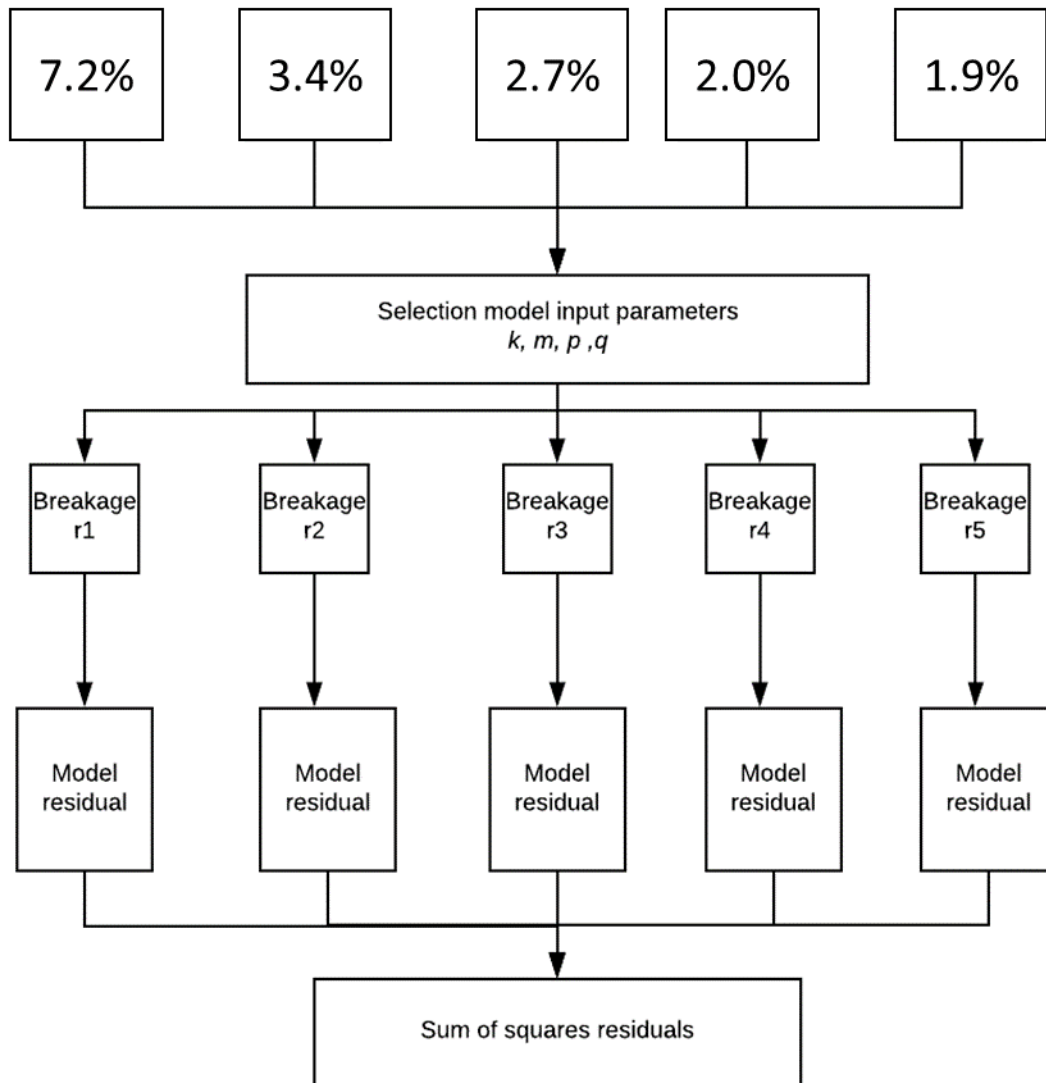


Fig. 5-15: A schematic diagram showing the steps undertaken to solve model input parameters for peanuts with different moisture contents after being removed from matrices when chewed at swallow point. The algorithm solves for one set of selection input parameters and five sets of breakage input parameters.

5.3.3 Fitted input parameters

Hutchings (2011) observed that higher moisture peanuts (after being removed in matrices), had a larger median particle size in the bolus at swallow-point. He proposed that the moisture content affects the physical properties of the peanut particles, which in turn influences the breakage function and the resulting particle size. The purpose of this section was to test this hypothesis. This is done by examining the input parameters which have been fitted to the observed data without bias and ask the question ‘Does the model predict more breakage for drier peanuts?’ on the role of breakage function in affecting the resulting particle size is tested in this section by model fitting.

The model output was best-fit to the experimental particle size data to determine the breakage input parameters in each type of peanuts studied. The two-way competition model was used to describe particle selection as it has been demonstrated to be sufficiently adequate to describe particle selection during an entire chewing sequence if chewing is started on a number of large particles (van der Glas et al., 2018). No variable was kept constant in the selection function for this case study as the subject (Hutchings, 2012) was different from the subject in section 6.6.1 (Flynn, 2012) and therefore is likely to have had different occlusal area and chewing behaviour. The best-fit parameters for the five different peanuts at the swallow-point are shown in Table 5-6 below. Fig. 5-16 shows the comparison between the fitted-model and experimental data of the PSD at swallow point for the five peanuts of different moisture contents that were removed from matrices.

Based on the best-fit results in Table 5-6, the following observations were made. The multiplication factor, k , in the power function describing the number of breakage sites and particle size relationship was 362.62, which is in good agreement with the range of values obtained in van der Glas et al. (2018). The power, m of the power function was greater than 2, which indicated that the number of breakage sites for all of the peanuts used in this study was dependent on a combination of projected area (X^2) of individual particles and a degree of piling at the initiation of breakage. The multiplication factor, p and the power q in the power function describing the affinity factor found in this study corroborates with the range of values obtained in van der Glas et al. (2018). The results of the fragmentation variable, r , which is an input parameter in the breakage function was highest for the peanuts of 2.0% moisture

content (2.05) and lowest for peanuts of 7.2% moisture content (1.02). The result agrees to the hypothesis being tested, that dryer peanuts will fragment more (a larger value of r denotes a greater degree of fragmentation of a particle, effectively the size distribution of broken particles (van der Glas et al., 1992; Lucas and Luke 1983a)). The results obtained from this study helps justify that the physical properties of the peanuts affect the breakage function from the different values of r obtained as seen in Table 5-6.

Table 5-6: Best fit model input parameters solved by the PSO algorithm to predict the PSD at swallow point for the five peanuts that were removed from matrices at different moisture contents. A good agreement between the model and data is found (R-squared > 0.96 for all peanuts)

Selection model of peanuts (%)	Moisture content of peanuts (%)	Selection model inputs				Breakage model input Fragmentation variable, r	Global best	
		Number of breakage sites, n_b		Affinity factor, σ_1			fitness value (Normalised SS residuals)	R -squared
		Multiplication factor, k	Power, m	Multiplication factor, p	Power, q			
<i>Two-way competition</i>	7.2	362.62	2.34	0.0016	2.27	1.02	0.015	0.98
<i>Two-way competition</i>	3.4	362.62	2.34	0.0016	2.27	1.33	0.015	0.98
<i>Two-way competition</i>	2.7	362.62	2.34	0.0016	2.27	1.69	0.004	0.99
<i>Two-way competition</i>	2.0	362.62	2.34	0.0016	2.27	2.05	0.045	0.96
<i>Two-way competition</i>	1.9	362.62	2.34	0.0016	2.27	1.69	0.008	0.99

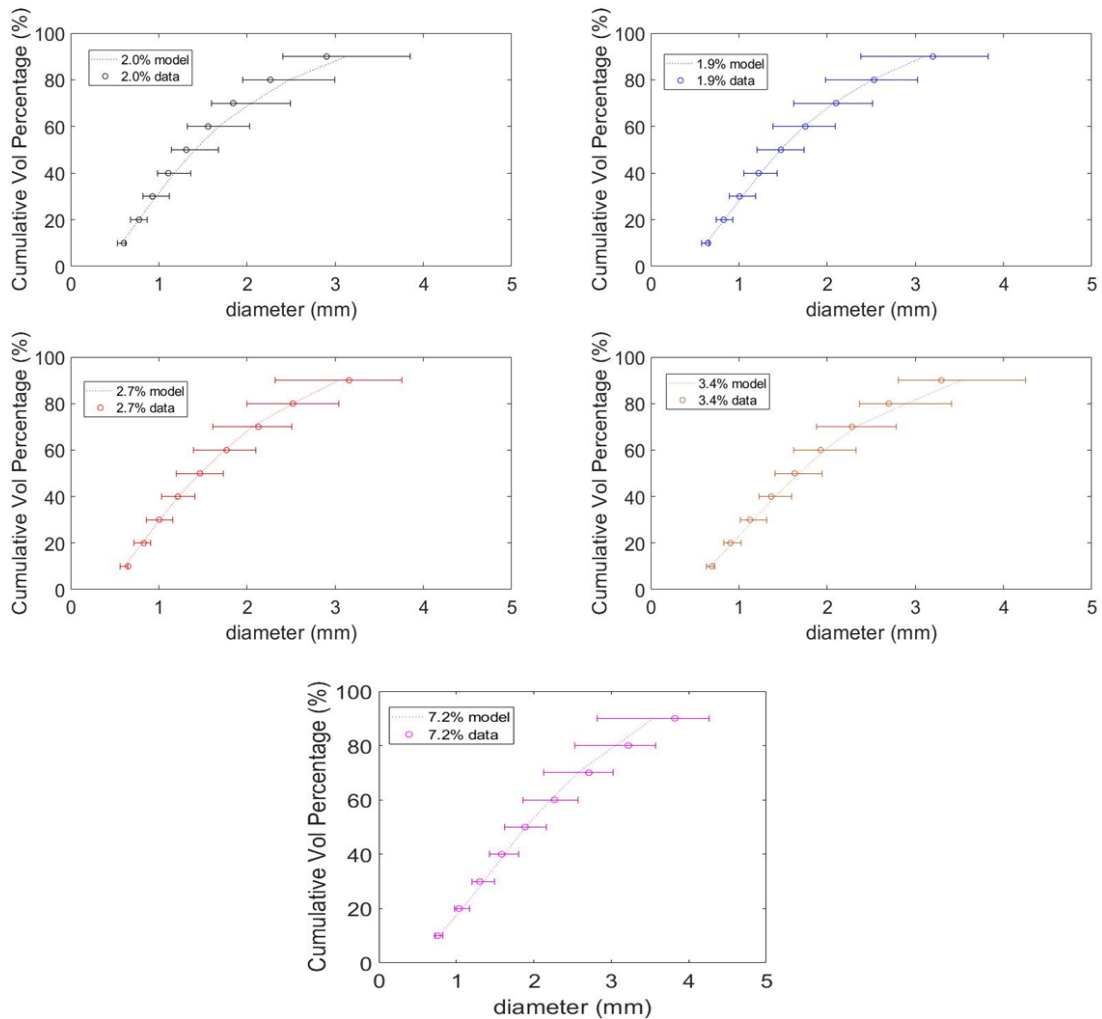


Fig. 5-16: A comparison between model predictions and experimental data of the PSD at swallow point for the five peanuts that were removed from matrices and have different moisture contents. Dotted lines are model predictions and open circles are the data. The error bar is the standard deviation of the model predictions after 50 simulations.

5.4 Chapter conclusion

In this chapter, two case studies were presented to test the application of the models developed in Chapter 3 in providing useful information for food design. The first aimed to understand which of the one-way or two-way competition models were more appropriate when the portion size of peanuts was varied. The second aimed to interrogate the model parameters, which were optimised without bias, to see whether they self-adjusted to reflect the variation in the physical properties of the peanuts.

The results of the first case study showed that the one-way competition model was sufficient to describe the particle selection for both the 2 g and 4 g peanuts. The 4 g portion had more peanuts, with a smaller fraction selected each chew, which was reflected by a higher power function describing the affinity factor when the one-way model was applied. The results of the second case study showed that

the value of the degree of fragmentation (r) varied to the changes in the initial moisture content, i.e., higher moisture content had lower r , hence coarser PSDs. The findings of the study are important because they help justify that the physical properties of the peanuts affect the breakage function.

The chewing models developed in Chapter 3 were successfully applied to peanuts to justify their application for food design. The next step will be to expand the models to account for a novel food system for which chewing influences digestion and sensorial outcomes. This aspect will be explored in the next few chapters.

Chapter 6 Influence of mastication on aroma release of rice

6.1 Introduction

During oral processing, the breakdown of particle size results in an increase in the surface area of food particles. The creation of new surfaces exposes volatiles and so helps their release by volatilisation and diffusion along a vapour pressure gradient. Taste and aroma compounds are then detected by the olfactory receptors in the nasal cavity (Chen, 2015). Harrison et al. (1998) modelled *in vivo* aroma release during chewing of solid foods and showed that it is dependent on selection and breakage functions during mastication. However, the model was never validated with experimental data. The most comprehensive validated model of aroma release during oral processing of solid foods was developed by Doyennette et al. (2014) for cheese. In a sensitivity analysis, they showed that the air-bolus contact surface area could affect aroma release, but the model was simplified by assuming that the bolus surface area increases linearly with time.

To date, there is still a gap in the literature in developing a validated and comprehensive mechanistic model that couples both mastication and mass transfer principles to predict flavour release, particularly for starch-based food systems. The chewing models can be integrated with flavour release to predict time-intensity flavour release profiles. If successful, the simulations can be used to formulate foods with a specific flavour profile, accounting for individual or group differences in chewing behaviour (Harrison et al., 1998).

Before the model was formulated, it was important to conduct *in vivo* experiments to provide insights on the role of chewing on the flavour release of a starch-based food system. The results of the experiments will help to understand specific mechanisms in chewing that affects aroma release so that a robust conceptual model and its relevant assumptions can be developed. Furthermore, the experimental data will also be used to validate model predictions.

Prior to the *in vivo* study, a series of experiments were conducted to select a novel starch-based food system for the model implementation. When the bolus properties of three different starch-based food systems were compared, it was found that cooked white rice was the most suitable food system as:

1. The bolus PSD and saliva content of cooked rice showed strong correlations with digestion in an *in vitro* study (see Appendix E for further details of this study).
2. It was found that the bolus saliva content increases linearly in all subjects with increasing mastication stages, which allowed a constant saliva flow rate to be assumed in the model (see Appendix F for further details of this study).
3. Cooked rice forms a particulate bolus during chewing which allows the competitive selection models to be used.
4. When the bolus losses were compared against two other starch-food systems, cooked rice had the highest bolus recovery (80-95%) (readers are referred to Appendix F for further details of this study).
5. Cooked rice is an aromatic food system.

The above reasons justified that the reasons why cooked rice was chosen as the food system for model application. Thus, the main objective of this chapter is to consider how the selection-breakage model could be adapted to the aroma release of cooked white rice. These factors could be identified by comparing the results of the physiological, oral processing, and aroma release parameters measured for five subjects against a conceptual model hypotheses. Hence, the study was divided into four sub-objectives:

1. To develop a conceptual model which links the subject's physiological and oral processing parameters to aroma release.
2. To measure the physiological variables for five subjects *in vivo*.
3. To measure the dynamics of bolus formation during oral processing of white rice for five subjects *in vivo*;
4. To measure the dynamics of aroma release during oral processing of white rice for five subjects *in vivo*.

6.2 Conceptual model relating the physiology and oral processing to aroma release

To explore the link between aroma release and the causative factors of physiology and oral processing, the related work on this topic was briefly reviewed. The retronasal aroma release during food consumption has been shown to depend on the physical structure of food, the physiology of the subject and their oral processing in the mouth (Foster et al., 2011; Ruijschop et al., 2011; Frank et al., 2012; Feron et al., 2014; Labouré et al., 2014; Jourdren et al., 2016;). The velum openings, swallowing, aroma interactions with the oral mucosa, the volume of the nasal cavity and the breath air flow rate and frequency were shown to impact retronasal aroma release when liquid and semi-liquid foods were consumed during *in vivo* experiments (Buettner et al., 2002; Trelea et al., 2007). For dairy-based products such as cheese, subjects who had the highest chewing activity, mouth coating and velum opening had the highest level of aroma release (Feron et al., 2014; Labouré et al., 2014).

Oral processing has been related to aroma release. For instance, the moisture content and the rheology of the bolus at swallow point have been shown to influence aroma release during consumption of model cheeses (Feron et al., 2014; Labouré et al., 2014; Guichard et al., 2017). However, for more semi-solid and solid-based products, the oral processing time is longer, requiring more chewing and tongue manipulation, and so these factors are also expected to be important to aroma release (Frank et al., 2012; Forde et al., 2017). Indeed, the bolus particle size distribution, which dynamically changes during mastication, has been shown to affect aroma release through a mechanistic model (Harrison et al., 1998; Doyennette et al., 2014). Breakdown generates new surface area, which helps expose and release taste and aroma compounds from the food matrix that are then detected by the olfactory receptors in the nasal cavity (Chen, 2015). Harrison et al. (1998) predicted using their model that *in vivo* aroma release during chewing of solid foods is dependent on selection and breakage functions during mastication, but the model was never validated with experimental *in vivo* data. Similarly, Doyennette et al. (2014) developed a mathematical model of *in vivo* aroma release of cheese and showed that the air-bolus contact surface area is essential. Despite these inferences from theoretical analysis,

there have been few attempts to experimentally relate the bolus particle size distribution to aroma release (Foster et al., 2011; Bornhorst et al., 2013; Doyennette et al., 2014).

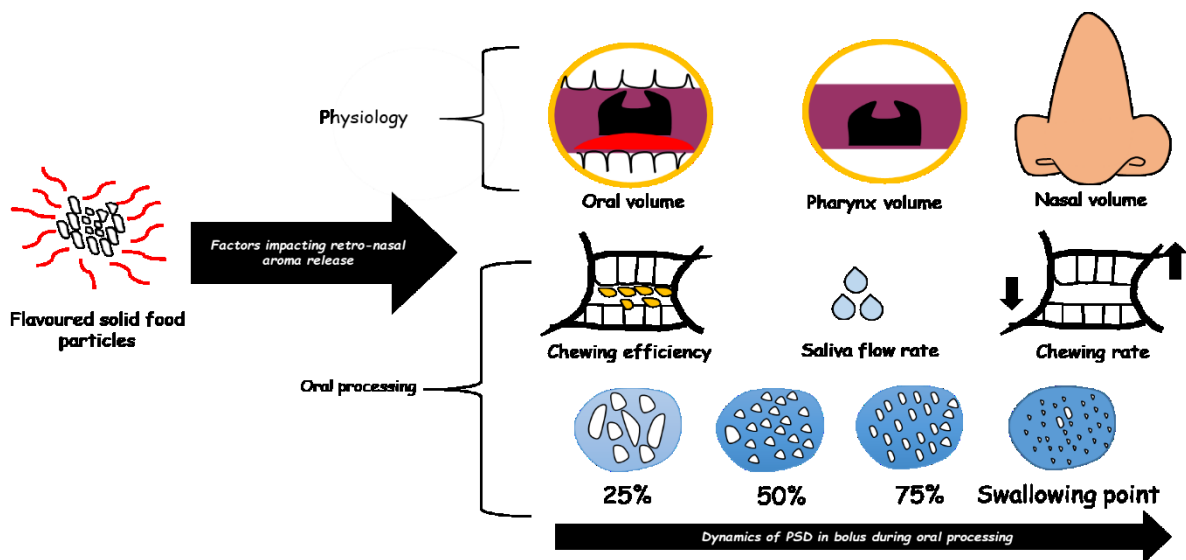


Fig. 6-1: A diagram to demonstrate the possible factors that can influence aroma release. Physiological parameters such as oral volume, pharynx volume and nasal volume can affect aroma release. Oral processing variables include the mastication efficiency, saliva flow rate, chewing frequency (rate) and the dynamics of the particle size distribution (PSD).

The above discussion demonstrates the clear link between aroma release and the causative factors of physiology and oral processing (Fig. 6-1). The interaction between these factors forms the basis for a concept-model, explained below.

Physiologically, subjects who have a large oral volume will also have a correlated large saliva flow rate at rest (Jourden et al., 2016). Thus, it would be expected that these subjects perceive a low retronasal aroma release because the saliva will coat, absorb and dilute the flavour compounds as they release from the food matrix during mastication (Doyennette et al., 2014). A second factor is a nasal volume. In a computer simulation of aroma release from yoghurts, subjects with small nasal volumes gave high-intensity peaks followed by a sharp decrease in the volatile concentration, while subjects with large nasal volumes gave low-intensity peaks but longer signal duration (Trelea et al., 2007). The third factor is pharynx volume, but this has not been shown to influence the aroma release (Doyennette et al., 2014), although it is possible that the pharynx volume may have an effect if the velopharyngeal opening is enormous, allowing a larger volume of air to exchange between the oral and the pharynx

cavities. It is also possible that with a larger pharynx, a larger layer of food deposits may remain as food residues in the pharynx, allowing the further release of aroma after mastication.

In terms of the effect of oral processing behaviour, three factors influence retronasal aroma detection. First, subjects with high masticatory efficiency and a high chewing rate are expected to produce a broader and finer particle size distribution during mastication. Subjects who produce boluses with smaller particles will have created more surface area and so are expected to perceive a higher retronasal aroma release intensities due to a faster release and movement of the taste and aroma compounds from the food matrix into the saliva and vapour phases. Second, subjects who have high saliva production rates are expected to have a weak perception of aroma release because of the reasons explained earlier. Lastly, subjects who have more food residues remaining in the mouth might perceive a more intense and lingering aroma released after swallowing. This completes the simple concept-model which forms the hypotheses of expected behaviour to compare against experimental data.

6.3 Materials and methods

6.3.1 Choice of the food system

No previous studies have looked at the influence of food oral processing on the retronasal aroma release of white rice. This study can be useful for parts of the population in the world that consume white rice in their diet, due to its impact on health issues when consumed excessively. For instance, white rice has been shown to significantly increase the risk of type 2 diabetes, especially among Asian (Chinese and Japanese) populations (Hu et al., 2012). In some parts of Asia, such as Malaysia and Singapore, rice is often flavoured with liquid products of high-fat content such as coconut milk and chicken broth or fried with a high amount of vegetable cooking oil, causing obesity issues (Nidhi et al., 2010; Lani et al., 2015; Umachandran et al., 2018). As such, improved understanding on what effects chewing of rice and the resultant impact on aroma release is useful.

6.3.1.1 Cooking recipe

White Jasmine rice (*Oryza sativa* L.) was purchased from a local supermarket (Auchan, Plaisir, France). Rice was cooked using a 1:2 ratio (125 g rice in 250 g water (Evian)) in a Microwave rice steamer

(Sistema®, New Zealand) using a microwave (Samsung, Model: MS23F300EAW) at 900 W for 9 minutes. A microwave rice steamer was used as rice can be cooked more quickly than using a standard rice cooker. The cooking recipe followed the manufacturer's recommendation. The rice was also cooked in three batches to check the repeatability of the cooking method. The moisture content results showed that the rice samples in all batches were within $\pm 0.9\%$ variation between batches.

6.3.2 Subjects used

Five healthy subjects (1 male and 4 female, aged from 24 to 40 years old) were recruited for the study. Each subject had good overall health, good natural dentition, and no dentures or prosthetic teeth. None of the subjects were taking any medication that could affect muscle function or saliva flow. Subjects gave their written informed consent to participate in the study (see Appendix C, for example of a consent form). They were asked not to eat or drink for at least one hour before the sessions. The study was given ethical approval by Massey University's Human Ethics Committees (4000020047) and was judged to be low risk.

6.3.3 Physiological variables

6.3.3.1 Oral cavity, pharynx and nasal cavity volume

Each subject's oral cavity, pharynx and nasal cavity volume were measured with an acoustic rhinopharyngometer from Eccovision® (Sleep Group Solutions, North Miami Beach, FL, USA). The volume was measured by asking subjects to breathe through their mouths. The rhinopharyngometer provided all the intermediate volume of compartments in the nasal cavity such as the left and right nostril compartments, the left and right anterior inferior turbinate compartments and the left and right posterior inferior turbinate compartments in cm^3 . The pharynx measurements included the oropharynx and the hypopharynx volumes. The total area of a compartment (oral cavity, pharynx and nasal cavity) was therefore the sum of all intermediate volumes that were measured by the rhinopharyngometer. (Doyennette et al., 2011). Three repetitions were made for each subject, and the average value was calculated.

6.3.3.2 Stimulated salivary flow rate and salivary flow rate at rest

Salivary flow rate at rest ($\text{g}\cdot\text{min}^{-1}$) was measured according to the method by Gavião et al., (2004). Subjects were asked to not swallow and to collect saliva in their mouth at rest and spit it out every 30 seconds into a pre-weighed cup for a total duration of 5 minutes. For the stimulated salivary flow ($\text{g}\cdot\text{min}^{-1}$), subjects were asked to chew a piece of 0.5 g of Parafilm (American National Can Company, Menasha, WI, USA) also for 5 minutes and to spit their saliva into a pre-weighed vessel every 30 seconds (Drago et al., 2011). The salivary flow rate was the ratio between the mass of saliva that was spat out and the sampling duration. Three repetitions were made for each subject, and the average value was calculated.

6.3.3.3 Individual masticatory index

The individual masticatory index was measured for each subject by chewing standardised cylinders (3 g ; $h: 1.8\text{ cm}$; $d: 1.4\text{ cm}$) of Optosil dental silicone during 20 chewing cycles as described by Panouillé et al., (2014). The particles were expectorated and then dried in an oven for 1 hour at 75°C . The index was determined as the ratio of the amount of dried sample that passed through a 4 mm sieve and the amount of expectorated sample. Triplicate trials were performed for each subject, and the average value was calculated.

6.3.3.4 Determination of the natural number of chews and oral processing time before swallowing

Five grams rice samples were transferred into small containers and were kept warm in a water bath at 60°C (Fig. 6-2). The rice was served to the subjects after cooling down to approximately 50°C , which is the temperature at which rice is usually consumed (Gray-Stuart, 2016; Trevan, 2018). A preliminary study with two subjects showed that the portion size per mouthful of rice using a tablespoon had a small range of $5.02 \pm 0.03\text{ g}$. The portion size per mouthful for the two subjects was determined by asking each subject to take rice using a tablespoon from a container as they would do under normal eating conditions; where the average in triplicate was the portion size per mouthful (Moongngarm et al., 2012). The rice in the container was weighed before and after the subject took a spoonful of rice to determine the portion size. Due to the small variation of the rice portion size between the two individuals, all five subjects were given 5 g of rice samples (wet basis) in the study.

The oral processing time before swallowing for all subjects was measured from the point when the 5 g rice sample was placed in the mouth and stopped when the subjects raised their hand to indicate they were ready to swallow. The number of chews taken to reach the swallowing point was counted by observing the upward and downward movement of the chin. Triplicate trials were performed for each subject, and the average value was calculated.

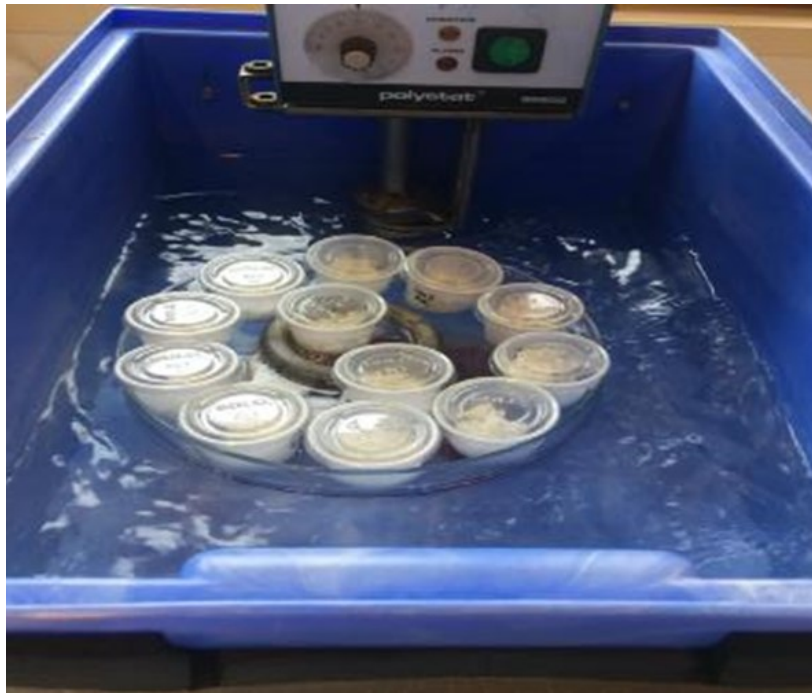


Fig. 6-2: Rice kept warm in 60°C water bath.

6.3.4 *In vivo* oral processing

6.3.4.1 Bolus collection

Each subject participated in two individual sessions of 30 minutes for bolus collection. One session was dedicated to particle size measurements and one session for the bolus moisture content, the amount of saliva incorporated, and the amount of residual bolus after expectorating. The bolus expectorated at 25%, 50%, 75%, 100% of their average total number of chews before swallowing (this parameter was already pre-determined as described in section 6.3.3.4) were collected. The researcher counted the number of chews (by observing the upward and downward movement of the chin) and told the subjects to expectorate their bolus (Erlenmeyer flask for PSD analysis and aluminium dishes for bolus moisture content) once the specified number of chews was taken at each mastication stage. Triplicate trials were

performed for each subject and all analysis were performed in the same day. Altogether, there were 120 boluses collected for the bolus properties analysis.

6.3.4.2 Particle size distribution analysis

The particle size distributions of the bolus samples were analysed by image analysis. Bolus samples were prepared as described by Le Bleis et al., (2013). Subjects were asked to expectorate their bolus in an Erlenmeyer flask and rinse their mouths with 30 mL of water (Evian) before and after chewing the rice. The rinsings were added to the Erlenmeyer flask. Each bolus sample was then diluted with 100 mL of glycerol (Sigma-Aldrich, USA) at room temperature for 20 minutes under constant shaking at 100 rpm (Fig. 6-3).



Fig. 6-3: Rice bolus diluted in glycerol under constant shaking at 100 rpm.

The high viscosity and density of glycerol aid in the separation of bolus particles (Le Bleis et al., 2013). After the dispersion of bolus particles in glycerol, solutions were poured into Petri dishes (diameter: 140 mm). To further aid the separation of bolus particles for image acquisition, the samples collected at higher oral processing times such as just prior to the swallow point (i.e., a chewing interval of 100%) were separated into 3 Petri dishes rather than 2 Petri dishes used for samples collected earlier in the mastication sequence. Particles that remained stuck together were gently separated with a plastic spatula prior to image acquisition (Fig. 6-4). Three replicates were performed for each chewing interval (25%, 50%, 75%, and 100%) of oral processing for all subjects. Before the *in vivo* experiments, the initial particle size distribution of the rice samples was also determined in triplicate. Particle images

were acquired using a Canon EOS 700D camera (Canon Inc., Japan) and a ScanCube 308 (Altawak Technologie, France) that conferred a standardised brightness (Fig. 6-5).

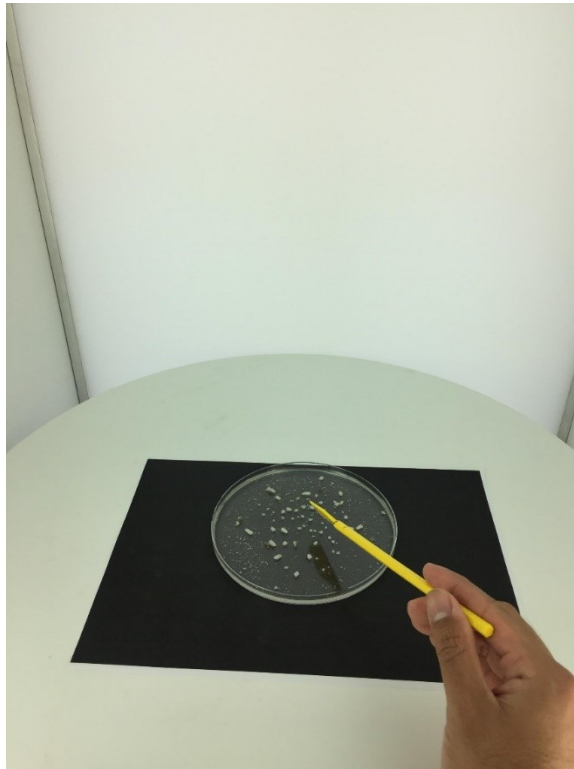


Fig. 6-4 Petri dish containing particles and glycerol which are gently separated using a plastic spatula prior to image acquisition.



Fig. 6-5: Petri dishes containing the boluses were placed inside ScanCube 308 which conferred a standardised brightness. A camera is used to capture the image of the bolus.

The particle size distribution (PSD) analysis was performed using ImageJ software (version 1.52a, National Institutes of Health, USA). A black and white threshold was applied to the images, and the software provided the projected area (mm²) of individual particles. The data was then exported to Excel (2016, Microsoft Corporation, USA).

6.3.4.2.1 Calculation of volume from projected area

The volume of a single particle in the image was predicted by multiplying the projected area with an assumed height (Eq. 6.1). The height was calculated by multiplying a characteristic dimension of the projected area with a constant factor (Eq. 6.2). A circular shape was assumed to calculate the characteristic dimension of the projected area (diameter in mm). Thus,

$$V = h \cdot A \quad (6.1)$$

where V is the volume in mm³, h is the assumed height in mm, and A is the projected area of a single particle in mm². h is calculated as

$$h = f \cdot \left(\frac{4 \cdot A}{\pi} \right)^{\frac{1}{2}} \quad (6.2)$$

where f is a factor.

The factor, f was obtained by minimising the residual sum of squares between the total predicted volume of particles calculated in Eq. 6.1 and the experimental recovered volume of bolus (Gray-Stuart, 2016) (Fig. 6-6). As the recovered volume of the bolus used for the particle size analysis was not known due to the difficulty of separating the particles from the glycerol, it was assumed that the volume of the recovered bolus was the same as the recovered bolus determined from the moisture content analysis. The median equivalent diameter d_{50} (mm), the quartiles d_{75} (mm), d_{25} (mm) and the interquartile ratio d_{75}/d_{25} (no unit) were obtained to describe the degree of degradation and the spread of the PSD respectively (Jourdren et al., 2017). According to Gray-Stuart (2016), particle size reduction of rice during oral processing follows a ‘cleave and paste’ breakage mechanism where a fraction of each particle undergoes fracture to break into a discrete number of daughter particles and the remaining fraction is pasted to become suspended solids within the liquid phase of the bolus. These pasted particles and any fractured daughter particles that are smaller than 0.355 mm were assigned to the suspended

solids phase and were no longer considered to participate in size reduction. Following the analysis as above, the volume of the particles greater than the threshold size of 0.355 mm was summed and the difference with the total volume of bolus was determined to calculate the volume of bolus, which was considered pasted. The ratio of the volume of pasted particles to the total volume of particles measured after image analysis was deemed as the pasted fraction.

6.3.4.3 Bolus moisture content, the amount of saliva incorporated and the amount of residual bolus after expectorating

For the remaining bolus characterisation measurements, subjects were asked to expectorate their bolus into pre-weighed aluminium dishes (at the various mastication stages as described above). Subjects were also asked to rinse their mouths with 30 mL of water before and after chewing the rice. The moisture content of the expectorated bolus (g per 100 g of bolus) was determined in triplicate for each oral processing moment by drying the bolus samples in an oven at 110°C for a minimum of 15 hours (Jourden et al., 2017). The amount of incorporated saliva in the bolus (g saliva per 100 g of dry matter) and the amount of rice remaining in the mouth after spitting (w/w % residues) were calculated as described by Drago et al., (2011) and Motoi et al., (2013).

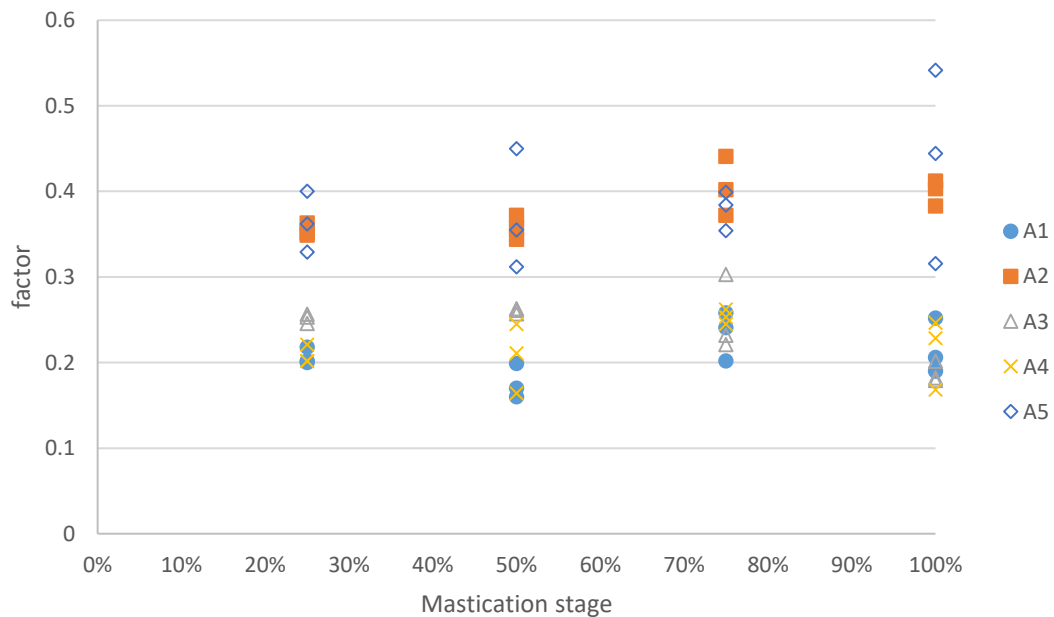


Fig. 6-6 The factor, f from Eq.6.2 to calculate the height of the particle at different mastication stages (3 replicates each), obtained by minimising the residual sum of squares between the total volume of particles calculated in Eq. 6.1 and the experimental recovered volume of bolus.

6.3.5 Rice flavouring

6.3.5.1 Selection of rice

As described above, Jasmine rice was used in *in vivo* experiments in this study. Prior to making this selection, a comparison between Basmati and Jasmine rice was conducted. A preliminary *in vitro* aroma release analysis was first performed to compare the differences in aroma compounds between the two types of rice.

The first part of the *in vitro* test was conducted using a Dynamic Headspace (DHS) - Gas Chromatography (GC) coupled with a Mass Spectrometer (MS) (DHS : MPS autosampler from Gerstel, GC: Agilent 7890B, MS: Agilent 5977B MSD, Agilent Technologies, Santa Clara, USA). The experimental protocol was carried out as follows. Three grams of cooked rice sample were weighed in 20 ml vial (Gerstel, Muihe in der Ruhr, Germany). Each sample was then incubated at 40°C for 3 min with agitation at 500 rpm. The headspace was then purged with a constant flow of helium at 30 ml/min for 10 min at 30°C and aroma compounds were trapped on an adsorption unit (Tenax TA). The trap was dried for 6 minutes under a stream of helium to remove traces of water. Then the trap unit was desorbed from 30°C to 270°C with a rate of 60°C /min and an isotherm of 7 min (270°C) in a cool injection system at -100°C. The column head injection was carried out from -100°C to 270°C with a rate of 12°C /min and an isotherm of 5 min (270°C).

The GC oven temperature was programmed from 40°C with an isotherm of 5 min, to 155°C with a rate of 4°C/min, then to 250°C with a rate of 20°C/min with a final isothermal stage of 5 min. The GC was equipped with an apolar capillary column (Agilent, DB-5MS, 60 m x 320 µm x 1 µm) and with a helium flow of 1.6 mL/min (carrier gas). A mass spectrometer was used to characterize aroma compounds. It was performed in the electron impact mode at 70 eV, in full scan from m/z 29 to 300 U.M.A. (United Mass Atomic or Dalton). The ionisation source was set at 230°C and the quad at 150°C. The compounds were identified by comparison of their mass spectra with those of the NIST 2017 Mass Spectral Library. The retention times were also used for characterization. The data was reported as peak area for each molecule detected. Quantification data were obtained from the integration of the areas from the total ion current (TIC).

Table 6-1 Aroma compounds of Basmati and Jasmine Rice after measurement in DHS-GC-MS

Chemical compound name	Formula	Molar mass	Retention time (min)	Jasmine rice	Basmati Rice
2-butanone	C4H8O	72	7.9	346914	114527
Pentanal	C5H10O	86	12	1122128	102953
1-pentanol	C5H12O	88	15.3	396215	59403
hexanal	C6H12O	100	17	15437433	1579141
acetic acid, butyl ester	C6H12O2	116	17.6	430816	392230
heptanone	C7H14O	114	21.3	663823	45906
2n-butyl-furan	C8H12O	124	21.5	208035	/
heptanal	C7H14O	114	22	468885	77191
2-acetyl-1-pyrroline	C6H9NO	111	23	121177	184365
cis-arbusculone	C9H14O2	154	24.7	165945	/
1-octen-3-ol	C8H16O	128	25.5	241938	14242
5-hepten-2-one,6-methyl	C8H14O	126	25.7	246875	53329
2-octanone	C8H16O	128	26	121951	/
Furan-2-pentyl	C9H14O2	138	26	1621839	196306
octanal	C8H16O	128	26.7	318399	73816
2-hexenal-2-ethyl	C8H14O	126	26.8	129487	/
acetophenone	C6H8O	120	29.7	306230	266556
2-nonanone	C9H18O	142	30.4	81657	/
nonanal	C9H18O	142	31	611457	311549
decanal	C10H20O	156	34.8	156577	107444
2-octenal-2-butyl	C12H22O	182	38.1	264402	/
octanoic acid, octyl ester	C16H32O2	256	42.9	572900	392690

When comparing the two types of rice, as shown in Table 6-1 above, jasmine rice was more aromatic than basmati. This is because jasmine rice contains more aroma compounds than basmati. Although it was shown that rice possesses a distinct “pop-corn” like aroma (2-acetyl-1-pyrroline) in previous studies (Lin et al., 1990; Buttery et al., 1993), it was found that hexanal was present in the greatest amount in both types of rice from the DHS-GC-MS results (highlighted in red in Table 6-1). Because jasmine rice was more aromatic than basmati, it was used in the following in vitro test using the PTR-MS.

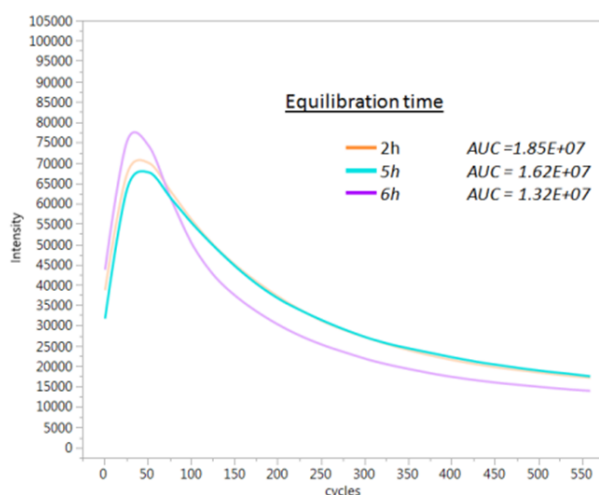
6.3.5.2 *In vitro and in vivo PTR-MS tests*

The second part of the *in vitro* test was conducted using a Proton Transfer Reaction Mass Spectrometry (PTR-MS). Ten-gram samples of cooked rice were stored at 37°C for 2 hours in 100 mL flasks that were equipped with valved caps (GL 45, Duran Group, Wertheim, Germany). The equilibration time was determined after observing the total concentration of hexanal in the rice (area under the curve) (m/z 83) at three different periods (2 hours, 5 hours and 6 hours) in the headspace which it showed that the total concentration was smaller due to losses after 5 and 6 hours respectively (Fig. 6-7). These losses could be attributed to the dilution of room air slowly leaking into the flasks despite the valved caps being kept closed throughout the experiments. Another possible explanation may be due to the ability

of aroma compounds to partition with the wall of the flasks over time which could contribute to the losses (Matsunaga & Ziemann 2010). Thus, due to the losses associated with longer equilibration time, it was assumed that the optimum equilibration time was reached after 2 hours. It will be beneficial however to measure the concentration at intervals before 2 hours (e.g. 30 minutes and 1 hour) in the future to see if the concentration decreases after 2 hours.

A highly sensitive PTR-MS apparatus (PTR-MS Control 2.7, Ionicon Analytik, Innsbruck, Austria) was operated at a drift tube temperature, voltage and pressure of 60°C, 600.1 (\pm 0.4) V and 2.0 (\pm 0.01) mbar, respectively, resulting in a field density ratio (E/N) of 151.4 (\pm 1.4 Td) (Doyennette et al., 2014; Jourden et al., 2017). The PTR-MS was used in a SCAN mode over a mass range of m/z 20-200 with a response time of 100 ms per peak. In the first five cycles of the measurement (90 s), the volatile compounds in the ambient air (i.e., the background signal) was measured. The next 15 cycles (290 s) were then dedicated to measuring the sample headspace (Jourden et al., 2017). The volatile compounds present in the sample headspace were then introduced into the system through a capillary line heated to 110°C at a flow rate of 100 mL/min.

a. Intensity (a.u) vs number of cycles



b. Area under the curve

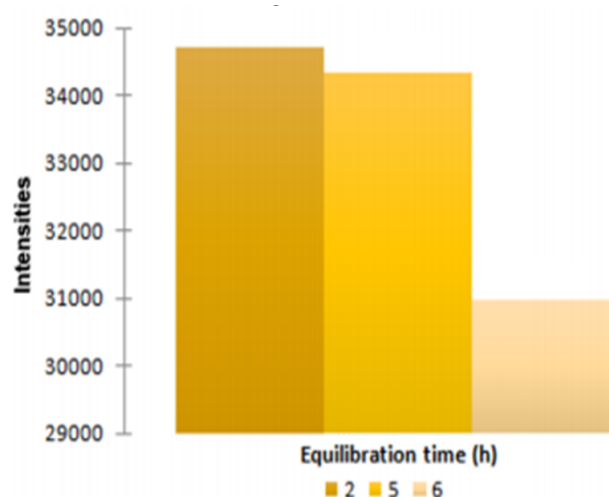


Fig. 6-7 Data showing the intensity vs number of measurement cycles (a) and area under the curve (b) of PTR-MS results of hexanal (m/z 103) in cooked rice at different equilibration time which was measured *in vitro*.



Fig. 6-8: *In vitro* set up to measure aroma compounds in rice using the PTR-MS

In all three batches of rice, two fragmented protonated molecular ions that represented hexanal (m/z 55 and m/z 83) were observed as the top two protonate molecular ions that were detected. Previous studies have also shown that hexanal is an aroma compound typically found in cooked rice (Buttery et al., 1983; Wei et al., 2017; Dias et al., 2019). Although 2-acetyl-1-pyrroline is the aroma compound that gives the rice its distinct flavour (Buttery et al., 1983; Wei et al., 2017; Dias et al., 2019), it was difficult to trace the protonated molecular ion that belonged to 2-acetyl-1-pyrroline (m/z 112). 2-acetyl-1-pyrroline is an unstable chemical compound in the presence of oxygen and moisture (Pico et al., 2018), therefore once protonated, the compound breaks into smaller fragmented protonated ions when PTR-MS is used. The presence of smaller fragmented ions resulting from the reaction in PTR-MS made it challenging to classify ions that belong to 2-acetyl -1-pyrroline. As a result, it was decided that the protonated molecular ion representing hexanal was used for monitoring in multiple ion detection (MID) mode in the following *in vivo* trial. However, before conducting *in vivo* experimental trials with the five subjects, it was essential to run a preliminary trial with a smaller number of subjects (i.e. two subjects) to be certain that hexanal could be detected in the PTR-MS during *in vivo*.

Two subjects were recruited for the preliminary *in vivo* trial. The presence of aroma compounds available in the cooked rice was measured online in a SCAN mode using the PTR-MS. The PTR-MS instrument was operated in similar conditions to as described previously in the *in vitro* test. Both

subjects were served with 10 g of rice. The experiment was run in duplicate for each subject. Fig. 6-9 shows the top 20 area under the curves for various protonated molecular ions for the two subjects. The results show that during *in vivo* conditions, a lot of fragmented protonated molecular ions were formed, which made it challenging to choose ions for monitoring.

Additionally, comparing the results obtained between *in vivo* and *in vitro* tests, the AUC (area under the curve) values obtained during *in vivo* were much lower. There are several reasons why this may happen. It was shown during in-mouth conditions that aroma compounds could interact with the oral-pharyngeal-nasal mucosa layers (Délérís et al., 2016). The interaction between the starchy components of rice with the mucosa layers could reduce the intensity of the targeted aroma compounds when measured in the nose air-space. Additionally, it is also possible that the aroma compounds were diluted with an increased amount of saliva during oral processing. Thus, because of the difficulty to choose a specific aroma compound for monitoring, it was decided to cook the white rice with water spiked with food-grade chemical compounds that were known to be detectable during *in vivo* conditions.

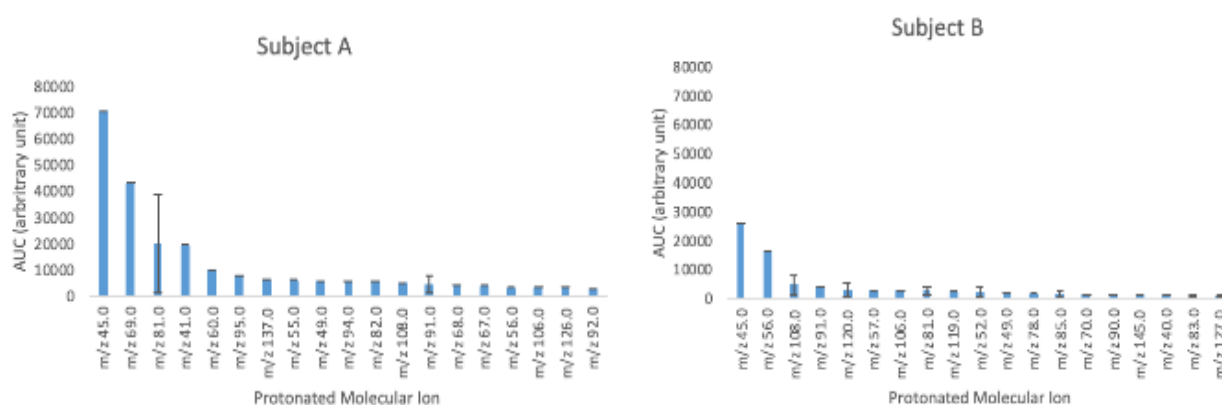


Fig. 6-9: The 20 highest protonated molecular ion (AUC) during experimental *in vivo* trial of two subjects when measured in SCAN mode of the PTR-MS

6.3.5.3 Flavouring the rice with food-grade aroma compounds

The cooked rice was spiked with 2-nonanone and ethyl propanoate. Both are chemical compounds that had been shown to be detectable in previous *in vivo* studies using PTR-MS (Doyennette et al., 2011; Labouré et al., 2014; Délérís et al., 2016). Moreover, 2-nonanone was also observed to be one of the

aroma compounds in the cooked rice when measured in the DHS-GC-MS as described in section 6.3.5.1. A mixture of 300 ppm of 2-nonanone and ethyl propanoate concentration (300 ppm each) was prepared by diluting the stock aroma solution with mineral water (Evian). Between the two chemical compounds, 2-nonanone has a lower solubility limit than ethyl propanoate with 371 mg/L for 2-nonanone at 25°C (PubChem, 2020) and 19,200 mg/L for ethyl propanoate at 25°C (Yalkowsky and Dannenfelser, 1992). Because the rice was cooked in a microwave, it was essential to choose the highest concentration possible (in this case, it was the solubility limit of 2-nonanone (371 mg/L)) to reduce the amount of volatile compounds that were lost during the cooking process. The boiling point of ethyl propanoate is 102.3°C and 2-nonanone is 184.65°C (estimated with EPI Suite™ programme), and therefore significant losses of both volatile compounds were expected during the cooking process because of the high temperature of the microwave.

The conditions to cook the rice was the same as described earlier for the non-flavoured rice, except the aroma solution was used to substitute the water. The concentrations of the cooked rice after cooking were 4.8 mg/L for 2-nonanone and 0.15 mg/L for ethyl propanoate which means over 98% of the aroma compounds were lost during the cooking process. The aroma compound was not added to the cooked rice after cooking as it would be a challenge to have the samples in a consistent and repeatable manner. A separate preliminary study was made to check if the flavoured samples prepared in different cooking batches were repeatable. The compounds, 2-nonanone and ethyl propanoate, in the newly flavoured rice samples prepared from three different batches, were tested in a Gas Chromatography Mass-Spectrometry (GC-MS) and the moisture content of the rice sample (by drying in the oven for a minimum of 15 hours) was also measured from each batch. The results showed that the coefficient of variation (CV) of the Total Ion Chromatogram (TIC) for all the samples were $\pm 10.4\%$ for 2-nonanone and $\pm 18\%$ for ethyl propanoate respectively. The moisture content results showed that the rice samples between all batches were within $\pm 0.9\%$ of the variation.

6.3.6 *In vivo* aroma release during oral processing

The dynamic release of aroma compounds during *in vivo* experiments was measured online using a PTR-MS (PTR-MS Control 2.7, Ionicon Analytik, Innsbruck, Austria). The PTR-MS

instrument was operated in similar conditions, as described in section 6.3.5.2. Measurements were performed with the MID mode on specific masses with a dwell time of 100 ms per mass. 2-nonanone was monitored with m/z 143 (protonated molecular ion) and ethyl propanoate m/z 103 (protonated molecular ion) and 75 (protonated molecular fragment ion) respectively. Acetone (m/z 59) was also monitored as a breath marker with a dwell time of 50 ms as described by (Doyennette et al., 2011). Masses m/z 21 (signal for $\text{H}_3^{18}\text{O}^+$) and m/z 37 (signal for water clusters $\text{H}_2\text{O}-\text{H}_3\text{O}^+$) were monitored to check the instrument performances and cluster ion formation (Jourden et al., 2017).

6.3.6.1 Temperature of served cooked rice

The partition coefficient of aroma compounds that were flavoured in the cooked rice (2-nonanone and ethyl propanoate) can vary with temperature. For instance, when the temperature dependence of the water-air partition coefficients (Henry's constants) of 2-nonanone was investigated between 20-49°C, the Henry constant varied from 0.008 to 0.033 respectively (Avison et al., 2015). Thus, to minimise the changes of the partition coefficient due to the changes in temperature once the cooked rice is placed inside the mouth, it was decided to serve the rice at the body temperature of 37°C.

After cooking, flavoured rice samples were transferred into glass Schott vials (5 g in each vial), equipped with caps. The glass vials, which now contained the flavoured rice samples, were placed in a warmer held at 50°C (Fig. 6-10). The flavoured rice samples were then moved to a metallic tablespoon and served to subjects after cooling down to approximately 37°C. The temperature of the rice was examined using a digital thermometer.

6.3.6.2 In vivo experiments with five subjects

For each subject, air from the nose space was sampled by two inlets of a stainless steel nosepiece, inserted into the subject's nostrils (Fig. 6-11). The gas produced from the samples was transferred from the nosepiece to the PTR-MS through a capillary line with a mean flow rate of 100 mL/min, heated at 110°C.



Fig. 6-10: Rice samples in Schott Vials placed inside warmer that was set at 50°C.

A minimum of five replicates were performed for all *in vivo* measurements. Between each sample, subjects were asked to clean their mouth with 30 mL of mineral water (Evian). Each *in vivo* analysis started with 10 s measurement of ambient air. The subjects were then asked to breathe normally for the next 30 s before they were instructed to put the samples into their mouths. For data analysis, the release curves were divided into three periods: (i) the phase before the sample was introduced (phase 0); (ii) the phase before the first swallow (phase 1); (iii) the phase after the first swallow (phase 2). For each sample, the mean PTR-MS signal from phase 0 was subtracted from phases 1 and 2 (Dél ris et al., 2016). From each subject's release curve in phases 1 and 2, the following quantitative release parameters were extracted: (i) maximal intensities indicating the maximum concentration reached by the aroma compound ($I_{\max 1}$ and $I_{\max 2}$); (ii) areas under the curve, related to the total amount of aroma molecules released (AUC_1 and AUC_2); and (iii) the time at which I_{\max} occurred ($T_{\max 1}$ and $T_{\max 2}$) to reflect temporal release parameters (D l ris et al., 2016).

To study the dynamics of aroma release during oral processing, AUC and intensity values (I) were also extracted at 25%, 50%, 75% and 100% of the subjects first swallowing point time.

6.3.7 Statistical Analysis

All statistical analysis was carried out with XLStat software (Version 2019.2.2, Addinsoft, New Zealand). A Kruskal-Wallis non-parametric test ($p < 0.05$) was performed with a multiple comparison test (Dunn test) to determine if the change in bolus properties during oral processing and the difference between the measured properties were statistically significant.



Fig. 6-11: Measuring *in vivo* aroma release using the PTR-MS.

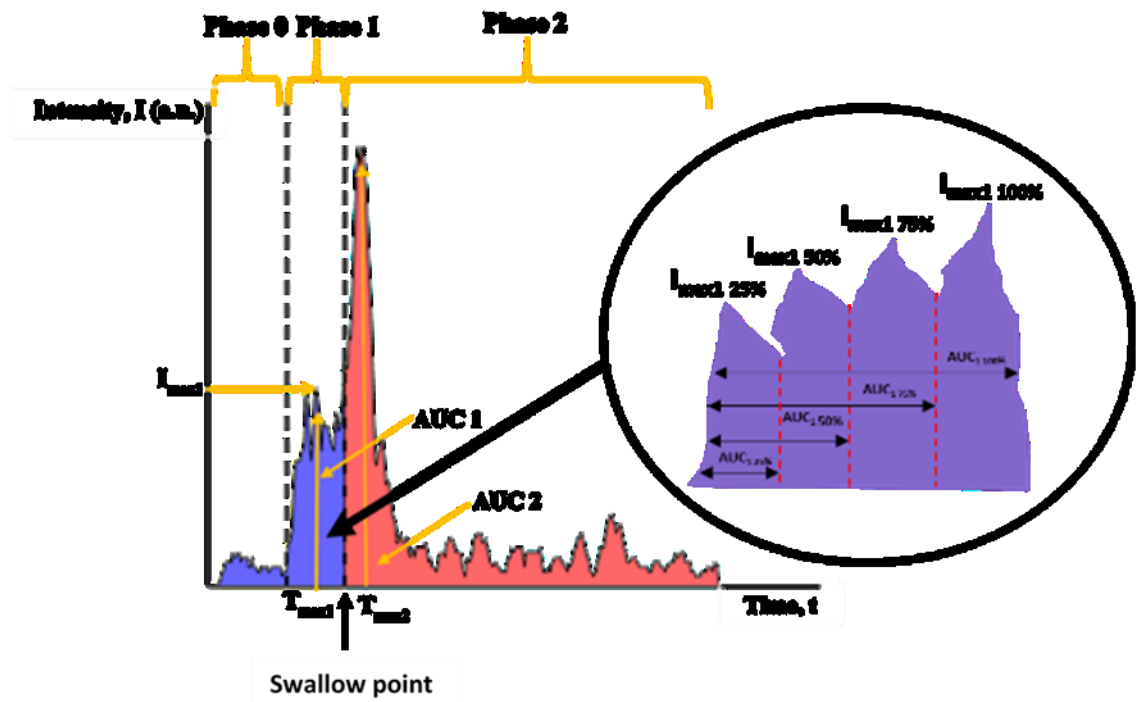


Fig. 6-12: Aroma release curve profile. The total amount of aroma released (AUC 1 & AUC 2), the maximum intensity (I_{max1} & I_{max2}), the time at which I_{max} occurred (T_{max1} & T_{max2}) as well as the intensity and AUC during multiple stages during mastication (25%, 50%, 75% and 100% of the time when first swallow occurred) were determined from the aroma release curve (Image redrawn from Dél ris et al. (2016)).

A Principal Component Analysis (PCA) was performed on the bolus properties and aroma release parameters to differentiate the oral breakdown pathways and aroma release dynamics between all five

subjects. The principal components from the PCA analysis of bolus properties and aroma release were also compared to gain a qualitative insight into the relationship of the two groups of variables.

6.4 Results and discussions

6.4.1 Subject's physiological parameters

Fig. 6-13 compares the physiological volumes for all subjects. Because only five subjects were used, there are no apparent trends. When compared to the values found in the literature measured among 8 to 10 subjects (Jourdren et al., 2016; Molfenter, 2016), the oral cavity volume results represent the values at the top end of the range. The pharynx volume results lie at the bottom end to the range of values of 10 subjects in Molfenter (2016). The nasal volume results seem to be higher to the study by Landa et al. (2010) who measured 55 Caucasian subjects. The point to note is that the mouth volume is 5-7 times larger than either the pharynx or nasal cavity.

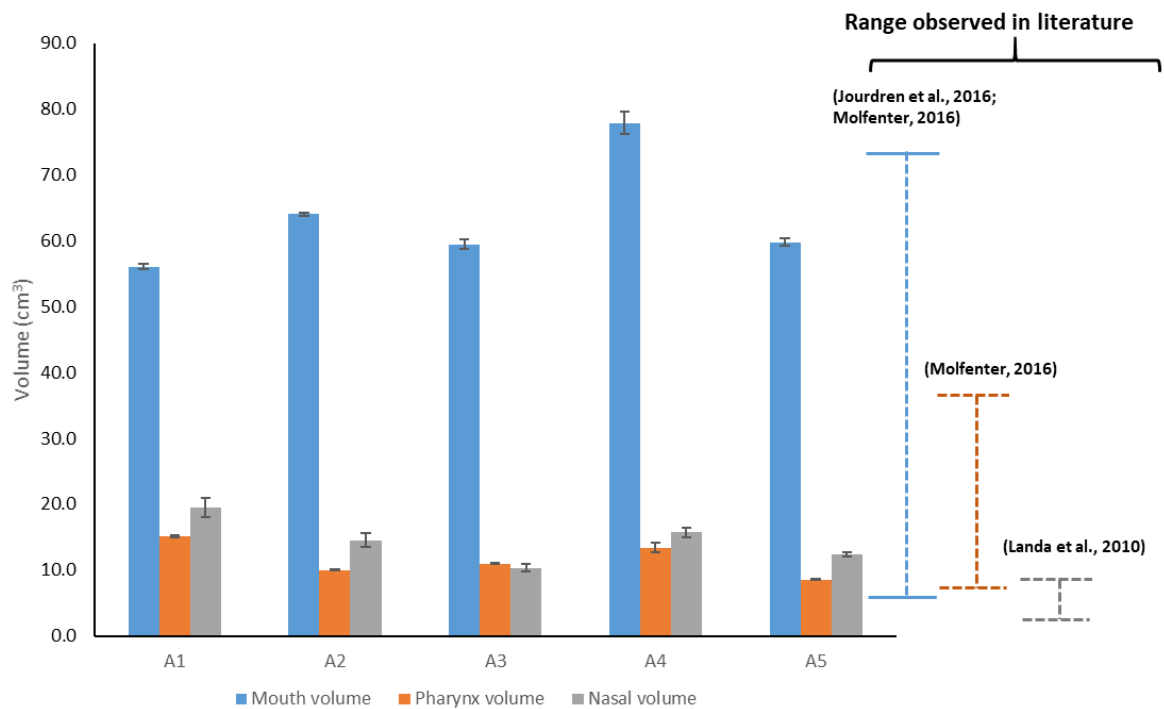


Fig. 6-13: Physiological volumes (Oral cavity, Pharynx and Nasal volume) of all subjects.

Fig. 6-14 shows the saliva flowrates at rest and during stimulation while chewing parafilm. The most obvious result is the large difference between the rest and stimulated states. No trend is apparent between the two saliva flows rate for the subjects. The results compare well to those obtained by Gavião et al. (2004) and Jourdren et al. (2016).

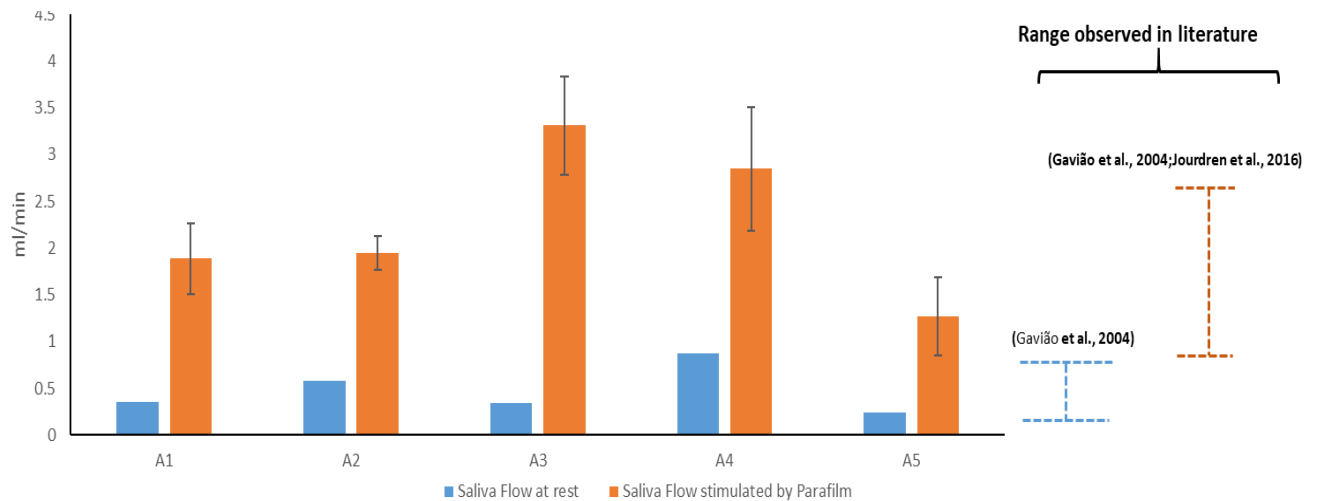


Fig. 6-14: Saliva flowrates of all subjects.

Fig. 6-15 shows the masticatory efficiency results of all subjects. These figures are at the lower end of the range found in the literature (24% to 77% efficiency) using the same method to determine the masticatory efficiency (Jourdren et al., 2016).

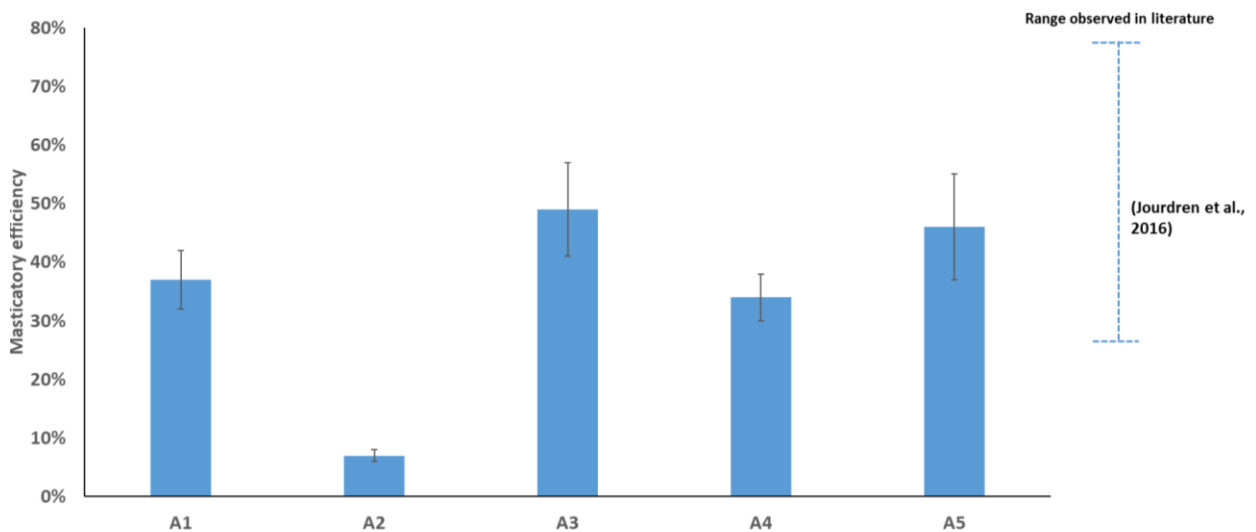


Fig. 6-15: Masticatory efficiency of all subjects

The above physiological parameters results highlight that wide variation occurs within a population. The focus of this work is not about developing population statistics, but to investigate whether models of mastication enhance the model predictive capability for the aroma release models developed by (Doyennette et al., 2014). Here, the models will be coupled. Therefore, because these same five individuals are also the subjects for the aroma release measurements, the mastication model will be tailored to each subject. In this way, the applicability of the combined mastication-aroma release

model will be established for the design of foods that deliver targeted digestion and sensory outcomes. The next step to make the models truly efficacious, which is outside the scope of the project here, is to establish the population range of input parameters that are needed for both the mastication model and the aroma release model.

6.4.2 Bolus characteristics

Fig. 6-16 compares the number of chews and time taken to swallow point. While chewing time and the number of chews are correlated, they show substantial variation between the small number of subjects but are within the ranges found in other studies involving mastication of rice (Moongngarm et al., 2012).

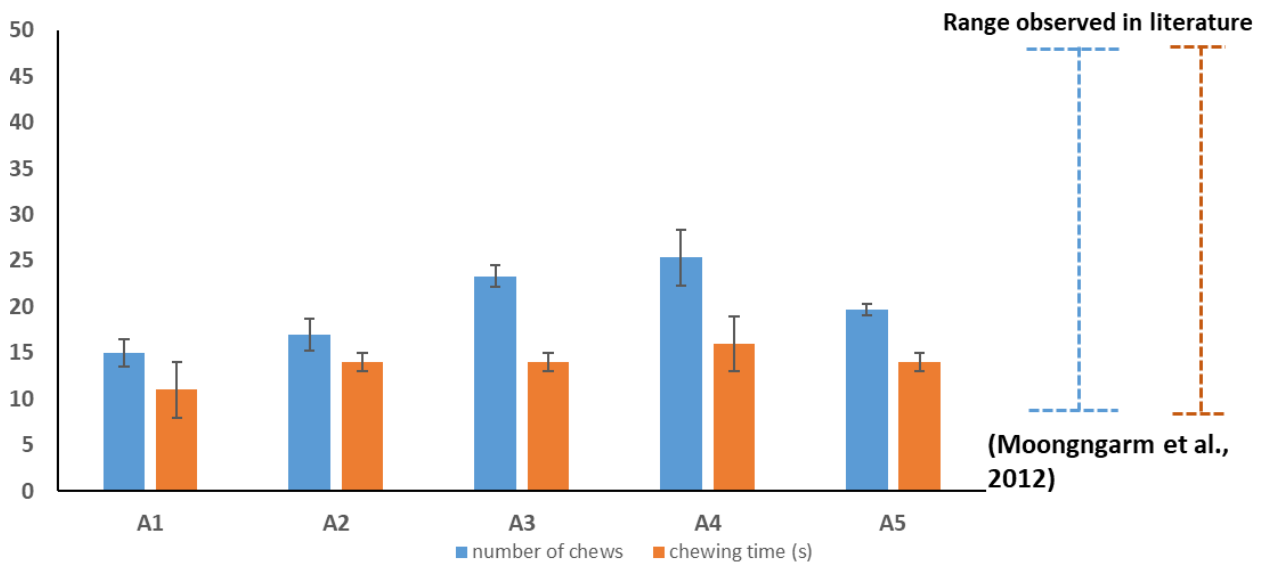


Fig. 6-16: Number of chews and chewing time (s) required to reach swallow point for all subjects.

Fig. 6-17 shows the percentage recovery of solids at the end of chewing, and the ratio of saliva mass to solids mass at the end of chewing for each subject. The unrecovered solids have probably fallen into the buccal pouches which are not cleared at expectoration (Flynn et al., 2011). Again, the results show wide variation between subjects.

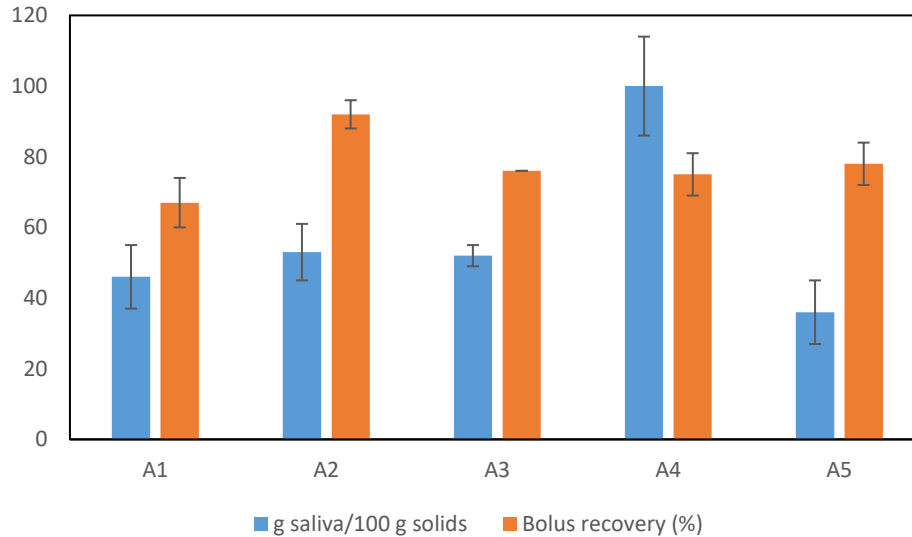


Fig. 6-17: The percentage recovery of solids and the ratio of saliva mass to solids mass (g saliva/100 g solids) at swallow point for each subject.

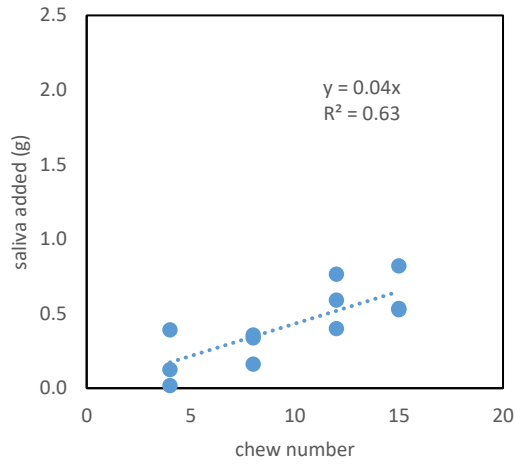
The bolus properties are interrogated with more detail in Table 6-2, where measurements were also made at 25, 50 and 75% of the mastication cycle. Each is discussed below in the order as presented in the table. Bolus moisture content increases with time ($p < 0.05$) although not by much, as the cooked rice already has a significant amount of moisture. This increase indicates some further absorption as the rice is disintegrated.

Table 6-2: Bolus properties at four stages of mastication (25%, 50%, 75% and 100%) for all five subjects (A1-A5). Each trial was performed three times, N=3. M is the mean of the bolus characteristic measured, and SE is the standard error. O/all is the overall mean and standard error for all subjects. Significance levels were encoded as follows: *: $p < 0.05$; **: $p < 0.01$; *: $p < 0.001$.**

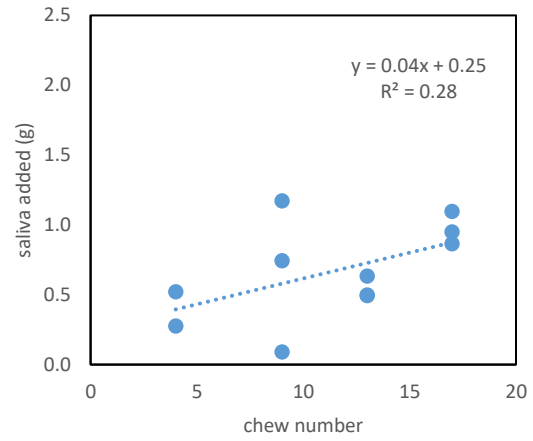
Parameter	Unit	Initial		25%		50%		75%		100%			
		M	SE	M	SE	M	SE	M	SE	M	SE		
Bolus moisture content	g /100 g bolus	**	61.0	1.0	O/all	65.2	2.6	65.3	1.4	66.5	1.1	67.7	0.9
					A1	62.9	2.2	64.8	1.3	66.7	1.4	66.9	1.0
					A2	67.5	6.2	65.4	3.5	64.7	0.6	67.6	0.9
					A3	63.6	1.6	64.3	0.1	66.2	1.2	66.8	0.35
					A4	68.0	1.7	68.6	0.6	70.5	1.8	71.7	1.1
					A5	63.8	1.4	63.3	1.25	64.3	0.57	65.4	1.1
Saliva incorporated	g /100 g dry matter	**	-	-	O/all	14.3	7.8	13.9	3.5	18.1	3.3	22.4	2.8
					A1	5.5	5.1	10.9	3.3	17.2	3.9	18.0	2.9
					A2	23.3	21.3	13.6	9.2	10.5	1.6	20.5	2.7
					A3	10.0	3.8	12.1	0.2	18.3	3.5	20.1	0.9
					A4	24.8	5.2	27.0	2.0	35.1	6.3	40.4	4.5
					A5	7.9	3.4	6.3	3.0	9.3	1.4	12.9	2.8

<i>Amount of residues</i>	%	*	-	-	O/all	13.8	3.6	17.3	3.9	16.3	4.3	20.3	3.8
					A1	33.9	6.4	48.2	2.6	32.8	3.4	31.3	5.8
					A2	4.8	1.0	1.0	3.8	3.1	4.5	5.2	3.3
					A3	4.5	2.2	4.6	0.7	13.2	4.1	22.3	0.1
					A4	13.0	6.2	17.5	5.8	19.5	5.8	22.5	5.1
					A5	12.5	2.1	15.1	6.7	12.8	3.8	20.2	4.8
<i>d₇₅</i>	mm	*	6.64	0.13	O/all	5.31	0.31	5.04	0.17	4.82	0.17	4.47	0.19
					A1	5.26	0.09	5.22	0.05	5.05	0.06	5.13	0.06
					A2	5.01	0.08	4.97	0.17	4.89	0.06	4.63	0.28
					A3	5.45	0.08	4.99	0.20	4.75	0.17	4.36	0.09
					A4	5.69	0.31	5.23	0.21	4.51	0.11	4.09	0.09
					A5	5.13	0.07	4.81	0.20	4.88	0.43	4.13	0.44
<i>d₅₀</i>	mm	***	6.48	0.11	O/all	4.76	0.14	4.24	0.21	3.98	0.10	3.62	0.12
					A1	4.95	0.16	4.81	0.25	4.49	0.04	4.29	0.07
					A2	4.64	0.10	4.24	0.29	4.08	0.06	3.72	0.15
					A3	4.69	0.13	4.08	0.09	3.89	0.20	3.51	0.02
					A4	5.07	0.19	4.15	0.17	3.62	0.06	3.31	0.05
					A5	4.46	0.10	3.91	0.27	3.80	0.16	3.29	0.29
<i>d₂₅</i>	mm	***	6.29	0.11	O/all	3.90	0.18	3.33	0.23	3.05	0.06	2.67	0.15
					A1	4.35	0.27	3.96	0.22	3.56	0.09	3.42	0.20
					A2	3.80	0.17	3.44	0.25	3.20	0.04	2.91	0.11
					A3	3.78	0.16	3.13	0.07	2.97	0.13	2.42	0.04
					A4	4.16	0.17	3.17	0.17	2.71	0.01	2.26	0.11
					A5	3.40	0.14	2.95	0.42	2.81	0.05	2.33	0.27
<i>d₇₅/d₂₅</i>	-	**	1.06	0.01	O/all	1.39	0.04	1.57	0.07	1.63	0.04	1.74	0.08
					A1	1.21	0.04	1.32	0.05	1.42	0.02	1.50	0.07
					A2	1.32	0.06	1.45	0.04	1.53	0.03	1.59	0.03
					A3	1.44	0.05	1.60	0.07	1.60	0.01	1.80	0.04
					A4	1.37	0.02	1.65	0.02	1.66	0.03	1.81	0.06
					A5	1.62	0.02	1.81	0.19	1.94	0.12	2.02	0.19
<i>Pasted fraction</i>	ml paste/100 ml bolus	***	-	-	O/all	0.41	0.10	0.75	0.15	0.71	0.10	1.10	0.19
					A1	0.07	0.01	0.48	0.06	0.10	0.07	0.28	0.22
					A2	0.64	0.27	1.01	0.05	1.07	0.22	1.17	0.14
					A3	0.43	0.04	0.60	0.08	0.65	0.08	1.25	0.08
					A4	0.23	0.11	0.64	0.08	0.68	0.05	1.34	0.23
					A5	0.70	0.07	1.02	0.48	1.05	0.10	1.47	0.28

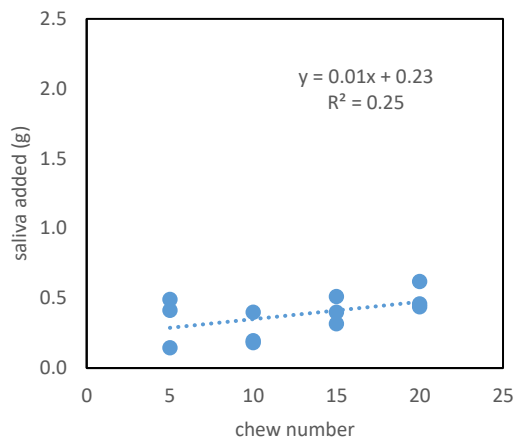
As expected, the saliva content increases steadily for each subject (significance, $p < 0.05$) although, as noted above, the final saliva contents at swallow point are quite different between subjects. To determine the saliva flow rate and the initial saliva volume in the mouth (prior to ingesting the food), these figures are plotted in Fig. 6-18 for all repeats at each stage of chewing. While the repeats show significant variability, the slope shows increasing saliva with mastication progress, varying from 0.012 to 0.043 g saliva/chew, which aligns with that found by Motoi et al. (2013).



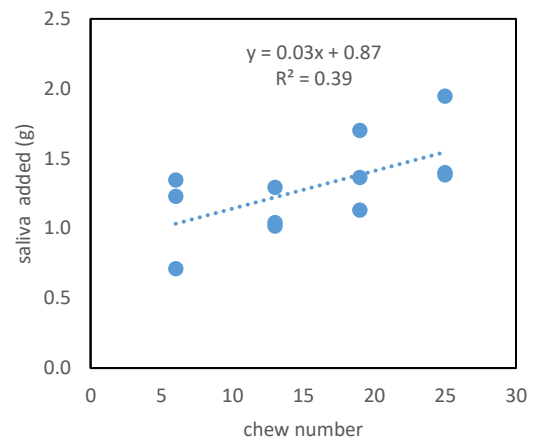
A1



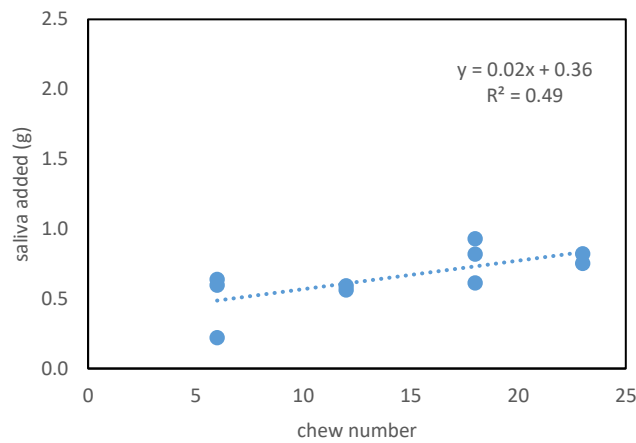
A2



A3



A4



A5

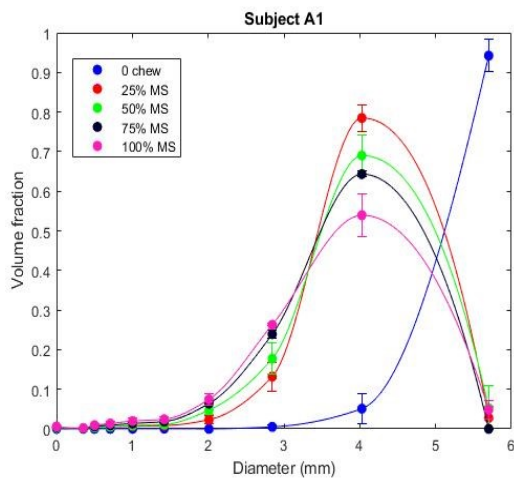
Fig. 6-18: Saliva content as a function of chew number for subjects A1-A5, showing the variation in both saliva rate and apparent initial saliva present. The initial quantity of 5 g rice was at 61.0% moisture content.

The amount of residue is the unrecovered fraction of the 5 g sample of rice given to subjects. This varies for each trial but appears to be relatively consistent for each subject; for example, subject A1 always had the highest unrecovered fraction and A2 the lowest. The change in rice bolus residue is significant over time ($p < 0.05$), and so some mechanism for residue accumulation must be taking place. It is likely that lubricated rice particles are not adhesive enough to clump and so remain in the main oral cavity during chewing but fall and lodge in interproximal spaces. The extent to which particles are retained in these subsidiary compartments is influenced by their physical properties such as size, tribology, adhesion and cohesion characteristics and viscoelasticity (Flynn et al., 2011).

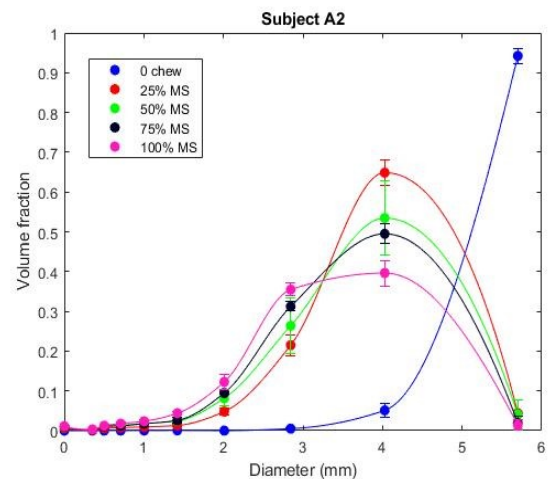
The bolus particle size distribution across all mastication stages, reported in Table 6-2 are also plotted in Fig. 6-19 as the fraction of the total volume of particles that were less than a specified sieve aperture of size for a range of sieve sizes from 5.7 down to 0.354 mm (followed a $2^{1/2}$ size series). The fraction that passed the 0.354 mm sieve are called the pasted fraction and are assumed to be suspended in the liquid phase. The particle size parameters d_{75} ($p < 0.05$), d_{50} ($p < 0.01$), d_{25} ($p < 0.01$) and d_{75}/d_{25} ($p < 0.01$), pasted fraction ($p < 0.01$) all changed significantly with increasing mastication stage. Generally, the subject that chewed for more chews reduced the particle size distribution the most.

It is interesting to interrogate just the 4 and 5.7 mm sieves. At the beginning, these sizes represent almost all the particles and therefore can be assumed to be the whole rice particles. Plotting the sum of these sieves versus chew number gives a measure of the breakdown of the rice without needing to consider the fracture mechanism, i.e., it represents the surviving whole rice grains. Fig. 6-20 shows two things; (i), the breakage of whole rice progresses approximately with chew number, meaning that the subject with the least number of chews to the swallow-point (A1) also produced the least breakdown; and (ii), all subjects exhibited more whole rice breakage in the first few chews than in later chewing. Indeed, at four chews (calculated using the trendline formulae), between 18-37% of whole rice had been broken down, or 4.66-9.36% loss of grains per chew. After the fourth chew, the breakage rate decreases to between 2 to 2.67% loss per chew (the trendline slopes), with subject A4 having the greatest loss rate. Interestingly, this subject also chewed for the longest. In seeking a reason for the variation between subjects, the saliva addition rate was explored with the hypothesis that higher saliva rate aids breakdown. Fig. 6-21 shows the salivation rates. Trend lines have been added and are here

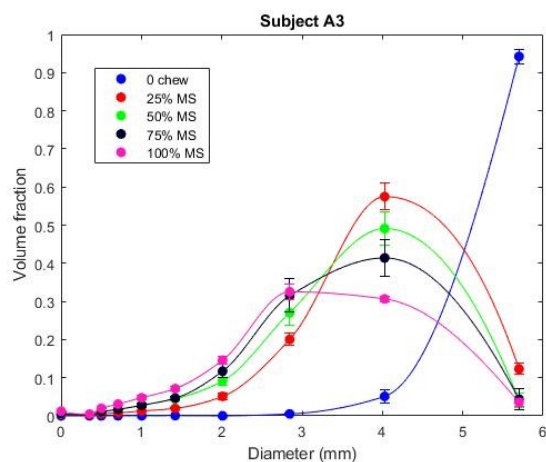
constrained to pass through the origin, which assumes that subjects had zero initial saliva content. This, of course, will not be true if they had been salivating prior to the food being placed in the mouth. The figure shows that prior salivation must occur for subject A4 (who has far higher overall saliva levels than the other subjects), and somewhat haphazardly for subject A2. For subject A4, the slope of the later extents of chewing yield a salivation rate of 1.83 ml/100 g dry matter, which is the highest compared to the rest of the subjects. Interestingly, subject A4 also had the greatest loss rate as shown in Fig. 6-20. Therefore, the hypothesis of the higher the saliva rate the higher the breakdown can be accepted for subject A4.



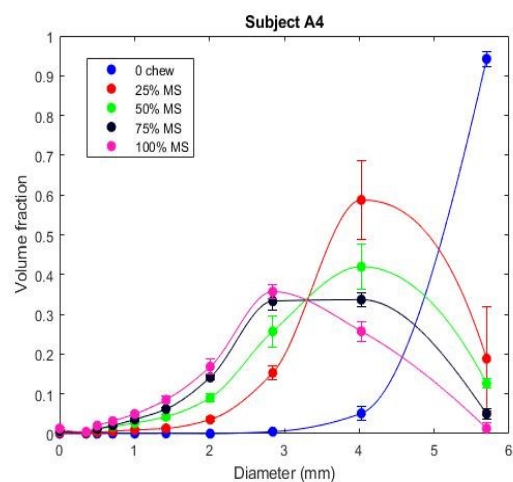
A1, $N_{100\%}=15$



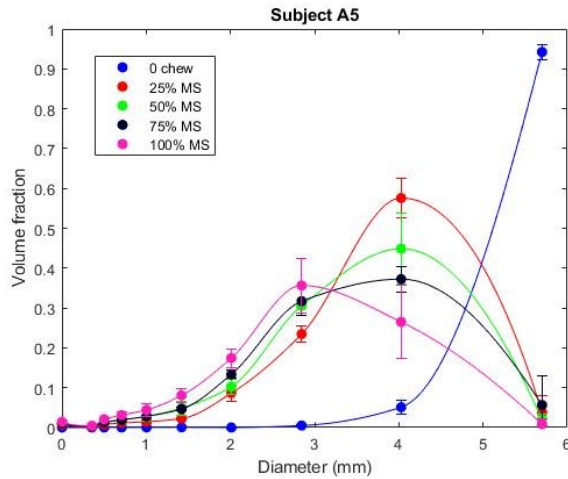
A2, $N_{100\%}=17$



A3, $N_{100\%}=23$



A4, $N_{100\%}=25$



A5, N_{100%}=20

Fig. 6-19: Bolus particle size distribution results for all subjects. The plotted curves are to guide the eye. Subject A1 and A4 clearly have a different number of chews to completion, N_{100%}, which means 25% of completion in subject A1 is about 4 chews while in subject A4 it is 6 chews.

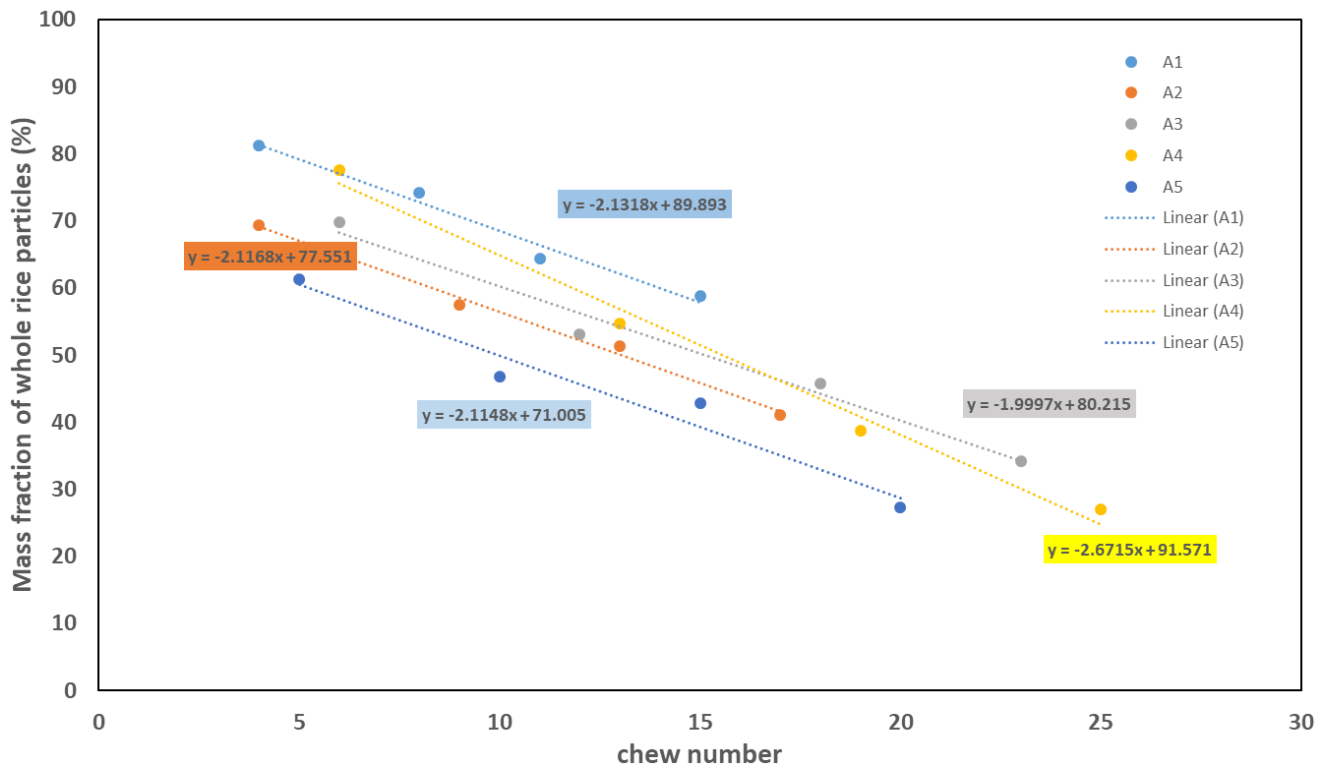


Fig. 6-20: Reduction in whole particles with chew number (with (0,100) point removed).

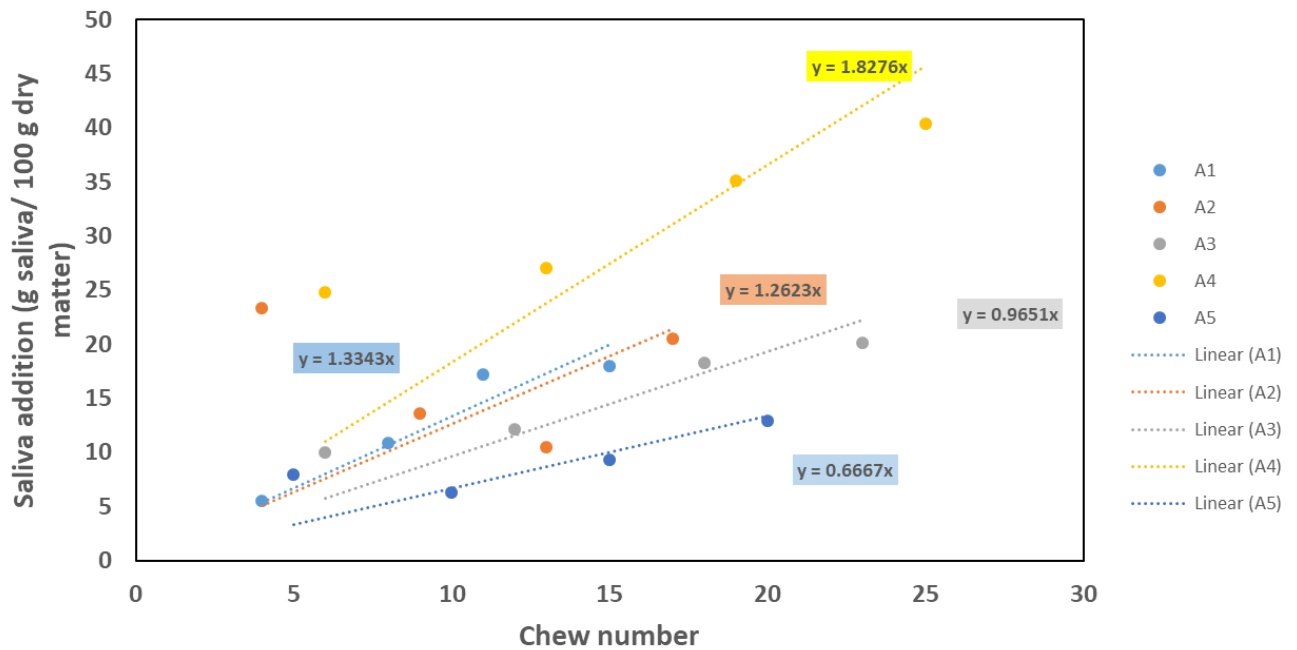


Fig. 6-21: Saliva addition rate. It is assumed that if the trend line is constrained to pass through (0,0) this will draw out the salivating effects of elevating the initial saliva content

The above discussion considers only the breakage of whole rice grains, assuming simplistically that all particles captured on the 4 and 5.7 mm sieves were whole grains of rice. The above discussion does not consider the mechanism of rice breakage. The mechanism of size reduction was interrogated for cooked brown rice by Gray-Stuart (2016). He discovered that the particle size distribution, when plotted as a frequency distribution of mass versus sieve size, became bimodal. This, he proposed, was because the rice particles were cleaved into one or several large particles and the remaining were pasted into small particles during occlusion. Gray-Stuart then suggested the concept of ‘cleave and paste’ mechanism applies for all starch-based foods. This is not as apparent here, because the bimodality is not seen in Fig. 6-19, even for subject A2 who consistently expectorated most of the rice with little loss and so therefore is the closest to achieving a mass balance. Here, the pasted fraction did increase over time, although it was still low (ranging from 0.28 to 1.47% at swallow point across five subjects) in comparison to ~15% observed at swallow point for brown rice when studied from a single subject (Gray-Stuart, 2016). However, the high pasted fraction obtained in the brown rice study are disputable for two reasons. Firstly, the author calculated the pasted fraction by back calculating from the unrecovered solids remained in the pan after wet sieving but did not include the quantity of bran layer

fragments which were seen to present in chewed brown rice (Bornhorst et al., 2013). Secondly, due to the soft nature of cooked rice, the wet sieving method used by the author to quantify the particle size distribution may cause further breakdown of the rice, yielding more pasted particles when recovered in the pan. In conclusion, the reduced pasted fraction seen here compared to that of Gray-Stuart (2016), provide support for breakdown to be more weighted to breakage than cleave-and-paste, although both are likely to occur to some extent.

6.4.2.1 The breakdown pathway of rice taken by subjects

The above discussion demonstrates that the breakdown mechanism of rice during mastication remains unclear. Here, this study has a limited number of subjects, where the reason for collecting individual data was to use them as case studies for the combined breakdown-aroma release model. Models require input parameters that relate to the physiology of the subjects and adjustable parameters relating to the food portion. Therefore, within the subject studies, it is important to look for relationships between these input parameters and the measured breakdown variables. As a first step in doing this, a PCA analysis was conducted to reduce the number of variables into a two-dimensional plot. Fig. 6-22 (a) portrays the factor loadings of the top two principal components describing the bolus characteristics in all subjects. Fig. 6-22 (b) shows the breakdown pathway taken for each subject with increasing mastication stages from left to right. By using Fig. 6-22 (b) as a guide, the differences in the rice breakdown pathway taken by each subject can be explained. For example, plots on the left of Fig. 6-22 (a) show bolus parameters during early mastication stages featuring large particle size (high d_{75} , d_{50} and d_{25}), low moisture and saliva content, narrow particle size distribution (low d_{75}/d_{25}), low pasted fraction and low amount of residues remaining in the mouth.

Moving towards the right side of the figure shows the plots of bolus properties towards the later stages of mastication where with smaller particle size, higher bolus moisture and saliva content, broader particle size distribution (high d_{75}/d_{25}), and an increased amount of pasted fraction and residues.

The variation of breakdown pathways between the subjects could also be investigated from the PCA plot. For example, Subject A1 who took the smallest number of chews and oral processing time to reach the swallowing point had a large bolus particle size and the lowest bolus moisture content at swallow point (see also Table 6-2), indicating a large particle size and low lubricating bolus threshold for safe

swallow. Subject A1 also had the largest amount of residue among all subjects (the lowest amount of bolus recovered), suggesting that the subject may need further chews to clear the remaining debris in the mouth. As the particles generated by the subject were large even towards the later stages of mastication, these particles may lodge in interproximal spaces of the teeth (Flynn et al., 2011). Comparatively, Subject A4 had a larger particle size at the early stages of chewing than others but had the smallest particle size at swallowing point. The subject had low mastication efficiency, which could explain why the particle size was quite large at the start, but also had the most prolonged duration of mastication that explained the small size of particles at swallowing point. Consequently, because of the prolonged duration of mastication, Subject A4 also had the highest bolus saliva content at the later chewing stages (Table 6-2). Subjects A3 and A5 had about the same level of factors for the percentage of residues, due to the same trend of their bolus particle size breakdown and moisture content increase during oral processing. Subject A2 being the least efficient chewer had a large particle size, even at swallowing point.

The influence of oral physiology on bolus properties could be further explored in Fig. 6-22 (a). Subject A4 who took the longest oral processing time and had the most substantial amount of saliva from the start had the highest amount of saliva incorporated in the bolus, a broad particle size distribution, smallest d_{25} and d_{75} and had a significant amount of pasted fraction compared to other subjects. Subject A1, being the opposite, had the largest particle size and low amount of saliva and pasted fraction at swallow point as the subject took the shortest time to chew. It was quite interesting to note that Subjects A3 and A5, despite being efficient chewers, both had a low amount of saliva incorporated in the bolus as their saliva flowrate was quite small at rest, contrary to subject A2. Due to the high amount of saliva flow at rest, Subject A2 had the lowest amount of residue in the mouth across all chews, as the bolus was highly lubricated, ensuring minimum losses when the bolus was spat out.

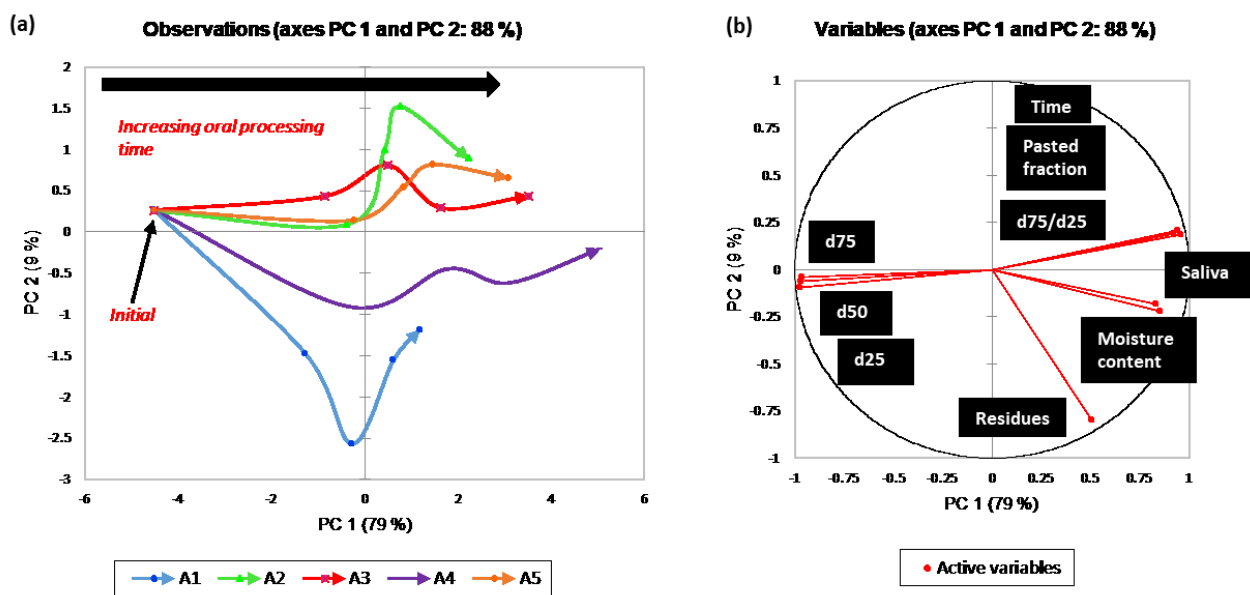


Fig. 6-22: Breakdown pathways of rice during oral processing from PCA analysis. (a) shows the plot when PC 1 and PC 2 of the bolus properties between subjects were compared. (b) shows the plot of the factor loadings of the bolus variables measured for all subjects and provides a guide for the breakdown pathway plot, in (a). Arrows are drawn from left to right to illustrate the breakdown pathway from the time when samples were introduced in the mouth (initial) to the swallowing point. The points between the initial and swallow point of each subject were the bolus properties at 25%, 50% and 75% of the subject's total oral processing time.

6.4.3 *In vivo* aroma release during oral processing

The aroma release parameters for all subjects are shown in Table 6-3 (the release of 2-nonanone, *m/z* 143) and Table 6-4 (the release of ethyl propanoate, *m/z* 103). A fragment ion belonging to ethyl propanoate, *m/z* 75, is not displayed as it followed a similar trend to *m/z* 103. In general, comparing the two aroma compounds studied, 2-nonanone seemed to have a higher intensity and AUC values for all subjects during chewing and after the first swallowing point than ethyl propanoate. The initial concentration of 2-nonanone in the cooked rice was 4.8 mg/L and for ethyl propanoate was 0.15 mg/L (data not shown here, but the calculations to estimate the initial concentration are shown in the next chapter). The boiling point of ethyl propanoate is 102.3°C in comparison to 2-nonanone, at 184.65°C (estimated with EPI Suite™ programme) therefore, losses of ethyl propanoate compound would have been more pronounced than 2-nonanone during the cooking process of rice. However, it may also be worthwhile to check the Henry's law constants for the two compounds as the losses could also be associated to the affinity of the chemical compounds to the air phase. The Henry's law constant for each aroma compound studied at 37°C was estimated using the following equation

$$H_i = H_{i,ref} \exp \left[\frac{-\Delta_{soln,w}H}{R} \left(\frac{1}{T} - \frac{1}{T_{ref}} \right) \right] \quad (6.3)$$

where R is the universal gas constant = 8.314 J/mol.K, $-\Delta_{soln,w}H = 61.0$ kJ/mol for 2-nonanone (Heynderickx et al., 2014) and 10.25 kJ/mol for ethyl propanoate (Fenclová et al., 2014). $H_{i,ref}$ is the Henry's law constant at 25°C for 2-nonanone which is 3.67×10^{-4} atm-m³/mol and ethyl propanoate at 2.51×10^{-4} atm-m³/mol (estimated from EPI Suite™ programme).

The Henry's law constants calculated using the equation above at 37°C for 2-nonanone was 1.42×10^{-4} atm-m³/mol and 2.14×10^{-4} for ethyl propanoate. Both compounds have Henry's law constants lower than the 'rule of thumb' suggested by the United States Environmental Protection Agency, 1996 (Katyal & Morrison, 2007); where compounds with a Henry's law constant greater than 10^{-3} atm-m³/mol are considered volatile. This means that both compounds are more attracted to water than the air phase. Thus, the drop of the concentration of the aroma compounds in the cooked rice after cooking would be explained by the losses of the aroma solution during the cooking process.

6.4.3.1 The dynamics of aroma release during oral processing

To illustrate the dynamics of aroma release during multiple stages of oral processing, the aroma release parameters, specifically the AUC and I_{max} values at 0%, 25%, 50% and 100% of each subject swallowing point were plotted in a PCA diagram (Fig. 6-23) The PCA plot summarises in just two-dimension plots the evolution of a large number of variables (5 variables) to visually differentiate between all subjects. Comparing between all subjects, as also observed through the aroma release parameters in Table 6-3 & Table 6-4, Subjects A4 and A1 are separated from other subjects with a higher aroma release parameters compared to other subjects who had fairly similar values. The differences in the aroma release parameters for all subjects during oral processing and after swallowing is further discussed below.

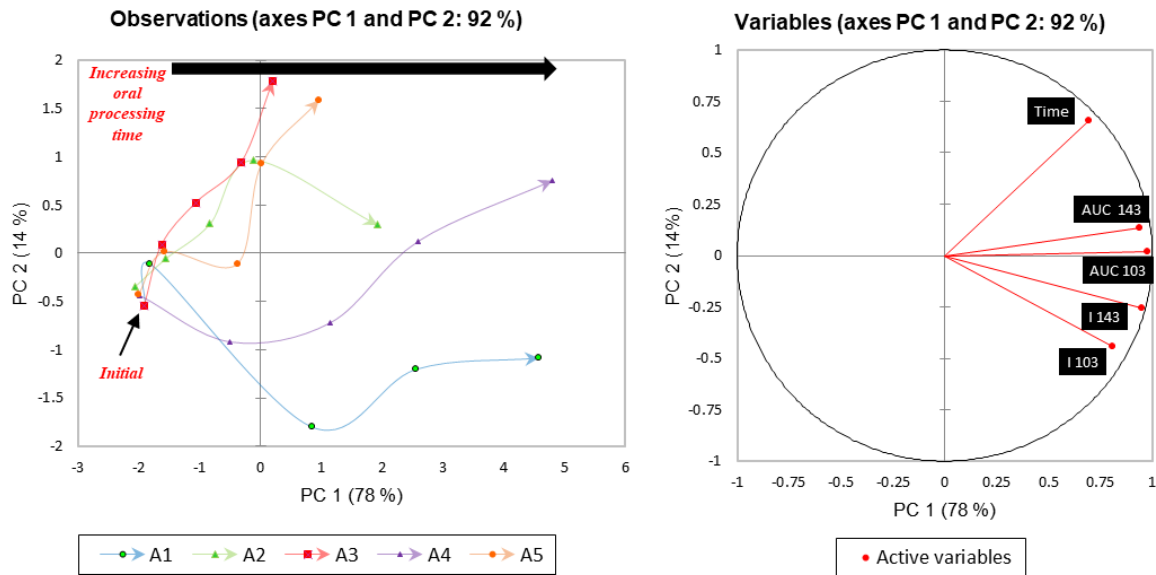


Fig. 6-23: The dynamics of aroma release parameters (AUC and I values) during oral processing between subjects. Subject A1 and A4 were differentiated from other subjects with higher I and AUC values while other subjects had similar I and AUC values during oral processing.

6.4.3.2 Influence of the dynamics of bolus properties during chewing on aroma release

The principal components of the bolus properties (PC 1 and PC 2 in Fig. 6-22) were compared with the principal components of the I_{\max} and AUC values measured at several stages of oral processing (PC 1 and PC 2 in Fig. 6-23) to provide a qualitative explanation on the effect of oral processing parameters on aroma release (Fig. 6-24). Previous studies on linking aroma release and mastication of solid foods have mostly looked at the effect of the bolus properties at swallow point on aroma release (Feron et al., 2014; Labouré et al., 2014) but since oral processing is a dynamic process, the bolus properties measured at different stages during oral processing should be taken into account as the impact of early and later stages of mastication on aroma release may be different. The generation of new surface area over time (measured from the bolus particle size distribution at several time points in this study) when masticating solid foods may be of importance as this will impact the rate of transfer of aroma compounds from the food product to the saliva phase as shown in model simulations of flavour release (Harrison et al., 1998; Wright & Hills, 2003; Doyennette et al., 2014). Although the generation of new surface area of food particles during oral processing was shown to affect aroma release from a mechanistic point of view, the effect of the particle size reduction due to the dynamics process of mastication is still poorly understood.

Table 6-3: Aroma parameters extracted from subject's aroma release curve for m/z 143 (2-nonanone).

Parameter	<i>2-nonanone</i> (<i>m/z 143</i>)	Subjects				
		A1	A2	A3	A4	A5
$I_{\max 1} \times 10^2$ (a.u.)	Mean	6.32	1.73	1.04	4.10	1.50
	S.E.	0.56	0.69	0.34	1.57	0.47
$AUC_1 \times 10^3$ (a.u.)	Mean	4.76	2.17	1.26	6.72	2.06
	S.E.	1.2	0.88	0.49	3.2	0.86
$T_{\max 1}$ (s)	Mean	14.4	21.5	25.4	26.8	24.3
	S.E.	1.3	3.3	4.9	3.4	6.0
$I_{\max 1}/T_{\max 1}$	Mean	44.1	7.9	4.2	15.2	6.2
	S.E.	6.3	2.1	1.8	4.8	0.9
$I_{\max 2} \times 10^2$ (a.u.)	Mean	5.28	2.31	2.21	5.92	1.95
	S.E.	1.45	0.29	0.83	2.35	0.68
$AUC_2 \times 10^3$ (a.u.)	Mean	8.33	5.62	9.80	16.70	5.70
	S.E.	2.18	1.80	3.70	9.90	2.60
$T_{\max 2}$	Mean	19.1	30.0	51.8	44.7	41.2
	S.E.	3.3	5.6	9.3	17.9	10.1
$I_{\max 2}/T_{\max 2}$	Mean	29.1	7.9	4.3	15.4	4.9
	S.E.	12.5	1.8	1.5	7.9	1.8

Table 6-4: Aroma parameters extracted from subject's aroma release curve for m/z 103 (Ethyl propanoate).

Parameter	<i>Ethyl propanoate</i> (<i>m/z 103</i>)	Subjects				
		A1	A2	A3	A4	A5
$I_{\max 1} \times 10^2$ (a.u.)	Mean	1.69	0.63	0.36	0.88	0.52
	S.E.	0.35	0.18	0.08	0.28	0.09
$AUC_1 \times 10^3$ (a.u.)	Mean	1.04	0.39	0.23	1.01	0.43
	S.E.	0.27	0.16	0.12	0.40	0.19
$T_{\max 1}$ (s)	Mean	12.3	18.7	19.3	19.7	21.0
	S.E.	3.0	9.2	5.2	8.2	4.3
$I_{\max 1}/T_{\max 1}$	Mean	14.5	4.2	1.9	5.0	2.6
	S.E.	4.8	2.9	0.3	2.3	0.9
$I_{\max 2} \times 10^2$ (a.u.)	Mean	0.52	0.53	0.49	1.09	0.46
	S.E.	0.16	0.26	0.18	0.41	0.15
$AUC_2 \times 10^3$ (a.u.)	Mean	0.32	0.32	0.46	1.01	0.40
	S.E.	0.13	0.09	0.21	0.36	0.21
$T_{\max 2}$	Mean	18.9	27.1	54.9	40.8	39.6
	S.E.	1.7	3.8	24.6	15.8	4.2
$I_{\max 2}/T_{\max 2}$	Mean	2.7	2.0	1.1	3.0	1.1
	S.E.	0.7	1.0	0.5	1.5	0.3

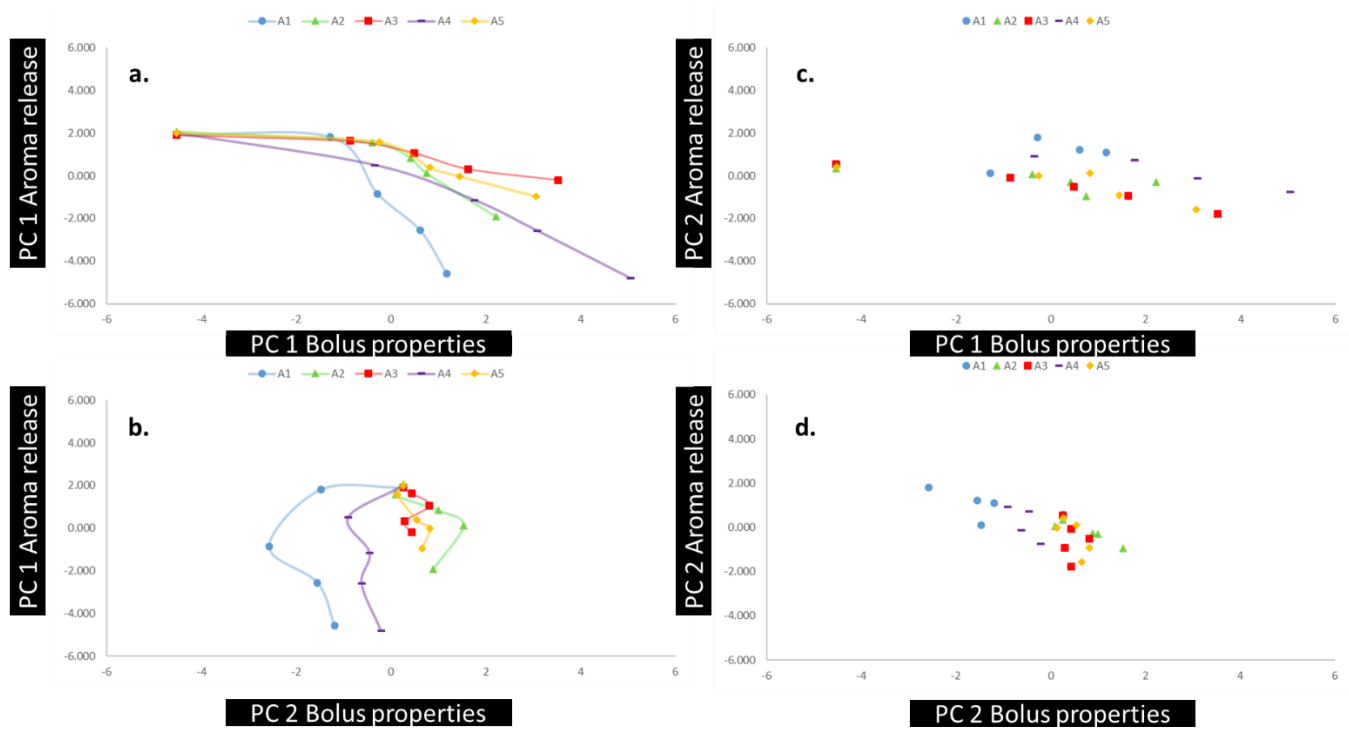


Fig. 6-24: Principal components of bolus properties compared with the principal components of intensity and AUC values of aroma release measured during several mastication stages. (a) shows the plot of PC 1 aroma release vs PC 1 bolus properties which explained most of the variation between subjects whereas (b) showed the impact of bolus residues on aroma release. No lines were drawn on (c) and (d) as both provided little information on the aroma release parameters.

6.4.3.2.1 Effect of physiological factors

The physiological variables measured in this study were the oral cavity volume, nasal cavity volume, saliva flow rate at rest and saliva flow rate when mechanically stimulated, masticatory efficiency and lastly the number of chews and the total time taken to reach swallow point. It can be observed in Fig. 6-24 (a) as well as in Fig. 6-23 that Subjects A4 and A1 were differentiated from other subjects with a high amount of aroma release (I_{\max} and AUC values). Thus, it seems reasonable to explain the association between the physiological variables and aroma release from these subjects.

Subject A4, had the highest number of chews and took the longest time to swallow the rice samples. The effect of oral processing time had been observed to affect aroma release, as shown in the literature. Studies with cheese (Tarrega et al., 2008; Labouré et al., 2014), confectioneries (Blissett et al., 2006) and custard (Ruijschop et al., 2011) have all shown that a longer duration of oral processing results in a higher amount of aroma release. A longer duration of oral processing would lead to an increased number of velum openings, allowing the more frequent renewal of the air phase in the oral

cavity, hence a larger amount of aroma would be extracted from the food matrix to the nasal cavity (Labouré et al., 2014). Additionally, the longer duration of oral processing is also related to a longer time for the transport of aromas to the headspace in the mouth. The concentration increases up to an equilibrium concentration. The Henry's law constants as described in section 6.4.3 for 2-nonanone and ethyl propanoate show that the compounds have a high affinity towards water, therefore it could be expected that it would take a longer time for the compounds to be released into the air phase.

Subject A4 also had the largest oral volume among all subjects, and the highest saliva flow rate at rest. Because both flavour compounds are attracted to the water phase more than the air phase, theoretically, it is expected that an increase in saliva flow rate will dilute the aroma concentration, therefore a smaller amount of aroma release parameters (compared to other subjects) should be expected in Subject A4. This is interesting because instead of diluting the flavour compounds, saliva may have a different role for starch-based food matrices such as rice. Previous studies have shown that the linear amylose fraction of starch can form inclusion complexes with flavour compounds during gelatinization which reduces the free flavour available for release (van Ruth & King, 2003; Conde-Petit et al., 2006). The presence of more saliva could weaken the physico-chemical interactions between starch and flavour compounds, resulting in a higher aroma release. Besides interactions with starch, the presence of mucins in saliva could also interact with aroma compounds, resulting in lowered retention of highly volatile compounds and increased retention of less volatile, hydrophobic compounds (van Ruth et al., 2001). This could also be a possible explanation to the observed results, although further studies with larger number of subjects will be required to confirm the speculation.

The nasal cavity and the pharynx volumes were observed to be the largest in Subject A1. It can also be observed from the aroma release results in Fig. 6-23 and Fig. 6-24 (a) that this subject had one of the highest aroma release parameters (I_{\max} and AUC values). The theoretical analysis showed that from previous studies, subjects with small nasal volumes gave high-intensity peaks followed by a sharp decrease in the volatile concentration, while subjects with large nasal volumes gave low-intensity peaks but longer signal duration (Trelea et al., 2007). It is possible that the pharynx volume may have an effect if the velopharyngeal opening is large, allowing a larger volume of air to exchange between the oral

and the pharynx cavities. The large nasal cavity and pharynx volumes of Subject A1 may explain the high aroma release parameters (I_{\max} and AUC values) observed.

Lastly, subject A3 who was the most efficient chewer had the lowest aroma release values as observed in Table 6-3 and Table 6-4 respectively. The theoretical analysis explained that a more efficient chewer would have produced boluses with smaller particles during mastication. This will have created more surface area and so are expected to perceive higher retronasal aroma release intensities due to a faster release and movement of the taste and aroma compounds from the food matrix into the saliva and air phases. However, this subject also had the smallest nasal cavity and pharynx volumes, as well as a low salivary flow rate at rest. It could be that these variables are more dominant than the surface area of the particles in influencing the aroma release.

6.4.3.2.2 Effect of bolus saliva content

As chewing time increases, the amount of saliva incorporated in the bolus also increases. From the theoretical analysis, an increase in saliva content would have diluted the flavour, causing a decrease in maximum flavour concentration, as also seen in other studies (Harrison et al., 1998; van Ruth & Roozen, 2000; Feron et al., 2014; Jourdren et al., 2017). Interestingly, Subject A4 who had the highest amount of saliva incorporated in the bolus (see Table 6-2) had the largest aroma release values (see Table 6-3 and Table 6-4) whereas subject A3, who had the lowest amount of saliva (Table 6-2) had the smallest aroma release values (see Table 6-3 and Table 6-4). In the previous section it was suggested that a possible reason for this is because saliva weakens the physico-chemical interactions between starch and the flavour compounds, resulting in a higher aroma release.

6.4.3.2.3 Effect of bolus particle size distribution and bolus residues

The theoretical analysis showed that subjects who produce boluses with smaller particles will have created more surface area and so are expected to perceive a higher retronasal aroma release intensities due to a faster release and movement of the taste and aroma compounds from the food matrix into the saliva and air phases. The particle size parameters (i.e. d_{75} , and d_{25}) of Subject A4 were the smallest at swallow point between all subjects (Table 6-2). The pasted fraction for this subject was also among the highest in all subjects (Table 6-2). As chewing progressed, particle size would reduce, resulting in an

increased surface area available for flavours to diffuse from the food matrix into the surrounding saliva and from the bolus to air (Harrison et al., 1998; Doyennette et al., 2014). The increase in surface area of particles would have also increased the rate of hydration of saliva, resulting in a faster dilution effect of saliva to the starch components in rice, as explained earlier. Starch-based food systems such as rice produce a portion of significantly small particles (pasted fraction) with every chew, which means not only that it provided a large surface area for transfer of aroma, but a lot of the starch components that interacted with the aroma compounds would have been diluted instantaneously with saliva. The findings of Subject A4 who had a high aroma release agreed with the theoretical analysis regarding the effect of particle size distribution on aroma release.

In contrast, Subject A1, who had the largest bolus particle size parameters (d_{75} , d_{50} , and d_{25}) had the second-highest aroma release. The findings from Subject A1 contradict the theoretical analysis on the role of particle size on aroma release. However, Subject A1 had the highest amount of rice bolus residues remaining in the mouth. What this means is that although Subject A1 had indicated (by raising hand to signal) he or she has swallowed, there were still a large portion of rice residues remaining in the mouth that could still be responsible for further release post-swallowing. However, having a larger amount of rice bolus residues does not guarantee there will be further release if starch does have the ability to retain the flavour compounds as explained previously for Subject A4. In a study looking at the influence of starch and amylopectin for 20 volatile flavour compounds in aqueous model food systems, it was found that increasing starch concentrations did not have any profound effect on volatile release under mouth conditions (van Ruth & King, 2003). The authors explained that although flavour compounds can bind with starch to reduce free flavour available for release, under mouth conditions, kinetic factors emerge as the primary factors determining the flavour release for their starch model systems. This is interesting because the driving force for transfer of volatile aroma compounds across the interface is the difference in flavour concentration between the food/saliva mixture and air phase under mouth conditions (van Ruth & King, 2003). Perhaps a higher amount of remaining rice bolus residues allowed diffusion from the rice-saliva mixture to the gas phase by the concentration gradients.

Subjects A2, A3 and A5 all possessed similar dynamic behaviour for aroma release (Fig. 6-23), which followed the trend of breakdown pathways as described in Fig. 6-22. The combined effect of

particle size and saliva content as explained for Subject A1 might explain their aroma release behaviour. Subjects A3 and A5, both efficient chewers, would have smaller particle size in the bolus resulting in a high transfer of aroma release but as they also had low saliva parameters (saliva flow at rest, stimulated saliva and saliva content in bolus), a lot of the aroma compounds would stay bound with the starch components as less was released into saliva. Similarly, Subject A2, despite being the least efficient chewer, had similar dynamics of aroma release with subjects A3 and A5 due to a high amount of saliva parameters that overruled the effect of particle size on aroma release.

The data obtained to link oral processing and aroma release agreed with the theoretical analysis in some ways. In particular, it was observed that Subject A4, who had the smallest particle size parameters had the highest aroma release behaviour. However, although in theory saliva can reduce flavour release through dilution, for starch-based matrices, it is suspected that this may be due to the role of saliva that could weaken the physico-chemical interactions between the flavour compounds and starch, thus, increases flavour release. Further study however would be needed to understand the effect of saliva on the flavour release of starch-based foods as it seems that during in mouth conditions, flavour release is governed by both thermodynamic and kinetic factors (van Ruth & King, 2003).

While the number of subjects used in this chapter is small, the aim of this chapter was not to justify flavour release from inter-individual differences in a population but rather to provide preliminary insights upon factors that can influence aroma release from an oral processing and physiology point of view. The theoretical analysis developed, and experimental data obtained in this study will be used as a basis for the development of a mathematical to predict aroma release in the subsequent chapter(s). Additionally, the experimental data obtained here will also be used to validate the model. By testing the implemented model against the real data, its underlying assumptions can be evaluated while considering the interactions between particle breakage, physiological parameters and saliva addition.

6.5 Chapter conclusion

Cooked white rice was chosen as a food system to further expand the application of the chewing models developed in Chapter 3, linking oral processing and sensorial outcomes. In this chapter, a series of experiments were conducted to understand the physiological and oral processing variables that affect

aroma release. The experimental data will also be used to provide model inputs and for model validation in the subsequent chapters.

A conceptual model was first developed to understand the role of subject's physiological and oral processing variables on aroma release of cooked white rice. The reliability of the conceptual model was then tested by comparing against the experimental *in vivo* aroma release data of five subjects with different physiology and oral processing behaviour. Results showed that the dynamic behaviour of aroma release for all subjects followed a similar trend with the breakdown pathways taken for each subject. Subjects with smaller particle size in their bolus had higher aroma release. This agrees with the theoretical analysis about the influence of a larger surface area of particles on increasing the rate of mass transfer of flavour compounds. In contrast, while the role of saliva should in theory reduce aroma release through dilution, experimentally, a conflicting result was observed because subjects who had high salivary flow rate seemed to have higher aroma release.

Because aroma release is influenced by many physiological factors which may have contrary effects it is difficult to identify which one had the dominant effect for a given individual to explain their release. A larger number of individuals could help to identify these trends more clearly because various combinations of physiological and release parameters would be statistically present in the database. A statistical model directly relating physiology and release could be built with a larger database. The development of a mechanistic model allows the theoretical basis to be tested directly.

Although preliminary, the chapter provides insights on the role of oral processing dynamics on flavour release from solid starch-based food products. The next chapter will aim to develop a mathematical model to predict the aroma release of rice using the theoretical analysis developed here as a basis. The experimental data will then be used for validation against the developed mathematical model.

Chapter 7 A mathematical model for *in vivo* aroma release

7.1 Introduction

During mastication, aroma compounds that are initially present in the food matrix have to reach the olfactory epithelium by the retronasal pathway in order to be perceived by a consumer (Trelea et al., 2007). However, the relationship between the release of the aroma compounds and the perception is complex and not well understood due to poorly understood mechanisms and their interactions (Trelea et al., 2007; Doyennette et al., 2011; Doyennette et al., 2014).

Mechanistic models can be a useful tool to predict aroma release and therefore are a key step in understanding, for example, the role of the product (e.g. composition and structure), the consumer (e.g. physiological parameters and individual experience) in the perceived flavour (Harrison et al., 1998; Trelea et al., 2007; Doyennette et al., 2011; Doyennette et al., 2014; Déléris et al., 2016). Additionally, they can also be used to understand the role of oral processing in flavour release, as well as to help design food products taking into account physiological characteristics of individuals (e.g. young or older people, or a people with clinical pathologies such as dysphasia) (Trelea et al., 2007). Consequently, the development of mathematical models can constitute a useful tool to predict aroma release and thus to identify the most essential physiochemical, anatomical and physiological parameters responsible for this release (Trelea et al., 2007).

Mathematical models predicting the aroma release of different food matrix types have been developed in the literature. The first model that predicts the aroma release of solid and semisolid foods was proposed by Harrison et al., (1998). The model was proposed on the basis of mass transfer theory; however, the models did not include experimental validation. Additionally, strong simplifying assumptions were made for the proposed model such as constant breath airflow and foods that were disintegrated during chewing did not further disintegrate and mix with saliva (Harrison et al., 1998; Trelea et al., 2007). Based on the model proposed by Harrison et al. (1998), improvements have been made by integrating a more realistic description of physiological mechanism; such as for mastication of semisolid products (Trelea et al., 2007; Wright & Hills, 2003; Wright et al., 2013), liquid products

(Rabe et al., 2004; Doyennette et al., 2011; Le Révérend et al., 2013) and for solid products (Doyennette et al., 2014; Harrison et al., 2014).

The most comprehensive model to predict aroma release during oral processing of solid foods to date was developed by Doyennette et al. (2014). The model was constructed using one-dimensional differential equations for mass transfer and flavour release and was validated against experimental *in vivo* data using cheese as the food system. A sensitivity analysis performed on the mathematical model showed that the air-bolus contact surface area could affect aroma release; however, the model did not include the coupling to any food breakdown model to predict the air-bolus contact surface area. Instead, the model assumes that the contact area between the solid product and the liquid bolus during mastication evolves linearly with time, which may not be true for pasty products such as cheese. The limitation of the model was acknowledged by the authors as the lack of coupling to a food breakdown model, stating that this would require complex experimental protocols which are challenging to implement (e.g. bolus spitting after a variable number of bites).

The main aim of Chapter 7 is, therefore, to develop a mechanistic model to predict *in vivo* aroma release using cooked white rice as a case study. The novelty aspect of this model is that it includes the food breakdown model developed in the previous chapters (a combined selection and breakage model) to predict the air-bolus contact area. In addition, the model would have to consider the mechanisms for mass transfer between the solid particles and liquid content of the bolus and how the interfacial area between the bolus and air phases change during mastication. This is the first study that uses cooked white rice as the food system to predict *in vivo* aroma release, developing the model based on the experimental study summarised in Chapter 7. This chapter will present the development of the mathematical model to predict *in vivo* aroma release of cooked white rice that was spiked with two aroma compounds (2-nonanone and ethyl propanoate).

7.2 Conceptual model development

7.2.1 Principles of the model

The aroma release model developed in this chapter is an extension to the model developed for solid products (cheese) developed by Doyennette et al. (2014). The extension of the model is the coupling

with the food breakdown model (selection and breakage function) to predict the air-bolus contact area during mastication. The model developed here only predicts the aroma release during the chewing step, i.e. the aroma release after the swallowing step is not considered as the particle size distribution of the rice that remains in the mouth were not measured in Chapter 6 to validate the food breakdown model. Fig. 7-1 shows the conceptual diagram for the interconnected compartments that are involved in flavour release during the consumption of cooked white rice. All variables and parameters of the interconnected compartments required for the model simulation are specified in Fig. 7-1.

From Fig. 7-1, the compartments that were involved in flavour release during food consumption were denoted as follows: the oral cavity (index O), the pharynx (index F), the nasal cavity (index N) and the trachea (index T). The model used here is an adaptation from a chemical engineering approach where the various parts of the upper respiratory tract are viewed as interconnected reactors, containing an air phase (index A) and the saliva phase, index (S). To take the retention effect of lubricated mucosa (index M) into account, the lubricated mucosa layers were also included in each compartment (oral cavity, pharynx and nasal cavity). The compartments were included as one of the aroma compounds used to spike the cooked white rice, 2-nonanone, was known to interact with the lubricated mucosa (Doyennette et al., 2014; Déléris et al., 2016).

The airflow rates (Q_{Na} , Q_{Ta} , Q_{Oa}), were considered to be positive if their direction is the one indicated by the arrows in Fig. 7-1 (inhalation) and negative when in the opposite case (exhalation). Aroma concentrations in all compartments (oral cavity, pharynx and nasal cavity) were calculated using mass transfer equations and mass balances. The mass balances include the flavour release at the saliva – product (rice) interface, air-saliva interface and the air and lubricated mucosa layer interface. In general, when two phases are in contact (e.g. air and saliva), volatile transfer occurs across the interfacial layers. At each side of the interface, the driving force is the concentration difference between the bulk phase and the interface. At the infinitely thin interface, local equilibrium is expressed via the partition coefficient between phases. The released volatile flux will depend on the contact area between phases and the transfer resistance in each phase, expressed via mass transfer coefficients. Other than the interfacial release, bulk flow may also occur between the various compartments. The volatile mass balances for this case involve the bulk concentrations and the bulk flow rates.

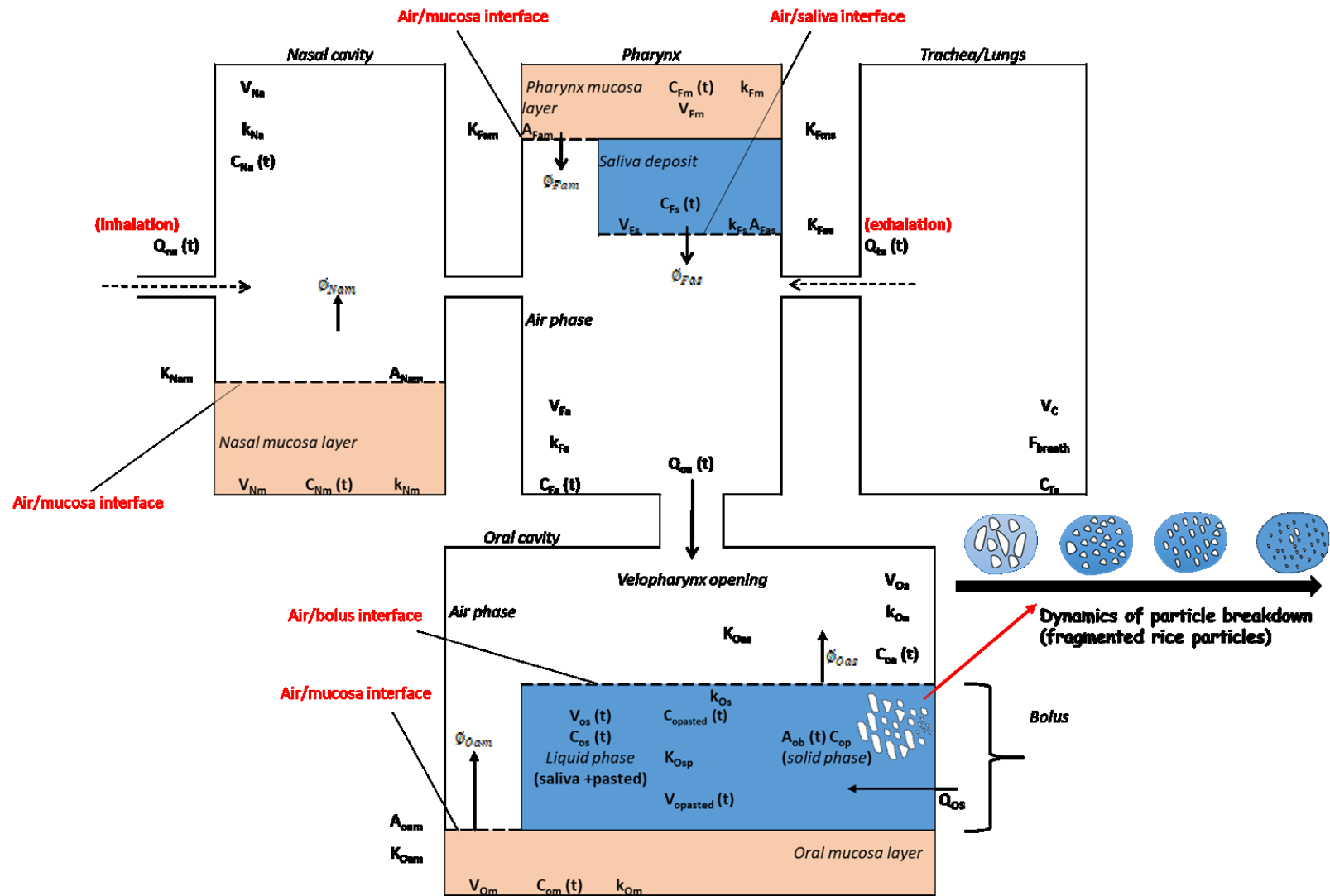


Fig. 7-1: Conceptual diagram of the interconnected compartments and the mechanisms involved in flavour release during the consumption of cooked white rice.

7.2.2 Assumption of the contact area between the rice and saliva phase

During mastication, the surface area of the food increases dramatically, allowing a greater proportion of the flavour to be released from the food matrix to the surrounding saliva (Harrison et al., 1998). The breakdown of a cooked rice particle follows a ‘cleave and paste’ mechanism (Fig. 7-2) where when a rice kernel is occluded, one or a few large particles are produced, and a fraction of the original kernel is pasted into very fine particles (paste) which become part of the liquid phase of the bolus (Gray-Stuart, 2016). It was found in the study by Gray-Stuart (2016) that during the mastication of rice from a single person, the rice bolus forms a bimodal particle size distribution when measured using a laser diffraction method. The size when particles become pasted were particles that have a size less than 0.355 mm. Pasting involves swelling of granules and it is known that normal rice starches have a granule size range of 1.9-26 μm (Desam et al., 2020) and that the granules can swell to a maximum of 2-48 times of their initial size when heated to various temperatures (Lii et al., 1996). Other than temperature, the swelling of starch granules can be enhanced with increasing shear rate (Svegmark & Hermansson, 1991) and the presence of excess water (Rao et al., 1997). Therefore due to the conditions during oral processing which involves a combination of vertical and lateral shearing of the teeth, heating and addition of saliva, the pasting size threshold of 0.355 mm as assumed here is a good starting point for the model development.

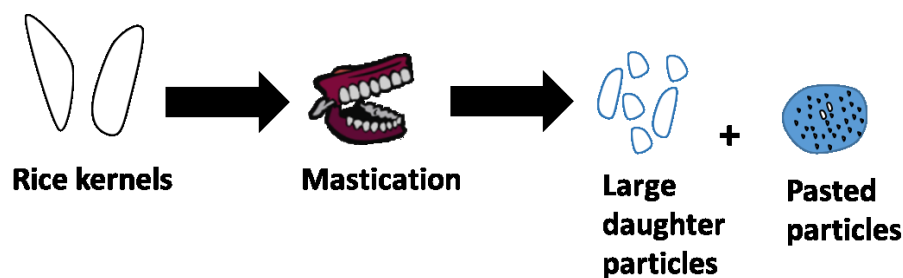


Fig. 7-2: ‘Cleave and paste’ mechanism during mastication of cooked rice

Therefore, during mastication of rice, two simultaneous phenomena can occur:

- the transfer of aroma compounds from the non-pasted daughter particles into the liquid phase of the bolus, particularly from newly exposed surface area generated during a chewing cycle, and
- the release of the aroma compounds contained in the pasted particles into the liquid phase of the bolus, where it was assumed because of their small size, that once transferred, the concentration of the aroma compounds in the pasted and liquid phases reach equilibrium instantaneously.

The direct transfer of aroma compounds from the solid surfaces into the air phase was assumed negligible as after ingestion there will be at least a thin layer of saliva/moisture present between these two phases and therefore aroma transfer always takes place through the liquid phase.

Because of the challenge to distinguish between the relative contributions of each mechanism, it was assumed initially that the release of the aroma compounds is dominated by the transfer of the aroma compounds from the pasted particles into the liquid phase of the bolus. This is a reasonable assumption as the surface area to volume ratio of the pasted particles will be significantly larger than the surface area to volume ratio of the particles that are greater than 0.355 mm. Similarly, the distances for diffusion in the pasted particles is very small. Thus, it is expected that the transfer of the aroma compounds from the pasted particles to the liquid phase of the bolus is significantly faster compared to the transfer from the larger particles.

Once in the liquid phase of the bolus, the concentration of the aroma compounds will be diluted by saliva flow into the oral cavity (Harrison et al., 1998). At the same time, volatiles partition from the saliva into the air phase, which then transports them to the pharyngeal compartment. During mastication, some aroma release to the pharynx and further to the nasal cavity is possible for panellists with imperfect velopharyngeal closure (Trelea et al., 2007). In the model, it is assumed that all subjects possess an imperfect velopharyngeal closure if the concentration of aroma compounds increases after food ingestion and continues to do so during the mastication period (i.e. the period before swallowing).

7.3 Model assumptions

Further to some of the main assumptions that were described in section 7.2.1 above, the following additional assumptions were made to develop the model equations.

- When a rice kernel is occluded, one or a few large particles are produced, and a fraction of the original kernel is pasted, which becomes part of the liquid (suspension) phase of the bolus.
- Isothermal conditions were assumed. That is, the temperature of the cooked rice which was served at 37°C, was constant throughout the duration of mastication. This is a reasonable assumption, considering the body temperature is at 37°C. This assumption also ensures the partition coefficient of aroma compounds will not change with temperature and avoids the need to include a heat transfer model.
- The air coming from the trachea (i.e. from the lungs) is assumed to be aroma free. This is because the contact area between the air and lungs is very large (~100 m²) (Trelea et al., 2007; Doyennette et al., 2011), thus it is reasonable to assume that the aroma compounds are quickly absorbed into the lungs.
- The transfer resistance on the air side ($1/k_{Oa}$) was assumed to be negligible compared to the transfer resistance on the liquid bolus side ($1/k_{Os}$). This is a reasonable assumption as the magnitude of the mass transfer coefficients representing the reciprocal of the resistances are 10^{-2} and 10^{-6} m/s, respectively (Doyennette et al., 2014).
- The ambient air coming during inhalation ($Q_{Na} \geq 0$) is assumed to be aroma free.
- The flow rate of saliva (Q_{Os}) is assumed to be constant over time.
- It is assumed that the food particles in the mouth were immediately coated with saliva at time zero.
- It is also assumed that at zero time, the concentration of flavour in both the liquid and air phases in all compartments is zero.
- The mass transfer coefficient is constant for all volatiles.
- The aroma compound concentration in the rice particles (non-pasted) remains constant over time.

- The release of aroma from the saliva to the mucosa layers in the oral cavity and pharynx is assumed negligible. This is because the volume of the saliva is significantly smaller than the volume of the mucosa layers in both compartments.
- Complete mixing is assumed when aroma is released in the air phases.
- The volume of air in nasal cavity and pharynx compartments are constant with time but the air volume in the oral cavity can change with time due to chewing movements which can create a cyclic variation of the air volume from the opening of velopharynx (Doyennette et al., 2014).
- Saliva residue can escape the oral cavity through the velopharynx during chewing and coats the pharyngeal wall.
- The partitioning of the aroma compounds in the air and liquid bolus/saliva phase follows Henry's law. This means it is assumed that the aroma compounds are not affected with the bolus composition due to interactions with the food components and/or saliva components (mucin) which can cause changes to the partition coefficient. This assumption is valid as the volume of pasted particles is significantly smaller than the volume of saliva.

7.4 Mathematical model formulation

In the previous section, the assumptions required in the model have been described in detail. While it was speculated in Chapter 6 that the interactions between the aroma compounds and the components in rice or mucins in saliva could affect aroma release, addressing these aspects lies beyond the scope of this model. To begin with, the model will not include such interactions to predict aroma release, but it could be an aspect to be revisited should the predictions disagree with the experimental data.

7.4.1 Air/bolus interfacial conditions in the oral cavity

Because the volume of the liquid bolus is largely composed of saliva compared to the pasted particles, the subscript 's' which denotes saliva will be used to describe the liquid bolus phase while keeping in mind that the liquid bolus includes both saliva and suspended pasted particles. As the mass transfer resistance on the air side $1/k_{Oa}$ was assumed to be negligible when compared to the mass transfer resistance on the liquid bolus side $1/k_{Os}$ as described above, the interfacial concentration of the aroma compound at the liquid bolus side is given as

$$C_{Os}(t) = \frac{C_{Oa}(t)}{K_{Oas}} \quad (7.1)$$

7.4.2 Liquid bolus in the oral cavity

The liquid bolus compartment is initially composed of pure saliva and is progressively flavoured by the addition of rice particles which were pasted. The volume increases by the addition of saliva (salivary flow rate) and with the addition of pasted particles.

The volume of the liquid bolus $V_{Ol(t)}$ can then be divided into two parts:

$$V_{Ol(t)} = V_{Os(t)} + V_{Opasted(t)} \quad (7.2)$$

where

$$\frac{dV_{Os(t)}}{dt} = Q_{Os} \quad (7.3)$$

7.4.3 Concentration of aroma compounds in the saliva phase

After each chewing cycle, new volumes of pasted particles are formed. This is then added to saliva, which becomes the liquid bolus phase. The concentrations of the aroma compounds in the saliva phase and pasted particles were assumed to reach equilibrium instantaneously. Therefore, after each chewing cycle, the mass of the aroma compounds in the saliva phase is a combination of the initial mass (before chewing) and the new mass of aroma being added from the pasted particles. The following word balance describes the mass balance of the aroma compounds in the saliva phase between a single chewing step.

Mass of aroma compounds in the liquid bolus phase (mass in saliva and pasted particles) before chew	+	New mass of aroma compounds in new pasted particles formed in next chew
=	Mass of aroma compounds in the liquid bolus phase (mass in saliva and pasted particles) after the chew	

And the balance was expressed mathematically as

$$V_{Os_i}C_{Os_i} + V_{Opasted_i}C_{Opasted_i} + (V_{Opasted_{i+1}} - V_{Opasted_i})C_{Op} = V_{Os_{i+1}}C_{Os_{i+1}} + V_{Opasted_{i+1}}C_{Opasted_{i+1}}$$

...(7.4)

The volatile concentration on the pasted particles side, using the partition conditions at the interface, is given by

$$C_{Opasted} = \frac{C_{Os}}{K_{Osp}} \quad (7.5)$$

After rearranging, the concentration of the aroma compound in the saliva after a single chew can be described as

$$C_{Os_{i+1}} = \frac{(V_{Os} + \frac{V_{Opasted}}{K_{Osp}})_i C_{Os_i} + (V_{Opasted_{i+1}} - V_{Opasted_i}) C_{Op}}{(V_{Os} + \frac{V_{Opasted}}{K_{Osp}})_{i+1}} \quad (7.6)$$

This step change in aroma concentration occurs instantaneously with each chew and then changes dynamically due to dilution with the addition of saliva or losses to the oral airspace. This is described in the word balance below.

rate of accumulation of mass of
aroma compound in the liquid

=

- Rate of mass loss to air caused
by the concentration difference
between the saliva
concentration and the
interfacial concentration.

And the balance was expressed mathematically as

$$\begin{aligned} \frac{d(V_{Os}(t)C_{Os}(t) + V_{Opasted}(t)C_{Opasted}(t))}{dt} &= -A_{Ob}(t)k_{Os} \left(C_{Os}(t) - \frac{C_{Oa}(t)}{K_{Oas}} \right) \\ \frac{d(V_{Os}(t)C_{Os}(t) + \frac{V_{Opasted}(t)C_{Os}(t)}{K_{Osp}})}{dt} &= -A_{Ob}(t)k_{Os} \left(C_{Os}(t) - \frac{C_{Oa}(t)}{K_{Oas}} \right) \\ \frac{d \left(V_{Os}(t) + \frac{V_{Opasted}(t)}{K_{Osp}} \right) C_{Os}(t)}{dt} &= -A_{Ob}(t)k_{Os} \left(C_{Os}(t) - \frac{C_{Oa}(t)}{K_{Oas}} \right) \end{aligned}$$

Applying the product rule on the left-hand side

$$V_{Os}(t) \frac{dC_{Os}(t)}{dt} + C_{Os}(t) \frac{dV_{Os}(t)}{dt} + C_{Os}(t) \frac{V_{Opasted}(t)}{K_{Osp}} = -A_{Ob}(t)k_{Os} \left(C_{Os}(t) - \frac{C_{Oa}(t)}{K_{Oas}} \right)$$

After rearranging,

$$\frac{dC_{Os}(t)}{dt} = \frac{-\left(Q_{Os}C_{Os}(t) + A_{Ob}(t)k_{Os}\left(C_{Os}(t) - \frac{C_{Oa}(t)}{K_{Oas}}\right)\right)}{\left(V_{Os}(t) + \frac{V_{Opasted}(t)}{K_{Osp}}\right)} \quad \dots (7.7)$$

7.4.4 The bolus surface area, A_{Ob}

The following derivation shows the steps required and assumptions made to calculate the bolus surface area.

For example, if each particle is assumed as a sphere (to provide clarity spherical shape is used here but the equations will be adaptable to other particle shapes as well), the volume of a particle is

$$V_p = \frac{4}{3}\pi r^3 \quad (7.8)$$

If it was assumed that each particle has an amount of fluid volume, V_{fluid} associated with it, the volume fraction of the fluid with respect to the volume of particle is

$$a = \frac{V_{fluid}}{V_p} \quad (7.9)$$

Therefore the V_{fluid} is

$$V_{fluid} = a \frac{4}{3}\pi r^3 \quad (7.10)$$

Assuming that each particle has an even and the same coating thickness, x (independent of size), the total volume of the particle and the fluid can be described as

$$V_{tot} = \frac{4}{3}\pi(r+x)^3 \quad (7.11)$$

where the V_{fluid} can also be calculated by subtracting V_{tot} with V_p . Hence,

$$V_{fluid} = \frac{4}{3}\pi(r+x)^3 - \frac{4}{3}\pi r^3 \quad (7.12)$$

Equating Eq.7.10 and Eq. 7.12, x can be described as

$$x = r(1+a)^{\frac{1}{3}} - r \quad (7.13)$$

Therefore, the surface area of a particle with a coating thickness can be described as

$$A_p = 4\pi(r+x)^2 \quad (7.14)$$

Substituting Eq. 7.13 into Eq. 7.14

$$A_p = 4\pi r^2(1+a)^{\frac{2}{3}} \quad (7.15)$$

If n_p is the total number of particles, the total surface area of all particles (before they coalesce due to saliva bonding) can be described as

$$4\pi(1+a)^{\frac{2}{3}} \sum_i^{n_p} r_i^2 \quad (7.16)$$

The bolus surface area can be predicted by emulating the concept of a sintering mechanism. In a sintering mechanism, the total surface area of the particles is reduced by growing bonds (bridges) between contacting particles during a heating process. The same concept can be applied here. As the number of chews increases, the amount of saliva incorporated in the bolus also increases. This also increases the number of saliva bridges among the particles in the bolus, which promotes the coalescence of the particles. For the sintering mechanism, a linear relationship was proposed between the surface area and the packing density where the surface area declines as the density increases (German, 2016). Thus, the surface area of a bolus can be described as

$$A_{Ob} = b\phi + c \quad (7.17)$$

Assuming that the initial packing density is ϕ_E , the initial surface area of the bolus is therefore

$$SA_E = b\phi_E + c \quad (7.18)$$

Assuming that the bolus forms a perfect sphere when the voidage between particles is 100% saturated with saliva ($\phi = 1$), the surface area of the bolus when at 100% saturation is

$$SA_{sphere} = b + c \quad (7.19)$$

Substituting Eq 7.19 into Eq. 7.18

$$SA_E = b(\phi_E - 1) + SA_{sphere} \quad (7.20)$$

Rearranging Eq. 7.20, the b constant can be described as

$$b = \frac{SA_{sphere} - SA_E}{1 - \phi_E} \quad (7.21)$$

Substituting Eq. 7.21 to Eq. 7.19, the c constant can be described as

$$c = SA_{sphere} - \frac{SA_{sphere} - SA_E}{1 - \phi_E} \quad (7.22)$$

Substituting Eq. 7.21 and Eq. 7.22 to Eq. 7.17, the surface area of the bolus can be described as

$$A_{Ob} = \frac{SA_{sphere} - SA_E}{1 - \phi_E} (\phi - 1) + SA_{sphere} \quad (7.23)$$

The initial surface area of the bolus, SA_E , can be estimated using equation 7.16. Thus,

$$SA_E = 4 \pi (1 + a)^{\frac{2}{3}} \sum_i^{n_p} r_i^2 \quad (7.24)$$

where

$$a = \frac{\varepsilon}{1 - \varepsilon} \cdot S \quad (7.25)$$

The total volume of particles can be described as below

$$V_{ptotal} = \frac{4}{3} \pi \sum_i^{n_p} r_i^3 \quad (7.26)$$

The total volume of the bolus is therefore

$$V_{bolus} = \frac{V_{ptotal}}{1 - \varepsilon} \quad (7.27)$$

If R is the radius of the bolus, the volume of the bolus can also be described as

$$V_{bolus} = \frac{4}{3} \pi R^3 \quad (7.28)$$

Equating Eq.7.27 and Eq. 7.28, the radius of the bolus can be calculated as follows

$$R = \left(\frac{\sum_i^{n_p} r_i^3}{1 - \varepsilon} \right)^{\frac{1}{3}} \quad (7.29)$$

Therefore, the surface area of the bolus when at 100% saturation (assuming spherical shape) is

$$SA_{sphere} = 4 \pi R^{\frac{2}{3}} \quad (7.30)$$

Finally, the packing density of the bolus in Eq. 7.23 can be estimated as described below

$$\phi = (1 - \varepsilon) + S \cdot \varepsilon \quad (7.31)$$

where the saturation of the bolus, S is calculated using the equation below

$$S = \frac{V_{opasted} + V_s}{V_{ptotal}} \cdot \left(\frac{1 - \varepsilon}{\varepsilon} \right) \quad (7.32)$$

The saturation of the bolus decides when Eq. 7.23 is used to estimate the bolus surface area. For any saturation value less than 1, Eq. 7.23 will be used to estimate the bolus surface area. For the bolus when the saturation surpasses the value of 1, the bolus surface area was estimated by evaluating

the radius of the bolus (assuming the bolus is spherical) using Eq. 7.28. The radius was then used to calculate the bolus surface area assuming the bolus is of a spherical shape.

7.4.5 Aroma compound retention by the lubricated mucosa in the oral cavity

The reservoir effect of the lubricated mucosa was also taken into account as one of the aroma compounds used in the study, 2-nonanone, was known to interact with the mucosa compartments (Doyennette et al., 2014; Dél  ris et al., 2016). It is assumed that the air in the mouth was in contact with the lubricated oral mucosa layer. Therefore, the rate of loss of volatile from the mucosa to the air phase is given by:

$$V_{Om} \frac{dO_m(t)}{dt} = -k_{Om} A_{Oam} \left(C_{Om}(t) - \frac{C_{Oa}(t)}{K_{Oam}} \right) \quad (7.33)$$

7.4.6 Air in the oral cavity

The mass balance of aroma compounds in the air phase contained in the oral cavity involves the addition from the aroma compound flux of the liquid bolus, the volatile flux from the oral mucosa and the aroma compounds from the air in the pharynx (for $Q_{Oa}(t) \geq 0$), which means that the air flows in the direction shown by the arrows in Fig. 7-1. The jaw movements during mastication induce velopharynx opening and cyclic air flow between the pharynx and the mouth (Marion Doyennette et al., 2014; Matsuo, Metani, Mays, & Palmer, 2010).

$$V_{Oa}(t) \frac{dC_{Oa}(t)}{dt} = A_{Ob} k_{Os} \left(C_{Os}(t) - \frac{C_{Oa}(t)}{K_{Oas}} \right) + k_{Om} A_{Oam} \left(C_{Om}(t) - \frac{C_{Oa}(t)}{K_{Oam}} \right) + \begin{cases} Q_{Oa}(t) (C_{Fa}(t) - C_{Oa}(t)) & \text{if } Q_{Oa}(t) \geq 0 \\ 0 & \text{if } Q_{Oa}(t) < 0 \end{cases} \quad \dots(7.34)$$

Because little information was known on the real change in V_{Oa} , it was assumed that the chewing movements create a cyclic variation of the air volume V_{Oa} around a mean value

$V_{Oa \text{ mean}}$ (Matsuo et al., 2010; Doyennette et al., 2014).

$$V_{Oa}(t) = V_{Oa \text{ mean}} + \Delta V_{Oa} \sin(2\pi f r_{\text{opening}} t) \quad (7.35)$$

Hence, the air flow rate coming from the mouth is calculated as follows:

$$Q_{Oa}(t) = \frac{dV_{Oa}(t)}{dt} = 2\pi f r_{\text{opening}} \Delta V_{Oa} \cos(2\pi f r_{\text{opening}} t) \quad (7.36)$$

where ΔV_{oa} was estimated to be 20% of $V_{oa\ mean}$ (Doyennette et al., 2014). The highest opening frequency $f_{r_{opening}}$, was coordinated with the chewing frequency, $f_{r_{chew}}$ and that the lowest opening frequency was coordinated with the breathing frequency, F_{breath} .

7.4.7 Bolus in the pharynx

The volatile release for the residual bolus in the pharynx to the adjacent air is given by:

$$V_{Fs} \frac{dC_{Fs}(t)}{dt} = -k_{Fs}A_{Fas} \left(C_{Fs}(t) - \frac{C_{Fa}(t)}{K_{Fas}} \right) \quad (7.37)$$

7.4.8 Aroma compound retention by the lubricated mucosa in the pharynx

The rate of loss of volatile from the mucosa in the pharynx to the air phase is given by:

$$V_{Fm} \frac{dC_{Fm}(t)}{dt} = -k_{Fm}A_{Fam} \left(C_{Fm}(t) - \frac{C_{Fa}(t)}{K_{Fam}} \right) \quad (7.38)$$

7.4.9 Air in the pharynx

The air in the pharynx receives aroma compounds from the residual bolus in the pharynx, the mucosa layer in the pharynx, as well as the air flow rates from the other compartments. This include the air flow from the mouth ($Q_{Oa}(t)$), the nose ($Q_{Na}(t)$) and the trachea ($Q_{Ta}(t)$).

The air balance in the pharynx is given by:

$$Q_{Na}(t) = -Q_{Ta}(t) + Q_{Oa}(t) \quad (7.39)$$

The mass balance of the aroma compound in the air phase of the pharynx gives the following equation:

$$V_{Fa} \frac{dC_{Fa}(t)}{dt} = k_{Fs}A_{Fas} \left(C_{Fs}(t) - \frac{C_{Fa}(t)}{K_{Fas}} \right) + k_{Fm}A_{Fam} \left(C_{Fm}(t) - \frac{C_{Fa}(t)}{K_{Fam}} \right) + \begin{cases} -Q_{Oa}(t)(C_{Oa}(t) - C_{Fa}(t)) & \text{if } Q_{Oa}(t) < 0 \\ Q_{Na}(t)(C_{Na}(t) - C_{Fa}(t)) & \text{if } Q_{Na}(t) \geq 0 \\ Q_{Ta}(t)(C_{Ta}(t) - C_{Fa}(t)) & \text{if } Q_{Ta}(t) \geq 0 \end{cases} \quad \dots(7.40)$$

7.4.10 Aroma compound retention by the lubricated mucosa in the nasal cavity

The rate of loss of volatile from the mucosa in the nasal cavity to the air phase is given by:

$$V_{Nm} \frac{dC_{Nm}(t)}{dt} = -k_{Nm}A_{Nam} \left(C_{Nm}(t) - \frac{C_{Na}(t)}{K_{Nam}} \right) \quad (7.41)$$

7.4.11 Air in the nasal cavity

The mass balance of the aroma compound in the air phase in the nasal cavity is given by:

$$V_{Na} \frac{dC_{Na}(t)}{dt} = k_{Nm} A_{Nam} \left(C_{Nm}(t) - \frac{C_{Na}(t)}{K_{Nam}} \right) + \begin{cases} Q_{Na}(t) (0 - C_{Na}(t)) & \text{if } Q_{Na}(t) < 0 \\ Q_{Na}(t) (C_{Fa}(t) - C_{Na}(t)) & \text{if } Q_{Na}(t) \geq 0 \end{cases} \dots (7.42)$$

7.4.12 The initial conditions

The initial concentration of aroma compounds in all compartments for the when the product was introduced in the mouth up to the first chewing cycle (chew 0 to chew 1), is zero. The initial volume of saliva to solve Eq. 7.3 was set as the volume of saliva at rest. Thus, the initial conditions from chew 0 to chew 1 are:

$$V_{Os}(t_0) = V_{Osrest}$$

$$C_{Os}(t_0) = C_{Oa}(t_0) = C_{Om}(t_0) = C_{Fs}(t_0) = C_{Fm}(t_0) = C_{Fa}(t_0) = C_{Nm}(t_0) = C_{Na}(t_0) = 0$$

After the 1st chew, rice will break into smaller particles, and some will be pasted which dissolves in the liquid bolus. The volatiles from the pasted particles are then transferred into the liquid bolus, and an instant equilibrium was assumed (see section 7.4.2, Eq. 7.6). Thus, the initial conditions are:

$$C_{Os}(t_0) = C_{Os}(t_{chew=1}) \text{ calculated from Eq. 7.6}$$

$$V_{Os}(t_0) = V_{Os}(t_{chew=1})$$

$$C_{Oa}(t_0) = C_{Oa}(t_{chew=1})$$

$$C_{Om}(t_0) = C_{Om}(t_{chew=1})$$

$$C_{Fs}(t_0) = C_{Fs}(t_{chew=1})$$

$$C_{Fm}(t_0) = C_{Fm}(t_{chew=1})$$

$$C_{Fa}(t_0) = C_{Fa}(t_{chew=1})$$

$$C_{Nm}(t_0) = C_{Nm}(t_{chew=1})$$

$$C_{Na}(t_0) = C_{Na}(t_{chew=1})$$

7.5 Numerical solution

The model was solved numerically using MATLAB program version R2019a using the ode45

function with a default relative error tolerance value of 0.001 which was shown to produce negligible

numerical error. The MATLAB code that was developed to numerically solve the ODE equations can be referred in Appendix A.

7.6 Coupling of the food breakdown model and the aroma release model

As described before, the food breakdown model developed in Chapter 3 was coupled with the ODE equations developed above to predict aroma release (quantified by the concentration of aroma compound in the nasal cavity). Fig. 7-3 shows a schematic model diagram describing the steps required to couple the models. The input parameters required for the selection and breakage models and the implementations have been described previously in Chapter 3. Once the selection and breakage models were applied to the initial PSD, the new PSD outputted the pasted daughter particles (diameter < 0.355 mm) and the non-pasted particles which were essentially particles with sizes that were greater than 0.355 mm. The simulation was repeated after the specified number of chews was completed. Once the PSD was predicted, the predictions were compared against experimental data, this was the *in vivo* bolus PSD data collected in Chapter 6. Since the model input parameters were not known, the PSO fitting approach developed in Chapter 4 was applied to solve the input parameters. The validated PSD model was then coupled to the aroma release models developed in this chapter (section 7.4). The pasted and non-pasted PSD outputs from the chewing model were used to calculate the bolus surface area, bolus saturation and the concentration of aroma compounds in the saliva phase. These consequential variables were needed to solve the mass transfer ODE equations in the various physiological compartments developed in section 7.4.

Finally, as the ODE equations could not be solved analytically, they were solved numerically using MATLAB. The concentration of aroma compound predicted in the nasal cavity was then compared against *in vivo* data (e.g *in vivo* aroma release data measured in Chapter 6) to test the validity of the model.

7.7 General model results

Fig. 7-4 shows the predicted time variations of 12 variables for the release of ethyl propanoate during the mastication of the cooked rice to demonstrate the model solutions.

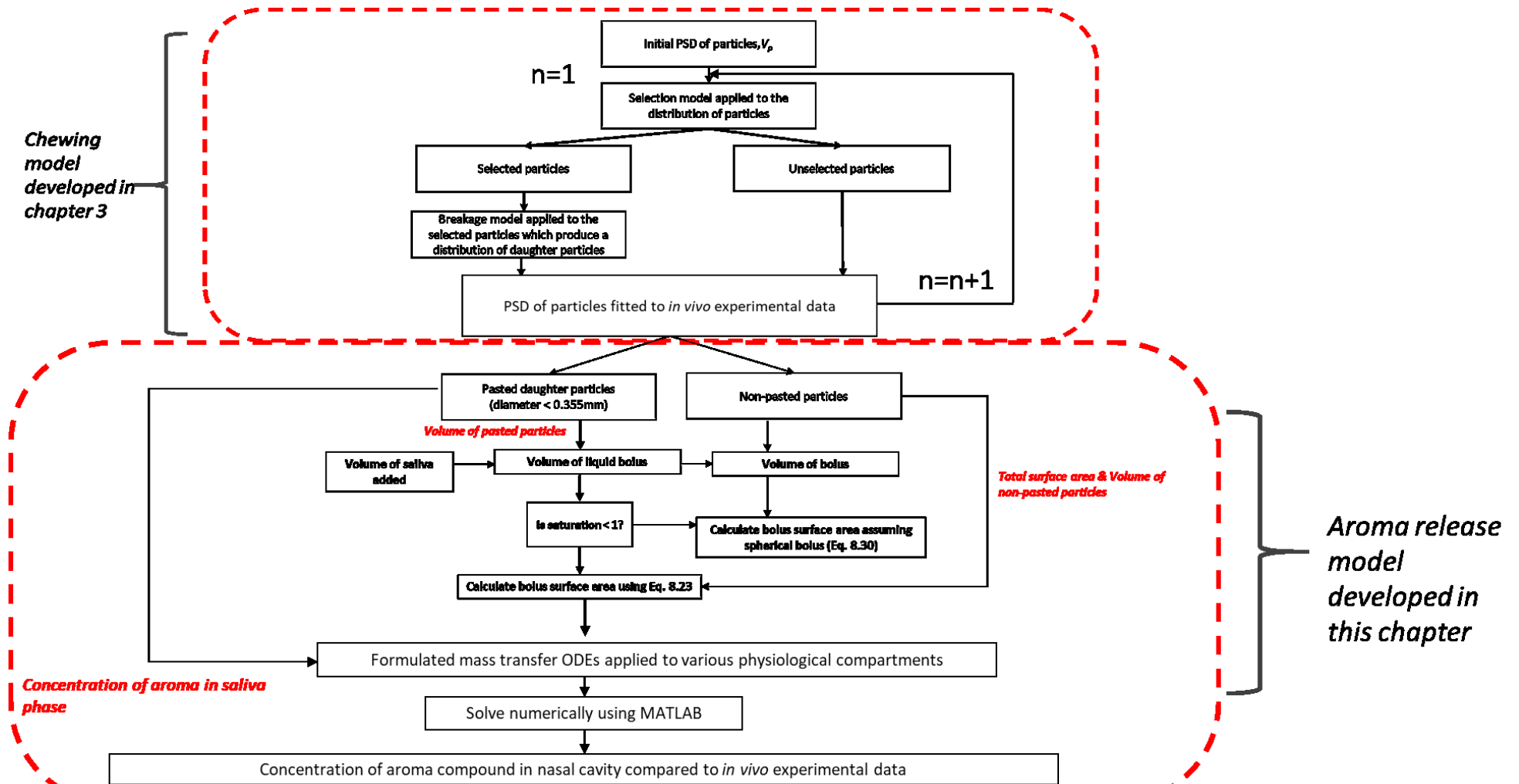


Fig. 7-3 Schematic diagram showing the model flow chart to couple the particle size reduction model developed in Chapter 3 and the models describing flavour release developed in this chapter

Subject A4 (m/z 103)

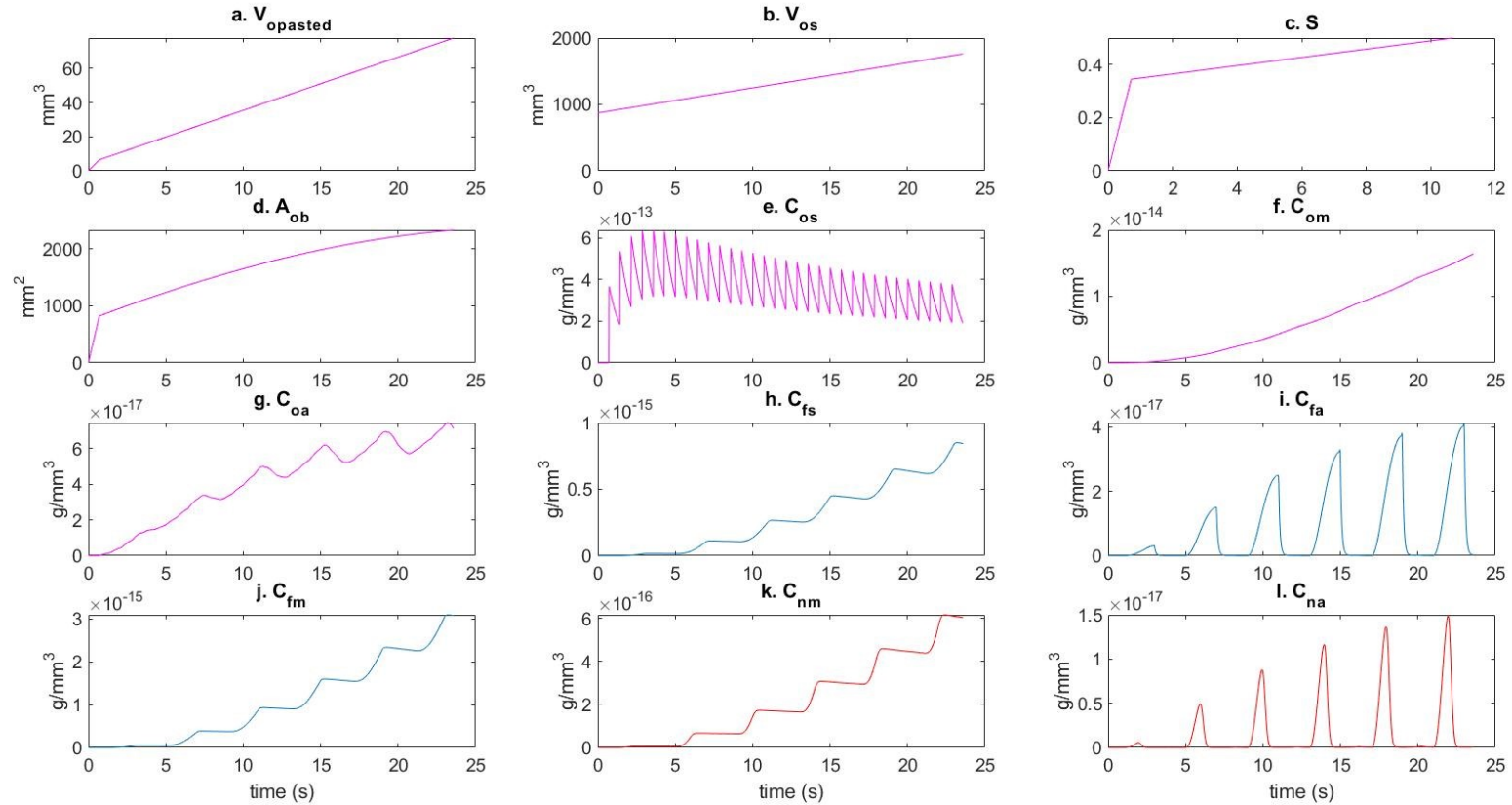


Fig. 7-4: Results of 12 model variables for the release of ethyl propanoate during the consumption of cooked white rice: (a) volume of pasted particles in the oral cavity, V_{opped} , (b) volume of saliva in the oral cavity, V_{os} , (c) liquid bolus saturation, S , (d) Surface area of bolus, A_{ob} , (e) Concentration of aroma in the liquid bolus of the oral cavity, C_{os} , (f) Concentration of aroma in the mucosa layer in the oral cavity, C_{om} , (g) Concentration of aroma in air phase in the oral cavity, C_{oa} , (h) Concentration of aroma in the liquid bolus in the pharynx, C_{fs} , (i) Concentration of aroma in the air phase in the pharynx, C_{fa} , (j) Concentration of aroma in the mucosa layer in the pharynx, C_{fm} , (k) Concentration of aroma in the mucosa layer in the nasal cavity, C_{nm} , (l) Concentration of aroma in the air phase in the nasal cavity, C_{na}

The values of physiological parameters were fixed to the values from one of the subjects used in Chapter 6 (Subject A4). The volume of pasted particles in the oral cavity, $V_{Opasted}$, increases with time, due to chewing which breaks the rice particles into paste and some larger daughter particles. The volume of saliva, V_{Os} started at the volume of saliva at rest (the y-intercept of the subject's bolus saliva content and chew number) and then increases in time as mastication progresses. The increase in the volume of saliva is dependent on Q_{Os} (the slope of the subject's bolus saliva content). Thus, the longer the chewing period, the larger the volume of saliva. The liquid bolus saturation, S , increases sharply after the first chew as pasted particles are formed and combine with the volume of saliva.

The increase in bolus saturation is dependent on the saliva flow rate, Q_{Os} as the volume of the pasted particles is relatively smaller than the volume of saliva (about 10 times higher). The bolus surface area, A_{Ob} also increases with time and seem to follow the increasing trend of the bolus saturation. This is consistent with the model assumption which uses the bolus saturation to calculate the bolus surface area. The concentration of the aroma in the liquid bolus in the oral cavity, C_{Os} increases at every chew due to the breakdown of rice which produce pasted particles which release their aroma into the liquid bolus. Between chews it decreases slowly due to the release into the air. At the end of chewing less rice is pasted, therefore less aroma is transferred to the liquid bolus phase and the dilution from saliva becomes dominant.

This explains the decrease in aroma compound concentration in the liquid phase of the bolus towards the end of chewing. The concentration of aroma in the air phase in the oral cavity, C_{Oa} increases due to mass transfer from the liquid bolus to the air. The increase in C_{Oa} is also contributed to by the desorption of aroma from the mucosa layer, C_{Om} . The velopharynx opening causes small cyclical depressions as it receives air from the pharynx. The concentration of aroma in the mucosa layer in the oral cavity, C_{Om} increases with time as it tries to reach equilibrium with C_{Oa} .

The concentration of aroma in the air phase in the pharynx, C_{Fa} gets pulses due to Q_{oa} which transport the aroma. C_{Fa} also receives aroma from the mucosa layer, C_{Fm} . The concentration of aroma in the liquid

bolus in the pharynx, C_{Fs} follows the trend of C_{Fa} as it tries to reach equilibrium. The concentration of aroma in the mucosa layer of the pharynx C_{Fm} follows the trend of C_{Fs} , to reach equilibrium with C_{Fa} .

The concentration of aroma in the air phase in the nasal cavity follows the pattern of C_{Fa} during exhalation and goes to zero during inhalation as the aroma compounds are swept out by the freshly inhaled air. Finally, the concentration of aroma in the mucosa layer of the nasal cavity, C_{Nm} increases with time as it tries to reach equilibrium with C_{Na} .

7.8 Chapter summary

A mathematical model describing the aroma release during the mastication of rice had been conceptualised and mathematically formulated. The ODE equations developed were numerically solved using MATLAB. The model was checked by comparing the solutions using different time steps and was shown to contain no significant numerical error. The next steps in the modelling process were to determine or estimate the best values and uncertainties of the input parameters before the model could be validated against the experimental data.

Chapter 8 Validation of the aroma release model

8.1 Introduction

In Chapter 7, conceptual and mathematical models to predict the aroma release of foods (applied to a starch-based food model - cooked white rice) were developed. It has been shown in the literature that mechanistic models describing aroma release from masticated foods have not been coupled to chewing due to the complexity of describing how the number and size of particles change as a function of time and the number of chews (Doyennette et al., 2014). In a previous study for cheese which the aroma release models of Chapter 7 were built on, the contact area between the solid and liquid phase of the bolus during mastication was assumed to evolve linearly with time (Doyennette et al., 2014). Indeed, the authors acknowledge that due to the challenges in quantifying the rate of change of contact area for pasty products like cheese, the assumption of linearly increasing contact area with time seems reasonable as long as some solid product is present in the mouth and a regular mastication behaviour was considered.

The key novelty of the model developed in Chapter 7 to predict aroma release is the coupling with the chewing model developed in Chapter 3. Through a combined model, aroma release can be predicted from selection and breakage behaviour of particles that could be measured independently. Because of the complexity of the combined model its application to the experimental data was developed in a staged manner.

The chewing behaviour and particle size distribution were measured at regular intervals for the same subjects that aroma release was monitored. This enables the application of the aroma release model on its own using the experimental bolus characteristics as inputs. By decoupling in this way, more direct exploration of the predictive capability of the aroma release model could be carried out. Similarly, the size reduction models developed in Chapter 3 could independently applied to predict the size distribution data. After validating the two separate components of the model, the combined model could then be validated against the experimental data. Consequently, this chapter was partitioned into three aims. The first objective was to validate the aroma release models developed in Chapter 8 where the chewing-related input parameters of the model was taken directly from the bolus PSD *in vivo*

experimental data. In addition, the physiological and physicochemical measurements conducted in Chapter 6 were used to predict the model. The second goal was to validate the aroma release models using the model coupling approach developed in Chapter 7. The final goal was to investigate the predictive capability of the combined model to predict aroma release.

8.2 Objective 1: Aroma model validation using *in-vivo* experimental bolus properties

The first validation stage aimed to validate the model predictions by directly taking the *in vivo* chewing experimental data conducted in Chapter 6 and using them as model inputs in the aroma release model. The input parameters required in the mathematical model were divided into three groups. These are the subject's chewing related parameters, the subject's physiological parameters, and aroma compound physicochemical parameters.

8.2.1 Subject's chewing parameters

The bolus PSD of each panellist during the consumption of cooked rice is required to predict aroma release. Two input parameters are required from the model developed in Chapter 7 to predict aroma release. Firstly, the volume of pasted rice particles at each chewing number as these particles are assumed to release most of the aroma compound. The volume of pasted particles is calculated by evaluating the total volume of particles, which have a size less than a specific size threshold (e.g. 0.354 mm) from the experimental data. The second input parameter required from the model is the total surface area of particles (particles that were greater than the pasted size threshold, mm²). This is required to calculate the bolus surface area as described in section 7.4.4, Chapter 7.

The bolus PSD data used in the model were the bolus PSD after 1 chew, 2 chews, 25%, 50%, 75% and 100% of each subject's swallow point. This is the same experimental data as shown in section 6.4.2 of Chapter 6, but the boluses were collected at two extra chew intervals in the early stages of mastication (1 and 2 chews) so the model could be provided with accurate PSD during the early stages of chewing. Fig. 8-1 shows the bolus PSD data for all subjects used in the model.

To uncouple the particle breakage and aroma release models, the total surface area of particles and the pasted volume inputs were directly obtained from the experimental data. As described in

Chapter 6 (refer section 6.3.4.2), image analysis method was used to measure the bolus PSD. The volume of a single particle was predicted by multiplying the measured projected area with an assumed height assuming it was a short cylinder (Eq. 6.1). The height was determined by minimising the residual sum of squares between the total predicted volume of particles and the experimental recovered volume of bolus (Eq. 6.2).

$$V = h.A \quad (6.1)$$

where V is the volume in mm^3 , h is the assumed height in mm, and A is the projected area of a single particle in mm^2 . h is calculated as a fraction (f) of the diameter, given by

$$h = f \cdot \left(\frac{4.A}{\pi} \right)^{\frac{1}{2}} \quad (6.2)$$

The mean f value across all mastication stages and their replicates (including the 1 chew and 2 chew data) for each subject measured in Chapter 6 is shown in Fig. 8-2. Due to the small variation of the f value between all chew numbers and replicates, it was assumed that the f value used to calculate the surface area of particles was constant (at the mean value) across all chew numbers specific to each subject.

Therefore, the total surface area of all particles assuming each particle is of cylindrical shape is given by

$$SA_{total} = \sum_{n=1}^n \pi D_{p_n} \left(h + \frac{D_{p_n}}{2} \right) \quad (8.1)$$

where SA_{total} is the total surface area of particles in mm^2 and D_{p_n} is the characteristic dimension of the projected area of a single particle (diameter in mm).

As the experimental pasted particles volume and the total surface area of particles consists of the data at 1 chew, 2 chews, 25%, 50%, 75% and 100% of the subject's swallowing point, a linear model was fitted to the data so the inputs can be interpolated at each intermediate chew number. Fig. 8-3- Fig. 8-7 shows the interpolated model against the experimental data. With the exception of subject A1, the model fits the experimental data well for all subjects (from the high R^2 value ($R^2 > 0.5$)). Potentially subject A1 had an intermediate swallow after about 5-6 chews as this break in the trend does not occur in the other four subjects where the linear fits were reasonable.

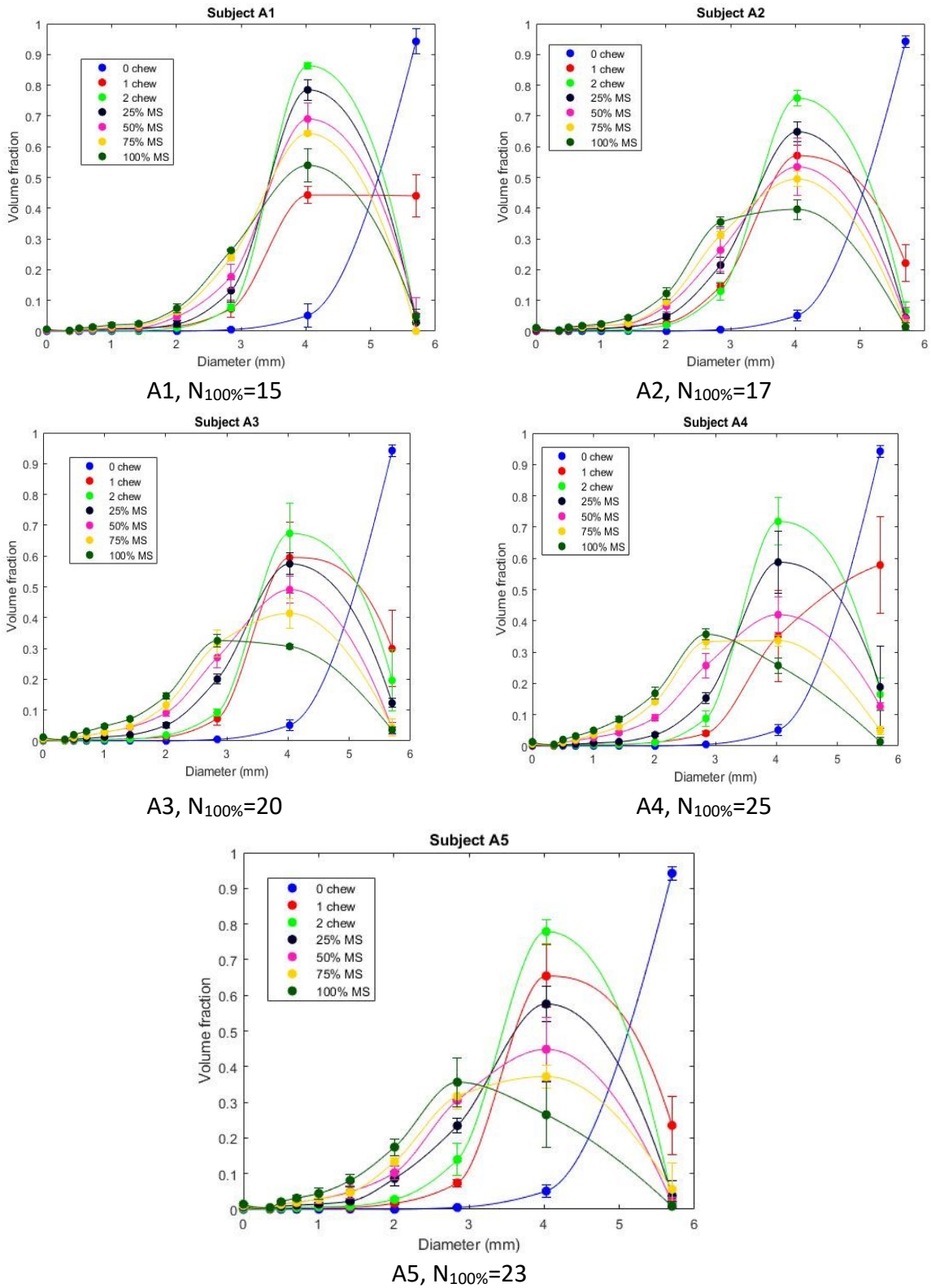


Fig. 8-1: Bolus particle size distribution results for all subjects. The line curves were plotted to guide the reader.

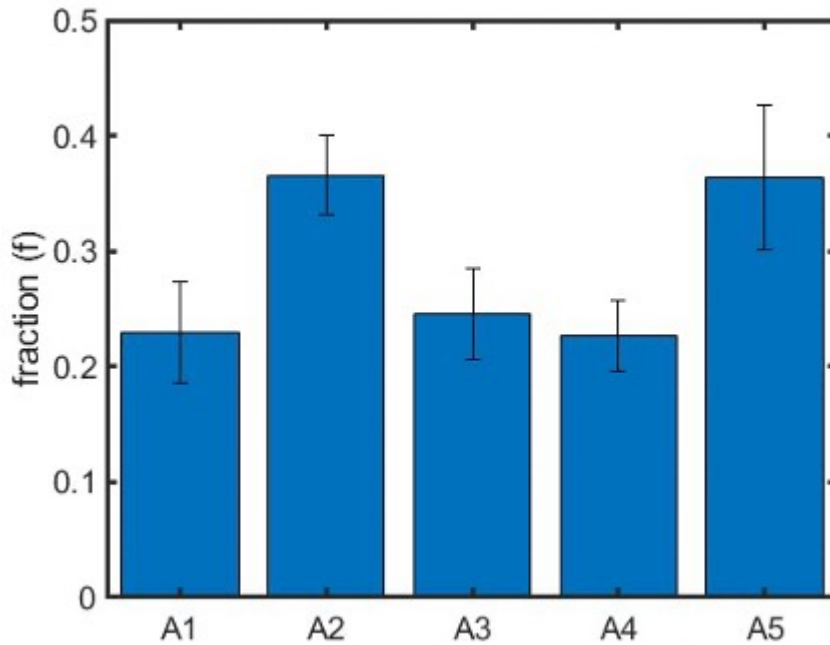


Fig. 8-2 The mean and standard deviation of the fraction, f of diameter across all mastication stages (measured in Chapter 7) to calculate the height of the particle in Eq. 6.2 obtained by minimising the residual sum of squares between the total volume of particles calculated in Eq. 6.1 and the experimental recovered volume of bolus.

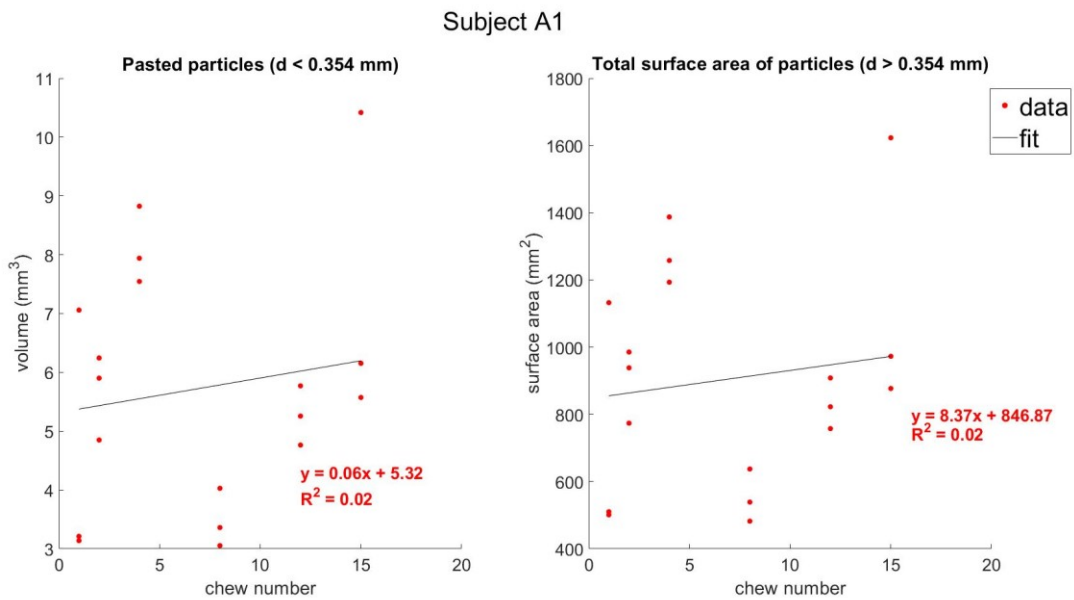


Fig. 8-3: Volume of pasted particles and total surface area of particles data for subject A1. A linear model (red line) was fitted to the data. The model does not fit the data well for subject A1 as demonstrated by the low R^2 value.

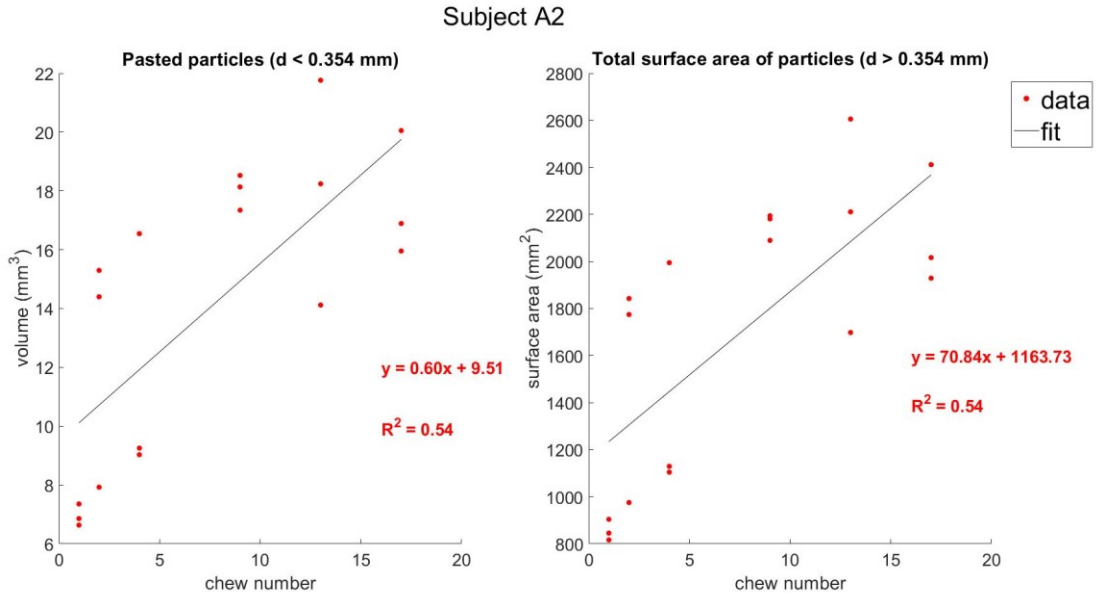


Fig. 8-4: Volume of pasted particles and total surface area of particles data for subject A2. A linear model (red line) was fitted to the data. The model fit the data well for subject A2 as demonstrated by the high R^2 value.

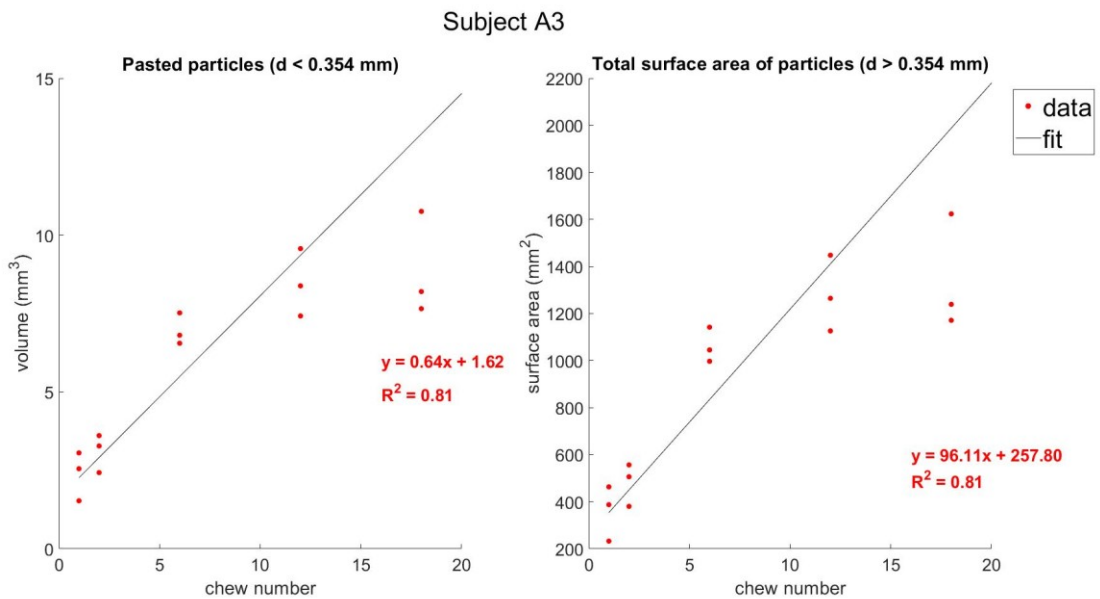


Fig. 8-5: Volume of pasted particles and total surface area of particles data for subject A3. A linear model (red line) was fitted to the data. The model fit the data well for subject A3 as demonstrated by the high R^2 value.

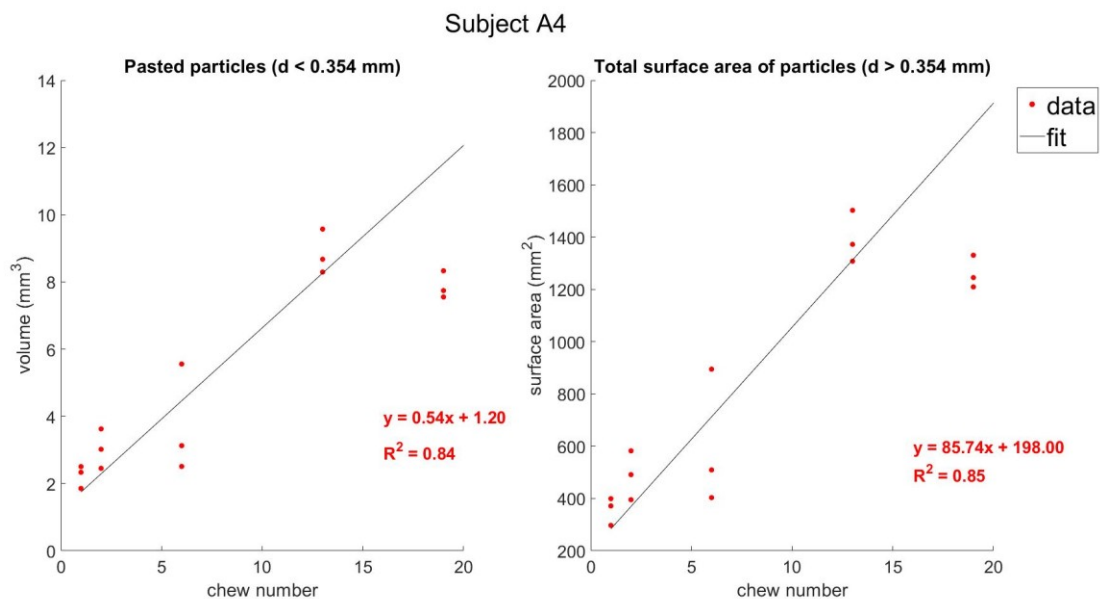


Fig. 8-6: Volume of pasted particles and total surface area of particles data for subject A4. A linear model (red line) was fitted to the data. The model fit the data well for subject A4 as demonstrated by the high R^2 value.

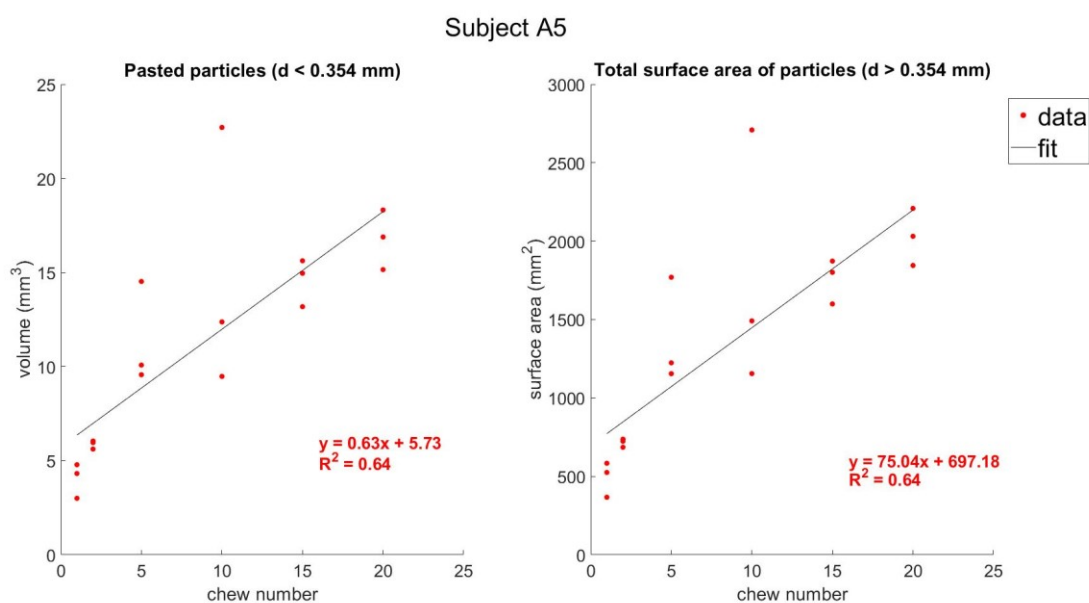


Fig. 8-7: Volume of pasted particles and total surface area of particles data for subject A5. A linear model (red line) was fitted to the data. The model fit the data well for subject A5 as demonstrated by the high R^2 value.

The linear equations as a function of chew number as displayed in the above figures were then used to calculate the volume of the pasted particles and the total surface area of particles at each chew number. Additionally, during the *in vivo* aroma release experiment, each subject was video recorded (with permission) in which their number of chews and the time taken to swallow were analysed to compare with the ones measured during the PSD measurement (Table 8-1).

As can be seen from the table below, the number of chews and the time taken to reach swallow point were higher during the *in vivo* aroma release experiments for almost all subjects (except subject A1). The fitted linear model as obtained above allows the volume of pasted particles and the total surface area of particles to be calculated at the chew number obtained from the *in vivo* aroma release experiments.

Table 8-1: Number of chews and time taken to swallow of all subjects determined from the PSD and *in vivo* aroma release experiments.

Subject	Number of chews		Time taken to swallow (s)	
	PSD experiment	<i>In vivo</i> aroma release	PSD experiment	<i>In vivo</i> aroma release
A1	15 ± 2	15 ± 2	11 ± 3	12 ± 2
A2	17 ± 2	25 ± 6	14 ± 1	21 ± 5
A3	23 ± 1	38 ± 3	14 ± 1	21 ± 3
A4	25 ± 3	35 ± 10	16 ± 3	24 ± 3
A5	20 ± 1	26 ± 6	14 ± 1	20 ± 5

8.2.2 Subject's physiological parameters

The physiological characteristics are critical input parameters required to predict aroma release. The input parameters were determined from the experimental measurements made in Chapter 6 or from the information found in the literature. Table 8-2 below summarises the physiological parameters required for the model, the values used and their source. The physiological input values, as described in Table 8-2 above, were determined through experiments and where they could not be measured due to limitation of resources, the values were obtained from the literature. The oral cavity volume, V_{Oamean} , the volume of air in the pharynx, V_{Fa} and the volume of air in the nasal cavity, V_{Na} were measured using the rhinopharyngometer as described in section 6.3.3.1 in Chapter 6. The volume of saliva at rest, V_{Osrest} and the saliva flow rate, Q_{Os} were obtained from the y-intercept and the slope of the subject's bolus saliva content and chew number relationship as previously described in section 6.4.2. The number of chews required to reach swallow point, n_{chews} , the chewing frequency, fr_{chew} and the time taken to

swallow, $t_{swallow}$ for each subject during the *in vivo* aroma release experiment were determined according to the protocol as previously described in section 6.3.3.4.

Table 8-2 Subject's physiological input values used in the model

Symbol	Unit	Description	Reference value	Range of variation	Source
A_O	mm ²	Total area in oral cavity	11600	5800-23200	(Déléris et al., 2016; Doyennette et al., 2014)
A_F	mm ²	Total area of the pharynx	6500	3250-13000	(Déléris et al., 2016; Doyennette et al., 2014)
A_{Oam}	mm ²	air/lubricated mucosa contact area in the oral cavity	$= 0.1 \times A_O$	$0.1 \times A_O - A_O$	(Déléris et al., 2016)
A_{Fam}	mm ²	air/lubricated mucosa in the pharynx	$= 0.1 \times A_F$	$0.1 \times A_F - A_F$	(Déléris et al., 2016)
A_{Fas}	mm ²	air/saliva contact area in the pharynx	$= A_F - A_{Fam}$	/	(Déléris et al., 2016)
A_{Nam}	mm ²	air/lubricated mucosa in the nasal cavity	15×10^3	$7.5 \times 10^2 - 3 \times 10^4$	(Déléris et al., 2016)
e_{Oam}	mm	Thickness of wetted mucosa in the oral cavity	5×10^{-2}	$5 \times 10^{-3} - 5 \times 10^{-1}$	(Déléris et al., 2016)
e_{Fam}	mm	Thickness of wetted mucosa in the pharynx	5×10^{-2}	$5 \times 10^{-3} - 5 \times 10^{-1}$	(Déléris et al., 2016)
e_{Nam}	mm	Thickness of mucosa in nasal cavity	5×10^{-2}	$5 \times 10^{-3} - 5 \times 10^{-1}$	(Déléris et al., 2016)
F_{breath}	number of cycles/s	breathing frequency	0.26	0.25-0.33	Experimental values
fr_{chew}	number of chews/s	chewing frequency	1.3	1.2-1.4	Experimental values
$fr_{opening}$	occurrence number/s	opening frequency of the velopharynx	$= F_{breath}$ or fr_{chew}	/	(Doyennette et al., 2014)
V_C	mm ³	current breath volume	8×10^5	$8 \times 10^5 - 16 \times 10^5$	(Déléris et al., 2016; Doyennette et al., 2014)
V_{Orest}	mm ³	volume of saliva at rest in the oral cavity	362	100-871	Experimental values
V_{Om}	mm ³	volume of mucosa in the oral cavity	$= e_{Oam} \times A_{Oam}$	/	(Déléris et al., 2016)
V_{Oamean}	mm ³	volume of air in the oral cavity	63720	56830-68100	Experimental values
V_{Fa}	mm ³	volume of air in the pharynx	33610	28500-41655	Experimental values

V_{Fs}	mm ³	volume of saliva in the pharynx	2×10^2	$10^2 - 4 \times 10^2$	(Déléris et al., 2016)
V_{Fm}	mm ³	volume of mucosa in the pharynx	$= e_{Fam} \times A_{Fam}$	/	(Déléris et al., 2016)
V_{Na}	mm ³	volume of air in the nasal cavity	14470	10320-19480	Experimental values
V_{Nm}	mm ³	volume of mucosa in the nasal cavity	$= e_{Nam} \times A_{Nam}$	/	(Déléris et al., 2016)
Q_{Os}	mm ³ /s	saliva flow rate in the oral cavity	40	18-60	Experimental values
$t_{swallow}$	s	time taken to swallow	20	12-20	Experimental values
n_{chews}		number of chews required to reach swallow point	28	15-38	Experimental values

The breathing frequency of the panellists during the consumption of the cooked rice was estimated from the acetone signal (m/z 59) measured in the nasal cavity which was recorded synchronously with the concentration of the target aroma compounds (Trelea et al., 2007). When ambient air is inhaled, the acetone concentration in the nasal cavity decreases due to dilution, whereas during exhalation, the concentration increases due to the contribution of the air coming from the lungs (Trelea et al., 2007). Fig. 8-8 below shows a single replicate of the acetone signal measured in one of the panellists. The breathing frequency was determined by measuring the time it takes to complete one breathing cycle. This was determined by identifying the point when the signal decreases and increases, as it symbolises when the subject inhales and exhales. The breathing frequency used in the model is the average of several breathing frequencies measured in all five replicates in the *in vivo* aroma release experiments.

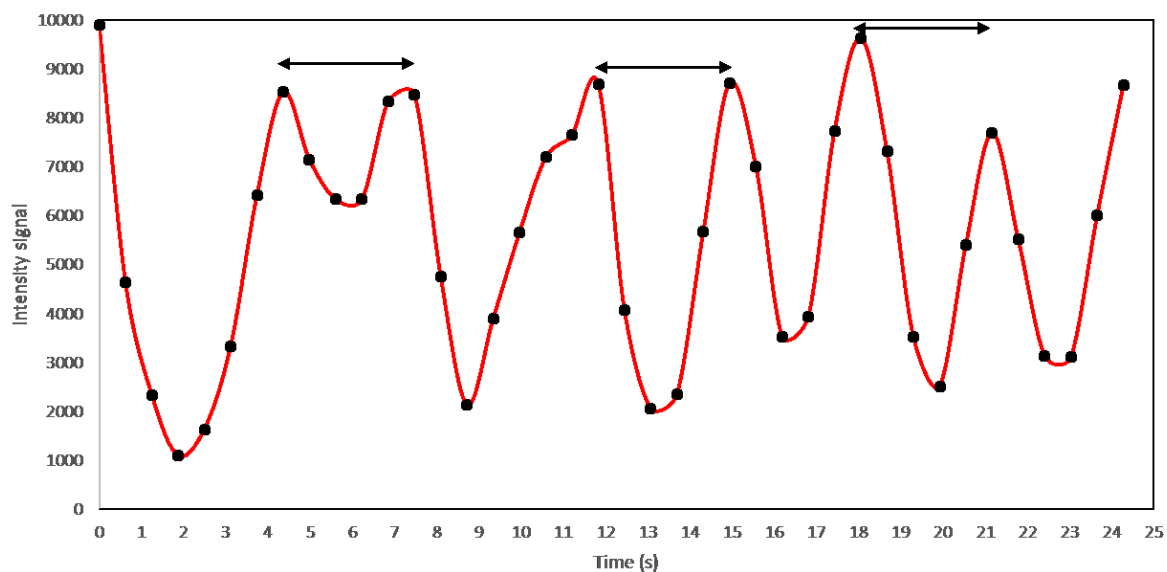


Fig. 8-8: An example to illustrate the dynamics of acetone signal during chewing. Data shown above is a single replicate from one of the panellists. The arrow in the figure shows the length of time in (s) for one breathing cycle, which determines the breathing frequency. For instance, it takes about 3-4 s for the subject to finish a breathing cycle. The breathing frequency used in the model is the average of several breathing frequencies measured in all five replicates in the *in vivo* aroma release experiments.

Other physiological variables including the area of the mucosa in all compartments (oral cavity, pharynx and nasal cavity), the thickness of the mucosa layer, and the breath volume/tidal volume were determined from the literature.

8.2.3 Physico-chemical input parameters

Other input parameters required for the model include the physico-chemical properties of the aroma compound that was spiked in the cooked rice, such as the partition coefficient between different phases. The mass transfer coefficient and the initial concentration were also required to predict aroma release. Table 8-3 below summarises the remaining parameters required for the model.

Table 8-3: Model input parameters which include the mass transfer coefficient, partition coefficient and the initial concentration of the aroma compounds that were spiked in the cooked white rice.

Symbol	Unit	Description	Reference value	Range of variation	Source
k_{Os}	mm/s	mass transfer coefficient in the saliva phase in the oral cavity	10^{-3}	10^{-5} - 10^{-1}	(Déléris et al., 2016)
k_{Fs}	mm/s	mass transfer coefficient in the saliva phase in the pharynx	10^{-3}	10^{-5} - 10^{-1}	(Déléris et al., 2016)
k_{Om}	mm/s	mass transfer coefficient in the	10^{-3}	10^{-5} - 10^{-1}	

K_{Fm}	mm/s	lubricated mucosa in the oral cavity mass transfer coefficient in the lubricated mucosa in the pharynx	10^{-3}	10^{-5} - 10^{-1}	(Déléris et al., 2016)
k_{Nm}	mm/s	lubricated mucosa in the nasal cavity mass transfer coefficient in the lubricated mucosa in the nasal cavity	10^{-3}	10^{-5} - 10^{-1}	(Déléris et al., 2016)
K_{Oas}		air/saliva partition coefficient in the oral cavity at 37°C	12.9×10^{-3} (Ethyl propanoate) 9.7×10^{-3} (2-nonanone)	/	(Déléris et al., 2016)
K_{Osp}		saliva/product(rice) partition coefficient in the oral cavity at 37°C	2.14 (Ethyl propanoate) 0.245 (2-nonanone)	/	Experimental values
K_{Oam}		air/lubricated mucosa partition coefficient in the oral cavity	10^{-3}	10^{-5} - 10^{-1}	(Déléris et al., 2016)
K_{Fas}		air/saliva partition coefficient in the pharynx	5×10^{-3}	5×10^{-4} - 5×10^{-2}	(Déléris et al., 2016)
K_{Fam}		air/lubricated mucosa partition coefficient in the pharynx	10^{-3}	10^{-5} - 10^{-1}	(Déléris et al., 2016)
K_{Nam}		air/lubricated mucosa partition coefficient in the nasal cavity	10^{-3}	10^{-5} - 10^{-1}	(Déléris et al., 2016)
C_{Op}	g/mm ³	aroma concentration in the product (rice) in the oral cavity	1.5×10^{-10} (ethyl propanoate) 4.8×10^{-9} (2-nonanone)	/	Experimental values

8.2.3.1 Partition coefficient determination

The air/rice partition coefficient at 37°C was determined using the phase ratio variation (PRV) method by headspace chromatography (Atlan et al., 2006; Doyennette et al., 2011). The method to determine the air/rice partition coefficient was adopted from (Doyennette et al., 2011). A known amount of rice (50 mg, 200 mg, 500 mg or 2000 mg) was placed in vials (20.5 cm³, Chromacol, France) and incubated at 37°C for 2.5 hours. The length of time was selected after preliminary experiments (measurements

every 30 min from 0 to 5 h) to ensure thermodynamic equilibrium was achieved. The temperature was selected as it was close to the body temperature (Doyennette et al., 2011).

After the equilibration time, 2 cm³ of the headspace above the rice was sampled and injected with an automatic HS CombiPal sampler (CTC Analytics, Switzerland) into a gas chromatograph HP (GC-FID HP6890, Germany) equipped with an HP-INNOWax polyethylene glycol semi capillary column (30 m x 0.53 mm, with a 1 µm-thick film) (J&W Scientific) and a flame ionisation detector (Doyennette et al., 2011). The temperatures of the gas chromatograph injector and detector (GC-FID HP6890, Germany) were set at 250°C. The oven program was 12 min, starting at 40°C for 5°C/min up to 60°C, then for 10°C/min up to 120°C, and 2 min for 120°C. Helium was used as the carrier gas at 8.4 cm³/min flow rate (corresponding to 57 cm/s average velocity at 50°C). The peak areas were measured using Hewlett-Packard Chemstation integration software. Three replicates were done for each amount of rice tested.

The basic PRV equation

The air to rice partition coefficient (K_{ap}) of an aroma compound is defined as the ratio between the air and the rice concentrations of the compound at thermodynamic equilibrium:

$$K_{ap} = \frac{C_a}{C_p} \quad (8.2)$$

In the PRV procedure, the target volatile compound (2-nonanone & ethyl propanoate) is first spiked in the rice matrix at initial concentration C_p^0 . As described previously, various volumes of rice are then introduced in closed vials until thermodynamic equilibrium is reached. The GC peak areas are the experimental measurements, which are proportional to the concentration of the target aroma compound in the air phase.

Based on mass balance, it was theoretically shown that the GC peak areas (A) are given by (Ettre et al., 1993):

$$A = \frac{F C_p^0}{K_{ap}^{-1} + \beta} \quad (8.3)$$

where F is the response factor of the detector and β is the volume ratio of the air and rice matrix phases in the vial:

$$\beta = \frac{V_a}{V_p} \quad (8.4)$$

The PRV equation (Eq. 9.3) can be rearranged to be linear with respect to the phase ratio, β :

$$\frac{1}{A} = x_1\beta + x_2 \quad (8.5)$$

Where the slope and intercept are;

$$x_1 = \frac{1}{FC_P^0} \quad (8.6)$$

$$x_2 = \frac{1}{FC_P^0 K_{ap}} \quad (8.7)$$

K_{ap} is then evaluated by dividing x_1 by x_2 .

The experimental results for the spiked aroma compounds (2-nonanone and ethyl propanoate) are shown in Fig. 8-9 and Fig. 8-10 respectively. The volume of the air inside the vial was determined from the difference of the volume of the vial and the volume of the rice (density of 1.27 g/cm³, determined by the water displacement method (Gray-Stuart, 2016)).

8.2.3.2 Determination of the initial concentration of aroma compounds

Another input that is required for the model is the initial concentration of the target aroma compounds in the rice matrix. The following describes how the initial concentrations of 2-nonanone and ethyl propanoate were evaluated.

For a given volume of rice in a vial that is in thermodynamic equilibrium, the mass of aroma compound in the rice matrix is given by the following mass balance:

$$V_p C_{op} = V_a C_{aeq} + V_p C_{peq} \quad (8.8)$$

where V_p is the volume of rice matrix in the vial (L), C_{op} is the initial concentration of the aroma compound (mg/L), V_a is the volume of air in the vial (L), C_{aeq} is the concentration of the aroma compound in the air phase when in thermodynamic equilibrium and C_{peq} is the concentration of the aroma compound in the rice matrix when in thermodynamic equilibrium.

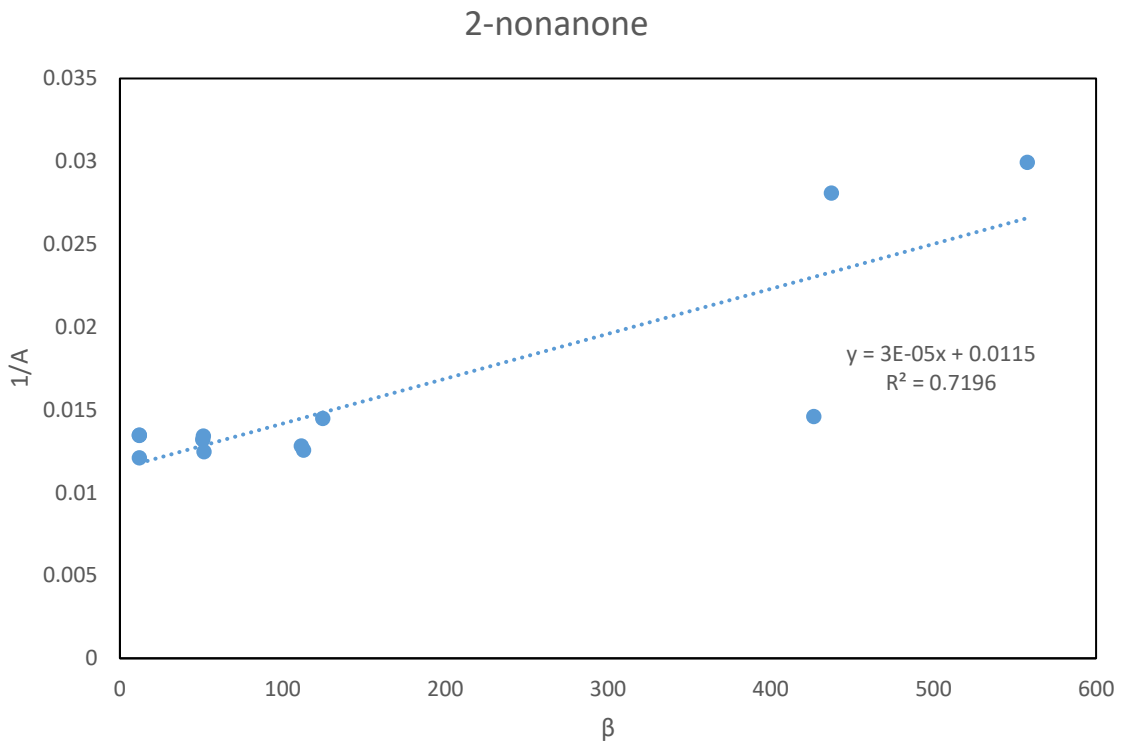


Fig. 8-9: $1/A$ vs β plot of 2- nonanone. The ratio of the slope and the y-intercept is K_{ap} .

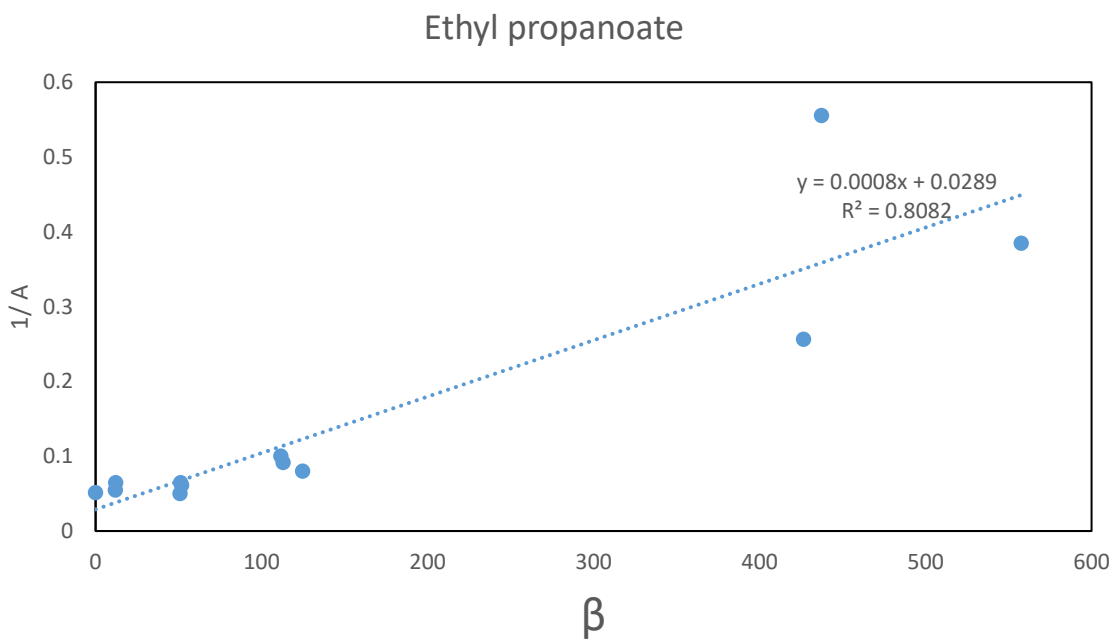


Fig. 8-10: $1/A$ vs β plot of ethyl propanoate. The ratio of the slope and the y-intercept is K_{ap} .

Using 2 g of rice as a reference value, the values of V_p and V_a can be evaluated. C_{aeq} and C_{peq} were determined by linear interpolation from the equilibrium concentrations when the aroma compound is in a liquid phase (H_2O). For a given volume of aroma solution in a vial that is in thermodynamic equilibrium, the mass of aroma compound in the liquid phase is given by the following mass balance:

$$V_l C_{ol} = V_a C_{aeq} + V_l C_{leq} \quad (8.9)$$

where V_l is the volume of liquid in the vial (L), C_{ol} is the initial concentration of the aroma compound (mg/L) in the liquid, C_{leq} is the concentration of the aroma compound in the liquid when in thermodynamic equilibrium.

The partition coefficient of the air/liquid phase is the ratio of the concentrations of the aroma compound in the air and the liquid phase:

$$K_{al} = \frac{C_{aeq}}{C_{leq}} \quad (8.10)$$

Using the information from Table 8-4 below and substituting Eq.8.10 to Eq. 8.9, C_{aeq} and C_{leq} can be evaluated.

Table 8-4: Physico-chemical characteristics of the target aroma compounds

Aroma compound	Volume of solution, V_l (L)	Initial Concentration of aroma solution, C_{ol} (mg/L)	Volume of vial (L)	Volume of air phase, V_a (L)	Air/Solution Partition coefficient at 37°C, K_{al}
2-nonanone	0.002	30	0.020498	0.018498	1.96×10^{-2}
ethyl propanoate	0.002	30	0.020498	0.018498	1.49×10^{-2}

Using the GC peak areas (A) of the aroma compounds in both the liquid and rice matrix phases and the C_{aeq} value in the liquid phase as calculated above, the C_{aeq} value in the rice matrix was calculated using linear interpolation. The A values for both aroma compounds when in 2 mL of water (30 ppm concentration each compound) were measured using the same conditions as described in section 8.2.3.1. Five replicates of samples were measured and the average was determined. The C_{peq} value in the rice matrix was then calculated from the partition coefficient of air to rice matrix that was

previously determined in section 8.2.3.1. The following table shows the GC peak area values for both the liquid and rice phases, as well as the concentrations of the aroma compounds in the liquid/rice/air phases when in thermodynamic equilibrium.

Table 8-5: GC peak areas and the concentration of aroma compounds in the liquid/rice/air phase when in thermodynamic equilibrium

Aroma compound	GC peak area, A, (liquid)	C_{aeq} (liquid) (mg/L)	GC peak area, A, (rice)	C_{aeq} (rice) (mg/L)	C_{peq} (rice) (mg/L)
ethyl propanoate	2219	0.393	17.7	0.003	1.14×10^{-1}
2-nonanone	3466.85	0.498	77.03	0.011	4.67

Now that C_{aeq} and C_{peq} values in the rice matrix have been determined, the initial concentration of the aroma compounds in the rice matrix could be calculated using Eq. 8.8.

8.2.4 Validation of the aroma release model

In the previous section, the input parameters information required for the model were established. In this section, the model was compared against the experimental data reported in Chapter 6 to test the validity of the model.

8.2.4.1 Comparison of model results and experimental data

In previous studies involving the modelling of aroma release, the model prediction is compared against experimental measurements by representing the data as a peak line (Doyennette et al., 2011; Doyennette et al., 2014). This is done by smoothing the breath-by-breath aroma release profiles by plotting a curve linking the maxima of the sinusoids (Doyennette et al., 2011). However, the nature of the *in vivo* aroma release experimental data collected in Chapter 6 makes it challenging to compare the peak curves. Fig. 8-11 below shows typical *in vivo* experimental data results for 2-nonanone during mastication (measured using PTR-MS).

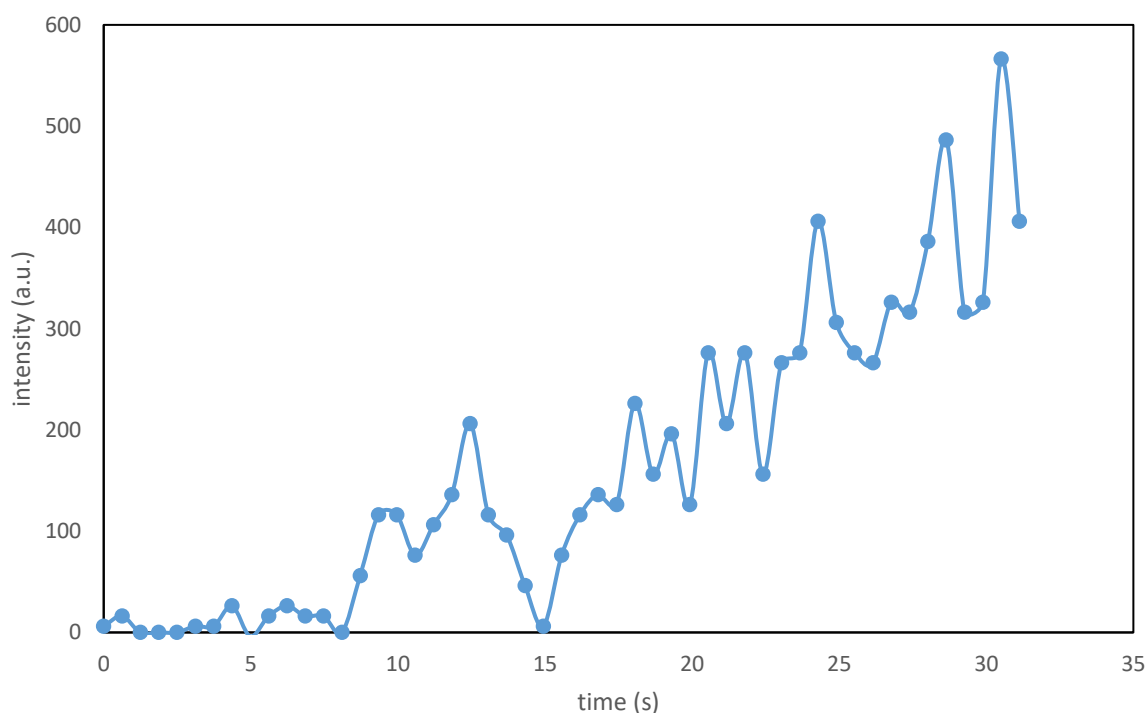


Fig. 8-11: Typical *in vivo* experimental data results of 2-nonanone that was measured using PTR-MS (single replicate).

Two issues arise from the experimental data (Fig. 8-11) above that makes it challenging to compare with the model. The first problem is the long sampling time of the experimental data. When a subject exhales, the person will bring aroma to his/her nasal cavity (this corresponds to the rising part of the sinusoid pattern of the aroma release curve) and when the subject inhales fresh air which is aroma free, the signal of concentration in the nasal cavity decreases to zero (Doyennette et al., 2011). However, looking at Fig. 8-11 above, particularly during inhalation, the concentration does not drop completely to zero. This is because the samples were taken every 0.622 s, which is the sum of the dwell time of all molecular ions that were tracked during the *in vivo* experiment. Specifically, these are m/z 21 (50 ms), m/z 32 (50 ms), m/z 37 (50 ms), m/z 59 (50 ms), m/z 83 (100 ms), m/z 143 (100 ms), m/z 103 (100 ms), m/z 75 (100 ms). An example to show the high sampling time effects the experimental data is shown in Fig. 8-12 below.

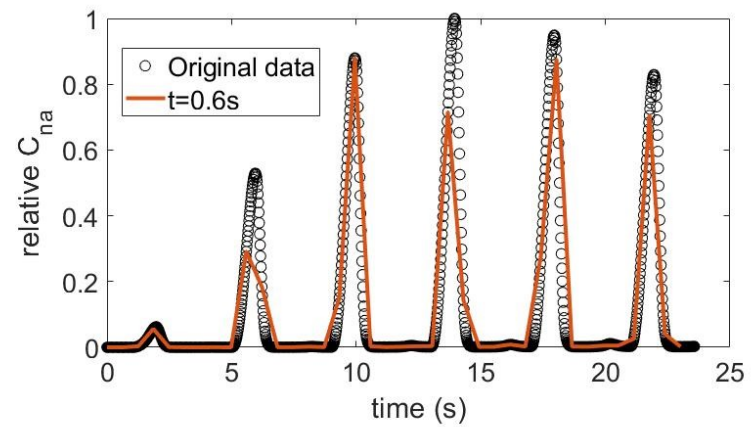
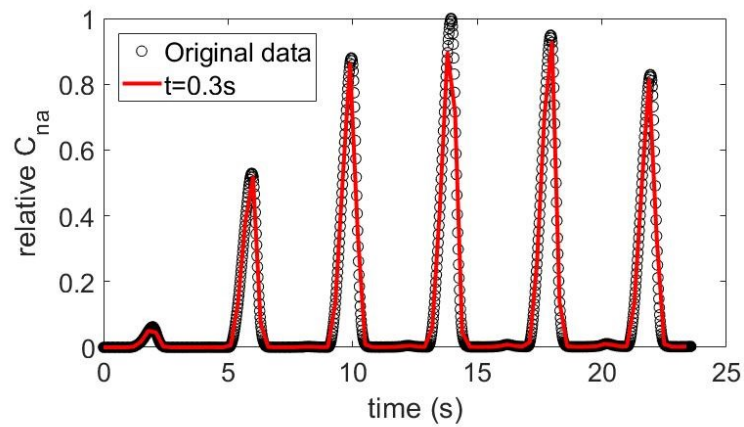
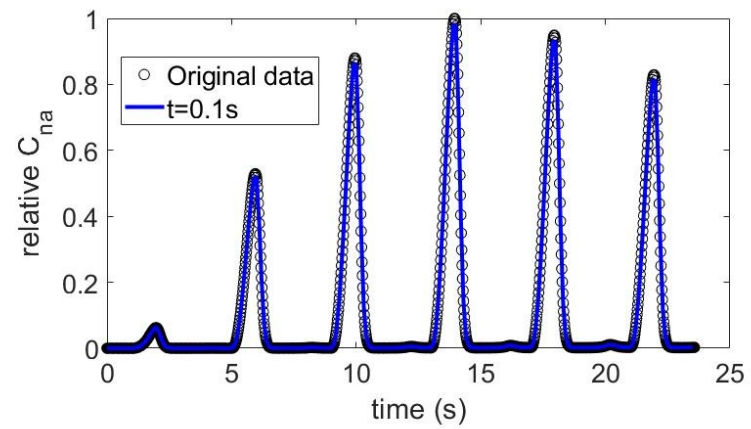
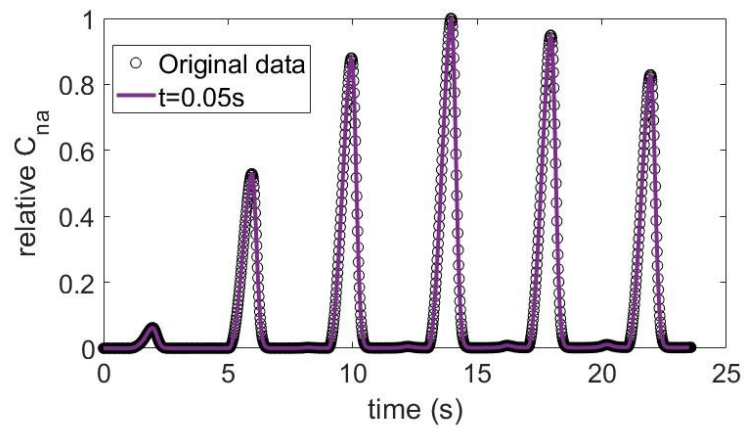


Fig. 8-12: Subplots to demonstrate the effect of different sampling time on the experimental data. The black symbol in the subplot refers to the original model results, while the other coloured curves referred to the curves that were taken at different sampling times.

To demonstrate the effect of different sampling times on the experimental data, the model results from Subject A4 were used as an example. The model results used here are the relative concentration in the nasal cavity (C_{na}), which is the ratio of the concentration and the maximum concentration observed experimentally. These are plotted as the black dashed line in Fig. 8-12 above. Each subplot in the above figure shows the effect when different sampling time was used, i.e. the sample was taken at every 0.05 s, 0.1 s, 0.3 s and 0.6 s respectively. The curve which was derived from different sampling rates (symbols) was then compared with the original model results (the black dashed line).

It can be observed from the above figure that the longer the sampling time, the more it deviates from the original model results. This shows the importance of having a faster sampling time so that the experimental data can be compared with the model results. The issue stems from the fact from the high number of molecular ions that were tracked in the PTR-MS measurement (the equipment can only track 8 molecular ions at a time). Because of that, it increases the sampling time as the Quadrupole-Ion-Detection System in the PTR-MS cannot measure all ions at the same time, but has to switch its filter (quad) between different ions (this is where the dwell time comes in) (Lindinger et al., 1998; Rndirk, 2017). Other instruments to measure *in vivo* aroma release such as Selected Ion Flow Tube Mass Spectrometry (SIFT-MS) (e.g. SIFT-MS developed by syft™ Technologies <https://www.syft.com/high-selectivity-real-time/>) might be useful as it has very high selectivity in real-time due to near-instant switching of the quadrupole.

The second issue stems in the fact to the time when sampling was initiated ($t=0$) relative to breathing. The chosen starting time was when the food product (rice) was introduced inside the mouth, but this was not coordinated with breathing or chewing frequency. As the starting time for the panellists' during the experiment was recorded by manual observation, it could be off by a few seconds. Fig. 8-13 below shows an example of how a difference in the starting time can be a challenge for the model validation.

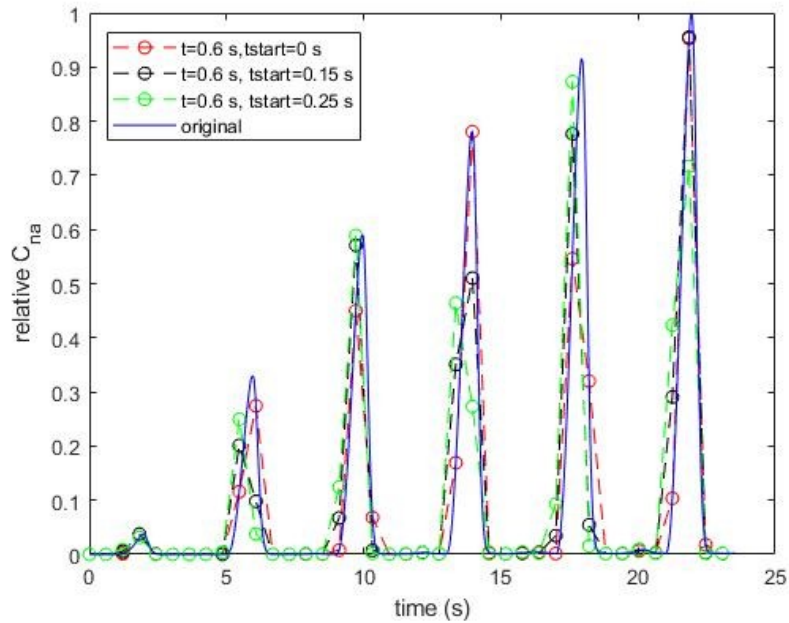


Fig. 8-13: Plot to demonstrate the effect of the different starting time of the experimental data. The blue curve in the plot refers to the original model results, while the other coloured curves referred to the curves that started at different time.

Similar to the data in Fig. 8-12, the model results from Subject A4 was used to demonstrate the effect of starting time offsets. As can be seen from Fig. 8-13 above, starting the plots at a different starting time (e.g. $t_{\text{start}}=0.15$ s and 0.25 s) causes the aroma release curve to desynchronise with the original data. Due to the two issues as highlighted above, it is a challenge to compare the experimental data with the model predictions from their peak curves. Therefore, a potential solution to this difficult problem was to compare the cumulative area under the curves as a function of time.

Fig. 8-14 shows the data when presented as the cumulative area the curve with different sampling times. Comparatively, it can be observed that presenting the results in terms of the cumulative area under the curve seems to match the original model results better although being sampled at different rates. This is a slightly unconventional way of solving this issue but is better than comparing the peak curves. Therefore, for model validation, the cumulative aroma release curve from both the model results and the experimental data are compared.

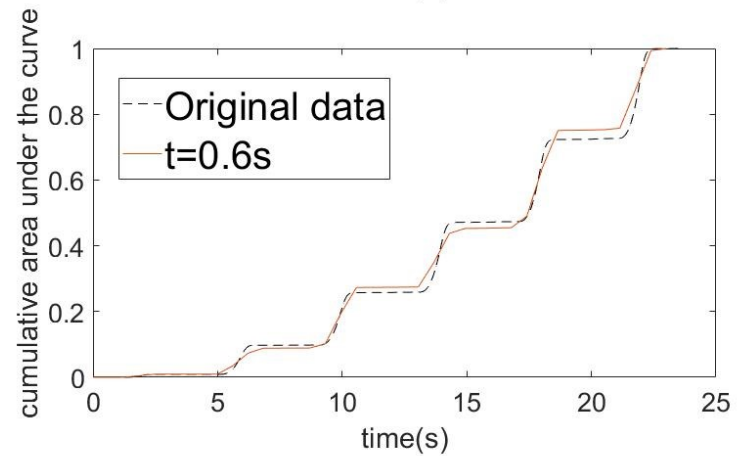
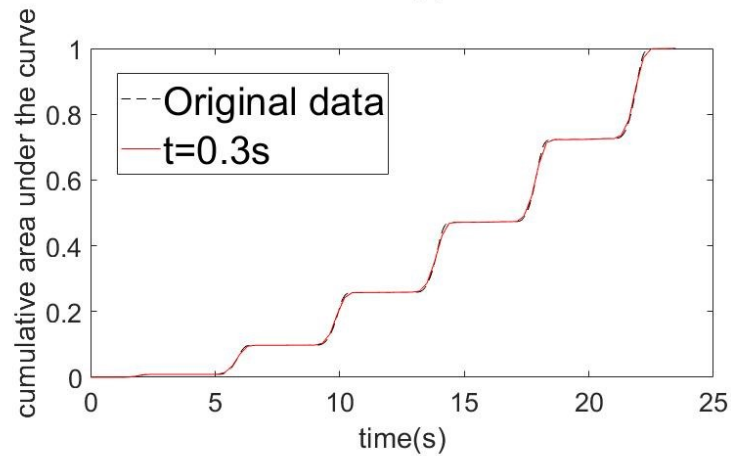
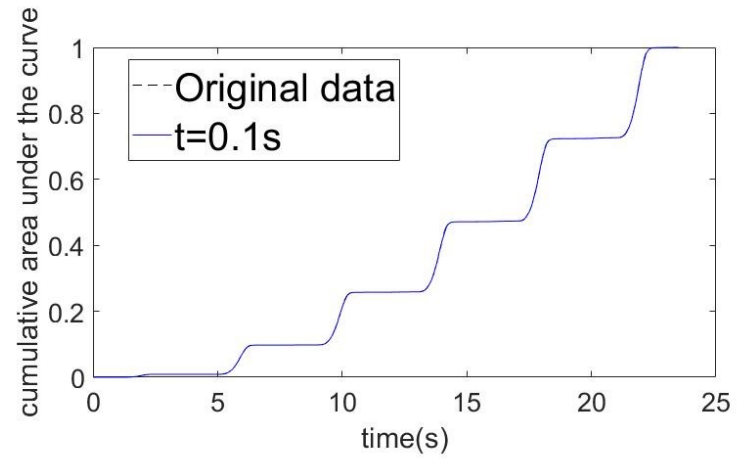
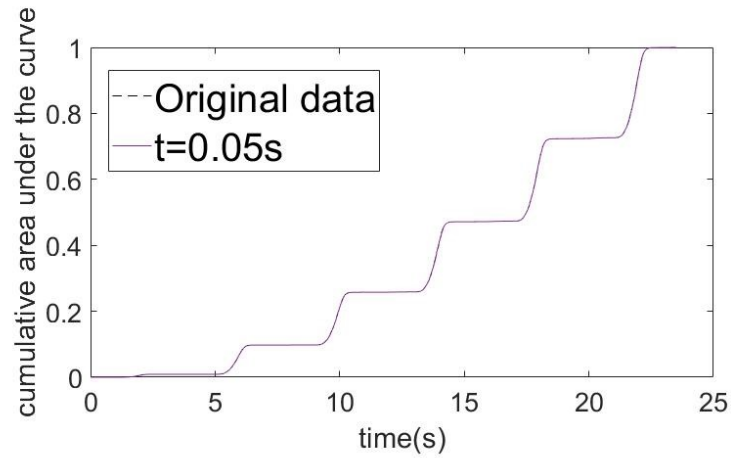


Fig. 8-14: Subplots to demonstrate the cumulative area the curve with different sampling time. The black dashed curve in the subplot refers to the original model results, while the other coloured curves referred to the curves that were taken at different sampling time.

8.2.4.2 Comparison of model predictions and experimental data

This section describes the comparison between the model predictions and the experimental data. The input parameters as described in the previous sections were applied. The physiological parameters that were specific to each subject were used in the model predictions for comparison against the *in vivo* aroma release data. The model predicts the concentration of 2-nonanone (*m/z* 143) and ethyl propanoate (*m/z* 103) in the nasal cavity in g/mm^3 . The concentration of the aroma compounds in the experimental data however was described as an intensity from the PTR-MS measurement, which is an arbitrary unit. Therefore, for comparison, the concentration of aroma compounds from both the model prediction and experimental data were normalised against the maximum concentration. The cumulative area under the curve were then obtained for the normalised concentrations and were then compared.

The main assumption of the model is that during chewing, aroma compounds are transferred to the saliva phase from the pasted rice particles instantaneously. The size threshold for when rice particles are pasted was set as 0.354 mm by Gray-Stuart (2016) in his work. Here, the model was predicted using different pasted size thresholds (0.2 mm, 0.354 mm, 0.5 mm and 1 mm) and compared against the experimental data to see if the difference in the threshold has a pronounced effect on the prediction. The five replicates of the experimental data were compared against the model prediction. It should be considered that for the particle breakdown model the threshold was set to describe particles that become too small to be actively broken down by occlusion. In terms of aroma release, the pasted particle threshold corresponds to particles that are assumed to instantaneously equilibrate their aroma compound with the liquid portion of the bolus.

Fig. 8-15 to Fig. 8-19 below shows the comparison of the model predictions against the experimental data for the five subjects.

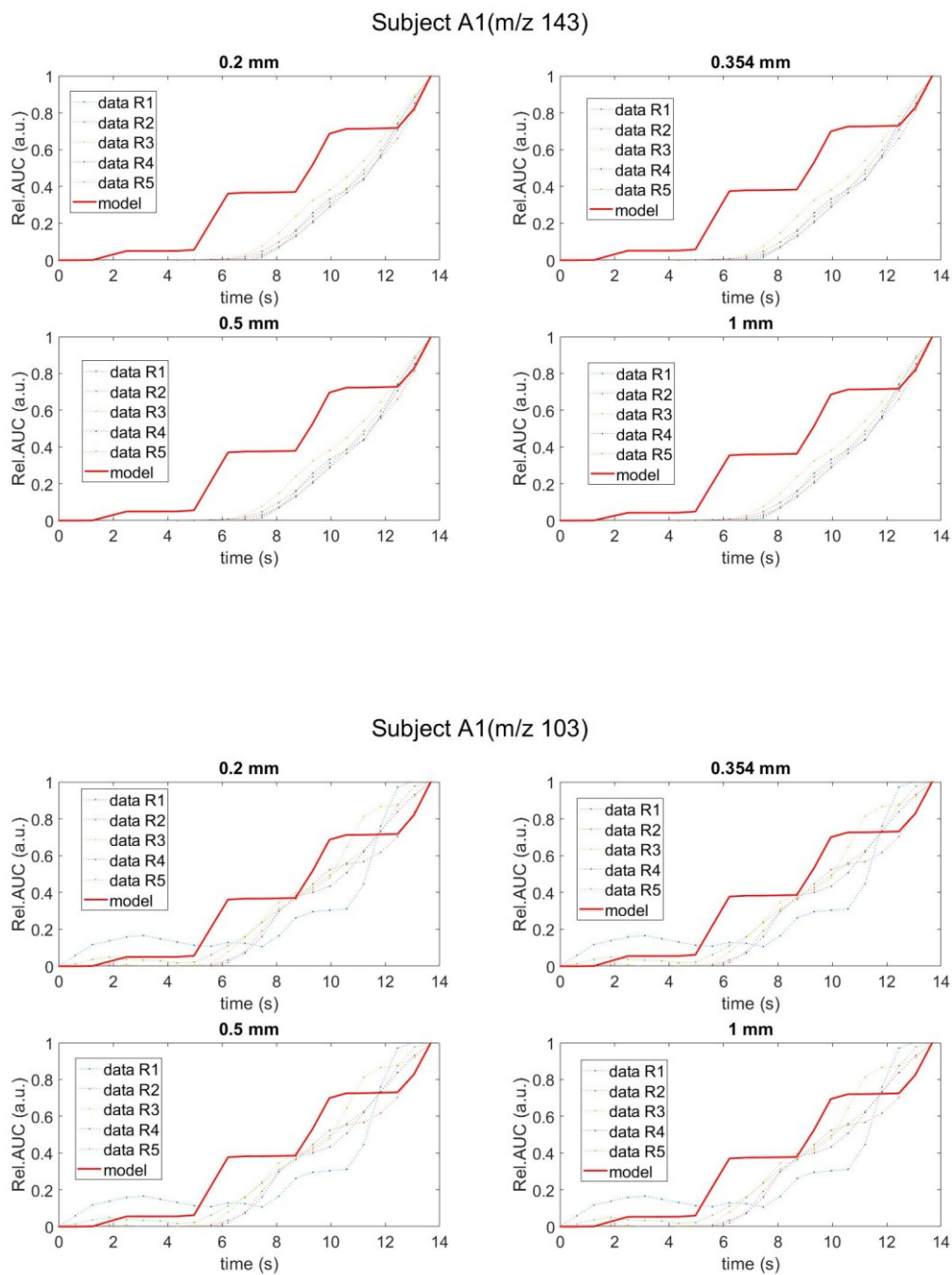


Fig. 8-15: Model prediction against experimental data of 2-nonanone (m/z 143) and ethyl propanoate (m/z 103) for Subject A1. Rel. AUC refers to the relative cumulative area under the curve, where the cumulative area under the curve was normalised against the total area under the curve. The model was also predicted using different pasted size threshold (0.2 mm, 0.354 mm, 0.5 mm and 1 mm) and compared against the five replicates of the experimental data.

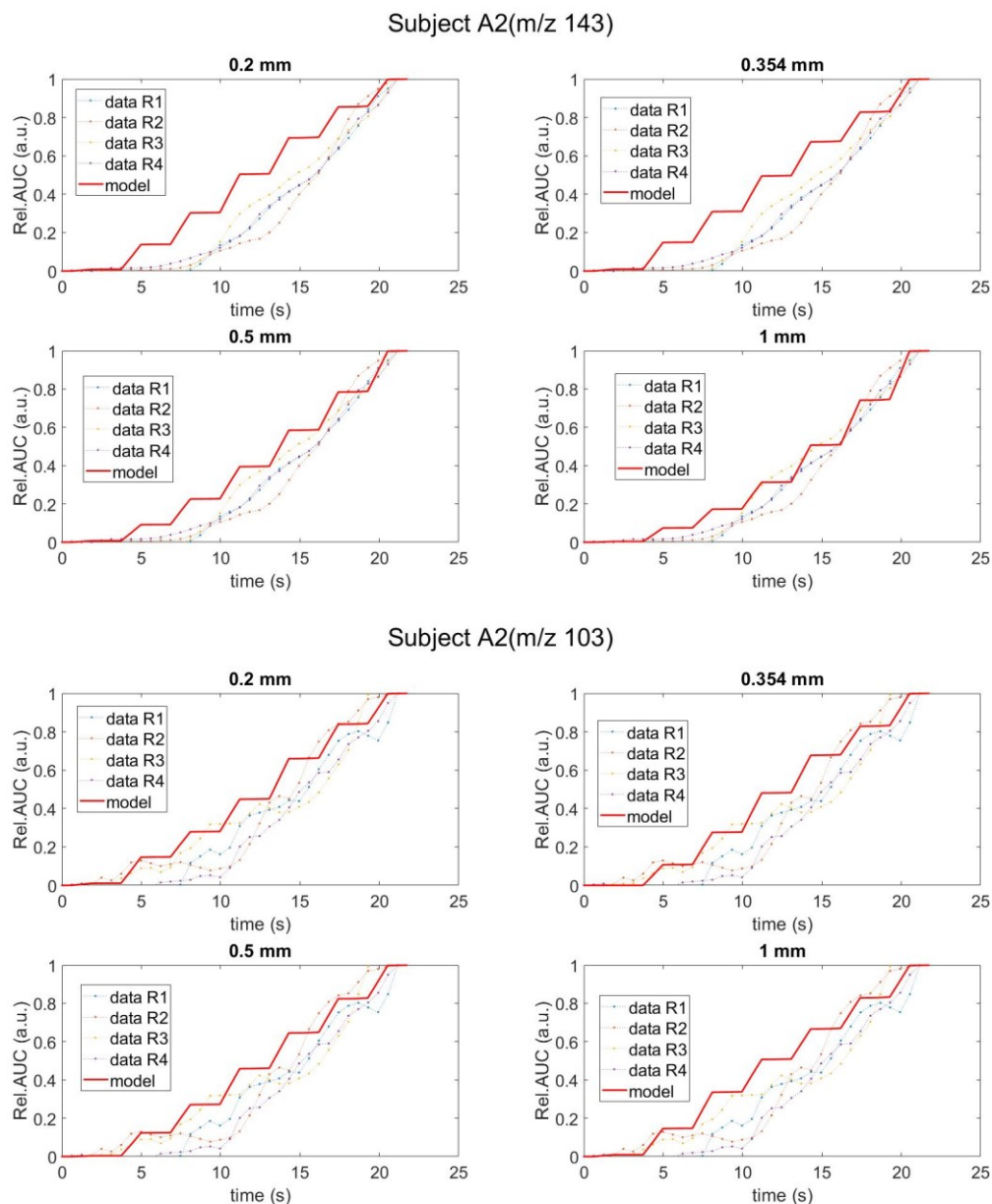


Fig. 8-16: Model prediction against experimental data of 2-nonanone (m/z 143) and ethyl propanoate (m/z 103) for Subject A2. Rel. AUC refers to the relative cumulative area under the curve, where the cumulative area under the curve was normalised against the total area under the curve. The model was also predicted using different pasted size threshold (0.2 mm, 0.354 mm, 0.5 mm and 1 mm) and compared against the five replicates of the experimental data.

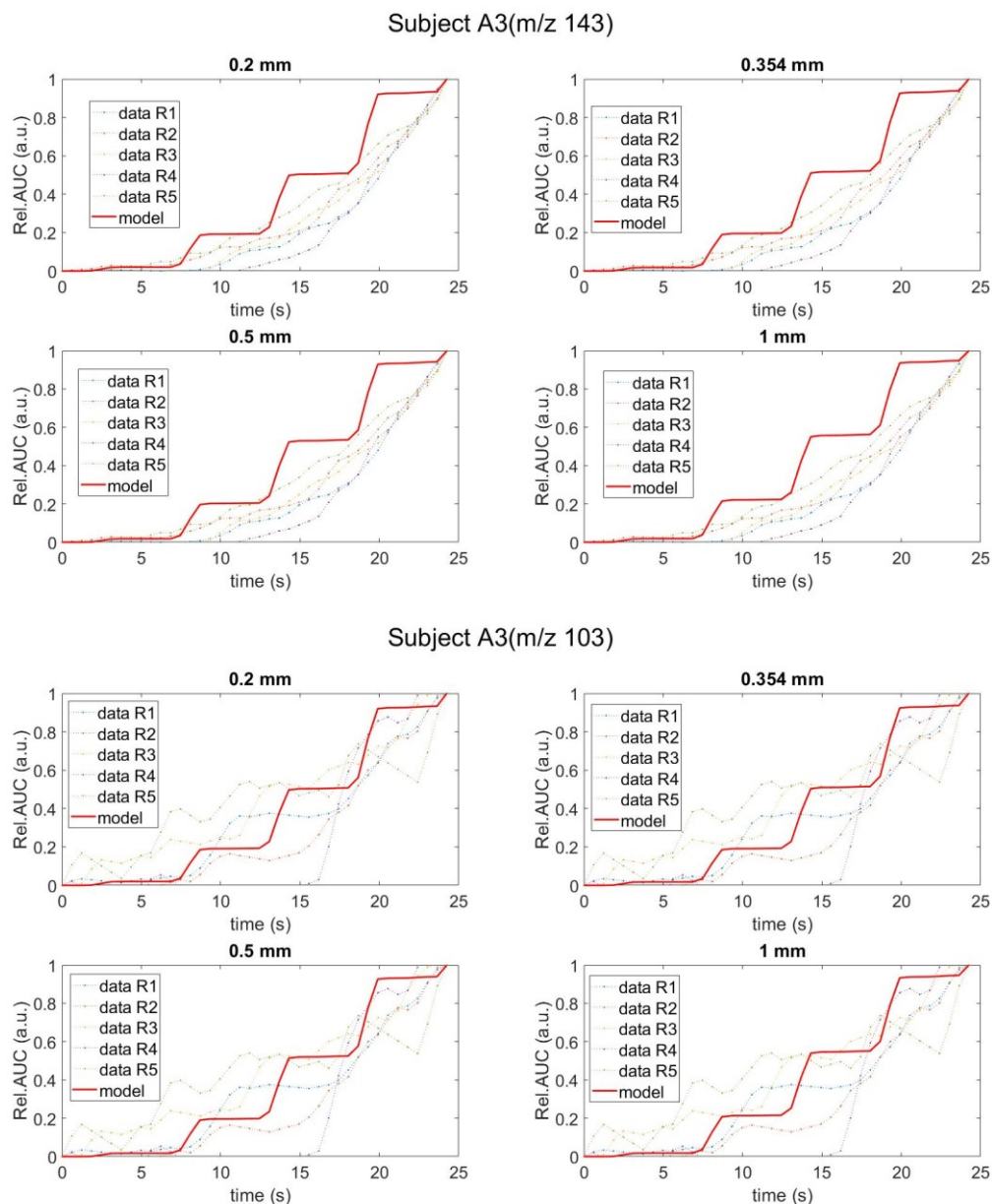


Fig. 8-17: Model prediction against experimental data of 2-nonanone (m/z 143) and ethyl propanoate (m/z 103) for Subject A3. Rel. AUC refers to the relative cumulative area under the curve, where the cumulative area under the curve was normalised against the total area under the curve. The model was also predicted using different pasted size threshold (0.2 mm, 0.354 mm, 0.5 mm and 1 mm) and compared against the five replicates of the experimental data.

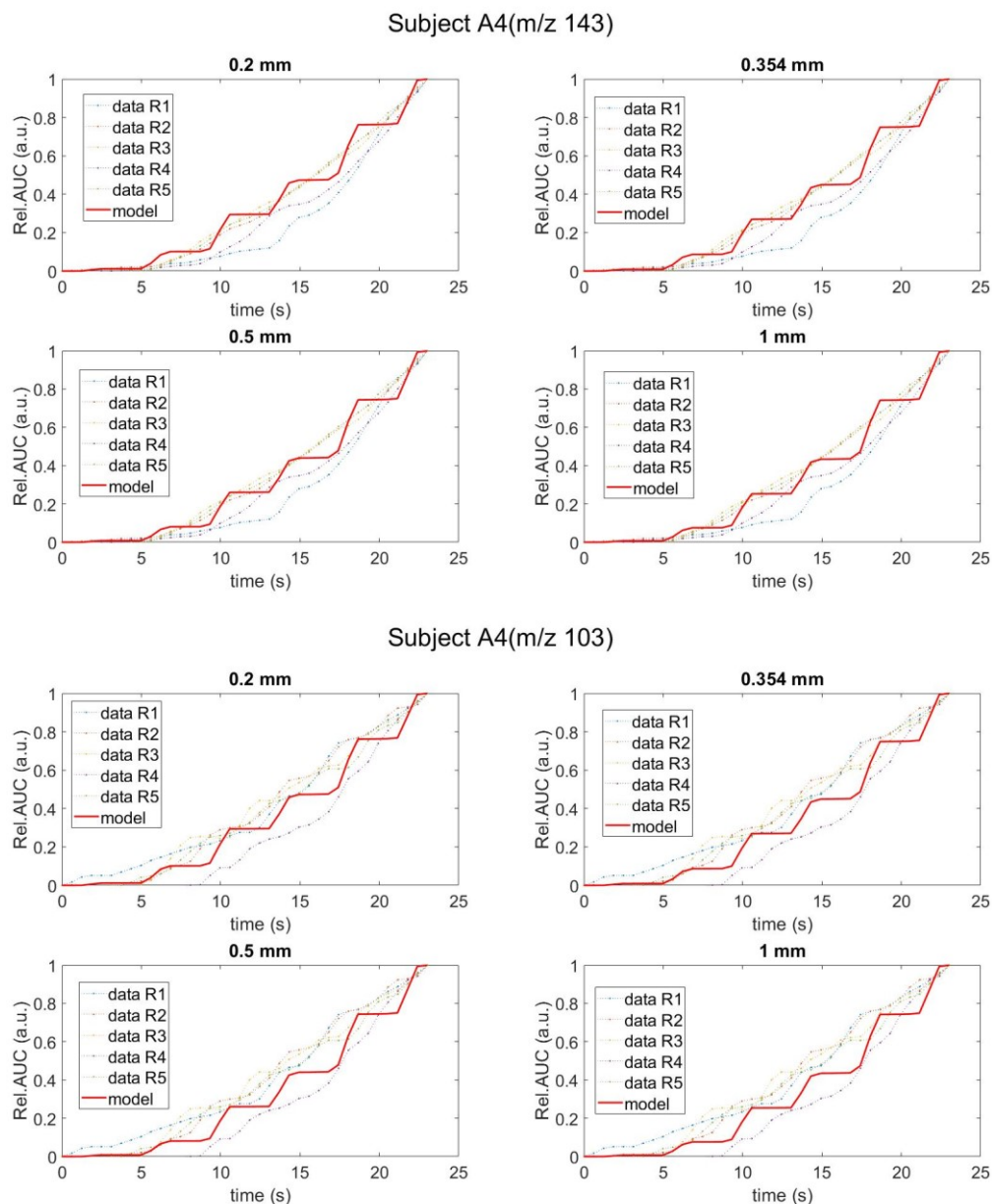


Fig. 8-18: Model prediction against experimental data of 2-nonanone (m/z 143) and ethyl propanoate (m/z 103) for Subject A4. Rel. AUC refers to the relative cumulative area under the curve, where the cumulative area under the curve was normalised against the total area under the curve. The model was also predicted using different pasted size threshold (0.2 mm, 0.354 mm, 0.5 mm and 1 mm) and compared against the five replicates of the experimental data.

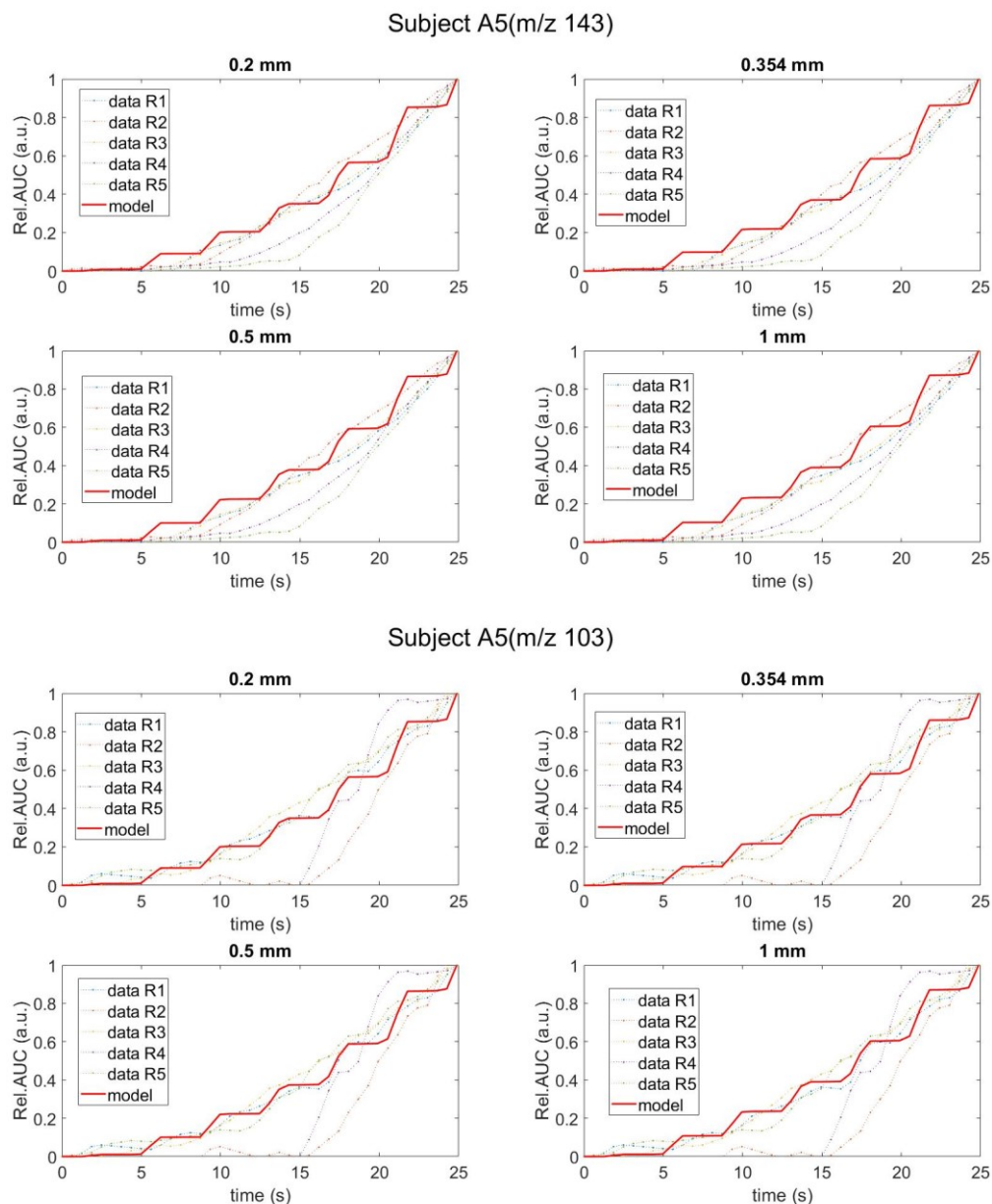


Fig. 8-19: Model prediction against experimental data of 2-nonanone (m/z 143) and ethyl propanoate (m/z 103) for Subject A5. Rel. AUC refers to the relative cumulative area under the curve, where the cumulative area under the curve was normalised against the total area under the curve. The model was also predicted using different pasted size threshold (0.2 mm, 0.354 mm, 0.5 mm and 1 mm) and compared against the five replicates of the experimental data.

As can be seen from Fig. 8-15 to Fig. 8-19, the model predictions agreed reasonably well with the experimental data across all subjects, except for 2-nonanone for Subject A1. This could be due to the lack of fit of the saliva flow rate and the volume of pasted particles input parameters for the subject. It can also be observed that the pasted size threshold has little impact on the predictions when the normalised concentrations were presented as the cumulative area under the curve. It should be noted

that the magnitude of the concentrations were different with greater concentrations being predicted when using the larger critical size used to determine the pasted fraction.

8.3 Objective 2: Validation using coupled chewing-aroma release models

This second case study aims to validate the aroma release model using the predicted bolus PSD from the chewing model developed in Chapter 3. As described above, two input parameters are required from the PSD model to predict aroma release. These are the volume of pasted particles at each chewing number and the total surface area of particles. Similarly, as previously done in Chapter 4 and 5, the input parameters for the chewing model were determined by best fitting the model to the experimental data.

8.3.1 The PSD model

The chewing model consists of selection and breakage sub-models. Each will be discussed.

8.3.1.1 Selection equations

The one-way and two-way competition selection models (Eq. 2.4 & 2.5) were applied and compared to identify which model was a best fit for the experimental data.

8.3.1.2 Breakage model equation

The breakage function used in the PSD model was as described in Eq. 2.11 below which was previously applied to brown rice (Gray-Stuart, 2016). The equation assumes that the pasted fraction is constant.

$$B(X, X_0) = (1 - P) \cdot \left[1 - \left(1 + r \cdot \frac{X}{X_0} \right) \cdot \left(1 - \frac{X}{X_0} \right)^r \right] \quad (2.11)$$

8.3.1.3 Discretised population model

The PSD was predicted using the discretised population balance model developed as described in section 3.2.3.

8.3.1.4 Model inputs

Input 1: Initial PSD

The 5 g initial PSD measured in Chapter 6 was used as the starting distribution in the model. Fig. 8-20 shows the initial PSD used in the model where most of the particles were between 5-6.5 mm in diameter.

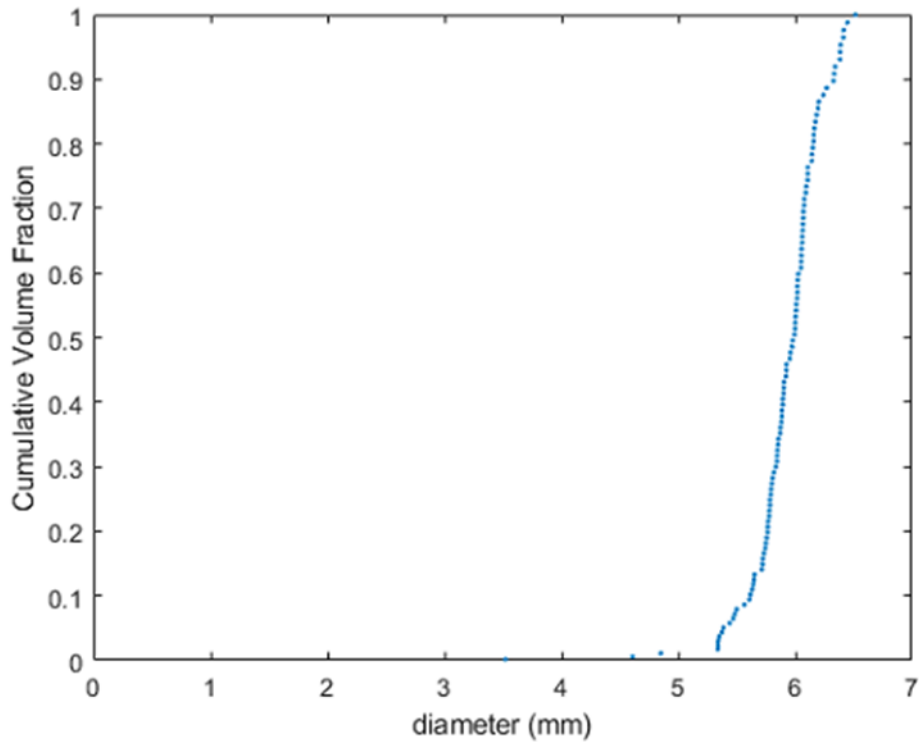


Fig. 8-20 Initial PSD used in the model (5 g).

Input 2: Selection and breakage model input parameters

The input parameters required for the one-way and two-way selection functions are the number of particles, the number of breakage sites and the affinity factor. The degree of fragmentation variable and the pasted fraction are required for the breakage function. The full details of the input parameters required for the selection and breakage functions have been discussed previously in Chapter 3.

9.3.1.5 Model fitting

Using the initial PSD as described above as the input to the model, the PSD after 1 chew, 2 chew, 25%, 50%, 75% and 100% of swallow point was determined for each subject. The PSO algorithm (as described in Chapter 4) was used to solve the model input parameters by minimising the normalised sum of squares residuals between the model and the experimental data. The residual was calculated from 10 d_x -values that were the intercepts for 10% (d_{10}), 20% (d_{20}), 30% (d_{30}), 40% (d_{40}), 50% (d_{50}), 60% (d_{60}), 70% (d_{70}), 80% (d_{80}), 90% (d_{90}) of the cumulative volume distribution of the model and the experimental data. The algorithm was also solved to minimise the normalised residual of the pasted fraction (defined as the volume fraction for particles less than 0.354 mm) of the model and experimental data. Due to the probabilistic nature of the way the selection and breakage models were implemented,

the model was repeated 50 times (see section 4.2.4 for the reason this number was chosen) and the average was determined to calculate the residual for the model fitting.

8.3.2 PSD model validation

Table 8-6 below shows the comparison of the best-fit input parameter results when the breakage function of Eq.2.11 was fixed, and when the one-way or two-way competition selection models were applied. The R-squared was calculated from equation 4.2 in section 4.2.3. Comparisons between the fitted *d*-values and pasted fraction against experimental data for all of the five subjects are shown in Fig. 8-21 to Fig. 8-25. The top images are for when the one-way competition selection model and a fixed breakage model were applied (Eq.8.1). The images at the bottom are for when the two-way competition model was used as the selection model. The plot on the left of the image is the comparison of the *d*-values of the best fit model and the experimental data whereas the plot on the right shows the comparison of the pasted fraction values. The error bar of the model is the standard deviation of 50 simulations. All 3 replicates of the measured data (three different markers) were plotted for comparison.

For most of the subjects, a better fit was achieved when the two-way competition model was used as the selection model. This is supported by the higher R-squared values when the two-way competition model was used across most subjects in Table 8-6 (except subject A1 and A2). Subject A1 had a better fit when the one-way competition model was used as it had a greater number of larger particles (particles between 4-5.7 mm) compared to other subjects even at the later stages of mastication (Fig. 8-1).

Therefore, the question of whether the one-way model or two-way model can describe the particle selection of the entire chewing sequence may be influenced on the person itself. Van der Glas et al., (2018) in their study, discussed that the two-way competition model may be sufficient to describe particle selection during the whole chewing sequence.

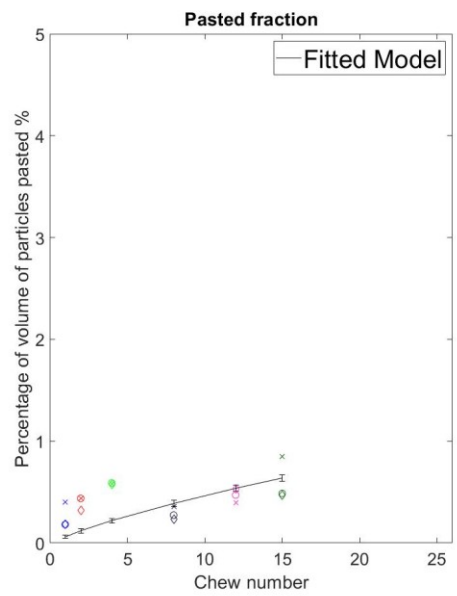
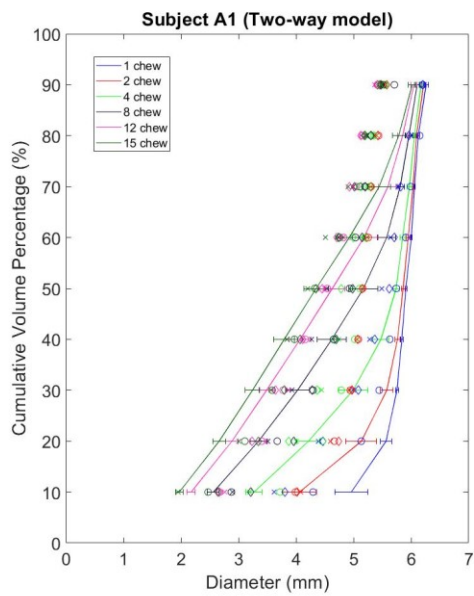
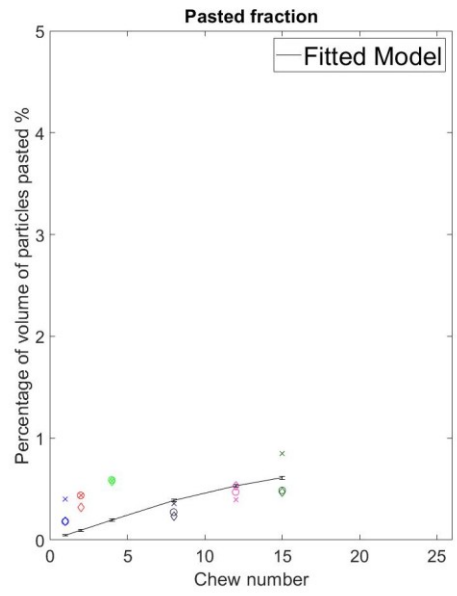
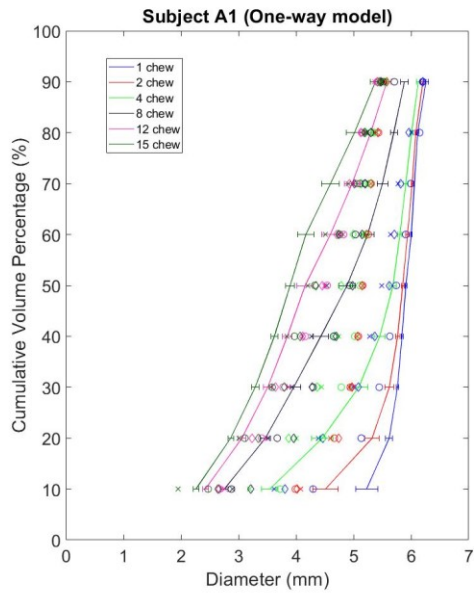


Fig. 8-21: Best-fit model against experimental data for Subject A1.

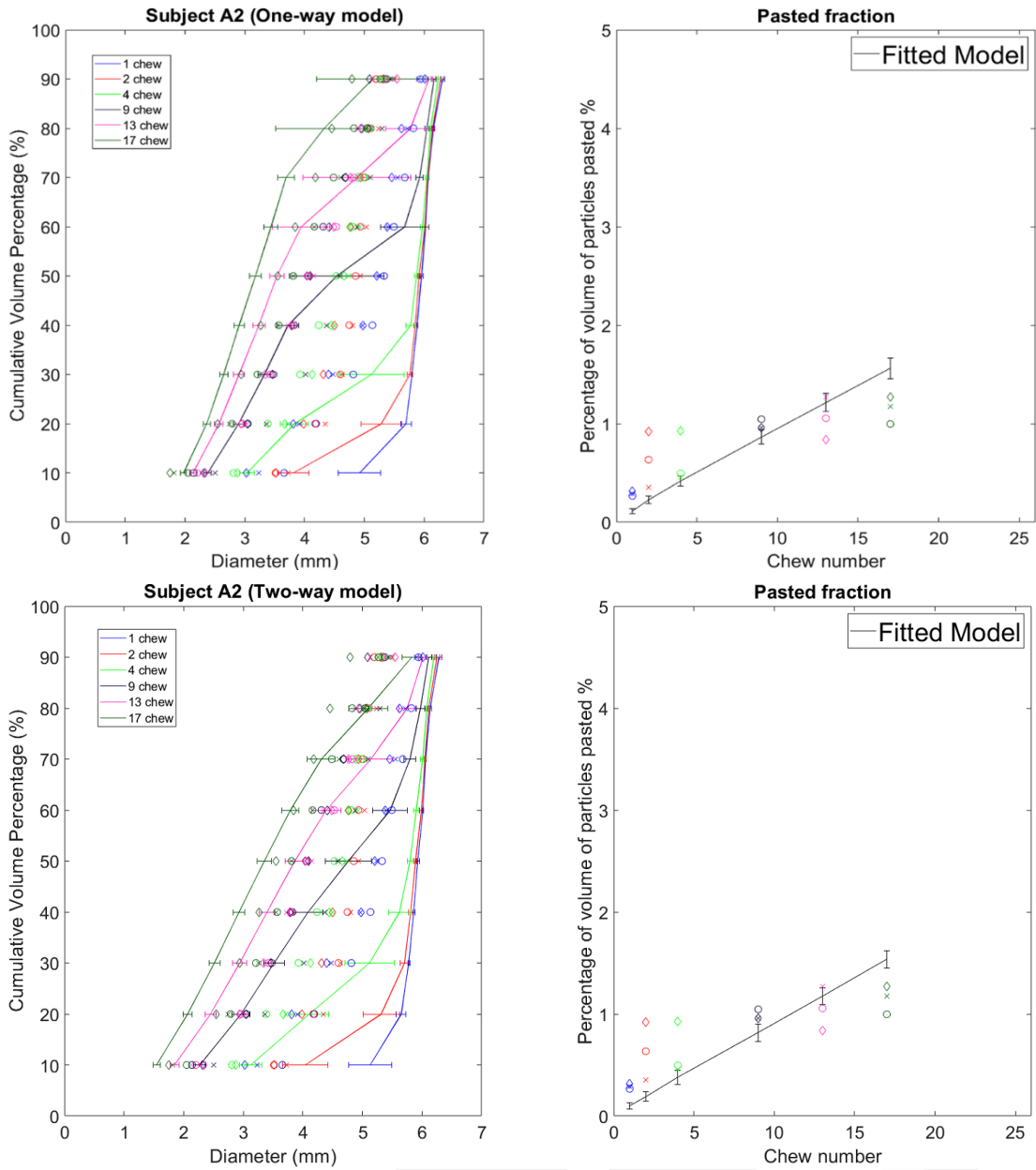


Fig. 8-22: Best-fit model against experimental data for Subject A2.

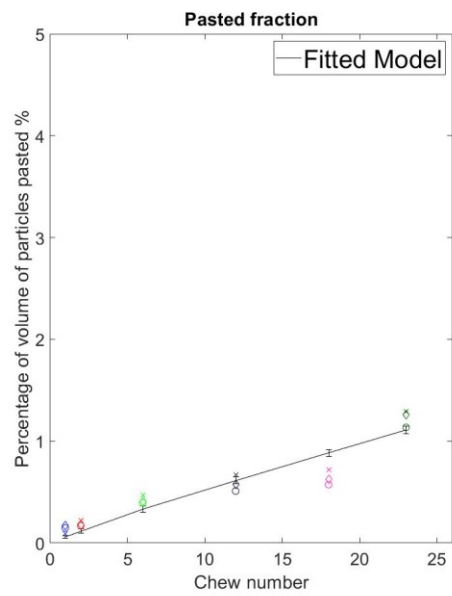
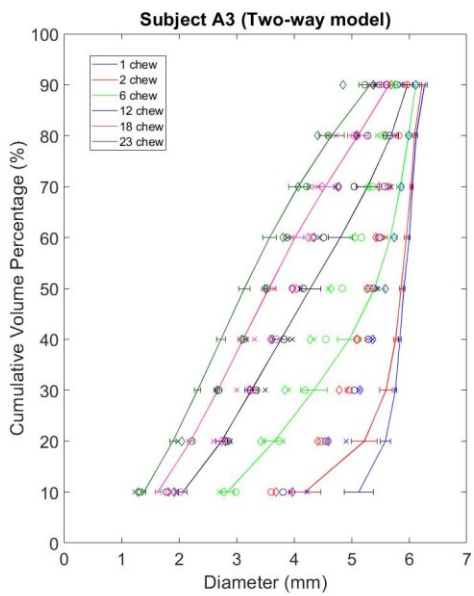
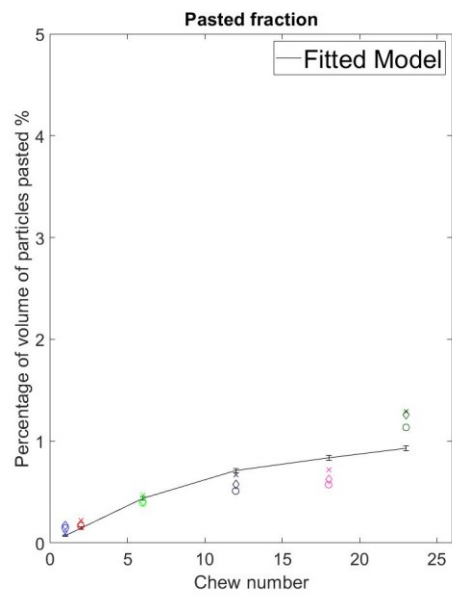
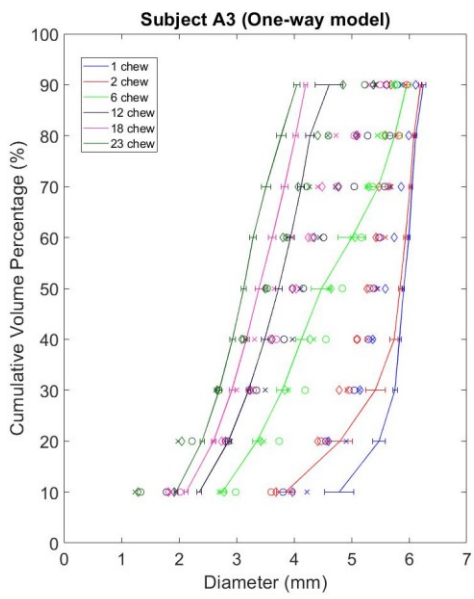


Fig. 8-23: Best-fit model against experimental data for Subject A3.

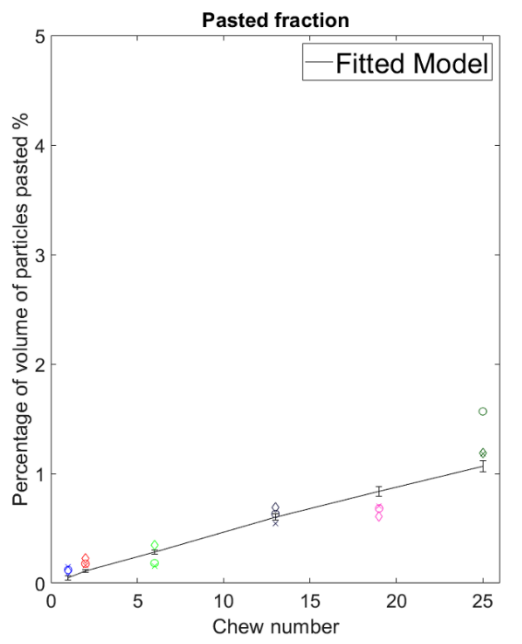
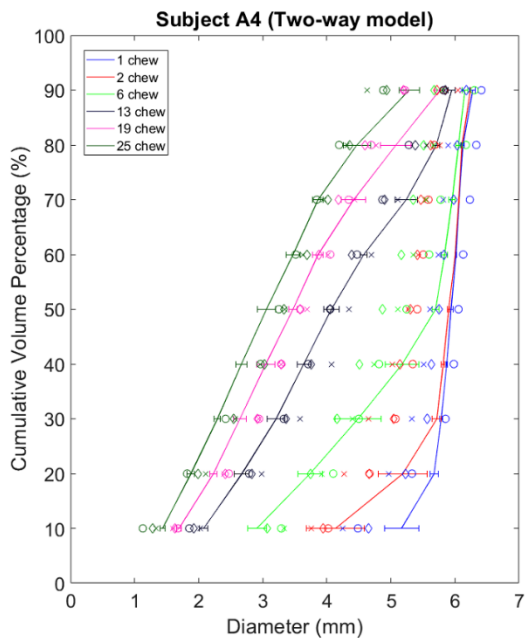
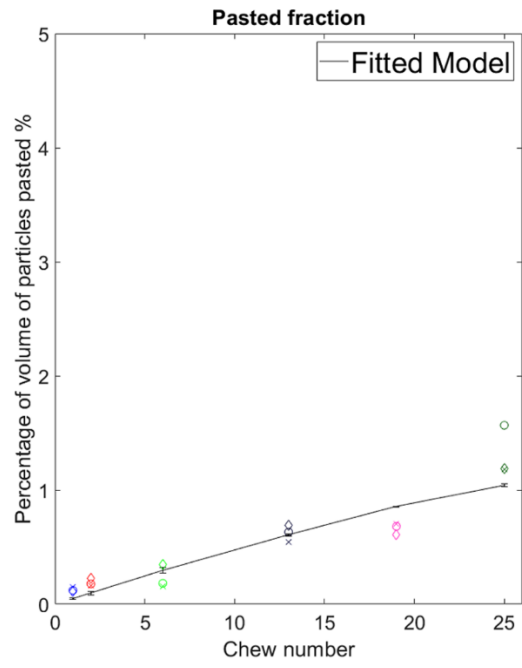
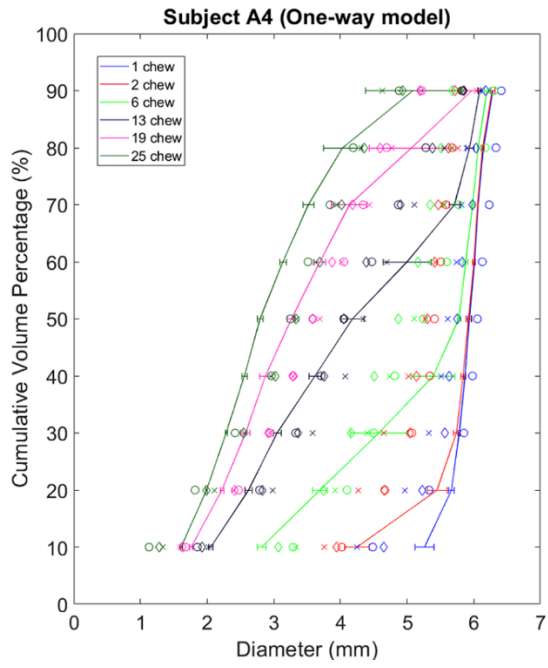


Fig. 8-24: Best-fit model against experimental data for Subject A4.

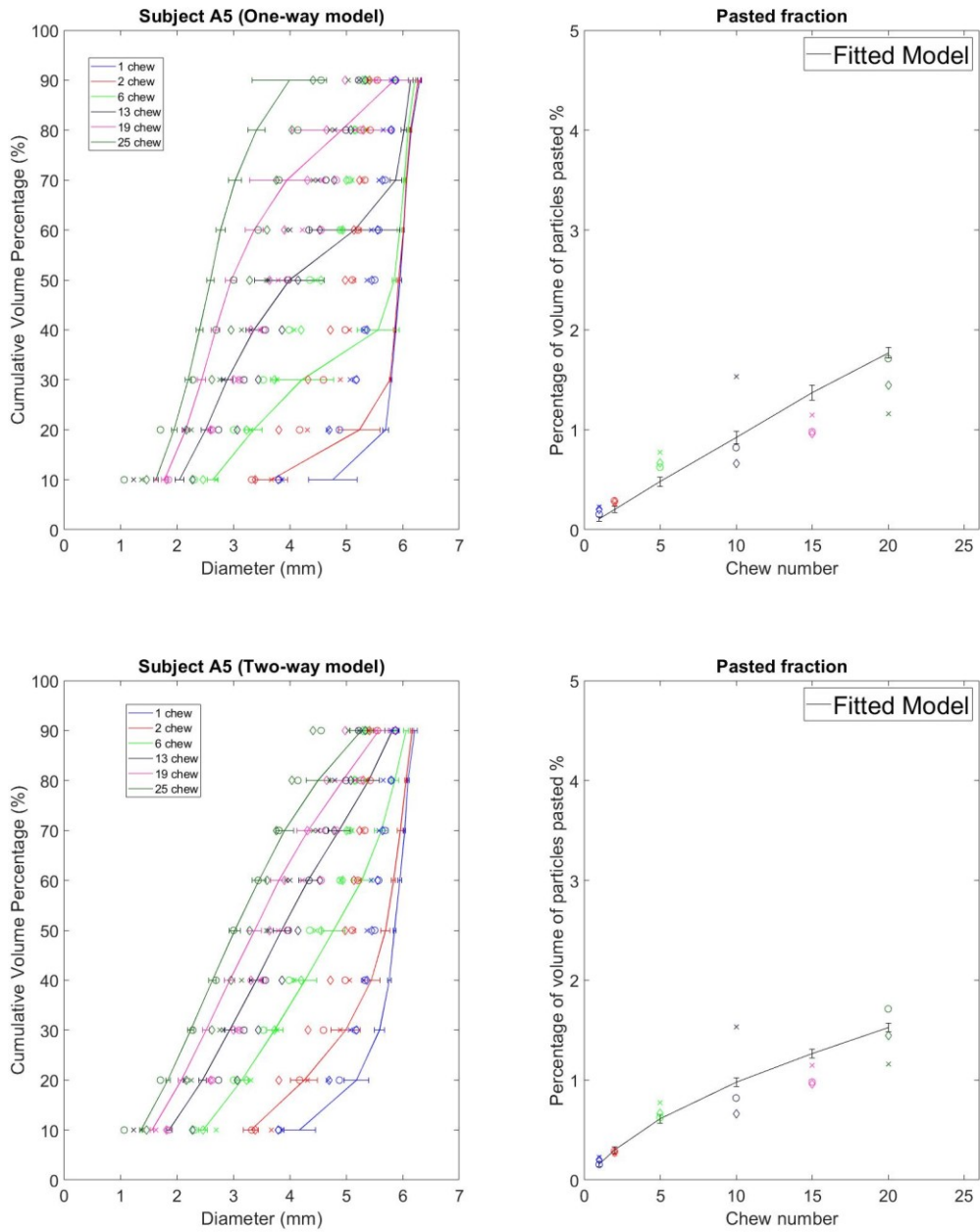


Fig. 8-25: Best-fit model against experimental data for Subject A5.

Table 8-6: Best fit input parameters of the PSD model evaluated from the PSO algorithm.

Subject	Selection model	Selection model inputs				Breakage model input		Normalised		
		Number of breakage sites, n_b		Affinity factor, α_1		Fragmentation variable, r	Pasted fraction, p	SS residuals	SS	R^2
		<i>Multiplication factor, k</i>	<i>Power, m</i>	<i>Multiplication factor, p</i>	<i>Power, q</i>					
		<i>One-way competition</i>	<i>Two-way competition</i>	<i>One-way competition</i>	<i>Two-way competition</i>					
A1	<i>One-way competition</i>	165.4	1.01	0.0016	1.77	0.16	0.001	2.49	13.3	0.92
	<i>Two-way competition</i>	133.1	1.25	0.0035	1.43	0.95	0.004	2.41	16.1	0.89
A2	<i>One-way competition</i>	237.6	2.25	0.0025	2.99	1.41	0.01	3.05	36.4	0.75
	<i>Two-way competition</i>	370.1	2.18	0.0015	2.97	2.43	0.011	3.45	36.4	0.75
A3	<i>One-way competition</i>	175.1	1.18	0.0036	2.17	0.26	0.002	1.42	13.8	0.92
	<i>Two-way competition</i>	331.65	1.81	0.0022	2.38	0.82	0.004	1.28	10.6	0.94
A4	<i>One-way competition</i>	163.3	1.87	0.0018	1.53	1.28	0.005	1.62	10.3	0.95
	<i>Two-way competition</i>	184.6	1.64	0.0029	2.44	1.41	0.005	0.91	5.32	0.97
A5	<i>One-way competition</i>	447.5	2.63	0.0015	2.96	1.72	0.01	2.38	30.9	0.82
	<i>Two-way competition</i>	169.9	1.02	0.0027	1.61	0.92	0.006	0.59	7.94	0.95

Van der Glas et al., (2018) explained that during the first few initial chewing cycles, when chewing is started on a batch of large particles, the difference between the one-way model and the two-way model regarding selection of large particles will be small because of a small affinity for small particles. Then after the initial phase of chewing, as more smaller fragments are produced, particle piling will occur extensively, which follows the two-way competition model. However, as seen here for subject A1 who chewed the shortest time at swallow point, particle selection followed the one-way competition model better because of the presence of larger particles at the later stages of mastication

(e.g. at the swallow point). The presence of some number of larger particles even towards the end of the chewing sequence could be explained through the fact that rice is a high moisture food (61 g water/100 g bolus as explained in section 6.4.2), therefore the existence of a few large particles in the bolus will not be an issue as they are lubricated enough to be swallowed safely.

The main conclusion that can be observed from the results above is that model fitting may give insights on the selection behaviour for different subjects and could be dependent on the type of food they consume. This could then provide opportunity for food manufacturers to design foods that are exclusively favourable for the behaviour described by the one-way or two-way model (Hutchings, 2011; van der Glas et al., 2018).

8.3.2.1 Lack of fit of the model

Although the two-way selection model provided a better fit than the one-way selection model in almost all of the subjects, based on the above figures (Fig. 8-21- Fig. 8-25), the model still does not fit the experimental data perfectly. For example, the model did not fit particularly well for the lower range of d -values (d_{10} - d_{50}) during the initial phase of chewing (1, 2 and 6 chews). The pasted fraction also did not fit particularly well for the number of chews at the early mastication stages for subject A1 and A2. The model fit particularly well using the two-way model for subject A3 but did not fit the experimental data well when the one-way model was used. Both one-way and two-way models fit reasonably well for subject A4, but not in the first few chewing cycles. The two-way model fitted the experimental data reasonably well for subject A5 but overestimated the breadth of the PSD when the one-way model was used. The lack of fit especially in the first few chewing cycles is to be expected as the selection and breakage functions are the most probabilistic during this stage. The study from Paphangkorakit et al. (2006) showed that as chewing progressed and as foods became softer and more dissociated, they found that subjects tend to use less lateral movement. Therefore as more lateral movements are used in the first few chews and less towards the late stage, it is expected that selection and breakage could change in the early phase of mastication but remains constant as the food softens towards the late stage of mastication. Furthermore, it was also observed in Chapter 4 to get a reasonable consistency in the model predictions, that at least 50 simulations were required. The PSD data used to fit the model here was

based on the mean of three bolus replicates, therefore if the experiment was to be repeated where another 3 bolus replicates were measured we may expect the mean PSD data to be quite different. In this manner, it seems sensible that the lack of fit was seen in the early phases of mastication.

In addition, the lack of fit of the model for some of the subjects may be explained due to the uncertainty of the range of the model input parameters used to be solved by the PSO algorithm. The range of parameters used was based on the data of five subjects who participated in one-chew experiments of Optosil® from van der Glas et al. (2018), which were different subjects to the ones participated in this study. Therefore, future studies involving coupling the PSD model and aroma release will require performing single chew experiments that are specific to the model food used to obtain the input parameters for the selection model. However, as mentioned previously in Chapter 2, single chew experiments are time-consuming, and it can be difficult to perform such experiments with real foods in a repeatable and consistent manner. The measurement of the occlusal area of the tested subjects with a chewing gum may be an alternative way to obtain some of the input parameters in the selection model in a fast and simple manner (see section 3.2.2.4.1, Chapter 3).

8.3.3 Validation of the coupled PSD-aroma release models

Despite the lack of fit of the PSD model, the model predictions were used as inputs to predict aroma release to observe the difference in the model validation compared to when it was taken directly from the experimental data. The PSD outputs from the PSD model were used to calculate the volume of the pasted particles and the total surface area of particles as described in section 8.2.1 previously. Both PSD outputs derived from the fittings of the one-way and two-way competition models were applied. Similarly, the physiological input parameters of each subjects and the physicochemical parameters as described in the previous sections were applied. The cumulative area under the curve were then obtained for the normalised concentrations of 2-nonanone (m/z 143) and ethyl propanoate (m/z 103) in the nasal cavity. The model was also predicted using different pasted size thresholds (0.2 mm, 0.354 mm, 0.5 mm and 1 mm) and compared against the experimental data to see if the difference in the threshold has a pronounced effect on the prediction. Fig. 8-26 to Fig. 8-30 shows the comparison of the model predictions against the experimental data for the five subjects.

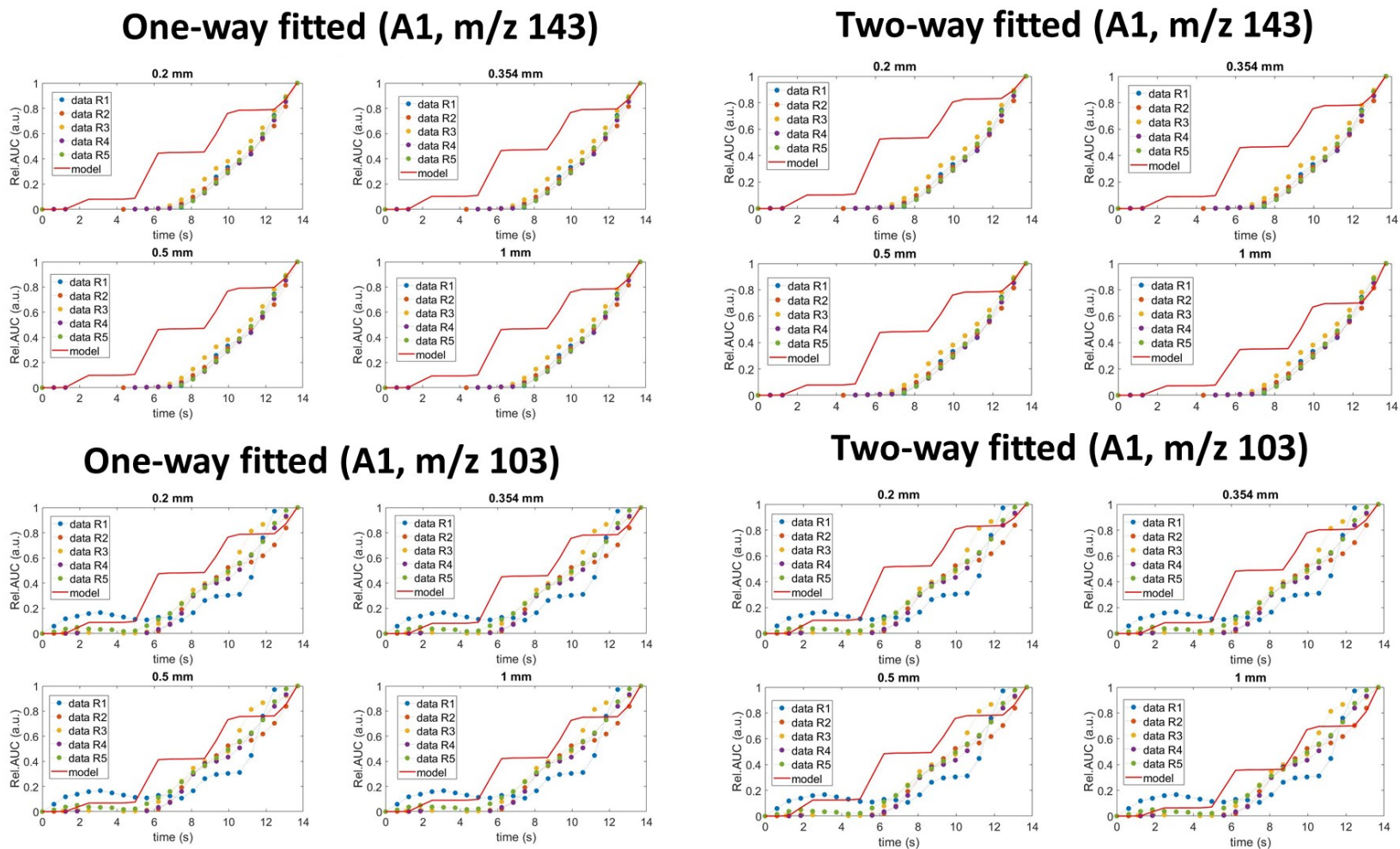
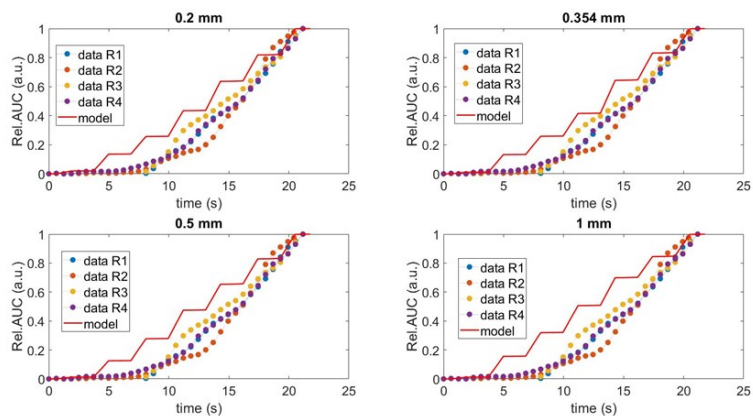
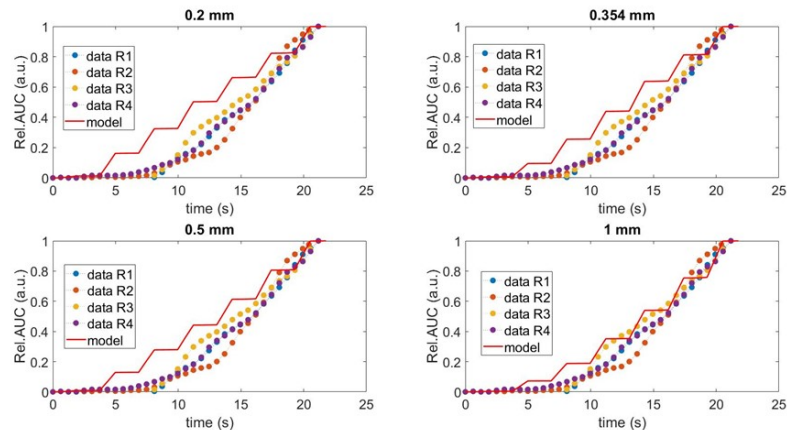


Fig. 8-26 Model prediction against experimental data of 2-nonanone (m/z 143) and ethyl propanoate (m/z 103) for Subject A1. Rel. AUC refers to the relative cumulative area under the curve, where the cumulative area under the curve was normalised against the total area under the curve. The model was also predicted using different pasted size threshold (0.2 mm, 0.354 mm, 0.5 mm and 1 mm) and different selection models (one-way and two-way competition) and compared against the five replicates of the experimental data.

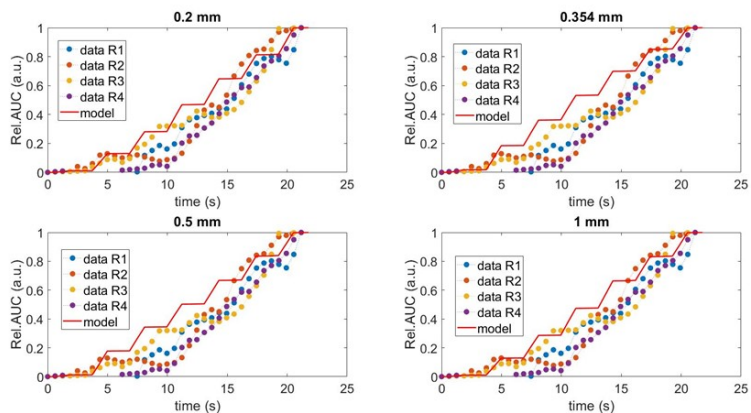
One-way fitted (A2, m/z 143)



Two-way fitted (A2, m/z 143)



One-way fitted (A2, m/z 103)



Two-way fitted (A2, m/z 103)

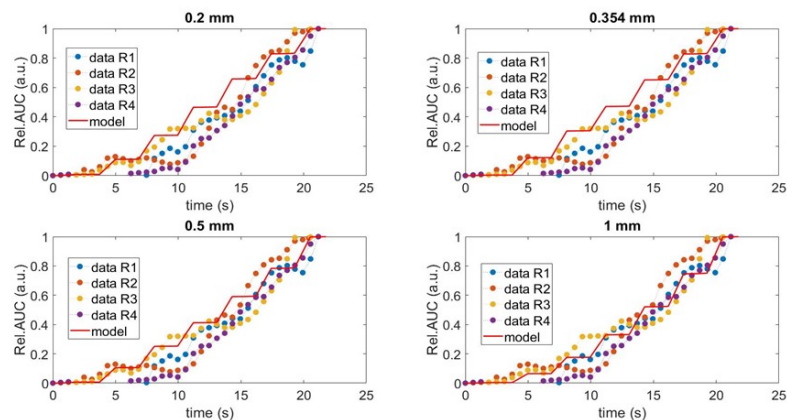


Fig. 8-27 Model prediction against experimental data of 2-nonanone (m/z 143) and ethyl propanoate (m/z 103) for Subject A2. Rel. AUC refers to the relative cumulative area under the curve, where the cumulative area under the curve was normalised against the total area under the curve. The model was also predicted using different pasted size threshold (0.2 mm, 0.354 mm, 0.5 mm and 1 mm) and different selection models (one-way and two-way competition) and compared against the five replicates of the experimental data.

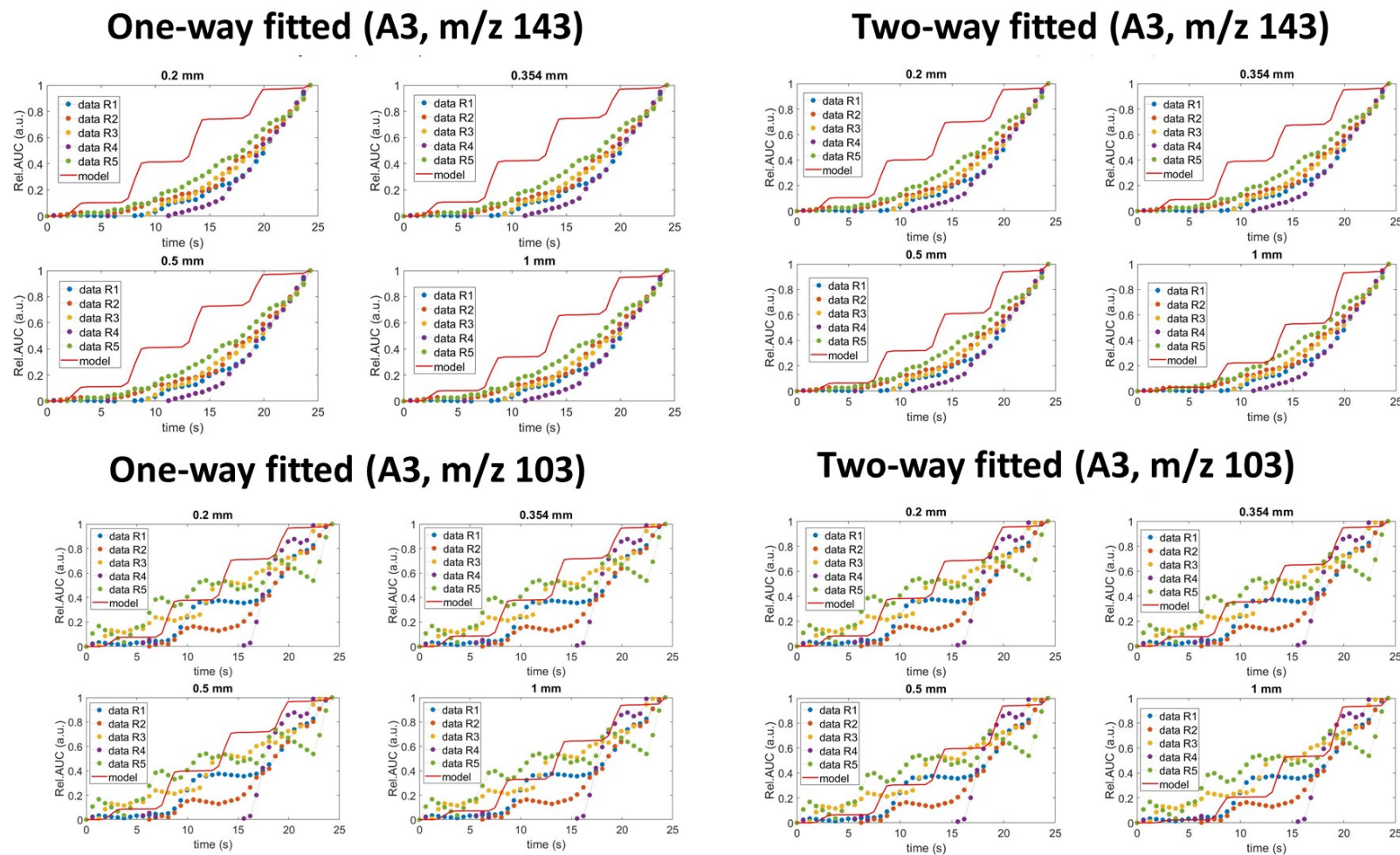


Fig. 8-28 Model prediction against experimental data of 2-nonanone (m/z 143) and ethyl propanoate (m/z 103) for Subject A3. Rel. AUC refers to the relative cumulative area under the curve, where the cumulative area under the curve was normalised against the total area under the curve. The model was also predicted using different pasted size threshold (0.2 mm, 0.354 mm, 0.5 mm and 1 mm) and different selection models (one-way and two-way competition) and compared against the five replicates of the experimental data.

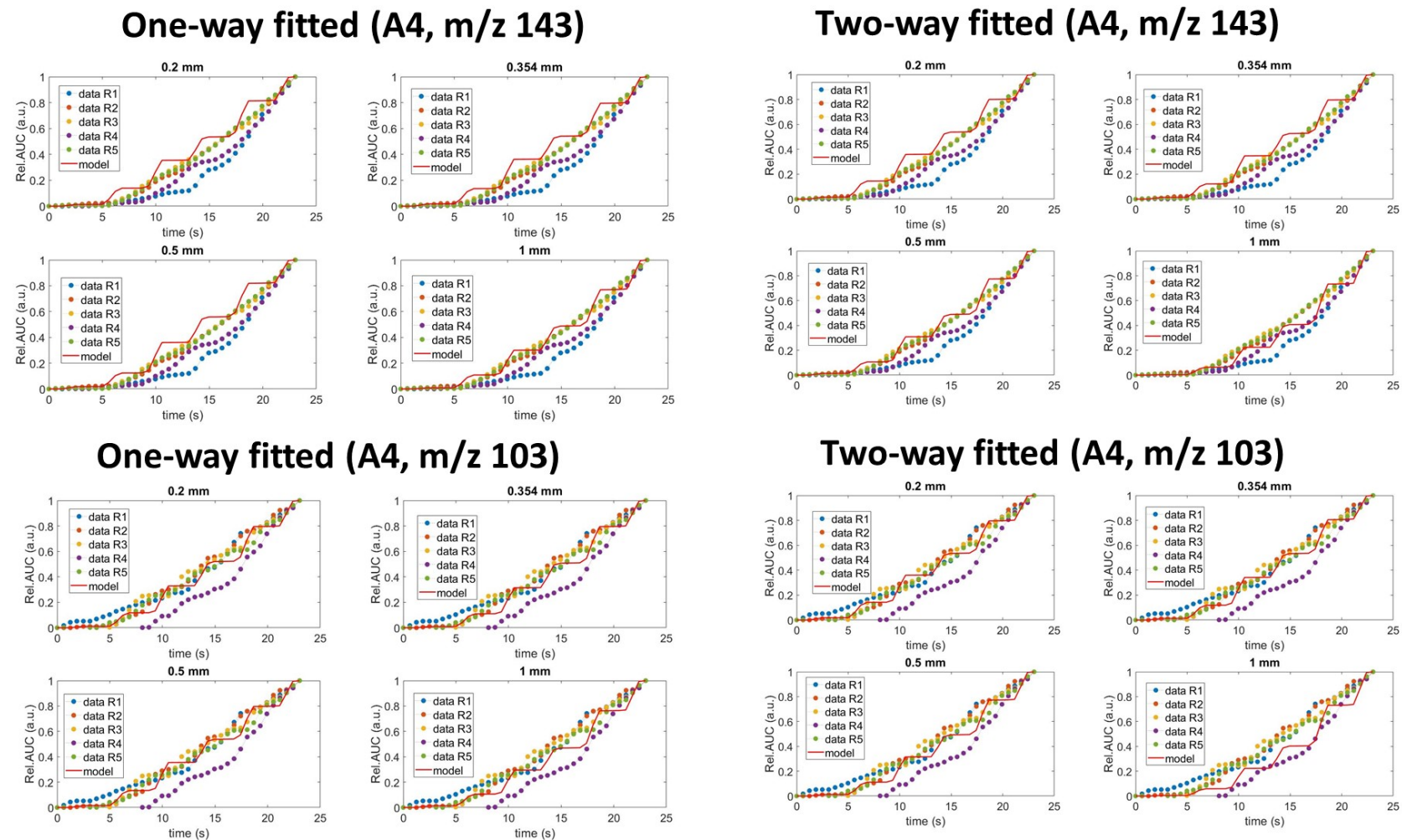
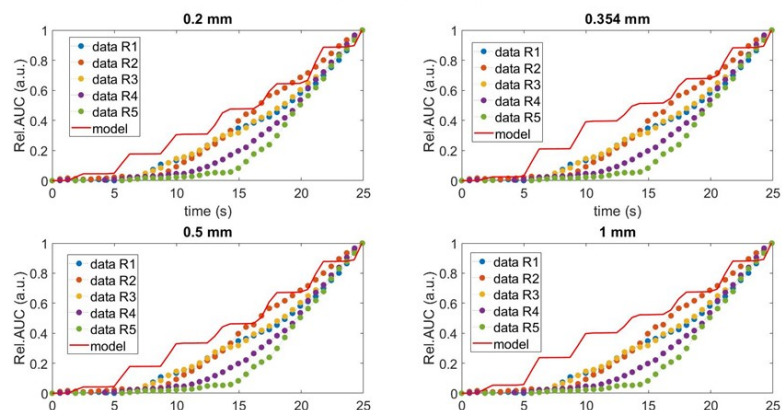
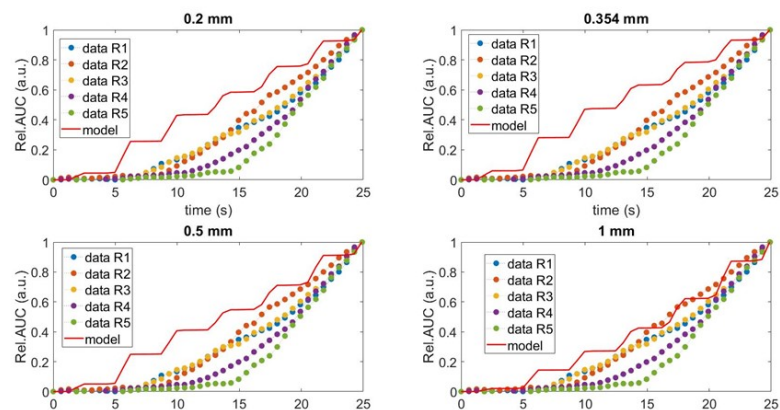


Fig. 8-29 Model prediction against experimental data of 2-nonanone (m/z 143) and ethyl propanoate (m/z 103) for Subject A4. Rel. AUC refers to the relative cumulative area under the curve, where the cumulative area under the curve was normalised against the total area under the curve. The model was also predicted using different pasted size threshold (0.2 mm, 0.354 mm, 0.5 mm and 1 mm) and different selection models (one-way and two-way competition) and compared against the five replicates of the experimental data.

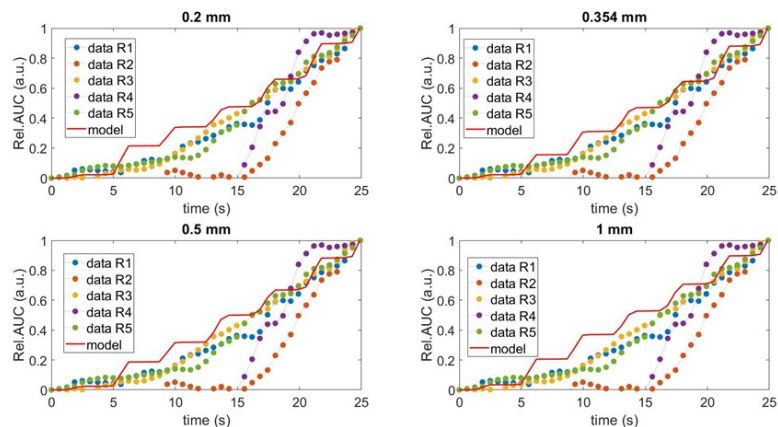
One-way fitted (A5, m/z 143)



Two-way fitted (A5, m/z 143)



One-way fitted (A5, m/z 103)



Two-way fitted (A5, m/z 103)

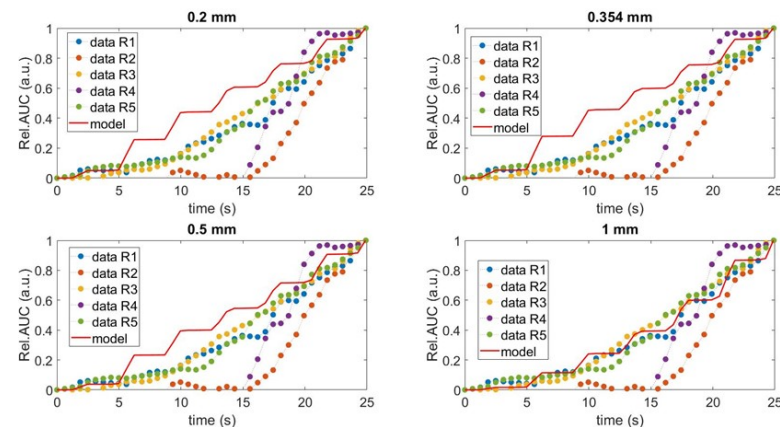


Fig. 8-30 Model prediction against experimental data of 2-nonanone (m/z 143) and ethyl propanoate (m/z 103) for Subject A5. Rel. AUC refers to the relative cumulative area under the curve, where the cumulative area under the curve was normalised against the total area under the curve. The model was also predicted using different pasted size threshold (0.2 mm, 0.354 mm, 0.5 mm and 1 mm) and different selection models (one-way and two-way competition) and compared against the five replicates of the experimental data.

A common trend can be seen from Fig. 8-26 to Fig. 8-30 is that the model predictions satisfactorily agreed with the experimental data well for ethyl propanoate (m/z 103) compared to 2-nonanone (m/z 143). However, when compared using the fitted PSD outputs from two different selection models, the two-way competition model seems to give closer predictions with the experimental data (e.g. subject A3, A4 and A5), although the difference is not eminent. This is mainly because the model assumed the aroma release to be largely contributed by the increase in the volume of pasted particles (particles < 0.354 mm) and both one-way and two-way models satisfactorily fitted the pasted particles experimental data as seen above. When the one-way competition fitted values were used, the model appears to slightly over-predict the data, for example subject A3 for m/z 143 and m/z 103 respectively. This makes sense as it is observed in section 8.3.2 for subject A3 that the PSD model over anticipated the size of particles when the one-way competition model was used, therefore resulted to a higher number of particles and hence, the sum of the surface area of particles. Therefore, a higher concentration of aroma release was to be expected in the model predictions. Nonetheless, overall, it appears that the model predictions find good agreement with subjects who had a validated PSD model. For example, subject A4 fitted the PSD data reasonably well in section 8.3.2 and compares well with the *in vivo* aroma release data seen above (Fig. 8-29).

For any case, it seems that using the PSD inputs taken directly from experimental data found a better agreement with the *in vivo* aroma release data compared to when the model was coupled with the PSD model. Thus, if one is only interested get the aroma release models validated then perhaps assuming that the PSD variables increases linearly with time seems reasonable particularly as the PSD model requires measurements of input parameters which can be time-consuming (from long simulation time and/or additional experimental protocols). However, the coupling with the mechanistic PSD model allows one to understand the role of chewing on aroma release more comprehensively, therefore provide opportunities to food scientists to design foods, which could influence the underlying chewing mechanisms and subsequently aroma release. For example, it was shown that the model fits were better when the one-way competition model was used. Therefore, if foods contain a mixture of particles with

various sizes, larger particles are preferentially selected for breakage. It may then be possible to maximise aroma release by adding aroma compounds to just the large particles. In terms of controlling the breakage function, perhaps the cooking method can be adjusted by adding more water to promote the swelling of rice granules therefore increases the chance of particles to be pasted. Anyhow, it was shown that the subject who had a well-fitted PSD model found a good agreement with the *in vivo* aroma release data. In the next chapter, the effect of each group of input parameters of the model will be discussed through one of the validated subjects (Subject A4) to demonstrate model application for food design.

8.4 Chapter conclusion

The objective of Chapter 8 was to validate the aroma release models developed in Chapter 7 with *in vivo* experimental data. Two different approaches were used to validate the model. The first approach was when the PSD outputs required for the model were taken directly from the experimental data. The second approach obtained the PSD outputs from the chewing model developed in Chapter 3. Other input parameters required for the model such as the physiological and physicochemical parameters were measured experimentally and those that could not be measured were obtained from the literature.

Due to issues related to the measurement of the experimental data, the model prediction for each subject was compared against the data in terms of its cumulative area under the curve. In the first approach, the model predictions satisfactorily agreed with the experimental data for all subjects except for 2-nonanone for Subject A1. The second approach showed that the model predictions compared well with the experimental data, particularly for subjects who found good agreement with the PSD data. The first approach appears to be a more sensible approach if the aroma release model only needs to be validated, however the downside is it does not give insights into the role of chewing on aroma release in a mechanistic way. Hence, to provide mechanistic insights of the aroma release of solid foods and to demonstrate model application for food design, the effect of each group of input parameters of the coupled PSD-aroma release model will be discussed through one of the validated subjects (Subject A4) in the next chapter.

Chapter 9 Application of the aroma release model

9.1 Introduction

In Chapter 7 models have been developed to predict the aroma release in food during mastication. The model to validate against experimental data for chewing white rice as described in Chapter 8. This builds on previous studies in the development of mechanistic models of flavour release of solid foods during mastication (Harrison et al., 1998; Wright & Hills, 2003; Doyennette et al., 2014). The ultimate aim of these developments is to be able to mathematically predict the effect of varying food composition, food structure, and mastication behaviour on the perceived time-intensity flavour release profile (Harrison et al., 1998).

In this chapter, the application of the models developed in Chapter 7 and Chapter 8 is demonstrated and discussed. Using the validated PSD model and the input parameters from one of the subjects (Subject A4), the aroma release of 2-nonanone in cooked rice (defined as the concentration of the aroma compound in the nasal cavity) was predicted. Input parameter values were then adjusted to demonstrate the application of the models in various situations which may interest food technologists/food manufacturers.

9.2 Using the model to provide insights for food design

9.2.1 The validated PSD model

The PSD model consists of selection and breakage sub-models. Each will be discussed.

9.2.1.1 Selection equations

The two-way competition model was applied as it was shown to provide a better fit with the PSD experimental data for subject A4 as described in Chapter 8 previously.

9.2.1.2 Breakage model equation

The breakage function used in the PSD model was as described in Eq. 2.11 below which was previously applied on brown rice (Gray-Stuart, 2016). The equation assumes that the pasted fraction is constant.

$$B(X, X_0) = (1 - P) \cdot \left[1 - \left(1 + r \cdot \frac{X}{X_0} \right) \cdot \left(1 - \frac{X}{X_0} \right)^r \right] \quad (2.11)$$

9.2.1.3 Discretised population model

The PSD will be predicted using the discretised population balance model developed as described in section 3.2.3.

9.2.1.3 PSD model inputs

Input 1: PSD after a single chew as a model input

Similar to the case study in Chapter 8, the 5 g initial PSD measured in Chapter 6 was used as the starting distribution in the model.

Input 2: Selection and breakage model input parameters

The input parameters required for the two-way competition model is the number of particles, the number of breakage sites and the affinity factor. The degree of fragmentation variable and the pasted fraction are required for the breakage function. The reference input parameters for subject A4 is shown in Table 9-1 below.

Table 9-1 PSD model input parameters which was previously fitted in Chapter 8.

Subject	Selection model	Selection model inputs				Breakage model input	
		Number of breakage sites, n_b		Affinity factor, α_1		Fragmentation variable, r	Pasted fraction, p
		<i>Multiplication factor, k</i>	<i>Power, m</i>	<i>Multiplication factor, p</i>	<i>Power, q</i>		
A4	Two-way competition	184.6	1.64	0.0029	2.44	1.41	0.005

9.2.2 Physiological and physicochemical input parameters

The remaining input parameters required for the model were the physiological parameters of the subject and the physicochemical parameters of 2-nonanone. The reference input values used are outlined in Table 9-2 and Table 9-3 below.

Table 9-2 Reference physiological parameters of subject A4.

Symbol	Unit	Description	Reference value
A_O	mm ²	Total area in oral cavity	11600
A_F	mm ²	Total area of the pharynx	6500
A_{Oam}	mm ²	air/lubricated mucosa contact area in the oral cavity	= 0.1 x A_O
A_{Fam}	mm ²	air/lubricated mucosa in the pharynx	= 0.1 x A_F
A_{Fas}	mm ²	air/saliva contact area in the pharynx	= $A_F - A_{Fam}$
A_{Nam}	mm ²	air/lubricated mucosa in the nasal cavity	15 x 10 ³
e_{Oam}	mm	Thickness of wetted mucosa in the oral cavity	5 x 10 ⁻²
e_{Fam}	mm	Thickness of wetted mucosa in the pharynx	5 x 10 ⁻²
e_{Nam}	mm	Thickness of mucosa in nasal cavity	5 x 10 ⁻²
F_{breath}	number of cycles/s	breathing frequency	0.25
fr_{chew}	number of chews/s	chewing frequency	1.5
$fr_{opening}$	occurrence number/s	opening frequency of the velopharynx	= F_{breath} or fr_{chew}
V_c	mm ³	current breath volume	8 x 10 ⁵
V_{Orest}	mm ³	volume of saliva at rest in the oral cavity	871
V_{Om}	mm ³	volume of mucosa in the oral cavity	= $e_{Oam} \times A_{Oam}$
V_{Oamean}	mm ³	volume of air in the oral cavity	78300
V_{Fa}	mm ³	volume of air in the pharynx	32000
V_{Fs}	mm ³	volume of saliva in the pharynx	2 x 10 ²

V_{Fm}	mm ³	volume of mucosa in the pharynx	= $e_{Fam} \times A_{Fam}$
V_{Na}	mm ³	volume of air in the nasal cavity	16000
V_{Nm}	mm ³	volume of mucosa in the nasal cavity	= $e_{Nam} \times A_{Nam}$
Q_{Os}	mm ³ /s	saliva flow rate in the oral cavity	38
$t_{swallow}$	s	time taken to swallow	24
n_{chews}		number of chews required to reach swallow point	35

Table 9-3 Reference physicochemical parameters used in the simulation

Symbol	Unit	Description	Reference value
k_{Os}	mm/s	mass transfer coefficient in the saliva phase in the oral cavity	10 ⁻³
k_{Fs}	mm/s	mass transfer coefficient in the saliva phase in the pharynx	10 ⁻³
k_{Om}	mm/s	mass transfer coefficient in the lubricated mucosa in the oral cavity	10 ⁻³
k_{Fm}	mm/s	mass transfer coefficient in the lubricated mucosa in the pharynx	10 ⁻³
k_{Nm}	mm/s	mass transfer coefficient in the lubricated mucosa in the nasal cavity	10 ⁻³
K_{Oas}		air/saliva partition coefficient in the oral cavity at 37°C	9.7 x 10 ⁻³ (2-nonanone)
K_{Osp}		saliva/product(rice) partition coefficient in the oral cavity at 37°C	0.245 (2-nonanone)
K_{Oam}		air/lubricated mucosa partition coefficient in the oral cavity	10 ⁻³

K_{Fas}		air/saliva partition coefficient in the pharynx	5×10^{-3}
K_{Fam}		air/lubricated mucosa partition coefficient in the pharynx	10^{-3}
K_{Nam}		air/lubricated mucosa partition coefficient in the nasal cavity	10^{-3}
C_{Op}	g/mm^3	aroma concentration in the product (rice) in the oral cavity	4.8×10^{-9} (2-nonanone)

Food manufacturers are interested in aroma release as it has been shown to be an important factor driving food acceptance (Ployon et al., 2017) and satiation (Ruijschop et al., 2009). Modelling can help to improve the understanding of the limiting mechanisms of aroma release by pointing out the most important parameters related to the product and to the individual. In this way, models can help to design food products that are targeted towards specific consumer groups such as the elderly, young children or people with specific disorders (Doyennette et al. 2014).

Fig. 9-1 shows the effects of some parameters related to the product and to the individual on the aroma release (concentration of aroma compound in the nasal cavity, C_{na}) which could be of interest to a food manufacturer and Table 9-4 shows the parameters varied in the simulation. It can be observed when the portion size increased (Fig. 9-1a), C_{na} increased. This is expected as the higher the portion size, the higher the volume of particles which will be broken into pasted particles during mastication. This is consistent with the main model assumption which assumes mass transfer of aroma compounds had only occurred from the paste to the saliva phase. Therefore, the higher the volume of particles that are pasted, the higher the C_{na} . The same trend can be observed when the initial particle size is varied (Fig. 9-1b). The larger the particle size, the higher the volume of a particle. Thus, the higher the volume of pasted particles will be formed, which results in a higher C_{na} . A higher C_{na} can also be observed when the initial aroma concentration is increased as to be expected (Fig. 9-1c).

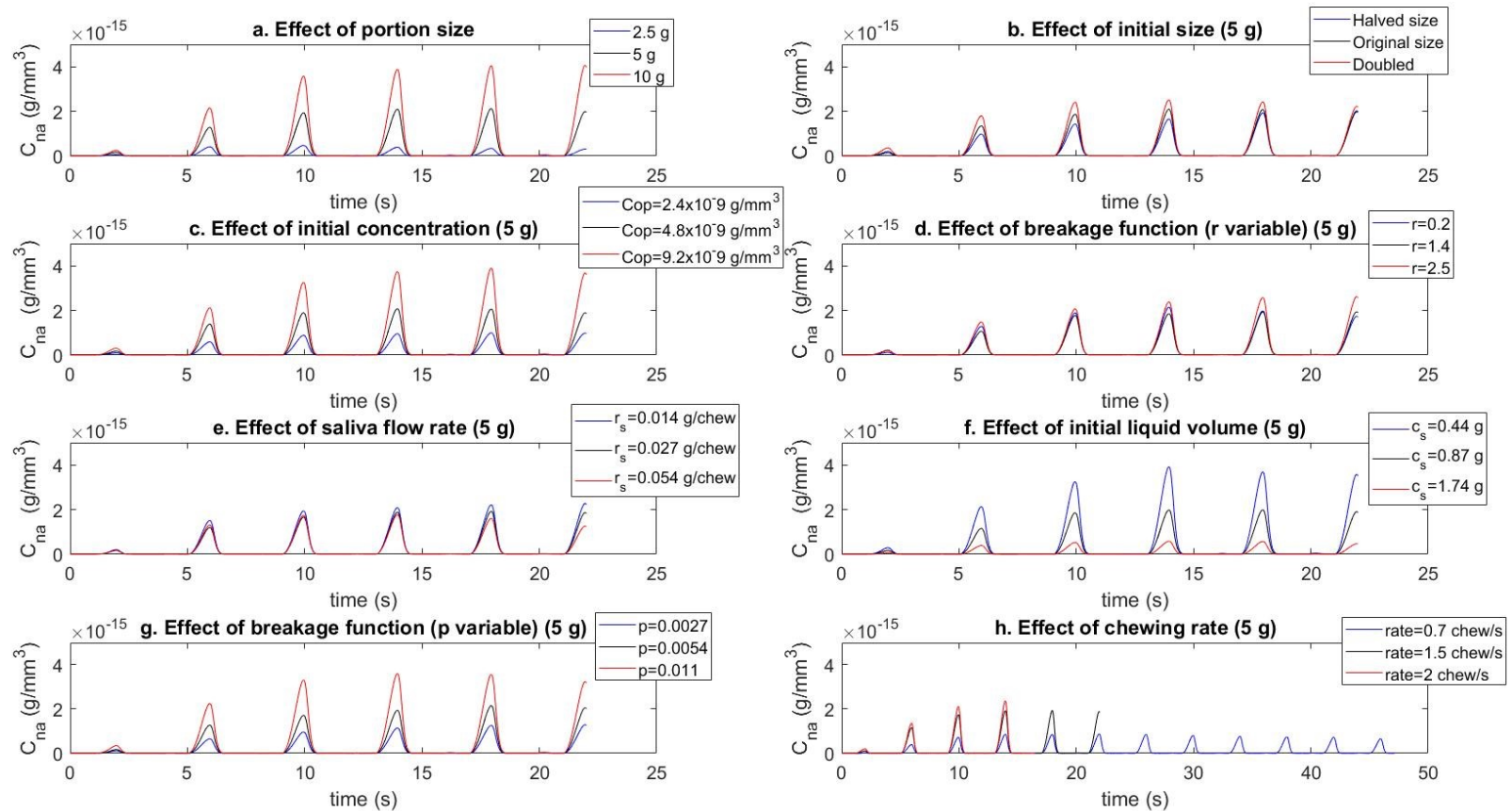


Fig. 9-1: Effect of parameters related to the product and individual which may be of interest to a food manufacturer. Using the physiological parameters of Subject A4, C_{na} of 2-nonanone was predicted. a. Aroma release (C_{na}) when portion size is varied (2.5 g, 5 g and 10 g of rice), b. Aroma release (C_{na}) when initial particle size is varied (halved, original and doubled size) for 5 g of rice c. Aroma release (C_{na}) when the initial concentration is varied for 5 g of rice, d. Aroma release (C_{na}) when the breakage function (represented by the fragmentation variable, r) is varied for 5 g of rice, e. Aroma release (C_{na}) when saliva flow rate is varied for 5 g of rice, f. Aroma release (C_{na}) when the initial liquid volume is varied for 5 g of rice, g. Aroma release (C_{na}) when the breakage function (represented by the pasted fraction, p) is varied for 5 g of rice, h. Aroma release (C_{na}) when the chewing rate (0.7 chew/s, 1.5 chew/s and 2 chew/s) is varied for 5 g of rice

Table 9-4 Product related and chewing parameters which may of interest to a food manufacturer

Parameters	Unit	Values simulated
Portion size	g	2.5, 5.0 and 10
Initial size	mm	½ original size, original size and 2x original size
Initial concentration	g/mm ³	2.4 x 10 ⁻⁹ , 4.8 x 10 ⁻⁹ and 9.2 x 10 ⁻⁹
Breakage function (degree of fragmentation)	-	0.2, 1.4 and 2.5
Breakage function (pasted fraction)		0.0027, 0.0054 and 0.011
Saliva flow rate (rate constant of saliva vs chew number)	g/chew	0.014, 0.027 and 0.054
Initial liquid volume (y- intercept of saliva vs chew number)	g	0.44, 0.87 and 1.74 g
Chewing rate	Chew/s	0.7 chew/s, 1.5 chew/s and 2 chew/s

The fragmentation variable, r was also varied to test the effect of the breakage function of foods on C_{na} . It can be observed from Fig. 9-1 d that the higher the r value, the higher the C_{na} . A higher r -value corresponds to a higher degree of fragmentation (faster breakdown) (Van der Glas et al., 1987). Therefore, a higher r value will produce a greater number of smaller daughter particles. It should be noted that in this model, when a particle is broken, some are produced into a number of larger daughter particles and some are pasted, which become part of the liquid bolus phase. The r value of the breakage function used in this model determines how much volume of the larger daughter particles will be produced whereas the pasted fraction, p determines how much are pasted. The bolus surface area is then calculated from the total surface area of the larger daughter particles. Therefore, with higher r value,

one may expect there will be more daughter particles being formed compared to a smaller r value. We will then have larger bolus surface area as there are more area of individual daughter particles. Therefore, the observation of a higher C_{na} when the food is highly fracturable (from higher r value) is expected.

As to be expected, the magnitude of C_{na} is also higher when p is larger, consistent with the main model assumption (Fig. 9-1 g). The higher the saliva flow rate (represented by the rate constant of the bolus saliva content data), the smaller the magnitude of C_{na} (Fig. 9-1 e), which is to be expected due to the renewal of fresh saliva present in the mouth and pharynx (Doyennette et al., 2014). The volume of saliva also determines the bolus saturation, which is a parameter required to calculate the bolus surface area. A higher salivary flow rate will result in the bolus reaching saturation faster, and therefore may decrease the surface area of the bolus. This results in a slower rate of transfer of aroma from the bolus to the air phase of the mouth, and hence explains the smaller C_{na} value. Thus, a food manufacturer may avoid the addition of additional chemical/components (such as citric acid) that may increase the saliva flow rate during mastication. The same trend can also be observed when the initial volume of liquid in the mouth is varied, where a higher initial liquid volume results in a smaller magnitude of C_{na} (Fig. 9-1 f). This example was used to demonstrate that when rice is served with liquid such as curries or soup which will reach bolus saturation immediately and will therefore have smaller bolus surface area. Finally, it is also interesting to test the effect of the chewing rate on C_{na} as it is dependent on the food structure (e.g. soft vs hard foods). Comparing the magnitude of C_{na} in the first 15 seconds in Fig. 9-1 h, chewing faster has a higher magnitude of aroma release as it takes a shorter time to swallow for the same initial mass of aroma compounds.

Besides the product, aroma release is also influenced by the physiological parameters of humans. This is a challenge for food technologists as humans show wide variation in these parameters and in the way they consume food (Taylor, 2002). Mathematical modelling can provide insights into understanding the role of individual physiological parameters as these parameters are defined in the model to predict aroma release. In this way, the model can be a tool to design food that can tailor to individual physiological characteristics.

9.3 Effect of physiological parameters on model predictions

Some of the physiological parameters that are used as the model inputs in Table 9-2 were manipulated to observe their effects on the aroma release predictions (Table 9-5). For clarity, only the impact of the most sensitive parameters on aroma release were shown in Fig. 9-2.

Table 9-5 Physiological values manipulated in the simulations.

Parameters	Unit	Values simulated
Breathing frequency	cycle/s	0.12, 0.25 and 0.32
Volume of oral cavity	mm ³	20000, 60000 and 100000
Volume of pharynx	mm ³	15000, 32000 and 60000
Volume of nasal cavity	mm ³	12000, 16000 and 40000
Thickness of oral mucosa	mm	5 x 10 ⁻³ , 5 x 10 ⁻² and 5 x 10 ⁻¹
Thickness of pharynx mucosa	mm	5 x 10 ⁻³ , 5 x 10 ⁻² and 5 x 10 ⁻¹
Thickness of nasal mucosa	mm	5 x 10 ⁻³ , 5 x 10 ⁻² and 5 x 10 ⁻¹
Tidal volume	mm ³	250000, 500000 and 1000000
Area of oral cavity	mm ²	5800, 11600 and 23200
Area of pharynx	mm ²	3250, 6500 and 13000
Air/mucosa contact area in nasal cavity (nose)	mm ²	7500, 16000 and 30000
Volume of saliva in pharynx	mm ³	100, 200 and 400

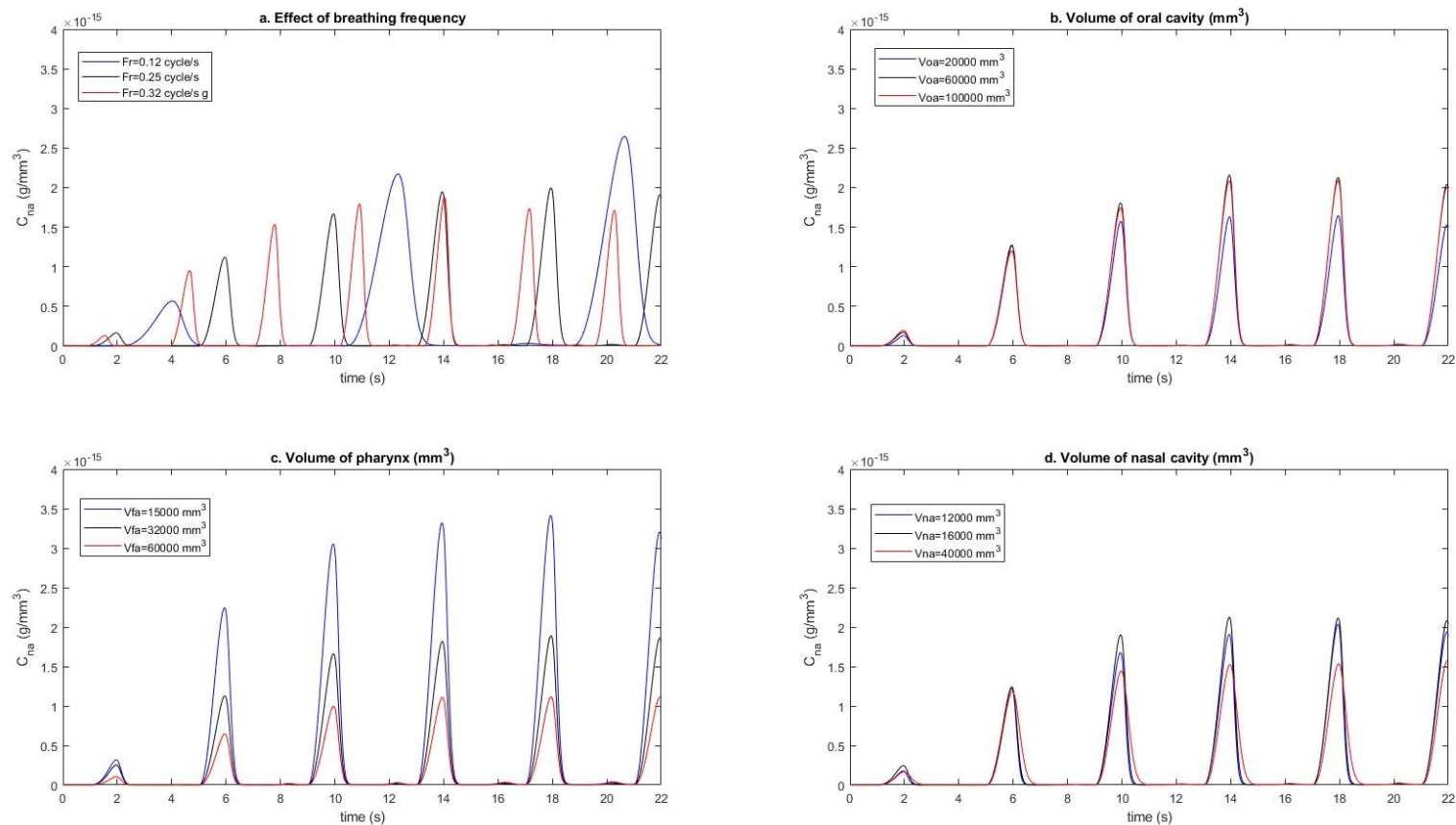


Fig. 9-2: Effect of physiological parameters on aroma release (C_{na}). Using the physiological parameters of Subject A4 as a reference value, C_{na} of 2-nonanone was predicted. a. Effect of breathing frequency on aroma release (C_{na}) (0.12 cycle/s, 0.25 cycle/s, 0.32 cycle/s), b. Effect of the oral cavity volume on aroma release (C_{na}) (20,000 mm³, 60,000 mm³, 100,000 mm³) c. Effect of the pharynx volume on aroma release (C_{na}) (15,000 mm³, 32,000 mm³, 60,000 mm³), d. Effect of the nasal cavity volume on aroma release (C_{na}) (12,000 mm³, 16,000 mm³, 40,000 mm³)

Aroma release was mostly impacted by the breathing frequency, the volume of pharynx, the volume of oral cavity and the volume of nasal cavity while the rest of the parameters seem to have a negligible effect. A higher breathing frequency reduces aroma concentration as it increases the removal of the aroma compound from the mouth. A higher aroma concentration is also observed with a larger oral cavity and it becomes more apparent towards the later stages of mastication. A larger volume of oral cavity indicates a larger volume of aroma-rich air in the oral cavity. Due to this, a higher concentration of aroma will be observed in the nasal cavity as it takes longer for the aroma-rich air in the oral cavity to be depleted during the course of breathing (for the same breath flow rate). The variation of the volume of pharynx gives a higher C_{na} when the volume is smaller. The same trend can be observed with the variation of the volume of nasal cavity. The effects can be explained from the combination of an aroma-rich air from the oral cavity/pharynx with aroma-free ambient air in the course of breathing. A lower pharynx/nasal cavity volume implies higher renewal rate; therefore it leads to a quicker increase and decrease of the aroma concentration (Trelea et al., 2007). The remaining physiological parameters seem to have a negligible effect on the simulated nasal aroma concentration. This indicates that the accurate knowledge of these parameters is not essential for running the model.

The substantial effects of some of the physiological parameters on the aroma concentration can provide knowledge to food manufacturers to design foods to a specific group of consumers. For example, race and gender are known to be the important factors affecting the oral and nasal structures (Xue & Hao, 2006). A study by Xue & Hao (2006) compared the vocal tract dimensions of 120 healthy adult subjects with equal numbers of men and women of three races (White American, African American and Chinese). The results showed that the men have a larger vocal tract dimensions (e.g. oral and pharynx volume) compared to women. Chinese people seem to have the largest oral and pharynx volume, followed by White American and African American. Thus, the physiological parameters of the subjects need to be considered by a food manufacturer in the food designing process. If a subject possesses a large oral volume, perhaps only a small initial concentration of aroma compound is required in the food to be able to perceive the 'right amount of flavor'.

Besides the physiological parameters, it is also known that other factors such as the nature of the food matrix and physicochemical factors can affect aroma release. It can be challenging to identify

the parameters that have the most effect on a subject through a series of lab experiments as these are time-consuming and expensive. Therefore, development of mechanistic models linking oral processing and aroma release provides tools to explore these interactions and can lead to the development of foods for sensorial and digestive outcomes.

9.4 Effect of physico-chemical parameters on model predictions

Physico-chemical factors such as partitioning, interfacial mass transport and diffusion are factors that can affect aroma release (Taylor, 2002). Food technologists are interested in this area as upon mastication, flavour components are released and the overall sensory appreciation is influenced by the way the components are distributed over the different phases (that make up the food microstructure) and the diffusion kinetics of flavor release and transport of the volatiles to the olfactory epithelium in the nasal cavity (Bruin, 1999). The manipulated parameters are shown in Table 9-6.

Table 9-6 Physicochemical parameters manipulated in the simulations.

Parameters	Unit	Values simulated
Saliva to rice partition coefficient	-	0.0245, 0.245 and 2.45
Air to saliva partition coefficient	-	9.7×10^{-4} , 9.7×10^{-3} and 9.7×10^{-2}
Air to oral mucosa partition coefficient	-	1×10^{-5} , 1×10^{-3} and 1×10^{-1}
Air to pharynx mucosa partition coefficient	-	1×10^{-5} , 1×10^{-3} and 1×10^{-1}
Air to nasal mucosa partition coefficient	-	1×10^{-5} , 1×10^{-3} and 1×10^{-1}
Air to saliva in pharynx partition coefficient	-	5×10^{-4} , 5×10^{-3} and 5×10^{-2}
Mass transfer coefficient in saliva in oral cavity	mm/s	10^{-5} , 10^{-3} and 10^{-1}

Mass transfer coefficient in saliva in pharynx	mm/s	10^{-5} , 10^{-3} and 10^{-1}
Mass transfer coefficient in oral mucosa in oral cavity	mm/s	10^{-5} , 10^{-3} and 10^{-1}
Mass transfer coefficient in mucosa of pharynx	mm/s	10^{-5} , 10^{-3} and 10^{-1}
Mass transfer coefficient in mucosa of nasal cavity	mm/s	10^{-5} , 10^{-3} and 10^{-1}

Almost all of the physico-chemical parameters have negligible effect on the simulated aroma concentration in the nasal cavity except the mass transfer coefficient for aroma transport from the saliva to air in the oral cavity (). This parameter was also pointed out to be one of the key factors governing the release of aroma compounds when a sensitivity analysis was carried out in the aroma release mechanistic model developed for cheese (Doyennette et al., 2014). The mass transfer coefficient could be influenced by the viscosity of the saliva and the stirring rate (tongue and cheek movements), both of which determine the thickness of the stagnant layer (Nahon et al., 2000). Increasing the viscosity of the surrounding fluid by addition of thickeners can therefore decrease the mass transfer coefficient and the rate of flavour release (Nahon et al., 2000). The rest of the physico-chemical parameters all seem to have a negligible effect on the aroma concentration, which indicate that their accurate knowledge is not essential to run the model. It is likewise intriguing to know the impacts of the partition coefficients of other aroma compounds on aroma release. Some compounds may have a higher affinity to water, therefore will not be released into the air phase as much.

Fig. 9-4 shows comparisons in the aroma release of three different aroma compounds with different partition coefficients. For example, ethyl butanoate which has a partition coefficient between the air and water phase of 1.83×10^2 (Le Thanh et al., 1993), shows the highest aroma release because of the higher affinity to the air phase. Ethyl butanoate has a fruity odour similar to pineapple and a key ingredient used as flavour enhancer in processed orange juices (Barba et al., 2018). In contrary,

Carvacrol, a spicy odour more attracted to water (partition coefficient of 5.95×10^{-5}) (Abdul Rahman, 2015) and had the lowest aroma release as expected. These predictions show higher concentrations would be seen for aroma compounds that partition more favourably in the air phase. However, this may not necessarily translate into greater perception of the flavours as that would depend on the mechanism of sensory receptors in the nasal cavity (Buettner & Schieberle, 2000).

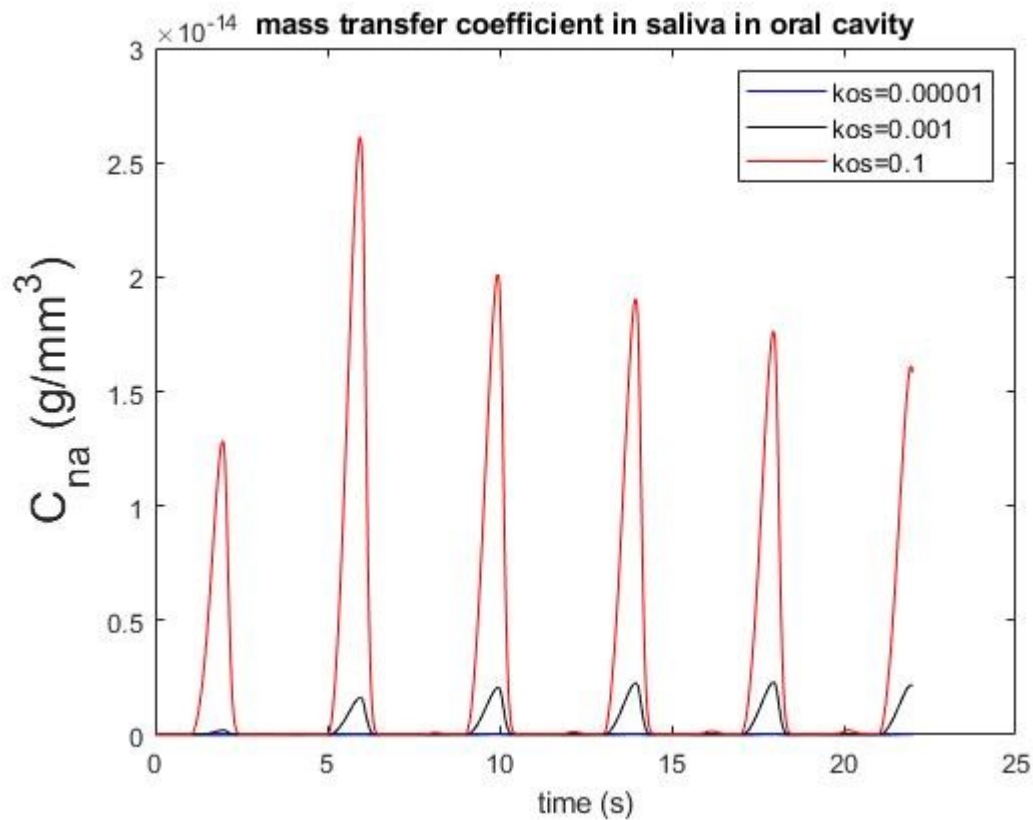


Fig. 9-3: Effect of mass transfer coefficient in saliva in oral cavity on aroma release (C_{na}) (0.00001 mm/s, 0.001 mm/s, 0.1 mm/s)

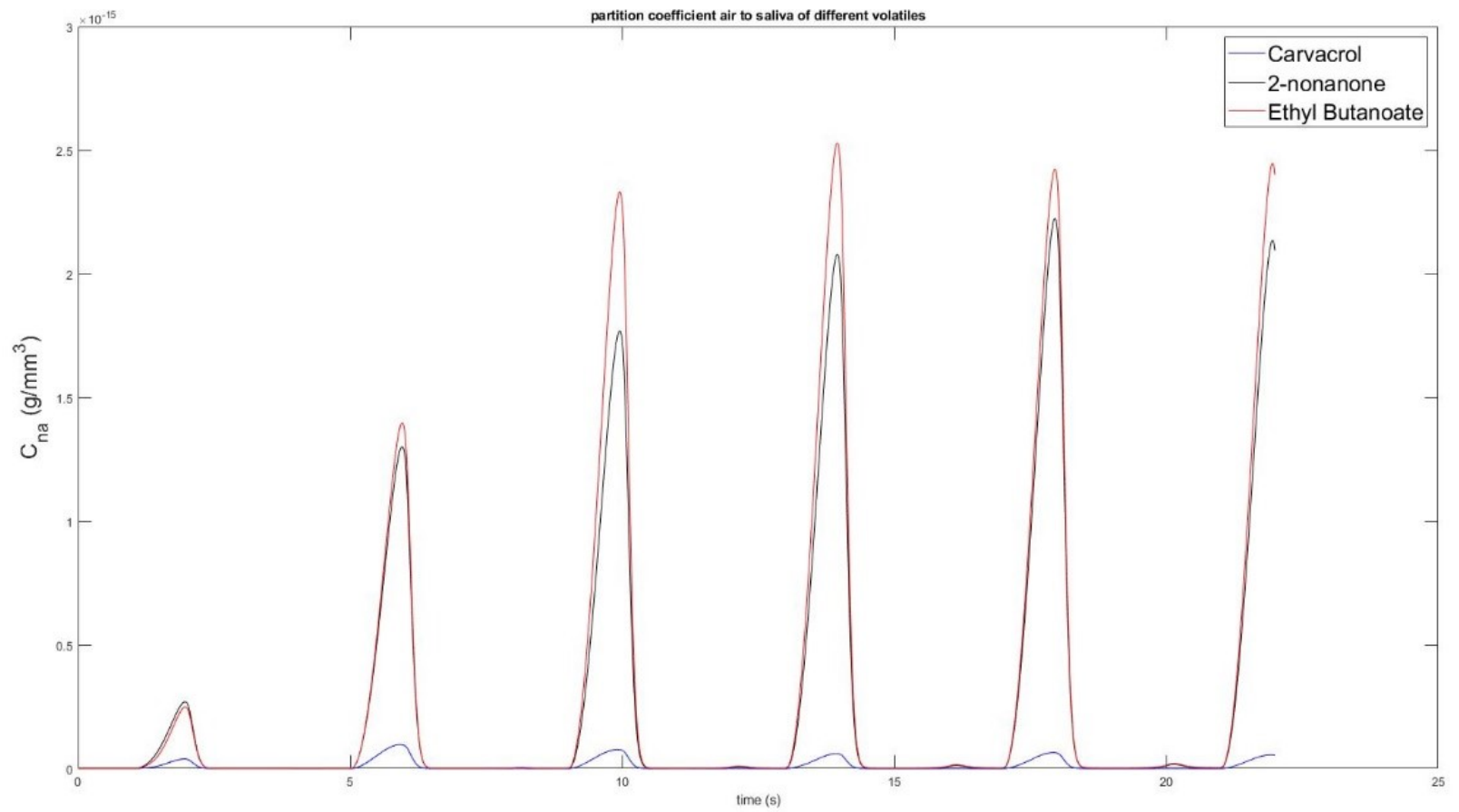


Fig. 9-4 Release of aroma compounds with different partition coefficients of air to saliva phase.

9.5 Chapter conclusion

The final chapter aimed to demonstrate the usage of the model to potentially provide insights for food technologists/manufacturers to design food. The first section summarises the list of parameters which are related to the product and individual which could provide clues for food manufacturers to design foods that could improve sensorial outcome. Factors that have the most impact on the aroma concentration include the portion size, initial concentration, initial liquid volume and the pasted fraction. Other than product related parameters, food technologists are also interested to understand the effects of individual physiological parameters so that food can be tailored to individual's specific needs. The model showed that the oral cavity volume, pharynx volume, nasal cavity volume and the breathing frequency were the factors that affect aroma concentration the most. Additionally, it was shown that the mass transfer coefficient of saliva has the most significant effect on the aroma release among all physico-chemical parameters. Depending upon the need, food technologists may add thickeners (to increase viscosity) or design foods that could influence the tongue and cheek movements in the mouth to influence the mass transfer coefficient. Finally, the effects of different aroma compounds of different partition coefficients were also investigated. As expected, the release of aroma compound which partition stronger into the air phase had the most elevated release compared to aroma compounds which had a higher affinity to water.

Conclusions and Recommendations for Future Work

Conclusions

Chewing is the first unit of the gastrointestinal tract but is often assumed less important as the total time spent chewing is relatively shorter compared to other digestive processes. However, studies have shown evidence that chewing has a huge impact on digestion and flavour release (Tarrega et al., 2008; Ranawana et al., 2010; Feron et al., 2014; Labouré et al., 2014; Ranawana et al., 2014). Despite these findings, due to the number of sub-processes occurring during chewing and their interactions, it can be difficult to explain experimental observations. Mathematical modelling can be a tool to explore these interactions and can lead to the development of foods to influence sensorial and digestive outcomes.

Chewing models have been developed in the literature to predict bolus PSD as a function of chewing number and have been adapted from selection and breakage functions applied in industrial comminution processes. In Chapter 3, selection and breakage models were used as a basis of the chewing model developed in this thesis. The chapter started with the development of a conceptual model and a discussion of assumptions to provide a comprehensive understanding of the underlying mechanisms and important processes involved to predict the bolus PSD during chewing. Examples were then provided to show how these models can be implemented using a discretised population model approach.

Chapter 4 and Chapter 5 aimed to test the implementation of the models developed in Chapter 3 on peanuts, which is a common food system used in the mastication literature. The input parameters of the models were determined using a powerful optimisation tool called the particle swarm optimization (PSO), which is useful when there are no obvious starting values and a large number of parameters are required. Because of the probabilistic nature of the selection models, it needs to be repeated for at least 50 times to obtain a reasonable consistency for model fitting.

In Chapter 4, the competitive selection models were combined to account for different stages of chewing, for instance, one-way selection model to describe the first few chews and two-way competition for the later stages of chewing, which have not been done in previous studies. However, because of the difference in the rate of bolus recovery between the model and experimental data, poor

fit was observed towards the late mastication stages. In addition, it was also found that when different breakage models were compared, all breakage models gave a good agreement with the experimental data. The advantage of using the most improved Austin (1971) breakage function were highlighted. Not only is the model mechanistic, but it also consists of only one parameter, therefore is highly portable (i.e. it can be easily reproduced in the future without the need to reuse modeler's software and calibration data).

The extension to the development of mechanistic models of chewing in the literature is whether they are useful to provide information for food design. This aspect is explored in Chapter 5 in two case studies. The first aimed to understand which of the competitive selection models were more appropriate when the portion size of peanuts was varied. The second aimed to interrogate the model parameters, which were optimised without bias, to see whether they self-adjusted to reflect the variation in the physical properties of the peanuts. Both the one-way and two-way competition models were shown to sufficiently described particle selection for both the 2 g and 4 g peanuts. A higher power function describing the affinity factor was observed for the 4 g peanuts when the one-way model was used. But no notable difference was observed when the two-way model was applied. This provides insight into the differences in particle selection when the food portion size is varied. The results of the second case study showed that the value of the degree of fragmentation of the breakage function varied according to the trend in moisture content as expected. The findings of the modelling study justify that the physical properties of the peanuts affect the breakage function.

The chewing model developed in Chapter 3 was shown to work and useful for peanuts through Chapter 4 and 5. This provided confidence for its application to a different food system which is known to have strong linkage with digestion and flavour release. Cooked white rice was chosen the bolus expectorated by each subject investigated in a preliminary experiment was consistent with the model assumptions described in Chapter 3. In addition, white rice is also aromatic, and the food bolus PSD and saliva content showed strong correlations with *in vitro* glucose release. These aspects made white rice a perfect food system to be studied in the subsequent chapters.

A series of experiments were conducted in Chapter 6 to understand the role of physiological and chewing parameters on aroma release of five subjects when chewing white rice. In addition, the data were also used as input parameters for the model and model validation. A conceptual model was developed to relate aroma release with an individual physiological and chewing variables. The conceptual findings were then compared against the experimental *in vivo* aroma release data of the subjects. Interestingly, the dynamic behaviour of aroma release for all subjects followed a similar trend with the breakdown pathways taken by each subject where subjects with smaller particle size in their bolus had higher aroma release. However, a conflicting result was also observed for subjects who had high salivary flow rate, where they possessed higher aroma release. Despite the interesting results, due to the small number of subjects in the study, it was challenging to identify which physiological and chewing effects that had the most dominant effect on aroma release. However, the study paved the first step in understanding the role of chewing on flavour release of solid starch rich food products.

The results obtained in Chapter 6 were used as basis for the model development relating chewing and physiological variables with aroma release. In Chapter 7, the model developed by Doyennette et al. (2014) was adapted to predict the aroma release of rice, where the models in Chapter 3 were incorporated to describe the chewing process. The added chewing model, how aroma compounds interact between phases (solid, saliva and air) and the type of food used (rice) were the novelties of the study. The main assumptions and equations required to predict aroma release were described in the chapter.

Chapter 8 described the validation of the models developed in Chapter 7. Two different approaches were used to validate the model. The first approach was when the PSD outputs required for the model were taken directly from the experimental data. This was done by fitting a linear model to the experimental particle size input parameters to calculate the total surface area of particles and the total volume of pasted particles which were needed for the model. The second approach obtained the PSD outputs from the chewing model developed in Chapter 3. Other input parameters required for the model such as the physiological and physicochemical parameters were measured experimentally and those that could not be measured were obtained from the literature.

Finally, Chapter 9 then demonstrated how the flavour release model, when coupled with a chewing model, can aid in the design of foods which meet the unique demands of consumers. The model application was showed using a validated coupled chewing-aroma release model from one of the subjects in Chapter 8. The product characteristics, the physiology of consumers and the flavour compound physico-chemical parameters can all influence flavour release. Among the product related parameters studied, it was shown that the portion size, initial concentration of aroma, initial liquid volume and the pasted fraction have the most impact on the aroma concentration. Physiologically, the model showed that the oral cavity volume, pharynx volume, nasal cavity volume and the breathing frequency were the variables that affect aroma concentration the most. The mass transfer coefficient of saliva has the most significant effect on the aroma release among all physico-chemical parameters studied in the model. The effects of the partition coefficient of different aroma compounds were also explored where aromas that had the highest affinity in air showed the highest aroma release. All in all, this thesis provides the first step upon the development of mechanistic models that can lead to the development of foods for sensorial and digestive outcomes.

Recommendations for Future Work

The following aspects need to be considered in future studies to improve the models developed in this study and to further strengthen the knowledge in understanding the role of chewing on digestion and aroma release.

The limitation of the chewing model developed in Chapter 3 is that it does not take into account for mass flow between the main bolus and buccal pouches (losses). The study from Flynn et al. (2011) showed that during mastication, a significant proportion of solids remained in the oral cavity after swallowing or expectoration. In addition, the particle size distribution of the expectorated boluses and the solids remaining in the mouth in her study were significantly different suggesting a recirculation of particles between the active bolus and residue compartments. It is recommended in further research to include a 'bolus loss' function in the model so the predictions can be more accurately compared to real-life particle size measurements. To do so, the mechanisms of losses and their dependence on particle size and saliva will need to be fully understood through a structured experimental investigation.

One of the main assumptions of the model is a constant breakage function, therefore the study was limited to foods that are around physiological temperature and resist moisture uptake by being high fat or already saturated in moisture. Therefore, this research can be expanded to foods that can change its breakage function during occlusion. For example, a dry and brittle food such as a rice cracker will fracture in the first few chewing cycles but loses its structural integrity relatively quickly as chewing progresses due to the increasing absorption of saliva. Studies as such can be useful to design foods that can meet demands of elderly consumers or dysphagia patients who need foods with a certain texture/consistency at a specific mastication stage or swallow point.

Another aspect which needs improvement is the simple method developed to obtain one of the selection model input parameters by measuring the occlusal area using a chewing gum. Although the method has the potential to reduce the number of time-intensive experiments, more investigations involving a larger number of subjects will be needed before conclusive evidence can be obtained. In addition, future research should also include subjects that chew both sides of the occlusal area as the study was only limited to subjects who had a preferred side (e.g. left or right). This is because it has been shown that chewing was more efficient on the side where there was a greater occlusal area (Wilding, 1993).

Another aspect that could be improved is the starting PSD used in the chewing simulations. In this thesis, the PSD after the 1st chew was used because the experimental data used to fit the model which was obtained from literature did not include details of the starting PSD. However, in Chapter 4, it was shown that the model predictions compared well with the data when an assumed uniform-sized initial PSD was used from the fits of the 1st chew PSD data. Nevertheless, using the original PSD as the starting PSD in the future will ensure more accurate model predictions.

Model fitting using the particle swarm optimization (PSO) algorithm is an efficient way to obtain input parameters of the selection and breakage model as it reduces the time required to perform experiments. In the current study, five to six input parameters of the selection and breakage models were solved by the PSO algorithm. It is recommended that to reduce the number of degrees of freedom for the optimization. The input parameter(s) of the breakage model should be evaluated as the experiments are relatively faster compared to the one-chew experiments to obtain the input parameters

of the competitive selection model. Indeed, the degree of freedom of the optimization was also constrained by an upper and lower-bound values obtained from a published study by (van der Glas et al., 2018). However, the upper and lower-bound values were based on the data of five subjects, therefore the fitted parameters may not accurately represent the input parameters for the subjects used in this thesis. In the future, although laborious and time-consuming, one-chew experiments which are conventionally done to evaluate selection model input parameters in the literature will need to be performed to the foods studied in this thesis to validate against the fitting method. Alternatively, if conducting one-chew experiments prove a challenge on real foods, then it should be done with an artificial test food that mimics the physical properties of the food (such as Optosil® as used in the literature) but to a larger number of subjects. This will allow the optimization to solve input parameters from a larger database, which may increase the accuracy of the solved parameters.

The weakness of the *in vivo* experiments conducted in this thesis to relate chewing and aroma release is that they were performed on a small number of subjects (n=5), therefore future experiments should be conducted in a larger number of subjects to provide a more convincing evidence. Furthermore, measurements performed on a larger number of subjects will enhance the model reliability and has the potential to allow the definition of classes of consumers, representative of a population using the model input parameters. For example, chewing motion (lateral, vertical) could be parameterized with the breakage function parameter ' r '. Selection behaviour could be trapped by the number of breakage sites (' k ' and ' m ' parameters) and affinity factors (' p ' and ' q ' parameters).

Future studies can also include other starch rich food products such as pasta or other rice types such as basmati. To date, previous studies linking oral processing and aroma release have mostly focused on bread (Jourdren et al., 2016; Jourdren et al., 2017a, 2017b; Pu et al., 2019). Additionally, the long sampling time of the instrument used in the study to measure aroma release (PTR-MS) made it difficult to compare against model predictions. Future studies of *in vivo* aroma release could be conducted in instruments with a short sampling time such as the Selected Ion Flow Tube Mass Spectrometry (SIFT-MS) developed by syft™ Technologies (<https://www.syft.com/high-selectivity-real-time/>). Furthermore, the input parameters used in the model describing aroma release can also be improved. Parameters such as the mass transfer coefficient, tidal volume and the breathing frequency

can be determined experimentally. For some foods (e.g. cheese), the partition coefficient and mass transfer coefficients of 2-nonanone and ethyl propanoate (which are the same aroma compounds studied in this thesis) are shown to depend on the bolus saliva content (Doyennette et al., 2011). It will be interesting to see the relationship between saliva and the partition and mass transfer coefficients when different food matrices are used (such as rice used in this study). Another aspect of the model that can be improved is in predicting the aroma release post-swallowing especially as it has been shown in the literature that some aroma compounds (e.g. 2-nonanone) tend to release more during post-swallowing especially for high-fat foods such as cheese products (Frank et al., 2012; Repoux et al., 2012; Feron et al., 2014; Labouré et al., 2014).

The current aroma release model assumes the pasted rice particles as the dominant mechanism in contributing the release of aroma to the liquid bolus phase in the mouth can also be improved. The model can include the changes in the surface area of the whole particle distribution where the predictions can be compared against the model simulations from the current assumption. In addition, in Chapter 10, it was also observed there were many parameters (product, physiological and physico-chemical) that have profound effects on aroma release. However, further *in vivo* experiments will be required to validate the observations from the model simulations.

This thesis demonstrated how a chewing model can be coupled successfully into a different model that describes aroma release. Besides aroma release, the chewing model can also be coupled to digestion models in the proximal regions of the stomach to further expand the work to relate chewing and digestion.

The models developed in this work provide a sound platform for these extensions discussed above. Future improvements will improve the utility of the models, but they can already provide useful functionality for food design. By working and applying these models with food product developers, the value of the modelling approach can be realised and clear priorities for which areas future model development should focus on will become apparent.

References

- Abdul Rahman, M. (2015). *Measurement of minimum inhibitory concentration (MIC) of individual and combinations of essential oil volatiles in food*. Massey University, New Zealand (Doctoral dissertation).
- Afoakwa, E. O., Paterson, A., Fowler, M., & Ryan, A. (2009). Matrix effects on flavour volatiles release in dark chocolates varying in particle size distribution and fat content using GC–mass spectrometry and GC–olfactometry. *Food Chemistry*, *113*(1), 208-215.
- Agrawal, K. R., Lucas, P. W., & Bruce, I. C. (2000). The effects of food fragmentation index on mandibular closing angle in human mastication. *Archives of Oral Biology*, *45*(7), 577-584.
- Almotairy, N., Kumar, A., & Grigoriadis, A. (2020). Effect of food hardness on chewing behavior in children. *Clinical oral investigations*, pp.1-14.
- Aps, J. K. M., & Martens, L. C. (2005). Review: The physiology of saliva and transfer of drugs into saliva. *Forensic Science International*, *150*(2), 119-131.
- Arvisenet, G., Billy, L., Poinot, P., Vigneau, E., Bertrand, D., & Prost, C. (2008). Effect of Apple Particle State on the Release of Volatile Compounds in a New Artificial Mouth Device. *Journal of Agricultural and Food Chemistry*, *56*(9), 3245-3253.
- Atlan, S., Trelea, I. C., Saint-Eve, A., Souchon, I., & Latrille, E. (2006). Processing gas chromatographic data and confidence interval calculation for partition coefficients determined by the phase ratio variation method. *Journal of Chromatography A*, *1110*(1-2), 146-155.
- Austin, L.G. (1971): A Review: Introduction to the Mathematical Description of Grinding as Rate Process, *Powder Technology*, *5*, 1-17.
- Austin, L. G., & Luckie, P. T. (1972). The estimation of non-normalized breakage distribution parameters from batch grinding tests. *Powder Technology*, *5*(5), 267-271.
- Avison, S., van Gruijthuisen, K., Pascu, M., Parker, A., & Bodnár, I. (2015). Novel Methodology for Measuring Temperature-Dependent Henry's Constants of Flavor Molecules. *Journal of agricultural and food chemistry*, *63*(28), 6313-6318.

- Barba, C., Beno, N., Guichard, E., & Thomas-Danguin, T. (2018). Selecting odorant compounds to enhance sweet flavor perception by gas chromatography/olfactometry-associated taste (GC/O-AT). *Food chemistry*, 257, 172-181.
- Berenbaum, R. (1961). Analysis of the shatter breakage of coal using a matrix method: *Jour. Inst. Fuel*, 34, 367-374.
- Blissett, A., Hort, J., Taylor, A.J. (2006) Influence of chewing and swallowing behavior on volatile release in two confectionery systems. *Journal of Texture Studies*, 37(5), 476-496.
- Boehm, M. W., Warren, F. J., Moore, J. E., Baier, S. K., Gidley, M. J., & Stokes, J. R. (2014). Influence of hydration and starch digestion on the transient rheology of an aqueous suspension of comminuted potato snack food. *Food & Function*, 5(11), 2775-2782.
- Bornhorst, G. M., & Singh, R. P. (2012). Bolus Formation and Disintegration during Digestion of Food Carbohydrates. *Comprehensive Reviews in Food Science and Food Safety*, 11(2), 101-118.
- Bornhorst, G. M., & Singh, R. P. (2013). Kinetics of in Vitro Bread Bolus Digestion with Varying Oral and Gastric Digestion Parameters. *Food Biophysics*, 8(1), 50-59.
- Bornhorst, G.M., Kostlan, K., Singh, R.P. (2013) Particle Size Distribution of Brown and White Rice during Gastric Digestion Measured by Image Analysis. *Journal of Food Science* 78(9), E1383-E1391.
- Bornhorst, G. M., Rutherford, S. M., Roman, M. J., Burri, B. J., Moughan, P. J., & Singh, R. P. (2014). Gastric pH distribution and mixing of soft and rigid food particles in the stomach using a dual-marker technique. *Food Biophysics*, 9(3), 292-300.
- Bornhorst, G. M., Hivert, H., & Singh, R. P. (2014). Rice bolus texture changes due to α -amylase. *LWT - Food Science and Technology*, 55(1), 27-33.
- Bornhorst, G. M. (2017). Gastric mixing during food digestion: Mechanisms and applications. *Annual review of food science and technology*, 8, 523-542.
- Borrirukwisitsak S, Keenan HE, Gauchotte-Lindsay C (2012) Effects of salinity, pH and temperature on the octanol-water partition coefficient of bisphenol A. *International Journal of Environmental Science and Development*, 3(5), 460.

- Broadbent, S., & Callcott, T. (1956). Coal breakage processes: II. A matrix representation of breakage. *J. Inst. Fuel*, 29(121), 524-528.
- Bruin, S. (1999). Phase equilibria for food product and process design Invited lecture, 8th International Conference on Properties and Phase Equilibria for Product and Process Design, April 26–May 1, 1998, Noordwijkerhout, The Netherlands.1. *Fluid Phase Equilibria*, 158-160, 657-671.
- Bryant, R. J., & McClung, A. M. (2011). Volatile profiles of aromatic and non-aromatic rice cultivars using SPME/GC–MS. *Food Chemistry*, 124(2), 501-513.
- Buettner, A., & Schieberle, P. (2000). Influence of mastication on the concentrations of aroma volatiles—some aspects of flavour release and flavour perception. *Food Chemistry*, 71(3), 347-354.
- Buettner, A., Beer, A., Hannig, C., Settles, M., Schieberle, P. (2002) Physiological and analytical studies on flavor perception dynamics as induced by the eating and swallowing process. *Food Quality and Preference*, 13(7), 497-504.
- Buettner, A. (2002). Influence of human saliva on odorant concentrations. 2. Aldehydes, alcohols, 3-alkyl-2-methoxypyrazines, methoxyphenols, and 3-hydroxy-4,5-dimethyl-2(5H)-furanone. *Journal of Agricultural and Food Chemistry*, 50(24), 7105-7110.
- Buttery, R. G., Ling, L. C., Juliano, B. O., & Turnbaugh, J. G. (1983). Cooked rice aroma and 2-acetyl-1-pyrroline. *Journal of Agricultural and Food Chemistry*, 31(4), 823-826.
- Butterworth, P. J., Warren, F. J., & Ellis, P. R. (2011). Human alpha-amylase and starch digestion: An interesting marriage. *Starch-Starke*, 63(7), 395-405.
- Buschang, P. H., Throckmorton, G. S., Travers, K. H., & Johnson, G. (1997). The effects of bolus size and chewing rate on masticatory performance with artificial test foods. *Journal of Oral Rehabilitation*, 24(7), 522-526.
- Carpenter, G. (2012). Role of Saliva in the Oral Processing of Food. In *Food Oral Processing: Fundamentals of Eating and Sensory Perception* (pp. 45-60).
- Carpenter, G. H. (2013). The secretion, components, and properties of saliva. *Annual Review of Food Science and Technology*, 4, 267-276.

- Cassady, B. A., Hollis, J. H., Fulford, A. D., Considine, R. V., & Mattes, R. D. (2009). Mastication of almonds: effects of lipid bioaccessibility, appetite, and hormone response. *The American Journal of Clinical Nutrition*, 89(3), 794-800.
- Chen, J. (2009). Food oral processing—A review. *Food Hydrocolloids*, 23(1), 1-25.
- Chen, S. Constrained Particle Swarm Optimization (2009-2018). MATLAB File Exchange. <https://www.mathworks.com/matlabcentral/fileexchange/25986>.
- Chen, J. (2015). Food oral processing: Mechanisms and implications of food oral destruction. *Trends in Food Science & Technology*, 45(2), 222-228.
- Cheong, Y. S., Reynolds, G. K., Salman, A. D., & Hounslow, M. J. (2004). Modelling fragment size distribution using two-parameter Weibull equation. *International Journal of Mineral Processing*, 74, S227-S237.
- Conde-Petit, B., Escher, F., Nuessli, J. (2006) Structural features of starch-flavor complexation in food model systems. *Trends in Food Science & Technology*, 17 (5), 227-235
- Déléris, I., Saint-Eve, A., Saglio, A., Souchon, I., Trelea, I.C. (2016) Insights in aroma compound retention by mucosa during consumption through mathematical modelling. *Journal of Food Engineering*, 190, 123-138.
- Desam, G. P., Li, J., Chen, G., Campanella, O., & Narsimhan, G. (2020). Swelling kinetics of rice and potato starch suspensions. *Journal of Food Process Engineering*, 43(4), e13353.
- Dias, L.G., Duarte, G.H.B., Mariutti, L.R.B., Bragagnolo, N. (2019) Aroma profile of rice varieties by a novel SPME method able to maximize 2-acetyl-1-pyrroline and minimize hexanal extraction. *Food Research International*, 123, 550-558.
- Doyennette, M., de Loubens, C., Deleris, I., Souchon, I., Trelea, I.C. (2011) Mechanisms explaining the role of viscosity and post-deglutitive pharyngeal residue on in vivo aroma release: A combined experimental and modeling study. *Food Chemistry*, 128 (2), 380-390.
- Doyennette, M., Deleris, I., Saint-Eve, A., Gasiglia, A., Souchon, I., Trelea, I.C. (2011) The dynamics of aroma compound transfer properties in cheeses during simulated eating conditions. *Food Research International*, 44 (10), 3174-3181.

- Doyennette, M., Déléris, I., Féron, G., Guichard, E., Souchon, I., & Trelea, I.C. (2014). Main individual and product characteristics influencing in-mouth flavour release during eating masticated food products with different textures: Mechanistic modelling and experimental validation. *Journal of Theoretical Biology*, 340, 209-221.
- Drago, S. R., Panouillé, M., Saint-Eve, A., Neyraud, E., Féron, G., & Souchon, I. (2011). Relationships between saliva and food bolus properties from model dairy products. *Food Hydrocolloids*, 25(4), 659-667.
- Drechsler, K. C., & Bornhorst, G. M. (2018). Modeling the softening of carbohydrate-based foods during simulated gastric digestion. *Journal of Food Engineering*, 222, 38-48.
- Dresselhuis, D. M., de Hoog, E. H. A., Cohen Stuart, M. A., Vingerhoeds, M. H., & van Aken, G. A. (2008). The occurrence of in-mouth coalescence of emulsion droplets in relation to perception of fat. *Food Hydrocolloids*, 22(6), 1170-1183.
- Ebbesen, S., Kiwitz, P., & Guzzella, L. (2012, 27-29 June 2012). A generic particle swarm optimization Matlab function. Paper presented at the 2012 American Control Conference (ACC).
- Engelen, L., de Wijk, R. A., Prinz, J. F., van der Bilt, A., & Bosman, F. (2003). The relation between saliva flow after different stimulations and the perception of flavor and texture attributes in custard desserts. *Physiology & Behavior*, 78(1), 165-169.
- Epstein, B. (1947). The mathematical description of certain breakage mechanisms leading to the logarithmico-normal distribution. *Journal of the Franklin Institute*, 244(6), 471-477.
- Ettre, L. S., Welter, C., & Kolb, B. (1993). Determination of gas-liquid partition coefficients by automatic equilibrium headspace-gas chromatography utilizing the phase ratio variation method. *Chromatographia*, 35(1), 73-84.
- Fenclová, D., Blahut, A., Vrbka, P., Dohnal, V., & Böhme, A. (2014). Temperature dependence of limiting activity coefficients, Henry's law constants, and related infinite dilution properties of C4–C6 isomeric n-alkyl ethanoates/ethyl n-alkanoates in water. Measurement, critical compilation, correlation, and recommended data. *Fluid Phase Equilibria*, 375, 347-359.

- Feron, G., Ayed, C., Qannari, E. M., Courcoux, P., Laboure, H., & Guichard, E. (2014). Understanding aroma release from model cheeses by a statistical multiblock approach on oral processing. *PLoS one*, 9(4), e93113.
- Flynn, C. S., Foster, K. D., Bronlund, J. E., Lentle, R. G., Jones, J. R., & Morgenstern, M. P. (2011). Identification of multiple compartments present during the mastication of solid food. *Archives of Oral Biology*, 56(4), 345-352.
- Flynn, C. S. (2012). *The particle size distribution of solid foods after human mastication*, Massey University, New Zealand (Doctoral dissertation).
- Forde, C., Leong, C., Chia-Ming, E., McCrickerd, K. (2017) Fast or slow-foods? Describing natural variations in oral processing characteristics across a wide range of Asian foods. *Food & function*, 8 (2), 595-606
- Foster, K. D., Woda, A., & Peyron, M. A. (2006). Effect of Texture of Plastic and Elastic Model Foods on the Parameters of Mastication. *Journal of Neurophysiology*, 95(6), 3469-3479.
- Foster, K. D., Grigor, J. M., Cheong, J. N., Yoo, M. J., Bronlund, J. E., & Morgenstern, M. P. (2011). The role of oral processing in dynamic sensory perception. *Journal of Food Science*, 76(2), R49-R61.
- Frank, O. (2005). Network sampling and model fitting. *Models and methods in social network analysis*, 31-56.
- Frank, D. C., Eyres, G. T., Piyasiri, U., & Delahunty, C. M. (2012). Effect of food matrix structure and composition on aroma release during oral processing using in vivo monitoring. *Flavour and Fragrance Journal*, 27(6), 433-444.
- Freitas, D., Le Feunteun, S., Panouille, M., & Souchon, I. (2018). The important role of salivary alpha-amylase in the gastric digestion of wheat bread starch. *Food & Function*, 9(1), 200-208.
- Froehlich, D. A., Pangborn, R. M., & Whitaker, J. R. (1987). The effect of oral stimulation on human parotid salivary flow rate and alpha-amylase secretion. *Physiology & Behavior*, 41(3), 209-217.
- Gao, J., Tan, E. Y. N., Low, S. H. L., Wang, Y., Ying, J., Dong, Z., & Zhou, W. (2020). From bolus to digesta: How structural disintegration affects starch hydrolysis during oral-gastro-intestinal digestion of bread. *Journal of Food Engineering*, pp. 110161.

- Gavião, M. B. D., Engelen, L., & Van Der Bilt, A. (2004). Chewing behavior and salivary secretion. *European Journal of Oral Sciences*, 112(1), 19-24.
- Gaudin, A.M. and Meloy, T.P. (1962). Model and a Comminution Distribution Equation for Single Fracture, *Trans AIME*, 223, 40-43.
- German, R. M. (2016). Sintering Trajectories: Description on How Density, Surface Area, and Grain Size Change. *JOM*, 68(3), 878-884.
- Gray-Stuart, E. M. (2016). *Modelling food breakdown and bolus formation during mastication*, Massey University, New Zealand (Doctoral dissertation).
- Gray-Stuart, E. M., Jones, J. R., & Bronlund, J. E. (2017). Defining the end-point of mastication: A conceptual model. *Journal of texture studies*, 48(5), 345-356.
- Grundy, M. M., Grassby, T., Mandalari, G., Waldron, K. W., Butterworth, P. J., Berry, S. E., & Ellis, P. R. (2014). Effect of mastication on lipid bioaccessibility of almonds in a randomized human study and its implications for digestion kinetics, metabolizable energy, and postprandial lipemia. *The American Journal of Clinical Nutrition*, 101(1), 25-33.
- Guichard, E., Repoux, M., Qannari, E., Labouré, H., Feron, G. (2017) Model cheese aroma perception is explained not only by in vivo aroma release but also by salivary composition and oral processing parameters. *Food & Function*, 8 (2):615-628
- Harris, C. C. (1968). The application of size distribution equations to multi-event comminution processes. *Trans SME/AIME*, 241, 343-58.
- Harrison, M., & Hills, B. P. (1996). A mathematical model to describe flavour release from gelatine gels. *International Journal of Food Science & Technology*, 31(2), 167-176.
- Harrison, M., Campbell, S., & Hills, B. P. (1998). Computer Simulation of Flavor Release from Solid Foods in the Mouth. *Journal of Agricultural and Food Chemistry*, 46(7), 2736-2743.
- Harrison, S. M., & Cleary, P. W. (2014). Towards modelling of fluid flow and food breakage by the teeth in the oral cavity using smoothed particle hydrodynamics (SPH). *European Food Research and Technology*, 238(2), 185-215.

- Harrison, S. M., Cleary, P. W., Eyres, G., Sinnott, M. D., & Lundin, L. (2014a). Challenges in computational modelling of food breakdown and flavour release. *Food & Function*, 5(11), 2792-2805.
- Harrison, S. M., Eyres, G., Cleary, P. W., Sinnott, M. D., Delahunty, C., & Lundin, L. (2014b). Computational modeling of food oral breakdown using smoothed particle hydrodynamics. *Journal of Texture Studies*, 45(2), 97-109.
- Hawkins, D. M. (2004). The problem of overfitting. *Journal of chemical information and computer sciences*, 44(1), 1-12.
- Heynderickx, P. M., Španěl, P., & Van Langenhove, H. (2014). Quantification of octanol–water partition coefficients of several aldehydes in a bubble column using selected ion flow tube mass spectrometry. *Fluid Phase Equilibria*, 367, 22-28.
- Hills, B. P., & Harrison M. (1995). Two-film theory of flavour release from solids. *International Journal of Food Science & Technology*, 30(4), 425-436.
- Hiiemae, K. (2004). Mechanisms of food reduction, transport and deglutition: How the texture of food affects feeding behaviour. *Journal of Texture Studies*, 35(2), 171-200.
- Hoebler, C., Karinthi, A., Devaux, M.-F., Guillon, F., Gallant, D. J. G., Bouchet, B., Barry, J.L. (1998). Physical and chemical transformations of cereal food during oral digestion in human subjects. *British Journal of Nutrition*, 80(05), 429-436.
- Hu EA, Pan A, Malik V, Sun Q (2012) White rice consumption and risk of type 2 diabetes: meta-analysis and systematic review. *BMJ*, 344, e1454.
- Hutchings, S. C. (2011). *Oral processing of heterogeneous foods*. Massey University, New Zealand (Doctoral dissertation).
- Hutchings, S. C., Foster, K. D., Bronlund, J. E., Lentle, R. G., Jones, J. R., & Morgenstern, M. P. (2012). Particle breakdown dynamics of heterogeneous foods during mastication: Peanuts embedded inside different food matrices. *Journal of Food Engineering*, 109(4), 736-744.
- Inoue, H., Ono, K., Masuda, W., Morimoto, Y., Tanaka, T., Yokota, M., & Inenaga, K. (2006). Gender difference in unstimulated whole saliva flow rate and salivary gland sizes. *Archives of Oral Biology*, 51(12), 1055-1060.

- Jalabert-Malbos, M. L., Mishellany-Dutour, A., Woda, A., & Peyron, M. A. (2007). Particle size distribution in the food bolus after mastication of natural foods. *Food quality and Preference*, 18(5), 803-812.
- Jourdren, S., Panouille, M., Saint-Eve, A., Deleris, I., Forest, D., Lejeune, P., Souchon, I. (2016) Breakdown pathways during oral processing of different breads: impact of crumb and crust structures. *Food & Function*, 7 (3):1446-1457
- Jourdren, S., Saint-Eve, A., Pollet, B., Panouillé, M., Lejeune, P., Guichard, E., Souchon, I. (2017). Gaining deeper insight into aroma perception: An integrative study of the oral processing of breads with different structures. *Food Research International*, 92, 119-127.
- Jourdren, S., Masson, M., Saint-Eve, A., Panouille, M., Blumenthal, D., Lejeune, P., Délérís, I., Souchon, I. (2017) Effect of bread crumb and crust structure on the in vivo release of volatiles and the dynamics of aroma perception. *Journal of Agricultural and Food Chemistry*, 65(16), 3330-3340
- Katyal, A., & Morrison, R. D. (2007). In B. L. Murphy & R. D. Morrison (Eds.), Introduction to Environmental Forensics (Second Edition) (pp. 513-575). *Burlington: Academic Press*.
- Kennedy, J., & Eberhart, R. (1942). Particle swarm optimization (PSO). *In Proceedings of the IEEE International Conference on Neural Networks*, Perth, Australia (Vol. 27).
- Kevin M., W., & Brian P., H. (2003). Modelling flavour release from a chewed bolus in the mouth: Part II. The release kinetics. *International Journal of Food Science and Technology*, 38, 361-368.
- Kim, E., Wilson, A., Motoi, L., Mishra, S., Monro, J., Parkar, S., Rosendale, D., Jobsis, C., Stoklosinski, H., Wadamori, Y., Hedderley, D., Morgenstern, M. 2020. Impact of chewing behaviour on carbohydrate digestion: 1. Using simulated gastrointestinal digestion and colonic fermentation models. *Food Research International*. Submitted
- Kohyama, K., Sakai, T., & Azuma, T. (2001). Patterns Observed in the First Chew of Foods with Various Textures. *Food Science and Technology Research*, 7(4), 290-296.
- Kohyama, K., Hatakeyama, E., Sasaki, T., Dan, H., Azuma, T., & Karita, K. (2004). Effects of sample hardness on human chewing force: a model study using silicone rubber. *Archives of Oral Biology*, 49(10), 805-816.

- Kohyama, K., Yamaguchi, M., Kobori, C., Nakayama, Y., Hayakawa, F., & Sasaki, T. (2005). Mastication Effort Estimated by Electromyography for Cooked Rice of Differing Water Content. *Bioscience, Biotechnology, and Biochemistry*, 69(9), 1669-1676.
- Kumar, D. S., Kumar, B. J., & Mahesh, H. M. (2018). Quantum nanostructures (QDs): an overview. In *Synthesis of Inorganic Nanomaterials* (pp. 59-88). Woodhead Publishing.
- Labouré, H., Repoux, M., Courcoux, P., Feron, G., Guichard, E. (2014) Inter-individual retronasal aroma release variability during cheese consumption: Role of food oral processing. *Food Research International*, 64, 692-700.
- Landa, J., Rich, A., Finkelman, M. (2010) Confirming Nasal Airway Dimensions Observed on Panoramic and Posterior-Anterior Cephalometric Radiographs Using An Acoustic Rhinometer. *European Archives of Paediatric Dentistry*, 11 (3), 115-121.
- Lani, M., Matsor, N., Nasution, Z., Ku, P., Yusof, A. (2015) Substitution Effects of Coconut Milk with Soymilk on Sensory Acceptance and Shelf Life of 'Nasi Lemak'. *British Journal of Applied Science & Technology*, 7 (4), 377.
- Le Bleis, F., Chaunier, L., Della Valle, G., Panouillé, M., Réguerre, AL. (2013) Physical assessment of bread destructure during chewing. *Food Research International*, 50 (1), 308-317.
- Lemmens, L., Van Buggenhout, S., Van Loey, A. M., & Hendrickx, M. E. (2010). Particle size reduction leading to cell wall rupture is more important for the β -carotene bioaccessibility of raw compared to thermally processed carrots. *Journal of Agricultural and Food Chemistry*, 58(24), 12769-12776.
- Le Révérend, B. J., Norton, I. T., & Bakalis, S. (2013). Modelling the human response to saltiness. *Food & Function*, 4(6), 880-888.
- Le Thanh, M., Voilley, A., & Phan Tan Luu, R. (1993). The influence of the composition of model liquid culture medium on vapor liquid partition coefficient of aroma substances. *Sciences des Aliments (France)*.
- Li-Hui, W., Chuan-Quan, L., Long, Y., Ru-Liu, L., Long-Hui, C., & Wei-Wen, C. (2016). Gender differences in the saliva of young healthy subjects before and after citric acid stimulation. *Clinica Chimica Acta*, 460, 142-145.

- Lii, C. Y., Tsai, M. L., & Tseng, K. H. (1996). Effect of amylose content on the rheological property of rice starch. *Cereal chemistry*, 73(4), 415-420.
- Lim, K. S., Ibrahim, Z., Buyamin, S., Ahmad, A., Naim, F., Ghazali, K. H., & Mokhtar, N. (2013). Improving vector evaluated particle swarm optimisation by incorporating nondominated solutions. *The Scientific World Journal*, 2013
- Lin, C. F., Hsieh, T. C. Y., & Hoff, B. J. (1990). Identification and Quantification of the “Popcorn”-like aroma in louisiana aromatic Delia rice (*Oryza sativa*, L.). *Journal of Food Science*, 55(5), 1466-1467.
- Lindinger, W., Hansel, A., & Jordan, A. (1998). On-line monitoring of volatile organic compounds at pptv levels by means of proton-transfer-reaction mass spectrometry (PTR-MS) medical applications, food control and environmental research. *International Journal of Mass Spectrometry and Ion Processes*, 173(3), 191-241.
- Liu, H., Wang, X., Chen, J., & der Glas, H. W. v. (2020). The Influence of Initial Breakage on Size Reduction during Habitual Chewing of a Solid Test Food. *Archives of Oral Biology*, 118, 104852.
- Liu, D. X., Ren, X., Asimi, S., Peng, J., & Zhang, M. (2020). Changes in oral processing parameters of three rice varieties. *Journal of Texture Studies*.
- Low, D. Y., D'Arcy, B., & Gidley, M. J. (2015). Mastication effects on carotenoid bioaccessibility from mango fruit tissue. *Food Research International*, 67, 238-246.
- Lucas, P. W., & Luke, D. A. (1983a). Computer simulation of the breakdown of carrot particles during human mastication. *Archives of Oral Biology*, 28(9), 821-826.
- Lucas, P. W., & Luke, D. A. (1983b). Methods for analysing the breakdown of food in human mastication. *Archives of Oral Biology*, 28(9), 813-819.
- Lucas, P. W., & Luke, D. A. (1984). Optimum mouthful for food comminution in human mastication. *Archives of Oral Biology*, 29(3), 205-210.
- Lucas, P. W., Prinz, J. F., Agrawal, K. R., & Bruce, I. C. (2002). Food physics and oral physiology. *Food Quality and Preference*, 13(4), 203-213.

- Malone, M. E., & Appelqvist, I. A. M. (2003). Gelled emulsion particles for the controlled release of lipophilic volatiles during eating. *Journal of Controlled Release*, *90*(2), 227-241.
- Mandalari, G., Parker, M. L., Grundy, M. M.-L., Grassby, T., Smeriglio, A., Bisignano, C., Wilde, P. J. (2018). Understanding the Effect of Particle Size and Processing on Almond Lipid Bioaccessibility through Microstructural Analysis: From Mastication to Faecal Collection. *Nutrients*, *10*(2), 213.
- Matsuo, K., Metani, H., Mays, K. A., & Palmer, J. B. (2010). Effects of respiration on soft palate movement in feeding. *Journal of Dental Research*, *89*(12), 1401-1406. 10.1177/0022034510377336
- Matsunaga, A., & Ziemann, P. J. (2010). Gas-wall partitioning of organic compounds in a Teflon film chamber and potential effects on reaction product and aerosol yield measurements. *Aerosol Science and Technology*, *44*(10), 881-892.
- Mayr, D., van Ruth, S. M., & Märk, T. D. (2003). Evaluation of the influence of mastication on temporal aroma release of ripe and unripe bananas, using a model mouth system and gas chromatography-olfactometry. *European Food Research and Technology*, *217*(4), 291-295.
- Mohan, V., Ruchi, V., Gayathri, R., Bai, M. R., Shobana, S., Anjana, R. M., & Sudha, V. (2017). Hurdles in brown rice consumption. In *Brown rice* (pp. 255-269). Springer, Cham.
- Molfenter, SM. (2016) The Reliability of Oral and Pharyngeal Dimensions Captured with Acoustic Pharyngometry. *Dysphagia*, *31*(4), 555-559.
- Moongngarm, A., Bronlund, J., Grigg, N., & Sriwai, N. (2012). Chewing behavior and Bolus Properties as Affected by Different Rice Types. *International Journal of Medical and Biological Sciences*, *6*.
- Mosca, A. C., & Chen, J. (2017). Food-saliva interactions: Mechanisms and implications. *Trends in Food Science & Technology*, *66*, 125-134.
- Motoi, L., Morgenstern, M. P., Hedderley, D. I., Wilson, A. J., & Balita, S. (2013). Bolus Moisture Content of Solid Foods during Mastication. *Journal of Texture Studies*, *44*(6), 468-479.

- Nahon, D. F., Harrison, M., & Roozen, J. P. (2000). Modeling flavor release from aqueous sucrose solutions, using mass transfer and partition coefficients. *Journal of Agricultural and Food Chemistry*, 48(4), 1278-1284.
- National Center for Biotechnology Information. PubChem Database. 2-Nonanone, CID=13187, <https://pubchem.ncbi.nlm.nih.gov/compound/2-Nonanone> (accessed on May 6, 2020)
- Ng, G. C. F., Gray-Stuart, E. M., Morgenstern, M. P., Jones, J. R., Grigg, N. P., & Bronlund, J. E. (2017). The slip extrusion test: a novel method to characterise bolus properties. *Journal of Texture Studies*, 48(4), 294-301
- Ng, G. C. F. (2018). *Novel methods to characterise texture changes during food breakdown*. Massey University, New Zealand (Doctoral dissertation).
- Nidhi, G., Ming Kai, C., Jingzhen, Y., Balasekaran, G., Michael, C., Robert, NG., Christopher, RE., Magdalena, Mo Ching M. (2010) Obesity prevention in Singapore: Collaborative efforts among government, health professionals and the community.
- Nishinari, K., Fang, Y., Rosenthal, A. (2019) Human oral processing and texture profile analysis parameters: Bridging the gap between the sensory evaluation and the instrumental measurements. *Journal of Texture Studies*.
- Norris, M. B., Noble, A. C., & Pangborn, R. M. (1984). Human saliva and taste responses to acids varying in anions, titratable acidity, and pH. *Physiology & Behavior*, 32(2), 237-244. [http://dx.doi.org/10.1016/0031-9384\(84\)90136-7](http://dx.doi.org/10.1016/0031-9384(84)90136-7)
- Panouillé, M., Saint-Eve, A., Déléris, I., Le Bleis, F., Souchon, I. (2014) Oral processing and bolus properties drive the dynamics of salty and texture perceptions of bread. *Food Research International* 62, 238-246.
- Paphangkorakit, J., Thothongkam, N., & Supanont, N. (2006). Chewing-side determination of three food textures. *Journal of oral rehabilitation*, 33(1), 2-7.
- Paravisini, L., Soldavini, A., Peterson, J., Simons, CT., Peterson, DG. (2019) Impact of bitter tastant sub-qualities on retronasal coffee aroma perception. *PloS one*, 14 (10):e0223280-e0223280.
- Pereira, L. J., de Wijk, R. A., Gavião, M. B. D., & van der Bilt, A. (2006). Effects of added fluids on the perception of solid food. *Physiology & Behavior*, 88(4), 538-544.

- Peyron, M. A., Mishellany, A., & Woda, A. (2004). Particle Size Distribution of Food Boluses after Mastication of Six Natural Foods. *Journal of Dental Research*, 83(7), 578-582.
- Pico, J., Khomenko, I., Capozzi, V., Navarini, L., Bernal, J., Gómez, M., Biasioli, F. (2018) Analysis of volatile organic compounds in crumb and crust of different baked and toasted gluten-free breads by direct PTR-ToF-MS and fast-GC-PTR-ToF-MS. *Journal of Mass Spectrometry*, 53(9):893-902.
- Pionnier, E., Chabanet, C., Mioche, L., Le Quéré, J.-L., & Salles, C. (2004). 1. In Vivo Aroma Release during Eating of a Model Cheese: Relationships with Oral Parameters. *Journal of Agricultural and Food Chemistry*, 52(3), 557-564.
- Ployon, S., Morzel, M., & Canon, F. (2017). The role of saliva in aroma release and perception. *Food Chemistry*, 226, 212-220.
- Prinz, J. F., & Lucas, P. W. (1997). An optimization model for mastication and swallowing in mammals. *Proceedings of the Royal Society B: Biological Sciences*, 264(1389), 1715-1721.
- Pu, D., Zhang, H., Zhang, Y., Sun, B., Ren, F., Chen, H., & He, J. (2019). Characterization of the aroma release and perception of white bread during oral processing by gas chromatography-ion mobility spectrometry and temporal dominance of sensations analysis. *Food Research International*, 123, 612-622.
- Rabe, S., Krings, U., & Berger, R. G. (2004). Dynamic flavour release from Miglyol/water emulsions: modelling and validation. *Food Chemistry*, 84(1), 117-125.
- Ranawana, V., Monro, J. A., Mishra, S., & Henry, C. J. K. (2010). Degree of particle size breakdown during mastication may be a possible cause of interindividual glycaemic variability. *Nutrition Research*, 30(4), 246-254.
- Ranawana, V., Leow, M. K., & Henry, C. J. (2014). Mastication effects on the glycaemic index: impact on variability and practical implications. *European Journal of Clinical Nutrition*, 68(1), 137-139.
- Rao, M. A., Okechukwu, P. E., Da Silva, P. M. S., & Oliveira, J. C. (1997). Rheological behavior of heated starch dispersions in excess water: role of starch granule. *Carbohydrate polymers*, 33(4), 273-283.

- Read, N. W., Welch, I. M., Austen, C. J., Barnish, C., Bartlett, C. E., Baxter, A. J., Worlding, J. (1986). Swallowing food without chewing; a simple way to reduce postprandial glycaemia. *British Journal of Nutrition*, 55(1), 43-47.
- Rémond, D., Machebeuf, M., Yven, C., Buffière, C., Mioche, L., Mosoni, L., & Mirand, P. P. (2007). Postprandial whole-body protein metabolism after a meat meal is influenced by chewing efficiency in elderly subjects. *The American Journal of Clinical Nutrition*, 85(5), 1286-1292.
- Repoux, M., Labouré, H., Courcoux, P., Andriot, I., Sémon, É., Yven, C., Guichard, E. (2012). Combined effect of cheese characteristics and food oral processing on in vivo aroma release. *Flavour and Fragrance Journal*, 27(6), 414-423.
- Rndirk. (2017). Dwekk time, Cycles in LC-MS/MS. Retrieved from https://www.chromforum.org/viewtopic.php?t=38691&fbclid=IwAR3Su7_z4tTEtTN79iie-uqm0_hAZEzJzDDWh3dLQ2OvjEvdqHRFNp09T4
- Rosenblum, J. L., Irwin, C. L., & Alpers, D. H. (1988). Starch and glucose oligosaccharides protect salivary-type amylase activity at acid pH. *American Journal of Physiology*, 254(5 Pt 1), G775-780.
- Routray, W., & Rayaguru, K. (2018). 2-Acetyl-1-pyrroline: A key aroma component of aromatic rice and other food products. *Food reviews international*, 34(6), 539-565.
- Rozenblat, Y., Grant, E., Levy, A., Kalman, H., & Tomas, J. (2012). Selection and breakage functions of particles under impact loads. *Chemical engineering science*, 71, 56-66.
- Ruijschop, R. M. A. J., Boelrijk, A. E. M., de Graaf, C., & Westerterp-Plantenga, M. S. (2009). Retronasal Aroma Release and Satiating: a Review. *Journal of Agricultural and Food Chemistry*, 57(21), 9888-9894.
- Ruijschop, R. M., Zijlstra, N., Boelrijk, A. E., Dijkstra, A., Burgering, M. J., de Graaf, C., & Westerterp-Plantenga, M. S. (2011). Effects of bite size and duration of oral processing on retro-nasal aroma release—features contributing to meal termination. *British Journal of Nutrition*, 105(2), 307-315.

- Saleh, A. S., Wang, P., Wang, N., Yang, L., & Xiao, Z. (2019). Brown rice versus white rice: Nutritional quality, potential health benefits, development of food products, and preservation technologies. *Comprehensive Reviews in Food Science and Food Safety*, 18(4), 1070-1096.
- Schuhmann Jr, R. (1940). Principles of comminution, I-size distribution and surface calculations. *Am. Inst. Min. Met. Eng., Tech. Pub.*, 1189, 1-11.
- Singh, H., & Gallier, S. (2014). In M. Boland, M. Golding, & H. Singh (Eds.), *Food Structures, Digestion and Health* (pp. 51-81). San Diego: Academic Press.
- Sumonsiri, P., et al. (2019). Assessment of the relationship between masticatory performance, occlusal contact area, chewing time and cycles, and gastric emptying scintigraphy in dentate subjects. *Journal of Oral Rehabilitation*, 46(9), 787-791.
- Svegmark, K., & Hermansson, A. M. (1991). Distribution of amylose and amylopectin in potato starch pastes: effects of heating and shearing. *Food Structure*, 10(2), 2.
- Tarrega, A., Yven, C., Sémon, E., Salles, C. (2008) Aroma release and chewing activity during eating different model cheeses. *International Dairy Journal*, 18(8), 849-857.
- Tavares, L. M. (2004). Optimum routes for particle breakage by impact. *Powder Technology*, 142(2-3), 81-91.
- Taylor, A. J. (2002). Release and Transport of Flavors In Vivo: Physicochemical, Physiological, and Perceptual Considerations. *Comprehensive Reviews in Food Science and Food Safety*, 1(2), 45-57.
- Trelea, I. C. (2003). The particle swarm optimization algorithm: convergence analysis and parameter selection. *Information Processing Letters*, 85(6), 317-325.
- Trelea, I.C., Atlan, S., Déléris, I., Saint-Eve, A., Marin, M., Souchon, I. (2007) Mechanistic mathematical model for in vivo aroma release during eating of semiliquid foods. *Chemical Senses*, 33 (2),181-192
- Treva, MD. (2018) Dying to Eat: Health, Heresy and Hysteria. *Cambridge Scholars Publishing*.
- Umachandran, K., Sawicka, B., Nasir, NA-N., Pasqualone, A. (2018) Nutritional features of Biryani as the basis for the formation of an entrepreneurial mode in Biryani Market.

- van der Bilt, A., Olthoff, L. W., van der Glas, H. W., van der Weelen, K., & Bosman, F. (1987). A mathematical description of the comminution of food during mastication in man. *Archives of Oral Biology*, 32(8), 579-586.
- van der Bilt, A., van der Glas, H. W., & Bosman, F. (1992). A Computer Simulation of the Influence of Selection and Breakage of Food on the Chewing Efficiency of Human Mastication. *Journal of Dental Research*, 71(3), 458-465.
- van der Bilt, A., van der Glas, H. W., Olthoff, L. W., & Bosman, F. (1991). The Effect of Particle Size Reduction on the Jaw Gape in Human Mastication. *Journal of Dental Research*, 70(5), 931–937.
- van der Bilt, A., Engelen, L., Pereira, L. J., van der Glas, H. W., & Abbink, J. H. (2006). Oral physiology and mastication. *Physiology & Behavior*, 89(1), 22-27.
- van der Glas, H. W., van der Bilt, A., Olthoff, L. W., & Bosman, F. (1987). Measurement of Selection Chances and Breakage Functions During Chewing in Man. *Journal of Dental Research*, 66(10), 1547-1550.
- van der Glas, H. W., van der Bilt, A., & Bosman, F. (1992). A selection model to estimate the interaction between food particles and the post-canine teeth in human mastication. *Journal of Theoretical Biology*, 155(1), 103-120.
- van der Glas, H. W., Kim, E. H. J., Mustapa, A. Z., & Elmanaseer, W. R. (2018). Selection in mixtures of food particles during oral processing in man. *Archives of Oral Biology*, 85, 212-225.
- van Ruth, S.M., Roozen, JP. (2000) Influence of mastication and saliva on aroma release in a model mouth system. *Food Chemistry*, 71 (3), 339-345.
- van Ruth, S.M., Grossmann, I., Geary, M., & Delahunty, C. M. (2001). Interactions between artificial saliva and 20 aroma compounds in water and oil model systems. *Journal of Agricultural and Food Chemistry*, 49(5), 2409-2413.
- van Ruth, S.M., King, C. (2003) Effect of starch and amylopectin concentrations on volatile flavour release from aqueous model food systems. *Flavour and Fragrance Journal*, 18 (5), 407-416
- Vogel, L., & Peukert, W. (2002). Characterisation of grinding-relevant particle properties by inverting a population balance model. *Particle & Particle Systems Characterization: Measurement and*

- Description of Particle Properties and Behavior in Powders and Other Disperse Systems*, 19(3), 149-157.
- Wang, S., Huang, W., Xiang, M.F. (2011) Effect of temperature on the partition coefficient of isoflurane and sevoflurane in perflurocarbon emulsion (Oxygent(TM)). *Nan Fang Yi Ke Da Xue Xue Bao*, 31 (10), 1718-1720
- Watanabe, S., & Dawes, C. (1988). The effects of different foods and concentrations of citric acid on the flow rate of whole saliva in man. *Archives of Oral Biology*, 33(1), 1-5.
- Victorin, L., & Lundberg, M. (1971). Cineradiographic studies of bolus position during chewing. *The Journal of Prosthetic Dentistry*, 26(3), 236-246.
- Wilding, R. J. C. (1993). The association between chewing efficiency and occlusal contact area in man. *Archives of oral biology*, 38(7), 589-596.
- Woolnough, J. W., Bird, A. R., Monro, J. A., & Brennan, C. S. (2010). The effect of a brief salivary alpha-amylase exposure during chewing on subsequent in vitro starch digestion curve profiles. *International Journal of Molecular Sciences*, 11(8), 2780-2790.
- Wei, X., Handoko, D.D., Pather, L., Methven, L., Elmore, J.S. (2017) Evaluation of 2-acetyl-1-pyrroline in foods, with an emphasis on rice flavour. *Food Chemistry*, 232, 531-544.
- Wright, K. M., Sprunt, J., Smith, A. C., & Hills, B. P. (2003). Modelling flavour release from a chewed bolus in the mouth: Part I. Mastication. *International Journal of Food Science & Technology*, 38(3), 351-360.
- Wright, K. M., & Hills, B. P. (2003). Modelling flavour release from a chewed bolus in the mouth: Part II. The release kinetics. *International Journal of Food Science & Technology*, 38(3), 361-368.
- Xue, S. A., & Hao, J. G. (2006). Normative Standards for Vocal Tract Dimensions by Race as Measured by Acoustic Pharyngometry. *Journal of Voice*, 20(3), 391-400.
- Xu, W., Kuhnert, L., Foster, K., Bronlund, J., Potgieter, J., & Diegel, O. (2007). Object-oriented knowledge representation and discovery of human chewing behaviours. *Engineering Applications of Artificial Intelligence*, 20(7), 1000-1012.

- Xu, W. L., Lewis, D., Bronlund, J. E., & Morgenstern, M. P. (2008). Mechanism, design and motion control of a linkage chewing device for food evaluation. *Mechanism and Machine Theory*, 43(3), 376-389.
- Yalkowsky, S.H., Dannenfelser, R.M.; The AQUASOL dATABASE of Aqueous Solubility. Fifth ed, Tucson,AZ: Univ Az, College of Pharmacy (1992)
- Yu, L., Witt, T., Bonilla, M.R., Turner, M., Fitzgerald, M., Stokes, J. (2019) New insights into cooked rice quality by measuring modulus, adhesion and cohesion at the level of an individual rice grain. *Journal of Food Engineering*, 240, 21-28
- Yurkstas, A. A. (1965). The masticatory act. *Journal of Prosthetic Dentistry* 15: 248-260
- Zhang, Y., Liu, T., Wang, X., Chen, J., & van der Glas, H. W. (2019). Locking up of food between posterior teeth and its influence on chewing efficiency. *Archives of Oral Biology*, 107, 104524.

Appendices

Appendix A: MATLAB codes used in the thesis

1. General MATLAB code used to apply the selection and breakage model developed in Chapter 3

```
%% Initial PSD
%Single chew data from Christine
thedata=load('Christineallchewsdata.mat'); %4g portion size
Dp=thedata.d_onechew;

%% Generate size classes
sieve=thedata.sieve;
sieve=sieve(1:8);
numclass=thedata.numclass;

%% Choose selection models
% Competition model Input parameters
k=54.85;
g=0.5358;
h=0.001055;
let=0.8277;

vanDerGlas=[k,g,h,let];

%Power law model Input parameters
v=0.1;
w=0.1;
lucas=[v,w];

% Selection function

% Model 1: Two-way competition model (k,g,h,let)
% Model 2: One-way competition model (k,g,h,let)
% Model 3: Power law model (v,w)
% Model 4: Single-sized model (k,g,h,let)

%Params=vanDerGlas (Van der glas models)
%Params=lucas (Lucas and luke models)

modelS=2;

ParamS=vanDerGlas;

chew=35;

%% Choose Breakage function
% model 1 is  $B=(1-p)*1-(1+r*xf).*(1-xf).^r$  where params=[r,p]
% model 2 is  $B=(1-p)*s*(1/xf).^r$  where params=[r,p,s] (Lucas & Luke, 1983)
% model 3 is  $B=(1-p)*1-s*(1-1/xf).^r$  where params=[r,p,s] (Lucas & Luke,
% 1983) %mechanistic
% model 4 is  $B=(1-\exp(1/xf)/(1-\exp(-1)))$  where params =p (B & C 1956)

modelB=1;
% r=0.8;
params=[r]; %fragmentation variable

Paste=0;
```

```

for countchewloop=1:chew

Vp=(1/2.03)*(2/3)*pi()*Dp.^3;

if modelS==1||2||4

%% Implement selection model
np=zeros(numclass,1);
    for i=1:numclass %
        np(i)=numel(find(Dp>sieve(i)));
    end
np(2:end)=np(2:end)-np(1:end-1);

S=selectionfuncs(sieve,np,modelS,ParamS);

Sizeclass=ones(size(Dp));

Sel=zeros(size(Dp));
    for i=1:numclass
        j=numclass+1-i; %9:1
        Sizeclass(Dp>=sieve(j))=j; %
        Sel(Dp>=sieve(j))=S(j);
    end
elseif modelS==3
S=selectionfuncs(Dp,[],modelS,ParamS);
Sel=S;
else
S=[];
end

% Applying the selection function to the Particle Size Distribution
RollDice=rand(size(Dp));%create random probability for every particle
IsSel=RollDice<=Sel;
SelDp=Dp(IsSel==1); %Selected diameter of particles
SelVp=Vp(IsSel==1); %Selected diameter of particles
UnSelDp=Dp(IsSel==0); %UnSelected diameter of particles
UnSelVp=(1/2.03)*(2/3)*pi()*UnSelDp.^3;%Unselectedvolumes
TotalV=sum(SelVp)+sum(UnSelVp); %check volume is conserved or not

%% Apply Breakage function

Daughters1=[];
Pastevol=[];

    for i=1:size(SelDp,1)
[Daughters NewPaste]=NewDaughters(SelDp(i),modelB,params,10);
Daughters1=[Daughters1,Daughters];
Pastevol=[Pastevol,NewPaste];
    end

Daughters1=sort(Daughters1');
daughters=(1/2.03)*(2/3)*pi()*Daughters1.^3;
Pasted_stuff=sum(Pastevol);

NewVp=sort([UnSelVp;daughters;]);

NewVp=NewVp(~isnan(NewVp));
NewVp=NewVp(NewVp~=0);
NewDp=((3.*NewVp*2.03)/(2.*pi)).^(1/3);

```

```

NewDp1=NewDp;

Cumulative=cumsum (NewVp./sum (sum (NewVp)+Pasted_stuff));

%% Parameters
% d90
n=0.9;
dist    = abs(Cumulative-n);
minDist = min(dist);
idx     = find(dist==minDist);
d90=NewDp1 (idx);
if isempty(d90)
    d90=sieve(end);
end

% d80
n1=0.8;
dist1   = abs(Cumulative-n1);
minDist1 = min(dist1);
idx1    = find(dist1==minDist1);
d80=NewDp1 (idx1);
if isempty(d80)
    d80=sieve(end);
end

% d75
n2=0.70;
dist2   = abs(Cumulative-n2);
minDist2 = min(dist2);
idx2    = find(dist2==minDist2);
d70=NewDp1 (idx2);

if isempty(d70)
    d70=sieve(end);
end

% d60
n3=0.6;
dist3   = abs(Cumulative-n3);
minDist3 = min(dist3);
idx3    = find(dist3==minDist3);
d60=NewDp1 (idx3);

if isempty(d60)
    d60=sieve(end);
end

% d50

n4=0.5;
dist4   = abs(Cumulative-n4);
minDist4 = min(dist4);
idx4    = find(dist4==minDist4);
d50=NewDp1 (idx4);
if isempty(d50)
    d50=sieve(end);
end

% d25

```

```

n5=0.4;
dist5 = abs(Cumulative-n5);
minDist5 = min(dist5);
idx5 = find(dist5==minDist5);
d40=NewDp1(idx5);
if isempty(d40)
    d40=sieve(end);
end
% d10
n6=0.3;
dist6 = abs(Cumulative-n6);
minDist6 = min(dist6);
idx6 = find(dist6==minDist6);
d30=NewDp1(idx6);
if isempty(d30)
    d30=sieve(end);
end

n7=0.2;
dist7 = abs(Cumulative-n7);
minDist7 = min(dist7);
idx7 = find(dist7==minDist7);
d20=NewDp1(idx7);
if isempty(d20)
    d20=sieve(end);
end

n8=0.1;
dist8 = abs(Cumulative-n8);
minDist8 = min(dist8);
idx8 = find(dist8==minDist8);
d10=NewDp1(idx8);

if isempty(d10)
    d10=sieve(end);
end

ParameterS=[d90;d80;d70;d60;d50;d40;d30;d20;d10];%Paste_fraction

Dp=NewDp;

DpRecord{countchewloop}=Dp;
Selected_record(countchewloop)=sum(SelVp);
Total_record(countchewloop)=sum(NewVp);
ParameterRecord{countchewloop}=ParameterS;
CumulativeRecord{countchewloop}=Cumulative;

end

Allparameters=[ParameterRecord{:,:}];

Model=[Allparameters(:,1),Allparameters(:,3),Allparameters(:,5),Allparameters(:,7),Allparameters(:,9),Allparameters(:,14),Allparameters(:,19),Allparameters(:,24),Allparameters(:,29),Allparameters(:,34)];

Model=transpose(Model);
end

```

2. Matlab script for the *randfixedsum* function used in Chapter 3

```
function [x,v] = randfixedsum(n,m,s,a,b)

% [x,v] = randfixedsum(n,m,s,a,b)
%
% This generates an n by m array x, each of whose m columns
% contains n random values lying in the interval [a,b], but
% subject to the condition that their sum be equal to s. The
% scalar value s must accordingly satisfy  $n*a \leq s \leq n*b$ . The
% distribution of values is uniform in the sense that it has the
% conditional probability distribution of a uniform distribution
% over the whole n-cube, given that the sum of the x's is s.
%
% The scalar v, if requested, returns with the total
% n-1 dimensional volume (content) of the subset satisfying
% this condition. Consequently if v, considered as a function
% of s and divided by  $\sqrt{n}$ , is integrated with respect to s
% from  $s = a$  to  $s = b$ , the result would necessarily be the
% n-dimensional volume of the whole cube, namely  $(b-a)^n$ .
%
% This algorithm does no "rejecting" on the sets of x's it
% obtains. It is designed to generate only those that satisfy all
% the above conditions and to do so with a uniform distribution.
% It accomplishes this by decomposing the space of all possible x
% sets (columns) into n-1 dimensional simplexes. (Line segments,
% triangles, and tetrahedra, are one-, two-, and three-dimensional
% examples of simplexes, respectively.) It makes use of three
% different sets of 'rand' variables, one to locate values
% uniformly within each type of simplex, another to randomly
% select representatives of each different type of simplex in
% proportion to their volume, and a third to perform random
% permutations to provide an even distribution of simplex choices
% among like types. For example, with n equal to 3 and s set at,
% say, 40% of the way from a towards b, there will be 2 different
% types of simplex, in this case triangles, each with its own
% area, and 6 different versions of each from permutations, for
% a total of 12 triangles, and these all fit together to form a
% particular planar non-regular hexagon in 3 dimensions, with v
% returned set equal to the hexagon's area.
%
% Roger Stafford - Jan. 19, 2006

% Check the arguments.
if (m~=round(m)) | (n~=round(n)) | (m<0) | (n<1)
    error('n must be a whole number and m a non-negative integer.')
elseif (s<n*a) | (s>n*b) | (a>=b)
    error('Inequalities  $n*a \leq s \leq n*b$  and  $a < b$  must hold.')
end

% Rescale to a unit cube:  $0 \leq x(i) \leq 1$ 
s = (s-n*a)/(b-a);

% Construct the transition probability table, t.
% t(i,j) will be utilized only in the region where  $j \leq i + 1$ .
k = max(min(floor(s),n-1),0); % Must have  $0 \leq k \leq n-1$ 
s = max(min(s,k+1),k); % Must have  $k \leq s \leq k+1$ 
s1 = s - [k:-1:k-n+1]; % s1 & s2 will never be negative
```

```

s2 = [k+n:-1:k+1] - s;
w = zeros(n,n+1); w(1,2) = realmax; % Scale for full 'double' range
t = zeros(n-1,n);
tiny = 2^(-1074); % The smallest positive matlab 'double' no.
for i = 2:n
    tmp1 = w(i-1,2:i+1).*s1(1:i)/i;
    tmp2 = w(i-1,1:i).*s2(n-i+1:n)/i;
    w(i,2:i+1) = tmp1 + tmp2;
    tmp3 = w(i,2:i+1) + tiny; % In case tmp1 & tmp2 are both 0,
    tmp4 = (s2(n-i+1:n) > s1(1:i)); % then t is 0 on left & 1 on right
    t(i-1,1:i) = (tmp2./tmp3).*tmp4 + (1-tmp1./tmp3).*(~tmp4);
end

% Derive the polytope volume v from the appropriate
% element in the bottom row of w.
v = n^(3/2)*(w(n,k+2)/realmax)*(b-a)^(n-1);

% Now compute the matrix x.
x = zeros(n,m);
if m == 0, return, end % If m is zero, quit with x = []

        rt = rand(n-1,m); % For random selection of simplex type

rs = rand(n-1,m); % For random location within a simplex

s = repmat(s,1,m);
j = repmat(k+1,1,m); % For indexing in the t table
sm = zeros(1,m); pr = ones(1,m); % Start with sum zero & product 1
for i = n-1:-1:1 % Work backwards in the t table
    e = (rt(n-i,:) <= t(i,j)); % Use rt to choose a transition
    sx = rs(n-i,:).^ (1/i); % Use rs to compute next simplex coord.
    sm = sm + (1-sx).*pr.*s/(i+1); % Update sum
    pr = sx.*pr; % Update product
    x(n-i,:) = sm + pr.*e; % Calculate x using simplex coords.
    s = s - e; j = j - e; % Transition adjustment
end
x(n,:) = sm + pr.*s; % Compute the last x

% Randomly permute the order in the columns of x and rescale.

rp = rand(n,m); % Use rp to carry out a matrix 'randperm'

[ig,p] = sort(rp); % The values placed in ig are ignored
x = (b-a)*x(p+repmat([0:n*n*(m-1)],n,1))+a; % Permute & rescale x

return

```

3. *Matlab script for the second numerical approach to address the conservation of volume developed in Chapter 3.*

```
function [Daughters NewPaste]=NewDaughters(Dp,model,Params)

Vp=4/3*pi().*(Dp/2).^3;
Pasted=0;
j=1;
vTot=0;
miss=0;

for i=1:1000
    if (Vp-Pasted-vTot)<(4/3*pi().*(0.354/2)^3) %if particle is a pasted
particle, it doesnt need breakage
        Pasted=Pasted+(Vp-Pasted-vTot);
        i=1001; % stop the loop as it doesnt need breakage
    end

    d=ItBreak(rand(),model,Params)*Dp;
    vP=4/3*pi().*(d/2)^3;

    if d<0.354
        Pasted=Pasted+vP;

    elseif vP>(Vp-Pasted-vTot)
        miss=miss+1;
    else
        dP(j)=d;
        vTot=vTot+vP;
        j=j+1;
    end

    if (vTot+Pasted)>=Vp
        i=1001;
    end

end

NewPaste=Pasted;

if ~exist('dP','var')
    Daughters=[];
else
    Daughters=dP;
end
end
```

```

function xf=ItBreak(B,model,params)

xfin=[0:0.01:1];
Bin=BreakIt(xfin,model,params);
Bin(isinf(Bin)|isnan(Bin)) = 0;
xf=interp1(Bin,xfin,B);

function B=BreakIt(xf,model,params)
%% Breakage function
% returns cumulative breakage function for input xf = x/xo
% model 1 is B=1-(1+r*xf).*(1-xf).^r where params=r
% model 2 is B=(1-exp(xf)/(1-exp(-1))) where params=[]
if model==1
    r=params(1);
    B=1-(1+r*xf).*(1-xf).^r;
elseif model==2
    B=(1-exp(-xf))/(1-exp(-1));
elseif model==3
    r=params(1);
    b=params(2);
    B=b.*(xf).^r;
elseif model==4
    r=params(1);
    b=params(2);
    B=1-b.*((1-(xf)).^r);
else
    B=0;
end
end

```

4. Matlab script to generate discrete number of particles from sieve data in Chapter 4

```

%% Data
%Mass fraction for the 1st chew
christine=load('differentchewsfinal.mat');

noofchews=11;

numclass=8;
sieve=christine.all(1,:);

i=1:length(sieve);
j=length(sieve):-1:1;

%Reorder sieve from largest to smallest
sieve(i)=sieve(j);

%Mass in each size class
real_mass=[3.36;3.13;2.7;2.3;1.95;1.7;1.46;1.67;1.15;1.27;0.9];

mass_inclass=christine.all(2:end,:).*real_mass;

%Convert to volume
density=1.12/1000; %(g/mm3)

%volume on sieves
Pvols=mass_inclass./density;

```



```

Pvols(:,i)=Pvols(:,j);

sized=[4,2.800000000000000,2,1.400000000000000,1,0.710000000000000,0.50000000
0000000,0.355000000000000];

Pvols=Pvols(:,1:8);

%Min volumeMinVols
MinVols=(1/2.03)*(2/3*pi()*sieve(1:8).^3);

%Adjust
for i=1:size(Pvols,1)%Number of rows
    for j=1:(size(Pvols,2)-1) %Numberofcolumns

        if Pvols(i,j)==0

            elseif Pvols(i,j)< MinVols(:,j)

                a=Pvols(i,j);
                b=Pvols(i,j+1);
                Pvols(i,j+1)=a+b;
                Pvols(i,j)=0;

            end

        end

    end

end

%% Generate particles
%Volume of a halved peanut particle
sieve_top=sieve(1)*(2.^(1/2));
Volume=(1/2.03)*(2/3)*pi()*sieve_top.^3;

%All particles
all_P=cell(noofchews,numclass);

Numberofparticlesrequired=zeros(size(Pvols,1),numclass);

for ii=1:size(Pvols,1) %Number of rows

    Average=zeros(1,numclass);
    % Average(1,numclass+1)=mean(Pasteparticles);

        for i=2:numclass
            Average(1,i)=(MinVols(i)*MinVols(i-1))^(1/2);
        end

        Average(1,1)=(Volume*MinVols(1))^(1/2);

        Average = repmat(Average,size(Pvols,1),1);

        for j=1:numclass

Numberofparticlesrequired(ii,j)=Pvols(ii,j)./Average(ii,j);

        end

```

```

end

Numberofparticlesrequired(Numberofparticlesrequired==0) = NaN;
Number=round(Numberofparticlesrequired);

Number(isnan(Number)) = 0;
Number=abs(Number);
daughters=cell(size(Pvols,1),numclass);

for j=1:size(Pvols,1)

    for i=1:numclass

        if Pvols(j,i)==0

            daughters{j,i}=0;
        elseif Number(j,i)==0
            daughters{j,i}=0;
        elseif i==1
            daughters{j,i} =
randfixedsum(Number(j,i),1,Pvols(j,i),MinVols(i),Volume);
        else
            daughters{j,i} =
randfixedsum(Number(j,i),1,Pvols(j,i),MinVols(i),MinVols(i-1));
        end
    end
end

end

%Volume of particles
daughter_onechew=sort(cat(1,daughters{1,:}));
s_1=sum(daughter_onechew);

daughter_twochew=sort(cat(1,daughters{2,:}));
daughter_fourchew=sort(cat(1,daughters{3,:}));
daughter_sixchew=sort(cat(1,daughters{4,:}));
daughter_eightchew=sort(cat(1,daughters{5,:}));
daughter_tenchew=sort(cat(1,daughters{6,:}));
daughter_fifteenchew=sort(cat(1,daughters{7,:}));
daughter_twentychew=sort(cat(1,daughters{8,:}));
daughter_twentyfivechew=sort(cat(1,daughters{9,:}));
daughter_thirtychew=sort(cat(1,daughters{10,:}));
daughter_thirtyfivechew=sort(cat(1,daughters{11,:}));

%Diameter of particles
d_onechew=((3.*daughter_onechew(1:end)*2.03)/(2.*pi()).^(1/3);
d_twochew=((3.*daughter_twochew(1:end)*2.03)/(2.*pi()).^(1/3);
d_fourchew=((3.*daughter_fourchew(1:end)*2.03)/(2.*pi()).^(1/3);
d_sixchew=((3.*daughter_sixchew(1:end)*2.03)/(2.*pi()).^(1/3);
d_eightchew=((3.*daughter_eightchew(1:end)*2.03)/(2.*pi()).^(1/3);
d_tenchew=((3.*daughter_tenchew(1:end)*2.03)/(2.*pi()).^(1/3);
d_fifteenchew=((3.*daughter_fifteenchew(1:end)*2.03)/(2.*pi()).^(1/3);
d_twentychew=((3.*daughter_twentychew(1:end)*2.03)/(2.*pi()).^(1/3);

```

```

d_twentyfivechew=((3.*daughter_twentyfivechew(1:end)*2.03)/(2.*pi()).^(1/3
));
d_thirtychew=((3.*daughter_thirtychew(1:end)*2.03)/(2.*pi()).^(1/3);

d_thirtyfivechew=((3.*daughter_thirtyfivechew(1:end)*2.03)/(2.*pi()).^(1/3
));

% check volume conserved
sumPvols=sum(Pvols,2);

%Volume fraction
volfrac_onechew=cumsum(daughter_onechew./sumPvols(1));
volfrac_twochew=cumsum(daughter_twochew./sumPvols(2));
volfrac_fourchew=cumsum(daughter_fourchew./sumPvols(3));
volfrac_sixchew=cumsum(daughter_sixchew./sumPvols(4));
volfrac_eightchew=cumsum(daughter_eightchew./sumPvols(5));
volfrac_tenchew=cumsum(daughter_tenchew./sumPvols(6));
volfrac_fifteenchew=cumsum(daughter_fifteenchew./sumPvols(7));
volfrac_twentychew=cumsum(daughter_twentychew./sumPvols(8));
volfrac_twentyfivechew=cumsum(daughter_twentyfivechew./sumPvols(9));
volfrac_thirtychew=cumsum(daughter_thirtychew./sumPvols(10));
volfrac_thirtyfivechew=cumsum(daughter_thirtyfivechew./sumPvols(11));

```

5. Matlab script to generate discrete number of particles from sieve data of different portion size in Chapter 5

```

%% Data
%Convert mass distribution to volume distribution

christine=load('differentchewsfinal.mat');

sieve=christine.all(1,:);
sieve=[0,sieve];
sieve(end)=5.7;

real_mass=[3.36;3.13;2.7;2.3;1.95;1.7;1.46;1.67;1.15;1.27;0.9];

mass_inclass=christine.all(2:end,:).*real_mass;

Paste_mass=[0.0112;0.02;0.06;0.08;0.145;0.19;0.27;0.39;0.25;0.33;0.20];

Exp_mass=real_mass+Paste_mass;

ratios=4./Exp_mass;

All_mass=[Paste_mass,mass_inclass];
Mass_frac=All_mass./Exp_mass;

%single chew
cum_singlechew=cumsum(Mass_frac(1,:));
cum_singlechew1=cum_singlechew;

%15 chews
cum_fifteenchew=cumsum(Mass_frac(7,:));

%30 chews

```

```

cum_thirtychew=cumsum(Mass_frac(10,:));

%Convert to volume
density=1.12/1000; %(g/mm3)

j=1;
Mp=Exp_mass(1); %portion size
mTot=0;
miss=0;

for i=1:1000

[cum_singlechew, index] = unique(cum_singlechew);
dparticle = interp1(cum_singlechew, sieve(index), rand());

vP=(1/2.03)*(2/3)*pi().*dparticle.^3;
mP=vP*density;
if mP>(Mp-mTot)
    miss=miss+1;
else
    dP(j)=dparticle;
    mTot=mTot+mP;
    j=j+1;
end

if mTot>=Mp
    i=1001;
end

end

Newdist=dP;
NewvP=(1/2.03)*(2/3)*pi().*Newdist.^3;
NewmP=sort(NewvP*density);
Newcum=cumsum(NewmP./nansum(NewmP));

```

6. *MATLAB script to convert sieve data of different peanuts moisture content in Chapter 5.*

Score matrix spreadsheet.

```

data=[0 0
      0.47 0
      0.5 4.1
      0.72 20.9
      1.01 38.98
      1.43 58.59
      2.02 75.93
      2.85 88.18
      4.03 97.14
      5.7 100.0];
data(:,2)=data(:,2)./100;

```

Note the added the first two lines.

- Line 1 is the 0,0

- Line 2 is where the data would cross the x-axis. This is crucial as below they will be interpolated linear between these two points and then using a curved interpolation between the other points.

Now create a series and interpolate values for Fs from them

The nomenclature

- F = cumulative
- f = probability density function
- subscripts (s=surface area, v=volume, n=number)

```
d=[0:0.05:6]';
i=find(d>=data(2,1),1);
Fs=zeros(size(d));
Fs(1:i)= interp1(data(:,1),data(:,2),d(1:i), 'linear');
Fs(i:end)= interp1(data(:,1),data(:,2),d(i:end), 'pchip');
```

Plot this as a graph

```
F=figure;
plot(d,Fs, ':')
hold on
plot(data(:,1),data(:,2), 'ob')
xlabel('diameter (mm)')
ylabel('F')
legend('data', 'interpolated')
```

Find the derivative as $f_s = d/dx(F_s)$

```
fs=gradient(Fs,d);
fs=fs/sum(fs);
% normalise so area under curve = 1
f=figure;
plot(d,fs)
xlabel('diameter (mm)')
ylabel('f')
```

convert to volume fraction as probability distribution function

```
fv=d.*fs;
fv=fv/sum(fv);
% normalise so area under curve = 1
hold on
plot(d,fv)
legend('fs', 'fv')
```

convert to cumulative volume distribution function

```
Fv=cumsum(fv);
figure(F);
plot(d,Fv, 'r')
legend('Fs', 'Fs data', 'Fv')
```

convert area to number probability distribution function just in case it is needed

```
fn=fs./d;  
fn(1)=0;  
fn=fn/sum(fn);  
figure(f)  
plot(d,fn,'g')  
legend('fs','fv','fn')
```

convert to number cumulative distribution

```
Fn=cumsum(fn);  
figure(F)  
plot(d,Fn,'g')  
legend('Fs','Fs data','Fv','Fn')
```

The converted data as a cumulative volume distribution

```
OutputData=[d,Fv]
```

7. General Matlab script to use the PSO in chapter 4, 5 and 9

```
%% Fitted data

helo1=load('Christineallchewsdata.mat');
helo2=load('realmassdata.mat');

data=helo1.alldata; %1 chew to swallow point
data=data(2:11,:); % 2 chew to swallow point

%% Fitness function
fitnessfcn=@(x0) sse(x0,data);

lbound=[90;1;0.0007;1;0];
ubound=[500;3;0.004;3;2];
nvars=length(y);

initial_values=[100.89,2.57,0.0018,2.85,0.76];

options=psoptimset('Generations',200,'PopulationSize',40,'PlotFcns',{@psoplotbestf,@psoplotswarmsurf},'InitialPopulation',initial_values);
dbstop if error
tic
[y PSO, fval, exitflag, output, population, scores]=pso(fitnessfcn,nvars,[],[],[],[],lbound,ubound,[],options);
toc

%% Sum of Squares Fitness function
function [ss]=sse(x0,data1)

%%Model predictions
[MeanC]=modelmeanruns(x0);

%%Normalised residuals
residuals=(MeanC-data1)./data1;

ss=sum(sum((residuals.^2)));

end

%% Mean of 50 simulations function
function [MeanC,stdC]=modelmeanruns(x0)
count=50;
Allop=cell(1,count);

for i=1:count
Allop{1,i}=thelatestmodel(x0);
end

MeanC = mean(cat(3, Allop{:}), 3);
stdC = std(cat(3, Allop{:}), [], 3);

end
```

8. General MATLAB script to solve ODE equations developed in Chapter 8.

```
%% chewing input parameters

k=y(1);
g=y(2);
h=y(3);
let=y(4);
r=y(5);
pfrac=y(6);

%% Input parameters
InitialPSD=load('initialnewPSD.mat');
Factor=[0.169 0.158 0.148 0.237 0.185 0.229 0.258 0.263 0.261 0.221 0.2020
0.2016 0.164 0.211 0.245 0.262 0.245 0.253 0.24657 0.22857 0.16837];

Meanf=mean(Factor);
Dp=sort(InitialPSD.Dp);

%%Size class classification for model that requires size class
biggestsieveclass=5.742;
smallestsieveclass=0.354;
numclass=9;

vanDerGlas=[k,g,h,let];

ParamS=vanDerGlas;

params=r; %r

Paste_vols=0;

for countchewloop=1:chew
    Vp=(pi()*Meanf.*Dp.^3)./4;

chks=sum(Vp);

if modelS==1||2||4

sieve=logspace(log10(biggestsieveclass),log10(smallestsieveclass),numclass)
; %Size in each sieve in mm;

%Count number of particles on sieves
np=zeros(numclass,1); %np means number of particles %Create array of zeros,
10 rows, 1 column
    for i=1:numclass
        np(i)=numel(find(Dp>sieve(i)
    end

np(2:end)=np(2:end)-np(1:end-1);

S=selectionfuncs(sieve,np,modelS,ParamS);
```



```

    Sizeclass=ones (size (Dp));
    Sel=zeros (size (Dp));
    for i=1:numclass
        j=numclass+1-i; %9:1
        Sizeclass (Dp>=sieve (j))=j;
        Sel (Dp>=sieve (j))=S (j);
    end

elseif modelS==3
S=selectionfuncs (Dp, [], modelS, ParamS);
Sel=S;

else

S=[];

end

    RollDice=rand (size (Dp));%create random probability for every particle
    IsSel=RollDice<=Sel;
    SelDp=Dp (IsSel==1); %Selected diameter of particles
    SelVp=Vp (IsSel==1); %Selected diameter of particles
    UnSelDp=Dp (IsSel==0); %UnSelected diameter of particles
    UnSelVp= (pi () .*Meanf .* (UnSelDp.^3))./4; %Unselected volumes

% Pasted particles
Pparticles=pfrac.*SelVp;

%Unpasted particles volume
NewParticles=SelVp-Pparticles;

%Unpasted particles diameter
NewDps= ((4.*NewParticles)./(pi () *Meanf)).^(1/3);

%daughters of unpasted
Daughters1=[];
Pastevol=[];

for i=1:size (NewDps,1)
    [Daughters , NewPaste]=NewDaughters (NewDps (i), modelB, params, 10, Meanf);
    Daughters1=[Daughters1, Daughters];
    Pastevol=[Pastevol, NewPaste];
end

Daughters1=sort (Daughters1');
daughters=(pi () .*Meanf .* (Daughters1.^3))./4;

%All new particles
NewVp=sort ([UnSelVp; daughters;]);

NewVp (isnan (NewVp))=[];

Pastevol (isnan (Pastevol))=0;
Pparticles (isnan (Pparticles))=0;

```

```

%sum of new particles generated
sumnew=sum(NewVp)+sum(PasteVol)+sum(Pparticles);

%check vol conserved or not
balV=chks-sumnew;

%New particles diameter
NewDpChew=((4.*NewVp)/(pi()*Meanf)).^(1/3);
RealDp=NewDpChew;
RealVp=NewVp;

%Find if there is pasted
NewDppasted=NewDpChew(find(NewDpChew<pasted_size));
VolDppasted=(pi()*Meanf.*(NewDppasted.^3))./4;
sumRemainingpasted=sum(VolDppasted);

%Deletethepastedones
NewDpChew(NewDpChew<pasted_size)=[];
NewVp(NewVp<(pi()*Meanf.*(pasted_size.^3))./4)=[];

%Pasted vols
Paste_volume=Paste_vols+sum(PasteVol)+sum(Pparticles)+sumRemainingpasted;
%combine paste from inputs and new paste
Paste_fraction=Paste_volume./chks;

if isempty(Paste_fraction)
    Paste_fraction = 0;
end
if isnan(Paste_fraction)
    Paste_fraction = 0;
end

chiki=sum(NewVp)+Paste_volume;

Cumulative=cumsum(RealVp./chks);

NewDp1=RealDp;

newarea=pi()*NewDpChew.*(NewDpChew.*Meanf+NewDpChew./2);
total_area=sum(newarea);
Dp=NewDpChew;
Paste_vols=Paste_volume;

% ParameterRecord{countchewloop}=ParameterS;
Paste_record(countchewloop)=Paste_volume;
pastedfracrecord(countchewloop)=Paste_fraction;
AreaRecord(countchewloop)=total_area;
Total_record(countchewloop)=chiki;
Nonpastedvol(countchewloop)=chiki-Paste_volume;

end

```

```

%% Outputs from The PSD model

[AreaRecord,Total_record,paste_new]=modeldata1(y,chew,modelS,modelB,pasted_
size);

Nonpastedvol=Total_record-paste_new;

%Saliva volume

a=0.027; %g/chew (gradient constant of linear model)
c=0.8714; %g (vol saliva at rest)

[Volsaliva]= salivamodel(a,chew,c); %in ML
Volsaliva=Volsaliva*1000; %in mm3

%Volume of liquid bolus (mm3) (Vol pasted + Vol saliva)
Liquidvol=paste_new+Volsaliva;

%Volume of bolus
Volumeofbolus=Liquidvol+Nonpastedvol;

%Saturation
Saturation=(Liquidvol./Total_record).*((1-Voidfraction)/Voidfraction);

%% Calculate surface area of bolus
rcubed=(3.*Nonpastedvol)./(4*pi()); %work out from volume of particles
PhiE=0.50;
por=1-PhiE;
S=Saturation;
Phi=(1-por)+por*S;
pors=por*S/(1-por);

SaExp=((1+pors).^(2/3)).*AreaRecord; %Surface area of outer layer
%mm24.*pi()*.*
SaSph=4.*pi()*.*(rcubed./(1-por)).^(2/3); %surface area of bolus
SaBol=((SaSph-SaExp).*Phi+SaExp-PhiE*SaSph)./(1-por);%mm2

% IF SATURATION GREATER THAN 1 ASSUME SPHERICAL BOLUS- WORK OUT FROM BOLUS
% VOLUME
S_m1=find(S>=1);
SaBol(S_m1)=4*pi()*((3.*Volumeofbolus(S_m1))./(4*pi()))^(2/3);

%% Global variables

global ks
global Kas
global Ksr
global kom
global koeq
global kfeq
global kfs
global Afas
global eom
global Kam
global Kfas
global Kfam
global frmasticatory
global fr
global Voamean

```

```

global Vfa
global Vna
global kfm
global efm
global knm
global enm
global tdeg
global tlag
global Vt
global Qs
global Aoam
global Afam
global Anam
global Vfs
global Koam
global Knam

Kas=Kasi;
Ksr=Ksri;

frmastatory=chewingrate; %Chewing frequency %chew/s
tlag=0; %swallowingtime (s)
tdeg=33/chewingrate;
ks=1e-3;% Mass transfer coefficient of liquid bolus (mm/s)
Kas=12.9e-3;% Partition coefficient of air to saliva for 2-nonanone at 37oC
(9.7+/-1.39 e-3) Ethyl propanoate, 12.9+/-5.5 e-3
Ksr=2.14; %Partition coefficient of saliva to rice for 2-NONANONE,0.245 at
37oC Ethyl propanoate, 2.14
kom=1e-3;% Mass transfer coefficient of oral mucosa %mm/s
eom=5e-2; %Thickness of oral mucosa mm
Kam=1e-3; %Partition coefficient of air to oral mucosa
fr=0.25; %Respiratory frequency %cycle/s 0.240.240.25
Voamean=78300; %mean oral volume (mm3)
Vfa=32000; %mean pharynx volume (mm3)
Vna=16000; %mean nasal cavity volume (mm3)20000
% e=0.0342; %Residual thickness layer of liquid bolus in pharynx (mm)
kfm=1e-3; %mass transfer coefficient of pharynx mucosa (mm/s)
efm=5e-2; %thickness of pharynx mucosa (mm)
knm=1e-3;%mass transfer coefficient of cavity mucosa (mm/s)
enm=5e-2; %thickness of nasal cavity mucosa (mm)
Vt=470000; %tidal volume (mm3)800000
Qs=37.8;%mm3/s34.63228.842.12
Cop=0.1512e-9;%g/mm3 %Initial concentration of particles4.8e-9 %2-nonanone
ethyl %0.1512
Vsalrest=c*1000; %mm3
Koms=Kas/Kam;
koeq=1/ks+Koms/kom;
kfs=1e-3;
Kfms=Kfas/Kfam;
kfeq=1/kfs+Kfms/kfm;
Af=6500; %mm2
Afam=0.1*Af;
Afas=Af-Afam;
Kfas=5e-3;
Kfam=1e-3;
Koam=1e-3;
Knam=1e-3;
Ao=11600;
Aoam=0.1*Ao;
Anam=16000;
Vfs=200;

```

```

%% Get simulation time information
chewtime=zeros(1,chew);

for n=1:chew
    chewtime(n)=n/chewingrate;
end

tstep=1/frmasticatory;
Initialconditions=[Vsalrest,0,0,0,0,0,0,0,0];
Ab=0;
Vpaste=0;
opts = odeset('RelTol',1e-3);
[t,y]=ode45(@ (t,y)Newmodell1(t,y,Ab,Vpaste),0:tstep:chewtime(1),Initialcondi
tions); %integrate from 0 to 1 chew

% integrate 1st chew until end of chew
for n=1:chew-1
Vsal=y(end,1);
Csold=y(end,2);
Csnew=((Vsal+paste_new(n)/Ksr)*Csold+(paste_new(n+1)-
paste_new(n))*Cop)/(Vsal+paste_new(n+1)/Ksr);
Ab=SaBol(n);
Vpaste=paste_new(n);
[tn,yn]=ode45(@ (t,y)Newmodell1(t,y,Ab,Vpaste),chewtime(n):tstep:chewtime(n+1
),[y(end,1),Csnew,y(end,3),y(end,4),y(end,5),y(end,6),y(end,7),y(end,8),y(e
nd,9)],opts);
t=[t;tn(2:end)];
y=[y;yn(2:end,:)];
end

Vs=y(:,1);
Cs=y(:,2);
Coa=y(:,4);
% Cfa=y(:,7);
Cna=y(:,9);
maxCna=max(Cna);
relCna=Cna./maxCna;

end

%% ODE equations

function [ode]=Newmodell1(t,y,Ab,Vpaste)

global ks
global Kas
global Ksr
global kom
global kfs
global Afas
global eom
global Koam
global Knam
global Kfas
global Kfam
global frmasticatory
global fr
global Voamean

```

```

global Vfa
global Vna
global kfm
global efm
global knm
global enm
global tdeg
global tlag
global Vt
global Qs
global Aoam
global Afam
global Anam
global Vfs

%% Calculate new values for dependent variables
Vs=y(1);
Cos=y(2);
Com=y(3);
Coa=y(4);
Cfs=y(5);
Cfm=y(6);
Cfa=y(7);
Cnm=y(8);
Cna=y(9);

%% Oral cavity
fropening=fr;%or frrespiratory %frmasticatory
Voa=Voamean*(1+0.2*sin(2*pi()*fropening*t)); %Volume of air in oral cavity
Qoa=0.4*pi()*Voamean*fropening*cos(2*pi()*fropening*t); %Oral cavity air
flow rate
Vom=eom*Aoam;
Vnam=enm*Anam;
Vfam=efm*Afam;

%Consequential variables pharynx
Qna=-pi()*fr*Vt*sin(pi()*2*fr*(t-tlag)); %Nasal cavity air flow rate-tdeg
Qta=Qoa-Qna;

% Liquid bolus (saliva)phase
%Dilution by saliva
%Loss of aroma to the air phase
ode=zeros(9,1);

%Saliva flow rate
ode(1)=Qs;

if t>tdeg
    ode(1)=0;
end
% Mass balance in saliva phase
ode(2)=(-(Ab*ks*(Cos-Coa/Kas))-Vs*Cos)/(Vs+Vpaste/Ksr);

%Mass balance in oral mucosa
ode(3)=- (kom*Aoam*(Com-Coa/Koam))/Vom;

%Air phase
%From liquid bolus,lubricated mucosa and air from pharynx
if Qoa<0

```

```

ode(4) = ((Ab.*ks*(Cos-Coa/Kas))./Voa) + (((kom*Aoam)*(Com-
Coa/Koam))./Voa);
else
ode(4) = ((Ab.*ks*(Cos-Coa/Kas))./Voa) + (((kom*Aoam)*(Com-
Coa/Koam))./Voa) + ((Qoa*(Cfa-Coa))./Voa);
end

%% Pharynx

%Liquid bolus phase
ode(5) = -(kfs*Afas*(Cfs-Cfa/Kfas))./Vfs;

%Lubricated pharynx mucosa
ode(6) = -(kfm*Afam*(Cfm-Cfa/Kfam))./Vfam;

% Air phase
if Qoa < 0
ode(7) = ((kfs*Afas*(Cfs-Cfa/Kas))./Vfa) + (((kfm*Afam)*(Cfm-Cfa/Kfam))./Vfa) -
((Qoa/Vfa)*(Coa-Cfa));
elseif Qna > 0
ode(7) = ((kfs*Afas*(Cfs-Cfa/Kas))./Vfa) + (((kfm*Afam)*(Cfm-
Cfa/Kfam))./Vfa) + ((Qna/Vfa)*(Cna-Cfa));
elseif Qta > 0
ode(7) = ((kfs*Afas*(Cfs-Cfa/Kas))./Vfa) + (((kfm*Afam)*(Cfm-
Cfa/Kfam))./Vfa) + ((Qta/Vfa)*(0-Cfa));
end

%% Nasal cavity

% Nasal cavity mucosa

ode(8) = -(knm*Anam*(Cnm-Cna/Knam))./Vnam;

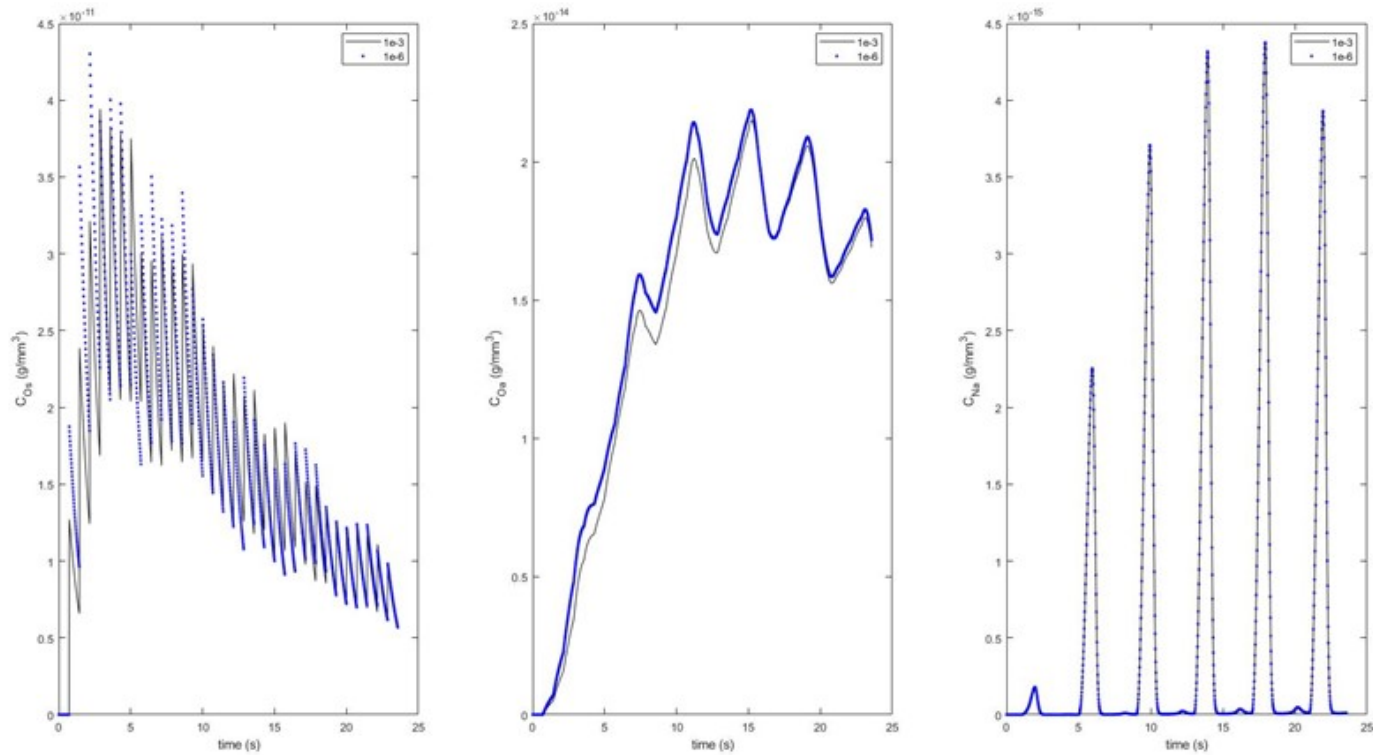
%Air phase in nasal cavity

if Qna < 0
ode(9) = (((knm*Anam)*(Cnm-Cna/Knam))./Vna) - ((Qna/Vna)*(Cfa-Cna)); %/Vna
elseif Qna > 0
ode(9) = (((knm*Anam)*(Cnm-Cna/Knam))./Vna) + ((Qna/Vna)*(0-Cna)); %/Vna
end
end

```

Numerical error checking

1. The figure below shows a comparison of model predictions when different relative tolerances were used to numerically solve the ODE equations developed in Chapter 8. C_{os} , C_{oa} and C_{na} were compared where when relative tolerance of 1×10^{-6} was used it is denoted as the blue dot marker and 1×10^{-3} as the black line.



Appendix B: PSO algorithm formulation

B-1 Formulation and the default parameters that were implemented in the PSO algorithm

The following formulation was implemented in the PSO algorithm of Chen (2009) in Matlab.

$$v_i^{k+1} = \phi^k v_i^k + \alpha_1 [\gamma_{1,i} (P_i - x_i^k)] + \alpha_2 [\gamma_{2,i} (G - x_i^k)] \quad (A - 1)$$

$$x_i^{k+1} = x_i^k + v_i^{k+1} \quad (A - 2)$$

The vectors, x_i^k and v_i^k are the current position and the velocity of the i th particle in the k th generation. P_i refers to the personal best position of each individual, and G is the global best position observed among all the particles up to the current generation. The parameters $\gamma_{1,2} \in [0,1]$ are uniformly distributed random values and α_1 and α_2 are acceleration constants. The function ϕ is the particle inertia which gives rise to a certain momentum of the particles.

The PSO algorithm also implemented the following to ensure the stability of the swarm.

These conditions guarantee convergence to a stable equilibrium.

The conditions are

$$\alpha_1 + \alpha_2 < 4 \quad (A - 3)$$

and

$$\frac{\alpha_1 + \alpha_2}{2} - 1 < \phi < 1 \quad (A - 4)$$

The input and output arguments of the PSO function in MATLAB can be described in Table B- and Table B-, respectively.

Table B-1 Input arguments used in the MATLAB function. For instance, `fitnessfcn` refers to the sum of squares residuals, `nvars` refers to the number of parameters being solved, `lb` and `ub` refers to the upper and lower bound that were set in the algorithm for the solved parameters.

<code>fitnessfcn</code>	Function handle of fitness function
<code>nvars</code>	Number of design variables
<code>Aineq</code>	A matrix for linear inequality constraints
<code>bineq</code>	b vector for linear inequality constraints
<code>Aeq</code>	A matrix for linear equality constraints
<code>beq</code>	b vector for linear equality constraints
<code>lb</code>	Lower bound on x
<code>ub</code>	Upper bound on x
<code>nonlcon</code>	Function handle of nonlinear constraint function
<code>options</code>	Options structure created by calling <code>pso</code> with no inputs and a single output

Table B-2 Output arguments of the PSO algorithm implemented in MATLAB. For example, `x` refers to the parameters that are being solved, `fval` refers to the sum of squares residual.

<code>x</code>	Variables minimising fitness function
<code>fval</code>	The value of the fitness function at x
<code>exitflag</code>	Integer identifying the reason the algorithm terminated
<code>output</code>	Structure containing output from each generation and other information about the performance of the algorithm

The `pso` function is called in MATLAB using the syntax as described in Table B-.

Table B-3 PSO syntax

```
[x, fval, exitflag, output] = pso(fitnessfcn, ...  
                               nvars, A, b, Aeq, Beq, lb, ub, nonlcon, options)
```

The options structure controls the behaviour of the PSO function. The default options structure is described in Table B-.

Table B-4 Default options structure in the PSO function. Empty bracket is denoted as [] where not default value is used.

Option structure	Definition	Default values
PopInitRange	Range of random initial population	0;1
PopulationSize	Number of particles in swarm	40
Generations	Maximum number of generations	200
TimeLimit	Maximum time before pso terminates	Inf
FitnessLimit	Fitness value at which pso terminates	-inf
StallGenLimit	Terminate if fitness value changes less than TolFun over StallGenLimit	50
StallTimeLimit	Terminate if fitness value changes than TolFun over StallTimeLimit	Inf
TolFun	Tolerance on fitness value	1e-6
TolCon	Acceptable constraint violation	1e-6
HybridFcn	Function called after pso terminates	[]
Display	Display output in command window.	'final'
OutputFcns	User specified output function called after each generation.	-
PlotFcns	User specified plot function called after each generation	-
Vectorised	Specify whether fitness function is vectorised.	'off'
InitialPopulation	Initial position of particles	[]
InitialVelocities	Initial velocities of particles.	[]
CognitiveAttraction	Attraction towards personal best	0.5
SocialAttraction	Attraction towards global best.	1.25
VelocityLimit	Limit absolute velocity of particles.	[]

BoundaryMethod	Set method of enforcing constraints.	'penalize'
----------------	--------------------------------------	------------

B-2 MATLAB code to record the state of swarm after each generation

```
function [state,options,changed,str] = SaveOut(options,state,flag)
    file_name = 'SaveBest.mat'; %File name
    if strcmp(flag,'init')
        var = state.Population; %Parameters in the specified population
        var2=state.Generation; %Number of generations, e.g. 200
        var3=state.Score; %Fitness value for each parameter
        var4=state.fGlobalBest; %Best fitness value
        var5=state.xGlobalBest; %Parameters at best fitness value
        save(file_name, 'var','var2','var3','var4','var5')
    elseif strcmp(flag,'iter')
        (Global best)
        ibest = state.fGlobalBest(end); %Best objective function
        ibest = find(state.Score == ibest,1,'last'); % Personal bests
        bestx = state.Population(ibest,:);
        bestx2=state.Generation;
        bestx3=state.Score;
        bestx4=state.fGlobalBest;
        bestx5=state.xGlobalBest;
        bestx6=state.Population;

        previous = load('SaveBest.mat');
        var = [previous.var;bestx];% Read Previous Results, Append New
Value
        var2 = [previous.var2;bestx2];
        var3 = [previous.var3;bestx3];
        var4 = [previous.var4;bestx4];
        var5 = [previous.var5;bestx5];
        var6=[previous.var;bestx6];
        save(file_name, 'var','var2','var3','var4','var5','var6')
    % Write 'Best Individual' To File
    end
        changed = true; %
    end
```

B-3 MATLAB code used to implement the PSO algorithm

Files were obtained from <http://www.mathworks.com/matlabcentral/fileexchange/25986>

Appendix C: Information sheet and consent forms



Rice Chewing Studies

You are invited to take part in a study investigating the breakdown of white rice and during chewing.

If you are aged between 18 and 30 years, have a healthy and complete set of teeth, are happy to have your chewed food analysed, and would like to find out more about the study, please contact:

Muhammad Syahmeer How
PhD student
School of Food and Advanced Technology
Massey University, Palmerston North
Email: M.How@massey.ac.nz

Subjects will be compensated for participating

"This project has been evaluated by peer review and judged to be low risk. Consequently it has not been reviewed by one of the University's Human Ethics Committees.

If you have any concerns about the conduct of this research that you want to raise with someone other than the researcher(s), please contact Professor Craig Johnson, Director (Research Ethics), email humanethics@massey.ac.nz.



Measuring the bolus properties and in vivo aroma release of chewed white rice during chewing

INFORMATION SHEET

Hello,

My name is Muhammad How; I am a PhD student in the School of Food and Advanced Technology, Massey University, New Zealand. I will be working with Prof Isabelle Souchon in this lab for 3 months. My PhD is about modelling the breakdown and the aroma release of rice during oral processing. I wish to obtain *in-vivo* experimental data during my stay here in order to validate the mathematical model that was developed during my PhD.

This study is divided into three parts. First the study aims to measure the properties of expectorated boluses, to obtain data to validate the particle breakdown model. The second part is to obtain *in-vivo* data to validate the aroma release model. The final part includes measuring the oral physiology of the subjects. This will include the saliva flow rate, mastication efficiency and the oral, nasal and pharynx volumes.

Participant involvement

Bolus collection

The trials will involve you chewing on cooked white rice; the samples will consist of a specific mass prepared by the researcher. The samples will be served to you, and you will be required to chew the samples naturally and expectorate the chewed samples in a container. The expectorated samples will be collected and analysed by the researcher.

Saliva collection

This will involve you chewing on a piece of parafilm for several minutes and to spit the saliva in a container. The saliva sample will be collected and analysed by the researcher.

Oral, nasal and pharynx volume

This will involve you to breathe through an acoustic device in order to measure your oral, nasal and pharynx volumes.

In-vivo aroma release

This will involve you to breathe in a nose-piece which will be inserted into your nostrils while chewing cooked white rice samples.

To protect your privacy, all of your data will be placed under a code so that you will not be identified in any publications, and a summary of the findings will be posted to you after data analysis and writing up.

You are under no obligation to accept this invitation. If you decide to participate, you have the right to:

- decline to answer any particular question
- withdraw from the study at anytime
- ask any questions about the study at any time during participation;
- provide information on the understanding that your name will not be used unless you give permission to the researcher
- be given access to a summary of the project findings when it is concluded.

If you are interested in taking part, or have any further questions about the project, please do not hesitate to contact any of the researchers listed below. Your interest will be greatly appreciated. A screening questionnaire will be given to see if you're eligible to take part.

Project Contacts:

Muhammad How

M.How@massey.ac.nz

Prof John Bronlund

J.E.Bronlund@massey.ac.nz

Prof Isabelle Souchon

isabelle.souchon@inra.fr

List of the ingredients that will be used in the test foods

Rice (White)

May contain traces of nuts

Measuring the bolus properties of chewed white rice and aroma release during chewing

Primary questionnaire

Thank you for expressing interest in this study. Prior to your participation, please answer the following questions.

Thank you for expressing interest in this study. Prior to your participation, please answer the following questions.

1. Is your age between 18 and 30?
Y N
2. Do you have 8 post canine teeth?
Y N
3. Do you experience any pain/discomfort while chewing?
Y N
4. Have you suffered any serious jaw injuries in the past?
Y N
5. Do you currently wear tooth braces?
Y N
6. Do you have a problem with dry mouth or salivary flow?
Y N
7. Do you wear dentures?
Y N
8. Do you currently take any medication that might affect saliva flow, such as oxybutynin or amitriptyline?
Y N
9. Do you have a disorder of the mouth?
Y N
10. Do you currently have any significant problems with tooth decay or gum disease?
Y N
11. Have you noticed any tooth grinding or excessive tooth clenching while chewing?
Y N
12. Are you aware of any other health problems that may inhibit your ability to take part in this study or put your health at risk in any way?
Y N
13. Do you suffer from any blood-borne infectious disease?
Y N
14. Are you allergic to any of the ingredients that will be used in this study? (Listed in information sheet)
Y N

If you are able to answer YES to Q1 and NO to all other questions above, you are invited to come and look at the laboratory where the experiments will take place and discuss the project and the role of a participant in more detail.

*Measuring the bolus properties and in vivo aroma release of
chewed white rice during chewing*

PARTICIPANT CONSENT FORM - INDIVIDUAL

I have read the Information Sheet and have had the details of the study explained to me. My questions have been answered to my satisfaction, and I understand that I may ask further questions at any time.

I agree to participate in this study under the conditions set out in the Information Sheet.

Signature: Date:.....

Full Name –printed

Appendix D: Data used in Chapter 4, 5 and 6.

1. 4 g peanut bolus data from Flynn (2012) used in Chapter 4, 5 and 6

Peanuts bolus mean mass (g) of recovered solids (\pm SEM)

Chew cycles	Sieve aperture											
	<0.124 mm		0.125 mm		0.18 mm		0.25 mm		0.355 mm		0.5 mm	
	Mean	\pm SEM	Mean	\pm SEM	Mean	\pm SEM	Mean	\pm SEM	Mean	\pm SEM	Mean	\pm SEM
1	0.00E+00	0.00E+00	6.17E-03	3.04E-03	4.00E-03	1.21E-03	1.77E-03	3.27E-04	7.63E-03	9.91E-04	4.23E-03	1.76E-03
2	0.00E+00	0.00E+00	9.50E-03	3.26E-03	5.63E-03	2.34E-03	4.33E-03	1.42E-03	4.83E-03	3.43E-03	8.53E-03	4.62E-03
4	0.00E+00	0.00E+00	2.66E-02	2.74E-03	1.97E-02	2.31E-03	1.81E-02	1.87E-03	2.74E-02	2.21E-03	3.57E-02	4.36E-03
6	0.00E+00	0.00E+00	3.53E-02	1.86E-02	2.27E-02	1.01E-02	2.27E-02	1.13E-02	3.26E-02	1.56E-02	4.41E-02	2.18E-02
8	0.00E+00	0.00E+00	4.92E-02	1.43E-02	5.33E-02	2.41E-02	4.21E-02	4.58E-03	5.64E-02	7.67E-03	7.31E-02	6.66E-03
10	0.00E+00	0.00E+00	6.10E-02	1.62E-02	5.27E-02	8.24E-03	5.50E-02	4.08E-03	8.79E-02	1.03E-02	9.60E-02	1.49E-02
15	0.00E+00	0.00E+00	1.09E-01	1.62E-02	7.66E-02	7.83E-03	7.97E-02	3.72E-03	1.06E-01	4.88E-03	1.38E-01	5.66E-03
20	0.00E+00	0.00E+00	1.38E-01	2.56E-02	1.13E-01	3.47E-02	1.37E-01	4.16E-02	1.60E-01	4.01E-02	1.80E-01	3.26E-02
25	0.00E+00	0.00E+00	9.03E-02	1.27E-02	6.98E-02	5.90E-03	8.56E-02	1.17E-02	1.10E-01	1.00E-02	1.35E-01	9.30E-03
30	0.00E+00	0.00E+00	1.12E-01	2.57E-02	1.12E-01	2.96E-02	1.10E-01	3.17E-02	1.57E-01	5.69E-02	1.79E-01	5.39E-02
35	0.00E+00	0.00E+00	6.88E-02	1.13E-02	5.96E-02	6.06E-03	7.55E-02	3.76E-03	1.07E-01	3.06E-03	1.36E-01	2.97E-03

Chew cycles	Sieve aperture											
	0.71 mm		1.0 mm		1.4 mm		2.0 mm		2.8 mm		4.0 mm	
	Mean	\pm SEM	Mean	\pm SEM	Mean	\pm SEM	Mean	\pm SEM	Mean	\pm SEM	Mean	\pm SEM
1	6.07E-03	4.27E-03	1.24E-02	4.88E-03	1.00E-02	5.62E-03	3.34E-02	8.63E-03	4.63E-02	2.11E-02	3.22E+00	1.62E-01
2	1.18E-02	7.26E-03	1.60E-02	1.10E-02	1.60E-02	1.52E-02	2.23E-02	1.77E-02	6.73E-02	6.66E-02	2.96E+00	3.12E-01
4	4.05E-02	1.87E-03	4.35E-02	1.17E-02	7.63E-02	1.38E-02	1.24E-01	3.06E-03	1.47E-01	1.90E-02	2.15E+00	7.32E-03
6	5.66E-02	2.63E-02	6.09E-02	2.20E-02	9.97E-02	3.80E-02	1.08E-01	4.17E-02	1.49E-01	6.28E-02	1.67E+00	3.38E-01
8	9.22E-02	7.34E-03	1.33E-01	2.41E-02	1.60E-01	4.03E-02	1.69E-01	2.63E-02	2.25E-01	1.07E-02	8.74E-01	5.36E-01
10	1.23E-01	1.40E-02	1.32E-01	1.53E-02	2.06E-01	6.49E-03	2.45E-01	4.16E-03	2.27E-01	2.07E-02	4.14E-01	1.33E-01
15	1.63E-01	4.00E-03	1.99E-01	1.15E-02	2.31E-01	1.36E-02	1.53E-01	2.37E-02	1.41E-01	3.60E-02	5.91E-02	4.50E-02
20	1.85E-01	2.57E-02	1.93E-01	1.75E-02	1.83E-01	6.12E-03	1.71E-01	8.31E-03	1.43E-01	2.85E-02	6.00E-02	4.18E-02
25	1.59E-01	1.24E-02	1.66E-01	1.59E-02	1.47E-01	9.45E-03	1.08E-01	1.46E-02	5.08E-02	1.19E-02	2.13E-02	2.61E-02
30	1.71E-01	4.04E-02	1.76E-01	3.41E-02	1.28E-01	3.61E-03	1.10E-01	3.47E-02	1.84E-02	1.27E-02	0.00E+00	0.00E+00
35	1.40E-01	9.56E-03	1.46E-01	1.37E-02	1.06E-01	3.05E-03	6.73E-02	8.34E-03	1.87E-02	1.68E-02	0.00E+00	0.00E+00

Fig. D-1 4 g peanut bolus data from Flynn (2012).

2. Peanut bolus data of 2 g and 4 g portion sizes from Flynn (2012) used in Chapter 6.

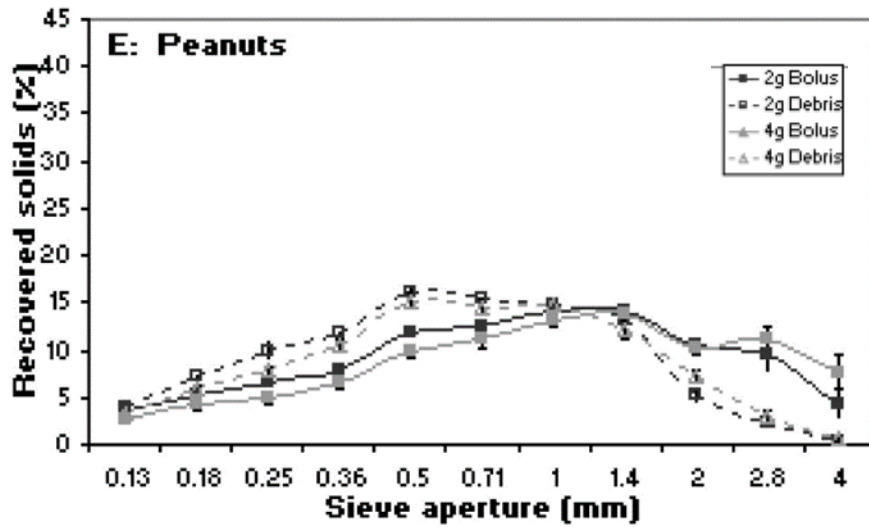


Fig. D-2 Peanut bolus data of 2 g and 4 g portion sizes from Flynn (2012).

3. Peanut bolus data embedded in various matrices (and removed) from Hutchings (2011) used in Chapter 6.

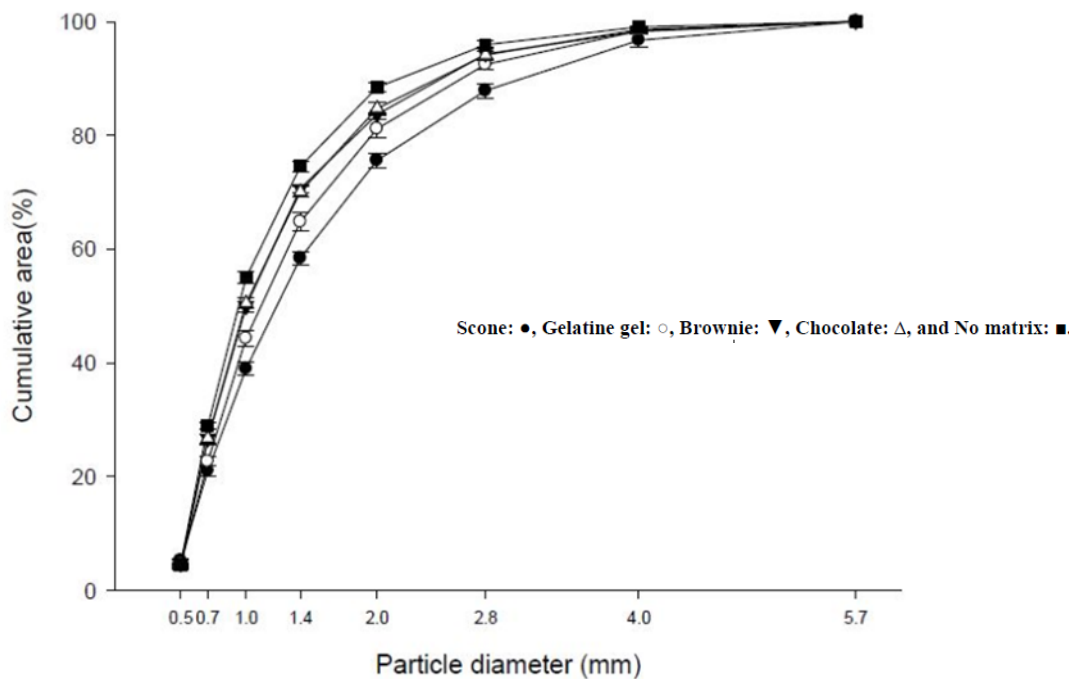


Fig. D-3 Cumulative particle size distribution of peanut particles in the bolus where peanuts which were embedded in matrices were removed.

Appendix E: Effect of chewing on *in vitro* digestion of brown rice

E.1 Introduction

Chewing is known to influence digestion and sensory outcomes. For instance, the PSD of a food bolus, which is an outcome of chewing, is known to influence the breakdown of starch-based foods during *in vitro* digestion (Ranawana et al., 2010; Bornhorst & Singh, 2012; Gao et al., 2020). The increase of bolus saliva content during chewing increases the bolus disintegration rate, which influences the breakdown of bread during simulated gastric digestion (Bornhorst & Singh, 2013). Furthermore, for starch-based foods, the amount of saliva added in the bolus plays a significant role in the breakdown in the proximal regions of the stomach due to the increased presence of α -amylase (Hoebler et al., 1998; Woolnough et al., 2010; Bornhorst & Singh, 2012). The bolus PSD also influences sensory outcomes by increasing the surface area exposure for release of volatiles from the food matrix (Harrison et al., 1998; Wright & Hills, 2003; Wright et al., 2003; Foster et al., 2011; Doyennette et al., 2014).

Chapter 4 and 5 showed how the chewing model developed in Chapter 3 can be applied to a real food system (peanuts). Due to the benefits of chewing on digestion and flavour release, the next step was to test if the model can be applied to a food system which has a direct influence on digestion and that possesses aromatic compounds. If successful the model can be further expanded to include other digestive and/or flavour release models. In order to link such models with chewing, an understanding of the effects of chewing on digestion and flavour release is required. The understanding will help to decide with certainty the inputs and outputs required for the chewing model.

Therefore, Appendix E was aimed at understanding the effects of chewing on digestion of starch rich foods, using brown rice as the model food system. A series of experiments were carried out by a fellow collaborator in Plant and Food Research, Lincoln, New Zealand where 29 subjects were asked to chew cooked brown rice, and their boluses were collected and acidified (to arrest salivary amylase activity). In the study, the bolus PSD and bolus moisture content were measured. In addition, each subject's oral physiological parameters such as the basal saliva flow rate and salivary amylase activity were also measured. To account for digestibility outcomes, the amount of sugar released after an *in-*

vitro digestion was also investigated. The first part of this chapter will therefore aimed to discuss the results of this study in terms of the requirements a chewing model needs to have for starch-based foods.

E.2 Influence of mastication of rice on digestion (An experiment conducted by Plant and Food Research, Lincoln, New Zealand)

E.2.1 Methodology

This section presents a brief description of the experimental methodology conducted by a team of researchers from Plant and Food Research, Lincoln, New Zealand to determine the influence of mastication on digestion. For a more detailed description of the experiments conducted, readers are referred to Kim et al. (2020). In the study, 29 participants (17 female and 12 male, mean age of 26.8 ± 8.4 years, mean BMI of 25.4 ± 3.9) were selected. The subjects were asked to chew cooked brown rice (at their average mouthful volume) at their average chewing time and then expectorate the bolus into a pre-weighed 70 mL plastic screw-cap container (or aluminium drying dish). Three replicates were collected from each subject for bolus particle size, bolus moisture content and *in vitro* digestion (9 samples altogether).

The bolus particle size was analysed using wet sieving and laser diffraction. The proportion of particles bigger (or smaller) than 2 mm (%) was determined from wet sieving. Meanwhile the PSD of the particles smaller than 2 mm, which were suspended in wash water, was measured using a laser diffraction particle size analyzer (Mastersizer 2000, Malvern Instruments Ltd, Malvern, UK). The PSD was described by surface area (μm^2) and the d_{50} , which is the diameter of particle below which 50% of the sample lies. The moisture content of the expectorated bolus on a wet basis (g per 100 g of bolus) was then determined in triplicate. The bolus moisture content was then used to calculate the amount of saliva added to the bolus (g/g dry rice). Lastly, digestion outcomes were investigated by measuring the sugar released after *in vitro* gastric digestion followed by a pancreatic digestion. The acquired data was expressed as mg glucose/g dry bolus sample.

Other than bolus measurements, physiological characteristics of the subjects were accounted for by measuring the subject's basal saliva flow rate and salivary α -amylase activity. Below shows a diagram that briefly describes the experimental setup. Full details of the experiments can be referred in Kim et al. (2020).

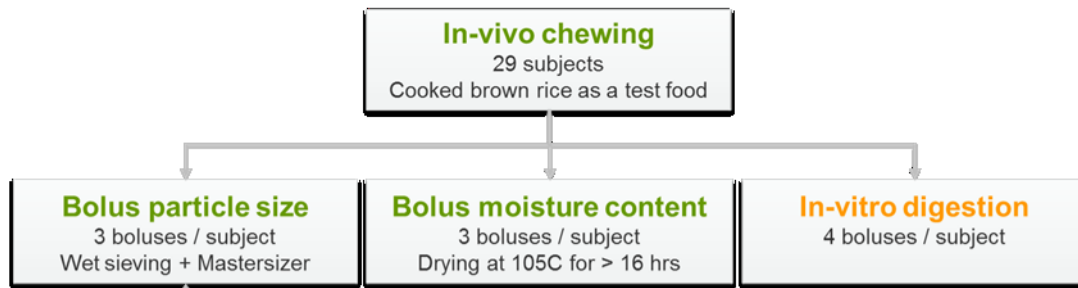


Fig. E-1: A diagram showing the experimental set up to study the influence of oral processing on digestion. Oral processing was accounted for by measuring the bolus particle size and saliva content. Boluses were also used in an *in vitro* digestion where the amount of sugar released was measured. Figure from Kim et al. (2020).

E.2.2 Results and discussion

While some data analysis of the results was carried out in Kim et al (2020), the analysis reported in the remainder of this chapter was carried out as part of this work to explore how chewing links to digestive outcomes. The mean and standard deviation of all of the variables measured for the 29 subjects are described in Table E-1.

Table E-1: Mean and Standard Deviation of oral processing parameters and the amount of sugar released after 120 minutes of *in vitro* digestion for all 29 subjects. Data from Kim et al. (2020)

Variable	Mean	Std. deviation
d_{50} of the particles smaller than 2 mm (μm)	212.12	43.78
Surface area (μm^2)	0.12	0.03
Bolus moisture content (g water/ g wet bolus)	0.65	0.03
Saliva added (g/g dry food)	0.63	0.30
Chew time (s)	22.35	8.42
Proportion of particles smaller than 2 mm (%)	27.63	15.15
Proportion of particles bigger than 2 mm (%)	72.37	15.15
Salivary amylase activity (U/mL)	84.95	79.48
Saliva flow rate at rest (g/min)	0.72	0.30
Sugar released after 120 minutes of <i>in vitro</i> digestion (mg/g dry sample)	682.04	49.09

Table E-2 displays the correlation values of all the measured variables. As can be seen from Table E-2, only a few variables have significant correlation values ($p < 0.05$). The bolus moisture content and the amount of saliva added in the rice bolus (which was derived from the bolus moisture content) were both positively correlated with the amount of sugar released after *in vitro* digestion ($p < 0.05$, $r > 0.4$). The

chewing time was also positively correlated with the amount of sugar released ($p < 0.05$, $r > 0.4$). The proportion of particles greater than 2 mm (%) was negatively correlated with the amount of sugar released but was not significant. The percentage of particles less than 2 mm (%) was positively correlated with the amount of sugar released. Particle size parameters that were derived from particles that were less than 2 mm, such as the surface area (μm^2) and d_{50} (μm) were negatively correlated with the amount of sugar released. Lastly, the saliva flow rate at rest (g/min) and the salivary amylase activity (U/mL) were positively correlated with the amount of sugar released.

Several inferences can be made from the results obtained. Saliva specific parameters such as the amount of saliva added in the bolus, saliva flow rate at rest, the amylase activity and the bolus moisture content all positively correlated with the amount of sugar released. An increase in the amount of saliva would mean there would be an increase in the amount of salivary amylase that can hydrolyse the rice particles in the oral phase or during *in vitro* digestion. This agrees with a previous study which examined the role of salivary amylase during oral processing (Hoebler et al. 1998). They had subjects consume white wheat bread and the bread boluses had more saliva (g/g food) incorporated than the pasta at swallow point and significantly more starch (50%) in the bread bolus was hydrolysed and transformed into molecules of smaller molecular mass compared to pasta (25%) (Hoebler et al., 1998). The authors argued that the lubrication of bread required greater volumes of saliva to coat particles, so a greater amounts of salivary amylase were likely to hydrolyse food starch. However, the authors also mentioned that during mastication, about 31% of starch granules were released from the gluten network, so they were more accessible to amylase compared to spaghetti.

Particle size parameters such as the proportion of large particles % (particles > 2 mm), the surface area of particles that were less than 2 mm (μm^2) and d_{50} (μm) were negatively correlated with the amount of sugar released. This makes sense as larger particles would have a smaller specific surface area; therefore, less surface area will be available for enzymatic hydrolysis relative to their volume. This was also supported with the findings that the proportion of particles less than 2 mm (%) was positively correlated with the amount of sugar released after 120 minutes of *in vitro* digestion. The proportion of particles that were smaller than 500 μm was also found to be significantly correlated with subjects *in vitro* glucose response.

The finding here is comparable with results from published studies looking at the effect of masticated particle size on starch hydrolysis. Hoebler et al. (1998) found that white bread that was masticated into smaller particles than pasta had 50% of the initial starch content hydrolysed and transformed into smaller molecular masses compared to pasta (25% hydrolyses as described above). The author discussed that because the masticated pasta particles were relatively large and the salivary impregnation was relatively low, starch hydrolysis was not significant as it only occurred at the surface of the pasta particles. In another study involving mastication of white Basmati rice, Ranawana et al. (2010) found that subjects who masticated rice to smaller particles showed a higher percentage of rapidly digested starch content in their boluses. Additionally, it was also found that the degree of mastication (15 vs 30 chews) affects the total glycemic response; where the glycemic response when chewing longer was significantly higher (Ranawana et al., 2014). Moreover, in a recent study investigating the impact of different *in vitro* mastication methods (i.e. cutting, cut-and-pestle, blending and grinding) and bread structures (i.e. baked bread, steamed bread and baguette), it was found that the *in vitro* mastication method has significant impact on digestion (smaller particle size has higher starch hydrolysis) while the bread type had no impact (Gao et al., 2020).

The findings as above showed the importance of particle size and saliva to influence digestion. This strengthens the need to predict the PSD and saliva/amylase incorporation when developing models for starch-based food systems.

E.3 Conclusion

Appendix E aimed to identify the main bolus properties that influence digestion from 29 subjects who masticated brown rice. It was found that both particle size and saliva content had significant correlation with the amount of sugar released after *in vitro* digestion, which strengthens the need to model these parameters when oral processing is accounted for to model the overall digestion process.

Table E-2: Pearson correlations between bolus properties (particle size and saliva parameters) and key digestion measures (sugar release after *in vitro* digestion). Values in bold are significant ($p < 0.05$).

Variables	Saliva flow rate at rest (g/min)	Salivary amylase activity (U/mL)	d_{50} (μm)	Specific surface area (μm^2)	Saliva added (g/g dry food)	Bolus MC wet (g water/g wet bolus)	Proportion of particles bigger than 2 mm (%)	Proportion of particles smaller than 2 mm (%)	Chew time (s)	Sugar release (mg/g dry sample)
Saliva flow rate at rest (g/min)	1	-0.376	0.093	0.171	0.213	0.232	-0.087	0.087	0.255	0.085
Salivary amylase activity (U/mL)	-0.376	1	0.035	-0.265	0.040	0.040	0.153	-0.153	0.032	0.339
d_{50} (μm)	-0.093	0.035	1	-0.908	0.406	0.395	-0.240	0.240	0.119	-0.029
Specific surface area (μm^2)	0.171	-0.265	0.908	1	-0.514	-0.513	0.301	-0.301	0.040	-0.103
Saliva added (g/g dry food)	0.213	0.040	0.406	-0.514	1	0.988	-0.732	0.732	0.361	0.409
Bolus MC wet (g water/ g wet bolus)	0.232	0.040	0.395	-0.513	0.988	1	-0.738	0.738	0.376	0.433
Proportion of particles bigger than 2 mm (%)	-0.087	0.153	0.240	0.301	-0.732	-0.738	1	-1.000	0.556	-0.219
Proportion of particles smaller than 2 mm (%)	0.087	-0.153	0.240	-0.301	0.732	0.738	-1.000	1	0.556	0.219
Chew time (s)	-0.255	0.032	0.119	-0.040	0.361	0.376	-0.556	0.556	1	0.421
Sugar release (mg/g dry sample)	0.085	0.339	0.029	-0.103	0.409	0.433	-0.219	0.219	0.421	1

Appendix F: A comparison of the bolus properties of starch-based food systems

Appendix F was aimed at selecting a food system for the model by investigating the bolus properties of three different types of starch-based foods: white rice, *Orzo* pasta and rice crackers. Parameters such as particle size, bolus moisture content, saliva added, and bolus loss were measured and to help decide the most suitable food system to focus model development on. The food system needs to have a minimal bolus loss to be consistent with the assumptions made in the particle breakdown model described in Chapter 3. In addition the bolus properties data have to be reliable to allow a valid comparison against the model predictions. In this study, white rice was chosen rather than brown rice as it is a more popular consumer choice globally (Mohan et al, 2017; Saleh et al.,2019). In addition, it has also been shown to significantly increase the risk of type 2 diabetes, especially among Asian (Chinese and Japanese) populations (Hu et al., 2012). Thus, greater understanding of the role of mastication on this food system can be useful for parts of the population in the world that consume white rice in their diet. *Orzo* was chosen as it has not been featured prominently in the literature on oral processing. Additionally, both white rice and *Orzo* foods form a particulate bolus, and therefore they can be applied to the mechanistic competition models for selection developed by van der Glas et al. (1992). Rice crackers were chosen for preliminary investigation as they may have the potential to break down differently (than rice and *Orzo*) due to their shape and therefore could be an interesting system to test the model against and/or rethink the breakage function, at least for the first few chews. Therefore, the results from this investigation help determine if the foods chosen are suitable for validating the mathematical models developed in this thesis.

F.1 The bolus properties of starch-based foods: a preliminary study

This section aimed to investigate the bolus properties of different types of starch-based foods in a preliminary study by measuring parameters such as PSD, bolus moisture content, saliva added, and bolus loss among four subjects chewing three starch based food systems. The results from this investigation would help determine if the foods chosen were suitable for validating the mathematical models developed in this thesis. Three starch-based foods differing in their physical structure were used in this study; cooked white rice, cooked *orzo* pasta and plain rice crackers. Cooked rice and *orzo* pasta

generally have a soft texture (Kohyama et al., 2005; Drechsler & Bornhorst, 2018) while rice crackers are hard, crispy and brittle (Kohyama et al., 2001).

F.1.1 Preparation of cooked white rice

White Medium Grain rice (Calrose variety, SunRice, Australia) was purchased from a local supermarket (Pak n Save, Palmerston North, New Zealand). Rice was cooked using a 1:2 ratio (125 g rice in 250 g tap water (25°C) in a 2.6 L microwave rice cooker (Sistema®, New Zealand) at 1000 W for 8 minutes using a microwave (Panasonic, Model: NN-7852). After cooking, cooked rice was transferred into a separate container, covered and cooled to room temperature (~ 21°C) prior to in vivo trials. Cooked rice is commonly served at approximately 40-50°C in previous studies (Moongngarm, 2012; Gray-Stuart, 2016) however, as the study was preliminary and because the focus of this work was not about developing population statistics, it was acceptable to serve the cooked rice at room temperature. Moreover, it is challenging to maintain the cooked rice at a specific temperature of 40-50°C as heat from the rice would have been lost immediately after the rice was transferred inside the container for serving. Heating the cooked rice with a microwave or warmer would have resulted in further moisture loss from the rice which could potentially affect the texture.

Rice cooked with different amounts of water has been shown to exhibit different textures; impacting the chewing behaviour of subjects (Kohyama et al., 2005). To evaluate the repeatability of the cooking procedure, rice was cooked in three batches. In each batch, 10 g of cooked rice was taken for moisture content measurement in triplicate. The moisture content measurement followed the methodology as described in section E.1.1 where samples are dried at 105°C in an air-dried oven for a minimum of 16 hours. The moisture content results showed that the rice samples between all batches were within 5% (0.57 ± 0.03 g water/g wet sample) of variation.

F.1.2 Preparation of cooked *Orzo* pasta

Orzo pasta (Riscossa, Italy) was purchased from a local supermarket (Countdown, Palmerston North, New Zealand). *Orzo* pasta was cooked according to the method given by Drechsler and Bornhorst (2018). 500 mL of water was brought to boil on a laboratory hot plate set at 400°C. Once boiled, the hot plate temperature was adjusted to 200°C and 200 g *orzo* pasta was added and cooked for 9 minutes. After cooking, the *Orzo* pasta was drained using a sieve and transferred into a separate container,

covered and cooled to room temperature ($\sim 21^{\circ}\text{C}$) prior to *in vivo* trials. *Orzo* pasta was also cooked in three batches and the moisture content measured to monitor sample consistency. The moisture content measurement followed the methodology as described above for white rice. The batches showed 5% of variation (0.58 ± 0.03 g water/g wet sample).

F.1.3 Rice crackers

Rice crackers (Original flavour, Peckish, New Zealand) were purchased from a local supermarket (Pak n Save, Palmerston North, New Zealand). The average mass of the rice crackers (15 rice crackers) was 1.96 ± 0.16 g. The moisture content measurement followed the methodology as described above. The variation of moisture content between three rice crackers showed 3 % variation (0.0335 ± 0.0009 g water/g wet sample).

F.1.4 Recruitment of subjects

Four healthy subjects (one male and three females, aged from 22 to 28 years old) were recruited for the study. All of the subjects had good overall health, good natural dentition, and no dentures or prosthetic teeth. None of the subjects were taking any medication that could affect muscle function or saliva flow. Subjects gave their written informed consent to participate in the study. They were asked not to eat or drink for at least one hour before the sessions. The study was given ethical approval by Massey University's Human Ethics Committees (4000020047) and was judged to be low risk.

F.1.5 Determination of the number of chews and oral processing time before swallowing for all foods studied

For the cooked rice, 10 g of samples were transferred into small containers in triplicate to determine the number of chews and oral processing time before swallowing. A preliminary study with all four subjects showed that the portion size per mouthful of rice using a tablespoon had a range of 10 ± 2.9 g. The portion size per mouthful for all subjects was determined by asking each subject to take rice using a tablespoon from a container as they would do under normal eating conditions; where the average of three portions was the portion size per mouthful (Moongngarm et al., 2012). The rice in the container was weighed before and after the subject took a spoonful of rice to determine the portion size. Due to the small variation of the rice portion size between all individuals, all four subjects were given 9.98 ± 0.35 g of rice samples (average and standard deviation of 60 samples) in the study.

A similar methodology was employed to obtain the number of chews required to swallow orzo pasta. The portion size per mouthful for all subjects consuming orzo pasta was 8.5 ± 2.0 g. All subjects were then served with 8.68 ± 0.29 g (average and standard deviation of 60 samples) of pasta to determine the number of chews required to swallow.

All subjects took only a single rice cracker when asked to take naturally from a bowl filled with rice crackers. All of them put the whole rice cracker in their mouth for mastication. Because of that, a whole rice cracker was then used to determine the number of chews required to swallow.

The oral processing time before swallowing for all subjects and all foods were measured from the point when the food sample was placed in the mouth and stopped when the subjects raised their hand to indicate they were ready to swallow. The number of chews taken to reach the swallowing point was counted by observing the upward and downward movement of the chin. Triplicate trials were performed for each subject, and the average value was calculated.

F.1.6 Bolus collection

Each subject participated in three sessions (one session for each food type) of 1 hour in the morning, to avoid any circadian variation, on three separate days. They were asked not to eat any food or drink (except water) for at least 1 hour before the sessions. Subjects were asked to chew and expectorate boluses at different stages of the mastication time. These stages were determined according to the number of chews needed to form a bolus of each food type ready for swallowing as described in F.1.5 previously. The number of chews needed to reach the swallowing point was considered to have a mastication stage of 100%. Three data points were selected before the swallowing point by calculating the number of chews that corresponded to 25, 50 and 75% of the total number of chews. One data point was selected after the swallowing point by asking the subjects to hold the food in the mouth and continue to chew for a chew number 25% beyond the swallow point (125% mastication stage). The subjects produced three replicates for each stage of the mastication in each food type. The samples were collected in a randomised order for each participant. A total of 180 boluses corresponding to different mastication stages for the three food types studied were analysed for moisture content, and 15 boluses were analysed for particle size for one of the subjects.

F.1.7 Bolus moisture content, the amount of saliva added and the percentage of recovered bolus

Subjects were asked to expectorate their bolus in pre-weighed aluminium dishes and then asked to rinse their mouths with 30 mL of water before and after chewing the rice to ensure the oral cavity was clean before each sample. The rinsings (remaining particles dispersed in the mouth) were not collected. The moisture content of the expectorated bolus (g per g of bolus) was determined in triplicate for each oral processing moment by drying the bolus samples in an oven at 110°C for a minimum of 15 hours (Jourden et al., 2017). The moisture content was calculated as $MC_{wet} = (m_0 - m_1)/m_0$, where m_0 is the mass before drying (g) and m_1 is the mass after drying (g). The moisture content on a dry basis was calculated using the formula: $MC_{db} = MC_{wet}/(1 - MC_{wet})$. The amount of saliva added to the bolus (g) was calculated as $(MC_{db, bolus} - MC_{db, food}) \times m_1$ where $MC_{db, bolus}$ represents the moisture content of the collected bolus on a dry basis and $MC_{db, food}$ represents the dry basis food moisture content before chewing. The percentage of recovered bolus were calculated by subtracting the initial dry weight of the food from the dry weight of the bolus (Drago et al. 2011; Motoi et al., 2013).

F.1.8 Preliminary particle size measurements

A preliminary study was conducted to measure the PSDs of the bolus samples by image analysis to check if the measurements provided for the three foods were reliable enough for model validation. Because particle size analysis is a laborious process, a single subject was first asked to chew a single replicate of each food type as an ‘instrumental’ measure. The image analysis method was adapted from Hutchings et al. (2011). The bolus and debris washings sample were sieved across a 355 µm sieve with warm water for 30 seconds, which caused the bulk of the food matrix to be washed through the sieve. The retained food particles (rice, *Orzo* and rice crackers) were then placed onto two plastic Petri dishes (140 mm diameter) (Biolab, Auckland, New Zealand) and 30 mL of absolute ethanol (Thermo Fisher Scientific New Zealand, Albany, New Zealand) was added (in each petri dish) to disperse the particles. Particles in the Petri dish were then scanned at 800 dpi using a flatbed desktop scanner (Epson Perfection V30). The scanned images were then analysed using ImageJ® (version 1.52a, National Institute of Health, USA). A black and white threshold was applied to the images to convert to binary where the number of particles and projected area were measured using a nucleus counter. The particle size measurements from ImageJ were saved in Microsoft Excel files. The projected area of each particle was then assumed circular, and the area-based diameter was derived.

The representative images of the scanned bolus particles at 25% and 100% mastication stage for the studied subject are shown in Fig. F-1 to provide clarity to the reader. The PSDs (diameter vs cumulative projected area fraction) across all mastication stages is shown in Fig. F-3. Comparing between the food types visually (Fig. F-1), there were many small particles present in the rice crackers bolus, followed by rice and *Orzo* respectively. The presence of these small particles present several issues to the particle size measurements. Firstly, these small particles abutted, and were difficult to separate even after dispersion with ethanol (Fig. F-2). The presence of these agglomerated particles will affect the reliability of the particle size results. For instance, the d_{50} (diameter of particles at the 50th percentile) for rice is 2.8 mm at 25% mastication stage and 4.2 mm at 100% mastication stage Fig. F-3) which clearly suggests particle agglomeration. For *Orzo* pasta which possess the least amount of small particles, the particle size reduction is to be expected with increasing chewing number. For some food, the washing process prior to scanning and dispersion in ethanol seem to dissolve some of the bolus significantly, as can be observed in rice crackers especially at the swallow point (Fig. F-1). This is certainly an issue for this study as more bolus will be lost, therefore the assumption of negligible bolus losses in the model cannot be valid should rice cracker was used as the model food system.

Because of the challenges to characterise PSD using the method above, particle size was not measured for the rest of the subjects. Clearly, for the foods used in this study, modifications need to be made to the particle size method above to obtain a reliable and valid data to validate the model developed in this thesis. The bolus will need to be pre-processed to separate the abutting particles prior to image analysis. For example, in the literature, particle size measurements on a starch-based food (bread) boluses were dispersed in a highly viscous medium (glycerol) and put under constant shaking to aid in separation of particles prior to image analysis (Le Bleis et al., 2013; Jourdren et al., 2016; Gao et al., 2020).

F.1.9 Results and discussions

F.1.9.1 Bolus moisture content, amount of saliva added and % of bolus recovered during mastication of starch-based foods

The number of chews conforming to all subjects 25, 50, 75% and 125% of the total number of chews (100%) and their corresponding chewing time are summarised in Table F-1. The total number of chews required to swallow for all three foods were pre-determined as described in section F.1.5. In general,

cooked white rice required a greater number of chews compared to *Orzo* pasta and rice crackers in all subjects (except subject D who chewed *Orzo* the greatest).

Table F-1: Number of chews and mastication time corresponding to the subjects 25, 50, 75 and 125% of the total number of chews (100%) for all foods.

Parameter	Unit	25%	50%	75%	100%	125%
Number of chews (rice)	A	9	17	26	34	43
	B	5	11	16	21	26
	C	6	11	17	22	28
	D	8	15	23	30	38
Number of chews (<i>Orzo</i>)	A	8	16	24	32	40
	B	5	9	14	18	23
	C	5	10	14	19	24
	D	9	17	26	34	43
Number of chews (cracker)	A	7	13	20	26	33
	B	3	5	8	10	13
	C	8	16	24	32	40
	D	5	11	16	21	26
Mastication time (rice)	A	7.3 ± 0.5	14.3 ± 0.5	20.0 ± 0.8	27.7 ± 1.7	35.7 ± 1.3
	B	2.6 ± 0.2	5.4 ± 0.1	6.9 ± 1.1	11.1 ± 0.8	12.4 ± 0.5
	C	6.0 ± 0.0	11.0 ± 0.8	15.7 ± 0.5	23.7 ± 4.6	25.0 ± 0.0
	D	5.3 ± 0.1	10.5 ± 0.9	15.7 ± 0.5	18.6 ± 0.6	23.4 ± 0.3
Mastication time (<i>Orzo</i>)	A	5.7 ± 0.0	12.1 ± 0.5	17.9 ± 0.5	23.3 ± 0.5	29.9 ± 0.6
	B	2.6 ± 0.2	4.4 ± 0.2	6.6 ± 0.1	8.4 ± 0.0	10.7 ± 0.3
	C	5.3 ± 0.3	9.8 ± 0.5	12.9 ± 1.9	18.2 ± 1.3	22.4 ± 0.9
	D	6.0 ± 0.8	9.7 ± 0.5	14.3 ± 0.9	20.0 ± 0.8	24.7 ± 0.5
Mastication time (cracker)	A	4.5 ± 0.4	10.8 ± 1.8	14.9 ± 0.2	20.5 ± 1.7	25.5 ± 1.1
	B	1.2 ± 0.1	2.2 ± 0.4	3.5 ± 0.1	4.4 ± 0.4	5.7 ± 0.3
	C	6.2 ± 0.9	11.3 ± 0.3	17.6 ± 0.4	25.5 ± 1.0	29.2 ± 0.6
	D	2.9 ± 0.4	6.5 ± 0.7	8.4 ± 0.2	10.6 ± 0.6	13.1 ± 0.5

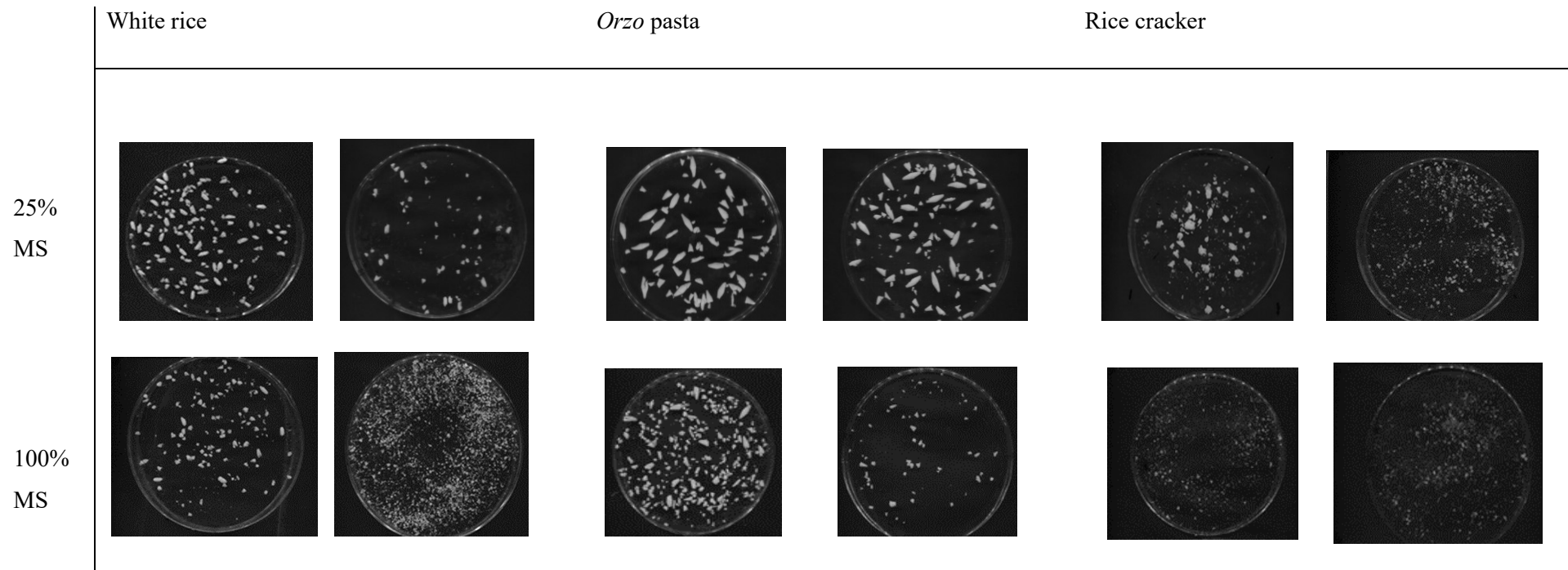


Fig. F-1 Representative scanned images of rice, *Orzo* and rice cracker boluses at 25% and 100% MS (mastication stages) (single replicate). The two pictures in each MS and food type represent the two petri dishes used to analyse the bolus. The subject's swallow point (100% MS) for rice is 30 chew, *Orzo*, 34 chew and rice cracker, 21 chew.

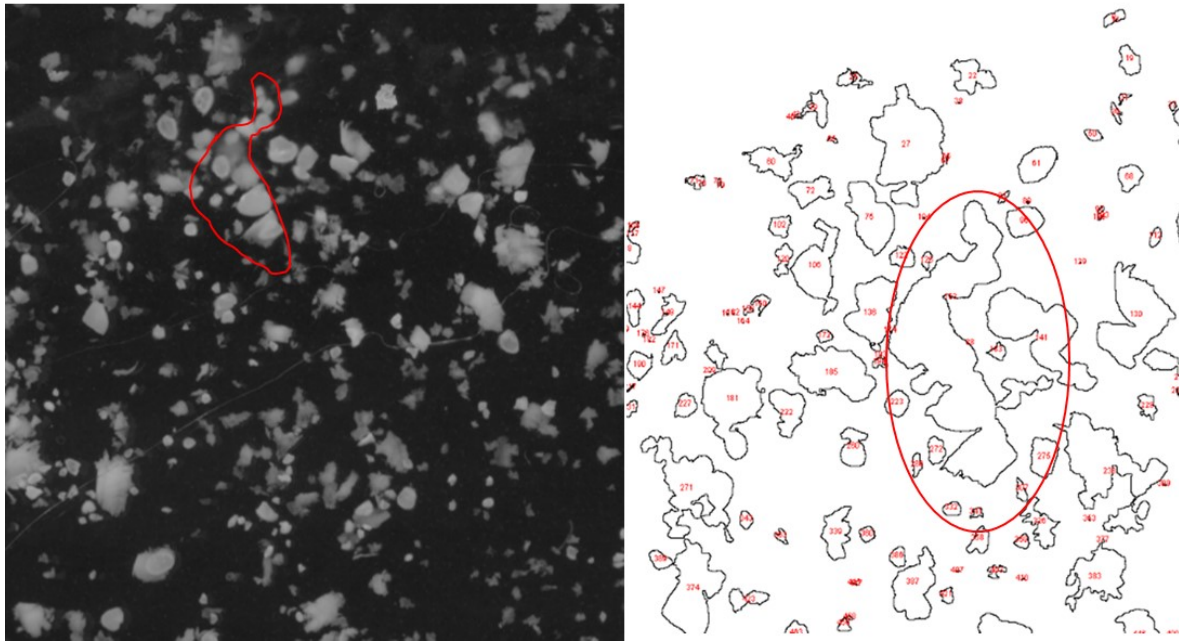


Fig. F-2 Images to show the effect of abutting rice particles on the particle size analysis. Image on the left is before analysis and on the right is after analysis by ImageJ. It can be seen from the figure that because the particles are close to each other, ImageJ considers the particles as a single particle. This will result to an erroneous PSD output, which makes it challenging to compare against model predictions.

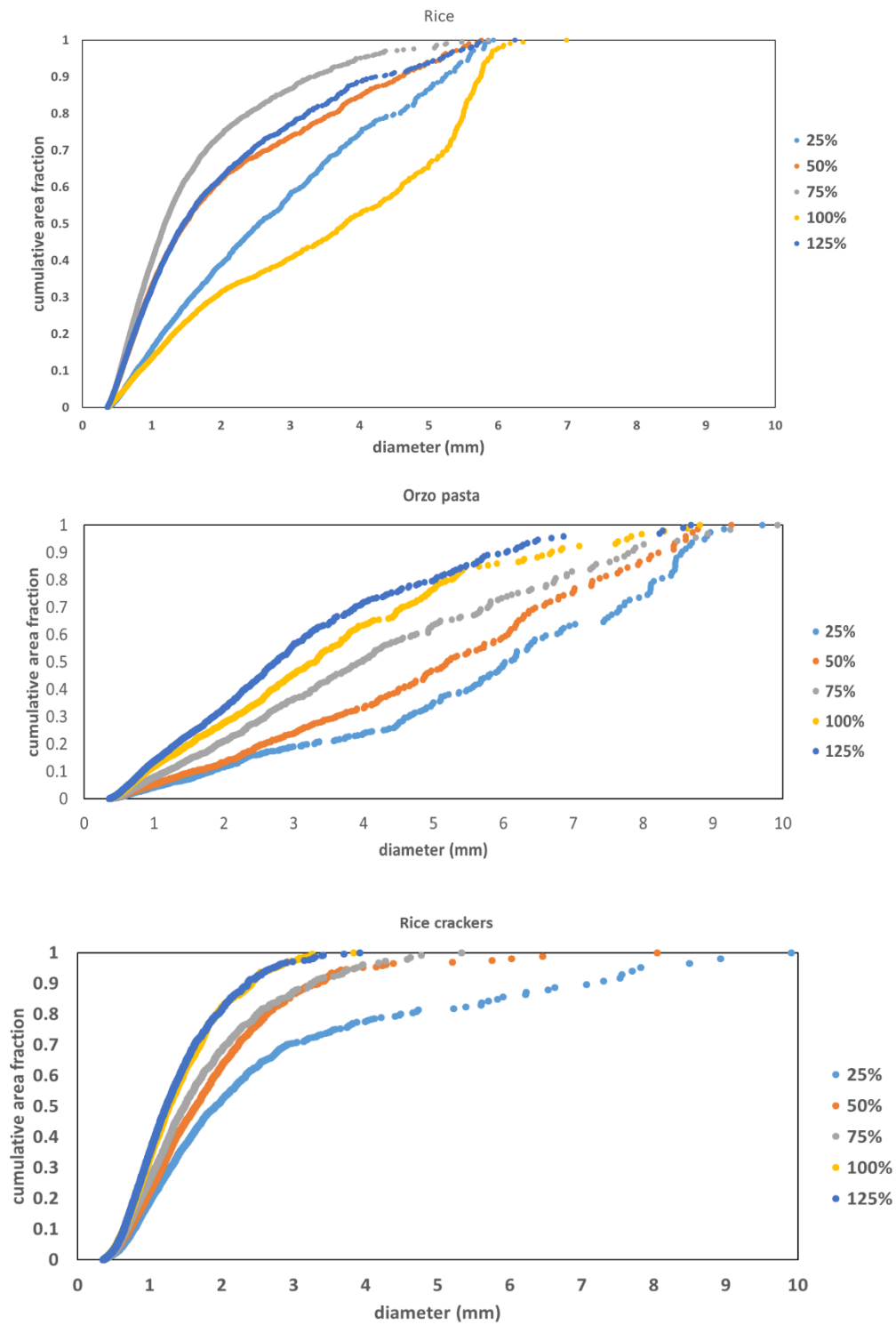
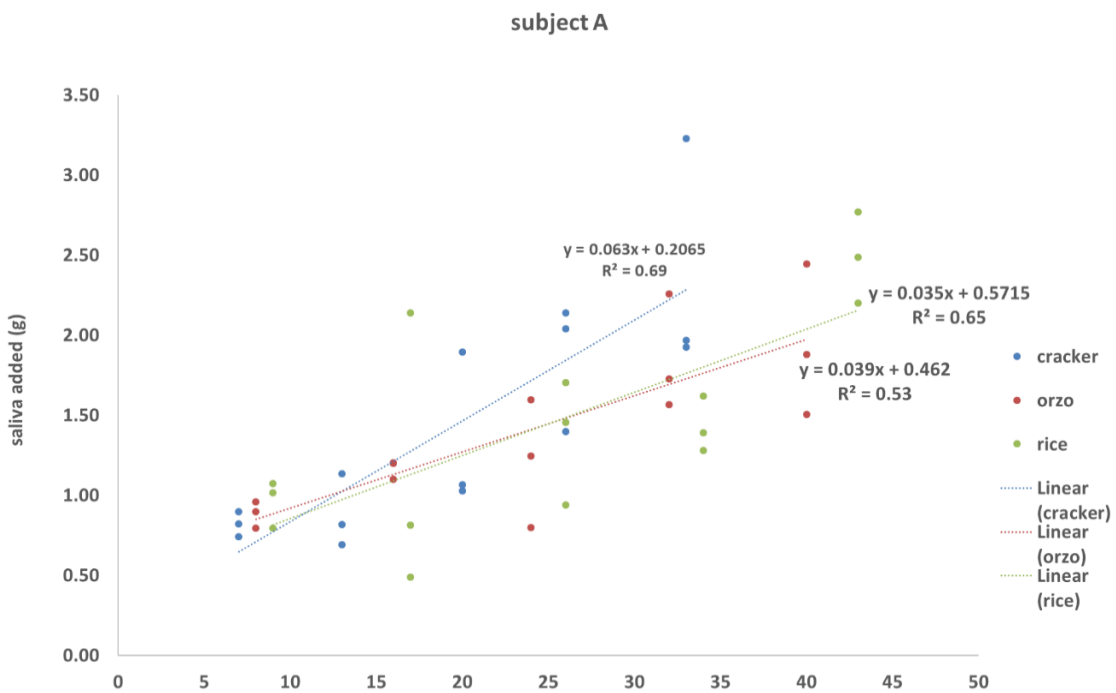
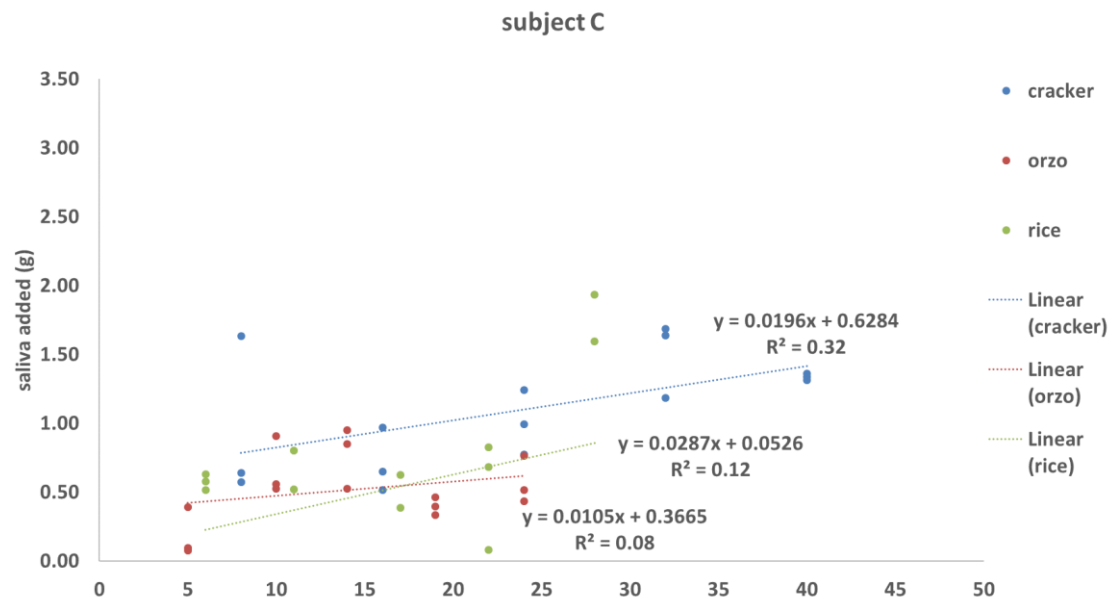
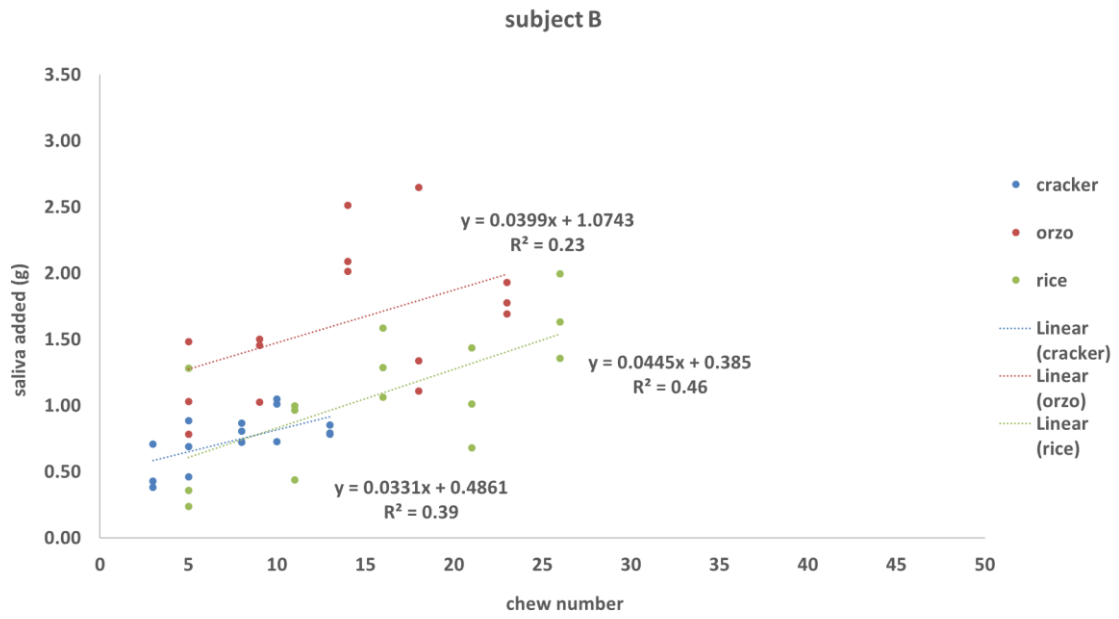


Fig. F-3 PSD presented as diameter (mm) vs cumulative projected area fraction for rice, orzo and rice cracker (single replicate). The subject's swallow point (100% MS) for rice is 30 chew, *Orzo*, 34 chew and rice cracker, 21 chew.

In general, the amount of saliva addition increased with increasing numbers of chews for all three foods, although they were not as pronounced for subjects B and C. Using a regression model to fit linear slopes to each food, saliva addition was reasonably linear over the number of chews for subjects A and D ($R^2 > 0.5$) (Fig. F-4). For these two subjects, the increase in saliva addition with mastication stages was more correlated with the rice crackers (A, $R^2=0.69$, D, $R^2=0.76$) followed by rice (A, $R^2=0.65$, D, $R^2=0.61$) and *Orzo* (A, $R^2=0.53$, D, $R^2=0.55$). When the slopes between different foods were compared for subject A, the change was somewhat similar for cooked white rice and *Orzo* pasta, but the gradient for rice crackers was two times higher.





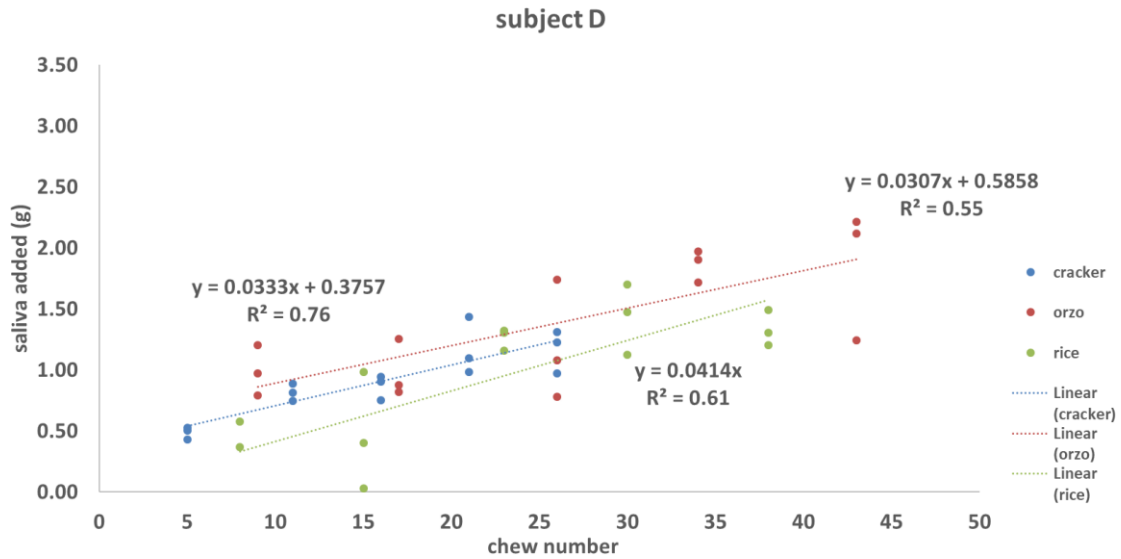


Fig. F-4: Saliva addition vs chew number for all subjects.

Similar work has also been reported by others in the literature, in particular for rice. When studying the effect of chew number on saliva secretion in 10 subjects using three varieties of rice, it was shown as the number of chews increased, saliva continued to increase linearly (Liu et al., 2020).

Fig. F-5 shows the bolus moisture content results in all subjects. In general, the bolus moisture content of the rice crackers was the lowest when comparing between all foods. The moisture content of the rice crackers increases sharply as chewing number increases and was reasonably constant for rice and *Orzo* due to the difference in serving sizes (rice cracker ~ 2.0 g, rice ~ 10.0 g, *Orzo* ~ 9.0 g). The percentage of bolus recovered % for all subjects is shown in Fig. F-6.

As shown in Fig. F-6, in general, rice crackers had the lowest percentage of bolus recovered when comparing with all foods. The loss could be attributed to a mixture of processes such as the dissolution of soluble components in the foods during oral processing, the melting and extraction of fats, transport of the bolus to the oropharynx prior to swallowing and intermediary swallows (Flynn et al., 2011).

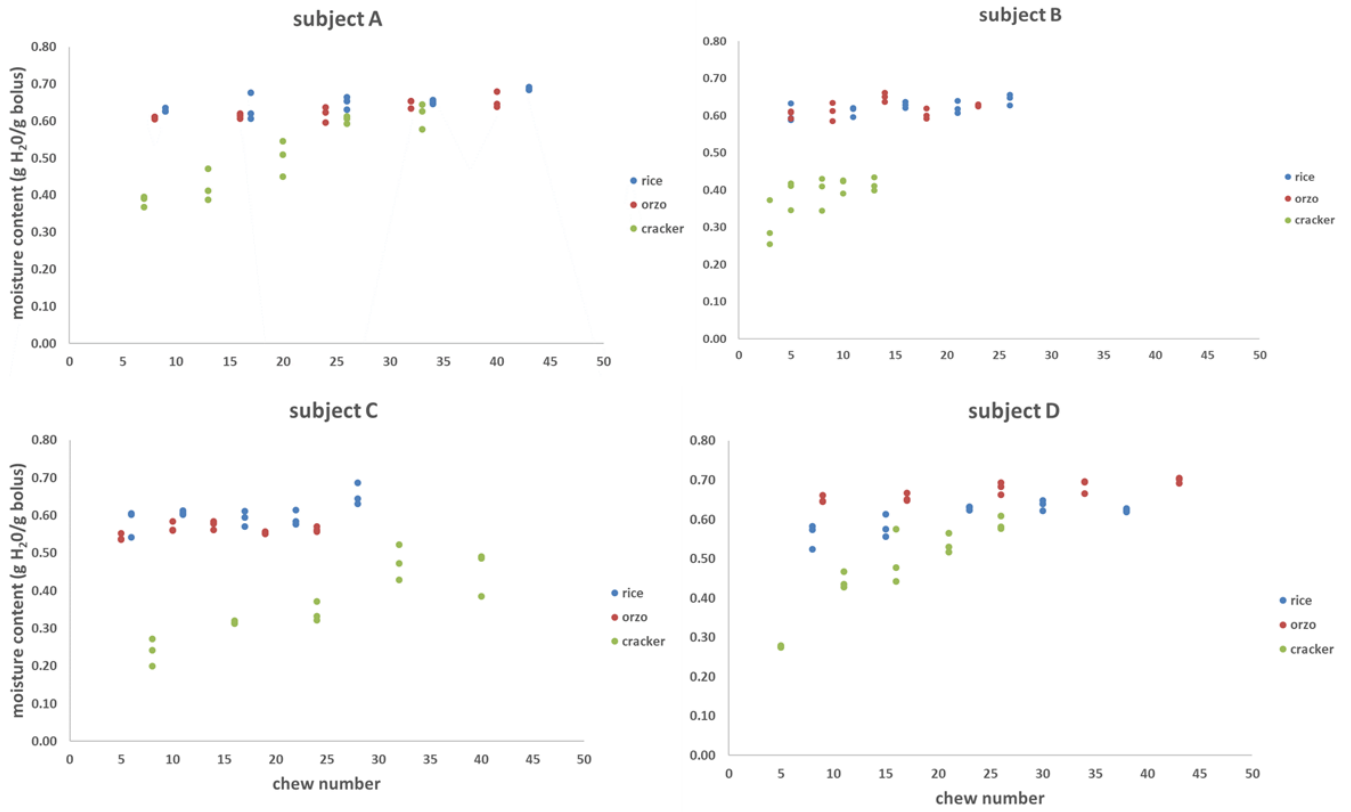


Fig. F-5: Bolus moisture content vs chew number for all subjects.

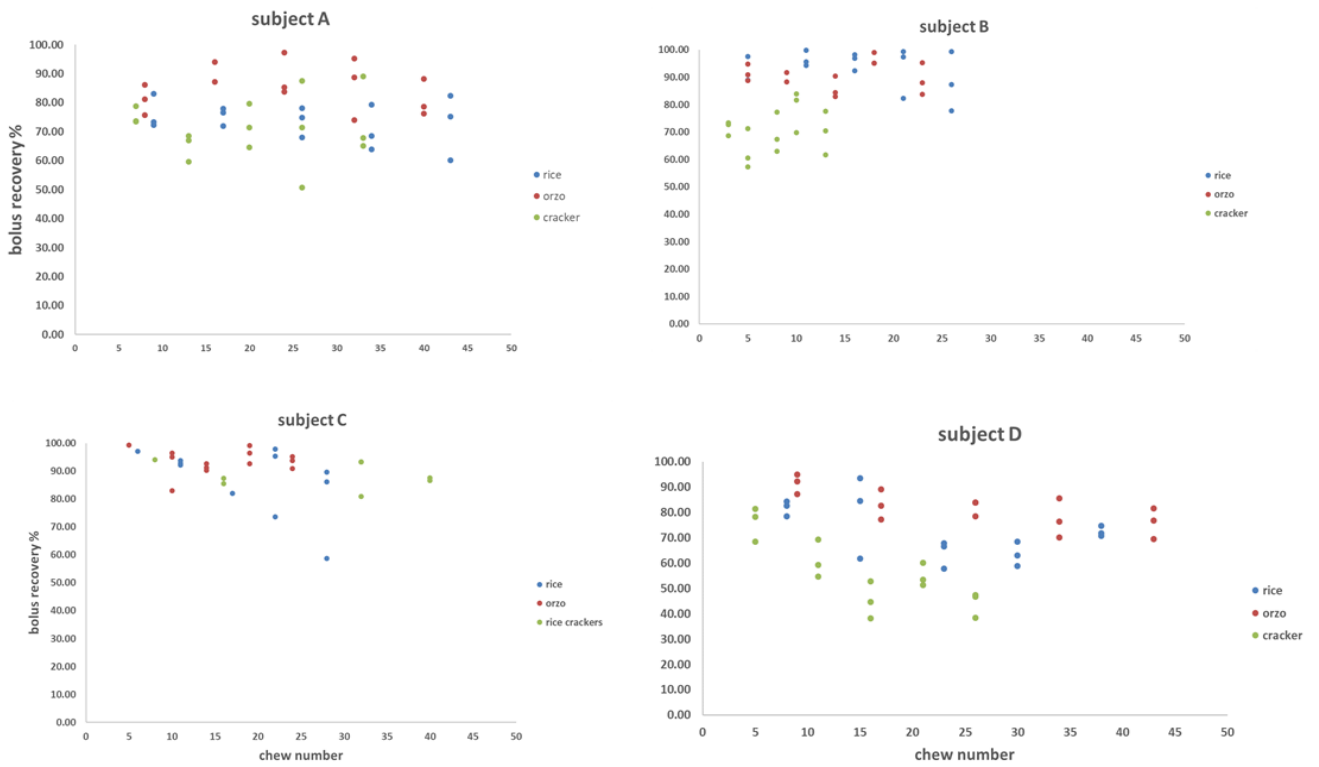


Fig. F-6: Percentage of bolus recovered for all subjects.

F.1.9.2 Selection of food for modelling study

This work investigated the bolus properties of three starch-based foods to gain insights into selecting a model food to validate the models developed in this thesis. Because of the assumption of negligible bolus losses in the chewing model, the food needed to have minimal bolus losses after mastication. The model also requires a saliva addition function, and this is normally obtained from the slope of the saliva added vs chew number where a linear model is fitted (Doyennette et al., 2014; Gray-Stuart, 2016). In this way, the model can approximate saliva addition with a constant saliva flow rate. Thirdly, the food also needs to be aromatic if the chewing model is coupled with model that describes flavour release. Preliminary studies on the bolus PSD showed that the rice cracker bolus was dissolved during analysis, causing further loss of the bolus. When the amount of saliva addition in the bolus of all food types were explored, it increased linearly for all foods but was more pronounced in rice cracker. However, the moisture content experiment revealed the rice cracker had the highest bolus losses, therefore the assumption of negligible bolus losses is not valid should rice crackers be used. The bolus losses of rice and *Orzo* were relatively smaller compared to rice cracker, however the increase in saliva with chew number seems to fit the linear model better for rice compared to *Orzo*. This finding is also backed up with the results in the literature on mastication of rice of 10 people who found that the amount of saliva added increases linearly with chew number (Liu et al., 2020). In addition, some rice varieties such as basmati and jasmine rice are aromatic (Bryant & McClung, 2011; Routray & Rayaguru, 2018), therefore rice was selected as the model food system to test against a coupled chewing and aroma release model.

F.2 Conclusion

Appendix F aimed to investigate the bolus properties (e.g. PSD, bolus moisture content, saliva added and bolus losses) among three potential model foods to help identify which food was the most suitable for applying the mathematical models developed in this thesis.

The PSD results showed that due to presence of abutting particles during analysis, the method needs to be modified to obtain a reliable data for modelling. In addition, it was also observed from scanned images that rice cracker boluses had significant losses during the bolus pre-processing stage. Therefore, the assumption of negligible bolus losses of the chewing model cannot be applied should rice cracker be used. When the bolus moisture content results were compared, all foods increased

linearly with chew number but this was more obvious in rice crackers for two of the subjects. Rice cracker also had the highest bolus losses when the amount of recovered solids were measured. The increase in saliva addition also increases reasonably linearly for white rice, followed by *Orzo* for two of the subjects studied.

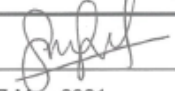

In view of these results, white rice was chosen because it had low bolus losses, a constant saliva flow rate during chewing and aromatic properties.



GRADUATE
RESEARCH
SCHOOL

STATEMENT OF CONTRIBUTION DOCTORATE WITH PUBLICATIONS/MANUSCRIPTS

We, the candidate and the candidate's Primary Supervisor, certify that all co-authors have consented to their work being included in the thesis and they have accepted the candidate's contribution as indicated below in the *Statement of Originality*.

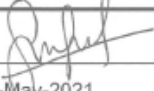

Name of candidate:	Muhammad Syahmeer How Mohd Firdaus How
Name/title of Primary Supervisor:	Professor John Bronlund
In which chapter is the manuscript /published work: 6	
Please select one of the following three options:	
<input checked="" type="radio"/> The manuscript/published work is published or in press <ul style="list-style-type: none"> • Please provide the full reference of the Research Output: How, M. S., Jones, J. R., Morgenstern, M. P., Gray-Stuart, E., Bronlund, J. E., Saint-Eve, A., ... & Souchon, I. (2021). Modelling the role of oral processing on in vivo aroma release of white rice: Conceptual model and experimental validation. <i>LWT</i>, 141, 110918. 	
<input type="radio"/> The manuscript is currently under review for publication – please indicate: <ul style="list-style-type: none"> • The name of the journal: • The percentage of the manuscript/published work that was contributed by the candidate: • Describe the contribution that the candidate has made to the manuscript/published work: 	
<input type="radio"/> It is intended that the manuscript will be published, but it has not yet been submitted to a journal	
Candidate's Signature:	
Date:	17-May-2021
Primary Supervisor's Signature:	
Date:	17-May-2021

This form should appear at the end of each thesis chapter/section/appendix submitted as a manuscript/publication or collected as an appendix at the end of the thesis.



STATEMENT OF CONTRIBUTION DOCTORATE WITH PUBLICATIONS/MANUSCRIPTS

We, the candidate and the candidate's Primary Supervisor, certify that all co-authors have consented to their work being included in the thesis and they have accepted the candidate's contribution as indicated below in the *Statement of Originality*.

Name of candidate:	Muhammad Syahmeer How Mohd Firdaus How
Name/title of Primary Supervisor:	Professor John Bronlund
In which chapter is the manuscript /published work: 3 and 4	
Please select one of the following three options:	
<input type="radio"/> The manuscript/published work is published or in press <ul style="list-style-type: none"> • Please provide the full reference of the Research Output: 	
<input checked="" type="radio"/> The manuscript is currently under review for publication – please indicate: <ul style="list-style-type: none"> • The name of the journal: Journal of Food Engineering • The percentage of the manuscript/published work that was contributed by the candidate: 80.00 • Describe the contribution that the candidate has made to the manuscript/published work: Conceptualization, Methodology, Investigation, Visualization, Formal analysis, Writing - original draft. 	
<input type="radio"/> It is intended that the manuscript will be published, but it has not yet been submitted to a journal	
Candidate's Signature:	
Date:	17-May-2021
Primary Supervisor's Signature:	
Date:	17-May-2021

This form should appear at the end of each thesis chapter/section/appendix submitted as a manuscript/publication or collected as an appendix at the end of the thesis.